frontiers | Research Topics

Development, assessment, improvement, and standardization of methods in herbal drug research

Edited by
Gunawan Indrayanto, Kornkanok Ingkaninan and Abdul Rohman

Published in
Frontiers in Pharmacology

ISSN 1664-8714
ISBN 978-2-83250-908-1
DOI 10.3389/978-2-83250-908-1

About Frontiers

Frontiers is more than just an open access publisher of scholarly articles: it is a pioneering approach to the world of academia, radically improving the way scholarly research is managed. The grand vision of Frontiers is a world where all people have an equal opportunity to seek, share and generate knowledge. Frontiers provides immediate and permanent online open access to all its publications, but this alone is not enough to realize our grand goals.

Frontiers journal series

The Frontiers journal series is a multi-tier and interdisciplinary set of open-access, online journals, promising a paradigm shift from the current review, selection and dissemination processes in academic publishing. All Frontiers journals are driven by researchers for researchers; therefore, they constitute a service to the scholarly community. At the same time, the *Frontiers journal series* operates on a revolutionary invention, the tiered publishing system, initially addressing specific communities of scholars, and gradually climbing up to broader public understanding, thus serving the interests of the lay society, too.

Dedication to quality

Each Frontiers article is a landmark of the highest quality, thanks to genuinely collaborative interactions between authors and review editors, who include some of the world's best academicians. Research must be certified by peers before entering a stream of knowledge that may eventually reach the public - and shape society; therefore, Frontiers only applies the most rigorous and unbiased reviews. Frontiers revolutionizes research publishing by freely delivering the most outstanding research, evaluated with no bias from both the academic and social point of view. By applying the most advanced information technologies, Frontiers is catapulting scholarly publishing into a new generation.

What are Frontiers Research Topics?

Frontiers Research Topics are very popular trademarks of the *Frontiers journals series*: they are collections of at least ten articles, all centered on a particular subject. With their unique mix of varied contributions from Original Research to Review Articles, Frontiers Research Topics unify the most influential researchers, the latest key findings and historical advances in a hot research area.

Find out more on how to host your own Frontiers Research Topic or contribute to one as an author by contacting the Frontiers editorial office: frontiersin.org/about/contact

Development, assessment, improvement, and standardization of methods in herbal drug research

Topic editors

Gunawan Indrayanto — University of Surabaya, Indonesia

Kornkanok Ingkaninan — Naresuan University, Thailand

Abdul Rohman — Gadjah Mada University, Indonesia

Citation

Indrayanto, G., Ingkaninan, K., Rohman, A., eds. (2022). *Development, assessment, improvement, and standardization of methods in herbal drug research*. Lausanne: Frontiers Media SA. doi: 10.3389/978-2-83250-908-1

Table of contents

frontiers | Frontiers in Pharmacology

TYPE Editorial
PUBLISHED 16 November 2022
DOI 10.3389/fphar.2022.1071194

OPEN ACCESS

EDITED BY
Javier Echeverria,
University of Santiago, Chile

REVIEWED BY
Dâmaris Silveira,
University of Brasilia, Brazil

*CORRESPONDENCE
Abdul Rohman,
bdulkimfar@gmail.com

SPECIALTY SECTION
This article was submitted to Ethnopharmacology, a section of the journal Frontiers in Pharmacology

RECEIVED 15 October 2022
ACCEPTED 26 October 2022
PUBLISHED 16 November 2022

CITATION
Rohman A, Indrayanto G and Ingkaninan K (2022), Editorial: Development, assessment, improvement, and standardization of methods in herbal drug research. *Front. Pharmacol.* 13:1071194. doi: 10.3389/fphar.2022.1071194

Editorial: Development, assessment, improvement, and standardization of methods in herbal drug research

Abdul Rohman[1]*, Gunawan Indrayanto[2] and Kornkanok Ingkaninan[3]

[1]Department of Pharmaceutical Chemistry, Faculty of Pharmacy and Center of Excellence, Institute for Halal Industry and Systems, Universitas Gadjah Mada, Yogyakarta, Indonesia, [2]Faculty of Pharmacy, Universitas Surabaya, Surabaya, Indonesia, [3]Centre of Excellence in Cannabis Research, Department of Pharmaceutical Chemistry and Pharmacognosy, Faculty of Pharmaceutical Sciences and Center of Excellence for Innovation in Chemistry, Naresuan University, Phitsanulok, Thailand

KEYWORDS

herbal drug, chemometrics, fingerprinting profiles, metabolomics, biological activities

Editorial on the Research Topic
Development, assessment, improvement, and standardization of methods in herbal drug research

Herbal drugs (HDs) or herbal medicines have been applied for a very long time as natural remedies for preventing and curing diseases and for improving human health. HDs are currently gaining increasing popularity globally as drugs, complementary and alternative medicines, nutraceuticals, food supplements, and cosmetics. HDs have gained wider interest among societies during the past decades due to their broad, synergistic actions on the physiological systems and the relatively lower incidence of adverse events compared to synthetic drugs (Noviana et al.). However, HD may not be entirely safe because some studies have reported adverse effects such as nephrotoxicity, hepatotoxicity, cardiotoxicity, neurotoxicity, and skin toxicity during the administration of HDs. These adverse effects may be due to the presence of some toxic metabolites or contaminants such as aflatoxins, or due to the falsification of HDs. Therefore, the quality assurance and authenticity of HDs must be assured (Heinrich, 2015). The complexity of HDs, which typically consist of many constituents, has raised major quality issues. The bioactive compounds of extracts and/or HD preparation are typically very complex and may vary. Thus, if the exact chemical composition is not determined accurately and specifically, the reported bioactivity or pharmacological effects may not always be reproducible. Assuring high-quality HDs with reproducible quality, efficacy, and safety is a challenging task. As a consequence, the availability of appropriate analytical methods is highly required, not only for the identification and standardization of HDs but also for the detection of adulterants and contaminants (Muyumba et al., 2021). The analytical methods used for the quality control of HDs, either chemical or biological-based methods, must be official

methods. Otherwise, the methods should first be validated according to the latest official guidelines. Without analytical method validation, the reliability of the data cannot be confirmed, and the results would be difficult to replicate by other scientists (Indrayanto, 2022).

The quality control and authentication of HDs are typically carried out by evaluating the biological characteristics and physicochemical properties along with microscopic and macroscopic observations. The characterization and discrimination of HDs by instrumental methods can be performed using three approaches: (1) single component analysis or targeted analysis using marker compounds responsible for biological activities, (2) fingerprint profiling (i.e., profile comparison of different HDs), and (3) metabolomic studies, either using targeted or untargeted metabolomics (Ruiz et al., 2016). Due to the large datasets obtained by these methods, the use of chemometrics is a must. Pattern recognition and multivariate calibration are among the widely used chemometrics techniques for the analysis of HDs (Zhu et al., 2014).

A total of 11 manuscripts are published in this Research Topic, including two review articles and nine original research articles. A narrative review by Noviana et al. highlights the use of metabolite fingerprint profiling based on chemical responses obtained from spectroscopy-based techniques (FT-IR and NMR spectroscopy), chromatographic techniques mainly thin layer chromatography (TLC), liquid chromatography (LC), and gas chromatography with different detection systems, electrophoretic methods, direct mass spectrometry, and DNA barcoding for the standardization and quality control of HDs. Since the instrumental analyses involve large datasets, in this review the authors also critically discuss some of the chemometrics tools applied. The combination of chemometrics of pattern recognition, multivariate calibrations, and validated instrumental methods for assisting the authentication analysis are also highlighted.

In a systematic review presented by Ibrahim et al., *Marantodes pumilum* (Blume) Kuntze, one of the Malay traditional herbal medicines, is critically discussed. Some aspects of this herbal medicine including the identification and authentication of the plant using different methods (organoleptic, microscopic, and macroscopic evaluation along with fingerprinting profiling using FT-IR spectroscopy, LC-MS, and DNA barcoding) are thoroughly discussed. Furthermore, the phytochemical constituents of the plant with known therapeutic activity are also described.

Nine original articles explored the biological activities of HDs either as a single component or in combination. Reported investigations include *in vitro* or *in vivo* studies, identification of chemical markers in HDs, and the relationship between the biological activities of HDs and chemical markers responsible for these activities.

Hu et al. identify chemical markers in the classes of phenolics and saponins from *Eleutherococcus senticosus* (Rupr. & Maxim.) leaves and their correlation with the hypoglycemic activity is measured by α-glucosidase inhibition assay. Ultra-performance liquid chromatography combined with tandem mass spectrometry (i.e., UPLC-QTOF-MS/MS and UPLC-QTRAP-MS/MS) is validated for the qualitative and quantitative analyses of the herb. Thirty compounds are identified including seven saponins and 20 phenolic compounds. Twelve of these compounds are isolated from *E. senticosus* for the first time. The newly isolated compounds are 5-O-caffeoylshikimic acid, quinic acid butyl ester, methyl 5-O-feruloylquinate, 5-O-p-coumaroylquinic acid butyl ester, 4-O-caffeoylquinic acid methyl ester, 5-O-feruloylquinic acid, 3,4-dihydroxybenzenepropionic acid methyl ester, quercetin 3-O-β-D-glucopyranosyl-(1→6)-β-D-glucopyranoside, (7S,8R)-urolignoside, *n*-butyl-1-O-α-L-rhamnopyranoside, (Z)-hex-3-en-1-ol O-β-D-xylopyranosyl-(1″-6′)-β-D-glucopyranoside, and hexenyl-rutinoside. The phenolic compounds can be used as markers for the hypoglycemic activity of this herb.

The effect of a combination of turmeric (*Curcuma longa* L.), grape (*Vitis vinifera* L.) seed, flaxseed (*Linum usitatissimum* L.), and psyllium (*Plantago ovata* L.) with bentonite as detoxification and cholesterol-lowering agents is investigated by Turgut et al. in hypercholesterolemic mice. The combination has a synergistic effect on reducing the risk of cardiovascular diseases. The chemical markers identified in turmeric using liquid chromatography and LC-MS/MS are curcuminoids (curcumin, desmethoxycurcumin, and bisdemethoxycurcumin), while chlorogenic acid, fumaric acid, (-)-epicatechin gallate, caffeic acid, vanillic acid, luteolin 7-glucoside, resveratrol, apigenin 7-glucoside, quercetin, luteolin, and apigenin are detected in grape seed.

Furthermore, Saggam et al. study the anti-cancer activity of extracts from two Ayurveda-based immunomodulatory herbs, *Asparagus racemosus* Willd and *Withania somnifera* (L.) Dunal, for therapeutic adjuvants in countering paclitaxel (PTX)-induced myelosuppression. The studied extracts significantly modulated 20 cytokines to evade PTX-induced leukopenia, neutropenia, and morbidity. Both extracts also prevented PTX-induced myelosuppression and morbidity signs by modulating associated cytokines. The results conclude that both HDs are potential therapeutic adjuvants in cancer management.

Sun et al. investigate the effects of Shuangxinfang, a formula of Traditional Chinese Medicine (TCM), in preventing S100A9-induced macrophage/microglial inflammation in rats after acute myocardial infarction. S100A9 is an important target protein in macrophage/microglial inflammation. The authors report that Shuangxinfang could promote the recovery of cardiac function and improve depression-like behavior.

Wang et al. study the effect of Yinhuapinggan granules, a TCM, as the adjuvant treatment of community-acquired

drug-resistant bacterial pneumonia (CDBP) caused by *Streptococcus pneumoniae*.

Lu et al. comprehensively explore the combination of pattern recognition chemometrics [i.e., similarity analysis (SA), cluster analysis (CA), and principal component analysis (PCA)] and chromatographic fingerprint analysis for the identification of quality markers (Q-marker) that contribute to the antioxidant activity of *Chrysanthemum morifolium* (CM) cv. (Juhua). The Q-marker is explored by correlating the concentrations of main constituents found in the HPLC chromatograms and the *in-vitro* radical scavenging capacity. The developed model is further used to evaluate the quality of 30 flower head samples of *C. morifolium*. The authors conclude that the combination of HPLC fingerprinting, *in-vitro* anti-oxidant activity evaluation, and chemometrics explain the therapeutic material basis and discovered Q-markers, providing a more comprehensive quality assessment of *C. morifolium*.

Rao et al. apply chromatographic fingerprinting based on UHPLC-Q-TOF MS and chemometrics of partial least square regression (PLSR), gray relational analysis models, and Spearman's rank correlation coefficient (SRCC) to discover active compounds in herbal medicine, *Zanthoxylum nitidum* (Roxb.) DC. Using this approach, a total of 48 compounds are identified or tentatively characterized, which include 37 alkaloids, seven coumarins, three phenolic acids, two flavonoids, and one lignan. This study also predicts that some compounds namely nitidine, chelerythrine, hesperidin, and oxynitidine are potential anti-inflammatory compounds.

Another study applying a combination of UPLC-TOF-MS and chemometrics (i.e., pattern recognition and multivariate statistical analysis) is reported by Li et al. to discover the markers in TCM of Wutou decoction, used for the treatment of rheumatoid arthritis. Using Pearson correlation analysis, Q-markers of aconitine, L-ephedrine, L-methylephedrine, quercetin, albiflorin, paeoniflorigenone, astragaline A, astragaloside II, glycyrrhetic acid, glycyrrhizic acid, licurazide, and isoliquiritigenin are determined to be key pharmacological components that regulate the metabolism of rheumatoid arthritis in rats.

Liu et al. explore a metabolomics approach based on desorption electrospray ionization mass spectrometry imaging (DESI-MSI) and chemometrics of PCA and partial least square-discriminant analysis (PLS-DA) for the investigation of a series of Aconitum alkaloids and for exploring the potential metabolic markers intended to understand the differentiation between raw and processed Fuzi, a herbal medicine used for the treatment of various diseases. Forty-two metabolic markers are identified to discriminate raw and steam-processed Fuzi. Six alkaloids, namely mesaconitine, aconitine, hypaconitine, benzoylmesaconine, benzoylaconine, and benzoylhypaconine can be used as markers for the differentiation of raw and processed Fuzi. DESI-MSI, combined with metabolomics, provides an efficient method to visualize the changeable rules and screen metabolic markers of Aconitum alkaloids during processing.

Overall, three approaches (single component analysis, metabolic fingerprinting, and metabolomics studies) are used by researchers to discover chemical markers related to biological activities, identification, differentiation, and classification of HDs. Furthermore, to produce reproducible results, these approaches must be properly validated before their routine applications.

Finally, research on HD derived from natural sources must rely on careful design, thoughtful execution, and detailed reporting of the study focusing on the pharmacological or biological activities of active compounds extracted from HDs. Heinrich et al. provide a "Four Pillars of Best Practice" as a reference/guideline for articles submitted to scientific journals focusing on pharmacology and ethnobotany of HDs, including (1) pharmacological requirements (i.e., traditional context, testing of the therapeutically relevant dose range, and credible experimental models), (2) composition requirements of HD (chemical and botanical compositions), (3) basic experimental and ethical requirements, and (4) specific requirements in relation to article types (Heinrich et al., 2020).

Author contributions

AR formulated the idea of the manuscript. AR and GI wrote the draft. AR, GI and KI reviewed and edited to the final manuscript.

Acknowledgments

The authors thank Dr. Eka Noviana from the Faculty of Pharmacy, Universitas Gadjah Mada for her assistance in editing.

Conflict of interest

The authors declare that the research was conducted in the absence of any commercial or financial relationships that could be construed as a potential conflict of interest.

Publisher's note

References

Heinrich, M., Appendino, G., Efferth, T., Fürst, R., Izzo, A. A., Kayser, O., et al. (2020). Best practice in research – overcoming common challenges in phytopharmacological research. *J. Ethnopharmacol.* 246, 112230. doi:10.1016/j.jep.2019.112230

Heinrich, M. (2015). Quality and safety of herbal medical products: Regulation and the need for quality assurance along the value chains. *Br. J. Clin. Pharmacol.* 80 (1), 62–66. doi:10.1111/bcp.12586

Indrayanto, G. (2022). The importance of method validation in herbal drug research. *J. Pharm. Biomed. Anal.* 214, 114735. doi:10.1016/j.jpba.2022.114735

Muyumba, N. W., Mutombo, S. C., Sheridan, H., Nachtergael, A., and Duez, P. (2021). Quality control of herbal drugs and preparations: The methods of analysis, their relevance and applications. *Talanta Open* 4, 100070. doi:10.1016/j.talo.2021.100070

Ruiz, G. G., Nelson, E. O., Kozin, A. F., Turner, T. C., Waters, R. F., and Langland, J. O. (2016). A lack of bioactive predictability for marker compounds commonly used for herbal medicine standardization. *PLoS ONE* 11 (7), 01598577–e159910. doi:10.1371/journal.pone.0159857

Zhu, J., Fan, X., Cheng, Y., Agarwal, R., Moore, C. M. V., Chen, S. T., et al. (2014). Chemometric analysis for identification of botanical raw materials for pharmaceutical use: A case study using panax notoginseng. *PLoS ONE* 9 (1), 874622–e87510. doi:10.1371/journal.pone.0087462

frontiers in Pharmacology

ORIGINAL RESEARCH
published: 06 December 2021
doi: 10.3389/fphar.2021.775789

Development of Cholesterol-Lowering and Detox Formulations Using Bentonite and Herbal Ingredients

Rana Turgut[1]*, *Murat Kartal*[2], *Esra Küpeli Akkol*[3]*, *İlker Demirbolat*[4] and *Hakkı Taştan*[5]

[1]Department of Pharmacognosy, Health Sciences Institute, Bezmialem Vakif University, Istanbul, Turkey, [2]Department of Pharmacognosy, Faculty of Pharmacy, Bezmialem Vakif University, Istanbul, Turkey, [3]Department of Pharmacognosy, Faculty of Pharmacy, Gazi University, Ankara, Turkey, [4]Bezmialem Center of Education, Practice, and Research in Phytotherapy, Bezmialem Vakif University, Istanbul, Turkey, [5]Department of Biology, Faculty of Science, Gazi University, Ankara, Turkey

Detoxification enzymes involved in human metabolism works to minimize the potential xenobiotic-induced damage constantly. Studies have revealed that toxin accumulation plays an important role in the etiology of cardiovascular disease. This study has been designed to provide evidence of medicinal use of bentonite, turmeric (*Curcuma longa* L.), grape (*Vitis vinifera* L.) seed, flaxseed (*Linum usitatissimum* L.), and psyllium (*Plantago ovata* L.) as detoxification and cholesterol-lowering agents using a hypercholesterolemic model in mice. The potential hypocholesterolemic effects and detoxification ability of these ingredients were evaluated at the same time: Total cholesterol, high-density lipoprotein cholesterol, low-density lipoprotein cholesterol, triglyceride, glucose, aspartate aminotransferase, alanine aminotransferase, malondialdehyde, plasma total antioxidant activity, nitric acid, leptin levels and glutathione, glutathione peroxidase, lipid peroxidation, superoxide dismutase and catalase values were measured. It was determined that GBTF group (grape seed extract, bentonite, turmeric, and flaxseed), GBTP group (grape seed extract, bentonite, turmeric, and psyllium), and GBT group (grape seed extract, bentonite, and turmeric) of the tested materials decreased the serum total cholesterol concentration by 64.8, 57.5, and 48.9%, respectively, in mice fed a high cholesterol diet. In addition, it was determined that some detoxification parameters such as superoxide dismutase, catalase, glutathione, and glutathione peroxidase were statistically significantly reversed in GBTF, GBTP, and GBT groups. Flaxseed, psyllium, and bentonite clay did not show significant effects in reducing total cholesterol; however, GBTF, GBTP, and GBT groups interventions had a significant effect in reducing total cholesterol levels. Moreover, it was observed that adding flaxseed or psyllium to the GBT group increased the cholesterol-lowering effect. Therefore, it can be thought that this significant effect is due to the synergistic effect of the raw materials. When the results obtained were evaluated, it was seen that the cholesterol-lowering and detoxification effects of the combinations were higher than from the effect of natural material used alone. As a result, combinations of some of these ingredients have a positive effect on reducing the risk of cardiovascular disease.

Keywords: detoxification, cholesterol, flaxseed, psyllium, turmeric, grape seed, bentonite

OPEN ACCESS

Edited by:
Kornkanok Ingkaninan, Naresuan University, Thailand

Reviewed by:
Haci Ahmet Deveci, University of Gaziantep, Turkey
Nanteetip Limpeanchob, Naresuan University, Thailand

***Correspondence:**
Rana Turgut
ranaturgut8@hotmail.com
Esra Küpeli Akkol
esrak@gazi.edu.tr

Specialty section:
This article was submitted to Ethnopharmacology, a section of the journal Frontiers in Pharmacology

Received: *14 September 2021*
Accepted: *16 November 2021*
Published: *06 December 2021*

Citation:
Turgut R, Kartal M, Akkol EK, Demirbolat İ and Taştan H (2021) Development of Cholesterol-Lowering and Detox Formulations Using Bentonite and Herbal Ingredients. Front. Pharmacol. 12:775789. doi: 10.3389/fphar.2021.775789

1 INTRODUCTION

We are exposed to many xenobiotics during our lifetime, including various pharmaceuticals and food components. Accumulated data suggest that an individual's ability to remove toxins from the body may play a role in the etiology or exacerbation of a range of chronic conditions and diseases. Detoxification is not one reaction but rather a process that involves multiple reactions and multiple players (Liska, 1998). The liver is the principal organ responsible for detoxifying xenobiotics, including drugs and toxic endogenous compounds. The detoxification process, also known as xenobiotic metabolism, involves three phases with different reactions: phase I (enzymatic functionalization), phase II (enzymatic conjugation), and phase III (transport) (Nakata et al., 2006). Numerous studies have elucidated the enzymes that are crucial in each phase, unraveling the cytochrome P450 (CYPs) in phase I, UDP glycosyltransferases (UGTs), glutathione-S-transferases (GSTs), glutathione peroxidase (GPx), and sulfotransferases (SULTs) in phase II and organic anion transporters (OATs), multidrug-resistance proteins (MDRs) and multidrug resistance-associated proteins (MRPs) in phase III (Chen et al., 2016). Also, to avoid reactive oxygen species (ROS) caused oxidative damage, higher organisms have evolved a complex antioxidant defense system comprising low-molecular-weight components such as ascorbate and glutathione, and enzymatic components such as SOD, peroxidase (POD), and catalase (CAT), which are involved in the detoxification of O_2 and H_2O_2, respectively, thereby preventing the formation of HO radicals (Valko et al., 2007). The detoxification systems are highly complex, show a significant amount of individual variability, and are incredibly responsive to an individual's environment, lifestyle, and genetic uniqueness (Liska, 1998). In general, the nature of studies indicates that specific foods may upregulate or favorably balance metabolic pathways to assist with toxin biotransformation and subsequent elimination. Therefore, it would seem that designing clinical recommendations to maximize the effects of food and reduce the impact of toxins is essential (Hodges and Minich, 2015).

Cholesterol is the principal sterol present in animal tissues. In mammals, cholesterol plays a vital role in life, being an essential component for the normal functioning of cells. However, cholesterol has gained a bad reputation in the World of health and nutrition, mainly because of its association with cardiovascular diseases. WHO predicted that by the year 2030, CVDs would remain a significant cause of death, affecting approximately 23.6 million people around the World (Cerqueira et al., 2016). Treatment of hypercholesterolemia is currently with a combination of diet and pharmaceutical treatments (Newby et al., 2005; Aarden et al., 2011). Cholesterol-lowering nutraceuticals and functional foods play an essential role in reducing the risk of coronary heart disease by improving the plasma lipoprotein profile (Chen et al., 2008).

Bentonite is a rock formed of highly colloidal and plastic clays composed mainly of montmorillonite, a clay mineral of the smectite group (Adamis et al., 2005). Montmorillonite has an extensive exchange capacity, and thus it can adsorb organic materials, bacteria, viruses, heavy metal ions, and other toxins (Uddin, 2018). In addition, the positive effects of montmorillonite in preventing hyperlipidemia suggest that it may be an excellent nutraceutical to adsorb excess lipids during the consumption of a fatty diet (Xu et al., 2016). Flaxseed's antioxidant and anti-inflammatory components (*Linum usitatissimum*) are associated with numerous health benefits, including cardiovascular benefits (Chikara et al., 2018). Flaxseed offers the unique opportunity to control different aspects of cardiovascular disease and its risk factors (Parikh and Pierce, 2019). Seeds from *Plantago ovata*, also known as psyllium, have a fiber-rich husk (Belorio and Gómez, 2020). Psyllium has been used traditionally since antiquity as a laxative, but at present, its new pharmacological uses have been discovered (Bannayan et al., 2008). Psyllium husk plays a crucial role in lowering serum cholesterol, so psyllium is considered a potential supportive agent in the therapy of hyperlipidemia (Xing et al., 2017). Turmeric (*Curcuma longa*) is a member of the Zingiberaceae family, and it grows in tropical and subtropical regions around the World (Paramasivam et al., 2009). Its most crucial active ingredient is curcuminoids: Curcumin, dimethoxy curcumin, and bisdemethoxycurcumin (Amalraj et al., 2017). Curcumin can be used as an antioxidant at 1.5% and an antilipidemic agent at 2.5% in the diet (Arshami et al., 2013). Grapes (*Vitis vinifera*) are one of the most highly consumed fruits across the World. In ancient Europe, grape plants' leaves and sap have been used in traditional treatment for ages. Besides being a wellspring for vitamins and fiber, the skin and seeds of grapes are highly rich in Polyphenols, specifically proanthocyanidins (Gupta et al., 2020).

The main objective of this study was to investigate the effects of potentially effective herbal ingredients and food-grade bentonite clay combinations in detoxifying and normalizing blood cholesterol levels to prevent cardiovascular diseases and develop effective formulations. In this study, bentonite, flaxseed (*Linum usitatissimum*), psyllium (*Plantago ovata*) seed, turmeric (*Curcuma longa*), and grape (*Vitis vinifera*) seed ingredients were determined as potential effective raw materials based on previous researches.

2 MATERIALS AND METHODS

2.1 Materials

Food-grade bentonite clay powder was provided by Alya Mineral Company, Ordu, Turkey. Fitovizyon Natural Products Company, Istanbul-Turkey, provided turmeric (*Curcuma longa*) extract. Flaxseed (*Linum usitatissimum*), grape (*Vitis vinifera*) seed, and psyllium (*Plantago ovata*) seed were provided by a local herbalist. Atorvastatin was obtained from the local pharmacy.

2.2 Animals

The study's experiments were performed on mice obtained from the SYLAB Experimental Animal Research and Breeding Laboratory (Ankara, Turkey). This study is a portion of the leading project submitted to comply with the requirements for the degree of Master in Pharmacognosy and Naturel Products Chemistry. This study was supported by the Bezmialem Vakıf

University (Istanbul, Turkey) Scientific Research Projects Unit, BAP. Male Swiss albino mice (20–25 g) were used in the study. They were accommodated at the Saki Yenilli Experimental Animal Research and Breeding Laboratory (Ankara, Turkey), where the surrounding temperature was controlled to be between 21 and 24°C for 12 h day and night period. Tap water and standard pellet feed were made freely available to all the animals. According to the National Institutes of Health Guide for Laboratory Animal Care and Use, animal ethical protocols were followed. The animal study was reviewed and approved by Saki Yenilli Experimental Animals Local Ethics Committee (Ethics Committee No: 03/15). At least seven animals were used in each group. All test materials were suspended in 0.5% sodium carboxymethyl cellulose (CMC) and administered to animals by gastric gavage. Two control groups were used in the study. Animals in the hypercholesterolemic group (positive control) were given a high cholesterol diet as in the test samples. The animals in the negative control group were given standard pellet feed without any intervention. Atorvastatin as a reference substance was administered orally to animals by gastric gavage at a dose of 10 mg/kg.

2.3 Analysis of Fixed Oils From Grape Seeds, Flaxseed, and Psyllium Seed

The seeds were powdered mechanically and extracted with hexane (180°C) for 5–6 h in a Soxhlet apparatus (Elektromag, Turkey). Removal of the solvent under reduced pressure gave the fixed oils. The fatty acid content of the fixed oils was investigated by GC analysis of their methyl esters. İnto the oils (0.5 ml) 5 ml 10% methanolic HCl was added. Methyl esters were prepared by transmethylation at 180°C 30 min heating under reflux. 5 ml of hexane, 25 ml of 10% $NaHCO_3$, and salt were added to the mixture, respectively, and shaken vigorously, and allowed to stand for 30 min. The upper layer was removed, and 1 µL was used for GC analysis (Houghton et al., 1995).

Gas Chromatography-Mass Spectrometry (GS-MS) is used to identify the fatty acid components of fixed oils, and Gas Chromatography Flame ionization Detector (GC-FID) is used to determine relative percentages. GC-FID analyses were performed using an Agilent 7890B Gas Chromatograph system with an Agilent DB-Wax capillary column (60 m × 0.25 mm × 0.25 µm) and helium as the carrier gas. Injector and detector (FID) temperatures were kept at 220°C. The split ratio was 50:1. Relative percentage amounts were calculated from the total area under the peaks by the software of the apparatus. GC–MS analyses of the oils were carried out on an Agilent 75977E Gas Chromatograph system. The oven temperature was as above; transfer line temperature 250°C; ion source temperature 230°C; carrier gas helium; ionization energy 70 eV; mass range 35–450 m/z.

2.4 Analysis of Swelling Index of Flaxseed and Psyllium Seed

The swelling index is the volume in ml taken up by the swelling of 1 g of plant material under specified conditions. For the characterization of mucilage content, the swelling index was determined according to the general and specified descriptions of European Pharmacopoeia by using *Linum usitatissimum* and *Plantago ovata* 1 g whole and powder seeds at the same time.

2.5 Preparation of Grape Seed Extract

The seeds were extracted for 5–6 h in a Soxhlet apparatus (Electromag, Turkey) with ethyl alcohol at different ratios (100% ethyl alcohol, 70% ethyl alcohol/water, and 50% ethyl alcohol/water) by temperature controlled. Evaporation was carried out at different temperatures for each solvent. As a result of the total phenolic/flavonoid content analysis, the appropriate solvent was determined as 50% ethanol/water. The above method was applied for the grape seed extract to be used in the study.

2.6 Analysis of Total Phenolic and Total Flavanoid Contents of Grape Seed Extract

Two different colorimetric methods determined the total phenolic and flavonoid content. The total phenolic content of the extract was determined by the Folin Ciocalteu reagent (FCR). UV-VIS Spectrophotometry device was used for the Folin Ciocalteu Method. After necessary dilution for the sample, the test solution was prepared with 104 µL of distilled water, 8 µL of the sample, 8 µL of FCR, and 80 µL of 7% Na_2CO_3. The test solution was kept in the dark for 90 min. Then, absorbance at 765 nm was determined against a blank containing all reagents, without the samples or the gallic acid. The total phenolic content is the number of gallic acid equivalents.

The total flavonoid content of the extract was determined by the aluminum chloride method, using quercetin as a reference compound. UV-VIS Spectrophotometry device was used for Aluminum Chloride Colorimetric Method. After necessary dilution for the sample, the test solution was prepared with 134 µL of distilled water, 20 µL of the sample, 6 µL of 10% AlCl3, and 40 µL of CH3COONH4. The test solution was kept in the dark for 10 min. Then, the same absorbance at 765 nm was determined under the same conditions. The total flavonoid content is the number of quercetin equivalents.

2.7 LC-HRMS Evaluation

Liquid Chromatography-High Resolution Mass Spectrometer (LC-HRMS) device was used for phenolic compound determination in grape seed extract. The extract was dissolved in MeOH-water, and a final concentration of 3 ppm was added from the 100 mg/L internal standard solutions. The sample was passed through a 0.45 µ filter, and 2 µ was added to the device. Separation was done on the C18 guard column and the mobile phase used was formic acid: water: Methanol. The rate of flow was constantly maintained at 0.35 ml per minute, and the peaks that appeared were recognized with the help of the mass scanning range 100–900 m/z. An MS detector was used for the segregation of phenolic compounds. The identification of these phenolic compounds was done by comparing the retention time and the spectral peaks previously obtained by the injection of

TABLE 1 | Study groups.

Groups	Intervention
1. Control group	Only standard diet
2. Hypercholesterolemic group	Only high cholesterol diet (HCD)
3. Reference group	HCD + Atorvastatin (10 mg/kg/day)
4. Bentonite group	HCD + bentonite clay (60 mg/day)
5. GBTF group	HCD + bentonite clay (60 mg/day) + flaxseed (7 mg/day) + grape seed extract (2.5 mg/day) + turmeric extract (2 mg/day)
6. GBTP group	HCD + bentonite clay (60 mg/day) + psyllium (7 mg/day) + grape seed extract (2.5 mg/day) + turmeric extract (2 mg/day)
7. GBT group	HCD + bentonite clay (60 mg/day) + grape seed extract (2.5 mg/day) + turmeric extract (2 mg/day)
8. Flaxseed group	HCD + flaxseed (7 mg/day)
9. Psyllium group	HCD + psyllium (7 mg/day)

Grape seed extract contains 24.81% palmitic acid, 6.02% palmitoleic acid, 6.10% stearic acid, 15.26% oleic acid, 43.61% linoleic acid, 4.20% linolenic acid, 24.6% phenolic substance and 1.48% flavonoid substance, flaxseed contains 9.27% palmitic acid, 5.9% stearic acid, 22.61% oleic acid, 17.83% linoleic acid, 44.27% linolenic acid and the swelling index 4.7 ml for ground flaxseed, psyllium contains 15.25% palmitic acid, 4.18% stearic acid, 25.96% oleic acid, 48.42% linoleic acid, 6.17% linolenic acid and the swelling index 17.8 ml for ground psyllium seed and turmeric extract contains 95% curcumin from the products used in this study.

standards. The calculation for their quantification was performed by external calibration.

2.8 Analysis of Curcumin in Turmeric Extract

10 mg of turmeric extract was dissolved in 10 ml of Methanol by staying in an ultrasonic bath for 10 min. 100 μL of the prepared solution was taken and diluted into 10 ml of mobile phase mixture. Curcumin amount was measured by HPLC-PDA Method (standard substance Curcumin; Sigma Aldrich).

2.9 Determination of Intervention Doses

Food-grade bentonite clay powder was determined as 60 mg/day for each mouse (Gershkovich et al., 2009; EFSA Panel on Additives and Products or Substances used in Animal Feed (FEEDAP), 2012). Flaxseeds (*Linum usitatissimum*) were determined as 7 mg/day for each mouse (Pan et al., 2009). Grape (*Vitis vinifera*) seed extract was determined as 2.5 mg/day for each mouse (EFSA Panel on Additives and Products or Substances used in Animal Feed (FEEDAP), 2016). Turmeric (*Curcuma longa*) extract was determined as 2 mg/day for each mouse (Qinna et al., 2012). Psyllium (*Plantago ovata*) was determined as 7 mg/day for each mouse (Wei et al., 2009).

2.10 Groups

When the mean difference was 4.77 units and the standard deviation was 3.52, the sample size was determined as six experimental animals for each group, a total of n = 54 (95% confidence level and 80% power at α = 0.05 significance level). The 54 adult male Swiss albino mice were divided into nine groups (n = 6) are shown in **Table 1**.

2.11 Hypercholesterolemia Experimental Design

Hypercholesterolemia was induced by the applying pellet feed containing 1% cholesterol to the experimental animals for 30 days. The test materials were administered simultaneously to the mice in the test group (except the control group). At the end of the 30-days experiment period, intracardiac blood samples and liver tissue were taken from the mice in all groups for biochemical determinations. At the end of the period, blood and tissue samples were taken from experimental animals;

1) Total cholesterol (TC), HDL cholesterol (HDL-C), LDL cholesterol (LDL-C) and Triglyceride (TG) values
2) Glucose, Aspartate aminotransferase (AST), Alanine aminotransferase (ALT), Malondialdehyde (MDA), Plasma total antioxidant activity (TAA), Nitric acid levels
3) Glutathione (GSH), Glutathione peroxidase (GPx), Lipid peroxidation (LPO), Superoxide dismutase (SOD), Catalase (CAT) values
4) Leptin levels were measured.

2.12 Estimation of Lipid Peroxidation Level in Serum

The method (Kurtel et al., 1992) was used for the measurement of lipid peroxidation levels in serum. In this method, 1 ml of serum, 2 ml of trichloroacetic acid (TCA; 15%)-thiobarbituric acid (TBA; 0.375%), 0.25 N HCl was mixed and centrifuged at 10,000 g for 5 min. After the supernatant was separated, it was mixed with 20 μL of butylhydroxytoluene (BHT) to prevent oxidation and kept in a hot water bath for 15 min. After cooling under running water, the precipitate was separated by centrifugation at 10,000 g for 5 min. The absorbance of the sample was then measured at 532 nm.

2.13 Determination of Antioxidant Parameters in Liver Tissue

The reduced glutathione (GSH) parameter, which is a non-enzymatic antioxidant, was determined by the method of Sedlak and Lindsay (Sedlak and Lindsay, 1968). With the method of Paglia and Valentine (Paglia and Valentine, 1967), the GPx parameter was determined. Enzymatic antioxidant superoxide dismutase (SOD) activity by the method developed by Misra and Fridovich (Misra and Fridovich, 1972) was determined. A catalase (CAT) activity test with the method determined by Takahara et al. (1960) was done. The lipid

peroxide (LPO) content in tissues was determined according to the method of Ohkawa et al. (1979).

2.14 Determination of Other Parameters

Serum high-density lipoprotein cholesterol (HDL-C) levels were determined using the Crescent Diagnostics Cholesterol Test Kit by precipitation of apolipoprotein B-containing lipoproteins with phosphotungstic acid and magnesium chloride. The cholesterol content of low-density lipoprotein (LDL-C) was determined using the Friedwald equation. Alanine aminotransferase and aspartate aminotransferase levels were determined using commercial kits from the Teco Diagnostics assay. Serum total protein, triglyceride, and cholesterol values were measured by enzymatic methods using commercially available kits (TECO Diagnostics, California, United States). Malondialdehyde was measured according to the method of Draper and Hardley (Draper and Hadley, 1990) based on the binding of MDA with thiobarbituric acid. The standard Fe-EDTA complex solution reacts with hydrogen peroxide in a Fenton-type reaction, leading to hydroxyl radicals (•OH). These reactive oxygen species break down the benzoate, causing the release of TBARS. Antioxidants cause suppression of TBARS production. The plasma total antioxidant activity test, which is based on the spectrophotometric measurement of the inhibition of color formation, defined as TAA, was measured according to the method of Koracevic et al. (2001). Nitric oxide metabolites (nitrates + nitrites, NOx) were tested in plasma by the colorimetric method of Griess (Miranda et al., 2001). Plasma leptin concentration was determined by the ELISA (Linco Research, Inc, St. Charles, United States) method using the enzyme kit (Cat. EZRL-83K).

2.15 Histopathological Analysis

The liver tissue of rats was dissected and then placed in formalin (10%) for 3 days. All tissues were detected using the Thermo Scientific Excelsior (ES) machine. The tissues were embedded in paraffin wax and blocks were prepared using the HistoCentre 2 machine. Subsequently, sections of 3.5 mm thickness were made from paraffin-embedded blocks using a Leica RM2255 microtome. The sections were stained with hematoxyline-eosin (HE) using the Shandon Varistan machine. Photographs of normal and pathological liver tissues were taken using Nikon Eclipse Ci with polarizing attachment and a Digital Image analysis system, then examined under a light microscope.

2.16 Gastric Ulcerogenic Effect

Potential risks for stomach damage were assessed due to the application of test samples over a long period, such as 30 days. For this purpose, after the hypocholesterolemic activity test was completed, the mice were killed using a high-dose anesthetic, and their stomachs were removed. It was examined under a dissecting microscope to determine the lesions or bleeding that may develop in the stomach.

2.17 Statistical Analysis

Experiment results were expressed as Mean Standard Error ± SEM. The effect of test samples on the parameters studied was compared with the results obtained in the hypercholesterolemic group, and statistical differences were evaluated by ANOVA and Student-Newman-Keuls posthoc tests. The difference in $p < 0.05$ was considered significant ($^{*}p < 0.05$; $^{**}p < 0.01$; $^{***}p < 0.001$).

2.18 Exclusion Criteria

1) Behavioral changes, goose pimples, hunched position, vomiting, diarrhea, formation of secondary skin lesions
2) Loss (ex) of animals during the experiment

No animals included in the study were excluded from the experiment, as no negative findings were found among the criteria mentioned above.

3 RESULTS

3.1 Gas Chromatography Analysis

The yield of the hexane extract obtained for the analysis of grape (*Vitis vinifera*) seed fixed oil was 9.4%. Findings of fixed oil acid components and relative percentages of fixed oils in grape seed are shown in **Figure 1**. The GC-FID chromatogram of the hexane extract of the grape seed found palmitic acid (24.81% ± 2.50), palmitoleic acid (6.02% ± 2.08), stearic acid (6.10% ± 1.22), oleic acid (15.26% ± 1.77), linoleic acid (43.61% ± 4.25), and linolenic acid (4.20% ± 0.94) present in the seed as fixed oil acid constituents (**Figure 1**).

The yield of the hexane extract obtained for the analysis of flax (*Linum usitatissimum*) seed fixed oil was 15.3%. Findings of fixed oil acid components and relative percentages of fixed oils in flaxseed are shown in **Figure 2**. The GC-FID chromatogram of the hexane extract of the flaxseed found palmitic acid (9.27% ± 0.62), stearic acid (5.9% ± 1.40), oleic acid (22.61% ± 2.14), linoleic acid (17.83% ± 0.47) and linolenic acid (44.27% ± 2.21) present in the seed as fixed oil acid constituents (**Figure 2**).

The yield of the hexane extract obtained for the analysis of psyllium (*Plantago ovata*) seed fixed oil was 2.3%. Findings of fixed oil acid components and relative percentages of fixed oils in psyllium seed are shown in **Figure 3**. The GC-FID chromatogram of the hexane extract of the psyllium seed found palmitic acid (15.25% ± 0.94), stearic acid (4.18% ± 1.05), oleic acid (25.96% ± 3.06), linoleic acid (48.42% ± 2.70) and linolenic acid (6.17% ± 0.21) present in the seed as fixed oil acid constituents (**Figure 3**).

3.2 Findings of the Swelling Index

It is stated in the European Pharmacopoeia that the swelling index for flaxseed should be at least 4 ml. According to the average of three parallel experiments, the swelling index was found to be 3.8 ml (±0.1) in whole flaxseed and 4.7 ml (±0.17) in-ground flaxseed.

It is stated in the European Pharmacopoeia that the swelling index should be at least 10 ml for psyllium seeds. According to the average of three experiments performed in parallel, the swelling index was found to be 9.3 ml (±0.56) in the whole psyllium seed and 17.8 ml (±0.45) in the ground psyllium seed.

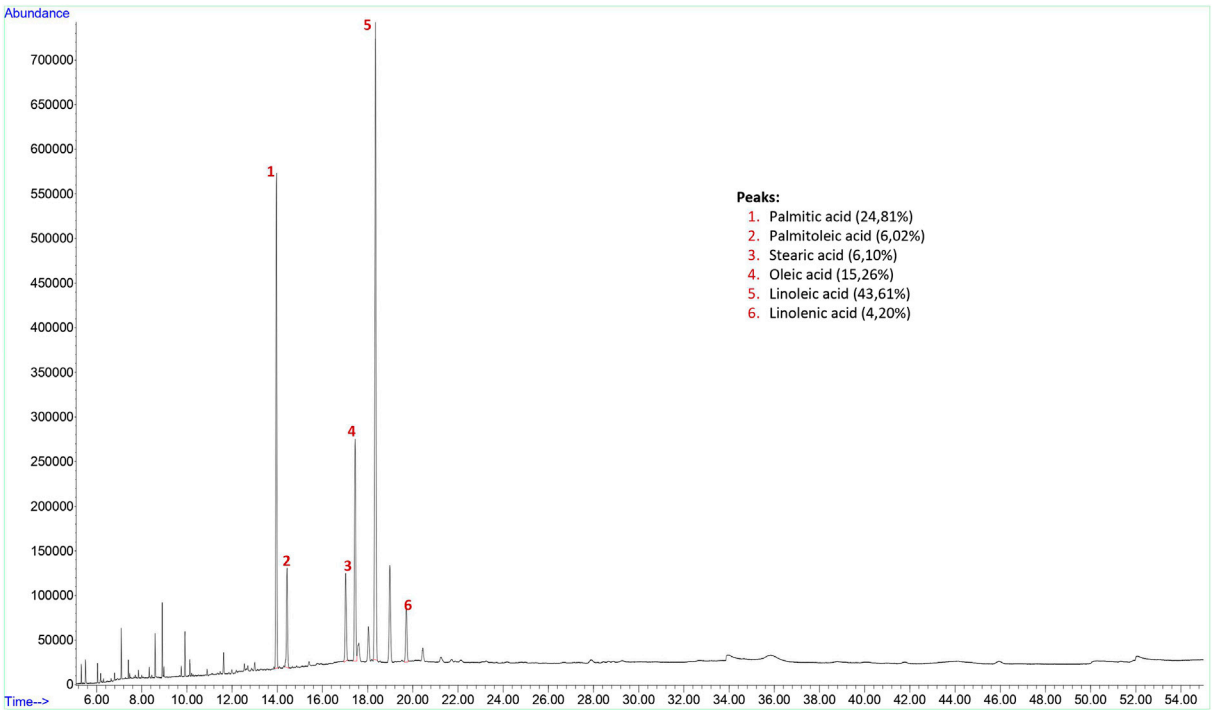

FIGURE 1 | GC-FID chromatogram of hexane extract of grape (*Vitis vinifera*) seed.

3.3 Total Phenolic and Total Flavonoid Contents of Grape Seed Extract

According to the analysis of total phenolic and flavonoid content in grape seed extracts obtained using different solvents (100% ethyl alcohol, 70% ethyl alcohol/water, and 50% ethyl alcohol/water), the final solvent was determined as 50% ethyl alcohol/water.

In the grape seed extracts obtained by using the final solvent, the phenolic substance content was 24.6% ± 5.57 and the flavonoid substance amount was 1.48% ± 0.38 in the average of the results of the three-repeated analysis.

3.4 Liquid Chromatography-High Resolution Mass Spectrometer Analysis

The analysis results of the determination of the number of phenolic substances in grape (*Vitis vinifera*) seed extract are shown in **Table 2**. According to the analysis results, the phenolic compounds in the grape seed extract were chlorogenic acid, fumaric acid, (-)-epicatechin gallate, caffeic acid, vanillic acid, luteolin 7-glucoside, resveratrol, apigenin 7-glucoside, quercetin, luteolin, and apigenin.

3.5 High-Performance Liquid Chromatographic Analysis

The HPLC chromatogram of the curcumin analysis result of the turmeric extract used in this study is shown in **Figure 4**. The sample was tested under the same conditions with the standard curcumin substance, and the amounts of curcumin were calculated from the peak areas in the same retention time. As a result, it was shown that the turmeric extract used in this study contains 95% curcumin.

3.6 Effect of the Interventions on Serum Biochemical Parameters

Our study determined that mice fed a high cholesterol diet had a higher serum total cholesterol concentration than mice fed a regular diet. The effects of test materials on serum lipid profile are shown in **Table 3**. Of the test materials, GBTF Group, GBTP Group, and GBT Group were found to reduce serum total cholesterol concentration by 64.8, 57.5, and 48.9%, respectively, without causing any ulcerogenic effect on the stomach surface in mice fed with a high cholesterol diet. Total cholesterol levels in blood samples obtained from GBTF Group and GBTP Group were significantly lower compared to the hypercholesterolemic group ($p < 0.01$). Although the total cholesterol levels obtained from the GBT Group were significant compared to the hypercholesterolemic group, the significance level was lower than GBTF Group and GBTP Group ($p < 0.05$). As shown in **Table 3**, all studied test samples showed increased serum HDL-C level activity, but this sign was higher in GBTF Group, GBTP Group, GBT Group, and Flaxseed Group. HDL-C levels were significantly higher in blood samples obtained from GBTP

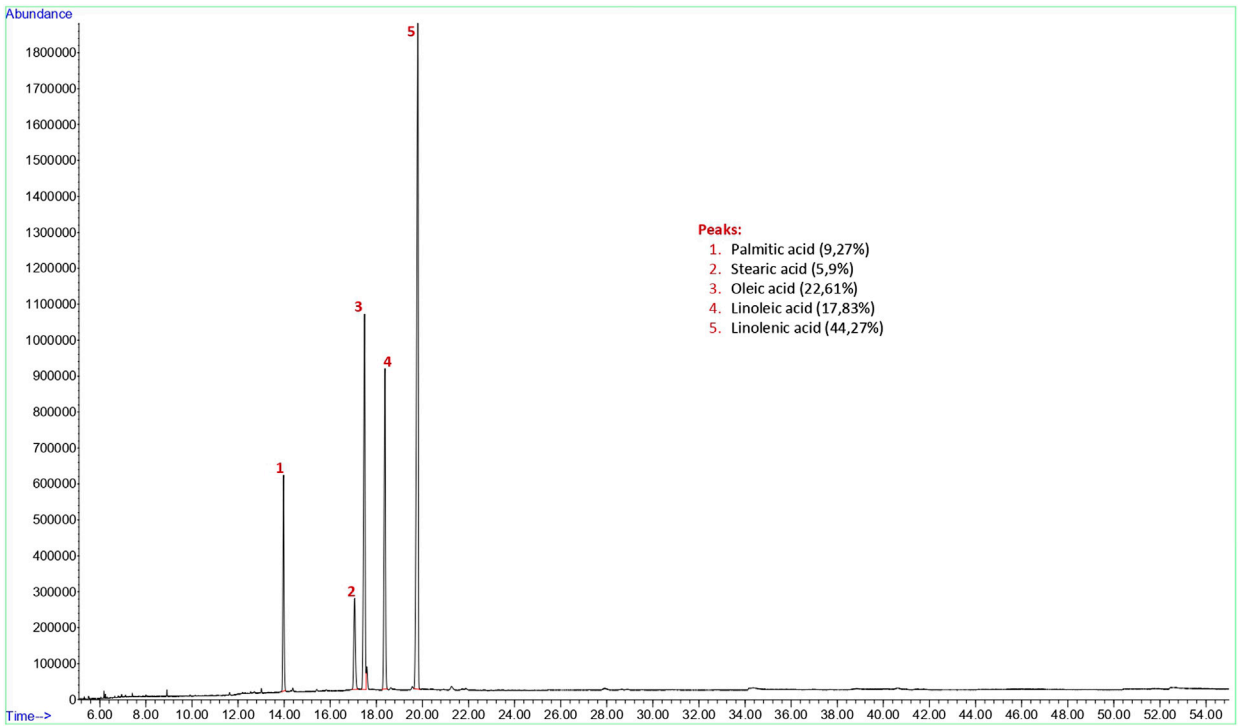

FIGURE 2 | GC-FID chromatogram of hexane extract of flax (*Linum usitatissimum*) seed.

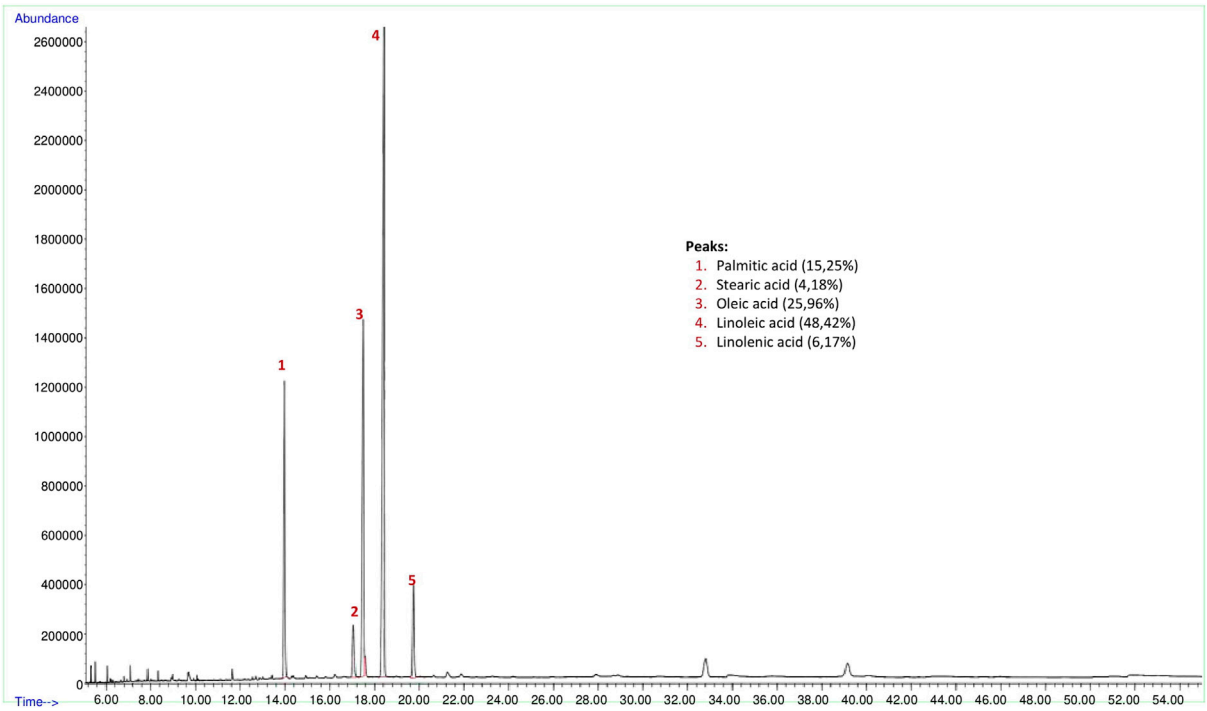

FIGURE 3 | GC-FID chromatogram of hexane extract of psyllium (*Plantago ovata*) seed.

TABLE 2 | Determined phenolic percentage components of grape seed extract.

Phenolic compounds	%
(-)-Epicatechin gallate	3.05
Apigenin	2.87
Apigenin 7-glucoside	3.59
Caffeic acid	3.74
Chlorogenic acid	3.58
Fumaric acid	2.88
Luteolin	3.42
Luteolin 7-glucoside	4.14
Quercetin	2.95
Resveratrol	2.87
Vanillic acid	3.49

Grape seed extract used in this study contains 24.6% phenolic substance and 1.48% flavonoid substance. These phenolic substances are chlorogenic acid, fumaric acid, (-)-epicatechin gallate, caffeic acid, vanillic acid, luteolin 7-glucoside, resveratrol, apigenin 7-glucoside, quercetin, luteolin, and apigenin as you can see ***Table 2****.*

Group than the hypercholesterolemic group ($p < 0.01$). Although HDL-C levels obtained from GBTF Group, GBT Group, and Flaxseed Group were significant compared to the hypercholesterolemic group, the significance level was lower than GBTP Group ($p < 0.05$).

It was determined that serum LDL-C and triglyceride levels were significantly reduced in GBTF Group, GBTP Group, and GBT Group. LDL-C levels were found to be significantly lower in blood samples obtained from GBTF Group and GBTP Group compared to the hypercholesterolemic group ($p < 0.01$). Although the LDL-C levels obtained from the GBT Group were significant compared to the hypercholesterolemic group, the level of significance was lower than GBTF Group and GBTP Group ($p < 0.05$). Triglyceride levels were significantly lower in blood samples obtained from GBTF Group and GBTP Group compared to the hypercholesterolemic group ($p < 0.01$). Although the triglyceride levels obtained from the GBT Group were significant compared to the hypercholesterolemic group, the significance level was lower than GBTF Group and GBTP Group ($p < 0.05$).

The effects of test materials on serum glucose, AST, ALT, MDA, TAA, nitric oxide, and leptin levels are shown in **Table 4**. Our study observed that none of the test materials caused a statistically significant change in serum glucose levels, but the inhibitory ratios in GBTF Group and GBTP Group were remarkable. Remarkable inhibitory effects on serum AST and ALT levels of hepatic marker enzymes were observed in almost all test materials. It was determined that the statistical significance in antihepatotoxic potential was especially in GBTF Group, GBTP Group and GBT Group. In addition, it was determined that the MDA concentration decreased significantly in GBTF Group, and GBTP Group. It was observed that the TAA decreased in the cholesterol-rich diet group compared to the control group. However, there was no statistically significant effect in modulating the decreased plasma TAA level, with a general tendency to normalize the TAA level.

Although the hypercholesterolemic diet caused a slight decrease in the plasma concentration of NO metabolites, the test samples showed significant (not statistically significant) increased activity. This study observed a significant increase in body weight and plasma leptin levels in the high-fat diet group compared to the control group animals. GBTF Group and GBTP Group interventions showed a 41.6 and 36.2% inhibition ratio in leptin concentration, respectively.

The lipid peroxidation level in the hypercholesterolemic group was relatively higher than in the control group. However, it was determined that statistically significant inhibitory activity on lipid peroxidation was shown in GBTF Group, GBTP Group, and GBT

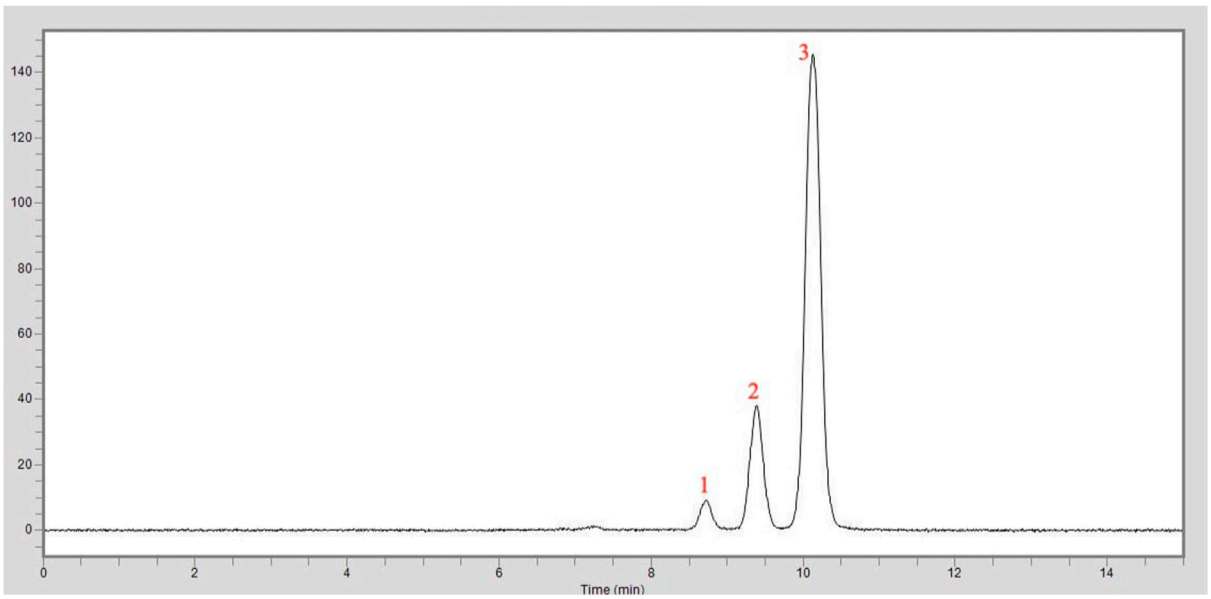

FIGURE 4 | HPLC chromatogram of the curcumin analysis in the turmeric extract: 1. Peak: Bisdemethoxycurcumin, 2. Peak: Demethoxycurcumin, 3. Peak: Curcumin.

TABLE 3 | Effects of test materials on serum TC, HDL-C, LDL-C, and TG levels.

Material	Total cholesterol (mg/dl) (%)	HDL-C (mg/dl) (%)	LDL-C (mg/dl) (%)	Triglyceride (mg/dl) (%)
Control group	127.3 ± 11.6	24.7 ± 1.5	80.7 ± 16.9	116.9 ± 21.3
Hypercholesterolemic group	202.8 ± 14.7#	20.1 ± 1.2	153.6 ± 21.5	171.4 ± 18.1
Bentonite group	151.2 ± 19.3 (–25.4)	26.7 ± 1.5 (+24.7)	172.6 ± 20.3 (+12.4)	193.6 ± 21.9 (+12.9)
GBTF group	**71.4 ± 9.5** (–64.8)**	**34.0 ± 1.7* (+40.8)**	**58.2 ± 17.1** (–62.1)**	**58.1 ± 12.7** (–66.1)**
GBTP group	**86.1 ± 7.9** (–57.5)**	**39.4 ± 1.7** (+48.9)**	**60.3 ± 6.2** (–60.7)**	**63.9 ± 14.1** (–62.7)**
GBT group	**103.6 ± 11.8* (–48.9)**	**30.6 ± 2.4* (+34.3)**	**81.7 ± 12.9* (–46.8)**	**91.7 ± 9.4* (–46.5)**
Flaxseed group	182.1 ± 23.4 (–10.2)	**29.1 ± 2.2* (+30.9)**	119.5 ± 13.7 (–22.2)	103.1 ± 9.7 (–39.8)
Psyllium group	173.1 ± 12.5 (–14.6)	23.4 ± 1.9 (+14.1)	159.1 ± 17.3 (+3.6)	118.2 ± 13.5 (–31.0)
Atorvastatin (10 mg/kg)	**98.5 ± 12.7* (–51.4)**	**40.3 ± 1.1** (+50.1)**	**68.2 ± 13.5** (–55.6)**	**79.2 ± 11.0* (–53.8)**

**p < 0.05; **p < 0.01; ***p < 0.001 (significance relative to hypercholesterolemic group); #: p < 0.05 (significance relative to control group).*
Bentonite Group: HCD + bentonite clay (60 mg/day); GBTF group: HCD + bentonite clay (60 mg/day) + flaxseed (7 mg/day) + grape seed extract (2.5 mg/day) + turmeric extract (2 mg/day); GBTP group: HCD + bentonite clay (60 mg/day) + psyllium (7 mg/day) + grape seed extract (2.5 mg/day) + turmeric extract (2 mg/day); GBT group: HCD + bentonite clay (60 mg/day) + grape seed extract (2.5 mg/day) + turmeric extract (2 mg/day); Flaxseed Group: HCD + flaxseed (7 mg/day); Psyllium Group: HCD + psyllium (7 mg/day).

TABLE 4 | Effects of test materials on serum Glucose, AST, ALT, MDA, TAA, Nitric oxide, and Leptin.

Material	Glucose (mg/dl) (%)	AST (IU/L) (%)	ALT (IU/L) (%)	MDA (nmol/ml) (%)	TAA (mmol/L) (%)	Nitric oxide (μmol/L) (%)	Leptin (μg/L) (%)
Control Group	89.3 ± 13.3	51.4 ± 14.9	11.5 ± 4.9	1.6 ± 0.9	1.22 ± 0.5	21.5 ± 4.3	2.11 ± 0.3
Hypercholesterolomic Group	67.1 ± 8.4	71.5 ± 10.6	39.3 ± 11.6	3.9 ± 1.7	0.94 ± 0.8	25.7 ± 5.8	8.26 ± 1.9
Bentonite Group	52.6 ± 14.1 (–21.6)	69.2 ± 14.7 (–3.2)	31.2 ± 12.4 (–20.6)	3.6 ± 1.1 (–7.7)	0.97 ± 0.3 (+3.2)	27.3 ± 3.2 (+6.2)	7.01 ± 0.7 (–15.1)
GBTF Group	87.5 ± 9.6 (+30.4)	**18.4 ± 5.7** (–74.3)**	**6.4 ± 5.0** (–83.7)**	**1.3 ± 0.2** (–66.7)**	1.13 ± 0.5 (+20.2)	33.8 ± 3.1 (+31.5)	**4.82 ± 1.4* (–41.6)**
GBTP Group	96.4 ± 11.8 (+43.7)	**23.7 ± 9.6** (–66.9)**	**8.7 ± 9.3** (–77.8)**	**2.0 ± 0.3* (–48.7)**	1.25 ± 0.3 (+32.9)	34.1 ± 7.4 (+32.7)	**5.27 ± 1.2* (–36.2)**
GBT Group	74.2 ± 12.4 (+10.6)	**41.5 ± 13.2* (–41.9)**	**10.5 ± 4.1** (–73.3)**	2.1 ± 0.6 (–46.2)	0.51 ± 0.6 (–45.7)	31.9 ± 4.0 (+24.1)	6.13 ± 1.1 (–25.8)
Flaxseed Group	48.1 ± 9.3 (–28.3)	47.1 ± 11.3 (–34.1)	**13.7 ± 9.2* (–65.1)**	2.3 ± 0.5 (–41.0)	1.05 ± 0.1 (+11.7)	31.4 ± 6.8 (+22.2)	6.28 ± 0.8 (–23.9)
Psyllium Group	44.6 ± 7.5 (–33.5)	61.4 ± 12.5 (–14.1)	21.1 ± 7.5 (–46.3)	2.5 ± 0.4 (–35.9)	1.09 ± 0.3 (+15.9)	29.6 ± 4.1 (+15.2)	6.94 ± 0.9 (–15.9)
Atorvastatin (10 mg/kg)	93.4 ± 8.3 (+39.2)	**26.2 ± 9.1** (–63.4)**	**7.9 ± 8.6** (–79.9)**	**2.1 ± 0.4* (–46.2)**	1.17 ± 0.2 (+24.4)	37.2 ± 4.9 (+44.7)	**3.92 ± 1.0** (52.5)**

**p < 0.05; **p < 0.01; ***p < 0.001 (significance relative to hypercholesterolemic group).*
Bentonite Group: HCD + bentonite clay (60 mg/day); GBTF group: HCD + bentonite clay (60 mg/day) + flaxseed (7 mg/day) + grape seed extract (2.5 mg/day) + turmeric extract (2 mg/day); GBTP group: HCD + bentonite clay (60 mg/day) + psyllium (7 mg/day) + grape seed extract (2.5 mg/day) + turmeric extract (2 mg/day); GBT group: HCD + bentonite clay (60 mg/day) + grape seed extract (2.5 mg/day) + turmeric extract (2 mg/day); Flaxseed Group: HCD + flaxseed (7 mg/day); Psyllium Group: HCD + psyllium (7 mg/day).

Group. Our study examined SOD, catalase, GSH, and GPx levels to evaluate oxidative damage in liver tissue. It was shown that all these biochemical parameters were statistically significantly reduced in GBTF Group, GBTP Group, and GBT Group.

According to histopathological analyses, it was determined that there was no degeneration in hepatocytes, hepatocyte cell plague, Kupffer cell, and sinusoids in the control group. While degenerative hepatocyte and degenerative hepatocyte plaques, mononuclear cell infiltration, sinusoid degeneration, and necrosis were observed to be quite intense in the hypercholesterolemic group, the presence of hepatocyte, endothelium, glycogen, and sinusoids were detected in the group where Atorvastatin, which is used as the reference drug, was administered. When the test samples were examined histopathologically, mononuclear cell infiltration, macro and microvesicles, hepatocyte cell degeneration, sinusoid endothelium, and granuloma formation in Bentonite Group, GBT, and Flaxseed Group. Blood cells in sinusoid, endothelial cells, capsules were seen in GBTF Group and GBTP Group. In the Psyllium Group fibrous tissue, degerative lobular formation, degenerative hepatocyte, and degenerative sinusoids were found to be quite prominent (**Figure 5**). In this context, it has been determined that histopathological data and biochemical parameters support each other.

4 DISCUSSION

Cholesterol and triglyceride, one of the naturally occurring fats in the body, are significant elements in the structure of biological membranes. They are used to both the biosynthesis of steroid hormones, bile acids, vitamin D, and the energy production for

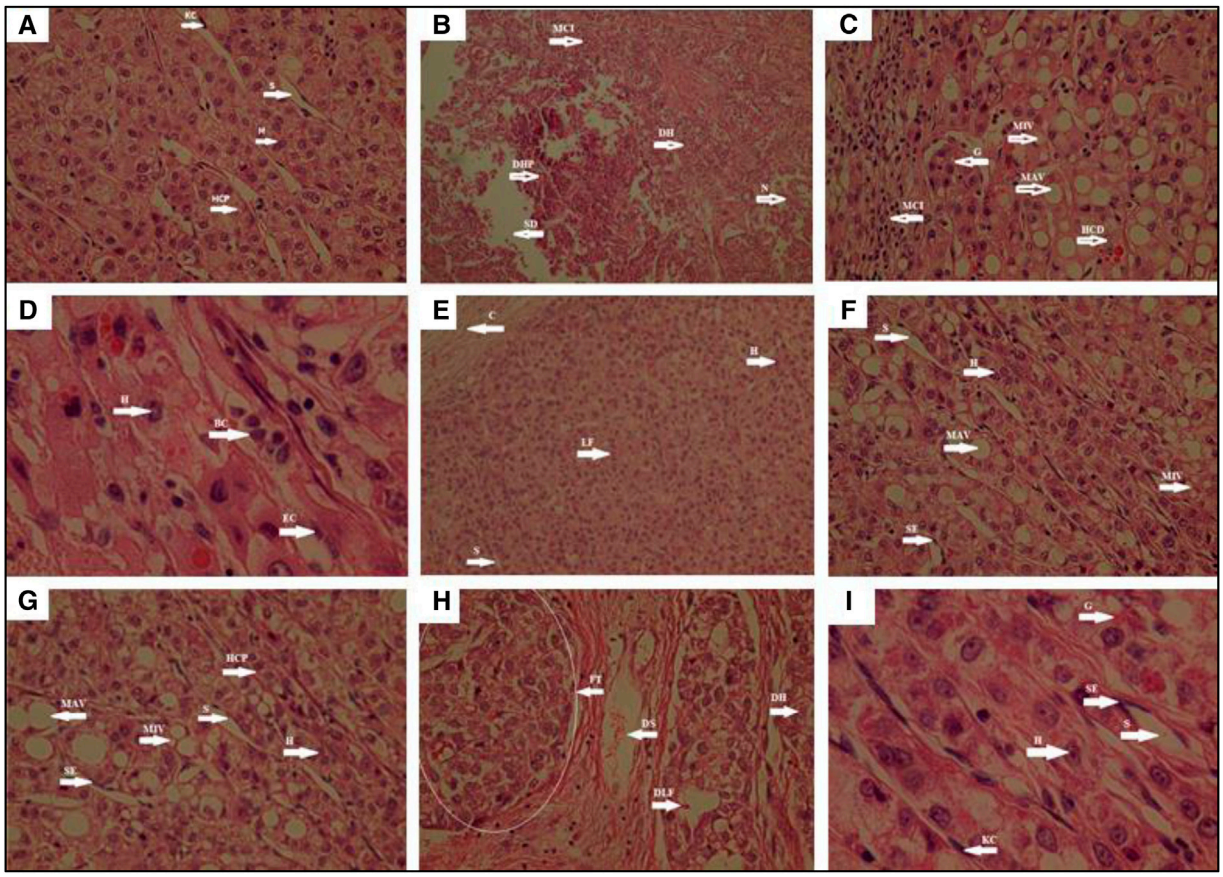

FIGURE 5 | Histopathological view of hepatic tissue in the control, hypercholesterolemia, test materials and reference drug Atorvastatin administered animals. Tissue sections was stained the hematoxylin and eosin (HE). The original magnification was ×100. Data are representative of six animal per group **(A)**: Control group; **(B)**: Hypercholesterolemic group; **(C)**: Bentonite Group; **(D)**: GBTF Group; **(E)**: GBTP Group; **(F)**: GBT Group; **(G)**: Flaxseed Group; **(H)**: Psyllium Group; **(I)**: Atorvastatin. BC, Blood cell in sinusoid; C, Capsule; DH, Degenerative hepatocyte; DHP, Degenerative Hepatocyte plague; DLF, Degenerative lobular formation; DS, Degenerative sinusoid; E, Endothelium; EC, Endothelial cell; FT, Fibrous tissue; G, Granuloma; H, Hepatocyte; HCD, Hepatocyte cell degeneration; HCP, Hepatocyte cell plague; KC, Kupffer cell; LF, Lobular formation; MCI, Mononuclear cell infiltration; MAV, Macrovesicle; MIV, Microvesicle; N, Necrosis; S, Sinusoid; SD, Sinusoid degeneration; SE, Sinusoid endothelium.

the body. However, high cholesterol concentration in the blood is associated with atherosclerosis and increases the risk of cardiovascular diseases. Total cholesterol concentration in the blood affects by both dietary cholesterol content and cholesterol synthesized in the liver (Avcı et al., 2006).

In our study, flaxseed, psyllium, and food-grade bentonite clay did not significantly reduce total cholesterol and LDL-C; however, GBTF Group, GBTP Group, and GBT Group interventions had a significant effect in reducing both total cholesterol levels and LDL-C levels. Therefore, it can be thought that this significant effect is due to the synergistic effect of the raw materials. It was observed that the addition of psyllium to the group with bentonite, grape seed extract, and turmeric extract (GBT Group) provided an 8.6% reduction in total cholesterol. Instead, the addition of flaxseed instead of psyllium to the same group (GBT Group) decreased total cholesterol by 15.9%. According to our results of fixed oil analysis, more amount of oil (better yield) is obtained from flaxseed than psyllium. The difference was found in the ratios of polyunsaturated fatty acids in flaxseed and psyllium, which have relatively the same ratios of saturated and monounsaturated fatty acids in fixed oil analysis. Linolenic Acid/Linoleic Acid (omega-3/omega-6) ratio in flaxseed seems to be more than in psyllium. Therefore, when studied at the same doses with flaxseed and psyllium, the group containing flaxseed (GBTF Group) had further total fatty acids and a higher omega-3/omega-6 ratio than the group containing psyllium (GBTP Group). This situation may explain the different effects on TC and LDL-C changes between these groups (GBTF Group—GBTP Group). In addition, Soltanian and Janghorbani (Soltanian and Janghorbani, 2019) previously stated that flaxseed has superior hypocholesterolemic effects compared to psyllium. Moreover, Brown et al. (1999) state that soluble fibers provide a reduction in serum TC and LDL-C. Similarly, in this study, more reductions in TC and LDL-C levels were observed with the addition of fiber-rich flaxseed or psyllium seeds to the group, which has food-grade bentonite clay, grape seed extract, and turmeric extract (GBT Group).

Low-density lipoprotein (LDL) transports cholesterol from the liver to the tissues, while high-density lipoprotein (HDL)

facilitates for transport of cholesterol from peripheral tissues to the liver. Therefore, it is recommended that increase the HDL-C ratio in serum while lowering LDL-C levels to reduce the risk of cardiovascular disease (Nofer et al., 2002). In this study, an increase in HDL-C was found higher in GBTF Group, GBTP Group, GBT Group, and Flaxseed Group than the other groups. Li et al. (2015) mentioned that anthocyanins had an additive effect on HDL-C. Therefore, the rich anthocyanin content of grape seed extract in GBTF Group, GBTP Group, and GBT Group may be responsible for this significant effect in the study. On the other hand, the significant increase in HDL-C only with flaxseed intervention (Flaxseed Group) was inconsistent with the data in the literature because there was no significant increase in HDL-C in previous intervention studies with flaxseed (Shakir and Madhusudhan, 2007).

As a result, considering the total cholesterol, HDL-C, LDL-C, and triglyceride serum concentrations in hypercholesterolemic mice, it was concluded that GBTF Group, GBTP Group, and GBT Group had a positive effect on reducing the risk of cardiovascular diseases such as atherosclerosis.

Hypercholesterolemia causes fatty liver and increases liver enzymes (Choe et al., 2001). Therefore, in this study, various serum parameters were also evaluated to reveal the effects of the test materials on hepatic markers and glucose (**Table 4**). Previous studies reported that both lipid peroxidation levels increased in serum (Das et al., 2000) and plasma MDA levels (Szczeklik et al., 1985). For this reason, the values measured in **Table 4**, such as MDA, are essential to evaluate the effects of hypercholesterolemia on the liver. It concluded that GBTF Group and GBTP Group interventions had a significant reducing effect on both MDA and liver enzymes, so these interventions may have positive effects on complications such as fatty liver that may occur as a result of hypercholesterolemia in this study. Moreover, the significant inhibitory effect of flaxseed intervention (Flaxseed Group) on liver enzymes suggests that even flaxseed intervention alone may be sufficient to exhibit liver-protective properties.

A high-fat diet causes lipid accumulation in visceral tissues and increases body weight (Milagro et al., 2006; Yang et al., 2006). The findings obtained due to increased leptin values in the hypercholesterolemic group compared to the control group are consistent with the literature (**Table 4**). GBTF Group and GBTP Group interventions reduced leptin levels in our study. Similarly, this kind of effect might be due to the synergistic effect of raw material components.

It is an critical issue to examine the correlation between the capacity of antioxidants for scavenging free radicals and that for inhibition of lipid peroxidation (Niki et al., 2008). A significant inhibitory effect on lipid peroxidation was observed in which turmeric extract containing 95% curcumin and grape seed extract rich in antioxidant properties were used (GBTF Group, GBTP Group, and GBT Group) as expected in this study (**Table 5**).

Reactive oxygen species (ROS) are reduced by non-enzymatic antioxidant defenses such as ascorbic acid (vitamin C), alpha-tocopherol (vitamin E), and GSH, or by enzymatic antioxidant defenses such as CAT, POD, and SOD (Seet et al., 2010). GSH is also the major non-protein thiol involved in antioxidant cellular defense (Di Pietro et al., 2010). These enzymes were evaluated as effective parameters in detoxification. These enzymes control the number of free radicals produced or scavenge them and prevent their binding to macromolecules. Moreover, the most crucial feature of the antioxidant defense system is that all synergistic components assign against reactive oxygen species for homeostasis. Combined oxidants/antioxidants are more effective than existing alone in the blood (Kaya et al., 2015). Significant increases in SOD, catalase, GSH, and GPx levels were observed in GBTF Group and GBTP Group. Similarly, this kind of effect can be attributed to the presence of curcumin and polyphenols. Also, it can be said that the presence of flaxseed in GBTF Group and psyllium seeds in GBTP Group was responsible for the significant effect on GSH and CAT levels. It is conceivable from other studies that flaxseed oil content and flaxseed lignan content may be responsible for the effects on these parameters. However, more research is necessary on the responsible component in psyllium seed that can be attributed to this kind of effect on these parameters. Contrary to expectations, bentonite did not have a significant effect on some detoxification parameters by itself. However, the short duration of the study can be a limiting factor for this kind of evaluation.

In conclusion, it was shown that GBTF Group, which contains bentonite, flaxseed, grape seed extract, turmeric extract, and GBTP Group, which contains bentonite, psyllium, grape seed extract, and turmeric extract, had significant positive effects on both detoxification parameters and serum cholesterol values when compared to the hypercholesterolemic group. According to a study, bentonite increases fecal lipid excretion by immobilizing lipids in the gastrointestinal system (Xu et al., 2016). The component responsible for the hypocholesterolemic effect of flaxseed is not clear. Nevertheless, we can say that fecal fat excretion was increased with flaxseed fiber (Kristensen et al., 2012). One of the components responsible for the cholesterol-lowering effect in flaxseed is lignans such as secoisolariciresinol diglucoside (SDG). However, the mechanism for the observed cholesterol-lowering effect of flaxseed lignan has not been elucidated (Fukumitsu et al., 2010). The phytoestrogen lignan may be similar to the selective estrogen receptor modulators for the cholesterol-lowering effect (Zhang et al., 2008). Psyllium has a cholesterol-lowering effect by increasing the excretion of bile acids, reducing intestinal cholesterol absorption, and reducing hepatic cholesterol synthesis. Especially high viscosity fibers such as psyllium significantly inhibit cholesterol absorption in the small intestine (Dikeman and Fahey, 2006). Curcumin can regulate the expression of genes involved in cholesterol homeostasis (Srinivasan and Sambaiah, 1991). Besides, It was reported that the anti hyperlipidemia effect of curcumin is similar to that of statins such as lovastatin and that curcumin mainly acts by reducing liver cholesterol biosynthesis by inhibiting HMG-CoA reductase (Zingg et al., 2013). Finally, grape seeds have cholesterol-lowering activity by inhibiting pancreatic cholesterol esterase, binding bile acids, and reducing the solubility of cholesterol in micelles, resulting in delayed cholesterol absorption (Ngamukote et al., 2011). Because of the different cholesterol-lowering mechanisms of all these components, it is

TABLE 5 | Effects of test materials on SOD, CAT, LPO, GSH and GPx levels.

Material	SOD (µg/mg protein)	CAT (µmol/mg)	LPO (nmol/mg)	GSH (nmol/g)	GPx (U/g Hb)
Control group	2.95 ± 0.51	22.3 ± 4.1	3.12 ± 0.51	1.16 ± 0.51	145.2 ± 5.13
Hypercholesterolomic group	1.57 ± 0.34	10.1 ± 4.0	4.98 ± 0.49	1.02 ± 0.58	102.6 ± 4.73
Bentonite Group	2.04 ± 0.23	19.4 ± 2.7	2.52 ± 0.37	1.18 ± 0.36	145.2 ± 5.13
GBTF Group	**5.72 ± 0.13***	**48.4 ± 3.1****	**1.75 ± 0.13***	**2.84 ± 0.09****	**229.4 ± 3.48****
GBTP Group	**4.39 ± 0.28***	**37.4 ± 2.5***	**1.86 ± 0.09***	**2.51 ± 0.11***	**215.1 ± 3.72****
GBT Group	**4.46 ± 0.31***	25.8 ± 1.3	**1.92 ± 0.27***	1.98 ± 0.22	**207.8 ± 4.06***
Flaxseed Group	3.69 ± 0.86	23.5 ± 3.2	2.20 ± 0.41	1.74 ± 0.25	192.3 ± 3.98
Psyllium Group	3.11 ± 0.27	22.6 ± 2.6	2.19 ± 0.36	1.81 ± 0.17	162.2 ± 3.21
Atorvastatin(10 mg/kg)	**4.37 ± 0.34***	**42.3 ± 1.5***	**1.43 ± 0.14***	**2.37 ± 0.14***	**198.7 ± 3.07****

*p < 0.05; **p < 0.01; ***p < 0.001 (significance relative to hypercholesterolemic group).
Bentonite Group: HCD + bentonite clay (60 mg/day); GBTF group: HCD + bentonite clay (60 mg/day) + flaxseed (7 mg/day) + grape seed extract (2.5 mg/day) + turmeric extract (2 mg/day); GBTP group: HCD + bentonite clay (60 mg/day) + psyllium (7 mg/day) + grape seed extract (2.5 mg/day) + turmeric extract (2 mg/day); GBT group: HCD + bentonite clay (60 mg/day) + grape seed extract (2.5 mg/day) + turmeric extract (2 mg/day); Flaxseed Group: HCD + flaxseed (7 mg/day); Psyllium Group: HCD + psyllium (7 mg/day).

hard to make a definitive judgment about the cholesterol-lowering mechanism of action of the combinations. On the other hand, it can be thought that the combinations provide inhibition of cholesterol absorption from the gastrointestinal tract. Studies on the cholesterol-lowering mechanism of these combinations may be conducted in the future. In this study, the model of hypercholesterolemia caused by a high cholesterol diet was studied. Therefore, we can not claim that these combinations would also positively affect a non-dietary hypercholesterolemia model. Also, these findings can be supported by clinical studies. The raw material doses used in the study can be applied to human nutrition, and formulations can be developed in line with this kind of positive effect.

DATA AVAILABILITY STATEMENT

The original contributions presented in the study are included in the article/Supplementary Material, further inquiries can be directed to the corresponding authors.

ETHICS STATEMENT

The animal study was reviewed and approved by Saki Yenilli Experimental Animals Local Ethics Committee (Ethics Committee No: 03/15). Written informed consent was obtained from the owners for the participation of their animals in this study.

AUTHOR CONTRIBUTIONS

MK created the idea, layout of the project and provided laboratory facilities. İD contributed to laboratory experiments. RT carried out laboratory experiments and preparation of the final manuscript. EA performed all *in vivo* experiments and revised the manuscript. HK performed the histopathological analysis. All authors approved it for publication.

FUNDING

This research was supported by the Scientific Research Unit of Bezmialem Vakif University with grant number 20200921.

ACKNOWLEDGMENTS

The manuscript has previously appeared online in a thesis (Turgut, 2021).

REFERENCES

Aarden, E., Van Hoyweghen, I., and Horstman, K. (2011). The Paradox of Public Health Genomics: Definition and Diagnosis of Familial Hypercholesterolaemia in Three European Countries. *Scand. J. Public Health* 39, 634–639. doi:10.1177/1403494811414241

Adamis, Z., Fodor, J., and Williams, R. B. (2005). Bentonite, Kaolin, and Selected Clay Minerals. *Environ. Health Criteria* 231, 1–175. doi:10.1016/0043-1354(85)90052-1

Amalraj, A., Pius, A., Gopi, S., and Gopi, S. (2017). Biological Activities of Curcuminoids, Other Biomolecules from Turmeric and Their Derivatives - A Review. *J. Tradit. Complement. Med.* 7 (2), 205–233. doi:10.1016/j.jtcme.2016.05.005

Arshami, J., Pilevar, M., Aami Azghadi, M., and Raji, A. R. (2013). Hypolipidemic and Antioxidative Effects of Curcumin on Blood Parameters, Humoral Immunity, and Jejunum Histology in Hy-Line Hens. *Avicenna J. Phytomed.* 3 (2), 178–185. doi:10.22038/ajp.2013.72

Avcı, G., Küpeli, E., Eryavuz, A., Yesilada, E., and Kucukkurt, I. (2006). Antihypercholesterolaemic and Antioxidant Activity Assessment of Some Plants Used as Remedy in Turkish Folk Medicine. *J. Ethnopharmacol* 107, 418–423. doi:10.1016/j.jep.2006.03.032

Bannayan, M., Nadjafi, F., Azizi, M., Tabrizi, L., and Rastgoo, M. (2008). Yield and Seed Quality of Plantago Ovata and Nigella Sativa under Different Irrigation Treatments. *Ind. Crops Prod.* 27 (1), 11–16. doi:10.1016/j.indcrop.2007.05.002

Belorio, M., and Gómez, M. (2020). Psyllium: A Useful Functional Ingredient in Food Systems. *Crit. Rev. Food Sci. Nutr.* 1-12, 1–12. doi:10.1080/10408398.2020.1822276

Brown, L., Rosner, B., Willett, W. W., and Sacks, F. M. (1999). Cholesterol-Lowering Effects of Dietary Fiber: A Meta-Analysis. *Am. J. Clin. Nutr.* 69 (1), 30–42. doi:10.1093/ajcn/69.1.30

Cerqueira, N. M., Oliveira, E. F., Gesto, D. S., Santos-Martins, D., Moreira, C., Moorthy, H. N., et al. (2016). Cholesterol Biosynthesis: A Mechanistic Overview. *Biochemistry* 55 (39), 5483–5506. doi:10.1021/acs.biochem.6b00342

Chen, Y., Xiao, J., Zhang, X., and Bian, X. (2016). MicroRNAs as Key Mediators of Hepatic Detoxification. *Toxicology* 368-369, 80–90. doi:10.1016/j.tox.2016.08.005

Chen, Z.-Y., Jiao, R., and Ma, K. Y. (2008). Cholesterol-Lowering Nutraceuticals and Functional Foods. *J. Agric. Food Chem.* 56 (19), 8761–8773. doi:10.1021/jf801566r

Chikara, S., Mamidi, S., Sreedasyam, A., Chittem, K., Pietrofesa, R., Zuppa, A., et al. (2018). Flaxseed Consumption Inhibits Chemically Induced Lung Tumorigenesis and Modulates Expression of Phase II Enzymes and Inflammatory Cytokines in A/J Mice. *Cancer Prev. Res. (Phila)* 11 (1), 27–37. doi:10.1158/1940-6207.CAPR-17-0119

Choe, S. C., Kim, H. S., Jeong, T. S., Bok, S. H., and Park, Y. B. (2001). Naringin Has an Antiatherogenic Effect with the Inhibition of Intercellular Adhesion Molecule-1 in Hypercholesterolemic Rabbits. *J. Cardiovasc. Pharmacol.* 38, 947–955. doi:10.1097/00005344-200112000-00017

Das, S., Vasisht, S., Das, S. N., and Srivastava, L. M. (2000). Correlation between Total Antioxidant Status and Lipid Peroxidation in Hypercholesterolemia. *Curr. Sci.* 78 (4), 486–487.

Di Pietro, G., Magno, L. A., and Rios-Santos, F. (2010). Glutathione S-Transferases: an Overview in Cancer Research. *Expert Opin. Drug Metab. Toxicol.* 6 (2), 153–170. doi:10.1517/17425250903427980

Dikeman, C. L., and Fahey, G. C. (2006). Viscosity as Related to Dietary Fiber: A Review. *Crit. Rev. Food Sci. Nutr.* 46 (8), 649–663. doi:10.1080/10408390500511862

Draper, H. H., and Hadley, M. (1990). Malondialdehyde Determination as Index of Lipid Peroxidation. *Methods Enzymol.* 186, 421–431. doi:10.1016/0076-6879(90)86135-i

EFSA Panel on Additives and Products or Substances used in Animal Feed (FEEDAP) (2016). Safety and Efficacy of Dry Grape Extract when Used as a Feed Favouring for All Animal Species and Categories. *EFSA J.* 14 (6), e04476. doi:10.2903/j.efsa.2016.4476

EFSA Panel on Additives and Products or Substances used in Animal Feed (FEEDAP) (2012). Scientific Opinion on the Safety and Efficacy of Bentonite as a Technological Feed Additive for All Species. *EFSA J.* 10 (7), 2787. doi:10.2903/j.efsa.2012.2787

Fukumitsu, S., Aida, K., Shimizu, H., and Toyoda, K. (2010). Flaxseed Lignan Lowers Blood Cholesterol and Decreases Liver Disease Risk Factors in Moderately Hypercholesterolemic Men. *Nutr. Res.* 30 (7), 441–446. doi:10.1016/j.nutres.2010.06.004

Gershkovich, P., Darlington, J., Sivak, O., Constantinides, P. P., and Wasan, K. M. (2009). Inhibition of Intestinal Absorption of Cholesterol by Surface-Modified Nanostructured Aluminosilicate Compounds. *J. Pharm. Sci.* 98 (7), 2390–2400. doi:10.1002/jps.21616

Gupta, M., Dey, S., Marbaniang, D., Pal, P., Ray, S., and Mazumder, B. (2020). Grape Seed Extract: Having a Potential Health Benefits. *J. Food Sci. Technol.* 57 (4), 1205–1215. doi:10.1007/s13197-019-04113-w

Hodges, R. E., and Minich, D. M. (2015). Modulation of Metabolic Detoxification Pathways Using Foods and Food-Derived Components: A Scientific Review with Clinical Application. *J. Nutr. Metab.* 2015, 760689. doi:10.1155/2015/760689

Houghton, P. J., Zarka, R., de las Heras, B., and Hoult, J. R. (1995). Fixed Oil of Nigella Sativa and Derived Thymoquinone Inhibit Eicosanoid Generation in Leukocytes and Membrane Lipid Peroxidation. *Planta Med.* 61 (01), 33–36. doi:10.1055/s-2006-957994

Kaya, I., Deveci, H., Ekinci, U., Karapehlivan, M., Kaya, M., and Alpay, M. (2015). The Effect of Ellagic Acid and Sodium Fluoride Intake on Total Sialic Acid Levels and Total Oxidant/antioxidant Status in Mouse Testicular Tissue. *ARRB* 7 (5), 329–335. doi:10.9734/arrb/2015/19327

Koracevic, D., Koracevic, G., Djordjevic, V., Andrejevic, S., and Cosic, V. (2001). Method for the Measurement of Antioxidant Activity in Human Fluids. *J. Clin. Pathol.* 54 (5), 356–361. doi:10.1136/jcp.54.5.356

Kristensen, M., Jensen, M. G., Aarestrup, J., Petersen, K. E., Søndergaard, L., Mikkelsen, M. S., et al. (2012). Flaxseed Dietary Fibers Lower Cholesterol and Increase Fecal Fat Excretion, but Magnitude of Effect Depend on Food Type. *Nutr. Metab. (Lond)* 9 (1), 8. doi:10.1186/1743-7075-9-8

Kurtel, H., Granger, D. N., Tso, P., and Grisham, M. B. (1992). Vulnerability of Intestinal Interstitial Fluid to Oxidant Stress. *Am. J. Physiol.* 263 (4), G573–G578. doi:10.1152/ajpgi.1992.263.4.G573

Li, S. G., Ding, Y. S., Niu, Q., Xu, S. Z., Pang, L. J., Ma, R. L., et al. (2015). Grape Seed Proanthocyanidin Extract Alleviates Arsenic-Induced Oxidative Reproductive Toxicity in Male Mice. *Biomed. Environ. Sci.* 28, 272–280. doi:10.3967/bes2015.038

Liska, D. J. (1998). The Detoxification Enzyme Systems. *Altern. Med. Rev.* 3 (3), 187–198.

Milagro, F. I., Campión, J., and Martínez, J. A. (2006). Weight Gain Induced by High-Fat Feeding Involves Increased Liver Oxidative Stress. *Obesity (Silver Spring)* 14, 1118–1123. doi:10.1038/oby.2006.128

Miranda, K. M., Espey, M. G., and Wink, D. A. (2001). A Rapid, Simple Spectrophotometric Method for Simultaneous Detection of Nitrate and Nitrite. *Nitric Oxide* 5, 62–71. doi:10.1006/niox.2000.0319

Misra, H. P., and Fridovich, I. (1972). The Role of Superoxide Anion in the Autoxidation of Epinephrine and a Simple Assay for Superoxide Dismutase. *J. Biol. Chem.* 247 (10), 3170–3175. doi:10.1016/s0021-9258(19)45228-9

Nakata, K., Tanaka, Y., Nakano, T., Adachi, T., Tanaka, H., Kaminuma, T., et al. (2006). Nuclear Receptor-Mediated Transcriptional Regulation in Phase I, II, and III Xenobiotic Metabolizing Systems. *Drug Metab. Pharmacokinet.* 21, 437–457. doi:10.2133/dmpk.21.437

Newby, L. K., Kandzari, D., Roe, M. T., Mulgund, J., Bhatt, D. L., DeLong, E., et al. (2005). Examining the Hypercholesterolemia Paradox in Acute Coronary Syndromes: Results from CRUSADE. *Circulation* 111, E329. doi:10.1002/clc.20518

Ngamukote, S., Mäkynen, K., Thilawech, T., and Adisakwattana, S. (2011). Cholesterol-lowering Activity of the Major Polyphenols in Grape Seed. *Molecules* 16 (6), 5054–5061. doi:10.3390/molecules16065054

Niki, E., Omata, Y., Fukuhara, A., Saito, Y., and Yoshida, Y. (2008). Assessment of Radical Scavenging Capacity and Lipid Peroxidation Inhibiting Capacity of Antioxidant. *J. Agric. Food Chem.* 56 (18), 8255–8260. doi:10.1021/jf800605x

Nofer, J. R., Kehrel, B., Fobker, M., Levkau, B., Assmann, G., and von Eckardstein, A. (2002). HDL and Arteriosclerosis: Beyond Reverse Cholesterol Transport. *Atherosclerosis* 161, 1–16. doi:10.1016/s0021-9150(01)00651-7

Ohkawa, H., Ohishi, N., and Yagi, K. (1979). Assay for Lipid Peroxides in Animal Tissues by Thiobarbituric Acid Reaction. *Anal. Biochem.* 95 (2), 351–358. doi:10.1016/0003-2697(79)90738-3

Paglia, D. E., and Valentine, W. N. (1967). Studies on the Quantitative and Qualitative Characterization of Erythrocyte Glutathione Peroxidase. *J. Lab. Clin. Med.* 70, 158–169. doi:10.5555/uri:pii:0022214367900765

Pan, A., Yu, D., Demark-Wahnefried, W., Franco, O. H., and Lin, X. (2009). Meta-Analysis of the Effects of Flaxseed Interventions on Blood Lipids. *Am. J. Clin. Nutr.* 90 (2), 288–297. doi:10.3945/ajcn.2009.27469

Paramasivam, M., Poi, R., Banerjee, H., and Bandyopadhyay, A. (2009). High-Performance Thin Layer Chromatographic Method for Quantitative Determination of Curcuminoids in Curcuma Longa Germplasm. *Food Chem.* 113 (2), 640–644. doi:10.1016/j.foodchem.2008.07.051

Parikh, M., and Pierce, G. N. (2019). Dietary Flaxseed: what We Know and Don't Know about its Effects on Cardiovascular Disease. *Can. J. Physiol. Pharmacol.* 97 (2), 75–81. doi:10.1139/cjpp-2018-0547

Qinna, N. A., Kamona, B. S., Alhussainy, T. M., Taha, H., Badwan, A. A., and Matalka, K. Z. (2012). Effects of Prickly Pear Dried Leaves, Artichoke Leaves, Turmeric and Garlic Extracts, and Their Combinations on Preventing Dyslipidemia in Rats. *ISRN Pharmacol.* 2012, 167979. doi:10.5402/2012/167979

Sedlak, J., and Lindsay, R. H. (1968). Estimation of Total, Protein-Bound, and Nonprotein Sulfhydryl Groups in Tissue with Ellman's Reagent. *Anal. Biochem.* 25 (1), 192–205. doi:10.1016/0003-2697(68)90092-4

Seet, R. C., Lee, C. Y., Lim, E. C., Tan, J. J., Quek, A. M., Chong, W. L., et al. (2010). Oxidative Damage in Parkinson Disease: Measurement Using Accurate Biomarkers. *Free Radic. Biol. Med.* 48 (4), 560–566. doi:10.1016/j.freeradbiomed.2009.11.026

Shakir, K. A., and Madhusudhan, B. (2007). Hypocholesterolemic and Hepatoprotective Effects of Flaxseed Chutney: Evidence from Animal Studies. *Indian J. Clin. Biochem.* 22 (1), 117–121. doi:10.1007/BF02912893

Soltanian, N., and Janghorbani, M. (2019). Effect of Flaxseed or Psyllium vs. Placebo on Management of Constipation, Weight, Glycemia, and Lipids: A Randomized Trial in Constipated Patients with Type 2 Diabetes. *Clin. Nutr. ESPEN.* 29, 41–48. doi:10.1016/j.clnesp.2018.11.002

Srinivasan, K., and Sambaiah, K. (1991). The Effect of Spices on Cholesterol 7 Alpha-Hydroxylase Activity and on Serum and Hepatic Cholesterol Levels in the Rat. *Int. J. Vitam. Nutr. Res.* 61, 364–369.

Szczeklik, A., Gryglewski, R. J., Domagala, B., Dworski, R., and Basista, M. (1985). Dietary Supplementation with Vitamin E in Hyperlipoproteinemias: Effects on Plasma Lipid Peroxides, Antioxidant Activity, Prostacyclin Generation and Platelet Aggregability. *Thromb. Haemost.* 54 (6), 425–430. doi:10.1055/s-0038-1657865

Takahara, S., Hamilton, H. B., Neel, J. V., Kobara, T. Y., Ogura, Y., and Nishimura, E. T. (1960). Hypocatalasemia: A New Genetic Carrier State. *J. Clin. Invest.* 39, 610–619. doi:10.1172/JCI104075

Turgut, R. (2021). *Development of Detox Formulations Using Bentonite and Herbal Raw Materials*. master's thesis. Istanbul: Bezmialem Vakif University.

Uddin, F. (2018). Montmorillonite: An Introduction to Properties and Utilization. *Curr. Top. Util. Clay Ind. Med. Appl.* 1. doi:10.5772/intechopen.77987

Valko, M., Leibfritz, D., Moncol, J., Cronin, M. T., Mazur, M., and Telser, J. (2007). Free Radicals and Antioxidants in Normal Physiological Functions and Human Disease. *Int. J. Biochem. Cel Biol.* 39 (1), 44–84. doi:10.1016/j.biocel.2006.07.001

Wei, Z. H., Wang, H., Chen, X. Y., Wang, B. S., Rong, Z. X., Wang, B. S., et al. (2009). Time- and Dose-dependent Effect of Psyllium on Serum Lipids in Mild-To-Moderate Hypercholesterolemia: a Meta-Analysis of Controlled Clinical Trials. *Eur. J. Clin. Nutr.* 63 (7), 821–827. doi:10.1038/ejcn.2008.49

Xing, L. C., Santhi, D., Shar, A. G., Saeed, M., Arain, M. A., Shar, A. H., et al. (2017). Psyllium Husk (Plantago Ovata) as a Potent Hypocholesterolemic Agent in Animal, Human and Poultry. *Int. J. Pharmacol.* 13 (7), 690–697. doi:10.3923/ijp.2017.690.697

Xu, P., Dai, S., Wang, J., Zhang, J., Liu, J., Wang, F., et al. (2016). Preventive Obesity Agent Montmorillonite Adsorbs Dietary Lipids and Enhances Lipid Excretion from the Digestive Tract. *Scientific Rep.* 6 (1), 1–12. doi:10.1038/srep19659

Yang, J. Y., Lee, S. J., Park, H. W., and Cha, Y. S. (2006). Effect of Genistein with Carnitine Administration on Lipid Parameters and Obesity in C57Bl/6J Mice Fed a High-Fat Diet. *J. Med. Food* 9, 459–467. doi:10.1089/jmf.2006.9.459

Zhang, W., Wang, X., Liu, Y., Tian, H., Flickinger, B., Empie, M. W., et al. (2008). Dietary Flaxseed Lignan Extract Lowers Plasma Cholesterol and Glucose Concentrations in Hypercholesterolaemic Subjects. *Br. J. Nutr.* 99 (6), 1301–1309. doi:10.1017/S0007114507871649

Zingg, J. M., Hasan, S. T., and Meydani, M. (2013). Molecular Mechanisms of Hypolipidemic Effects of Curcumin. *BioFactors* 39 (1), 101–121. doi:10.1002/biof.1072

Conflict of Interest: The authors declare that the research was conducted in the absence of any commercial or financial relationships that could be construed as a potential conflict of interest.

Publisher's Note: All claims expressed in this article are solely those of the authors and do not necessarily represent those of their affiliated organizations, or those of the publisher, the editors, and the reviewers. Any product that may be evaluated in this article, or claim that may be made by its manufacturer, is not guaranteed or endorsed by the publisher.

frontiers in Pharmacology

ORIGINAL RESEARCH
published: 07 February 2022
doi: 10.3389/fphar.2022.809482

Chemical Antioxidant Quality Markers of *Chrysanthemum morifolium* Using a Spectrum-Effect Approach

Yi-Fan Lu[1,2], *Ding-Xiang Li*[2], *Ran Zhang*[2], *Lin-Lin Zhao*[2], *Zhen Qiu*[2], *Yan Du*[2], *Shuai Ji*[2,3] *and Dao-Quan Tang*[2,3]*

[1]*The Second Clinical College, Xuzhou Medical University, Xuzhou, China,* [2]*Jiangsu Key Laboratory of New Drug Research and Clinical Pharmacy, Xuzhou Medical University, Xuzhou, China,* [3]*Department of Pharmaceutical Analysis, Xuzhou Medical University, Xuzhou, China*

Traditionally, the quality evaluation of *Chrysanthemum morifolium* (CM) cv. (Juhua) attributes its habitats and processing methods, however, this strategy of neglecting bioactive ingredients usually results in deviation of quality evaluation. This study aims to explore the quality marker (Q-marker) based on spectrum-effect relationship and quality control strategy of CMs. The chromatographic fingerprint of 30 flower head samples of CMs from five different habitats including Hang-baiju, Gongju, Huaiju, Taiju and Boju were constructed by high performance liquid chromatography and analyzed through chemometrics methods such as similarity analysis (SA), cluster analysis (CA) and principal component analysis (PCA). The common peaks were quantified by external standard method and relative correction factor method. The *in-vitro* radical scavenging capacity assays of DPPH·, ·OH and ABTS were carried out. The Q-marker was explored by the correlation analysis between the contents of common peaks and *in-vitro* radical scavenging capacity, and then used to evaluate the quality of 30 flower head samples of CMs. A total of eight common peaks were appointed in 30 flower head samples of CMs, and their similarities ranged from 0.640 to 0.956. CA results showed that 30 flower head samples of CMs could be divided into five categories with reference to the Euclidean distance of 5. PCA results showed that common peaks played a major role in differential contribution of CMs. The quantification of common peaks hinted that their contents possessed significant variation whether for different accessions or the same accessions of CMs. The correlation analysis showed that chlorogenic acid, 3,5-*O*-dicaffeoylquinic acid, unknown peak 1, 4,5-*O*-dicaffeoylquinic acid and kaempferol-3-*O*-rutinoside could be used as the Q-markers for the quality evaluation of 30 flower head samples of commercially available CMs. The analysis strategy that combines chromatographic fingerprint analysis, multiple ingredients quantification, *in-vitro* chemical anti-oxidant activity evaluation and spectrum-effect relationship analysis clarified the therapeutic material basis and discovered the Q-markers, which possibly offers a more comprehensive quality assessment of CMs.

Keywords: Q-marker, *Chrysanthemum* morifolium cv., chromatographic fingerprint, antioxidant activity, spectrum-effect relationship

OPEN ACCESS

Edited by:
Abdul Rohman,
Gadjah Mada University, Indonesia

Reviewed by:
Ahmad Arzani,
Isfahan University of Technology, Iran
Prasenjit Mitra,
Post Graduate Institute of Medical Education and Research (PGIMER), India

***Correspondence:**
Dao-Quan Tang
tangdq@xzhmu.edu.cn

Specialty section:
This article was submitted to Ethnopharmacology, a section of the journal Frontiers in Pharmacology

Received: *05 November 2021*
Accepted: *19 January 2022*
Published: *07 February 2022*

Citation:
Lu Y-F, Li D-X, Zhang R, Zhao L-L, Qiu Z, Du Y, Ji S and Tang D-Q (2022) Chemical Antioxidant Quality Markers of Chrysanthemum morifolium *Using a Spectrum-Effect Approach. Front. Pharmacol. 13:809482. doi: 10.3389/fphar.2022.809482*

INTRODUCTION

Chrysanthemum morifolium (CM) cv. (Juhua) is the dried flower head of *Chrysanthemum morifolium* (Ramat.) Hemsl., and has the effects of dispersing wind and clearing heat, calming the liver and clearing the eyes, and clearing heat and detoxifying the body (Tu et al., 2021; Yang et al., 2019). The *Compendium of Materia Medica* records that CM can benefit the five veins, regulate the extremities, and cure the head wind heat tonic. Modern pharmacological researches also show that CM possesses heat dissipation, detoxification, brightening eyes, lowering blood pressure and other effects (Hodaei et al., 2021a). The main active ingredients of CM include flavonoids (luteolin), phenolic acids (chlorogenic acid), and polysaccharides (Hodaei et al., 2018; Tian et al., 2020), and *Chrysanthemum* extracts containing different components have the ability to improve myocardial nutrition, remove reactive oxygen radicals, strengthen vascular resistance, and lower blood lipids (Zhang et al., 2019). For instance, phenolic acids extract has antibacterial, antiviral, anti-infective, and anti-inflammatory effects (Hodaei et al., 2021b; Youssef et al., 2020; Cho et al., 2021), while polysaccharides extract has anti-tumor and immunity enhancing effects (Jing et al., 2016). Among these effects, antioxidant capacity is the most important pharmacological efficacy of CM and the basis for the treatment of different diseases (Bai et al., 2018; Liu et al., 2018; Lin et al., 2010). The pharmaceutical value and safety of CM have enabled it to be broadly applied as a homogeneous medicinal herb for medical and edible purposes.

There are about 18 species of CMs in China, including 11 medicinal species, mainly cultivated in Zhejiang, Anhui, Henan and other provinces. Currently, about nine species of CMs are used in the market, such as Boju, Chuju, Gongju, Huaiju, Hangju, Taiju, Qiju, Jiju, and Chuanju, and five of them including Boju, Huaiju, Gongju, Hangju, and Chuju are recorded in the *Chinese Pharmacopoeia* (Ch.P.), according to their origins and processing methods. Moreover, there are a variety of wild CMs used in the clinical and food fields. The diversity of species, habitat, cultivation pattern and processing method results in the quality variation of CMs, effective quality control has thus become an important guarantee for the application of CMs in the medical and food fields (Song et al., 2018).

At present, the quality control strategies of CM mainly include multi-ingredients quantification, chromatographic fingerprint and/or their combination. For example, quantification of chlorogenic acid (ChA), luteolin-7-O-glucoside (L-7G), and 3,5-*O*-dicaffeoylquinic acid (3,5-DCQA) and chromatographic fingerprint analysis were respectively used to control the quality of CMs by Ch.P. or other scholars (He et al., 2021; Dai and Sun, 2021). These strategies have provided an assurance for the quality of CMs to a certain extent. Recently, the concept of quality marker (Q-marker) has provided a new idea for the quality control of traditional Chinese medicine (TCM) (Tian et al., 2019), which is based on the perspective of biological activity, and through a variety of ways to find the chemical components that can reflect biological effect of TCM (Chen et al., 2021). Among them, the strategy to explore Q-marker from the perspective of the correlation between the chromatographic spectrums and biological effect (spectrum-effect) has been widely used in the study of various TCMs (Chen L. et al., 2020; Li et al., 2020; Jiang et al., 2021). A predictive analysis on the Q-marker of CMs was conducted by the review of its chemical composition and pharmacological effects (Zhou et al., 2019), however, the study to explore the Q-marker for the quality control of CM from the aspect of spectrum-effect relation has not been published to now.

Antioxidant activity of CMs is the important basis for its edible and medicinal application. Hence, based on chemical antioxidant activity, this study aimed to explore the Q-marker of CMs from the aspect of spectrum-effect relation. Chromatographic fingerprint analysis of 30 flower head samples of five accessions of CMs was firstly performed by high performance liquid chromatography (HPLC) to find common peaks, and chemometric analysis such as similarity analysis (SA), cluster analysis (CA), and principal component analysis (PCA) were used to evaluate the difference of 30 flower head samples of CMs. Common peaks were quantified by external standard method and relative correction factor method. Meanwhile, the chemical antioxidant activities of 30 batches of CMs were evaluated by *in-vitro* free radical scavenging activity such as DPPH, OH and ABTS. The correlation analysis between the common peak and the chemical antioxidant activity was further performed to explore the Q-marker of CM, and the Q-marker was then validated by evaluating the quality of commercially available CMs.

MATERIALS AND METHODS

Materials and Reagents

Methanol and formic acid of chromatographic grade were purchased from Beijing Mreda technology Co., Ltd. (Beijing, China). The reference standards including L-7G, 3,5-DCQA, 4,5-*O*-dicaffeoylquinic acid (4,5-DCQA), apigenin-7-*O*-glucuronide (A-7G), and kaempferol-3-*O*-rutinoside (K-3R) were purchased from Sichuan Weikeqi Biological Technology Co., Ltd. (Chengdu, China), while ChA was purchased from Chengdu Purechem-standard Biological Technology Co., Ltd. (Chengdu, China). Their purities were all not less than 98%. Potassium persulfate, salicylic acid, 1,1-Diphenyl-2-picrylhydrazyl (DPPH), and 2,2′-biazo-bis-3-ethylbenzothiazoline-6-sulfonic acid (ABTS) of analytical grade were purchased from Shanghai Maclean Biochemical Technology Co., Ltd. (Shanghai, China), while ferrous sulfate heptahydrate was purchased from Shanghai Aladdin Biochemical Technology Co., Ltd. (Shanghai, China). Other reagents were of analytical grade and water was purified using a Milli-Q system (Millipore, Bedford, MA, United States).

A total of 30 flower head samples of CMs were collected and identified by Associate Professor Shuai Ji of our laboratory as the dried flower heads of *Chrysanthemum morifolium* (Ramat.) Hemsl. The information of the samples was shown in **Table 1**.

Preparation of Mixed Standard and Sample Solution

The standard substances of ChA, 3,5-DCQA, L-7G, 4,5-DCQA, A-7G and K-3R were weighed accurately and dissolved in

TABLE 1 | Information of 30 batches of CM samples.

No.	Accessions	Lot No.	Manufacturer	Place of production
JH-01	Gongju	191208	Bulk packaging in Xuzhou Deren Clinic	Huangshan, Anhui
JH-02	Gongju	20200621	Purchased online	Huangshan, Anhui
JH-03	Gongju	20200608	Purchased online	Huangshan, Anhui
JH-04	Gongju	20200825	Purchased online	Huangshan, Anhui
JH-05	Gongju	20200908	Purchased online	Huangshan, Anhui
JH-06	Gongju	20200404	Purchased online	Huangshan, Anhui
JH-07	Hang-baiju	200407	Suzhou Tianling Traditional Chinese Medicine Tablet Co., Ltd.	Zhejiang
JH-08	Hang-baiju	191219	Suzhou Tianling Traditional Chinese Medicine Tablet Co., Ltd.	Zhejiang
JH-09	Hang-baiju	191209	Suzhou Li-liangji Traditional Chinese Medicine Co., Ltd.	Zhejiang
JH-10	Hang-baiju	200815	Bulk packaging in Xuzhou Deren Clinic	Zhejiang
JH-11	Hang-baiju	200404	Suzhou Lei-yunshang Traditional Chinese Medicine Co., Ltd.	Zhejiang
JH-12	Hang-baiju	191102	Suzhou Lei-yunshang Traditional Chinese Medicine Co., Ltd.	Zhejiang
JH-13	Taiju	200107	Purchased online	Zhejiang
JH-14	Taiju	191201	Purchased online	Zhejiang
JH-15	Taiju	200816	Suzhou Tianling Traditional Chinese Medicine Tablet Co., Ltd.	Zhejiang
JH-16	Taiju	20200830	Bulk packaging in Xuzhou Deren Clinic	Zhejiang
JH-17	Taiju	200506	Suzhou Tianling Traditional Chinese Medicine Tablet Co., Ltd.	Zhejiang
JH-18	Taiju	20200401	Bulk packaging in Xuzhou Deren Clinic	Zhejiang
JH-19	Boju	20200809	Purchased online	Bozhou, Anhui
JH-20	Boju	20200901	Purchased online	Bozhou, Anhui
JH-21	Boju	20200701	Purchased online	Bozhou, Anhui
JH-22	Boju	20200716	Purchased online	Bozhou, Anhui
JH-23	Boju	20200911	Bozhou Fumei Biotech Co., Ltd.	Bozhou, Anhui
JH-24	Boju	20200908	Purchased online	Bozhou, Anhui
JH-25	Huaiju	20200905	Bulk packaging in Cai-zhizhai Chinese medicine store	Jiaozuo, Henan
JH-26	Huaiju	20191220	Xinyuan Huaiyao Medicine Co., Ltd.	Jiaozuo, Henan
JH-27	Huaiju	20200908	Purchased online	Jiaozuo, Henan
JH-28	Huaiju	20200901	Purchased online	Jiaozuo, Henan
JH-29	Huaiju	20200909	Purchased online	Wenxian, Henan
JH-30	Huaiju	20200919	Purchased online	Jiaozuo, Henan

methanol to obtain the mixed standards solution containing the standards at the concentrations of 0.212, 0.248, 0.628, 0.420, 0.217, 0.742 mg ml^{-1}, respectively. These standards solutions were sealed away from light and stored in −20°C refrigerator before use.

CM sample was crushed into powder. A total of 50 mg precisely-weighed powder was put into a 1.5 ml centrifuge tube, added 1 ml of 50% ethanol, and then sealed for extraction with ultrasonic treatment (500 W, 28 kHZ) for 30 min. After cooling, the solution was centrifuged at 12,000 rpm for 5 min at 4°C. A total of 0.5 ml supernatant was employed, diluted with 0.5 ml of methanol, and then filtered through 0.22 μm microporous membrane for use.

Chromatographic Conditions

Chromatographic analysis was performed on an Agilent 1260 Infinity HPLC system consisted of G4212B 1260 DAD, G1322A 1260 Degasser, G1312B 1260 Bin Pump, G4226A 1290 Sampler, and G1316C 1290 TCC column temperature chamber. Samples were separated on an Agilent ZORBAX SB-C18 (4.6 × 250 mm, 5 μm) column with methanol (A) and 0.1% formic acid water solution (B) as the mobile phase, and the gradient elution was performed as follows：85%–65%B, 5 min; 65%–55%B, 10 min; 55%–45%B, 20 min; 45%–35%B, 5 min; 35%–15%B, 5 min; and then 15%–85%B for 10 min to clean up the residues on the column. The flow rate was kept at 0.8 ml min^{-1} with detection wavelength of 348 nm, column temperature of 35°C, and injection volume of 15 μL.

Antioxidant Activity Assay

DPPH clearance capacity was determined referring to the previous method with a slight modification (Zhang X. et al., 2021). Briefly, appropriate concentration of sample was mixed with 1 ml of 0.2 mM DPPH solution. After the reaction was carried for 30 min, the absorbance of the solution was determined at the wavelength of 517 nm. OH clearance capacity was determined as the published method with a minor modification (Jia et al., 2020). In brief, proper concentration of sample solution was added 1 ml of 6 mM $FeSO_4$ and 1 ml of 8.8 mM H_2O_2. After being mixed and left for 10 min, 1 ml of 6 mM salicylic acid solution (dissolved in anhydrous ethanol) was added into it and mixed well, and then left it for another 30 min. After centrifuging at 12,000 rpm for 5 min, the absorbance of supernatant was measured at 510 nm. ABTS clearance capacity was measured according to the previous method with a slight modification (Gong et al., 2019). Briefly, suitable concentration of sample solution was added in 3.9 ml of ABTS working solution (1.76 ml of 140 mM potassium persulfate solution and 100 ml of 7 mM ABTS solution). After vortexing evenly and leaving at room temperature for 6 min, the absorbance of solution was recorded at 734 nm.

The blank control solution without free radical working solution and the negative control solution without antioxidants were prepared and determined as the same manner. The free radical scavenging capacity was calculated by **Eq. 1**.

$$\text{Free radical scavenging capacity } (\%) = \left(1 - \frac{A_a - A_b}{A_0}\right) \times 100\% \quad (1)$$

Where A_a is the absorbance of sample solution which is a mixture of free radical working solution and sample solutions; A_b is the absorbance of blank control solution without free radical work solution; A_0 is the absorbance of negative control solution without antioxidants.

Statistical Analysis

SA was performed by the professional software "Similarity Evaluation System for Chromatographic Fingerprint of Traditional Chinese Medicine (Version 2012)," which was recommended by National Medical Products Administration of China. Statistical analysis was carried out with SPSS 23.0 (IBM, Armonk, NY, United States) and data were expressed as means ± standard deviation of at least three independent experimental results. Comparison among multiple groups was performed by one-way ANOVA, while differences between two groups were analyzed by using two-tailed Student's *t*-test. The results with *p*-values of less than 0.05 were believed to be statistically significant.

RESULTS

Chromatographic Fingerprint Analysis

Sample (JH-07) was selected to validate the methodology of chromatographic fingerprint analysis. The precision was evaluated by the relative standard deviation (RSD) of relative retention time (RRT) and relative peak area (RPA) of characteristic peaks from six consecutive times analysis of sample. The values of RRT and RPA of characteristic peaks were calculated with 3,5-DCQA (peak 2) as the reference peak, and the results showed that the RSD values of RRT and RPA of characteristic peaks were all less than 0.05% or 0.1%, respectively, which indicated that this analytical method possessed a good precision. The stability of sample solution at room temperature was investigated by measuring the variation of RRT and RPA of characteristic peaks at 0, 2, 6, 12, 24, and 48 h. The results showed that the RSD values of RRT and RPA were all less than 0.2% or 2.9%, respectively, which indicated that the sample solution was stable within 48 h. Six sample solutions were prepared in parallel and used to evaluate the reproducibility. The results showed that the RSD values of RRT and RPA of characteristic peaks were not more than 0.5% or 3.7%, respectively, which indicated that the method was reproducible.

Thirty flower head samples of CMs were analyzed and their fingerprints were generated by using the average method with a time width of 0.1 (**Figure 1**). A total of eight peaks were identified as common peaks, and six characteristic peaks were identified as ChA, 3,5-DCQA, L-7G, 4,5-DCQA, A-7G and K-3R by comparing with the reference standards, respectively. By automatically matching the chromatographic peaks of 30 flower head samples of CMs to generate the average fingerprint, the similarities of different CMs were calculated by comparing them with the average fingerprint. The RPAs of eight common peaks of 30 flower head samples of CMs were calculated by the ratio of their peak areas with respect to the reference peak area (peak 2, 3,5-DCQA). From the **Table 2** and **Supplementary Table S1**, we could find that the similarities of most CMs were more than 0.8 except JH-21 and JH-22 with a similarity value of 0.64 or 0.665, but the variation (RSD% value) of RPA of common peaks ranged from 27.2% to 86.3%.

CA is a multivariate statistical technique for classifying sample or index components and is one of the most widely used multivariate statistical methods (Zhang Y. et al., 2021). The interval of intergroup connection and square Euclidean distance as the metric was used to establish a dendrogram of CA of 30 flower head samples of CMs, which is shown in **Figure 2**. The CA results of common peaks can basically classify different accessions of CMs into five classes at Euclidean distance of five and three classes at Euclidean distance of 10, and JH-01 was obviously far away from the others.

PCA is a multivariate statistical method widely used in multiple disciplines, which can be used to simplify data and quickly achieve visual identification of data (Cao et al., 2018). Factor analysis was performed on the eight common peaks of 30 flower head samples of CMs, and the component with an eigenvalue of more than 1 was taken as the extracted principal component (PC) according to the principle of principal component extraction (Liu et al., 2017). As shown in **Table 3**, the cumulative contribution of the first three PCs could reach 85.47%, indicating that the extracted three PCs could basically respond to the main information of the samples. The eigenvalue in PC1 reached 3.04 with the variance contribution rate of 38.04%, and the peaks with higher loadings were mainly ChA, L-7G, 4,5-DCQA, A-7G, and K-3R, indicating that these five peaks mainly reflected the information of PC1. The eigenvalue of PC2 was 2.284 with the variance contribution rate of 28.55%, and the peaks with higher loadings were ChA, 3,5-DCQA, and Peak 3 (unknown peak 1), indicating that these three peaks mainly reflected the information of PC2. The eigenvalue of PC3 was 1.511 with the variance contribution rate of 18.88%, and the peaks with higher loadings were A-7G and Peak 8 (unknown peak 2), indicating that the two peaks mainly reflected the information of PC3.

To further distinguish the effects of PCs, the data were imported into MetaboAnalyst 4.0 (http://www.metaboanalyst.ca) to obtain two-dimensional analysis plot and loadings plot using eight common peaks as variables and original grouping as a reference. According to the results of CA, some samples with excessive deviations were removed. The results in **Figure 3A** showed that the contribution values of PC1 and PC2 reached 67.4% and 22.8%, respectively, and the various accessions of CMs were well separated. As shown in **Figure 3B**, L-7G, K-3R, 4,5-DCQA, unknown peak 1, and 3,5-DCQA were the main components to distinguish the difference between Taiju,

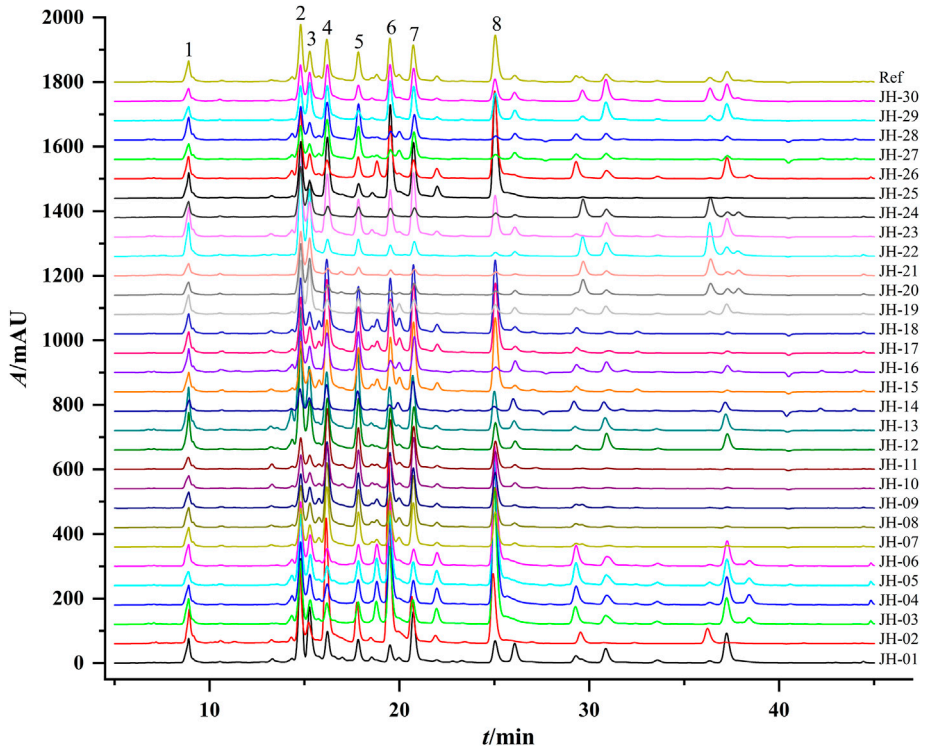

FIGURE 1 | Representative HPLC chromatograms of 30 flower head samples of CMs. CM represents *Chrysanthemum morifolium;* R means the reference average fingerprint; JH-01~JH30 mean 30 flower head samples of different accessions of CMs and their detailed information were listed in **Table 1**.

TABLE 2 | Similarity evaluation of different flower head samples of chrysanthemum samples.

No.	Accessions	Similarity	No.	Accessions	Similarity	No.	Accessions	Similarity
JH-01	Gongju	0.835	JH-11	Hang-baiju	0.903	JH-21	Boju	0.640
JH-02	Gongju	0.840	JH-12	Hang-baiju	0.917	JH-22	Boju	0.665
JH-03	Gongju	0.808	JH-13	Taiju	0.921	JH-23	Boju	0.956
JH-04	Gongju	0.827	JH-14	Taiju	0.807	JH-24	Boju	0.679
JH-05	Gongju	0.848	JH-15	Taiju	0.941	JH-25	Huaiju	0.909
JH-06	Gongju	0.831	JH-16	Taiju	0.845	JH-26	Huaiju	0.897
JH-07	Hang-baiju	0.931	JH-17	Taiju	0.952	JH-27	Huaiju	0.839
JH-08	Hang-baiju	0.932	JH-18	Taiju	0.946	JH-28	Huaiju	0.823
JH-09	Hang-baiju	0.923	JH-19	Boju	0.811	JH-29	Huaiju	0.923
JH-10	Hang-baiju	0.931	JH-20	Boju	0.681	JH-30	Huaiju	0.911

Huaiju, Hang-baiju, and Boju, while unknown peak 2 and A-7G were the main components to distinguish the difference between other kinds of CMs and Gongju.

Quantification of the Eight Common Peak Components in CMs

To accurately find the difference among 30 flower head samples of CMs, the common peaks were further quantified. Chromatographic separation of 30 flower head samples of CMs was performed under the set condition of this study, and the representative chromatograms of the reference standards and sample were shown in **Figure 4**. The resolutions of the eight common peaks were all more than 1.5, and their theoretical numbers of plate were all better than 8,000.

Determination of Relative Correction Factors

As two unknown common peaks (Peak 3 and Peak 8) could not be identified by comparing with chemical data and the reference standards of CM, thus, their quantifications were performed by the relative correction factor method referring to the previous studies (Hou et al., 2011; Zhao et al., 2021). This method assumed that if the structure of an unknown peak (without standard) was similar with a known peak (with the standard), the quantification of the unknown peak could be

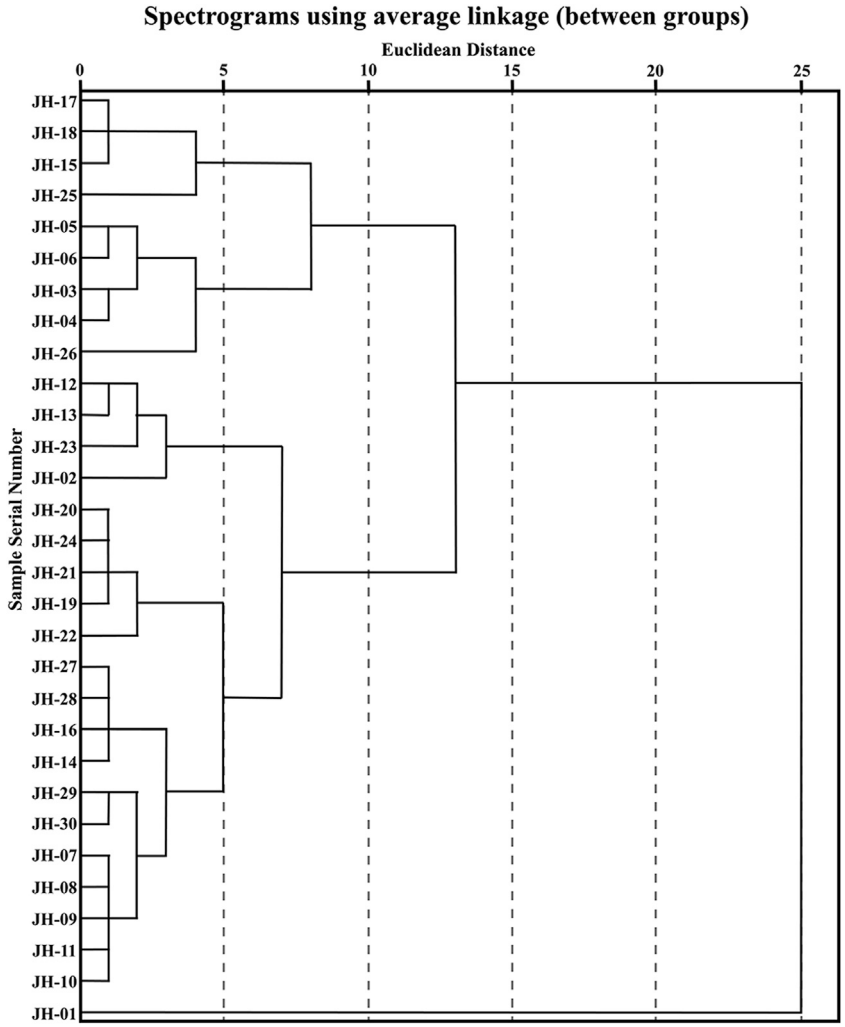

FIGURE 2 | Phylogenetic cluster analysis of 30 flower head samples of CMs.

TABLE 3 | Principal component analysis and factor loading matrix of 30 flower head samples of CMs.

	Principal components							
	1	**2**	**3**	**4**	**5**	**6**	**7**	**8**
Initial eigenvalue	3.04	2.28	1.51	0.56	0.40	0.12	0.06	0.03
Variance contribution rate (%)	38.04	28.55	18.88	6.99	4.96	1.52	0.70	0.35
Cumulative contribution rate (%)	38.04	66.60	85.47	92.47	97.43	98.95	99.65	100
Characteristic peak	**Principal component factor loading matrix**							
Peak 1 (ChA)	0.63	0.66	0.14	—	—	—	—	—
Peak 2 (3,5-DCQA)	0.45	0.85	0.11	—	—	—	—	—
Peak 3 (Unknown 1)	–0.14	0.93	–0.11	—	—	—	—	—
Peak 4 (L-7G)	0.82	–0.35	–0.30	—	—	—	—	—
Peak 5 (4,5-DCQA)	0.76	0.02	–0.41	—	—	—	—	—
Peak 6 (A-7G)	0.68	–0.22	0.61	—	—	—	—	—
Peak 7 (K-3R)	0.76	–0.24	–0.43	—	—	—	—	—
Peak 8 (Unknown 2)	0.38	–0.18	0.81	—	—	—	—	—

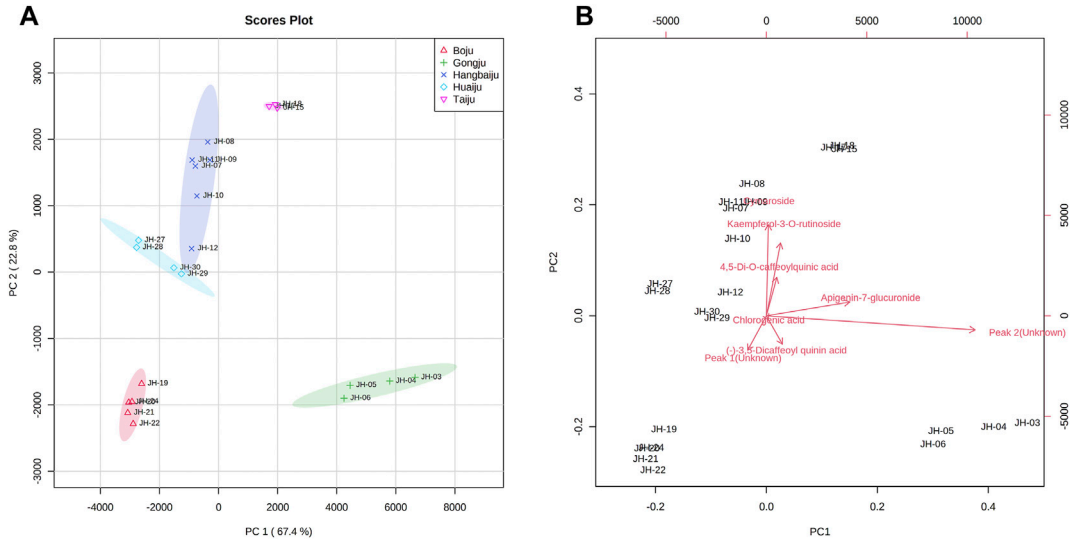

FIGURE 3 | Two-dimensional score plots **(A)** and loading plots **(B)** of PCA of different accessions of CMs.

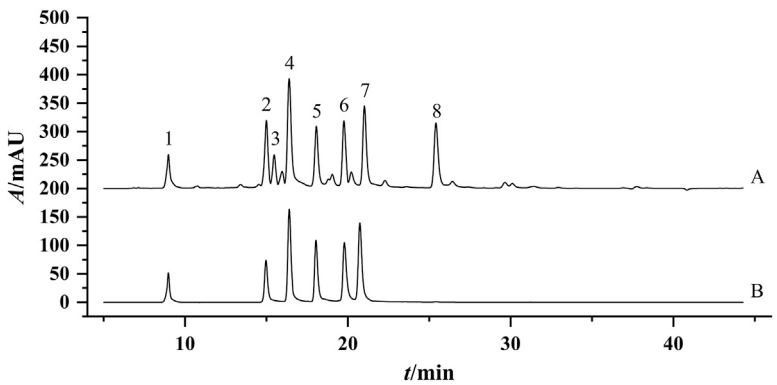

FIGURE 4 | Representative chromatogram of the Sample JH-07 **(A)** and mixed standard solution **(B)**. 1: ChA; Peak 2, 3,5-DCQA; Peak 3, Unknown peak 1; Peak 4, L-7G; Peak 5, 4.5-DCQA; Peak 6, A-7G; Peak 7, K-3R; Peak 8, Unknown peak 2.

performed by the content of the known peak multiplying by the relative correction factor.

In this study, to find the relative correction factors of two unknown peaks, different concentrations of the same sample solution were determined, and the relative correction factor (f_s) was determined by calculating **Eq. 2**, and the f_s with a constant value and lower variation (RSD%) was selected to quantify the unknown peak.

$$\text{Relative correction factor } f_s = \frac{A_s}{A_i} = \frac{C_s}{C_i} \quad (2)$$

where A_s and C_s represent the peak area and concentration of known compound including ChA, 3,5-DCQA, L-7G, 4,5-DCQA, A-7G, or K-3R, respectively. A_i and C_i mean the peak area and concentration of unknown compound (Peak 3 and Peak 8), respectively.

As shown in **Supplementary Tables S2, S3**, the RSD value of f_s of unknown peak 1 to L-7G was 1.95%, while the RSD value of f_s of unknown peak 2 to K-3R was 3.32%, which were much lower than that of other known compounds. Thus, the linear equation of L-7G and K-3R were used to calculate the concentration of unknown peak 1 or unknown peak 2 with a f_s value of 0.93 or 1.37, respectively.

Quantitative Method Validation

A total of five series of standard solutions of six compounds including ChA, 3,5-DCQA, L-7G, 4,5-DCQA, A-7G, and K-3R were used to determine the linear range by an external standard method. Calibration curves were generated by plotting the peak areas (y) versus the corresponding concentrations (x, μg mL^{-1}). A series of diluted solutions of six reference standards were used to determine limit of detection (LOD) and limit of quantification (LOQ), which were defined as the signal-to-noise (S/N) ratios of 3 and 10, respectively. As shown in **Table 4**, the correlation coefficients were all better than 0.9951 for all analytes and the

TABLE 4 | Linear relationship of standard substances from components of CMs.

Components	Regression equation[a]	R^2	Linear range (μg ml^{-1})	LOD[b] (μg ml^{-1})	LOQ[c] (μg ml^{-1})
ChA	$y = 8.6378x–20.26$	0.9989	16.4–81.8	0.05	0.16
3,5-DCQA	$y = 12.211x–111.77$	0.9984	19.1–95.7	0.06	0.19
L-7G	$y = 10.674x–0.386$	0.9985	48.5–242.4	0.14	0.49
4,5-DCQA	$y = 11.367x–293.87$	0.9895	32.4–162.1	0.09	0.32
A-7G	$y = 22.281x–297.62$	0.9951	16.8–83.8	0.05	0.17
K-3R	$y = 7.0582x–19.461$	0.9991	27.3–286.4	0.08	0.27

[a]*y and x are the peak areas and concentrations (μg·mL^{-1}) of the analytes, respectively.*
[b]*The limit of detection (LOD) was defined as the concentration for which the signal-to-noise ratio was 3.*
[c]*the limit of quantification (LOQ) was defined as the concentration for which the signal-to-noise ratio was 10.*

range of LODs and LOQs for all compounds were in the ranges of 0.05–0.14 μg ml^{-1}, and 0.12–0.51 μg ml^{-1}, respectively, which indicated that this method possessed a good linearity and sensitivity.

The precision of the proposed method was determined by injecting mixed standard solution for six consecutive times, and the RSD values of the peak areas of ChA, 3,5-DCQA, L-7G, 4,5-DCQA, A-7G, and K-3R were used to evaluate the precision. The results showed that the RSD values of six reference standards were 0.26%, 0.38%, 0.30%, 0.34%, 0.26%, and 0.27%, respectively. The repeatability was investigated with six independently prepared sample solutions of JH-07, one of which was injected into the apparatus at 0, 2, 4, 8, 12, and 24 h, separately, to determine the stability of the solution. The results showed that the RSD values of six analytes in the six independently prepared sample solutions were 1.84%, 0.64%, 0.97%, 1.48%, 1.06%, and 1.80%, respectively, and the RSD values of six analytes in one sample solution within 24 h were 0.65%, 0.73%, 1.81%, 0.88%, 1.82%, and 1.20%, respectively. These results hinted that this method possessed a good precision, repeatability, and stability.

The accuracy was confirmed by the recovery measured by standard addition method. Six different amounts of the reference standards were added to a real sample for which the concentrations of the compounds of interest were known. The mixtures were treated and analyzed using the method in this study. The accuracy was expressed as the percentage of the analytes recovered by the assay. As shown in **Supplementary Table S4**, the recoveries of the components ranged from 91.6% to 110.2% with the RSD values of 2.4%–6.2%, which indicated that the method enabled highly accurate simultaneous analysis of the six analytes.

Samples Determination

The validated method was used to determine the contents of eight common peaks in 30 flower head samples of CMs, among which 2 unknown peaks were quantified using the relative correction factor method, while six known peaks were assayed by the external standard method. As shown in **Table 5**, the variation (RSD) of the contents of eight common peaks of 30 flower head samples of different accessions of CMs ranged from 38.7% to 77.3%. Even for the same accessions of CM, the variation (RSD) of the contents of eight common peaks were still enormous, such as Gongju, Hang-baiju, Taiju, Boju, and Huaiju with the RSD value ranges of 21.4%–123.0%, 11.7%–64.7%, 31.3%–60.9%, 32.7%–119.8%, and 38.7%–77.3%, respectively. From the **Figure 5**, we could vividly observe the scattered distribution of the contents of eight common peaks in 30 flower head samples of CMs.

Prediction of Q-Marker of CMs Based on Antioxidant Activity

To find the Q-marker, the *in-vitro* chemical antioxidant activity of CMs was first determined, and then the correlation analysis between the chemical antioxidant activity and the contents of eight common peaks was performed. To minimize the deviation of Q-marker as much as possible, some CMs samples that were excessively deviated from most samples according to the results of chemometrics were removed. Finally, three samples of each accession of CMs and a total of 15 CMs were selected to be evaluated the chemical antioxidant activities. As shown in **Table 6**, the DPPH, OH, and ABTS clearance rate of different CMs ranged from 28.34% to 85.35%, 55.72% to 81.18%, and 49.65%–93.75%, respectively.

Pearson correlation analysis between the chemical antioxidant activities and the contents of eight common peaks was then further performed, and the results (**Table 7**) showed the contents of ChA, 3,5-DCQA, and unknown peak 1 were significantly correlated with ABTS·, DPPH·, and OH clearance capacities, while the contents of 4,5-DCQA and K-3R were significantly correlated with ABTS and DPPH clearance capacities. The correlation coefficients of the above five compounds with the antioxidant activity ranked as follows: 3,5-DCQA ˃ ChA ˃ unknown peak 1 ˃ 4,5-DCQA ˃ K-3R. Thus, the above five compounds were selected as the Q-markers of chemical antioxidant activity of CMs.

Quality Evaluation of Commercially Available CMs Using the Q-Marker of Antioxidant Activity

The contents of ChA, 3,5-DCQA, unknown peak 1, 4,5-DCQA, and K-3R in 30 flower head samples of different accessions of commercially available CMs were further determined, and the results were shown in **Table 8**. To evaluate the quality of CMs in a relatively objective way, this study set up four grades of excellent,

TABLE 5 | Contents of eight common peaks in 30 batches of CMs (%, g/g).

No.	Accessions	ChA	3,5-DCQA	Unknown peak 1	L-7G	4,5-DCQA	A-7G	K-3R	Unknown peak 2
JH-01	Gongju	0.65	1.00	1.38	2.36	0.72	1.64	1.28	0.94
JH-02		0.43	1.58	0.35	0.61	0.44	0.19	1.57	1.14
JH-03		0.44	0.93	0.16	0.27	0.46	0.80	0.68	0.50
JH-04		0.34	0.97	0.19	0.33	0.48	0.72	0.60	0.44
JH-05		0.24	1.06	0.16	0.27	0.48	0.63	0.59	0.43
JH-06		0.38	0.94	0.14	0.25	0.44	0.59	0.42	0.31
RSD[a]		33.1	23.1	123.0	122.2	21.4	62.9	53.4	53.0
JH-07	Hangbaiju	0.30	0.57	0.71	1.22	0.62	0.34	1.29	0.94
JH-08		0.31	0.62	0.78	1.34	0.67	0.33	1.52	1.11
JH-09		0.25	0.48	0.73	1.25	0.63	0.49	1.12	0.82
JH-10		0.21	0.51	0.44	0.76	0.70	0.31	1.53	1.12
JH-11		0.19	0.47	0.62	1.06	0.74	0.45	1.28	0.94
JH-12		0.69	1.66	0.54	0.93	0.95	0.39	1.31	0.96
RSD[a]		56.9	64.7	20.2	20.1	17.0	18.7	11.7	11.7
JH-13	Taiju	0.64	1.87	0.61	1.04	1.34	0.40	1.61	1.18
JH-14		0.22	0.33	0.27	0.46	0.42	0.11	0.91	0.66
JH-15		0.30	0.72	0.79	1.35	0.80	0.48	2.04	1.49
JH-16		0.36	0.65	0.42	0.72	0.76	0.15	1.09	0.79
JH-17		0.33	0.80	0.81	1.38	0.84	0.48	2.04	1.49
JH-18		0.31	0.79	0.82	1.40	0.85	0.48	1.99	1.45
RSD[a]		40.3	60.9	37.3	37.3	35.3	49.6	31.3	31.5
JH-19	Boju	0.34	0.76	0.13	0.21	0.33	0.15	0.45	0.33
JH-20		0.23	0.82	0.12	0.20	0.19	0.09	0.35	0.26
JH-21		0.23	0.71	0.09	0.15	0.23	0.09	0.17	0.12
JH-22		0.59	1.33	0.14	0.25	0.37	0.13	0.39	0.29
JH-23		0.45	1.45	0.80	1.37	0.71	0.43	1.97	1.44
JH-24		0.29	0.82	0.12	0.21	0.27	0.13	0.26	0.19
RSD[a]		39.8	32.7	119.2	119.8	53.7	76.2	113.5	113.2
JH-25	Huaiju	0.47	0.87	0.64	1.09	0.32	0.91	1.66	1.21
JH-26		0.38	1.05	0.17	0.30	0.43	0.48	0.48	0.35
JH-27		0.24	0.53	0.44	0.76	0.63	0.13	0.82	0.60
JH-28		0.35	0.51	0.42	0.71	0.71	0.12	0.75	0.54
JH-29		0.25	0.52	0.42	0.71	0.25	0.38	1.03	0.75
JH-30		0.24	0.56	0.42	0.72	0.33	0.35	0.95	0.70
RSD[a]		29.4	34.1	35.7	35.1	41.6	73.4	41.9	41.9
RSD[b]		38.7	44.4	66.5	66.3	44.6	77.3	53.3	53.2

RSD[a], represents the variation of the contents of eight common peaks from the same accessions of CM; RSD[b], represents the variation of the contents of eight common peaks from 30 flower head samples of different accessions of CM.

good, medium, and poor according to the contents of five compounds. As the content changes of five compounds were inconsistent among different accessions of CMs, we further set up five different sub-grades according to the contents of five different compounds. The top 10%, ranking of 11%–30%, 31%–90%, and 91%–100% of the contents of ChA, 3,5-DCQA, unknown peak 1, 4,5-DCQA, or K-3R were respectively set as the excellent, good, medium, and poor, and assigned the value of "1"; "2," "3," and "4," respectively. As the contribution degree of five compounds to the chemical antioxidant activity of CMs were different, the proportions of 3,5-DCQA, ChA, unknown peak 1, 4,5-DCQA, and K-3R in the calculation of final grade were set as 30%, 25%, 20%, 15%, and 10% referring to their corresponding rank, respectively. Thus, the final grades of different accessions of CMs were calculated by the following Equation: Grade = Sub-grade (3,5-DCQA) × 0.3 + Sub-grade (ChA) × 0.25 + Sub-grade (unknown peak 1) × 0.2 + Sub-grade (4,5-DCQA) × 0.15 + Sub-grade (K-3R) × 0.1, and shown in **Table 8**. From **Table 8**, we could find that 30 flower head samples of different accessions of CMs were sorted as different grades. Two of them (JH-12 and JH-13), respectively from Hang-baiju and Taiju, were assigned as the excellent; 11 of them were evaluated as the good; and two of them (JH-14 and JH-21), respectively from Taiju and Boju, were sorted as the poor. These results further hinted that there existed wide quality variation between different accessions of CMs, and even for the same accession of CMs.

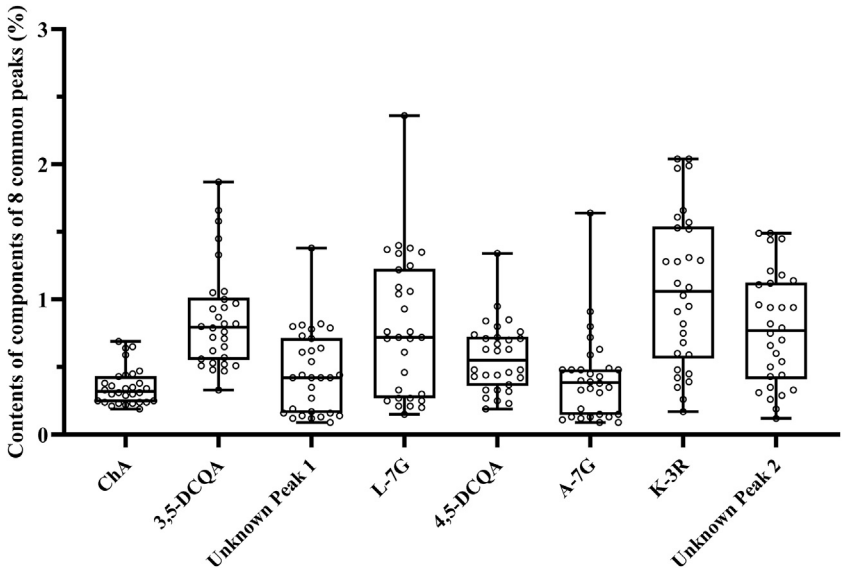

FIGURE 5 | The box diagram of the contents of eight common peaks in 30 flower head samples of CMs.

TABLE 6 | Free radical scavenging rate of different species of CMs (n = 3).

No.	Accessions	Free radical clearance rate (%)			No.	Accessions	Free radical clearance rate (%)		
		DPPH·	OH·	ABTS·			DPPH·	OH·	ABTS·
JH-02	Gongju	73.41 ± 0.40	79.25 ± 0.14	90.22 ± 0.48	JH-17	Taiju	50.37 ± 0.20	71.50 ± 0.07	79.20 ± 0.90
JH-04	Gongju	43.33 ± 0.23	71.14 ± 0.19	70.20 ± 0.90	JH-19	Boju	33.29 ± 0.38	72.37 ± 0.19	64.97 ± 0.74
JH-06	Gongju	37.92 ± 0.14	71.26 ± 0.14	69.21 ± 0.96	JH-23	Boju	58.88 ± 0.49	72.53 ± 0.07	90.01 ± 0.48
JH-09	Hang-baiju	42.93 ± 0.10	67.61 ± 0.26	70.52 ± 0.90	JH-24	Boju	28.51 ± 0.06	75.11 ± 0.07	67.13 ± 0.69
JH-10	Hang-baiju	43.44 ± 0.10	55.72 ± 0.25	72.53 ± 1.01	JH-28	Huaiju	38.59 ± 0.26	71.63 ± 0.07	66.42 ± 0.95
JH-12	Hang-baiju	70.77 ± 0.45	77.86 ± 0.12	88.21 ± 0.58	JH-29	Huaiju	32.51 ± 0.17	56.01 ± 0.07	59.92 ± 0.80
JH-13	Taiju	85.35 ± 0.16	81.18 ± 0.25	93.75 ± 0.11	JH-30	Huaiju	35.28 ± 0.79	72.28 ± 0.07	61.37 ± 0.85
JH-14	Taiju	28.34 ± 0.06	63.76 ± 0.38	49.65 ± 0.80					

The concentrations of sample solutions for the determination of DPPH, OH, or ABTS· clearance rate were 1.0, 10.0 or 5.0 mg/ml, respectively.

DISCUSSION

To obtain a chromatographic separation of CM, chromatographic conditions were first optimized. As CM is rich in flavonoids and phenolic acids, referring to our group's previous experience and study (Tang et al., 2010), Agilent ZORBAX SB-C18 column was thus selected as the stationary phase, and four mobile phase systems including methanol-water, methanol-0.1% formic acid water solution, methanol-0.2% formic acid water solution, and 0.1% formic acid methanol solution-0.1% formic acid water solution were investigated, respectively. The results showed that lower resolution and fewer chromatographic peaks could be obtained when using methanol-water as the mobile phase, while all components could be fully separated using the other three kinds of mobile phase. Considering the environmental protection and low consumption, methanol-0.1% formic acid water was finally chosen as the mobile phase in this study. The influences of column temperature at 30°C, 35°C, 37°C, and 40°C on the chromatographic separation were respectively observed, and the results showed that the column temperature at 35°C could obtain the lower back pressure, higher response, and better baseline. After repeated test, the optimal grade elution mode listed in this study was finally obtained.

Flavonoids and phenolic acids are the active substances responsible for the antioxidant activity of CM (Chen et al., 2015; Peng et al., 2019; Sun et al., 2021), thus, the contents of total phenolic acids and total flavonoids were thus selected as the evaluation indexes of extraction methods. In this experiment, extraction method, solvent, time and the ratio of liquid to solid were optimized for the preparation of the sample solution, respectively. Three extraction methods including water decoction, reflux extraction, and ultrasonic method were separately investigated, and the results showed that the extraction rate of ultrasonic extraction method was significantly higher than the other two extraction methods (**Supplementary Table S5**). The extraction solvents including pure water, 30%, 50%, 70%, 100% methanol or ethanol were then observed, and it was found that 50% ethanol could obtain the best extraction rate for the total phenolic acids and total flavonoids

TABLE 7 | Correlation analysis between the antioxidant activity and the contents of eight common peaks from the different CMs.

Characteristic peak	ABTS clearance capacity	DPPH clearance capacity	OH clearance capacity
ChA	0.778** (0.001)	0.799** (0.000)	0.709** (0.003)
3,5-DCQA	0.899** (0.000)	0.900** (0.000)	0.771** (0.001)
Unknown peak 1	0.582* (0.023)	0.628* (0.012)	0.650** (0.009)
L-7G	0.512 (0.051)	0.462 (0.083)	0.039 (0.890)
4,5-DCQA	0.713** (0.003)	0.800** (0.000)	0.377 (0.166)
A-7G	0.162 (0.565)	0.056 (0.843)	−0.008 (0.979)
K-3R	0.622* (0.013)	0.602* (0.018)	0.056 (0.844)
Unknown peak 2	0.073 (0.795)	−0.023 (0.986)	0.021 (0.942)

*The data means the correlation coefficient (*p *value).*

TABLE 8 | Evaluation of commercially available CMs by Q-marker based on antioxidant activity.

No.	Accessions	Contents (%, g/g)					Grade
		ChA	3,5-DCQA	Unknown peak 1	4,5-DCQA	K-3R	
JH-01	Gongju	0.65	1.00	1.38	0.72	1.28	Good
JH-02		0.43	2.20	0.35	0.44	1.57	Good
JH-03		0.44	1.27	0.16	0.46	0.68	Good
JH-04		0.34	1.32	0.19	0.48	0.60	Medium
JH-05		0.24	1.46	0.16	0.48	0.59	Medium
JH-06		0.38	1.29	0.14	0.44	0.42	Good
JH-07	Hang-baiju	0.30	0.76	0.71	0.62	1.29	Medium
JH-08		0.31	0.84	0.78	0.67	1.52	Medium
JH-09		0.25	0.64	0.73	0.63	1.12	Medium
JH-10		0.21	0.68	0.44	0.70	1.53	Medium
JH-11		0.19	0.62	0.62	0.74	1.28	Medium
JH-12		0.69	2.31	0.54	0.95	1.31	Excellent
JH-13	Taiju	0.64	2.60	0.61	1.34	1.61	Excellent
JH-14		0.22	0.43	0.27	0.42	0.91	Poor
JH-15		0.30	0.98	0.79	0.80	2.04	Good
JH-16		0.36	0.87	0.42	0.76	1.09	Medium
JH-17		0.33	1.09	0.81	0.84	2.04	Good
JH-18		0.31	1.08	0.82	0.85	1.99	Good
JH-19	Boju	0.34	1.03	0.13	0.33	0.45	Medium
JH-20		0.23	1.12	0.12	0.19	0.35	Medium
JH-21		0.23	0.96	0.09	0.23	0.17	Poor
JH-22		0.59	1.84	0.14	0.37	0.39	Good
JH-23		0.45	2.00	0.80	0.71	1.97	Good
JH-24		0.29	1.12	0.12	0.27	0.26	Medium
JH-25	Huaiju	0.47	1.19	0.64	0.32	1.66	Good
JH-26		0.38	1.44	0.17	0.43	0.48	Good
JH-27		0.24	0.70	0.44	0.63	0.82	Medium
JH-28		0.35	0.68	0.42	0.71	0.75	Medium
JH-29		0.25	0.69	0.42	0.25	1.03	Medium
JH-30		0.24	0.75	0.42	0.33	0.95	Medium

(**Supplementary Table S6**). The ultrasonic extraction for 10, 15, 20, 30, and 40 min was further investigated, and the results showed that when the extraction time was more than 30 min, the extraction rate could not be obviously increased (**Supplementary Table S7**). Finally, the ration of liquid to solid was optimized, and it was found that when the ratio was more than 1:20, the extraction rate could not be significantly elevated (**Supplementary Table S8**).

In the quality control of TCM, chromatographic fingerprint analysis plays an important role, which can give an overall view of the characteristics of nearly all the components. However, it can only show results of similarity calculated on the basis of the relative value using a pre-selected marker compound as a reference and cannot reveal the possible content variation (Tang et al., 2010). Our results also support this fact. In our study, the similarities of most CMs were more than 0.8 except JH-21 and JH-22, however, the peak area variation (RSD value) of common peak ranged from 42.4% to 86.3%. Chemometrics can provide further data mining of chromatographic fingerprint. For example, CA can group the similar samples into several classes (Zhao et al., 2020) and visually explore the similarity of different accessions of CMs. Our results of CA revealed that the same accessions of CMs were not clustered into one class, which hinted that the difference of CMs was related to not only the species, but also the origin, harvesting season, maturity, and storage and processing condition (Chen

X. et al., 2020; Khan et al., 2020). PCA is often used to explain differences between samples and to obtain information on the variables that primarily influence sample similarity and variability (Šamec et al., 2016). Our results of PCA indicated that the peak areas of the eight common peaks all contributed to the difference between different species of CMs.

The combination of chromatographic fingerprint and chemometrics can explore the similarity and the reason of the difference between different accessions of CMs. However, these analytical strategies are all based on the peak areas of common peaks. Thus, multiple ingredients quantification, especially the common peaks quantification, is considered as an important complementary to chromatographic fingerprint analysis for the quality control of TCM (Tang et al., 2010; Yang et al., 2011). Our results of accurate quantification of the common peaks further verified that the RSD values of their contents possessed significant variations whether for the different accessions of CMs or for the same accession of CMs. The results were consistent with the peak areas variation of the common peaks in the chromatographic fingerprint analysis, and further verified that the species, origin, harvesting season, maturity, and storage and processing conditions all contributed to the quality variation of CMs.

Although the quantification of the common peak can provide an important complementary to chromatographic fingerprint analysis for the quality control of TCM, however, different compounds in the common peaks possessed the different contribution to the biological activity of TCM. Thus, how to control the quality of TCM according to the contents of common peaks is still a challenge. Recently, Q-marker based on biological activity provides a new strategy for the quality control of TCM. As anti-oxidant activity is the basis of pharmacological effects of CM, the correlation analysis between the chemical anti-oxidant activity and the contents of common peaks was further performed to explore the Q-marker of CM in this study. Our results hinted that ChA, 3,5-DCQA, unknown peak 1, 4,5-DCQA, and K-3R might be used as the Q-markers of CMs, which was partly consistent with a previous study (Zhou et al., 2019). More importantly, we successfully utilized the Q-markers to evaluate the quality of 30 flower head samples of different accessions of commercially available CMs according to their contributions to the chemical anti-oxidant activity of CMs, and the results showed that the quality of JH-21 was consistent with the results of chromatographic fingerprint analysis. The synthesis and accumulation of phytochemical compositions in plant tissues are influenced by the genotype, growing environment, and their interaction (Kiani et al., 2021). Hang-baiju and Taiju, two famous-region drugs of Zhejiang Province of China, are generally considered as higher quality of CMs (Gong et al., 2019). Our results also showed that JH-12 and JH-13, respectively from Hang-baiju and Taiju, were assigned as the excellent based on the evaluation of Q-marker. However, JH-14, a flower head sample from Taiju, was sorted as the poor, which hinted that JH-14 might be an adulteration product. Those results also indicated that it was unreliable to evaluate the quality of CMs according to geographical origins.

Although this study preliminarily screened chemical anti-oxidant quality markers, there are also some limitations. Firstly, quality markers were screened only from eight components in this study, and some active components may be omitted. Therefore, the analysis of chemical components needs to be further expanded and screened. Secondly, the screening of anti-oxidant quality markers of CM was based on the DPPH, OH, and ABTS clearance rate. Those methods are simply chemical tests and cannot provide the definite evidence of anti-oxidant activity of CM. Thus, *in vivo* anti-oxidant activity using cell or animal as model needs to be further explored in future research. In addition, CM also has many kinds of activities include antiviral, anti-inflammatory, anti-bacterial, anti-tumor, anti-infective, and anti-inflammatory effects except anti-oxidant. Therefore, quality markers that can comprehensively mirror varies kinds of biological activities of CM need to be further studied.

This study identified the Q-markers of CM through the analysis of chromatographic fingerprint, quantification of common peaks, chemical anti-oxidant activity and the spectrum-effect relationship. The quality control of CM was implemented with the chromatographic fingerprint, multiple ingredients quantification and Q-marker determination. Overall, this study has discovered that the Q-marker based quality assessment of CM was feasible and practical. This study also serves as a reference for Q-marker selections and quality control of other TCMs.

DATA AVAILABILITY STATEMENT

The original contributions presented in the study are included in the article/**Supplementary Material**, further inquiries can be directed to the corresponding author.

AUTHOR CONTRIBUTIONS

Y-FL and D-XL performed the investigation and wrote the paper. RZ, L-LZ, and ZQ participated in the collection and preparation of samples. Y-FL, D-XL, RZ, and YD performed the analyses. SJ and D-QT designed the study and amended the paper. All authors reviewed and approved the final manuscript.

FUNDING

This work was financially supported by the Natural Science Foundation of Jiangsu Higher Education Institutions of China (No. 16KJA350001), Natural Science Foundation of Jiangsu Province of China (No. BK20181147 and BE2019640), and Students Science and Technology Innovation Activity Plan of Jiangsu Province (202110313001Z) and China (202110313001).

SUPPLEMENTARY MATERIAL

The Supplementary Material for this article can be found online at: https://www.frontiersin.org/articles/10.3389/fphar.2022.809482/full#supplementary-material

REFERENCES

Bai, G., Zhang, T., Hou, Y., Ding, G., Jiang, M., and Luo, G. (2018). From Quality Markers to Data Mining and Intelligence Assessment: A Smart Quality-Evaluation Strategy for Traditional Chinese Medicine Based on Quality Markers. *Phytomedicine* 44, 109–116. doi:10.1016/j.phymed.2018.01.017

Cao, X., Sun, L., Li, D., You, G., Wang, M., and Ren, X. (2018). Quality Evaluation of Phellodendri Chinensis Cortex by Fingerprint-Chemical Pattern Recognition. *Molecules* 23 (9), 2307. doi:10.3390/molecules23092307

Chen, J., Cheng, X. L., Li, L. F., Dai, S. Y., Wang, Y. D., Li, M. H., et al. (2022). A General Procedure for Establishing Composite Quality Evaluation Indices Based on Key Quality Attributes of Traditional Chinese Medicine. *J. Pharm. Biomed. Anal.* 207, 114415. doi:10.1016/j.jpba.2021.114415

Chen, L., Huang, X., Wang, H., Shao, J., Luo, Y., Zhao, K., et al. (2020a). Integrated Metabolomics and Network Pharmacology Strategy for Ascertaining the Quality Marker of Flavonoids for *Sophora Flavescens*. *J. Pharm. Biomed. Anal.* 186, 113297. doi:10.1016/j.jpba.2020.113297

Chen, L., Kotani, A., Kusu, F., Wang, Z., Zhu, J., and Hakamata, H. (2015). Quantitative Comparison of Caffeoylquinic Acids and Flavonoids in *Chrysanthemum Morifolium* Flowers and Their Sulfur-Fumigated Products by Three-Channel Liquid Chromatography with Electrochemical Detection. *Chem. Pharm. Bull. (Tokyo)* 63 (1), 25–32. doi:10.1248/cpb.c14-00515

Chen, X., Wang, H., Yang, X., Jiang, J., Ren, G., Wang, Z., et al. (2020b). Small-scale alpine Topography at Low Latitudes and High Altitudes: Refuge Areas of the Genus *Chrysanthemum* and its Allies. *Hortic. Res.* 7 (1), 184. doi:10.1038/s41438-020-00407-9

Cho, B., Shin, J., Kang, H., Park, J., Hao, S., Wang, F., et al. (2021). Anti-inflammatory E-ffect of Chrysanthemum Z-awadskii, P-eppermint, Glycyrrhiza G-labra H-erbal M-ixture in L-ipopolysaccharide-stimulated RAW264.7 M-acrophages. *Mol. Med. Rep.* 24 (1), 532. doi:10.3892/mmr.2021.12171

Dai, T., and Sun, G. (2021). The Analysis of Active Compounds in Flos *Chrysanthemi Indici* by UHPLC Q Exactive HF Hybrid Quadrupole-Orbitrap MS and Comprehensive Quality Assessment of its Preparation. *Food Funct.* 12 (4), 1769–1782. doi:10.1039/d0fo03053h

Gong, J., Chu, B., Gong, L., Fang, Z., Zhang, X., Qiu, S., et al. (2019). Comparison of Phenolic Compounds and the Antioxidant Activities of Fifteen *Chrysanthemum Morifolium* Ramat Cv. 'Hangbaiju' in China. *Antioxidants (Basel)* 8 (8), 325. doi:10.3390/antiox8080325

He, J., Zhang, Q., Ma, C., Giancaspro, G. I., Bi, K., and Li, Q. (2021). An Effective Workflow for Differentiating the Same Genus Herbs of *Chrysanthemum Morifolium* Flower and *Chrysanthemum Indicum* Flower. *Front. Pharmacol.* 12, 575726. doi:10.3389/fphar.2021.575726

Hodaei, M., Rahimmalek, M., and Arzani, A. (2021b). Variation in Bioactive Compounds, Antioxidant and Antibacterial Activity of Iranian *Chrysanthemum Morifolium* Cultivars and Determination of Major Polyphenolic Compounds Based on HPLC Analysis. *J. Food Sci. Technol.* 58 (4), 1538–1548. doi:10.1007/s13197-020-04666-1

Hodaei, M., Rahimmalek, M., and Behbahani, M. (2021a). Anticancer Drug Discovery from Iranian *Chrysanthemum* Cultivars through System Pharmacology Exploration and Experimental Validation. *Sci. Rep.* 11 (1), 11767. doi:10.1038/s41598-021-91010-y

Hodaei, M., Rahimmalek, M., Arzani, A., and Talebi, M. (2018). The Effect of Water Stress on Phytochemical Accumulation, Bioactive Compounds and Expression of Key Genes Involved in Flavonoid Biosynthesis in *Chrysanthemum Morifolium* L. *Ind. Crops Prod.* 120, 295–304. doi:10.1016/j.indcrop.2018.04.073

Hou, J. J., Wu, W. Y., Da, J., Yao, S., Long, H. L., Yang, Z., et al. (2011). Ruggedness and Robustness of Conversion Factors in Method of Simultaneous Determination of Multi-Components with Single Reference Standard. *J. Chromatogr. A.* 1218 (33), 5618–5627. doi:10.1016/j.chroma.2011.06.058

Jia, F., Liu, X., Gong, Z., Cui, W., Wang, Y., and Wang, W. (2020). Extraction, Modification, and Property Characterization of Dietary Fiber from *Agrocybe Cylindracea*. *Food Sci. Nutr.* 8 (11), 6131–6143. doi:10.1002/fsn3.1905

Jiang, Y. L., Xu, Z. J., Cao, Y. F., Wang, F., Chu, C., Zhang, C., et al. (2021). HPLC fingerprinting-based multivariate analysis of chemical components in *Tetrastigma Hemsleyanum* Diels et Gilg: Correlation to their antioxidant and neuraminidase inhibition activities. *J. Pharm. Biomed. Anal.* 205, 114314. doi:10.1016/j.jpba.2021.114314

Jing, S., Chai, W., Guo, G., Zhang, X., Dai, J., and Yan, L. J. (2016). Comparison of Antioxidant and Antiproliferative Activity between Kunlun *Chrysanthemum* Flowers Polysaccharides (KCCP) and Fraction PII Separated by Column Chromatography. *J. Chromatogr. B Analyt Technol. Biomed. Life Sci.* 1019, 169–177. doi:10.1016/j.jchromb.2016.01.004

Khan, I. A., Xu, W., Wang, D., Yun, A., Khan, A., Zongshuai, Z., et al. (2020). Antioxidant Potential of *chrysanthemum Morifolium* Flower Extract on Lipid and Protein Oxidation in Goat Meat Patties during Refrigerated Storage. *J. Food Sci.* 85 (3), 618–627. doi:10.1111/1750-3841.15036

Kiani, R., Arzani, A., and Mirmohammady Maibody, S. A. M. (2021). Polyphenols, Flavonoids, and Antioxidant Activity Involved in Salt Tolerance in Wheat, *Aegilops Cylindrica* and Their Amphidiploids. *Front. Plant Sci.* 12, 646221. doi:10.3389/fpls.2021.646221

Li, Y., Zhang, Y., Cao, B., Zhang, F., Niu, M., Bai, X., et al. (2020). Screening for the Antiplatelet Aggregation Quality Markers of *Salvia Yunnanensis* Based on an Integrated Approach. *J. Pharm. Biomed. Anal.* 188, 113383. doi:10.1016/j.jpba.2020.113383

Lin, G. H., Lin, L., Liang, H. W., Ma, X., Wang, J. Y., Wu, L. P., et al. (2010). Antioxidant Action of a *Chrysanthemum Morifolium* Extract Protects Rat Brain against Ischemia and Reperfusion Injury. *J. Med. Food* 13 (2), 306–311. doi:10.1089/jmf.2009.1184

Liu, C., Guo, D. A., and Liu, L. (2018). Quality Transitivity and Traceability System of Herbal Medicine Products Based on Quality Markers. *Phytomedicine* 44, 247–257. doi:10.1016/j.phymed.2018.03.006

Liu, Z., Wang, D., Li, D., and Zhang, S. (2017). Quality Evaluation of *Juniperus rigida* Sieb. et Zucc. based on phenolic profiles, bioactivity, and HPLC fingerprint combined with chemometrics. *Front. Pharmacol.* 8, 198. doi:10.3389/fphar.2017.00198

Peng, A., Lin, L., Zhao, M., and Sun, B. (2019). Classification of Edible *Chrysanthemums* Based on Phenolic Profiles and Mechanisms Underlying the Protective Effects of Characteristic Phenolics on Oxidatively Damaged Erythrocyte. *Food Res. Int.* 123, 64–74. doi:10.1016/j.foodres.2019.04.046

Šamec, D., Maretić, M., Lugarić, I., Mešić, A., Salopek-Sondi, B., and Duralija, B. (2016). Assessment of the Differences in the Physical, Chemical and Phytochemical Properties of Four Strawberry Cultivars Using Principal Component Analysis. *Food Chem.* 194, 828–834. doi:10.1016/j.foodchem.2015.08.095

Song, C., Liu, Y., Song, A., Dong, G., Zhao, H., Sun, W., et al. (2018). The *Chrysanthemum Nankingense* Genome Provides Insights into the Evolution and Diversification of Chrysanthemum Flowers and Medicinal Traits. *Mol. Plant* 11 (12), 1482–1491. doi:10.1016/j.molp.2018.10.003

Sun, J., Wang, Z., Chen, L., and Sun, G. (2021). Hypolipidemic Effects and Preliminary Mechanism of Chrysanthemum Flavonoids, its Main Components Luteolin and Luteoloside in Hyperlipidemia Rats. *Antioxidants (Basel)* 10 (8), 1309. doi:10.3390/antiox10081309

Tang, D., Yang, D., Tang, A., Gao, Y., Jiang, X., Mou, J., et al. (2010). Simultaneous Chemical Fingerprint and Quantitative Analysis of *Ginkgo Biloba* Extract by HPLC-DAD. *Anal. Bioanal. Chem.* 396 (8), 3087–3095. doi:10.1007/s00216-010-3536-8

Tian, D., Yang, Y., Yu, M., Han, Z. Z., Wei, M., Zhang, H. W., et al. (2020). Anti-inflammatory Chemical Constituents of Flos *Chrysanthemi Indici* Determined by UPLC-MS/MS Integrated with Network Pharmacology. *Food Funct.* 11 (7), 6340–6351. doi:10.1039/d0fo01000f

Tian, Z., Jia, H., Jin, Y., Wang, M., Kou, J., Wang, C., et al. (2019). Chrysanthemum Extract Attenuates Hepatotoxicity via Inhibiting Oxidative Stress *In Vivo* and *In Vitro*. *Food Nutr. Res.* 63. doi:10.29219/fnr.v63.1667

Tu, X., Wang, H. B., Huang, Q., Cai, Y., Deng, Y. P., Yong, Z., et al. (2021). Screening Study on the Anti-angiogenic Effects of Traditional Chinese Medicine - Part II: Wild Chrysanthemum. *J. Cancer* 12 (1), 124–133. doi:10.7150/jca.52971

Yang, D. Z., An, Y. Q., Jiang, X. L., Tang, D. Q., Gao, Y. Y., Zhao, H. T., et al. (2011). Development of a Novel Method Combining HPLC Fingerprint and Multi-Ingredients Quantitative Analysis for Quality Evaluation of Traditional Chinese

Medicine Preparation. *Talanta* 85 (2), 885–890. doi:10.1016/j.talanta.2011.04.059

Yang, J. L., Liu, L. L., and Shi, Y. P. (2019). Two New Eudesmane Sesquiterpenoids from the Flowers of *Chrysanthemum Indicum*. *Nat. Prod. Bioprospect* 9 (2), 145–148. doi:10.1007/s13659-019-0199-9

Youssef, F. S., Eid, S. Y., Alshammari, E., Ashour, M. L., Wink, M., and El-Readi, M. Z. (2020). *Chrysanthemum Indicum* and *Chrysanthemum Morifolium*: Chemical Composition of Their Essential Oils and Their Potential Use as Natural Preservatives with Antimicrobial and Antioxidant Activities. *Foods* 9 (10), 1460. doi:10.3390/foods9101460

Zhang, X., Sun, X., Li, W., Huang, X., Tao, L., Li, T., et al. (2021a). *In Vitro* and *In Vivo* Antioxidant Activities of Soy Protein Isolate Fermented with *Bacillus Subtilis* Natto. *J. Food Sci. Technol.* 58 (8), 3199–3204. doi:10.1007/s13197-020-04823-6

Zhang, X., Wu, J. Z., Lin, Z. X., Yuan, Q. J., Li, Y. C., Liang, J. L., et al. (2019). Ameliorative Effect of Supercritical Fluid Extract of Chrysanthemum Indicum Linnén against D-Galactose Induced Brain and Liver Injury in Senescent Mice via Suppression of Oxidative Stress, Inflammation and Apoptosis. *J. Ethnopharmacol* 234, 44–56. doi:10.1016/j.jep.2018.12.050

Zhang, Y., Wu, M., Xi, J., Pan, C., Xu, Z., Xia, W., et al. (2021b). Multiple-fingerprint Analysis of *Poria Cocos* Polysaccharide by HPLC Combined with Chemometrics Methods. *J. Pharm. Biomed. Anal.* 198, 114012. doi:10.1016/j.jpba.2021.114012

Zhao, C., Cheng, J., Li, C., Li, S., Tian, Y., Wang, T., et al. (2021). Quality Evaluation of *Acanthopanax Senticosus* via Quantitative Analysis of Multiple Components by Single Marker and Multivariate Data Analysis. *J. Pharm. Biomed. Anal.* 201, 114090. doi:10.1016/j.jpba.2021.114090

Zhao, X., Song, L., Jiang, L., Zhu, Y., Gao, Q., Wang, D., et al. (2020). The Integration of Transcriptomic and Transgenic Analyses Reveals the Involvement of the SA Response Pathway in the Defense of chrysanthemum against the Necrotrophic Fungus Alternaria Sp. *Hortic. Res.* 7 (1), 80. doi:10.1038/s41438-020-0297-1

Zhou, H. P., Ren, M. X., Guan, J. Q., Liu, Y. L., Xiong, Y. X., Zhong, Q. F., et al. (2019). Research Progress on Chemical Constituents and Pharmacological Effects of *Chrysanthemum Morifolium* and Predictive Analysis on Quality Markers. *Chin. Traditional Herbal Drugs* 50, 4785–4795.

Conflict of Interest: The authors declare that the research was conducted in the absence of any commercial or financial relationships that could be construed as a potential conflict of interest.

Publisher's Note: All claims expressed in this article are solely those of the authors and do not necessarily represent those of their affiliated organizations, or those of the publisher, the editors and the reviewers. Any product that may be evaluated in this article, or claim that may be made by its manufacturer, is not guaranteed or endorsed by the publisher.

frontiers in Pharmacology

ORIGINAL RESEARCH
published: 22 February 2022
doi: 10.3389/fphar.2022.835616

Ayurveda-based Botanicals as Therapeutic Adjuvants in Paclitaxel-induced Myelosuppression

*Akash Saggam[1,2], Prathamesh Kale[2], Sushant Shengule[2], Dada Patil[2], Manish Gautam[2], Girish Tillu[1], Kalpana Joshi[3], Sunil Gairola[2] and Bhushan Patwardhan[1]**

[1]AYUSH-Center of Excellence, Center for Complementary and Integrative Health, School of Health Sciences, Savitribai Phule Pune University, Pune, India, [2]Serum Institute of India Pvt. Ltd., Pune, India, [3]Department of Biotechnology, Sinhgad College of Engineering, Pune, India

Chemotherapy-induced myelosuppression is one of the major challenges in cancer treatment. Ayurveda-based immunomodulatory botanicals *Asparagus racemosus* Willd (AR/Shatavari) and *Withania somnifera* (L.). Dunal (WS/Ashwagandha) have potential role to manage myelosuppression. We have developed a method to study the effects of AR and WS as therapeutic adjuvants to counter paclitaxel (PTX)-induced myelosuppression. Sixty female BALB/c mice were divided into six groups—vehicle control (VC), PTX alone, PTX with aqueous and hydroalcoholic extracts of AR (ARA, ARH) and WS (WSA, WSH). The myelosuppression was induced in mice by intraperitoneal administration of PTX at 25 mg/kg dose for three consecutive days. The extracts were orally administered with a dose of 100 mg/kg for 15 days prior to the induction with PTX administration. The mice were observed daily for morbidity parameters and were bled from retro-orbital plexus after 2 days of PTX dosing. The morbidity parameters simulate clinical adverse effects of PTX that include activity (extreme tiredness due to fatigue), behavior (numbness and weakness due to peripheral neuropathy), body posture (pain in muscles and joints), fur aspect and huddling (hair loss). The collected samples were used for blood cell count analysis and cytokine profiling using Bio-Plex assay. The PTX alone group showed a reduction in total leukocyte and neutrophil counts (4,800 ± 606; 893 ± 82) when compared with a VC group (9,183 ± 1,043; 1,612 ± 100) respectively. Pre-administration of ARA, ARH, WSA, and WSH extracts normalized leukocyte counts (10,000 ± 707; 9,166 ± 1,076; 10,333 ± 1,189; 9,066 ± 697) and neutrophil counts (1,482 ± 61; 1,251 ± 71; 1,467 ± 121; 1,219 ± 134) respectively. Additionally, higher morbidity score in PTX group (7.4 ± 0.7) was significantly restricted by ARA (4.8 ± 1.1), ARH (5.1 ± 0.6), WSA (4.5 ± 0.7), and WSH (5 ± 0.8). (Data represented in mean ± SD). The extracts also significantly modulated 20 cytokines to evade PTX-induced leukopenia, neutropenia, and morbidity. The AR and WS extracts significantly prevented PTX-induced myelosuppression ($p < 0.0001$) and morbidity signs ($p < 0.05$) by modulating associated cytokines. The results indicate AR and WS as therapeutic adjuvants in cancer management.

Keywords: Ayurveda, *Asparagus racemosus*, *Withania somnifera*, Cancer Therapeutics, Chemotherapy, Paclitaxel, Myelosuppression, Cytokine Modulation

OPEN ACCESS

Edited by:
Kornkanok Ingkaninan, Naresuan University, Thailand

Reviewed by:
Basel A. Abdel-Wahab, Assiut University, Egypt
Behnam Ghorbanzadeh, Dezful University of Medical Sciences (DUMS), Iran

****Correspondence:***
Bhushan Patwardhan
bpatwardhan@gmail.com

Specialty section:
This article was submitted to Ethnopharmacology, a section of the journal Frontiers in Pharmacology

Received: *14 December 2021*
Accepted: *19 January 2022*
Published: *22 February 2022*

Citation:
Saggam A, Kale P, Shengule S, Patil D, Gautam M, Tillu G, Joshi K, Gairola S and Patwardhan B (2022) Ayurveda-based Botanicals as Therapeutic Adjuvants in Paclitaxel-induced Myelosuppression. Front. Pharmacol. 13:835616. doi: 10.3389/fphar.2022.835616

INTRODUCTION

Cancer is one of the leading causes of mortality worldwide. The GLOBOCAN 2020 data indicates more than 19 million new cases with more than 9 million deaths due to cancer in the year 2020 with increasing prevalence globally (GLOBOCAN 2020 Fact Sheet 2020). The therapeutic approaches of cancer include chemotherapy, radiotherapy, and surgery depending upon the stage of cancer and response to therapies. In recent years, immunotherapy has emerged as an effective therapeutic alternative (Arruebo et al., 2011). However, chemotherapy is a predominant approach in cancer therapeutics that restricts cancer development by using chemotherapeutic agents. The chemotherapeutic agents include alkylating agents, cytoskeletal disrupters, anthracyclines, and enzyme inhibitors etc. (Shewach and Kuchta 2009). Although chemotherapy has emerged as an effective therapeutic approach, there are several dose-limiting adverse effects (Chopra et al., 2016; Regnard and Kindlen 2019). Chemotherapy-induced myelosuppression is one of the major challenges in cancer therapeutics. The declined ability of bone marrow to produce blood cells is referred as myelosuppression that leads to neutropenia, leukopenia, and thrombocytopenia (Maxwell and Maher 1992).

In the present study, we used paclitaxel (PTX/taxane) as a prototype chemotherapeutic drug to induce myelosuppression in a mouse model. PTX is one of the extensively used anticancer drugs in the treatment of various types of cancers including breast cancer, ovarian cancer, pancreatic cancer, advanced non-small cell lung cancer, and liver cancer (Weaver 2014). The pharmacological activity of PTX is to stabilize the microtubules of cancer cells that leads to tumor suppression; however, the adverse effects of PTX remains a major concern. The clinical adverse effects of PTX include myelosuppression, fatigue, hypersensitivity reactions, hair loss, peripheral neuropathy (numbness and weakness), pain in muscles and joints etc. (Markman 2003). PTX is known to inhibit the proliferation of bone marrow cells. It induces apoptosis by activating caspase-3/7 and promotes DNA damage leading to myelosuppression (Hu et al., 2016). The hematopoietic growth factors especially granulocyte colony-stimulating factor (G-CSF) and granulocyte-macrophage colony-stimulating factor (GM-CSF) are employed in between chemotherapeutic cycles that increase blood cell count in patients to manage myelosuppression (Dale 2002). However, the notable toxicity risks limit the use of growth factors (Puhalla, Bhattacharya, and Davidson 2012). Additionally, active involvement of growth factors in carcinogenesis is speculated by researchers (Halper 2010). In such a scenario, a safe therapeutic adjuvant with better effectiveness to counter chemotherapy-induced myelosuppression is needed.

Ayurveda, a traditional medicine system, has a lot to offer to tackle myelosuppressive indications. The therapeutic approaches of Ayurveda focus on balancing the physiological processes and body constitution leading to homeostasis (Patwardhan et al., 2015). Ayurveda medicines have a long history of safe use and are being used in cancer management (Lele 2010; Raut et al., 2012; Patwardhan 2014). The *Rasayana* approach of Ayurveda strengthens physiological homeostasis through rejuvenating and adaptogenic effects (Chulet and Pradhan 2009). Ayurveda botanicals, *Asparagus racemosus* Willd. (AR) known as Shatavari and *Withania somnifera* (L.). Dunal (WS) known as Ashwagandha are *Rasayana* botanicals used as adaptogens and immunomodulators (Balasubramani et al., 2011). AR and WS are known for their multimodal pharmacological activities such as galactagogic, anti-ageing, nootropic, anti-inflammatory, and especially immunomodulation (N. Singh et al., 2011; Alok et al., 2013). The immunomodulatory activity of AR and WS can help to counter chemotherapy-induced myelosuppression. AR and WS have been reported to offer myeloprotection during cancer chemotherapy (Diwanay et al., 2004). The experimental methods replicated *Rasayana* approach of Ayurveda that recommends pre-administration and daily dosing of botanical extracts (Chulet and Pradhan 2009).

The present study reports a method and effects of AR and WS as therapeutic adjuvants to counter PTX-induced myelosuppression in BALB/c mice. This study explores the preventive effects of AR and WS extracts in PTX-induced myelosuppression. It also investigates the observational parameters of morbidity that simulate the clinical adverse effects of PTX as mentioned above. Furthermore, it also connects the myelosuppression and morbidity parameters to cytokine modulation.

MATERIALS AND METHODS

Materials

The commercially available clinical formulation of PTX-Mitotax®-300 (Dr Reddy's Laboratory) was procured from local pharmacists and was standardized for dosage regimen. The Cremophor EL® (polyoxyethylated castor oil) (Cat. No. 238470) and absolute ethanol were obtained from Millipore and SRL respectively. The standardized aqueous and hydroalcoholic extracts of *Asparagus racemosus* (ARA, ARH) and *Withania somnifera* (WSA, WSH) were obtained from Pharmanza Herbal Pvt. Ltd. as a gift. We have used standardized extracts prepared as per previously reported method (Borse et al., 2021).

Animals

The ethics approval (27/23-03/2021-R, dated-23/03/2021) was obtained from the Institutional Animal Ethics Committee of Serum Institute of India Pvt. Ltd. The female BALB/c mice were reared as per CPCSEA guidelines in the animal house of Serum Institute of India Pvt. Ltd. with *ad libitum* food and water. The mice weighing 13-18 gms were housed in polypropylene cages on ground corn cobs bedding at optimum room temperature with 12 h of light/dark cycle. The mortality and morbidity variables in the method development experiment suggest that the female mice were more tolerant to the high and consecutive doses of PTX. The model titers the dose regimen to balance myelosuppression and survival. Therefore, we used female mice in the present study.

Dosing

The animals were randomly allocated in 6 groups-vehicle control (VC), PTX alone (PTX), and PTX along with aqueous and hydroalcoholic extracts of AR (PTX + ARA and PTX + ARH) and WS (PTX + WSA and PTX + WSH) (**Figure 1A**). Each group contained 10 mice weighing 13-18 gms.

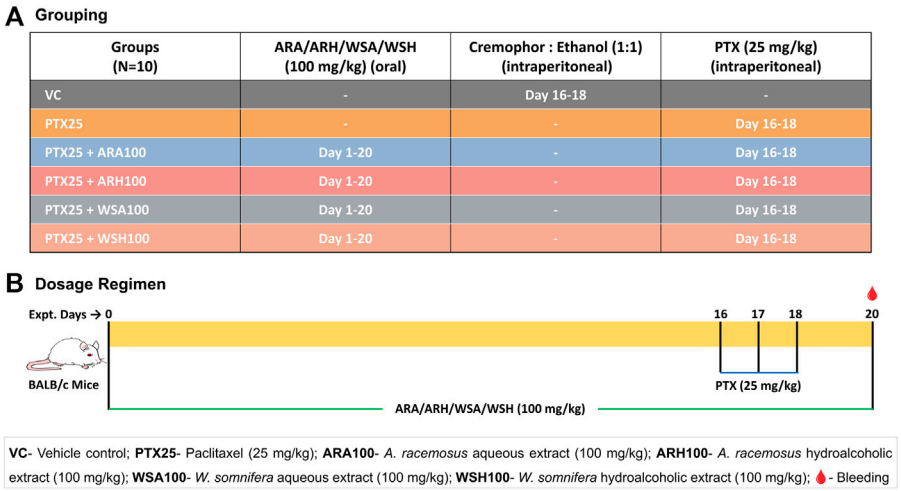

FIGURE 1 | Grouping and dosage regimen. **(A)** depicts grouping of mice to be dosed with botanical extracts and PTX for desired days. **(B)** illustrates the dosing regimen of botanical extracts as per Ayurveda (for 20 days) and that of PTX (on 16th, 17th and 18th day) as standardized for induction of myelosuppression. The blood samples were collected from retro-orbital plexus on 20th day for cell count and cytokine analysis.

The 59.125 mg/kg PTX dose per mouse is equivalent to that of the human dose of 175 mg/m^2. Although PTX is administered intravenously in humans, it was given through the intraperitoneal route in mice. Our earlier standardization experiments have suggested consistent results with intraperitoneal dosing in small animal models like mice. It also has a practical advantage over intravenous administration in mice (Ray et al., 2011). The commercially available clinical formulation of PTX was diluted with sterile saline to obtain the desired concentration. The mouse dose of botanical extracts was extrapolated from recommended clinical dose based on Ayurveda (Gogte 2000). Moreover, previous studies by the investigators' group have consistently demonstrated that the dose of 100 mg/kg of AR and WS extracts for consecutive 15 days is best for immunomodulation (Ziauddin et al., 1996; Gautam, et al., 2004a; Gautam, et al., 2004b).

As shown in the dosage regimen (**Figure 1B**), the mice were pre-administered with 100 mg/kg of botanical extracts orally every morning for 15 days prior to PTX dosing and continued throughout the experiment (up to 20th day). After a series of dose standardization experiments, 25 mg/kg of PTX dose was finalized to be administered intraperitoneally for 3 consecutive days (15th, 16th, and 17th day) to induce myelosuppression. The VC group was dosed with 1:1 solution of cremophor and absolute ethanol in the dose equivalent to the PTX since the commercially available PTX was dissolved in cremophor-ethanol solution. The mice were anesthetized by drop jar method using isoflurane and were bled from retro-orbital plexus 2 days after PTX cycle (on 20th day) (Anesthesia Guidelines Mice, 2021). These samples were analysed for blood cell count and plasma cytokine profiling.

Blood Cell Count Analysis

The primary outcome measures of myelosuppression were total leukocyte and neutrophil counts as indicators of myelosuppression. The blood collected in EDTA-coated vacutainers was subjected to Sysmex XN550 analyser. The total leukocyte count/mm^3 (TLC) and absolute neutrophil count/mm^3 (ANC) were considered for further analysis.

Morbidity Analysis

Along with the total leukocyte and neutrophil count, we also considered examining other clinical adverse effects of PTX in mice. Cancer chemotherapy especially with PTX is associated with several adverse effects (Marupudi et al., 2007). Such adverse effects may be the signs of morbidities. Previous studies have reported the methods for observational scoring in cancer therapeutics (Banipal et al., 2017; Banerjee and Prasad 2020). Therefore, the secondary outcome measures included morbidity parameters such as activity, behavior, fur aspect, huddling, and posture. The morbidity parameters simulated clinical adverse effects of PTX such as fatigue (extreme tiredness), peripheral neuropathy (numbness and weakness), hair loss (alopecia), and pain in muscles and joints (Batchelder et al., 1983; Paclitaxel Taxol, 2020; Clinical Signs of Pain and Disease in Laboratory Animals 2021) (**Table 1**).

The mice from all the groups were observed daily for morbidity parameters including activity, behavior, fur aspect, huddling, and body posture throughout the experiment. The morbidity scoring (**Table 2**) was derived based on literature survey (Banipal et al., 2017; Banerjee and Prasad 2020; Paclitaxel Taxol, 2020; Clinical Signs of Pain and Disease in Laboratory Animals, 2021; Batchelder et al., 1983) wherein score '0' represents normal and score '3' represents highest observed morbidity parameter. More the score indicates higher morbidity. The morbidity score of each group was calculated as the average of the sum of all the parameters of each mouse of the group (data are shared as **Supplementary Material S1**).

Cytokine Profiling

The panel of 20 cytokines (eotaxin, G-CSF, GM-CSF, IFN-γ, IL-1α, IL-1β, IL-2, IL-3, IL-4, IL-5, IL-6, IL-10, IL-13, IL-17A, KC,

TABLE 1 | Rationale of morbidity analysis.

Clinical adverse effects of PTX	Observations and signs in animals	Parameters
Fatigue (extreme tiredness)	Fatigue reduces general wandering of animal in cage	Activity
Peripheral neuropathy (numbness and weakness)	Abnormal behavior and lack of relocation is due to numbness	Behavior
Hair loss (alopecia)	Ruffled and fur loss represents alopecia	Fur aspect
	Adult mice huddle in response to cold caused by hair loss	Huddling/Grouping
Painful muscles and joints	Hunched posture is a general sign of pain or distress	Posture

References: (Batchelder et al., 1983; Paclitaxel Taxol, 2020; Clinical Signs of Pain and Disease in Laboratory Animals 2021).

TABLE 2 | Morbidity scoring system.

Score	0	1	2	3
Activity	Normal	Reduced	Only when provoked	Little or none with provocation
Behavior	Normal	Slow normal when disturbed	Abnormal when disturbed and relocation	Abnormal when disturbed and no relocation
Fur aspect	Normal coat/actively grooming	Slightly ruffled or mild loss of fur	Ruffled fur and moderate loss of fur	Ruffled fur, piloerection, and significant loss of fur
Huddling/ Grouping	Normal or no grouping	Mild grouping or social proximity	Moderate grouping or social proximity	High grouping or social proximity
Posture	Normal	Slightly hunched but moving freely	Hunched with stiff movement	Hunched with little or no movement

References: (Banipal et al., 2017; Banerjee and Prasad 2020; Paclitaxel Taxol, 2020; Clinical Signs of Pain and Disease in Laboratory Animals 2021; Batchelder et al., 1983).

MCP-1, MIP-1α, MIP-1β, RANTES, and TNF-α) was considered for cytokine profiling. Cytokines were measured using Bio-Plex multiplex that operates on the principle of capture sandwich immunoassay. The polystyrene magnetic beads coupled with antibodies of specific cytokines were incubated with the plasma samples on shaker at 850 ± 50 rpm for 30 min in a 96-well plate. The beads were washed thrice using wash buffer. The primary antibody-cytokine conjugate was incubated with secondary (detection) antibody for 30 min followed by washing thrice using wash buffer. Further, the secondary antibodies were tagged with streptavidin-phycoerythrin and incubated for 10 min. The beads were again washed thrice and resuspended in buffer. The plate was then subjected to Bio-Plex 200 system for reading.

Statistical Analysis

The experimental results of blood cell count, morbidity analysis, and cytokine profiling were analysed using GraphPad 9.0.0 software. The statistical significance of the data of blood cell count analysis (TLC and ANC), morbidity score, and observed concentrations of cytokines (pg/ml) was analysed by one-way ANOVA. The intergroup comparison was carried out using Tukey's statistical hypothesis testing with 95% confidence interval. The data is represented in mean ± SD.

RESULTS

The mice were observed healthy with normal activity and behavior at the time of housing.

AR and WS Prevented PTX-induced Myelosuppression

The pre-administration of botanical extracts significantly ($p < 0.0001$) prevented PTX-induced myelosuppression in BALB/c mice (**Figure 2**). The PTX group showed a reduction in total leukocyte and neutrophil counts (4,800 ± 606; 893 ± 82) when compared with that of a VC group (9,183 ± 1,043; 1,612 ± 100) respectively. The PTX-induced leukopenia and neutropenia were evident by reduced counts of total leukocytes and neutrophils respectively. The adjuvant groups with botanical extracts were found to maintain these counts. Pre-administration of ARA, ARH, WSA, and WSH extracts prevented PTX-induced reduction by normalizing total leukocyte counts (10,000 ± 707; 9,166 ± 1,076; 10,333 ± 1,189; 9,066 ± 697) and neutrophil counts (1,482 ± 61; 1,251 ± 71; 1,467 ± 121; 1,219 ± 134) respectively. The total leukocyte and neutrophil counts of adjuvant groups were adjacent to that of VC group. Thus, ARA, ARH, WSA, and WSH prevented leukopenia and neutropenia induced by PTX in BALB/c mice.

AR and WS Reduced PTX-induced Morbidity

The pre-administration of botanical extracts significantly ($p < 0.05$) reduced PTX-induced morbidity signs in BALB/c mice (**Figure 3A**). These signs included reduced activity and relocation, hunched posture (**Figure 3B**), huddling/grouping (**Figure 3C**), hair loss/alopecia (**Figure 3D**) that simulated clinical adverse effects of PTX. The morbidity score was significantly higher in PTX group (7.4 ± 0.7) than that of VC group (1 ± 0). The clinical adverse effects of PTX were observed in mice such as reduced activity or general wandering (fatigue),

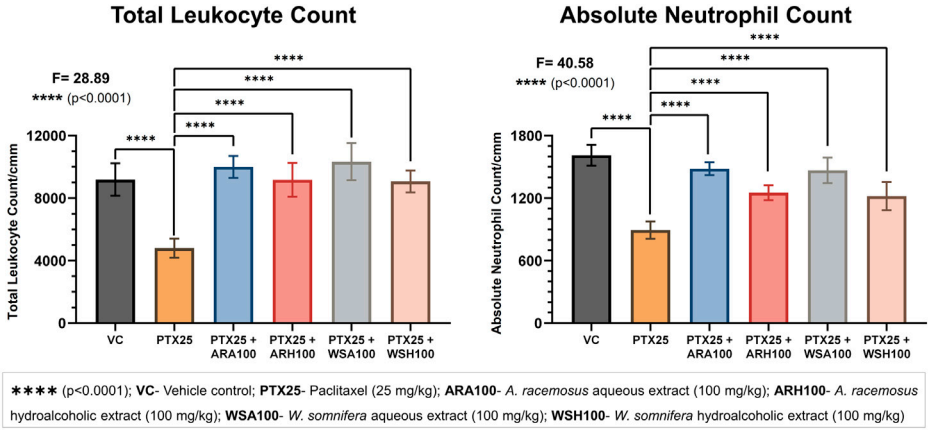

FIGURE 2 | Blood cell count analysis. The figure depicts that ARA, ARH, WSA, and WSH significantly prevented PTX-induced leukopenia and neutropenia. PTX at 25 mg/kg dose significantly ($p < 0.0001$) reduces the total leukocyte and neutrophil count. Pre-administration of botanical extracts ARA, ARH, WSA, and WSH at 100 mg/kg dose 15 days prior to PTX dosing significantly ($p < 0.0001$) prevents the reduction in total leukocyte and neutrophil count. All botanical extracts normalize the total leukocyte and neutrophil count comparable to VC group. The data points are represented as mean ± SD with n = 6.

abnormal behavior and lack of relocation (numbness and weakness due to peripheral neuropathy), hunched posture (pain in muscles and joints), notable hair loss and grouping due to cold (alopecia). The adjuvant groups with botanical extracts restricted the aforementioned morbidity signs. ARA (4.8 ± 1.1), ARH (5.1 ± 0.6), WSA (4.5 ± 0.7), and WSH (5 ± 0.8) decreased the morbidity score that was elevated by PTX. In all the adjuvant groups (those treated with extracts), it was observed that the activity and relocation of mice was improved with reduced stiffness of posture followed by negligible hair loss and grouping.

AR and WS Modulated PTX-induced Cytokine Alterations

The pre-administration of botanical extracts significantly (p=0.0086 for KC, p=0.0004 for IL-5, p=0.0001 for IL-4, and p<0.0001 for all other cytokines) mitigated PTX-induced cytokine alterations in BALB/c mice (**Figure 4**). PTX significantly (p<0.05) increased the plasma levels of cytokines (G-CSF, GM-CSF, IL-1α, IL-1β, IL-6, IL-10, and IL-13) and chemokines (KC and MCP-1). The botanical extracts modulated the PTX-induced cytokine alterations to maintain homeostasis. ARA and/or ARH reduced the expression of G-CSF, IL-1α and increased the expression of IL-13. WSA and WSH also reduced the expression of G-CSF, GM-CSF, IL-1α, IL-1β, IL-6, IL-10, and IL-13. Overall, WS was found to normalise the PTX-induced cytokine alterations to bring it back to the level of VC. ARA was found to decrease KC and increase TNF-α and IL-17A whereas ARH increased IL-3 and IL-4 levels in mouse plasma significantly (p<0.05).

DISCUSSION

The present study reports a method developed for induction of myelosuppression using chemotherapeutic drug PTX. The standardized PTX dose of 25 mg/kg (administered intraperitoneally for three consecutive days) significantly reduces total leukocyte and neutrophil count in mice. An application of clinically used PTX formulation mimics the model closer to the clinical scenarios. Therefore, this mouse model may be a better evidence-based option over reported predictive models of myelosuppression (Schurig et al., 1985; Schurig, Florczyk, and Bradner 1986; Friberg et al., 2002; Friberg and Karlsson 2003). The methods of this study are useful in screening therapeutic adjuvants in cancer chemotherapy. The data from this study suggests that AR and WS extracts prevented PTX-induced myelosuppression. The ARA, ARH, WSA, and WSH extracts significantly evaded the leukopenia, neutropenia, and morbidity induced by PTX in BALB/c mice. This preventive effect is corroborated with cytokine data (**Figure 4**).

AR and WS Restrict PTX-induced Inflammatory Response

PTX was found to induce inflammatory conditions evident by significant expression of pro-inflammatory cytokines (IL-1α, IL-1β, IL-6, and IL-13) and chemokines (KC, and MCP-1). AR and WS extracts and their phytoconstituents have been reported as potential anti-inflammatory agents acting through inhibition of pro-inflammatory cytokines released by several immune cells including monocytes, macrophages, dendritic cells, and keratinocytes etc. (Agarwal et al., 1999; Bani et al., 2006; Alok et al., 2013; Tiwari et al., 2017; Dubey et al., 2018; Saggam et al., 2021). In this study, the PTX-induced inflammation was significantly prevented by AR (downregulation of IL-1α and KC) and WS (downregulation of IL-1α, IL-1β, IL-6, IL-13, and MCP-1).

AR and WS Maintain Hematological Homeostasis

The AR and WS extracts prevented PTX-induced decrease in total leukocyte and neutrophil count in mice through

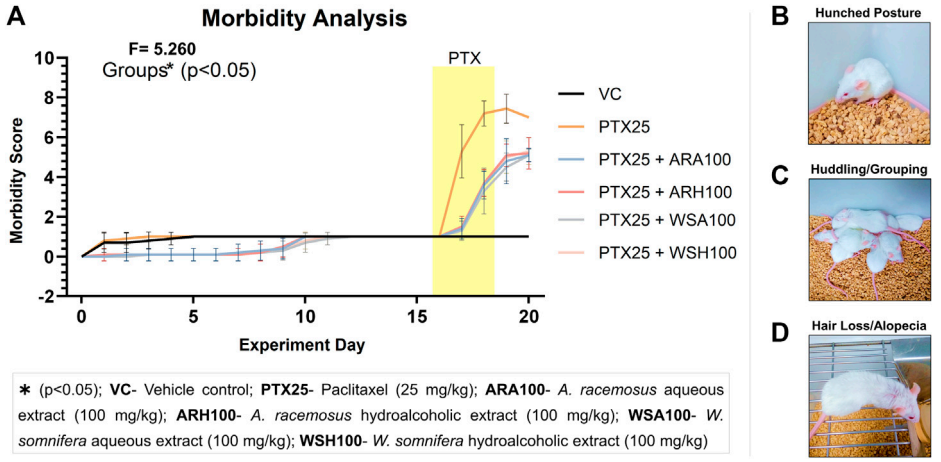

FIGURE 3 | Morbidity analysis. The figure represents that ARA, ARH, WSA, and WSH significantly prevented PTX-induced morbidity. **(A)** shows the graphical representation of morbidity score based on observations of mice. These observations included reduced activity and relocation, hunched posture **(B)**, huddling/grouping **(C)**, hair loss/alopecia **(D)** that simulated clinical adverse effects of PTX. The morbidity score of each group was calculated as the average of the sum of all the parameters of each mouse of the group. Therefore, more the score more would be the morbidity signs in mice. The yellow patch depicts the duration of PTX dosing on 16th, 17th, and 18th day of the experiment. The graph shows that consecutive dosing of PTX (25 mg/kg) increases morbidity score in mice from 16th day up to 20th day of the experiment. Pre-administration of botanical extracts ARA, ARH, WSA, and WSH at 100 mg/kg dose 15 days prior to PTX dosing significantly ($p < 0.05$) restricts the increased morbidity score. The data points are represented as mean ± SD with n = 10.

mitigation of cytokine alterations. The increased plasma level of G-CSF is well correlated with cyclic neutropenia clinically. The neutrophil count was found to be inversely proportional to the plasma G-CSF levels (Watari et al., 1989). The present study also demonstrated the PTX-induced neutropenia accompanied by the increased plasma level of G-CSF. Both of these parameters were found to reverse in all the adjuvant groups with AR and WS extracts. Furthermore, a clinical study reported an increase in IL-6, GM-CSF, IFN-γ levels in breast cancer patients undergoing PTX treatment (Tsavaris et al., 2002). The results of this study also support the significant increase in IL-6 and GM-CSF on PTX administration that was found to be normalised by WS. However, the increase in IFN-γ remained non-significant in PTX alone group.

TNF-α plays a central role in physiological homeostasis by regulating immunity (Silke and Hartland 2013). During an inflammatory condition, TNF-α maintains the persistence of hematopoietic stem cells and ensures myeloid regeneration (Yamashita and Passegué 2019). PTX administration triggered TNF-α expression that was found to be enhanced by ARA extract to maintain regeneration of blood cells matured from myeloid lineage. ARA extract also synergistically increased the expression of IL-17A that contributes to granulopoiesis and stimulates mobilization of mature granulocytes into the circulation (Krstic et al., 2012; Mojsilović et al., 2015). ARH extract facilitated the expression of IL-2 and IL-3 that promotes T-cell proliferation and granulocyte colony formation respectively (Groopman, Molina, and Scadden 1989; Murphy 1993; Metcalf 2008).

The results of present study suggested a significant increase in plasma levels of MCP-1 induced by PTX. The MCP-1 is reported for regulating monocyte infiltration from peripheral blood to surrounding tissue through vascular endothelium as an inflammatory response (Deshmane et al., 2009). Moreover, PTX is also known to trigger inflammation mediated through pro-inflammatory cytokines (Ilinskaya, Dobrovolskaia, and McNeil 2012). This underlines the possibility of PTX to induce monocyte depletion in peripheral blood as a result of inflammatory response through MCP-1. WS on the other hand reduces PTX-induced increase in MCP-1 levels and may contribute to maintaining monocyte homeostasis in peripheral blood. Additionally, WS reduced the expression of MIP-1α that inhibits the proliferation of hematopoietic stem cells (Cook 1996) and AR upregulated MIP-1β that reverses the myelosuppressive effect of MIP-1α (Broxmeyer et al., 1993). These results indicate the corrective measures of AR and WS in PTX-induced myelosuppression.

PTX induces IL-1β overexpression that subsequently promotes the invasiveness of malignant cells. Blocking IL-1β pathway using IL-1 receptor antagonist followed by PTX therapy slightly inhibits tumor growth (Voloshin et al., 2015). Therefore, an adjuvant that inhibits IL-1 cytokines along with PTX would be beneficial. The results of this study showed a significant reduction of IL-1α and IL-1β by AR and WS extracts induced by PTX. This indicates adjuvant potential of AR and WS in cancer therapeutics.

AR and WS Ameliorate PTX-induced Morbidity

The morbidity implications of PTX such as fatigue, peripheral neuropathy, hair loss, pain in muscles and joints were also restricted by AR and WS. Clinically, the increase in IL-6 and IL-10 on PTX administration is correlated with joint pain and

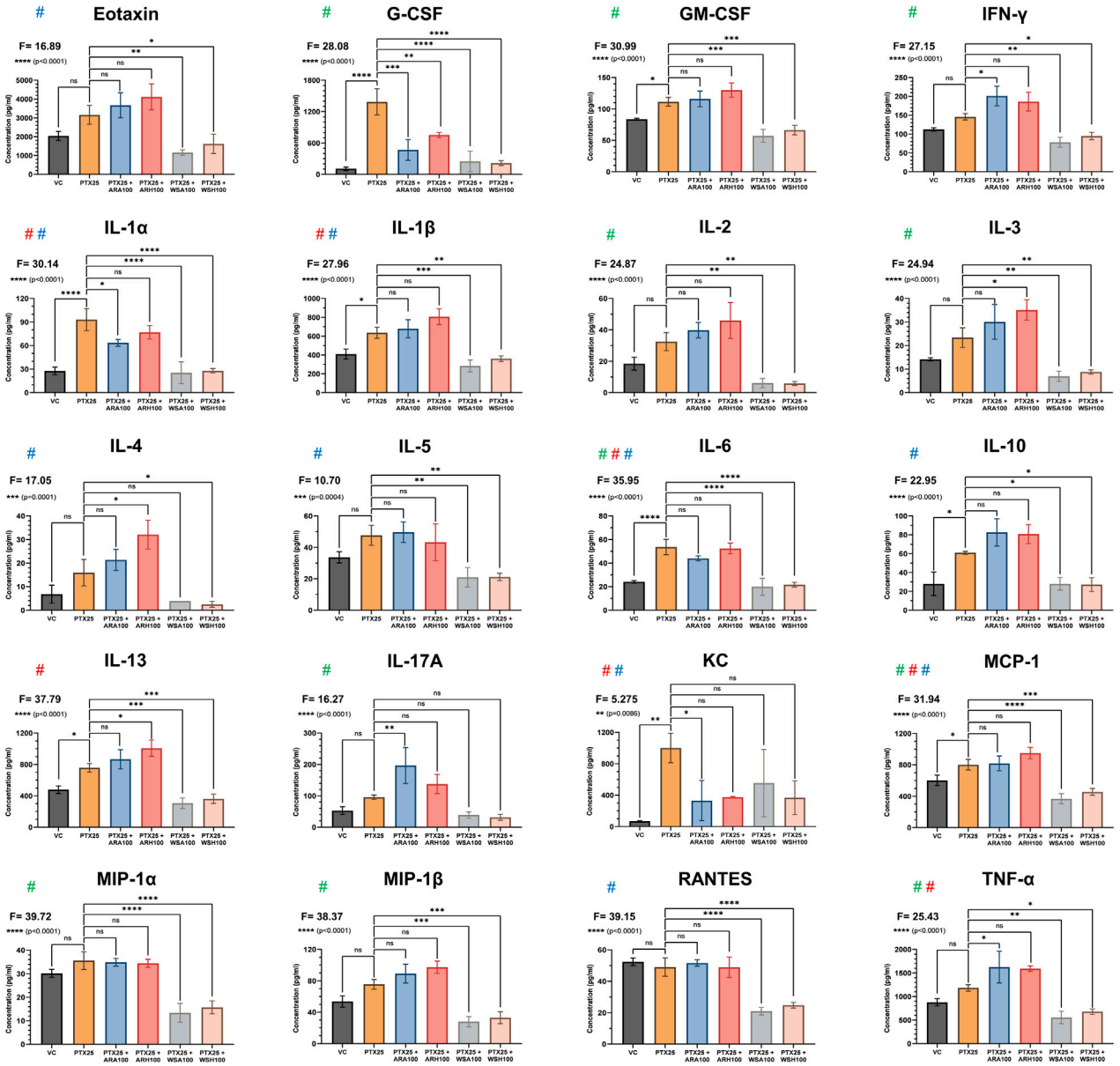

VC- Vehicle control; **PTX25**- Paclitaxel (25 mg/kg); **ARA100**- *A. racemosus* aqueous extract (100 mg/kg); **ARH100**- *A. racemosus* hydroalcoholic extract (100 mg/kg); **WSA100**- *W. somnifera* aqueous extract (100 mg/kg); **WSH100**- *W. somnifera* hydroalcoholic extract (100 mg/kg); **ns**- non-significant; ✱ ($p \leq 0.05$); ✱✱ ($p \leq 0.01$); ✱✱✱ ($p \leq 0.001$); ✱✱✱✱ ($p \leq 0.0001$); # Hematopoietic cytokines; # Inflammatory cytokines; # Morbidity cytokines

FIGURE 4 | Cytokine profiling. The figure shows that ARA, ARH, WSA, and WSH extracts modulated the plasma levels of cytokines altered by PTX-administration with different statistical significance (**p = 0.0086 to ****p < 0.0001). The cytokines are categorized by their involvement in the biological processes such as hematopoiesis, inflammation, and morbidity signs (fatigue, peripheral neuropathy, hair loss, and pain in muscles and joints). PTX administration (25 mg/kg) for three consecutive days significantly altered the plasma levels of cytokines. Pre-administration of ARA (G-CSF, IL-1α, and KC) and ARH (G-CSF) extracts (100 mg/kg) reversed the expressions of cytokines induced by PTX. Pre-administration of WSA and WSH extracts (100 mg/kg) normalized the PTX-altered cytokine levels comparable to that of VC group. The data points are represented as mean ± SD with n = 6.

fatigue respectively in cancer patients (Pusztai et al., 2004). Our study showed the increased morbidity score for hunched posture and reduced activity due to joint pain and fatigue respectively in mice. It was also confirmed by the increased levels of IL-6 and IL-10 in mouse plasma after PTX administration. WS significantly reduced the observed morbidity and plasma levels of IL-6 and IL-10 in mice.

Cytokine-induced inflammation is an established physiological link between fatigue and pain (Louati and Berenbaum 2015; Karshikoff, Sundelin, and Lasselin 2017). On the other hand,

cancer and chemotherapy-associated persistent fatigue is correlated with the increased levels of IL-1 and IL-6 (Bower 2014, 2007). Pain in muscles and joints is also associated with pro-inflammatory cytokines viz. IL-1 and IL-6 that acts either through sensory neurons or prostaglandin mediators (Ren and Torres 2009; Schaible 2014). The AR and WS extracts have ameliorated PTX-induced signs of fatigue (decreased wandering of mice in cages) and pain (hunched posture) that is evident by decreased plasma levels of IL-1 and IL-6. The patients with joint pain due to musculoskeletal disorder found to have greater levels of eotaxin (J. Singh, Noorbaloochi, and Knutson 2017). Therefore, reduction in hunched posture by WS may also be through downregulation of eotaxin as revealed in our study.

The signs of peripheral neuropathy such as numbness and weakness in mice were observed by abnormal behavior and lack of relocation on PTX-administration (Cavaletti et al., 1995; Höke 2012). The peripheral neuropathy is reported to be associated with MCP-1 induction (Zhang et al., 2013), IL-1β release (Hangping et al., 2020; Starobova et al., 2021), and high levels of IL-6 (Zheng et al., 2021). Both the extracts of WS significantly reduced the signs of peripheral neuropathy accompanied by reduction in PTX-induced high levels of MCP-1, IL-1β, and IL-6. Furthermore, KC was found to have a central role in the pathophysiological process of peripheral neuropathy also evident by a reduction in neuropathic pain upon pharmacological blockade of KC receptor-CXCR2 by the selective antagonist (Manjavachi et al., 2014; Piotrowska et al., 2019). ARA significantly reduced the increased levels of KC thereby signs of peripheral neuropathy induced by PTX. The prevention of chemotherapy-induced peripheral neuropathy is correlated with the active IL-4/STAT6 signaling pathway (Shi et al., 2018). Therefore, the reduced sign of peripheral neuropathy in mice on administration of ARH was evident by significant increase in plasma levels of IL-4. In addition, the chemokine RANTES is directly associated with the neuropathic pain (Liou et al., 2013). Though PTX was unable to induce RANTES in mice, WSA and WSH significantly reduced the RANTES expression. Therefore, the role of WS in reducing the neuropathic pain by RANTES depletion is worth investigating.

Chemotherapy-induced alopecia remains a major concern in cancer therapeutics (West 2017). IL-1α contributes to inflammatory alopecia (hair loss) by inhibiting the proliferation of hair follicles (Harmon and Nevins 1993). High serum levels of IL-4, IL-5, and IL-6 are also reported in patients with alopecia (Ito et al., 2020). AR significantly decreased IL-1α whereas WS significantly decreased IL-1α, IL-4, IL-5, and IL-6 in mouse plasma. This implies the possible function of aforementioned cytokines in preventing PTX-induced alopecia by AR and WS.

Implications in Clinical Management of Cancer

The *Rasayana* effect implies the rejuvenating and adaptogenic property (Saggam et al., 2021). It is an ability to achieve physiological homeostasis to restore health (Rege et al., 1999). The *Rasayana* effects of AR and WS are evident by exhibiting rejuvenating and adaptogenic potential endorsed by Ayurveda (Chulet and Pradhan 2009). The present study helped to generate scientific evidence of the *Rasayana* concept that emphasizes on strengthening physiological homeostasis by preventing myelosuppression and morbidity (Balasubramani et al., 2011). It also highlighted the importance of Ayurveda principles and recommended dosage regimen to achieve desired effects.

A couple of studies depicted the antitumor activities of AR with or without clinically utilised chemotherapeutic drugs (Mitra et al., 2012; Benil et al., 2020). Similarly, our team has previously mapped several pharmacological activities of WS reported in various cancer models indicating its ability to influence the classical hallmarks of cancer (Saggam et al., 2020). The clinical benefits of WS have been reported wherein marked improvement in quality of life was seen in cancer patients undergoing PTX-based chemotherapy regimen (Biswal et al., 2013). These results suggest a potential role of an Integrative Oncology approach using Ayurveda-based therapeutic adjuvants in mitigating the adverse effects of chemotherapy (Winters 2006; Saggam et al., 2020). However, the mechanism(s) underlying these clinical observations have not been well-studied.

The preclinical mouse model employed in our study has been utilised for investigating the pathophysiology of PTX-induced myelosuppression (Ray et al., 2011). Several studies have indicated that this experimental model recapitulates the clinical scenarios in this with reference to biochemical parameters, immuno-regulation, cytokine levels, inflammation and overall behaviour (Burke and Balkwill 1996; Frese and Tuveson 2007; Höke 2012; Lampreht Tratar, Horvat, and Cemazar 2018; Ireson et al., 2019).

Previously published clinical reports on PTX-induced changes in myelosuppressive immune response allow us to intuitively extrapolate our preclinical results into clinical translation. For example, patients with cyclic neutropenia showed elevated levels of G-CSF in neutropenic phase (Watari et al., 1989). In addition, breast cancer patients undergoing PTX treatment have been reported to demonstrate increased levels of GM-CSF in blood (Tsavaris et al., 2002). Indeed, the results of our preclinical study in mice are in alignment with these reported clinical scenarios. In this study, we have observed that the AR and WS extracts prevented neutropenia by normalizing the levels of colony stimulating factors (namely G-CSF and GM-CSF) which were elevated by PTX. Therefore, it is plausible to postulate that co-administration of AR and WS extracts with colony-stimulating factors may have salutary effects in managing chemotherapy-induced myelosuppression. Furthermore, carefully designed molecular studies will shed light on the mechanism(s) underlying the observed protective effect of AR and WS extracts in PTX-induced myelosuppression.

In addition, we observed alterations in cytokine levels associated with immune response which are in alignment with previously reported clinical literature. Marked increase in IL-6 and IL-10 levels subsequent to PTX administration in cancer patients have been reported to be associated with joint pain and fatigue (Tsavaris et al., 2002; Pusztai et al., 2004). In our study, WS extract was found to mitigate PTX-induced elevation of IL-6 and IL-10 levels and restored normal posture (reduced stiffness that occurred due to joint pain) and activity (reduced tiredness that occurred due to fatigue) in mice. In concurrence with the clinical reports from cancer patients, we similarly observed an increase in IL-10 levels after PTX dosing (Pusztai et al., 2004). Furthermore, we observed that the PTX-induced elevation in IL-

10 level was not observed when mice were dosed with WS extract prior to or during the course of PTX regimen.

Our study indicates that AR and WS extract offer protective effects against PTX-induced myelosuppression as indicated by experimental observations related to total leukocytes, neutrophils, cytokines and morbidity in mice. These promising preclinical observations potentially lay the foundation for well-designed clinical studies to investigate beneficial effects of Ayurveda-based *Rasayana* botanicals in cancer patients undergoing PTX-associated chemotherapy regimens. Such clinical studies along with molecular pharmacology investigations will be needed in future for exploring the promise of Ayurveda-based botanicals as therapeutic adjuvants in cancer management.

CONCLUSION

In conclusion, the present study revealed that AR and WS markedly increased the tolerance of mice towards PTX administration. The clinical adverse effects of PTX such as myelosuppression, fatigue (extreme tiredness), hair loss, peripheral neuropathy (numbness and weakness), pain in muscles and joints etc. can be managed by pre-administration of AR and WS (Markman 2003). Thus, AR and WS are promising cancer adjuvants to enhance the efficacy and reduce the adverse effects of chemotherapy. Further studies on the effects of AR and WS on PTX-induced myelosuppression in a cancer model are needed. Our study suggests well-designed clinical trials with a focus on molecular mechanisms as a future step towards safer and more effective cancer management.

DATA AVAILABILITY STATEMENT

The original contributions presented in the study are included in the article/**Supplementary Material**, further inquiries can be directed to the corresponding author.

ETHICS STATEMENT

The animal study was reviewed and approved by the Institutional Animal Ethics Committee of Serum Institute of India Pvt. Ltd.

AUTHOR CONTRIBUTIONS

AS: Protocol development, experimentation, biochemistry, ethnopharmacology, molecular mechanisms, data analysis, illustrations, manuscript writing PK: Protocol development, experimentation, molecular mechanism, manuscript writing SS: Protocol development, experimentation, manuscript writing DP: Protocol development, pharmacology, manuscript writing MG: Protocol development, pharmacology, molecular mechanism, manuscript writing GT: Protocol development, clinical aspect of Ayurveda, ethnopharmacology, manuscript writing. KJ: Molecular mechanism, ethnopharmacology, manuscript writing SG: Pharmacology, manuscript writing BP: Conceptualization, protocol development, biochemistry, ethnopharmacology, Ayurveda, biomedical science, manuscript writing.

FUNDING

This study was supported by Ministry of Ayush, Govt. of India (GoI-A-757) and Savitribai Phule Pune University.

ACKNOWLEDGMENTS

The authors highly acknowledge funding support from Ministry of Ayush, Govt. of India. Authors are grateful to Serum Institute of India Pvt. Ltd. for infrastructural support and Pharmanza Herbal Pvt. Ltd. for offering botanical extracts. Authors acknowledge Dr Santosh Dixit for his crucial inputs in clinical translation of the results. AS extends his gratitude towards Dr Sham Diwanay, Dr Preeti Chavan-Gautam and Dr Swapnil Borse for their crucial scientific contributions in this study. AS also thanks Ms Madhura Joshi, Ms Sanchita Sangle, and Ms Nupur Agrawal for thier edits in the manuscript. All the authors express their gratitude to Late Dr Suresh Jadhav from Serum Institute of India Pvt. Ltd. who was one of the investigators since conceptualization of this project. We dedicate this article in his memory!

SUPPLEMENTARY MATERIAL

The Supplementary Material for this article can be found online at: https://www.frontiersin.org/articles/10.3389/fphar.2022.835616/full#supplementary-material

Supplementary Data Sheet 1 | The scoring system of each parameter.

Supplementary Data Sheet 2 | The morbidity score (0–3) of each parameter/animal/group/day.

Supplementary Data Sheet 3 | The summation of score of all five parameters depicted as total morbidity score of each animal/group/day.

Supplementary Data Sheet 4 | The mean and standard deviation of total morbidity score of each group/day.

REFERENCES

Agarwal, R., Diwanay, S., Patki, P., and Patwardhan, B. (1999). Studies on Immunomodulatory Activity of Withania Somnifera (Ashwagandha) Extracts in Experimental Immune Inflammation. *J. Ethnopharmacol* 67 (1), 27–35. doi:10.1016/S0378-8741(99)00065-3

Alok, S., Jain, S., Verma, A., Kumar, M., Mahor, A., and Sabharwal, M. (2013). Plant Profile, Phytochemistry and Pharmacology of Asparagus Racemosus (Shatavari): A Review. *Asian Pac. J. Trop. Dis.* doi:10.1016/S2222-1808(13)60049-3

Anesthesia Guidelines Mice (2021). Anesthesia Guidelines: Mice. Available at: https://www.researchservices.umn.edu/services-name/research-animal-resources/research-support/guidelines/anesthesia-mice.

Arruebo, M., Vilaboa, N., Sáez-Gutierrez, B., Lambea, J., Tres, A., Valladares, M., et al. (2011). Assessment of the Evolution of Cancer Treatment Therapies. *Cancers (Basel)* 3 (3), 3279–3330. doi:10.3390/cancers3033279

Balasubramani, S. P., Venkatasubramanian, P., Kukkupuni, S. K., and Patwardhan, B. (2011). Plant-Based Rasayana Drugs from Ayurveda. *Chin. J. Integr. Med.* 17, 88–94. doi:10.1007/s11655-011-0659-5

Banerjee, R., and Prasad, V. (2020). Are Observational, Real-World Studies Suitable to Make Cancer Treatment Recommendations? *JAMA Netw. Open* 3 (7), e2012119. doi:10.1001/jamanetworkopen.2020.12119

Bani, S., Gautam, M., Sheikh, F. A., Khan, B., Satti, N. K., Suri, K. A., et al. (2006). Selective Th1 Up-Regulating Activity of Withania Somnifera Aqueous Extract in an Experimental System Using Flow Cytometry. *J. Ethnopharmacol* 107 (1), 107–115. doi:10.1016/j.jep.2006.02.016

Banipal, R. P. S., Singh, H., and Singh, B. (2017). Assessment of Cancer-Related Fatigue Among Cancer Patients Receiving Various Therapies: A Cross-Sectional Observational Study. *Indian J. Palliat. Care* 23 (2), 207–211. doi:10.4103/IJPC.IJPC_135_16

Batchelder, P., Kinney, R. O., Demlow, L., and Lynch, C. B. (1983). Effects of Temperature and Social Interactions on Huddling Behavior in Mus Musculus. *Physiol. Behav.* 31 (1), 97–102. doi:10.1016/0031-9384(83)90102-6

Benil, P. B., Nimisha, P., Arokiyaraj, S., Rajakrishnan, R., Alfarhan, A., and AlAnsari, A. (2020). "Antitumour and Anti-haematotoxic Activity of Asparagus Racemosus L Total Dissolved Solids in Co-administration with Cyclophosphamide in Mice." *J. King Saud Univ. - Sci.* 32 (5), 2582–2589. doi:10.1016/j.jksus.2020.04.016

Biswal, B. M., Sulaiman, S. A., Ismail, H. C., Zakaria, H., and Musa, K. I. (2013). Effect of Withania Somnifera (Ashwagandha) on the Development of Chemotherapy-Induced Fatigue and Quality of Life in Breast Cancer Patients. *Integr. Cancer Ther.* 12 (4), 312–322. doi:10.1177/1534735412464551

Borse, S., Joshi, M., Saggam, A., Bhat, V., Walia, S., Marathe, A., et al. (2021). Ayurveda Botanicals in COVID-19 Management: An In Silico Multi-Target Approach. *Plos One* 16, e0248479. doi:10.1371/journal.pone.0248479

Bower, J. E. (2014). Cancer-Related Fatigue--Mechanisms, Risk Factors, and Treatments. *Nat. Rev. Clin. Oncol.* 11 (10), 597–609. doi:10.1038/nrclinonc.2014.127

Bower, J. E. (2007). Cancer-Related Fatigue: Links with Inflammation in Cancer Patients and Survivors. *Brain Behav. Immun.* 21 (7), 863–871. doi:10.1016/j.bbi.2007.03.013

Broxmeyer, H. E., Cooper, S., Lu, L., Maze, R., Beckmann, M. P., Cerami, A., et al. (1993). Comparative Analysis of the Human Macrophage Inflammatory Protein Family of Cytokines (Chemokines) on Proliferation of Human Myeloid Progenitor Cells. Interacting Effects Involving Suppression, Synergistic Suppression, and Blocking of Suppression. *J. Immunol.* 150 (8 Pt 1), 3448–3458.

Burke, F., and Balkwill, F. R. (1996). Cytokines in Animal Models of Cancer. *Biotherapy* 8 (3), 229–241. doi:10.1007/BF01877209

Cavaletti, G., Tredici, G., Braga, M., and Tazzari, S. (1995). Experimental Peripheral Neuropathy Induced in Adult Rats by Repeated Intraperitoneal Administration of Taxol. *Exp. Neurol.* 133 (1), 64–72. doi:10.1006/exnr.1995.1008

Chopra, D., RehanRehan, H. S., Sharma, V., and Mishra, R. (2016). Chemotherapy-Induced Adverse Drug Reactions in Oncology Patients: A Prospective Observational Survey. *Indian J. Med. Paediatr. Oncol.* 37 (1), 42–46. doi:10.4103/0971-5851.177015

Chulet, R., and Pradhan, P. (2009). A Review on Rasayana. *Pharmacognosy Rev.* 3 (6), 229–234.

Clinical Signs of Pain and Disease in Laboratory Animals (2021). Clinical Signs of Pain and Disease in Laboratory Animals. Available at: https://your.yale.edu/policies-procedures/guides/4446-clinical-signs-pain-and-disease-laboratory-animals.

Cook, D. N. (1996). The Role of MIP-1 Alpha in Inflammation and Hematopoiesis. *J. Leukoc. Biol.* 59 (1), 61–66. doi:10.1002/jlb.59.1.61

Dale, D. C. (2002). Colony-stimulating Factors for the Management of Neutropenia in Cancer Patients. *Drugs* 62 (Suppl. 1), 1–15. doi:10.2165/00003495-200262001-00001

Deshmane, S. L., Kremlev, S., Amini, S., and Sawaya, B. E. (2009). Monocyte Chemoattractant Protein-1 (MCP-1): An Overview. *J. Interferon Cytokine Res.* 29 (6), 313–326. doi:10.1089/jir.2008.0027

Diwanay, S., Chitre, D., and Patwardhan, B. (2004). Immunoprotection by Botanical Drugs in Cancer Chemotherapy. *J. Ethnopharmacol* 90 (1), 49–55. doi:10.1016/j.jep.2003.09.023

Dubey, S., Yoon, H., Cohen, M. S., Nagarkatti, P., Nagarkatti, M., and Karan, D. (2018). Withaferin a Associated Differential Regulation of Inflammatory Cytokines. *Front. Immunol.* 9 (FEB), 195. doi:10.3389/fimmu.2018.00195

Frese, K. K., and Tuveson, D. A. (2007). Maximizing Mouse Cancer Models. *Nat. Rev. Cancer* 7 (9), 645–658. doi:10.1038/nrc2192

Friberg, L. E., Henningsson, A., Maas, H., Nguyen, L., and Karlsson, M. O. (2002). Model of Chemotherapy-Induced Myelosuppression with Parameter Consistency across Drugs. *J. Clin. Oncol.* 20 (24), 4713–4721. doi:10.1200/JCO.2002.02.140

Friberg, L. E., and Karlsson, M. O. (2003). Mechanistic Models for Myelosuppression. *Invest. New Drugs* 21 (2), 183–194. doi:10.1023/a:1023573429626

Gautam, M., Diwanay, S., Gairola, S., Shinde, Y., Patki, P., and Patwardhan, B. (2004b). Immunoadjuvant Potential of Asparagus Racemosus Aqueous Extract in Experimental System. *J. Ethnopharmacol* 91 (2–3), 251–255. doi:10.1016/j.jep.2003.12.023

Gautam, M., Diwanay, S. S., Gairola, S., Shinde, Y. S., Jadhav, S. S., and Patwardhan, B. K. (2004a). Immune Response Modulation to DPT Vaccine by Aqueous Extract of Withania Somnifera in Experimental System. *Int. Immunopharmacol* 4 (6), 841–849. doi:10.1016/j.intimp.2004.03.005

Globocan 2020 Fact Sheet (2020). *Global Cancer Observatory: Cancer Today*, 419. Available at: https://gco.iarc.fr/today/data/factsheets/populations/900-world-fact-sheets.pdf.

Gogte, B. K. (2000). *Ayurvedic Pharmacology and Therapeutic Uses of Medicinal Plants (Dravyagunavidnyan-Translation)*. Mumbai: The Academic Team of Bharatiya Vidya Bhavan's SPARC.

Groopman, J. E., Molina, J. M., and Scadden, D. T. (1989). Hematopoietic Growth Factors. Biology and Clinical Applications. *N. Engl. J. Med.* 321 (21), 1449–1459. doi:10.1056/NEJM198911233212106

Halper, J. (2010). Growth Factors as Active Participants in Carcinogenesis: A Perspective. *Vet. Pathol.* 47 (1), 77–97. doi:10.1177/0300985809352981

Hangping, Z., Ling, H., Lijin, J., Wenting, Z., Xiaoxia, L., Qi, Z., et al. (2020). The Preventive Effect of IL-1beta Antagonist on Diabetic Peripheral Neuropathy. *Endocr. Metab. Immune Disord. Drug Targets* 20 (5), 753–759. doi:10.2174/1871530319666191022114139

Harmon, C. S., and Nevins, T. D. (1993). IL-1 Alpha Inhibits Human Hair Follicle Growth and Hair Fiber Production in Whole-Organ Cultures. *Lymphokine Cytokine Res.* 12 (4), 197–203.

Höke, A. (2012). Animal Models of Peripheral Neuropathies. *Neurotherapeutics* 9 (2), 262–269. doi:10.1007/s13311-012-0116-y

Hu, W., Sung, T., Jessen, B. A., Thibault, S., Finkelstein, M. B., Khan, N. K., et al. (2016). Mechanistic Investigation of Bone Marrow Suppression Associated with Palbociclib and its Differentiation from Cytotoxic Chemotherapies. *Clin. Cancer Res.* 22 (8), 2000–2008. doi:10.1158/1078-0432.CCR-15-1421

Ilinskaya, A., Dobrovolskaia, M., and Scott, M. (2012). Induction of Pro-inflammatory Cytokines by Traditional and Nano Formulations of Anti-cancer Drug Paclitaxel (161.11). *J. Immunol.* 188 (1 Suppl. ment), 161–11161. Available at: https://www.jimmunol.org/content/188/1_Supplement/161.11.

Ireson, C. R., Alavijeh, M. S., Palmer, A. M., Fowler, E. R., and JonesJones, H. J. (2019). The Role of Mouse Tumour Models in the Discovery and Development of Anticancer Drugs. *Br. J. Cancer* 121 (2), 101–108. doi:10.1038/s41416-019-0495-5

Ito, T., Kageyama, R., Nakazawa, S., and Honda, T. (2017). "Understanding the Significance of Cytokines and Chemokines in the Pathogenesis of Alopecia Areata." *Exp. Dermatol.* 29 (8), 726–732. doi:10.1111/exd.14129

Karshikoff, B., Sundelin, T., and Lasselin, J. (2017). Role of Inflammation in Human Fatigue: Relevance of Multidimensional Assessments and Potential Neuronal Mechanisms. *Front. Immunol.* 8, 21. doi:10.3389/fimmu.2017.00021

Krstic, A., Mojsilovic, S., Jovcic, G., and Bugarski, D. (2012). The Potential of Interleukin-17 to Mediate Hematopoietic Response. *Immunol. Res.* 52 (1–2), 34–41. doi:10.1007/s12026-012-8276-8

Lampreht Tratar, U., Horvat, S., and Cemazar, M. (2018). Transgenic Mouse Models in Cancer Research. *Front. Oncol.* 8, 268. doi:10.3389/fonc.2018.00268

Lele, R. D. (2010). Beyond Reverse Pharmacology: Mechanism-Based Screening of Ayurvedic Drugs. *J. Ayurveda Integr. Med.* 1 (4), 257–265. doi:10.4103/0975-9476.74435

Liou, J. T., Mao, C. C., Ching-Wah Sum, D., Lai, Y. S., Li, J. C., and Day, Y. J. (2013). Peritoneal Administration of Met-RANTES Attenuates Inflammatory and Nociceptive Responses in a Murine Neuropathic Pain Model. *J. Pain* 14 (1), 24–35. doi:10.1016/j.jpain.2012.09.015

Louati, K., and Berenbaum, F. (2015). Fatigue in Chronic Inflammation - a Link to Pain Pathways. *Arthritis Res. Ther.* 17 (October), 254. doi:10.1186/s13075-015-0784-1

Manjavachi, M. N., Costa, R., QuintãoCalixto, N. L., and Calixto, J. B. (2014). The Role of Keratinocyte-Derived Chemokine (KC) on Hyperalgesia Caused by Peripheral Nerve Injury in Mice. *Neuropharmacology* 79 (April), 17–27. doi:10.1016/j.neuropharm.2013.10.026

Markman, M. (2003). Managing Taxane Toxicities. *Support Care Cancer* 11 (3), 144–147. doi:10.1007/s00520-002-0405-9

Marupudi, N. I., Han, J. E., Li, K., Renard, V. M., Tyler, B. M., and Brem, H. (2007). Paclitaxel: A Review of Adverse Toxicities and Novel Delivery Strategies. *Expert Opin. Drug Saf.* 6, 609–621. doi:10.1517/14740338.6.5.609

Maxwell, M. B., and Maher, K. E. (1992). Chemotherapy-Induced Myelosuppression. *Semin. Oncol. Nurs.* 8 (2), 113–123. doi:10.1016/0749-2081(92)90027-z

Metcalf, D. (2008). Hematopoietic Cytokines. *Blood* 111 (2), 485–491. doi:10.1182/blood-2007-03-079681

Mitra, S. K., Prakash, N. S., and Sundaram, R. (2012). Shatavarins (Containing Shatavarin IV) with Anticancer Activity from the Roots of Asparagus Racemosus. *Indian J. Pharmacol.* 44 (6), 732–736. doi:10.4103/0253-7613.103273

Mojsilović, S., Jauković, A., Santibañez, J. F., and Bugarski, D. (2015). Interleukin-17 and its Implication in the Regulation of Differentiation and Function of Hematopoietic and Mesenchymal Stem Cells. *Mediators Inflamm.* 2015, 470458. doi:10.1155/2015/470458

Murphy, M. J., Jr. (1993). The Hematopoietic Cytokines: An Overview. *Toxicol. Pathol.* 21 (2), 229–230. doi:10.1177/019262339302100215

Paclitaxel Taxol (2020). Paclitaxel Taxol. Available at: https://breastcancernow.org/information-support/facing-breast-cancer/going-through-treatment-breast-cancer/chemotherapy/paclitaxel-taxol.

Patwardhan, B., Mutalik, G., and Tillu, G. (2015). *Integrative Approaches for Health: Biomedical Research, Ayurveda and Yoga. Integrative Approaches for Health: Biomedical Research, Ayurveda and Yoga*. 1st ed. Amsterdam: Elsevier. doi:10.1016/C2013-0-19395-6

Patwardhan, B. (2014). Bridging Ayurveda with Evidence-Based Scientific Approaches in Medicine. *EPMA J.*, 5. doi:10.1186/1878-5085-5-19

Piotrowska, A., Rojewska, E., Pawlik, K., Kreiner, G., Ciechanowska, A., Makuch, W., et al. (2019). Pharmacological Blockade of Spinal CXCL3/CXCR2 Signaling by NVP CXCR2 20, a Selective CXCR2 Antagonist, Reduces Neuropathic Pain Following Peripheral Nerve Injury. *Front. Immunol.* 10, 2198. doi:10.3389/fimmu.2019.02198

Puhalla, S., Bhattacharya, S., and Davidson, N. E. (2012). Hematopoietic Growth Factors: Personalization of Risks and Benefits. *Mol. Oncol.* 6 (2), 237–241. doi:10.1016/j.molonc.2012.03.001

Pusztai, L., Mendoza, T. R., ReubenReuben, J. M., Martinez, M. M., Willey, J. S., Lara, J., et al. (2004). Changes in Plasma Levels of Inflammatory Cytokines in Response to Paclitaxel Chemotherapy. *Cytokine* 25 (3), 94–102. doi:10.1016/j.cyto.2003.10.004

Raut, A. A., Rege, N. N., Tadvi, F. M., Solanki, P. V., Kene, K. R., Shirolkar, S. G., et al. (2012). Exploratory Study to Evaluate Tolerability, Safety, and Activity of Ashwagandha (Withania Somnifera) in Healthy Volunteers. *J. Ayurveda Integr. Med.* 3 (3), 111–114. doi:10.4103/0975-9476.100168

Ray, M. A., Trammell, R. A., Verhulst, S., Ran, S., and Toth, L. A. (2011). Development of a Mouse Model for Assessing Fatigue during Chemotherapy. *Comp. Med.* 61 (2), 119–130. doi:10.1038/nrurol.2011.14

Rege, N. N., Thatte, U. M., and Dahanukar, S. A. (1999). Adaptogenic Properties of Six Rasayana Herbs Used in Ayurvedic Medicine, *Phytother Res.*, 13. 2-S, 275–291. doi:10.1002/(SICI)1099-1573(199906)13:4<275::AID-PTR510>3.0.CO;2-S

Regnard, C., and Kindlen, M. (2018). Chemotherapy: Side Effects. *Support. Palliat. Care Cancer*, 39–41. doi:10.1201/9781315378596-13

Ren, K., and Torres, R. (2009). Role of Interleukin-1beta during Pain and Inflammation. *Brain Res. Rev.* 60 (1), 57–64. doi:10.1016/j.brainresrev.2008.12.020

Saggam, A., Limgaokar, K., Borse, S., Chavan-Gautam, P., Dixit, S., Tillu, G., et al. (2021). Withania Somnifera (L.) Dunal: Opportunity for Clinical Repurposing in COVID-19 Management. *Front. Pharmacol.* 12, 623795. doi:10.3389/fphar.2021.623795

Saggam, A., Tillu, G., Dixit, S., Chavan-Gautam, P., Borse, S., Joshi, K., et al. (2020). Withania Somnifera (L.) Dunal: A Potential Therapeutic Adjuvant in Cancer. *J. Ethnopharmacol* 255 (March), 112759. doi:10.1016/j.jep.2020.112759

Schaible, H.-G. (2014). Nociceptive Neurons Detect Cytokines in Arthritis. *Arthritis Res. Ther.* 16 (5), 470. doi:10.1186/s13075-014-0470-8

Schurig, J. E., Florczyk, A. P., and Bradner, W. T. (1986). The Mouse as a Model for Predicting the Myelosuppressive Effects of Anticancer Drugs. *Cancer Chemother. Pharmacol.* 16 (3), 243–246. doi:10.1007/BF00293985

Schurig, J. E., Schlein, A., Florczyk, A. P., Farwell, A. R., and Bradner, W. T. (1985). Animal Models for Evaluating the Myelosuppressive Effects of Cancer Chemotherapeutic Agents. *Exp. Hematol.* 13 (Suppl. 1), 101–105.

Shewach, D. S., and Kuchta, R. D. (2009). Introduction to Cancer Chemotherapeutics. *Chem. Rev.* 109, 2859–2861. doi:10.1021/cr900208x

Shi, Q., Cai, X., Shi, G., Lv, X., Yu, J., and Wang, F. (2018). Interleukin-4 Protects from Chemotherapy-Induced Peripheral Neuropathy in Mice Modal via the Stimulation of IL-4/STAT6 Signaling. *Acta Cir Bras* 33 (6), 491–498. doi:10.1590/s0102-865020180060000003

Silke, J., and Hartland, E. L. (2013). "Masters, Marionettes and Modulators: Intersection of Pathogen Virulence Factors and Mammalian Death Receptor Signaling." *Curr. Opin. Immunol.* 25 (4), 436–440. doi:10.1016/j.coi.2013.05.011

Singh, J. A., Noorbaloochi, S., and Knutson, K. L. (2017). Cytokine and Neuropeptide Levels Are Associated with Pain Relief in Patients with Chronically Painful Total Knee Arthroplasty: A Pilot Study. *BMC Musculoskelet. Disord.* 18 (1), 17. doi:10.1186/s12891-016-1375-2

Singh, N., Bhalla, M., de Jager, P., and Gilca, M. (2011). An Overview on Ashwagandha: A Rasayana (Rejuvenator) of Ayurveda. *Afr. J. Tradit Complement. Altern. Med.* 8 (5 Suppl. l), 208–213. doi:10.4314/ajtcam.v8i5S.9

Starobova, H., Monteleone, M., Adolphe, C., Batoon, L., Sandrock, C. J., Tay, B., et al. (2021). Vincristine-induced Peripheral Neuropathy Is Driven by Canonical NLRP3 Activation and IL-1β Release. *J. Exp. Med.* 218 (5). doi:10.1084/jem.20201452

Tiwari, N., Gupta, V. K., Pandey, P., Patel, D. K., Banerjee, S., Darokar, M. P., et al. (2017). Adjuvant Effect of Asparagus Racemosus Willd. Derived Saponins in Antibody Production, Allergic Response and Pro-inflammatory Cytokine Modulation. *Biomed. Pharmacother.* 86 (February), 555–561. doi:10.1016/j.biopha.2016.11.087

Tsavaris, N., Kosmas, C., Vadiaka, M., Kanelopoulos, P., and Boulamatsis, D. (2002). Immune Changes in Patients with Advanced Breast Cancer Undergoing Chemotherapy with Taxanes. *Br. J. Cancer* 87 (1), 21–27. doi:10.1038/sj.bjc.6600347

Voloshin, T., Alishekevitz, D., Kaneti, L., Miller, V., Isakov, E., Kaplanov, I., et al. (2015). Blocking IL1β Pathway Following Paclitaxel Chemotherapy Slightly Inhibits Primary Tumor Growth but Promotes Spontaneous Metastasis. *Mol. Cancer Ther.* 14 (6), 1385–1394. doi:10.1158/1535-7163.MCT-14-0969

Watari, K., Asano, S., Shirafuji, N., Kodo, H., Ozawa, K., Takaku, F., et al. (1989). Serum Granulocyte Colony-Stimulating Factor Levels in Healthy Volunteers and Patients with Various Disorders as Estimated by Enzyme Immunoassay. *Blood* 73 (1), 117–122. doi:10.1182/blood.v73.1.117.bloodjournal731117

Weaver, B. A. (2014). How Taxol/Paclitaxel Kills Cancer Cells. *Mol. Biol. Cel* 25 (18), 2677–2681. doi:10.1091/mbc.E14-04-0916

West, H. J. (2017). Chemotherapy-Induced Hair Loss (Alopecia). *JAMA Oncol.* 3 (8), 1147. doi:10.1001/jamaoncol.2017.1026

Winters, M. (2006). Ancient Medicine, Modern Use: Withania Somnifera and its Potential Role in Integrative Oncology. *Altern. Med. Rev. : A J. Clin. Ther.* 11 (4), 269–277.

Yamashita, M., and Passegué, E. (2019). "TNF-α Coordinates Hematopoietic Stem Cell Survival and Myeloid Regeneration." *Cell Stem Cell* 25 (3), 357-e7. doi:10.1016/j.stem.2019.05.019

Zhang, H., Boyette-Davis, J. A., KosturakisKosturakis, A. K., Li, Y., Yoon, S. Y., Walters, E. T., et al. (2013). Induction of Monocyte Chemoattractant Protein-1 (MCP-1) and its Receptor CCR2 in Primary Sensory Neurons Contributes to Paclitaxel-Induced Peripheral Neuropathy. *J. Pain* 14 (10), 1031–1044. doi:10.1016/j.jpain.2013.03.012

Zheng, H., Sun, W., Zhang, Q., Zhang, Y., Ji, L., Liu, X., et al. (2021). Proinflammatory Cytokines Predict the Incidence of Diabetic Peripheral Neuropathy over 5 Years in Chinese Type 2 Diabetes Patients: A Prospective Cohort Study. *EClinicalMedicine* 31 (January), 100649. doi:10.1016/j.eclinm.2020.100649

Ziauddin, M., Phansalkar, N., Patki, P., Diwanay, S., and Patwardhan, B. (1996). Studies on the Immunomodulatory Effects of Ashwagandha. *J. Ethnopharmacol* 50 (2), 69–76. doi:10.1016/0378-8741(95)01318-0

Conflict of Interest: AS, PK, SS, DP, MG, and SG was employed by the Serum Institute of India Pvt. Ltd.

The remaining authors declare that the research was conducted in the absence of any commercial or financial relationships that could be construed as a potential conflict of interest.

Publisher's Note: All claims expressed in this article are solely those of the authors and do not necessarily represent those of their affiliated organizations, or those of the publisher, the editors and the reviewers. Any product that may be evaluated in this article, or claim that may be made by its manufacturer, is not guaranteed or endorsed by the publisher.

frontiers in Pharmacology

ORIGINAL RESEARCH
published: 09 March 2022
doi: 10.3389/fphar.2022.794277

Spectrum-Effect Relationship Analysis of Bioactive Compounds in *Zanthoxylum nitidum* (Roxb.) DC. by Ultra-High Performance Liquid Chromatography Mass Spectrometry Coupled With Comprehensive Filtering Approaches

Si-wei Rao[1], *Yuan-yuan Duan*[1], *Han-qing Pang*[2], *Shao-hua Xu*[1], *Shou-qian Hu*[1], *Ke-guang Cheng*[1], *Dong Liang*[1]* and *Wei Shi*[1]*

[1]State Key Laboratory for Chemistry and Molecular Engineering of Medicinal Resources, Collaborative Innovation Center for Guangxi Ethnic Medicine, School of Chemistry and Pharmaceutical Science, Guangxi Normal University, Guilin, China, [2]Institute of Translational Medicine, Medical College, Jiangsu Key Laboratory of Integrated Traditional Chinese and Western Medicine for Prevention and Treatment of Senile Diseases, Yangzhou University, Yangzhou, China

OPEN ACCESS

Edited by:
Abdul Rohman,
Gadjah Mada University, Indonesia

Reviewed by:
Ying-yuan Lu,
Peking University, China
Chang-hong Wang,
Shanghai University of Traditional Chinese Medicine, China

***Correspondence:**
Dong Liang
liangdonggxnu@163.com
Wei Shi
swv2012@163.com

Specialty section:
This article was submitted to Ethnopharmacology, a section of the journal Frontiers in Pharmacology

Received: 13 October 2021
Accepted: 31 January 2022
Published: 09 March 2022

Citation:
Rao S-w, Duan Y-y, Pang H-q, Xu S-h, Hu S-q, Cheng K-g, Liang D and Shi W (2022) Spectrum-Effect Relationship Analysis of Bioactive Compounds in Zanthoxylum nitidum (Roxb.) DC. by Ultra-High Performance Liquid Chromatography Mass Spectrometry Coupled With Comprehensive Filtering Approaches. Front. Pharmacol. 13:794277. doi: 10.3389/fphar.2022.794277

Zanthoxylum nitidum (Roxb.) DC. (ZN), with strong effects of anti-inflammation and antioxidant activities is treated as a core herb in traditional Chinese medicine (TCM) preparation for treating stomachache, toothache, and rheumatoid arthritis. However, the active ingredients of ZN are not fully clarified due to its chemical complexity. In the present study, a double spectrum–effect analysis strategy was developed and applied to explore the bioactive components in herbs, and ZN was used as an example. Here, the chemical components in ZN were rapidly and comprehensively profiled based on the mass defect filtering-based structure classification (MDFSC) and diagnostic fragment-ion-based extension approaches. Furthermore, the fingerprints of 20 batches of ZN samples were analyzed by high-performance liquid chromatography, and the anti-inflammatory and antioxidant activities of the 20 batches of ZN samples were studied. Finally, the partial least squares regression (PLSR), gray relational analysis models, and Spearman's rank correlation coefficient (SRCC) were applied to discover the bioactive compounds in ZN. As a result, a total of 48 compounds were identified or tentatively characterized in ZN, including 35 alkaloids, seven coumarins, three phenolic acids, two flavonoids, and one lignan. The results achieved by three prediction models indicated that peaks **4**, **12**, and **17** were the potential anti-inflammatory compounds in ZN, whereas peaks **3**, **5**, **7**, **12**, and **13** were involved in the antioxidant activity. Among them, peaks **4**, **5**, **7**, and **12** were identified as nitidine, chelerythrine, hesperidin, and oxynitidine by comparison with the standards and other references. The data in the current study achieved by double spectrum–effect analysis strategy had great importance to improve the quality standardization of ZN, and the method might be an efficiency tool for the discovery of active components in a complex system, such as TCMs.

Keywords: *Zanthoxylum nitidum* (Roxb.) DC., spectrum–effect relationship, chemical profiling, anti-inflammation, antioxidant activity

INTRODUCTION

Generally, traditional Chinese medicines (TCMs) achieve their therapeutic effects by initial interactions via multicomponents and multitargets. To understand how it works, it is necessary for researchers to study the relationship between TCMs' compounds and their efficacy from a holistic perspective (Jiang et al., 2010). A pharmacological study of single-compound and holistic studies of TCMs are not birds of a feather; however, their research ideas and methods cannot be generalized (Xie and Leung, 2009). Although the above studies contributed to reveal the mechanism of pharmacological efficacy of TCMs, it is also meaningful to unravel the details of TCMs' mechanism with important implications to quality control of TCMs and treatment of complicated diseases.

Zanthoxylum nitidum (Roxb.) DC. belongs to the genus *Zanthoxylum* of family Rutaceae (Seidemann, 2005; Rivera et al., 2014), and its underground roots (ZN) are used as the medicinal part recorded in the Chinese Pharmacopoeia (China Pharmacopoeia Commission, 2020). ZN has excellent curative effects, such as for the treatment of toothache, stomachache, traumatism, and rheumatoid arthritis. In daily life, ZN could be used as toothpaste and hand sanitizer. In a previous study, researchers were mainly focused on the chemical isolation and activity evaluation of ZN (Yang et al., 2008; Zhao et al., 2018; Nguyen et al., 2019). ZN extracts showed good anti-inflammatory and antioxidant activities (Xie, 2000; Liu et al., 2014). Alkaloids, the major component in ZN, have earned an increasing interest (Lu et al., 2020). Nitidine, a typical single alkaloid in ZN, has been found to have antifungal and anti-inflammatory activity (Zhang et al., 2014; Zhang et al., 2017). However, the components in ZN were very complicated, and some other active ingredients could also exist. To screen the active compounds rapidly, a comprehensive qualitative strategy and spectrum–effect relationship analysis is worth to establish.

The spectrum–effect relationship analysis is a tried-and-true method in using stoichiometric methods to figure out the connection between efficacy and components (Wang et al., 2019; Chen et al., 2021; Qiao et al., 2021). Zhang et al. developed the spectrum–effect relationship analysis strategy to discover the active compounds in Lycii Fructus; the results showed that chlorogenic acid, quercetin, kaempferol, and isorhamnetin are their potential bioactive components (Zhang et al., 2018). Moreover, a strategy-contained spectrum–effect relationship analysis was proposed to discover hepatotoxic equivalent markers from Psoraleae Fructus, and the results revealed that psoralen and isopsoralen are the hepatotoxic equivalent components (Zhang et al., 2021). The above studies have further verified the effectiveness of the spectrum–effect relationship analysis method, which were confirmed to effectively predict the active compounds in the complicated matrix.

In this study, a comprehensive filtering approach and spectrum–effect relationship were applied to discover the bioactive components in ZN (**Figure 1**). First, based on the mass defect filtering-based structure classification (MDFSC) and diagnostic fragment-ion-based extension (DFIBE) approaches, the chemical compounds of ZN were rapidly profiled by the ultrahigh-performance liquid chromatography-quadrupole time-of-flight mass spectrometry (UHPLC Q-TOF MS). Second, the fingerprints of 20 batches of ZN samples were established by high-performance liquid chromatography (HPLC), followed by similarity analysis (SA) and hierarchical cluster analysis (HCA). Furthermore, different activity tests including 3-(4,5-dimethylthiazol-2-yl)- 2,5-diphenyltetrazolium bromide (MTT) test, NO production assay, and the 2,2-diphenyl-1-picrylhydrazyl (DPPH) assay were determined, respectively. Finally, to discover the potential active compounds, the spectrum–effect relationship was modeled by chemometrics such as the partial least squares regression (PLSR), gray relational analysis (GRA), and Spearman's rank correlation coefficient (SRCC).

MATERIALS AND METHODS

Materials and Reagents

Twenty batches of ZN samples were collected from different areas in China, which contain the resource areas that are shown in **Supplementary Table S1**). The voucher specimens were identified by Prof. Dong Liang from the Department of Chemistry and Pharmacy in Guangxi Normal University and were stored in the State Key Laboratory for the Chemistry and Molecular Engineering of Medicinal Resources, Guilin, China.

Liquid chromatography mass spectrometry (LC-MS)-grade acetonitrile and methanol were bought from MEDIA (Fairfield, CT, United States). Formic acid was HPLC grade and purchased from Aladdin (Shanghai, China). Chelerythrine, diosmin, hesperidin, nitidine chloride, sanguinarine, magnoflorine, and dihydrochelerythrine, all with purity of ≥98%, were obtained from Chengdu Push Bio-Technology (Chengdu, China). Deionized water was purified using a Milli-Q water purification system (Millipore, United States). Dulbecco's modified Eagle's medium (DMEM) was produced by Gibco (Grand Island, NE, United States), and DPPH was produced by Tokyo Chemical Industry (Tokyo, Japan).

Preparation of *Zanthoxylum nitidum* (Roxb.) DC. Extracts

After being ground into powder and air-dried (filtered with a 50-mesh sieve), each ZN sample (5 g) was dissolved with 100 ml of 80% ethanol and extracted three times at 3, 2, and 1 h on a water bath at 80°C. Then a Rotavapor OSB-2200 from EYELA Co. (Tokyo, Japan) was used to remove the solvent. The extracts were powdered by an FD5-series vacuum freeze dryer (GOLD SIM, Newark, NJ, United States) and then stored for use.

Chromatographic and Mass Spectrometric Condition

Chemical Profiling of *Zanthoxylum nitidum* (Roxb.) DC. Sample by UHPLC Q-TOF MS

The comprehensive characterization of ZN samples was conducted on an Agilent 6545 UHPLC Q-TOF MS (Agilent Technologies, Santa Clara, CA, United States) with the

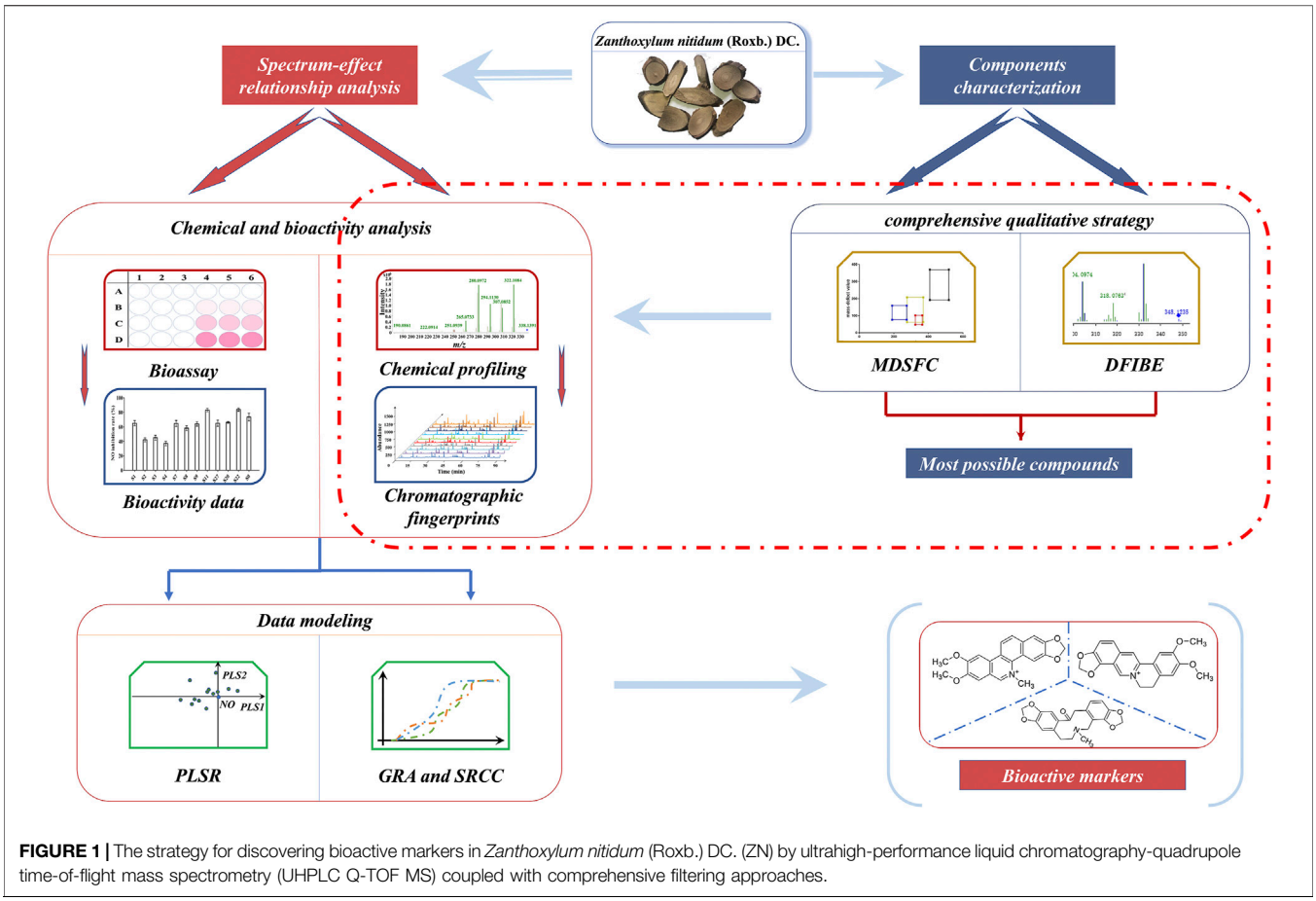

FIGURE 1 | The strategy for discovering bioactive markers in *Zanthoxylum nitidum* (Roxb.) DC. (ZN) by ultrahigh-performance liquid chromatography-quadrupole time-of-flight mass spectrometry (UHPLC Q-TOF MS) coupled with comprehensive filtering approaches.

monitoring of Agilent LC-QTOF/MS Mass Hunter Workstation Acquisition Software Version B.05.01 (Agilent Technologies, Santa Clara, CA, United States). Tested samples were separated on an Agilent Zorbax clipse Plus C18 column (2.1 × 50 mm, 1.8-μm, Agilent Corp., Santa Clara, CA, United States). The mobile phase consisted of acetonitrile (Santa Clara, CA, United States). The mobile phases were 0.1% formic acid (A) and acetonitrile (B) with the following gradient elutions: 5–15% B linear 0–3 min, 15–20% B linear 3–6 min, 20–22% B linear 6–7 min, 22% B isocratic 7–9 min, 22–26% B linear 9–12 min, 26–28% B linear 12–13 min, 28% B isocratic 13–15 min, 28–34% B linear 15–16 min, 34–38% B linear 16–18 min, 38–40% B linear 18–20 min, 40–55% B linear 20–24 min, 55–65% B linear 24–25 min, 65–85% B linear 25–28 min, and 85–95% B linear 28–30 min. The injection volume and the detection wavelength were set as 0.6 μl and at 254 nm, respectively. The flow rate was 0.6 ml/min, and the column temperature was maintained at 35°C.

Both MS and MS/MS were performed in positive ion mode, and the ion source is dual AJS ESI. The MS parameters were set as follows: capillary voltage, 3,500 V; nebulizer gas (N_2) pressure, 30 psig; drying gas flow rate, 8.0 L/min; drying gas (N_2) temperature, 320°C; shealth gas flow rate, 12.0 L/min; shealth gas (N_2) temperature, 350°C; OCT RF V, 750 V; skimmer, 65 V; fragmentor, 135 V. The scan ranges for product ions were *m/z* 100–3,000, and the collision energy was set at 20, 40, and 60 V. Before the analysis, mass spectrometer of the TOF was calibrated at *m/z* 121.0508 and 922.0098 in positive ion mode to ensure the mass accuracy. Data acquisition and analysis were obtained by Agilent LC-MS MassHunter Workstation Software (version B.08.00).

Chemical Fingerprint Analysis of *Zanthoxylum nitidum* (Roxb.) DC. Sample by HPLC

The SHIMADZU LC-20AT HPLC system was employed to perform the HPLC fingerprint analysis. The system consists of quad pump, online vacuum degassing machine, DAD detector, column temperature box, and automatic sampler (SHIMADZU LabTotal, Tokyo, Japan). Chromatographic separation was conducted on a column of symmetry columns (4.6 × 250 mm, 5 μm, Waters, Milford, CT, United States). The mobile phase consisted of water with 0.1% formic acid (A) and acetonitrile (B). The gradient conditions are shown in **Supplementary Table S2**. The temperature was set at 35°C. The purpose of the final 10 min is re-equilibrizing the column. The flow rate was at 1 ml/min, and the injection volume and detection wavelength were set at 10 μl and 254 nm, respectively.

Antioxidant and Anti-Inflammatory Bioactivity Assay

Antioxidant Activity Assay

In this study antioxidant activities were measured by the classic test DPPH assays. DPPH assay is a chemical analysis experiment, which is used in a basic *vitro* screening method for evaluating the radical scavenging activity (Heinrich et al., 2020). The radical scavenging activity (RSA) was calculated by the following formula:

$$RSA\,(\%) = \left[1 - \frac{\left(A_{sample} - A_{blank}\right)}{\left(A_{control} - A_{blank}\right)}\right] \times 100 \quad (1)$$

where $A_{control}$ is the absorbance of 100 μl of DPPH solution with 100 μl of ethanol, A_{blank} is the absorbance of 200 μl of ethanol, and A_{sample} is the absorbance of 100 μl of DPPH solution with 100 μl of sample or ascorbic acid solution.

The DPPH assay was performed based on the instructions described in the literature (Kang et al., 2011; Wang et al., 2017; Zhang et al., 2018). An aliquot of 100 μl of each sample in ethanol (10, 25, 50, 100, 200 μg/ml) was mixed with 100 μl of 0.2 mM DPPH ethanolic solution. Ascorbic acid was used as a positive drug. The mixture was incubated for 30 min in the darkroom, then the absorbance was measured at 517 nm. The determination was conducted in triplicates, and the antioxidant activity was expressed by the IC_{50} value.

Anti-Inflammatory Activity Assay

Raw264.7 cells (100 μl) were seeded at 2.5×10^4 cells per well into 96-Transwell insert plates and incubated in a 5% CO_2 atmosphere at 37°C. After 24 h, the powder of ZN extracts was dissolved in the new culture medium containing 1 μg/ml of LPS, configured as a solution of 80 μg/ml to replace the old culture medium. Cells were maintained in the incubator at 37°C for 24 h. The level of nitric (an indicator of NO synthesis) was measured using nitric oxide assay kit (Beyotime, Shanghai, China) according to the manufacturer's instructions. The OD value was measured at 540 nm with a microplate reader (BioTek, SynergyH1, United States). The calculation formula of inhibition rate of NO production is as follows:

$$\text{Rate}\,(\%) = \left[\frac{C_m - C_s}{C_m - C_n}\right] \times 100 \quad (2)$$

C_m is the NO concentration of the model group, C_s is the NO concentration of the samples, and C_n is the NO concentration of the normal control group. Finally, the original cells in 96-well plates were used to determine the cell viability by an MTT assay (Wang et al., 2019).

Spectrum–Effect Relationship Modeling

Establishing of HPLC Fingerprint and Hierarchical Cluster Analysis

Twenty batches of ZN samples were chemically profiled and matched automatically by using the "Chinese Medicine Chromatographic Fingerprint Similarity Evaluation System 2012." Then the common peaks of 20 fingerprints were calculated by the multipoint method, and the control chromatogram was generated automatically by the average method.

The HCA of different batches of ZN samples was carried out with the SPSS statistics software (SPSS version 19.0, IBM Corp., Armonk, NY, United States). The between-group linkage method and the squared Euclidean distance were used to establish the clusters.

Partial Least Squares Regression Model

PLSR is the statistical method, which is related to principal component regression, but is not a hyperplane that looks for the maximum variance between the response variable and the independent variable (Qiao et al., 2018). It is helpful in classification and biomarker discovery. The model is a multivariate calibration model used to find the inner relationship between an n × p data matrix X and an n × q response matrix Y (Martens and Naes, 1992). In this study, PLSR was used to model the fingerprint–activity relationship based on the SIMCA-P 14.0 Software (Umetrics AB, Umea, Sweden). The X-matrix was composed of the common peak areas in chromatographic fingerprints, and the Y-matrix was constructed with the anti-inflammatory and antioxidant activities.

$$X = TP^T + E \quad (3)$$

$$Y = UQ^T + F \quad (4)$$

where X is a prediction matrix of $n \times m$, Y is a prediction matrix of $n \times p$, TP^T approximates to the common peak areas and UQ^T to the activity values, and E and F contains the residuals of the regression model.

Grey Relational Analysis Model

The Grey relational analysis is often used to measure the degree of correlation among factors according to the degree of similarity or dissimilarity between the development trends of factors, which is also called "grey correlation degree" (Elena Arce et al., 2015; Jiang et al., 2018). The anti-inflammatory and antioxidant activities of 20 ZN samples were selected as the reference sequence, and 18 relative common peaks were defined as comparability sequences. Then the grey relational coefficients (GRC) between common peaks and bioactivities were conducted through the Data Processing System (DPS 9.01) software. The formula for calculation relational degree is as follows:

$$r_i = \frac{1}{N}\sum_{k=1}^{N} \xi_i\,(k) \quad (5)$$

where r_i is the correlation, ξ_i is the grey relational coefficient, and N is the total sample number.

Spearman's Rank Correlation Coefficient

Spearman's rank correlation coefficient (ρ) is a widely used method to measure the degree of correlation between two variables. A positive correlation coefficient value of ρ (from 0 to 1) implies that the two variables are positively correlated. On

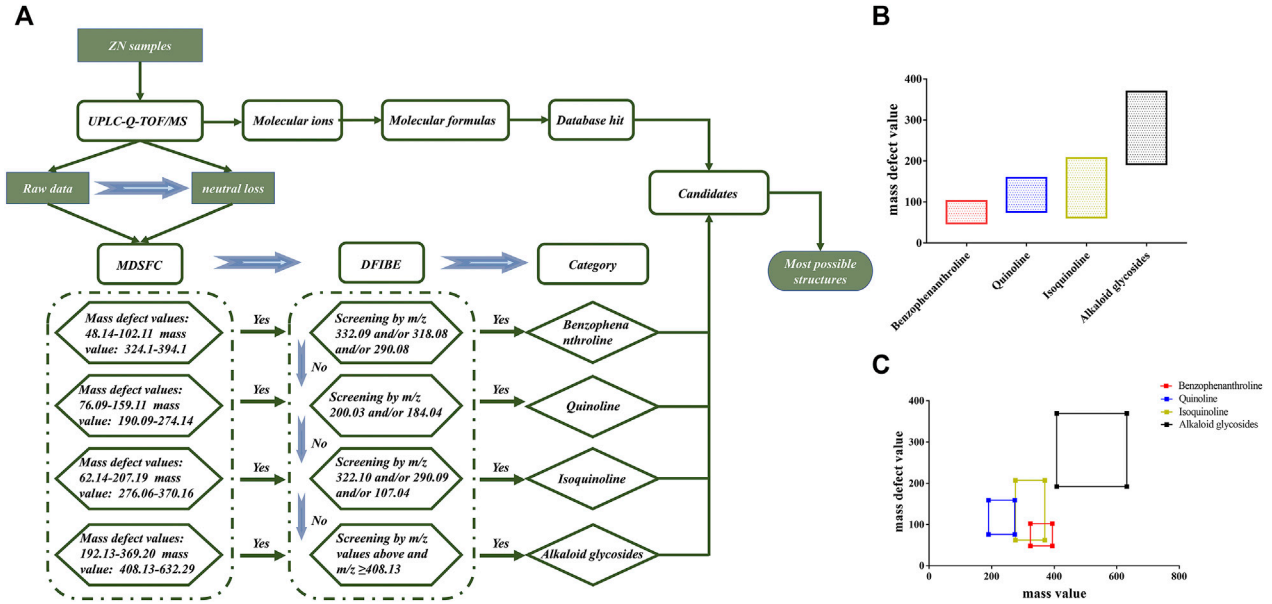

FIGURE 2 | The structure-diagnostic ion-oriented network **(A)**. The mass defect ranges of different types of alkaloids in ZN **(B)**; the correlations between the mass ranges and mass shifts of the basic skeletons of ZN alkaloids **(C)**. MDFSC, mass defect filtering-based structure classification; DFIBE, diagnostic fragment-ion-based extension.

the contrary (from −1 to 0), there is a negative correlation. Besides, a correlation coefficient value of 0 implies that the two variables are not related (Zar, 2005).

In this study, Spearman's rank correlation coefficient was used to quantify the correlation between 18 common peaks and bioactivities by using SPSS version 19.0 (IBM Corp., Armonk, NY, United States). The formula for the calculation of the relational degree is as follows:

$$\rho = \frac{\sum_i (x_i - \bar{x})(y_i - \bar{y})}{\sqrt{\sum_i (x_i - \bar{x})^2 \sum_i (y_i - \bar{y})^2}} \quad (6)$$

where *xi* is the rank of the data of the random variable X, *yi* is the rank of the data of the random variable Y, and $\bar{x}$ and $\bar{y}$ are the expectations of X and Y, respectively.

RESULTS AND DISCUSSION

Chemical Identification of *Zanthoxylum nitidum* (Roxb.) DC. Sample

Establishment of the Qualitative Strategy

In TCMs, the same chemical structure compounds can be classified as a category with a unique mother skeleton. These compounds with similar structure group share identical diagnostic ions and mass defect value, which could make the structural identification more efficient (Zhang et al., 2008; Zhang et al., 2009). In this study, a structure-diagnostic ion-oriented network (**Figure 2A**) was established for the rapid characterization of alkaloids compounds in ZN: 1) The mass fragment behaviors of the compounds in ZN were summarized by referring to the existing reviews and database (Sci-finder, Google Scholar, and PubMed). 2) Total ions and product ion scan were used to create the comprehensive chemical profiling of ZN (**Figures 2B,C**). 3) Then the mass defect filtering-based structure classification (MDFSC) and diagnostic fragment-ion-based extension (DFIBE) were applied to process the MS data. 4) With the help of the classification method, most alkaloid compounds in ZN were rapidly identified by their mass fragmentation rules. A diagram for rapid classification and identification of the chemical compounds in ZN is displayed in **Figure 2**.

MDFSC Approach for Structural Classification

With a well-preset mass defect window, the MDFSC approach can quickly find out the class of compound based on their similar mother skeleton over certain mass ranges, and can also obtain new compounds never found before (He et al., 2018; Zhou et al., 2018; Pang et al., 2019). Considering that alkaloids are just one part of compounds in ZN, the MDFSC strategy was only a preliminary structural classification for alkaloids in the whole identification of ZN.

On the basis of existing literatures (Jia et al., 2013; Yang et al., 2017; Fu et al., 2021) and authoritative database, we concluded the core substructures and corresponding substituents in ZN, and calculated their maximum and minimum mass defect values (the tolerance of mass defect is ±5 m Da). In total, the alkaloids can be divided into four categories: benzophenanthroline, quinoline, isoquinoline, and alkaloid

TABLE 1 | Characterization of chemical constituents of *Zanthoxylum nitidum* (Roxb.) DC. (ZN) sample.

No.	T_R (min)	Identification	Formula	Theoretical mass (*m/z*)	Measured mass (*m/z*)	Error (ppm)	In mode	MS/MS (*m/z*)
1	0.32	L-Arginine	$C_6H_{14}N_4O_2$	175.1190	175.1194	−2.28	$[M+H]^+$	158.0901, 144.1377, 130.0963, 116.0705, 100.0756
2	1.32	(E)-3-(3,4,5-trihydroxyphenyl) acrylaldehyde	$C_9H_8O_4$	181.0495	181.0492	1.66	$[M+H]^+$	153.0539, 140.0461, 125.0589, 110.0353
3	1.90	Chlorogenic acid	$C_{16}H_{18}O_9$	355.1024	355.1036	−3.38	$[M+H]^+$	266.0805, 193.0491, 163.0387, 135.0439, 117.0331
4	2.13	Magnocurarine A	$C_{19}H_{24}NO_3^+$	314.1756	314.1754	0.64	$[M]^+$	269.1164, 237.0899, 175.0747, 107.0482
5	2.38	Magnoflorine A	$C_{20}H_{24}NO_4^+$	342.1705	342.1709	−1.46	$[M]^+$	297.1124, 282.0891, 237.0911, 222.0678, 192.1021
6	3.14	Magnocurarine B	$C_{19}H_{24}NO_3^+$	314.1756	314.1771	−4.77	$[M]^+$	314.1760, 269.1174, 237.0909, 175.0751, 107.0489
7	3.20	3′-hydroxy-4′,6,7-trimethoxyl-N,N-dimethyltetrahydroisoquinoline	$C_{21}H_{28}NO_4^+$	358.2018	358.2024	−1.68	$[M]^+$	298.1196, 267.1011, 206.1171, 174.0617, 137.0594
8	3.42	D-Tertrahydropaimatine	$C_{21}H_{25}NO_4$	356.1869	356.1856	−3.65	$[M+H]^+$	192.1022, 177.0785, 137.0594
9	3.59	(Z)-3-(2-(2-hydroxypropan-2-yl)-2,3-dihydrobenzofuran-5-yl) acrylic acid	$C_{14}H_{16}O_4$	249.1130	249.1121	3.61	$[M+H]^+$	203.0703, 189.0548, 171.0437, 161.0590, 141.0694, 129.0695, 115.0538
10	4.00	Dimethyl 5-[(6-phenethylpyridin-3-yl) methyl] isophthalate	$C_{24}H_{23}NO_4$	390.1574	390.1559	3.84	$[M+H]^+$	330.0732, 295.0600, 254.0576, 209.0593, 167.0488
11	4.18	Protopine	$C_{20}H_{19}NO_5$	354.1336	354.1349	−3.67	$[M+H]^+$	320.0918, 247.0750, 192.1021, 149.0594, 107.0485
12	4.34	Analog of liriodenine	$C_{19}H_{17}NO_4$	324.1241	324.1230	3.39	$[M+H]^+$	309.0998, 281.1047, 266.0812, 192.1021, 177.0786, 145.0282, 117.0333
13	4.40	Tertrahydropaimatine	$C_{21}H_{25}NO_4$	356.1869	356.1856	3.65	$[M+H]^+$	340.1544, 192.1021, 177.0786, 145.0282
14	4.49	Analog of oxyavicine	$C_{21}H_{21}NO_5$	368.1492	368.1498	−1.63	$[M+H]^+$	352.1191, 324.1240, 310.1082, 292.0970, 264.0662, 204.0654
15	4.62	Magnoflorine B	$C_{20}H_{24}NO_4^+$	342.1705	342.1710	−1.17	$[M]^+$	297.1123, 282.0886, 237.0906, 222.0672, 207.0801
16	5.16	Palmatrubin	$C_{20}H_{19}NO_4$	338.1387	338.1401	−4.14	$[M+H]^+$	307.0841, 265.0735, 237.0783, 190.0863, 175.0628
17	5.19	Allocryptopine	$C_{21}H_{23}NO_5$	370.1649	370.1657	−2.16	$[M+H]^+$	336.1223, 290.0932, 252.0774, 206.0802, 188.0698, 149.0591
18	5.21	10-Methoxy-2,3-dihydro-7H-[1,4] dioxino [2,3-g] chromen-7-one	$C_{12}H_{10}O_5$	235.0601	235.0607	−2.55	$[M+H]^+$	205.0497, 191.0341, 177.0547, 163.0389, 149.0230, 135.0441, 121.0283, 107.0488
19	5.47	Jatrorrhizine	$C_{20}H_{19}NO_4$	338.1400	338.1391	2.66	$[M+H]^+$	322.1091, 294.1130, 280.0972, 265.0733, 222.0914
20	5.62	Diosmin	$C_{28}H_{32}O_{15}$	609.1814	609.1815	−0.16	$[M+H]^+$	463.1234, 301.0706, 285.0753, 263.0551, 245.0445, 177.0551
21	5.86	Hesperidin	$C_{28}H_{34}O_{15}$	611.1970	611.1995	−4.09	$[M+H]^+$	465.1351, 303.0872, 285.0754, 263.0553, 245.0448, 177.0550
22	6.35	Haplopine	$C_{13}H_{11}NO_4$	246.0761	246.0768	−2.84	$[M+H]^+$	231.0526, 216.0289, 188.0343, 160.0390
23	6.37	Isofagaridine	$C_{20}H_{16}NO_4^+$	344.1079	344.1069	2.91	$[M]^+$	319.0849, 291.0897, 276.0663, 262.0865
24	6.60	Palmatine	$C_{21}H_{22}NO_4$	352.1543	352.1555	−3.41	$[M+H]^+$	336.1236, 320.1285, 292.0972, 190.0859
25	6.71	Sanguinarine A	$C_{20}H_{14}NO_4^+$	332.0917	332.0932	−4.52	$[M]^+$	319.0842, 291.0892, 274.0870, 246.0915, 216.0808
26	6.77	Epiberberine	$C_{20}H_{17}NO_4$	336.1230	336.1242	−3.57	$[M+H]^+$	320.0919. 304.0968, 292.0970, 278.0814, 263.0936
27	7.16	Sanguinarine B	$C_{20}H_{14}NO_4^+$	332.0917	332.0934	−5.12	$[M]^+$	319.0843, 291.0890, 274.0866, 246.0914, 216.0806
28	8.06	Marmesin	$C_{14}H_{12}O_4$	245.0808	245.0813	−2.04	$[M+H]^+$	212.0460, 191.0337, 163.0387, 147.0436, 128.0616
29	8.32	Nitidine A	$C_{21}H_{18}NO_4^+$	348.1230	348.1246	−4.60	$[M]^+$	332.0926, 318.0763, 304.0974, 290.0818, 275.0939
30	8.71	Chelerythrine	$C_{21}H_{17}NO_4$	348.1230	348.1240	−2.87	$[M+H]^+$	332.0921, 318.0759, 304.0968, 290.0812

(Continued on following page)

TABLE 1 | (*Continued*) Characterization of chemical constituents of *Zanthoxylum nitidum* (Roxb.) DC. (ZN) sample.

No.	T_R (min)	Identification	Formula	Theoretical mass (*m/z*)	Measured mass (*m/z*)	Error (ppm)	In mode	MS/MS (*m/z*)
31	9.31	γ-Fagarine	$C_{13}H_{11}NO_3$	230.0812	230.0821	−3.91	$[M+H]^+$	215.0580, 200.0340, 186.0547, 172.0394, 158.0600
32	9.63	Skimmianine	$C_{14}H_{13}NO_4$	260.0917	260.0925	−3.08	$[M+H]^+$	227.0574, 200.0661, 199.0629, 184.0390, 170.0593
33	9.83	5-Methoxydictamnine	$C_{13}H_{11}NO_3$	230.0812	230.0819	−3.04	$[M+H]^+$	215.0579, 200.0340, 186.0547, 172.0398, 158.0594
34	9.86	Dictamnine	$C_{12}H_9NO_2$	200.0706	200.0715	−4.50	$[M+H]^+$	185.0474, 156.0446, 129.0576, 102.0466
35	10.16	Nitidine B	$C_{21}H_{18}NO_4^+$	348.1230	348.1240	−2.87	$[M]^+$	332.0922, 318.0763, 304.0969, 290.0813, 275.0937
36	10.90	Unknown	$C_{15}H_{14}O_5$	275.0914	275.0918	−1.45	$[M+H]^+$	229.0493, 217.0497, 203.0338, 175.0390, 161.0596
37	12.03	Analog of magnoflorine	$C_{36}H_{42}NO_9^+$	632.2875	632.2870	0.79	$[M]^+$	342.1700, 297.1124, 282.0890, 265.0862, 237.0912, 222.0673, 191.0852
38	15.13	Toddanone	$C_{16}H_{18}O_5$	291.1227	291.1236	−3.09	$[M+H]^+$	219.0652, 205.0496, 191.0702, 161.0597, 131.0488
39	16.42	Analog of jatrorrhizine	$C_{27}H_{41}NO_{13}$	610.2470	610.2448	3.61	$[M+Na]^+$	338.1390, 322.1077, 294.1123, 280.0973, 190.0862, 161.0595, 105.0700
40	16.79	Analog of nitidine	$C_{28}H_{31}NO_6^+$	477.2151	477.2150	0.21	$[M]^+$	348.1234, 332.0927, 318.0769, 304.0975, 290.0818, 275.0936
41	18.46	Oxynitidine	$C_{21}H_{17}NO_5$	364.1179	364.1192	−3.57	$[M+H]^+$	348.0867, 334.0716, 320.0919, 306.0766, 290.0455, 278.0809
42	18.77	5,7-Dimethoxy-8-(3-methyl-2-butenoxy) coumarin	$C_{16}H_{18}O_5$	291.1227	291.1233	−2.06	$[M+H]^+$	220.0366, 193.0134, 178.0259, 165.0184, 133.0284, 107.0486
43	19.49	6-Ethoxychelerythrine	$C_{23}H_{23}NO_5$	394.1654	394.1666	−3.04	$[M+H]^+$	376.1548, 361.1313, 346.1093, 318.1125, 330.1127, 288.0795, 260.0829
44	20.16	Phellopterin	$C_{17}H_{16}O_5$	301.1071	301.1081	−3.32	$[M+H]^+$	218.0210, 190.0255, 162.0309, 134.0361, 106.0409
45	21.54	Suberosin	$C_{15}H_{16}O_3$	245.1172	245.1181	−3.67	$[M+H]^+$	215.0698, 187.0389, 175.0389, 143.0488, 131.0488
46	23.25	Dihydronitidine	$C_{21}H_{19}NO_4$	350.1387	350.1399	−3.43	$[M+H]^+$	334.1078, 319.0838, 290.0816, 247.0759, 219.0805
47	23.64	Dihydrochelerythrine	$C_{21}H_{19}NO_4$	350.1387	350.1385	0.53	$[M+H]^+$	334.1085, 319.0848, 290.0821, 247.0756, 219.0804
48	25.67	Analog of nitidine	$C_{36}H_{32}NO_9^+$	622.2072	622.2090	−2.89	$[M]^+$	348.1230, 332.0920, 318.0760, 304.0969, 290.0814, 246.0912

glycosides. Respectively, mass defect values and mass values of these four categories are listed as follows: benzophenanthroline (mass defect values 48.14–102.11 m Da, mass values: 324.10–394.10 m Da), quinoline (mass defect values: 76.09–159.11 m Da, mass values: 190.09–274.14 m Da), isoquinoline (mass defect values: 62.14–207.19 m Da, mass values: 276.06–370.16 m Da), and alkaloid glycosides (mass defect values: 192.13–369.20 m Da, mass values: 408.13–632.29 m Da). Using the MDFSC approach, we could preliminarily sort part of the detected ions as the certain chemical homologs and discovered that some alkaloid glycosides have mother skeletons, which are compounds classified in the former three categories. For example, the mother skeleton of compound 39 was similar to jatrorrhizine; its MS/MS spectra had fragment peaks of 338.1390, 322.1077, and 294.1123 m/*z*, which correspond to jatrorrhizine.

Structure Classification and Identification of Alkaloids in *Zanthoxylum nitidum* (Roxb.) DC. Sample

Combined with the MDFSC approach and DFIBE, the structure-diagnostic ion-oriented strategy was employed to rapidly speculate the chemical constituents, and in total, 48 compounds were inferred from ZN. Among them, alkaloids accounted for 35 of the 48, which indicate the significance of alkaloids. All the detailed information is listed in **Table 1**, and the fragmentation pattern together with mass spectrogram of representative compounds are shown in **Figure 3**.

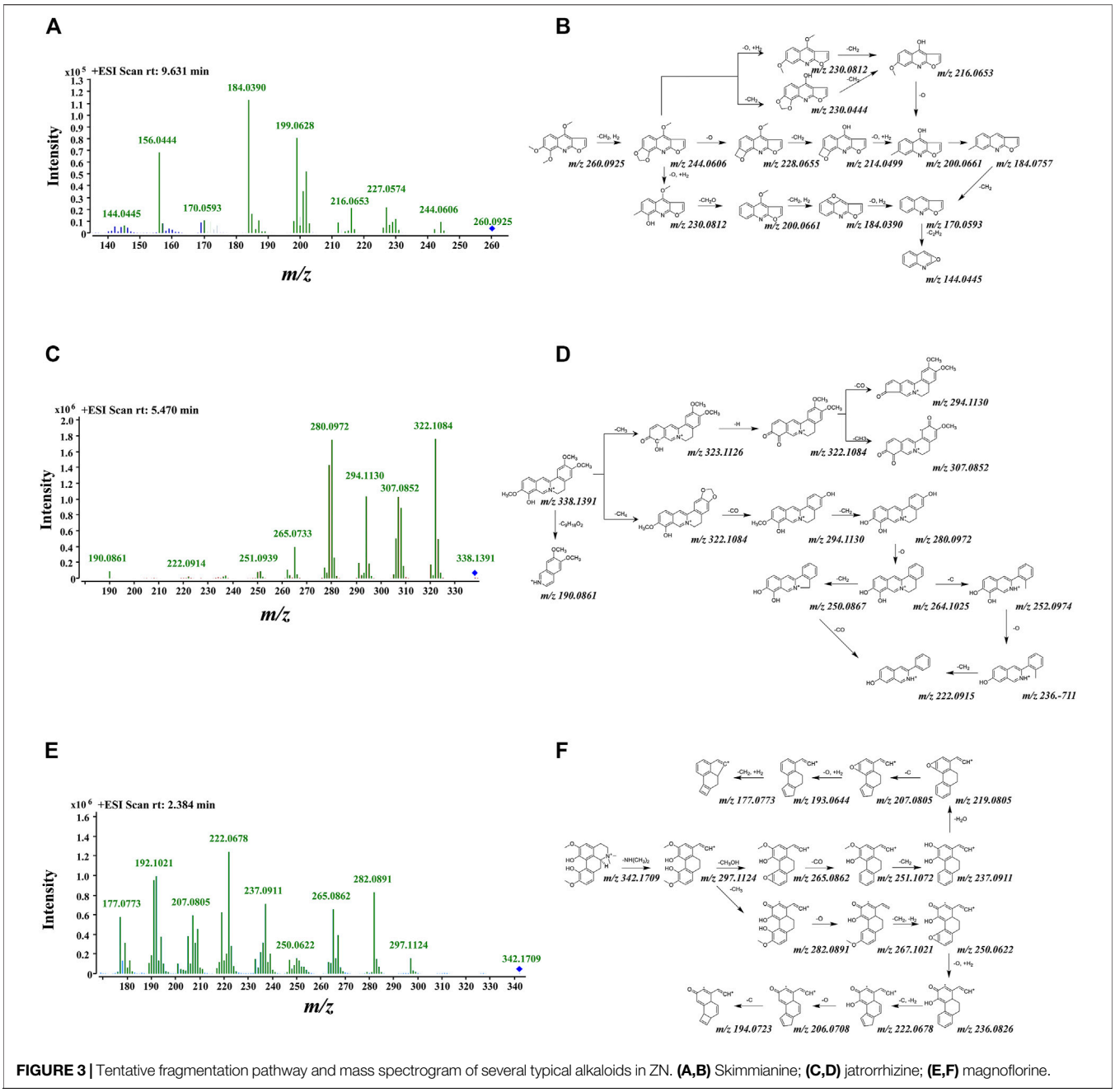

FIGURE 3 | Tentative fragmentation pathway and mass spectrogram of several typical alkaloids in ZN. **(A,B)** Skimmianine; **(C,D)** jatrorrhizine; **(E,F)** magnoflorine.

Characterization of Typical Benzophenanthroline

For benzophenanthrolines, their basic carbon framework consists of a benzene and a phenanthridine. Benzophenanthrolines are the most studied category of compounds in ZN, such as NC and chelerythrine (Li et al., 2017; Lin et al., 2020). In the MS/MS spectra of benzophenanthrolines, some certain product ions at *m/z* 332.09, 318.08, and 290.08 were presented, and consecutive losses of CH_2 (14 Da), CO (28 Da), and O (16 Da) could be easily found. Nitidine ($[M]^+$ at *m/z* 348.1246) is the typical compound, eluted at 8.71 min, and its molecular formula was determined as $C_{21}H_{18}NO_4^+$. In the positive MS/MS spectra, its MS/MS spectra had fragment peaks of 332.0926 $[M\text{-}O]^+$ and 318.0763 $[M\text{-}O\text{-}CH_2]^+$, which correspond to the core substructures of benzophenanthrolines. Its tentative fragmentation pathway is shown in **Supplementary Figures S1A,B**. By integrating data inquiries, MDFSC and DFIBE approaches, nitidine, oxynitidine, and dihydronitidine were confirmed (Cesar et al., 2015).

Characterization of Typical Quinoline

Quinoline consists of a benzene connecting to pyridine and other groups. The product ions of $[M+H-14]^+$, $[M+H-30]^+$, and $[M+H-16]^+$ were available in the MS/MS spectra of quinoline,

and certain product ions at *m/z* 200.03, 184.04 were the basis of DFIBE judgment. According to the patterns above, skimmianine ($[M+H]^+$ at *m/z* 260.0925) was identified rapidly. It was eluted at 9.63 min, and its molecular formula was determined as $C_{14}H_{13}NO_4$. It had fragment peaks of 200.0661[M+H-CH_2+H_2-O+H_2-CH_2O]$^+$ and 184.0390 [M+H-CH_2+H_2-O+H_2-CH_2O-CH_2+H_2]$^+$, which were equal to the core substructures. Then the skimmianine was identified with the support of integrating data bases (Wang, 1980), and its tentative fragmentation pathway is shown in **Figures 3A,B**. Besides, γ-fagarine and dictamnine are inferred as quinoline alkaloids.

Characterization of Typical Isoquinoline

For isoquinoline, the basic carbon framework consists of a phenanthridine connecting to pyridine. Its MS/MS spectra provided several certain product ions at *m/z* 322.10, 290.09, and 107.04, and consecutive losses of CH_2 (14 Da), C (12 Da), CO (28 Da), and O (16 Da) could be easily found (Xiao et al., 2018). The typical compound is jatrorrhizine ($[M+H]^+$ at *m/z* 338.1400), which was eluted at 5.47 min, and its main molecular formula was determined as $C_{20}H_{20}NO_4^+$. Its fragment peaks contain 322.1091 [M+H-CH_4]$^+$, 294.1130 [M+H-CH_4-CO]$^+$, and 280.0972 [M+H-CH_4-CO-CH_2]$^+$. After integrating data bases, jatrorrhizine was confirmed. During the whole characterization of isoquinoline, we found that the overall structure and fragmentation pathway of magnoflorine is very interesting. Tentative fragmentation pathways of jatrorrhizine and magnoflorine are shown in **Figures 3C–F**.

Characterization of Typical Alkaloid Glycosides

With the assistance of MDFSC and DFIBE approaches, several alkaloid glycosides and alkaloids of larger relative molecular weights were found in ZN. It is attractive that the mother nucleuses of these compounds are similar to the known alkaloids we discovered. Take compound 40, for example; its mother nucleus is nitidine, which is described in the previous section, and its tentative fragmentation pathway is shown in **Supplementary Figures S1A,B**, and the tentative fragmentation pathways of oxynitidine and dihydronitidine are shown in **Supplementary Figures S1C–F**. Unfortunately, we could not suspect the accurate structure of these compounds and the attached groups.

Characterization of Other Types of Compounds

Several alkaloids do not belong to the above four categories or cannot be found in medium to low polarity, such as magnocurarine B ($[M]^+$ at *m/z* 314.1760). It is a benzylisoquinoline alkaloid, and is eluted at 3.14 min in high polarity. Its fragment peaks contain 269.1174 [M+H-C_2H_8N]$^+$, 237.0909 [M+H-$C_3H_{12}NO$]$^+$, 107.0489 [M+H-$C_{12}H_{18}NO_2$]$^+$, etc. After integrating the databases and DFIBE approach, magnocurarine B was identified. Its tentative fragmentation pathway is shown in **Supplementary Figures S2A,B**. This result indicates that the MDFSC and DFIBE approaches cannot only be applied in the characterization of alkaloids but also can be used in other types of compounds. Finally, the tentative fragmentation pathways of all remaining identified compounds are sorted out in **Supplementary Figures S4–S45**.

Chromatographic Fingerprint Analysis of *Zanthoxylum nitidum* (Roxb.) DC. Samples

Under the optimized experimental conditions, the chromatographic fingerprints of ZN samples are neatly lined up in **Figure 4**. To evaluate the validation of the HPLC method, we selected and analyzed a random sample (S18) for its validation tests in terms of precision, stability, and repeatability. The RSDs of precision, stability, and repeatability were all less than 5% (shown in **Supplementary Table S3**), which indicated that the established method was reliable and repeatable.

Then the fingerprint of 20 batches of ZN samples was generated automatically by the software Similarity Evaluation System for Chromatographic Fingerprint of Traditional Chinese Medicine (2012A Version, Committee of Chinese Pharmacopeia). HPLC fingerprints were provided in **Figure 4A**, and reference spectra are shown in **Supplementary Figure S3**, respectively. Eighteen common characteristic peaks were chosen as research object, which covered more than 80% of the whole peak areas in the fingerprint. Subsequently, we performed the similarity analysis to evaluate the similarity of all the chromatographic profile of the samples, which was based on vector cosine calculations. It could be noted that most of similarity values were higher than 0.90, while similarity values of several batches from Guangdong province were 0.81–0.89 (**Supplementary Table S1**). The results showed that the chemical fluctuation among the random samples is pretty small in major producing areas (Sun and Liu, 2007), and it proved that the established fingerprint was reliable.

Hierarchical Cluster Analysis of *Zanthoxylum nitidum* (Roxb.) DC. Samples

Based on the SPSS 19.0 software, we took the relative area of each common peak as the index for HCA (Liu et al., 2016). The sample similarity was measured by correlation coefficient as distance. The results are shown in **Figure 4B**, and 20 batches of ZN samples could be grouped into six categories: S1–S5, S6–S11 and S16–S20, S14–S15, S12, and S13 were, respectively, classified to one group. More importantly, the six groups belonged to the four resource provinces, and the group contains S16–S20 was from Guangxi with good similarity and intragroup similarity. The results indicated that ZN from different areas have good stability.

Bioactivities of *Zanthoxylum nitidum* (Roxb.) DC. Samples

Anti-Inflammatory Activity of *Zanthoxylum nitidum* (Roxb.) DC. Samples

The inhibition of NO production is positively correlated with the anti-inflammatory activity (Chen et al., 2019). Thus, the inhibition of

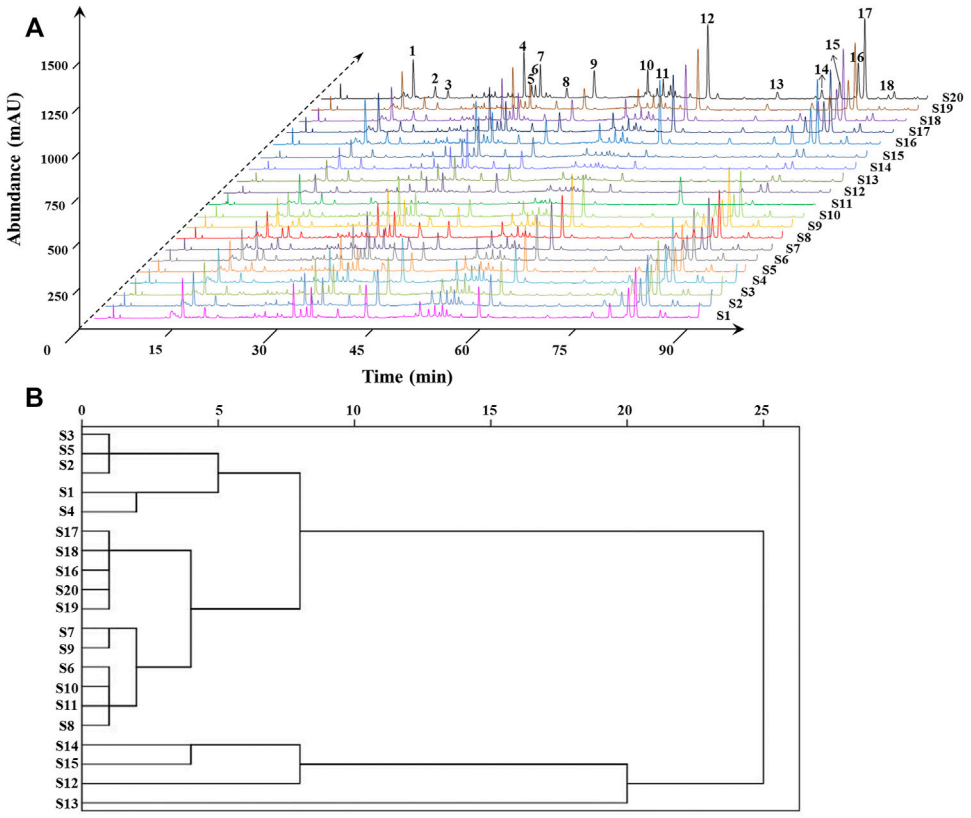

FIGURE 4 | HPLC fingerprints and common peaks of 20 batches of ZN samples **(A)**. Cluster analysis of 20 batches of ZN samples **(B)**.

NO production was set as the index to assess the anti-inflammatory property of ZN samples in the present study. The results showed that cell viability (**Supplementary Table S4**) was from 77.4 ± 2.4 to 107 ± 1.3%, which means ZN inhibits the production of NO while not producing a toxic effect *in vitro*. Moreover, as is shown in **Supplementary Table S4**, the range of NO inhibition rate was 37.1 ± 2.9 to 83.9 ± 2.2%, and S10 (83.2 ± 2.3%), S11 (81.8 ± 1.7%), S12 (83.9 ± 3.8%), and S19 (83.9 ± 2.2%) were higher than 80% (**Figure 5A**). Among them, the sample S19 from Guangxi province showed best inhibition of NO production (83.9 ± 2.2%). The data indicated that most batches of ZN samples from different areas showed better anti-inflammatory activity.

Antioxidant Activity of *Zanthoxylum nitidum* (Roxb.) DC. Samples

The IC_{50} value is the indicator to evaluate the antioxidant property of ZN samples, and it is negatively correlated with the antioxidant activity (Wang et al., 2017). As was shown in **Supplementary Table S5**, the IC_{50} values were from 47.21 ± 0.33 to 109.34 ± 1.43 μg/ml, and S10 (53.48 ± 0.29 μg/ml), S12 (47.21 ± 0.33 μg/ml), and S20 (55.22 ± 0.64 μg/ml) were lower than 60 μg/ml (**Figure 5B**). Besides, the sample S12, S20 showed strong antioxidant activity (47.21 ± 0.33 μg/ml; 55.22 ± 0.64 μg/ml), whereas the antioxidant activity of S17 (109.36 ± 1.43 μg/ml) was weak. The results revealed that most batches of ZN samples have better antioxidant activity.

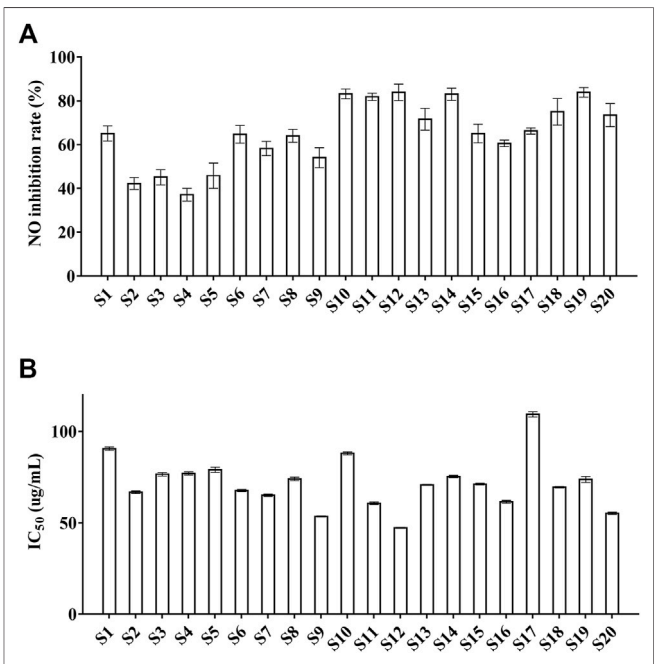

FIGURE 5 | The NO inhibition and the antioxidant activities of 20 batches of ZN samples. **(A)** NO inhibition; **(B)** DPPH. Values represent means ± SD, $n = 5$ **(A)**; $n = 3$ **(B)**.

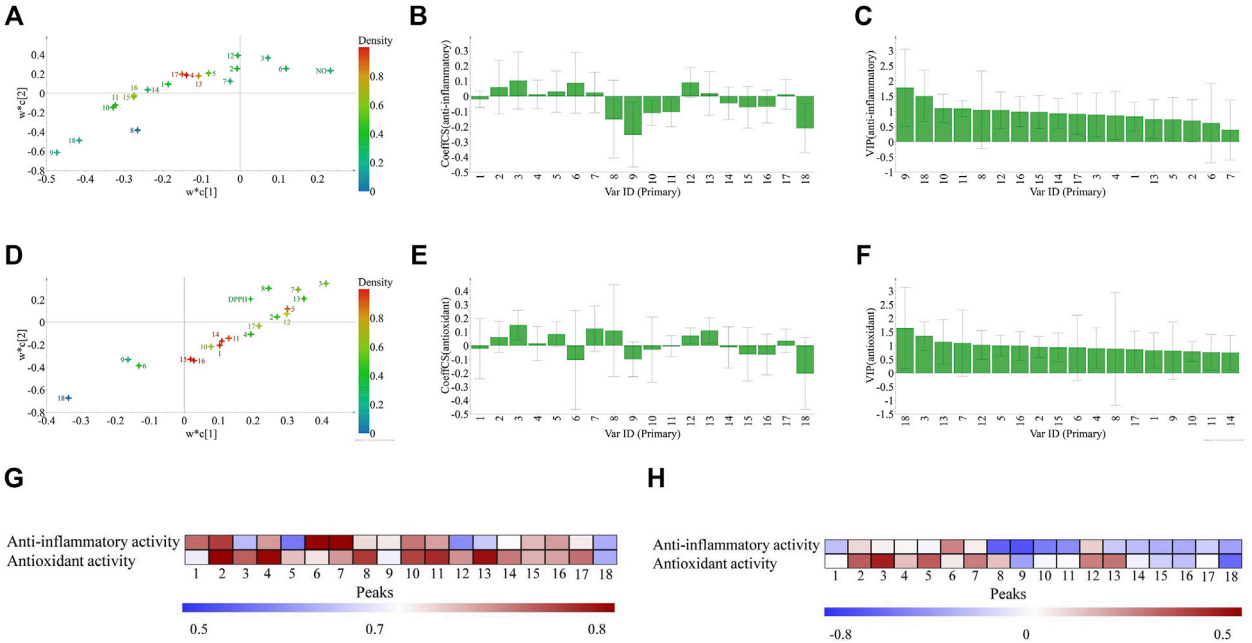

FIGURE 6 | The three pharmacodynamic models to discover principal bioactive components. The results of partial least squares regression (PLSR, **A–F**): the loading scatters of PLSR **(A**: anti-inflammatory; **D**: antioxidant, colored according to density**)**; regression coefficient between the 18 common peaks and the anti-inflammatory, antioxidant activities, respectively **(B**: anti-inflammatory; **E**: antioxidant**)**, and VIP values **(C**: anti-inflammatory; **F**: antioxidant**)**. The heat map of bioactivities of 18 compounds by GRA analysis **(G)** and Spearman's rank correlation coefficient (SRCC) **(H)** in ZN samples. Peaks 1–18 represent the common peaks.

Discovery of Principal Bioactive Components by Partial Least Squares Regression, Gray Relational Analysis, and Spearman's Rank Correlation Coefficient

In the past decades, artemisinin and ephedrine were regarded as gifts that the TCMs bring to the world (Tu, 2016; Leung and Xu, 2020). They were both isolated substances from TCMs and have undergone the modernization of traditional medicines. It proved that we can clarify the effectiveness of TCMs by finding out the bioactive components, but this is desperately not enough; the efficacy of TCMs does not come from a single compound, and TCMs usually consists of hundreds of components (Ma et al., 2016; Zhang et al., 2019). Thus, the search of the biological constituents of TCMs are a complex task. To solve this problem, the spectrum-effect relationship analysis might be a suitable choice. In this study, stoichiometric methods (PLSR, GRA, and SRCC) were applied to rapidly discover bioactive compounds from ZN samples.

First, the results of GRA showed that the GRC between the relative contents of 18 common peaks and anti-inflammatory activity were in the range of 0.5691–0.8139 (**Figure 6G**). Peaks 1, 2, 4, 6, 7, and 10 showed significant influence to anti-inflammatory activity of ZN, and peaks 16, 11, 15, 8, 9, 17 showed influence to anti-inflammatory activity of ZN. The contribution order of chromatographic peaks to the anti-inflammatory activity was P6 > P7 > P2 > P1 > P10 > P4 > P16 > P11 > P15 > P8 > P9 > P17. Similarly, GRC between the relative contents of 18 common peaks and antioxidant activity were in the range of 0.5908–0.8520 (**Figure 6G**). Peaks 2, 3, 4, 7, 11, 12, 13, 14, and 17 showed an important effect to antioxidant activity of ZN, and peaks 5, 10, 15, and 16 showed influence to antioxidant activity of ZN. The contribution order of chromatographic peaks to the antioxidant activity was P2 > P4 > P13 > P11 > P3 > P17 > P14 > P12 > P7 > P16 > P15 > P10 > P5.

Second, the PLSR model was used to discover the potential active compounds by correlating the fingerprint chromatographic data, antioxidant or anti-inflammatory activities. The X matrix of dimensions (20 × 18) from common peak areas and the Y matrix of DPPH and the NO inhibition activities were used in this model (**Figure 5** and **Supplementary Tables S4, S5**. The R^2 of NO inhibition is 0.764, and R^2 of DPPH is 0.762, respectively). Then the PLSR loading scatters were performed (**Figures 6A,D**), where Y-variables are situated near the X-variables and positively correlated to them.

For the anti-inflammatory activity of ZN samples, we found that peaks 2, 3, 4, 5, 6, 7, 12, 13, and 17 were positively correlated to the anti-inflammatory activity (**Figure 6B**). Furthermore, we employed the parameter VIP to screen the variables responsible for the anti-inflammatory activity. Variables above the VIP value threshold of 1.0 were filtered out as candidate bioactive compounds. Among them, peaks 4 (nitidine), 12, and 17 were screened out and considered as the potential anti-inflammatory

compounds of ZN (**Figure 6C**). For the antioxidant activity of ZN samples, similarly, peaks 3, 5 (chelerythrine), 7 (hesperidin), 12 (oxynitidine), and 13 appeared in a cluster trend. These compounds were positively correlated to the antioxidant activity, and the VIP value was above 1.0 (**Figures 6E,F**). According to the above results, we preliminarily inferred that the peaks 3, 4, 5, 7, 12, 13, and 17 were more relevant to the measured activities.

Finally, the results of SRCC (shown in **Figure 6H**) indicated that peaks 2, 3, 4, 6, 7, and 12 showed an influence to the anti-inflammatory activity of ZN, and peaks 2, 3, 5, 7, 12, and 13 have an important influence on the antioxidant activity of ZN.

By combining the results of PLSR, GRA, and SRCC, it can be concluded that peaks 4, 12, and 17 are tentatively assigned as candidate ingredients accounting for the anti-inflammatory activity, and peaks 3, 5, 7, 12, and 13 are the candidate ingredients for antioxidant activity. Among them, owning to the high content and bioactive activities in ZN, nitidine has attracted much attention. It has been found that nitidine could inhibit LPS-induced TNF alpha, IL-1beta, and IL-6 production by the inhibition of phosphorylation of MAPK in the RAW264.7 cell test (Wang et al., 2012). Taken together, nitidine might be the main anti-inflammatory component in ZN. What is more, peaks 12 and 17 might also be the potential anti-inflammatory compounds of ZN, which warrant further investigation. Among the antioxidant candidate compounds, hesperidin was identified to have an oxidative damage protective effect against γ-radiation-induced tissue damage in Sprague–Dawley rats (Pradeep et al., 2012). Additionally, peaks 3, 12, and 13 might also be the potential antioxidant compounds of ZN. As a complicated system, the potential synergistic and/or antagonism effects arising from multicomponents in ZN must be taken into consideration. Thus, it could be found that peaks 3, 4, 5, 7, 12, 13, and 17 might be the main bioactive compounds in ZN samples, and among them, peaks 4, 12, and 17 were the principal anti-inflammatory components and peaks 3, 5, 7, 12, and 13 were regarded as the principal antioxidant components, respectively.

Verification of Bioactive Compound Activities

In order to confirm the reliability of the correlation analysis, the anti-inflammatory activity of nitidine and the antioxidant activity of chelerythrine and hesperidin were determined by the antioxidant and anti-inflammatory bioactivity assays. The result of nitidine (**Supplementary Figure S46A**) showed that the IC_{50} value of nitidine is 87.241 ± 1.752 μM, which indicated that nitidine might be the main anti-inflammatory component of ZN. The results of chelerythrine and hesperidin (**Supplementary Figures S46B,C**) showed that chelerythrine has an antioxidant activity, and hesperidin showed a weaker antioxidant activity, which indicated that chelerythrine and hesperidin might be the main antioxidant components of ZN. Besides, according to the results of the correlation analysis, it could be noticed that diosmin has no antioxidant activity, which is in accordance with the results of these previous studies (Khlebnikov et al., 2007; Naso et al., 2016), and all these results verified the reliability of the correlation analysis.

CONCLUSION

In order to solve the challenge of discovering bioactive compounds in ZN, a comprehensive filtering approach and a spectrum–effect relationship were performed in our work. A total of 48 compounds were identified from ZN by the structure-diagnostic ion-oriented network, and 35 of them were alkaloids. During the identification of chemical components in ZN by integrating the MDFSC and DFIBE approaches, some new alkaloid analogs were found, such as compounds **37**, **39**, **40**, and **48**. Meanwhile, we discovered the principal bioactive components of ZN by using the GRA, PLSR, and SRCC models. Among the bioactive compounds, peaks **4** (nitidine), **12** (oxynitidine), and **17** might be the potential anti-inflammatory compounds in ZN, and peaks **3**, **5** (chelerythrine), **7** (hesperidin), **12**, and **13** might contribute to the antioxidant activity of ZN. Our study not only revealed the plant metabolites of anti-inflammatory and antioxidant activities of ZN, but it could also be an applicable data support for the discovery of active components of other TCMs. Our future studies will perform more comprehensive and reliable methods to verify the anti-inflammatory and antioxidant activities of ZN *in vitro* and *in vivo*.

DATA AVAILABILITY STATEMENT

The original contributions presented in the study are included in the article/**Supplementary Material**, further inquiries can be directed to the corresponding authors.

AUTHOR CONTRIBUTIONS

S-WR conducted the analysis of the experiment and data analysis, and contributed to the manuscript writing. Y-YD conducted the pharmacological and antioxidant experiment and manuscript revision. WS supervised the project and designed the study. S-HX, H-QP, and S-QH participated in the related auxiliary experiments. K-GC and DL guided the experiment. All authors read and approved the manuscript.

FUNDING

This work was supported by the BAGUI Young Scholar Program of Guangxi, the State Key Laboratory for Chemistry and Molecular Engineering of Medicinal Resources (CMEMR2018-A04), the Basic Ability Promotion Project for Young and Middle-aged Teachers of Guangxi Universities (No. 2020KY02036), and the Guangxi Natural Science Foundation of China (No. 2020GXNSFBA297085).

SUPPLEMENTARY MATERIAL

The Supplementary Material for this article can be found online at: https://www.frontiersin.org/articles/10.3389/fphar.2022.794277/full#supplementary-material

REFERENCES

Cesari, I., Grisoli, P., Paolillo, M., Milanese, C., Massolini, G., and Brusotti, G. (2015). Isolation and Characterization of the Alkaloid Nitidine Responsible for the Traditional Use of *Phyllanthus Muellerianus* (Kuntze) Excell Stem Bark against Bacterial Infections. *J. Pharm. Biomed. Anal.* 105, 115–120. doi:10.1016/j.jpba.2014.11.051

Chen, G. L., Fan, M. X., Wu, J. L., Li, N., and Guo, M. Q. (2019). Antioxidant and Anti-inflammatory Properties of Flavonoids from lotus Plumule. *Food Chem.* 277, 706–712. doi:10.1016/j.foodchem.2018.11.040

Chen, Y. H., Bi, J. H., Xie, M., Zhang, H., Shi, Z. Q., Guo, H., et al. (2021). Classification-based Strategies to Simplify Complex Traditional Chinese Medicine (TCM) Researches through Liquid Chromatography-Mass Spectrometry in the Last Decade (2011-2020): Theory, Technical Route and Difficulty. *J. Chromatogr. A.* 1651, 462307. doi:10.1016/j.chroma.2021.462307

China Pharmacopoeia Commission (2020). *Chinese Pharmacopeia*. 2020 Edition, I. Beijing: China Medical Science Press, 176–177.

Elena Arce, M., Saavedra, Á., Míguez, J. L., and Granada, E. (2015). The Use of Grey-Based Methods in Multi-Criteria Decision Analysis for the Evaluation of Sustainable Energy Systems: A Review. *Renew. Sust. Energ. Rev.* 47, 924–932. doi:10.1016/j.rser.2015.03.010

Fu, J. L., Yang, L. M., Fan, X. Y., Guo, Q. O., Zhou, W. M., and Zhang, J. Y. (2021). Research Progress on Chemical Constituents and Pharmacological Activities of *Zanthoxylum Nitidum* (Roxb.) DC. *Acta Pharm. Sin.* 1, 39. doi:10.16438/j.0513-4870.2020-1718

He, M., Jia, J., Li, J., Wu, B., Huang, W., Liu, M., et al. (2018). Application of Characteristic Ion Filtering with Ultra-high Performance Liquid Chromatography Quadrupole Time of Flight Tandem Mass Spectrometry for Rapid Detection and Identification of Chemical Profiling in *Eucommia Ulmoides Oliv. J. Chromatogr. A.* 1554, 81–91. doi:10.1016/j.chroma.2018.04.036

Heinrich, M., Appendino, G., Efferth, T., Fürst, R., Izzo, A. A., Kayser, O., et al. (2020). Best Practice in Research - Overcoming Common Challenges in Phytopharmacological Research. *J. Ethnopharmacology* 246, 112230. doi:10.1016/j.jep.2019.112230

Jia, C. P., Huang, X. L., Li, Y., and Feng, F. (2013). HPLC-DAD/ESI-Q-TOF-MS Analysis of Alkaloids in *Zanthoxylum Nitidum* (Roxb.) DC. *China J. Chin. Mater. Med.* 38 (8), 1198–1202. doi:10.4268/cjcmm20130816

Jiang, Y., David, B., Tu, P., and Barbin, Y. (2010). Recent Analytical Approaches in Quality Control of Traditional Chinese Medicines-Aa Review. *Anal. Chim. Acta* 657, 9–18. doi:10.1016/j.aca.2009.10.024

Jiang, Z., Zhao, C., Gong, X., Sun, X., Li, H., Zhao, Y., et al. (2018). Quantification and Efficient Discovery of Quality Control Markers for Emilia Prenanthoidea DC. By Fingerprint-Efficacy Relationship Modelling. *J. Pharm. Biomed. Anal.* 156, 36–44. doi:10.1016/j.jpba.2018.04.020

Kang, W.-Y., Song, Y.-L., and Zhang, L. (2011). α-Glucosidase Inhibitory and Antioxidant Properties and Antidiabetic Activity of Hypericum Ascyron L. *Med. Chem. Res.* 20, 809–816. doi:10.1007/s00044-010-9391-5

Khlebnikov, A. I., Schepetkin, I. A., Domina, N. G., Kirpotina, L. N., and Quinn, M. T. (2007). Improved Quantitative Structure-Activity Relationship Models to Predict Antioxidant Activity of Flavonoids in Chemical, Enzymatic, and Cellular Systems. *Bioorg. Med. Chem.* 15, 1749–1770. doi:10.1016/j.bmc.2006.11.037

Leung, E. L., and Xu, S. (2020). Traditional Chinese Medicine in Cardiovascular Drug Discovery. *Pharmacol. Res.* 160, 105168. doi:10.1016/j.phrs.2020.105168

Li, W., Yin, H., Bardelang, D., Xiao, J., ZhengRuibing, Y. W., and Wang, R. (2017). Supramolecular Formulation of Nitidine Chloride Can Alleviate its Hepatotoxicity and Improve its Anticancer Activity. *Food Chem. Toxicol.* 109, 923–929. doi:10.1016/j.fct.2017.02.022

Lin, Q., Ma, C., Guan, H., Chen, L., Xie, Q., Cheng, X., et al. (2020). Metabolites Identification and Reversible Interconversion of Chelerythrine and Dihydrochelerythrine *In Vitro/In Vivo* in Rats Using Ultra-performance Liquid Chromatography Combined with Electrospray Ionization Quadrupole Time-Of-Flight Tandem Mass Spectrometry. *J. Pharm. Biomed. Anal.* 189, 113462. doi:10.1016/j.jpba.2020.113462

Liu, H., Feng, J., Feng, K., and Lai, M. (2014). Optimization of the Extraction Conditions and Quantification by RP-LC Analysis of Three Alkaloids in *Zanthoxylum Nitidum* Roots. *Pharm. Biol.* 52 (2), 255–261. doi:10.3109/13880209.2013.826244

Liu, X., Huang, C. Y., Yang, Y. F., Xu, Y. F., and Zhao, J. G. (2016). HPLC Fingerprint of Dan'e Fukang Decocted Extract Based on Hierarchical Clus. *Chin. Med. Sci. J.* 47 (11), 1388–1393. doi:10.16522/j.cnki.cjph.2016.11.011

Lu, Q., Ma, R., Yang, Y., Mo, Z., Pu, X., and Li, C. (2020). *Zanthoxylum Nitidum* (Roxb.) DC: Traditional Uses, Phytochemistry, Pharmacological Activities and Toxicology. *J. Ethnopharmacol.* 260, 112946. doi:10.1016/j.jep.2020.112946

Ma, X., Lv, B., Li, P., Jiang, X., Zhou, Q., Wang, X., et al. (2016). Identification of "multiple Components-Multiple Targets-Multiple Pathways" Associated with Naoxintong Capsule in the Treatment of Heart Diseases Using UPLC/Q-TOF-MS and Network Pharmacology. *Evid. Based Complement. Alternat Med.* 2016, 9468087. doi:10.1155/2016/9468087

Martens, H., and Naes, T. (1992). *Multivariate Calibration*. Great Britain: John Wiley & Sons.

Naso, L., Martínez, V. R., Lezama, L., Salado, C., Valcarcel, M., Ferrer, E. G., et al. (2016). Antioxidant, Anticancer Activities and Mechanistic Studies of the Flavone Glycoside Diosmin and its Oxidovanadium(IV) Complex. Interactions with Bovine Serum Albumin. *Bioorg. Med. Chem.* 24, 4108–4119. doi:10.1016/j.bmc.2016.06.053

Nguyen, T. H. V., Tran, T. T., Cam, T. I., Pham, M. Q., Pham, Q. L., Vu, D. H., et al. (2019). Alkaloids from *Zanthoxylum Nitidum* and Their Cytotoxic Activity. *Nat. Product. Commun.* 14 (5), 1934578X1984413. doi:10.1177/1934578X19844133

Pang, H. Q., An, H. M., Yang, H., Wu, S. Q., Fan, J. L., Mi, L., et al. (2019). Comprehensive Chemical Profiling of Yindan Xinnaotong Soft Capsule and its Neuroprotective Activity Evaluation *In Vitro*. *J. Chromatogr. A.* 1601, 288–299. doi:10.1016/j.chroma.2019.05.023

Pradeep, K., Ko, K. C., Choi, M. H., Kang, J. A., Chung, Y. J., and Park, S. H. (2012). Protective Effect of Hesperidin, a Citrus Flavanoglycone, against γ-radiation-induced Tissue Damage in Sprague-Dawley Rats. *J. Med. Food* 15, 419–427. doi:10.1089/jmf.2011.1737

Qiao, J., Wang, G., Li, W., and Li, X. (2018). A Deep Belief Network with PLSR for Nonlinear System Modeling. *Neural Netw.* 104, 68–79. doi:10.1016/j.neunet.2017.10.006

Qiao, R., Zhou, L., Zhong, M., Zhang, M., Yang, L., Yang, Y., et al. (2021). Spectrum-effect Relationship between UHPLC-Q-TOF/MS Fingerprint and Promoting Gastrointestinal Motility Activity of *Fructus Aurantii* Based on Multivariate Statistical Analysis. *J. Ethnopharmacol.* 279, 114366. doi:10.1016/j.jep.2021.114366

Rivera, D., Allkin, R., Obón, C., Alcaraz, F., Verpoorte, R., and Heinrich, M. (2014). What Is in a Name? the Need for Accurate Scientific Nomenclature for Plants. *J. Ethnopharmacology* 152, 393–402. doi:10.1016/j.jep.2013.12.022

Seidemann, J. (2005). *World Spice Plants*. Berlin, Heidelberg, New York: Springer-Verlag. doi:10.1007/3-540-27908-3

Sun, G., and Liu, J. (2007). Qualitative and Quantitative Assessment of the HPLC Fingerprints of *Ginkgo Biloba* Extract by the Involution Similarity Method. *Anal. Sci.* 23, 955–958. doi:10.2116/analsci.23.955

Tu, Y. (2016). Artemisinin-a Gift from Traditional Chinese Medicine to the World (Nobel Lecture). *Angew. Chem. Int. Ed. Engl.* 55, 10210–10226. doi:10.1002/anie.201601967

Wang, F., Wang, B., Wang, L., Xiong, Z. Y., Gao, W., Li, P., et al. (2017). Discovery of Discriminatory Quality Control Markers for Chinese Herbal Medicines and Related Processed Products by Combination of Chromatographic Analysis and Chemometrics Methods: Radix Scutellariae as a Case Study. *J. Pharm. Biomed. Anal.* 138, 70–79. doi:10.1016/j.jpba.2017.02.004

Wang, M. X. (1980). Study on the Chemical Components of Zanthoxylum Nitidum. *J. Sun Yat-sen Univ. (Med. Sci).* 1 (4), 341–349. doi:10.13471/j.cnki.J.sun.yat-sen.univ(med.Sci).1980.0065

Wang, Y. L., Zhang, Q., Yin, S. J., Cai, L., Yang, Y. X., Liu, W. J., et al. (2019). Screening of Blood-Activating Active Components from Danshen-Honghua Herbal Pair by Spectrum-Effect Relationship Analysis. *Phytomedicine* 54, 149–158. doi:10.1016/j.phymed.2018.09.176

Wang, Z., Jiang, W., Zhang, Z., Qian, M., and Du, B. (2012). Nitidine Chloride Inhibits LPS-Induced Inflammatory Cytokines Production via MAPK and NF-kappaB Pathway in RAW 264.7 Cells. *J. Ethnopharmacol.* 144, 145–150. doi:10.1016/j.jep.2012.08.041

Xiao, J., Song, N., Lu, T., Pan, Y., Song, J., Chen, G., et al. (2018). Rapid Characterization of TCM Qianjinteng by UPLC-QTOF-MS and its Application in the Evaluation of Three Species of *Stephania*. *J. Pharm. Biomed. Anal.* 156, 284–296. doi:10.1016/j.jpba.2018.04.044

Xie, P. S., and Leung, A. Y. (2009). Understanding the Traditional Aspect of Chinese Medicine in Order to Achieve Meaningful Quality Control of Chinese Materia Medica. *J. Chromatogr. A.* 1216, 1933–1940. doi:10.1016/j.chroma.2008.08.045

Xie, Y. F. (2000). Antioxidation Effect of *Zanthoxylum Nitidum* (Roxb.) DC. Extracts. *Lishizhen Med. Mater. Med. Res.* 11 (1), 1–2.

Yang, C. H., Cheng, M. J., Chiang, M. Y., Kuo, Y. H., Wang, C. J., and Chen, I. S. (2008). Dihydrobenzo[c]phenanthridine Alkaloids from Stem Bark of Zanthoxylum Nitidum. *J. Nat. Prod.* 71 (4), 669–673. doi:10.1021/np700745f

Yang, P., Qing, Z. X., Xiang, F., Mo, C. M., and Tang, Q. (2017). HPLC-Q-TOF/MS Method for Identification of Alkaloids in *Zanthoxylum Nitidum* and *Zanthoxylum Echinocarpum*. *Chin. Tradit. Pat. Med.* 39 (8), 1646–1650. doi:10.3969/j.issn.1001-1528.2017.08.022

Zar, J. H. (2005). Spearman Rank Correlation. *Encyclopedia of biostatistics* 7. doi:10.1002/0470011815.b2a15150

Zhang, C., Qian, D. D., Yu, T., Yang, H., Li, P., and Li, H. J. (2021). Multi-parametric Cellular Imaging Coupled with Multi-Component Quantitative Profiling for Screening of Hepatotoxic Equivalent Markers from Psoraleae Fructus. *Phytomedicine* 93, 153518. Available online 17 February 2021. doi:10.1016/j.phymed.2021.153518

Zhang, H., Zhang, D., Ray, K., and Zhu, M. (2009). Mass Defect Filter Technique and its Applications to Drug Metabolite Identification by High-Resolution Mass Spectrometry. *J. Mass. Spectrom.* 44 (7), 999–1016. doi:10.1002/jms.1610

Zhang, H., Zhu, M., Ray, K. L., Ma, L., and Zhang, D. (2008). Mass Defect Profiles of Biological Matrices and the General Applicability of Mass Defect Filtering for Metabolite Detection. *Rapid Commun. Mass. Spectrom.* 22 (13), 2082–2088. doi:10.1002/rcm.3585

Zhang, H. L., Gan, X. Q., Fan, Q. F., Yang, J. J., Zhang, P., Hu, H. B., et al. (2017). Chemical Constituents and Anti-inflammatory Activities of Maqian (*Zanthoxylum Myriacanthum Var. Pubescens*) Bark Extracts. *Sci. Rep.* 7, 45805. doi:10.1038/srep45805

Zhang, W., Huai, Y., Miao, Z., Qian, A., and Wang, Y. (2019). Systems Pharmacology for Investigation of the Mechanisms of Action of Traditional Chinese Medicine in Drug Discovery. *Front. Pharmacol.* 10, 743. doi:10.3389/fphar.2019.00743

Zhang, X. F., Chen, J., Yang, J. L., and Shi, Y. P. (2018). UPLC-MS/MS Analysis for Antioxidant Components of Lycii Fructus Based on Spectrum-Effect Relationship. *Talanta* 180, 389–395. doi:10.1016/j.talanta.2017.12.078

Zhang, Y., Luo, Z., Wang, D., He, F., and Li, D. (2014). Phytochemical Profiles and Antioxidant and Antimicrobial Activities of the Leaves of *Zanthoxylum Bungeanum*. *ScientificWorldJournal* 2014, 181072. doi:10.1155/2014/181072

Zhao, L. N., Guo, X. X., Liu, S., Feng, L., Bi, Q. R., Wang, Z., et al. (2018). (±)-Zanthonitidine A, a Pair of Enantiomeric Furoquinoline Alkaloids from Zanthoxylum Nitidum with Antibacterial Activity. *Nat. Prod. Bioprospect* 8 (5), 361–367. doi:10.1007/s13659-018-0169-7

Zhou, W., Shan, J., and Meng, M. (2018). A Two-step Ultra-high-performance Liquid Chromatography-Quadrupole/time of Flight Mass Spectrometry with Mass Defect Filtering Method for Rapid Identification of Analogues from Known Components of Different Chemical Structure Types in Fructus Gardeniae-Fructus Forsythiae Herb Pair Extract and in Rat's Blood. *J. Chromatogr. A.* 1563, 99–123. doi:10.1016/j.chroma.2018.05.067

Conflict of Interest: The authors declare that the research was conducted in the absence of any commercial or financial relationships that could be construed as a potential conflict of interest.

Publisher's Note: All claims expressed in this article are solely those of the authors and do not necessarily represent those of their affiliated organizations or those of the publisher, the editors, and the reviewers. Any product that may be evaluated in this article, or claim that may be made by its manufacturer, is not guaranteed or endorsed by the publisher.

frontiers in Pharmacology

ORIGINAL RESEARCH
published: 10 March 2022
doi: 10.3389/fphar.2022.842890

Unveiling Dynamic Changes of Chemical Constituents in Raw and Processed Fuzi With Different Steaming Time Points Using Desorption Electrospray Ionization Mass Spectrometry Imaging Combined With Metabolomics

*Yue Liu[1,2], Xuexin Yang[3], Chao Zhou[3], Zhang Wang[2], Tingting Kuang[2], Jiayi Sun[4], Binjie Xu[4], Xianli Meng[4], Yi Zhang[2] and Ce Tang[1,2]**

[1]State Key Laboratory of Southwestern Chinese Medicine Resources, Chengdu University of Traditional Chinese Medicine, Chengdu, China, [2]School of Ethnic Medicine, Chengdu University of Traditional Chinese Medicine, Chengdu, China, [3]Waters Technology (Beijing) Co., Ltd., Beijing, China, [4]Innovative Institute of Chinese Medicine and Pharmacy, Chengdu University of Traditional Chinese Medicine, Chengdu, China

OPEN ACCESS

Edited by:
Abdul Rohman,
Gadjah Mada University, Indonesia

Reviewed by:
Bin Hu,
Jinan University, China
Katy Margulis,
Hebrew University of Jerusalem, Israel

***Correspondence:**
Ce Tang
tangce@cdutcm.edu.cn

Specialty section:
This article was submitted to Ethnopharmacology, a section of the journal Frontiers in Pharmacology

Received: 24 December 2021
Accepted: 16 February 2022
Published: 10 March 2022

Citation:
Liu Y, Yang X, Zhou C, Wang Z, Kuang T, Sun J, Xu B, Meng X, Zhang Y and Tang C (2022) Unveiling Dynamic Changes of Chemical Constituents in Raw and Processed Fuzi With Different Steaming Time Points Using Desorption Electrospray Ionization Mass Spectrometry Imaging Combined With Metabolomics. Front. Pharmacol. 13:842890. doi: 10.3389/fphar.2022.842890

Fuzi is a famous toxic traditional herbal medicine, which has long been used for the treatment of various diseases in China and many other Asian countries because of its extraordinary pharmacological activities and high toxicity. Different processing methods to attenuate the toxicity of Fuzi are important for its safe clinical use. In this study, desorption electrospray ionization mass spectrometry imaging (DESI-MSI) with a metabolomics-combined multivariate statistical analysis approach was applied to investigate a series of *Aconitum* alkaloids and explore potential metabolic markers to understand the differences between raw and processed Fuzi with different steaming time points. Moreover, the selected metabolic markers were visualized by DESI-MSI, and six index alkaloids' contents were determined through HPLC. The results indicated visible differences among raw and processed Fuzi with different steaming times, and 4.0 h is the proper time for toxicity attenuation and efficacy reservation. A total of 42 metabolic markers were identified to discriminate raw Fuzi and those steamed for 4.0 and 8.0 h, which were clearly visualized in DESI-MSI. The transformation from diester-diterpenoid alkaloids to monoester-diterpenoid alkaloids and then to non-esterified diterpene alkaloids through hydrolysis is the major toxicity attenuation process during steaming. DESI-MSI combined with metabolomics provides an efficient method to visualize the changeable rules and screen the metabolic markers of *Aconitum* alkaloids during steaming. The wide application of this technique could help identify markers and reveal the possible chemical transition mechanism in the "Paozhi" processes of Fuzi. It also provides an efficient and easy way to quality control and ensures the safety of Fuzi and other toxic traditional Chinese medicine.

Keywords: Fuzi, DESI-MSI, diterpenoid alkaloids, toxicity attenuation, processing

1 INTRODUCTION

Fuzi, the lateral root of *Aconitum carmichaelii* Debeaux (Fam. Ranunculaceae), primarily cultivated in Jiangyou and Butuo in Sichuan, China, has been an indispensable herb in traditional Chinese medicine (TCM) for thousands of years (Chinese Pharmacopoeia Commission, 2020). Jiangyou Fuzi and Butuo Fuzi are not only well-known genuine medicinal materials but also important agricultural products of Sichuan Province. The initial record of Fuzi can be dated back to the Han Dynasty in the earliest Chinese material medical classic work "Shennong Bencao Jing," wherein it is listed in the inferior category because of its highly toxic properties (Singhuber et al., 2009; Zhou et al., 2015). However, Fuzi also has potent efficacy to restore from collapse, reinforce fire and Yang, and dispel cold to relieve pain (Luo et al., 2019; Chinese Pharmacopoeia Commission, 2020). It is usually combined with other herbs in formulations such as Si Ni Tang, Shen Fu Tang, and Fuzi Lizhong Wan to treat cold-damp-type illness (Singhuber et al., 2009). Given its outstanding clinical effects, Fuzi is one of "The Four Pillars" of TCM, together with *Ginseng Radix et Rhizoma*, *Rehmanniae Radix*, and *Rhei Radix et Rhizoma* (Dong et al., 2020). Modern studies have indicated that Fuzi has cardiotonic, anti-inflammatory, analgesic, and anti-tumor activities, which can be utilized to heal heart failure, shock, and hypotension subsequent to acute myocardial infarction, coronary heart disease, rheumatic heart disease, rheumatoid arthritis, tumors, skin wounds, depression, and diarrhea (Li et al., 2012; Zhao et al., 2012; Wu et al., 2018; Chinese Pharmacopoeia Commission, 2020). However, the toxicity of Fuzi coexists with its pharmaceutical activities, and thousands of Fuzi poisoning cases have been reported worldwide (Yang et al., 2018; Lei et al., 2021). Therefore, Fuzi is only used internally after processing, and various processing methods have been established by which the highly toxic alkaloids were transformed to lowly toxic and non-toxic forms through processing. The studies of toxic components and their mechanisms and the proper methods to attenuate the toxicity and reserve efficacy are the primary concern of scholars.

A literature survey has revealed that over 100 alkaloids have been isolated and identified in this herb, including C_{20}-, C_{19}-, and C_{18}-diterpenoid alkaloids and double diterpenoid alkaloids, which are the main source of biological activities and toxicities. Among these alkaloids, the aconitine type, which belongs to C_{19}-diterpenoid alkaloids, can be further divided into four categories: diester-diterpenoid alkaloids (DDAs), monoester-diterpenoid alkaloids (MDAs), non-esterified diterpene alkaloids (NDAs) (**Figure 1**), and lipo-diterpenoid alkaloids (LDAs). In recent years, numerous studies have demonstrated that the high toxicity of Fuzi is primarily attributed to DDAs (Tong et al., 2013). Based on previous studies, the main toxic effect of Fuzi is that it can affect the central nervous system, heart, and muscle tissues because of the interaction with voltage-dependent sodium channels, modulation of neurotransmitter release and related receptors, promotion of lipid peroxidation, and induction of cell apoptosis in the heart, liver, or other organs (Fu et al., 2006; Zhou et al., 2015; Liu et al., 2017). Therefore, the pretreatment method to reduce such toxic components is highly essential for the safe use of Fuzi.

The appropriate processing methods, which are known as "Paozhi" in Chinese, for TCM are usually necessary to reduce the toxicity while retaining or enhancing its pharmacological activities. Various methods can be used to process Fuzi, such as soaking, saturating, steaming, and decocting. According to the Chinese Pharmacopeia (CP) (2020 Edition), soaking in Danba (halogen solution), then continuous soaking with salt, steaming or decocting, long rinsing, and oven drying are the major processing methods for Fuzi (Chinese Pharmacopoeia Commission, 2020). During these heating procedures, the highly toxic DDAs were hydrolyzed to low toxic MDAs and non-toxic NDAs (Wang et al., 2003; Zhao et al., 2010; Tan et al., 2016). However, toxic *Aconitum* alkaloids are also responsible for the pharmacological activity and therapeutic efficacy of Fuzi, and

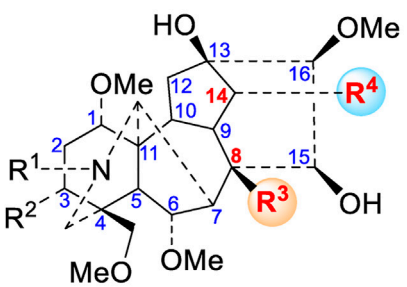

Type	Compound	R^1	R^2	R^3	R^4
DDAs	Aconitine	Et	OH	OAc	OBz
	Mesaconitine	Me	OH	OAc	OBz
	Hypaconitine	Me	H	OAc	OBz
MDAs	Benzoylaconine	Et	OH	OH	OBz
	Benzoylmesaconine	Me	OH	OH	OBz
	Benzoylhypaconine	Me	H	OH	OBz
NDAs	Aconine	Et	OH	OH	OH
	Mesaconine	Me	OH	OH	OH
	Hypaconine	Me	H	OH	OH

FIGURE 1 | Main C_{19}-diterpenoid alkaloids of Fuzi.

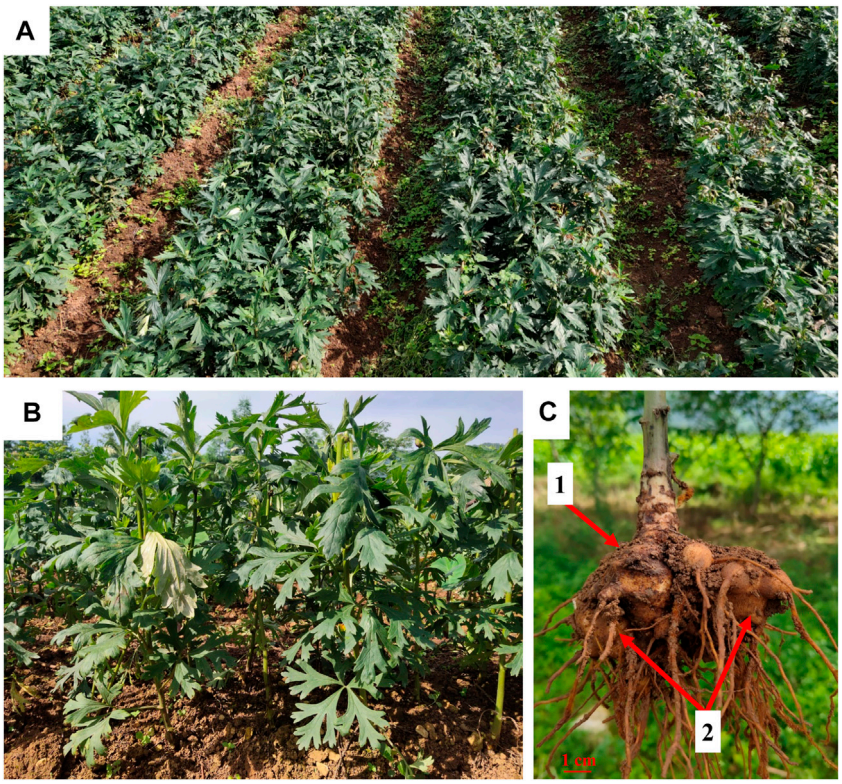

FIGURE 2 | Fuzi planting base in Jiangyou, Sichuan **(A,B)**. The mother root (1) and lateral root (2) of *A. carmichaelii* **(C)**.

efficacy preservation should be observed during toxicity attenuation. Recent research has indicated that DDAs, MDAs, and water-soluble active constituents have a massive loss after soaking in Danba and subsequent rinsing. Moreover, inorganic impurities are easily introduced to Fuzi (Ye et al., 2019). Thus, a Danba-free process becomes a more recognized processing approach for Fuzi. Nevertheless, the visual changes and distribution of DDAs and MDAs during steaming are rarely investigated. Therefore, a suitable methodology to explore these variation characteristics is highly necessary.

At present, the high-performance liquid chromatography (HPLC) and liquid chromatography coupled with mass spectrometry (LC-MS) are commonly used methods for alkaloid analysis of Fuzi (Yue et al., 2009; Xu et al., 2014; Yang et al., 2014; Miao et al., 2019; Sun et al., 2020). However, these techniques require complex preparation procedures, especially extraction from crushed samples. The ambient ionization MS, such as direct analysis in real-time mass spectrometry (DART-MS), was also utilized for direct analysis of Fuzi and other processed herbal medicine. Nevertheless, this method still needs sample pretreatment (Zhu et al., 2012). Therefore, analyzing and recognizing the distribution of specific alkaloids in original Fuzi has become challenging.

Mass spectrometry imaging (MSI) integrates sensitivities and high-throughput screening mass spectrometry with spatial and temporal chemical information and enables the visualized distribution of specific metabolites within non-destructive tissues (Stoeckli et al., 2001; Garza et al., 2018; Parrot et al., 2018). Matrix-assisted laser desorption/ionization (MALDI) and desorption electrospray ionization (DESI) are the commonly used ionization techniques for MSI (Parrot et al., 2018; Xu et al., 2019). Compared with MALDI-MSI, DESI-MSI allows 2D polar biomolecular distribution analysis with minimal sample pretreatment. Furthermore, no matrix is needed at ambient conditions (Takáts et al., 2004).

The extensive application of DESI-MSI to determine natural products (primary and secondary metabolites) demonstrated its power and good practicability (Dill et al., 2009; Li et al., 2012; Hemalatha and Pradeep, 2013; Hemalatha et al., 2015; Liao et al., 2019; Mohana Kumara et al., 2019).

In this study, an easy-handling and comprehensive method combining DESI-MSI with metabolomics was applied to investigate the variation of key ester-diterpenoid alkaloids and identify the metabolic markers in raw and processed Fuzi with different steaming time points. In addition, the contents of six ester-type alkaloids were determined through HPLC.

2 MATERIALS AND METHODS

2.1 Materials and Reagents

The reference standards (>98%, quantification grade) of aconitine (**40**), mesaconitine (**22**), hypaconitine (**36**), benzoylaconine (**34**), benzoylmesaconine (**32**), and benzoylhypaconine (**29**) were

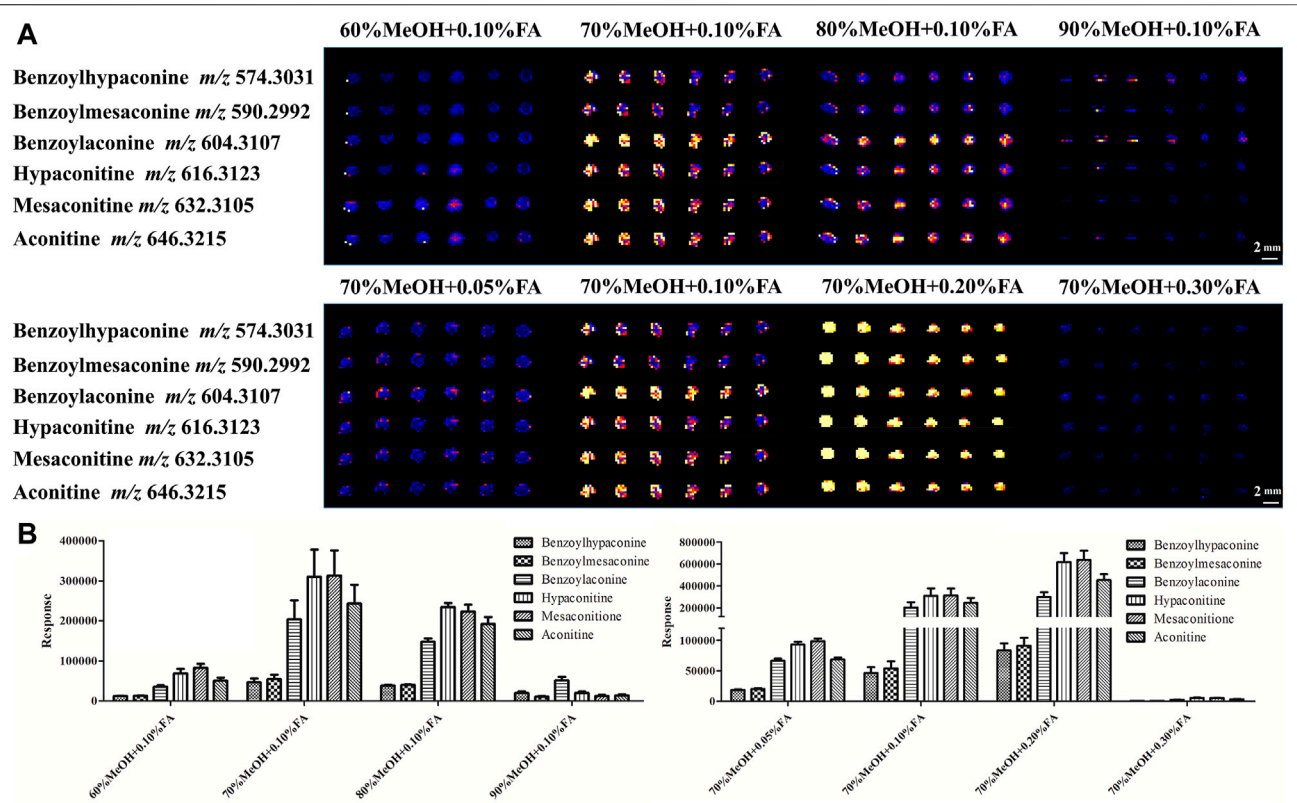

FIGURE 3 | DESI-MS images **(A)** and responses **(B)** of six alkaloids using different concentrations of MeOH with different proportions of FA.

TABLE 1 | Content determination of six ester-type alkaloids through HPLC (n = 3).

Steaming time (h)	Content of MDAs (mg/g)			Proportion of MDAs (%)	Content of DDAs (mg/g)			Proportion of DDAs (%)
	BMAC (32)	BAC (34)	BHAC (29)		MAC (39)	AC (40)	HAC (36)	
0	0.0478	0.0126	—	0.006	0.6694	0.7095	0.3830	0.176
1.0	0.6698	0.1659	0.3179	0.115	—	0.3385	—	0.034
2.0	0.6053	0.1851	0.6687	0.146	—	0.2664	—	0.027
3.0	0.4103	0.0664	0.6561	0.113	—	0.1627	—	0.016
4.0	0.3639	0.0951	0.5022	0.096	—	0.0064	—	0.006
5.0	0.4212	0.1551	0.5578	0.113	—	—	—	—
6.0	0.3412	0.0646	0.7582	0.116	—	—	—	—
7.0	0.4145	0.0770	0.7992	0.129	—	—	—	—
8.0	0.4912	0.0817	0.7918	0.137	—	—	—	—
9.0	0.2623	0.0282	0.8971	0.119	—	—	—	—
10.0	0.3112	0.1098	0.4433	0.086	—	—	—	—

obtained from Chengdu Herbpurify Co., Ltd. (Chengdu, China). LC-MS-grade methanol (MeOH), formic acid (FA), acetonitrile, and isopropanol were purchased from Sigma-Aldrich (Sigma-Aldrich, United States). Ammonium acetate of HPLC grade was obtained from Chengdu Chron Chemical Co., Ltd. (Chengdu, China). The Elga Labwater Purelab system (Elga-Veolia, High Wycombe, United Kingdom) was used to obtain purified water for UPLC analyses. All other reagents were of analytical grade.

A batch of crude Fuzi was collected from Jiangyou (Sichuan, China) and authenticated by Professor Yi Zhang from Chengdu University of TCM (**Figure 2**). The voucher specimens were deposited in the School of Ethnic Medicine, Chengdu University of TCM, China.

2.2 Sample Preparation and DESI-MSI Analysis

Cleaned raw Fuzi were randomly divided into 11 groups, one of which was selected as raw Fuzi (without steaming), and the rest were placed into a suitable container for steaming for 1.0, 2.0, 3.0, 4.0, 5.0, 6.0, 7.0, 8.0, 9.0, and 10.0 h. All the samples were directly

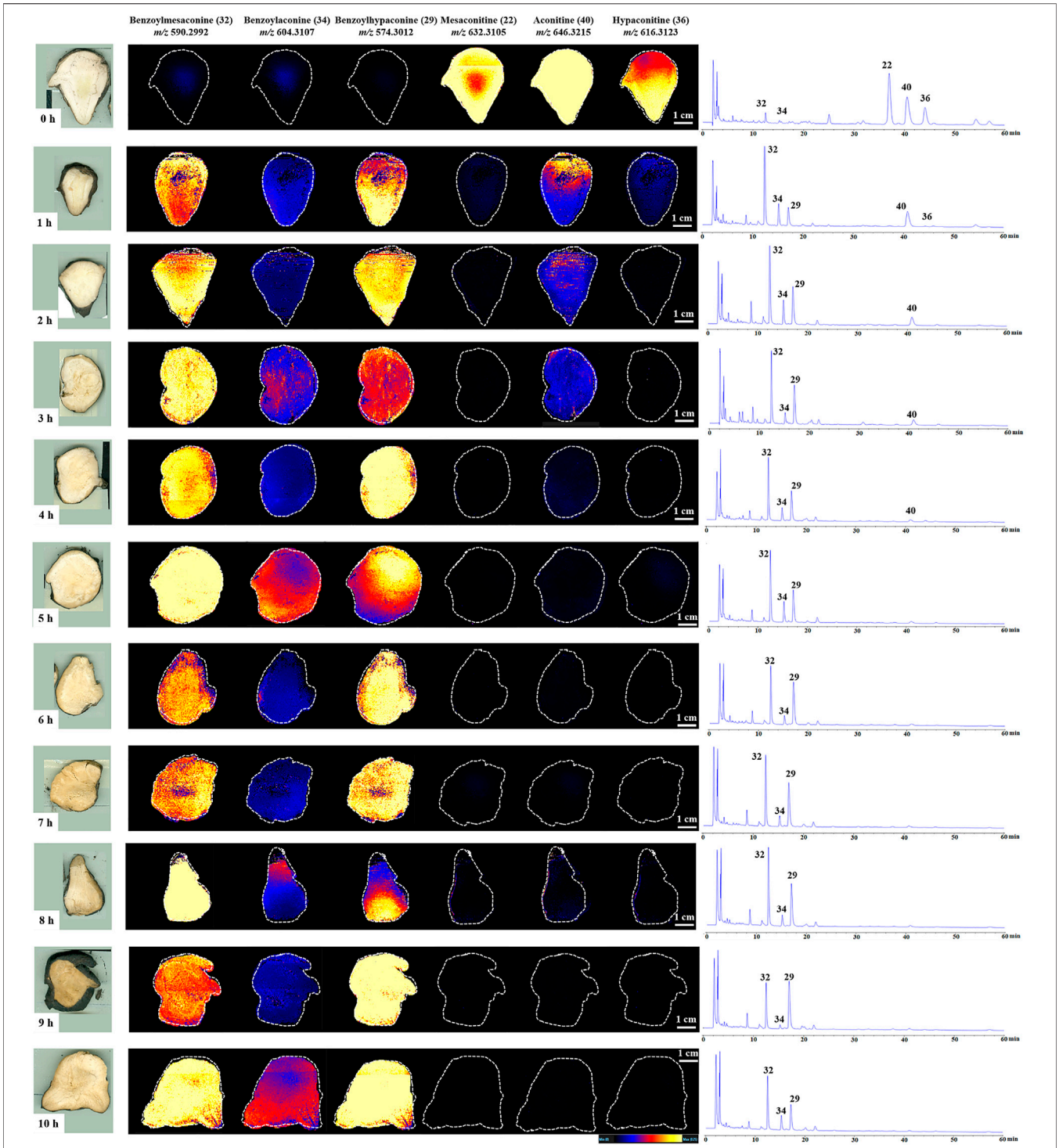

FIGURE 4 | DESI-MS images and the corresponding HPLC chromatograms of six ester-type alkaloids in raw and processed Fuzi steamed for different time points.

sliced, and the thickness of cross-sectional slices was approximately 5 mm. Subsequently, the sample was glued onto glass slides using double-sided tape and then subjected to DESI-MSI analysis.

Imaging experiments were conducted using a Waters Xevo G2-XS QTof mass spectrometer equipped with a DESI source (Waters Corporation, Milford, MA, United States). The following DESI parameters were optimized to obtain good signal intensity: nebulizing gas (dry nitrogen) pressure: 0.45 MPa; spray solvent 70% MeOH, 30% H_2O, 0.2% FA, and 0.1 mM leucine enkephalin (LE) delivered at 2 μl/min; capillary voltage: 4.5 kV; and

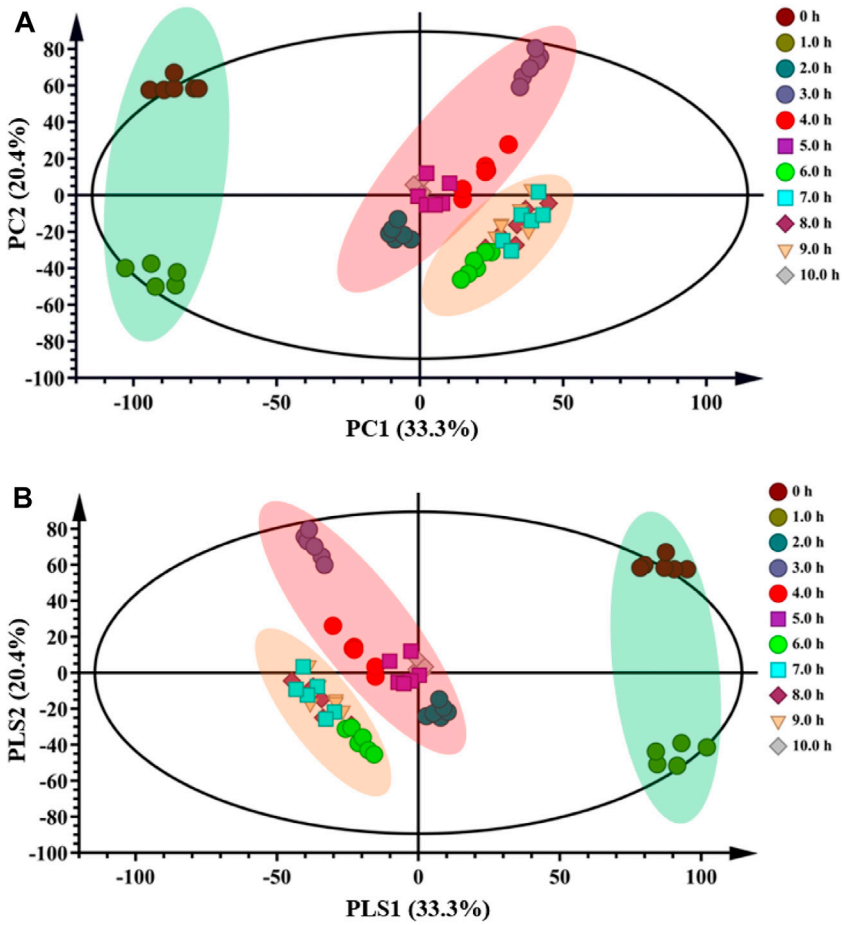

FIGURE 5 | PCA **(A)** and PLS-DA **(B)** score plots of raw and processed Fuzi steamed for different time points.

ionization mode: positive. The pixel size (X and Y pixel size of 200 μm) was determined on the basis of the total scan time of the mass spectra and the x–y scanner speed. A mass range of *m/z* 100–1,000 and the scan rate of 400 μm/s were used for imaging, and the images were viewed using high-definition image (HDI) v1.5 software (Waters Corporation, Milford, MA, United States). The MS images were created from Raw MS files through HDI with LE as the lockmass (m/z 556.2766) for resolution MS.

2.3 Desorption Electrospray Ionization Mass Spectrometry Imaging Data Processing and Statistical Analysis

MS raw data files were imported into HDI for imaging. The regions of interest (ROIs) were selected from root areas. Each sample had six ROIs that were converted into a data matrix of mass *m/z* and signal intensity. The data matrix was imported into SIMCA-P 13.0 (Umetrics, Umea, Sweden) to establish PAC, PLS-DA, and OPLS-DA models for distinguishing classification analysis and selecting crucial variable constituents for Fuzi steaming for different time points. The data were standardized using a Pareto-scaling technique.

2.4 Sample Preparation and HPLC Analysis

According to the CP (2020 Edition) (Chinese Pharmacopoeia Commission, 2020), all the processed or raw samples were oven-dried at 50°C for 24 h. Then, the dried samples were finely powered and passed through a 50-mesh sieve. Each sample powder (2.0 g) was weighed and then extracted by ultrasonication with 3 ml of ammonia TS and 50 ml of isopropanol–ethyl acetate (1/1, *v/v*) for 30 min (300 w, 40 kHz). Following extraction, isopropanol–ethyl acetate (1/1, *v/v*) was added to compensate for the lost weight during extraction and then filtered. 25 ml of filtrate was accurately measured and evaporated under reduced pressure at 40°C to dryness. Three milliliters of 0.05 M hydrochloric acid–methanol solution was precisely added to dissolve the residue. The supernatants were used as the sample solution after being centrifuged at 15,000 rpm for 30 min. The concentration of aconitine (AC, **40**), mesaconitine (MAC, **22**), hypaconitine (HAC, **36**), benzoylaconine (BAC, **34**), benzoylmesaconine (BMAC, **32**), and benzoylhypaconine (BHAC, **29**) in every sample was calculated on the basis of established calibration curves.

The filtered sample was analyzed using Agilent Technology 1260 Infinity (Agilent Technologies, Santa Clara, CA,

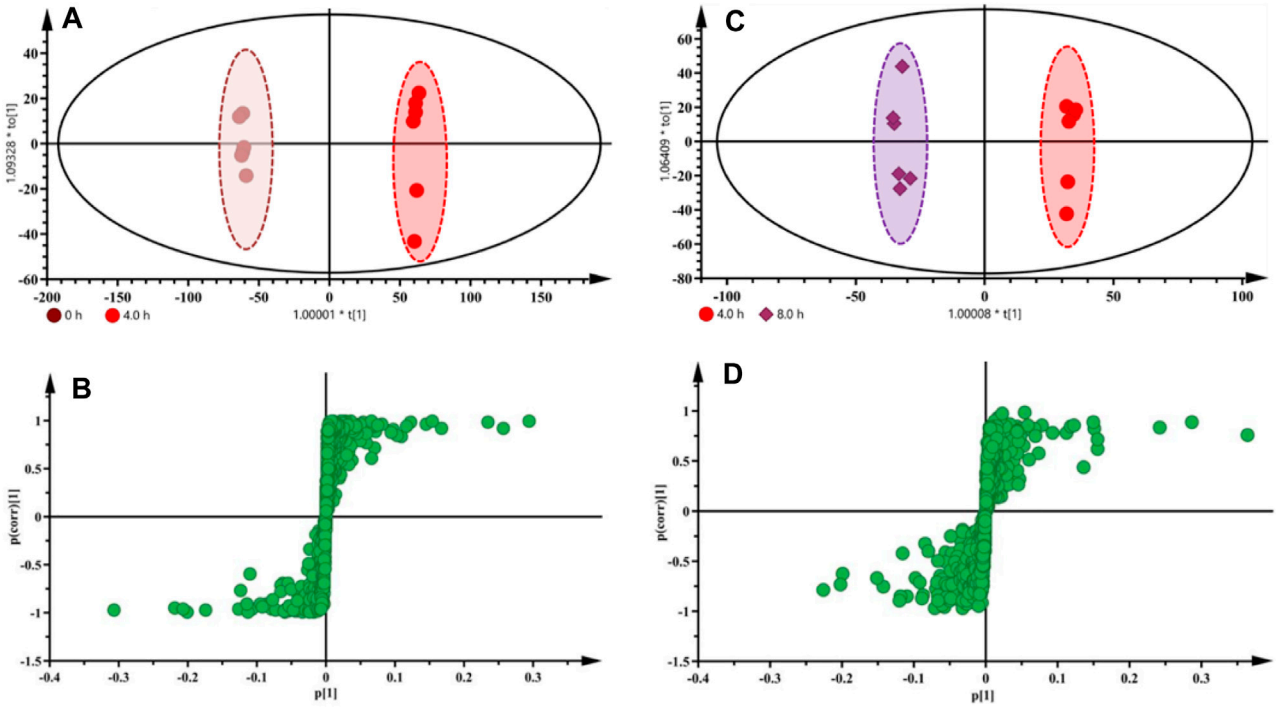

FIGURE 6 | OPLS-DA score plots and S-plots based on raw and processed Fuzi steamed for 4.0 h **(A,B)** and Fuzi steamed for 4.0 and 8.0 h **(C,D)** from DESI-MSI data.

United States) equipped with a binary pump, mobile phase degasser, temperature-controlled autosampler, column thermostat, and diode array detector (1260-DAD). HPLC separation was performed on an Agilent Eclipse XDB C_{18} column (4.6 mm × 250 mm, 5 μm) and maintained at 30°C. The mobile phase consisted of 0.04 M of ammonium acetate solution (solvent A, adjusting pH to 8.5 with an ammonia solution) and acetonitrile (solvent B) using the following gradient: 20%–28% B for 0–10 min, 28%–30% B for 10–20 min, 30%–35% B for 20–50 min, and 35%–38% B for 50–60 min. The flow rate was kept at 1 ml/min, and the injection volume was 10 μl. The UV detection wavelength was set at 235 nm.

HPLC-DAD was validated with regard to linearity, stability, recovery, repeatability, and precision. The storage solutions of six compounds were used in the regression equations between the peak areas and concentrations of six compounds. The limit of detection (LOD) and quantification (LOQ) were determined at signal-to-noise ratios of 3 and 10, respectively.

3 RESULTS

3.1 Optimization of Spray Solvent for Desorption Electrospray Ionization Mass Spectrometry Imaging Analysis

In DESI analysis, the ratio selection of solvent and acid is an important step to achieve sensitive and high MS signal response to target compounds. The solvent compositions are selected based on the analyte of interest and the tissue surface, which play a major role in the elution of each category of the compound (Claude et al., 2017). A large number of literature studies indicate that Fuzi primarily contains alkaloids. Therefore, a mixture of MeOH and water (with optional FA for positive ion mode analysis) is used as the DESI spray solvent for alkaloid analysis (Kumara et al., 2016). In the present experiment, the volume ratio of water to MeOH and FA concentration were evaluated (**Supplementary Figure S1**). As shown in **Figures 3A,B**, using 70% MeOH with 0.2% FA provided high response and uniform detection of six ester-type alkaloids across the Fuzi sample. Therefore, this solvent condition was used in the following MSI experiments.

3.2 Effects of Steaming on Toxicity and Active Components of Fuzi

As a highly toxic medicinal material, improper use of Fuzi will seriously affect the safety of people. According to the CP (2020 edition), DDAs shall not exceed 0.020% with regard to the total amount of mesaconitine (MAC, **22**), hypaconitine (HAC, **36**), and aconitine (AC, **40**). In addition, the total amount of MDAs, including benzoylmesaconine (BMAC, **32**), benzoylaconine (BAC, **34**), and benzoylhypaconine (BHAC, **29**), should not be less than 0.010%.

The changes of the six aforementioned alkaloids in the samples of Fuzi steamed for different time points were

TABLE 2 | Chemical information of 42 metabolic markers of Fuzi for different steaming time points.

No.	Putative identification	Molecular formula	$[M+H]^+$		Delta (ppm)	MDa	VIP	
			Theoretical (*m/z*)	Measured (*m/z*)			$VIP_{0h/4h}$	$VIP_{4h/8h}$
1	Hetisine	$C_{20}H_{27}NO_3$	330.2069	330.2090	6.4	2.1	3.29	—
2	Fuzitine	$C_{20}H_{23}NO_4$	342.1705	342.1706	0.3	0.1	2.13	4.55
3	Denudatine/Guanfu base H	$C_{22}H_{33}NO_2$	344.2590	344.2597	2	0.7	—	2.69
4	3-*epi*-Ignavinol	$C_{20}H_{27}NO_4$	346.2018	346.2000	–5.2	–1.8	2.49	2.84
5	Dictysine	$C_{21}H_{33}NO_3$	348.2539	348.2546	2	0.7	—	1.51
6	Songorine	$C_{22}H_{31}NO_3$	358.2382	358.2386	1.1	0.4	3.06	6.65
7	Napelline	$C_{22}H_{33}NO_3$	360.2539	360.2543	1.1	0.4	—	4.26
8	16-Hydroxycardiopetaline	$C_{21}H_{33}NO_4$	364.2488	364.2479	–2.5	–0.9	1.37	3.58
9	Karakanine	$C_{22}H_{33}NO_4$	376.2488	376.2495	1.9	0.7	1.22	1.51
10	Karacoline	$C_{22}H_{35}NO_4$	378.2644	378.2618	–6.9	–2.6	2.54	8.23
11	Karacolidine/Chuanfumine	$C_{22}H_{35}NO_5$	394.2593	394.2613	5.1	2	3.32	2.55
12	Nevadenine	$C_{23}H_{35}NO_5$	406.2593	406.2585	–2	–0.8	—	1.86
13	Isotalatizidine/Talatizidine	$C_{23}H_{37}NO_5$	408.2750	408.2755	1.2	0.5	5.29	7.22
14	Talatisamine	$C_{24}H_{39}NO_5$	422.2906	422.2891	–3.6	–1.5	2.28	4.39
15	Senbusine A/B	$C_{23}H_{37}NO_6$	424.2699	424.2707	1.9	0.8	2.68	—
16	Guiwuline	$C_{24}H_{37}NO_6$	436.2699	436.2690	–2.1	–0.9	1.28	1.07
17	Neoline	$C_{24}H_{39}NO_6$	438.2856	438.2841	–3.4	–1.5	8.17	11.09
18	Condelphine	$C_{25}H_{39}NO_6$	450.2856	450.2849	–1.6	–0.7	1.05	—
19	Fuziline	$C_{24}H_{39}NO_7$	454.2805	454.2823	4	1.8	3.79	—
20	14-*O*-acetyltalatizamine	$C_{26}H_{41}NO_6$	464.3012	464.3033	4.5	2.1	1.45	—
21	Hypaconine	$C_{24}H_{39}NO_8$	470.2754	470.2760	1.3	0.6	2.31	3.38
22	Mesaconine	$C_{24}H_{39}NO_9$	486.2703	486.2706	0.6	0.3	1.87	3.32
23	8-Acetyl-15-hydroxyneoline	$C_{26}H_{41}NO_8$	496.2910	496.2905	–1	–0.5	2.83	—
24	Episcopalisine	$C_{29}H_{39}NO_6$	498.2856	498.2887	6.2	3.1	1.28	—
25	Aconicarchamine B	$C_{31}H_{41}NO_7$	540.2961	540.2941	–3.7	–2	1.23	—
26	Dehydrated benzoylhypaconine	$C_{31}H_{41}NO_8$	556.2910	556.2920	1.8	1	1.80	—
27	Straconitines A	$C_{31}H_{43}NO_8$	558.3067	558.3067	0	0	1.14	—
28	6-*O*-benzoyleldelidine	$C_{32}H_{43}NO_8$	570.3067	570.3087	3.5	2	1.63	—
29	Benzoylhypaconine	$C_{31}H_{43}NO_9$	574.3016	574.3012	–0.7	–0.4	9.03	6.65
30	Pyraconitine	$C_{32}H_{43}NO_9$	586.3016	586.3032	2.7	1.6	3.00	—
31	Benzoyldeoxyaconine	$C_{32}H_{45}NO_9$	588.3173	588.3150	–3.9	–2.3	2.10	—
32	Benzoylmesaconine	$C_{31}H_{43}NO_{10}$	590.2965	590.2992	4.6	2.7	7.24	—
33	*N*-demethylhypaconitine	$C_{32}H_{43}NO_{10}$	602.2965	602.3012	7.8	4.7	1.24	—
34	Benzoylaconine	$C_{32}H_{45}NO_{10}$	604.3122	604.3107	–2.5	–1.5	—	2.12
35	10-Hydroxybenzoylmesaconine	$C_{31}H_{43}NO_{11}$	606.2914	606.2922	1.3	0.8	3.63	—
36	Hypaconitine	$C_{33}H_{45}NO_{10}$	616.3122	616.3123	0.2	0.1	9.45	2.24
37	10-Hydroxybenzoylaconine	$C_{32}H_{45}NO_{11}$	620.3071	620.3085	2.3	1.4	1.23	—
38	Indaconitine	$C_{34}H_{47}NO_{10}$	630.3278	630.3278	0	0	6.17	—
39	Mesaconitine	$C_{33}H_{45}NO_{11}$	632.3071	632.3105	5.4	3.4	6.85	—
40	Aconitine	$C_{34}H_{47}NO_{11}$	646.3227	646.3215	–1.9	–1.2	6.37	—
41	Beiwutine	$C_{33}H_{45}NO_{12}$	648.3020	648.3047	4.2	2.7	3.33	—
42	Aconifine	$C_{34}H_{47}NO_{12}$	662.3177	662.3190	2	1.3	2.26	—

analyzed by HPLC and DESI-MSI. The HPLC data (**Table 1**) showed that the content of three DDAs decreased under 0.020%, and MDAs increased above 0.010% in the investigated samples after 3.0 h of steaming. However, the MDA levels slightly declined to 0.096% after 4.0 h of steaming and then stabilized over 0.100% until 9.0 h of steaming. At 10.0 h of steaming, the total content of three MDAs reduced again. Therefore, the requirements stipulated by the CP can be met by steaming Fuzi for over 3.0 h. In addition, three DDAs of Fuzi could not be detected by HPLC (below the detection limit) after 5.0 h. The results of the methodological study are shown in **Supplementary Tables S1, S2**.

In situ molecular detection was conducted in simulated industrial sections of Fuzi using DESI-MS with a mass range of m/z 100–1,000 in the positive ion mode to explore the change process of six alkaloids specified by the CP during different steaming time points of Fuzi. As shown in the MS images (**Figure 4**), six alkaloids, namely, mesaconitine (**22**, *m/z* 632.3105), aconitine (**40**, *m/z* 646.3215), hypaconitine (**36**, *m/z* 616.3123), benzoylmesaconine (**32**, *m/z* 590.2992), benzoylaconine (**34**, *m/z* 604.3107), and benzoylhypaconine (**29**, *m/z* 574.3012), were visually presented and compared. With the extension of steaming time, the concentrations of three DDAs decreased sharply, whereas the three MDAs increased significantly, among which mesaconitine (**22**) and hypaconitine (**36**) decreased faster than aconitine (**40**) and could not be visualized after 1.0 h, and the intensity of benzoylmesaconine (**32**) and benzoylhypaconine (**29**)

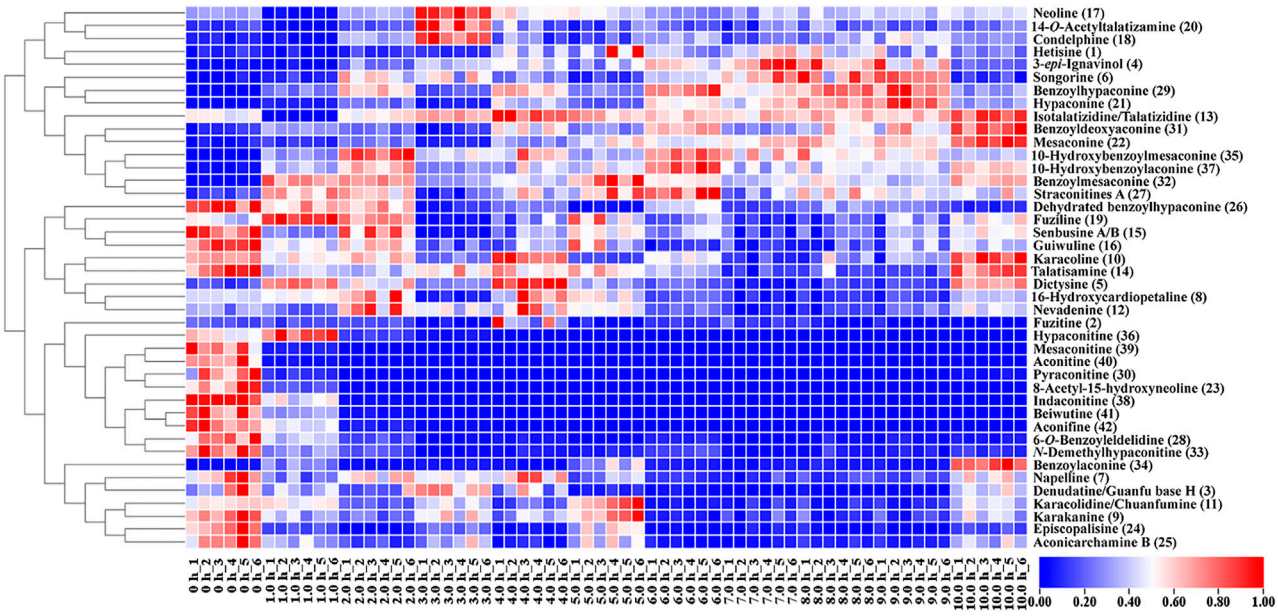

FIGURE 7 | Heat map of metabolic markers of raw and processed Fuzi steamed for different time points.

increased faster than that of benzoylaconine (**34**). The DESI-MSI results are consistent with those of HPLC experiments, which indicated its reliability.

3.3 PCA and PLS-DA of Raw and Processed Fuzi With Different Steaming Hours

A data matrix of mass *m*/*z* and signal intensity from DESI-MSI was submitted to PCA and PLS-DA to discriminate the variations of Fuzi with different steaming time points, visualize the underlying trend, and understand the metabolic differentiation among them. The PCA score plot (R^2X = 0.884 and Q^2 = 0.798) showed that all the ingredients could be classified into three major groups (**Figure 5A**). Raw Fuzi and processed Fuzi steamed only for 1.0 h were highly different from Fuzi steamed for more than 2.0 h. The ingredients of Fuzi steamed for 2.0–5.0 h were grouped together, but those steamed for 3.0 h were located relatively far away from the other samples. This may be due to the insufficient hydrolysis reaction from DDAs to MDAs. Fuzi steamed for 6.0–9.0 h were in a separate cluster. However, samples steamed for 10.0 h were back into the 2.0–5.0 h steaming group. The classification results also indicated that, after steaming for 5.0 h, these ingredients were located closer compared with those steamed for a short time. PLS-DA discrimination (R^2X = 0.916, R^2Y = 0.775, and Q^2 = 0.701) (**Figure 5B**) was in good agreement with the PCA model, and all samples were separated into three groups. In addition, the samples steamed for a longer time were distributed closer. The close points indicated that these samples share similar chemical components. Combined with the results of HPLC, DESI-MSI, and multivariate statistical analysis, 4.0 h is demonstrated to be the appropriate steaming time for toxicity attenuation and efficacy reservation of Fuzi.

3.4 Metabolic Markers for the Identification of Raw and Processed Fuzi With Different Steaming Hours

Based on the HPLC, DESI-MSI, PCA, and PLS-DA results, 4.0 and 8.0 h were selected as the key steaming time points to uncover the metabolic markers. OPLS-DA was applied to compare the metabolic changes between the 0 and 4.0 h groups and the 4.0 and 8.0 h groups. As shown in **Figures 6A,C**, the Fuzi samples with different steaming time points were separated from one another, indicating that the metabolic perturbation significantly occurred in raw Fuzi and processed Fuzi steamed at different time points. As shown in the corresponding S-plot (**Figures 6B,D**), the ions away from the origin contributed significantly to the separation between the 0 and 4.0 h groups and the 4.0 and 8.0 h groups. Therefore, the ions may be regarded as the discrimination metabolites for raw and processed Fuzi steamed for different hours. After combining the results of the S-plots, the VIP value (VIP >1) was obtained from OPLS-DA analysis, and the corresponding metabolites could be selected. The chemical structures of the metabolites were identified using online databases such as SciFinder (https://scifinder.cas.org/), and further confirmation was obtained through comparisons with authentic standards and published literature (Wang et al., 2002; Yue et al., 2007; Hu et al., 2009; Yan et al., 2010; Sun et al., 2012; Zhang et al., 2012; Sun et al., 2013; Xu et al., 2014; Yang et al., 2014; Luo et al., 2016; Zhang et al., 2017; Lei et al., 2021).

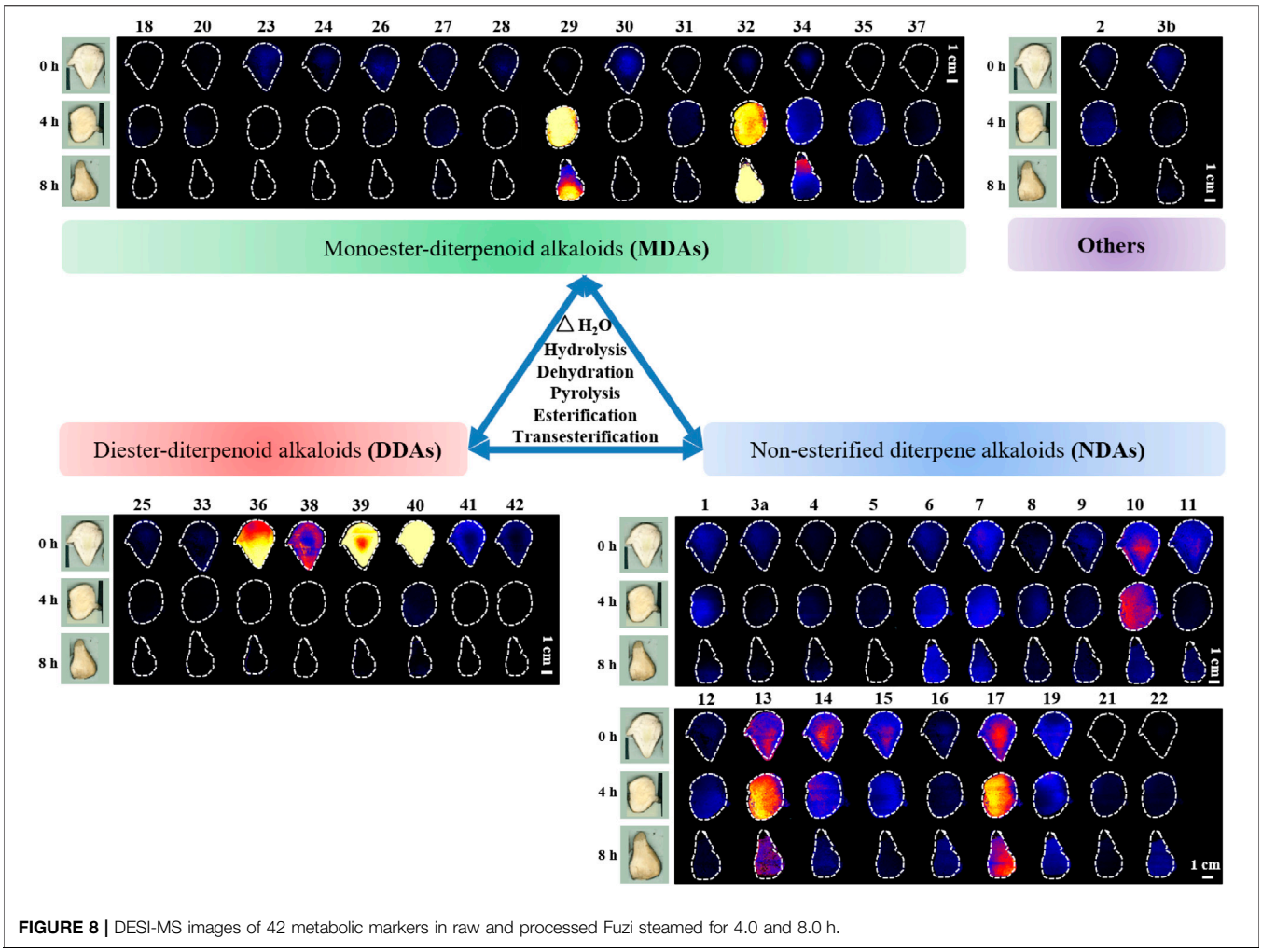

FIGURE 8 | DESI-MS images of 42 metabolic markers in raw and processed Fuzi steamed for 4.0 and 8.0 h.

A total of 42 discriminating metabolites were tentatively identified, and the detailed information is given in **Table 2** and **Supplementary Figure S2**. All 42 metabolites were visualized using DESI-MSI (**Supplementary Figure S3**). The intensities of 37 metabolites, including hypaconitine (**36**, *m/z* 616.3123), benzoylhypaconine (**29**, *m/z* 574.3012), neoline (**17**, *m/z* 438.2841), benzoylmesaconine (**32**, *m/z* 590.2992), mesaconitine (**39**, *m/z* 632.3105), aconitine (**40**, *m/z* 646.3215), and indaconitine (**38**, *m/z* 630.3278), changed after steaming for 4.0 h. Thus, these metabolites were considered as chemical markers to distinguish raw Fuzi and processed Fuzi steamed for 4.0 h. In addition, a total of 20 metabolites, such as neoline (**17**, *m/z* 438.2841), karacoline (**10**, *m/z* 378.2618), isotalatizidine/talatizidine (**13**, *m/z* 408.2755), benzoylhypaconine (**29**, *m/z* 574.3012), songorine (**6**, *m/z* 358.2386), fuzitine (**2**, *m/z* 342.1706), and talatisamine (**14**, *m/z* 422.2891), were set as the markers to distinguish Fuzi steamed for 4.0 and 8.0 h.

A heat map was used to visualize the changes in the content of the 42 metabolites in raw Fuzi and processed Fuzi for different steaming hours. As shown in **Figure 7**, the content of 15 metabolites increased, whereas that of 27 metabolites decreased. Metabolites with increased content are primarily MDAs. However, the content of most DDAs, including three highly toxic ones, mesaconitine (**22**), aconitine (**40**), hypaconitine (**36**), and some of the MDAs decreased dramatically within two steaming hours. The content of napelline (**7**), denudatine/Guanfu base H (**3**), karakolidine/Chuanfumine (**11**), karakanine (**9**), episcopalisine (**24**), and aconicarchamine B (**25**) declined to low levels after steaming for 4.0–5.0 h, but such content increased again when steaming was continued for 10.0 h. Nine metabolites, including dehydrated benzoylhypaconine (**26**), fuziline (**19**), senbusine A/B (**15**), guiwuline (**16**), karacoline (**10**), talatisamine (**14**), dictysine (**5**), 16-hydroxycardiopetaline (**8**), and nevadenine (**12**), showed volatility decreases, and most of them belong to NDAs. As an isoquinoline alkaloid, fuzitine (**2**) generally exists in the form of salt, which showed a particular changing rule during steaming. The content reached the highest on steaming after 4.0 h and decreased or transformed to other metabolites with the extension of steaming time. The heat map also indicated that some of the metabolites were unstable when steamed for 3.0 h and then tended to be stable. When steamed for 10.0 h, the content of metabolites became similar to samples steamed for 4.0–5.0 h. This phenomenon corresponds to the aforementioned PCA and PLS-DA results (**Figure 6**).

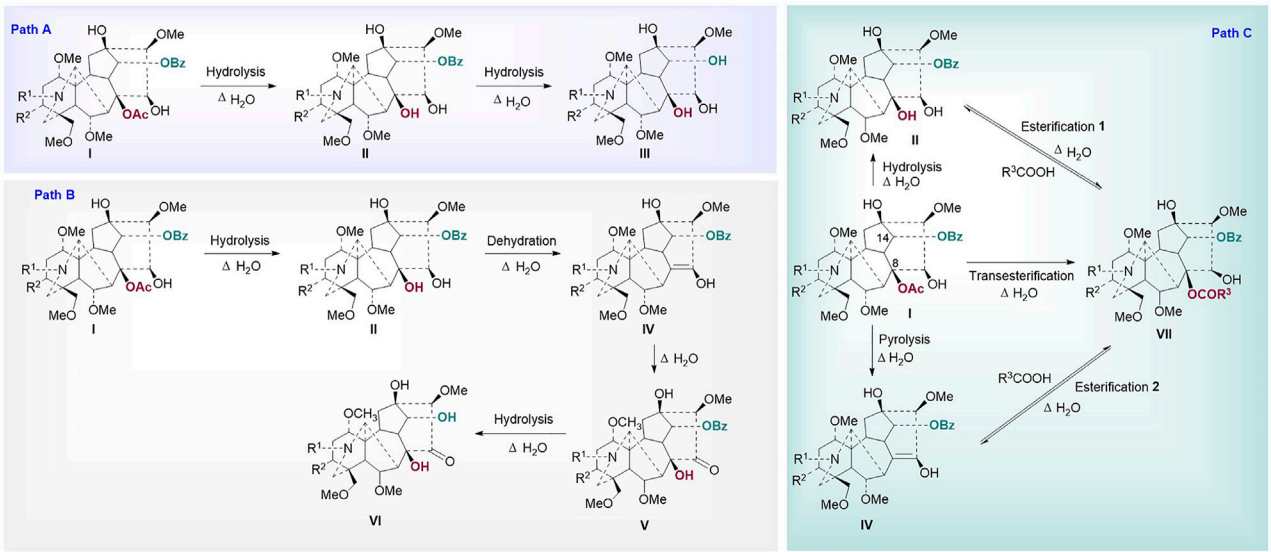

FIGURE 9 | Proposed mechanism for the transformation of ester type alkaloids (Path **(A)**: hydrolysis reactions; Path **(B)**: hydrolysis and dehydration reactions; Path **(C)**: esterification and transesterification reactions I: diester-diterpenoid alkaloids, II: monoester-diterpenoid alkaloids; III: non-esterified diterpene alkaloids; IV: enol-type monoester-diterpenoid alkaloids; V: ketone-type monoester-diterpenoid alkaloids; VI: ketone-type non-esterified diterpene alkaloids; VII: lipo-diterpenoid alkaloids).

4 DISCUSSION

As a typical toxic traditional herbal medicine that is known for its extraordinary pharmacological activities and toxicity, Fuzi has long been used as an irreplaceable traditional herbal medicine in TCM, Kampo medicine, and homeopathy for thousands of years (Zhou et al., 2015; Wu et al., 2018; Qiu et al., 2021).

As toxicity and efficacy are interdependent in Fuzi, the toxicities of processed products such as Yanfuzi, Heishunpian, Baifupian, Danfupian, and Paofupian dramatically decreased compared with raw Fuzi (Zhou et al., 2012; Zhao et al., 2014), but the efficacy also decreased. Considering that Danba is needed during the aforementioned procedures, which would induce halide ions and inorganic impurities into Fuzi, the alkaloids will be lost with a long rinsing time (Ye et al., 2019). Recent studies indicated that the total alkaloids and various ester-diterpenoid alkaloids' levels were high in directly steamed, stir-fried, or baked Fuzi, which showed better detoxification and efficacy reservation effects than Danba-used procedures (Liu et al., 2019; Ye et al., 2019). Thus, this study focused on direct steaming, discussed changeable rules of the key ester-diterpenoid alkaloids, and identified the metabolic markers in raw and processed Fuzi steamed at different time points through DESI-MSI combined with metabolomics.

Investigations of basal metabolism are important to improve the quality control of TCMs (Jiang et al., 2022). DDAs, the major pharmaceutical and toxic secondary metabolites, are important to determine the quality, safety, and efficacy of Fuzi, which were hydrolyzed during heating processing procedures, such as steaming. However, the changeable patterns during steaming are rarely reported. Here, DESI-MSI provides an easy and effective way to explore the change characteristics of the key ester-diterpenoid *Aconitum* alkaloids. Combining metabolism and multivariate statistical analysis, the metabolites and important markers would be identified, which are essential to assess the quality of steamed Fuzi.

HPLC was initially applied to determine variation in the content of three MDAs and three DDAs. A total of 10 steaming time points were set, and HPLC data indicated that the content limit of steamed Fuzi met the requirements of the CP after 3.0 h of steaming and became steady after 4.0 h. DESI-MSI was performed to visualize the HPLC results with high resolutions in mass and space: three MDAs were difficult to detect, and three DDAs were highly visible in raw Fuzi. The images showed an increase in MDAs and a decrease in DDAs during steaming. After 4.0 h of steaming, DDAs and MDAs met the standards of CP, and parts of the DDAs still remain. PCA and PLS-DA analyses also illustrated that the samples after steaming for over 4.0 h were grouped closer and located in the coordinate origin region. Consequently, 4.0 h of steaming was recommended for the toxicity attenuation and efficacy reservation of Fuzi.

Chemometric analysis was combined with a heat map to identify the significant metabolic markers, and 4.0 h was set as the key time node. The DESI-MSI comparison of the 42 metabolites of raw Fuzi and processed Fuzi steamed for 4.0 and 8.0 h showed that the content of highly toxic DDAs decreased dramatically, and a large part of the content of MDAs and NDAs fluctuated during steaming, which indicated a reversible process (**Figure 8**). DDAs and MDAs were the major metabolic markers between raw and processed

Fuzi steamed for 4.0 h, whereas NDAs were identified as the predominant markers of Fuzi steamed for 4.0 and 8.0 h. During 0–4.0 h of steaming, hydrolysis was conducted to convert DDAs to MDAs and then to NDAs, which are considered as the major chemical transformations based on the present results and published literature (Liu et al., 2008; Chen et al., 2013; Qiu et al., 2021), and three main paths for the transformation of C_{19}-ester-diterpenoid alkaloids were proposed (**Figure 9**). Except for conventional hydrolysis and dehydration processes (**Figures 9A,B**), esterification reactions **1** and **2** in path C also indicated two important reversible processes, which explained why some of the alkaloids' content fluctuated during steaming. However, NDAs were the important hydrolysis products after long and continuous steaming, and the pharmaceutical activities will then decrease.

5 CONCLUSION

In this study, the combination of DESI-MSI and metabolomics for rapid and high-resolution characterization of ester alkaloids in raw and steamed Fuzi was developed. The changes in alkaloids of raw and processed Fuzi with different steaming time periods were observed, and the results of HPLC, DESI-MS coupled with PCA, PLS-DA, and OPLS-DA all indicated that 4.0 h of steaming was appropriate for toxicity attenuation and efficacy reservation of Fuzi. In addition, a total of 37 metabolic markers to distinguish raw and processed Fuzi steamed for 4.0 h and 22 metabolites to distinguish Fuzi steamed for 4.0 and 8.0 h were identified through DESI-MSI-based metabolomics. Moreover, three major chemical transformation pathways of C_{19}-ester alkaloids were summarized. Therefore, the novel method provides an efficient approach to visualize the changeable rules and screen the metabolic markers of alkaloids during steaming. The wide application of the method could help to identify biomarkers and reveal the possible chemical transition mechanism in the "Paozhi" processes of TCM.

DATA AVAILABILITY STATEMENT

The raw data supporting the conclusion of this article will be made available by the authors, without undue reservation.

AUTHOR CONTRIBUTIONS

YL wrote the main manuscript, drew the figures, and conducted part of the experiments. TK, ZW, XY, CZ, JS, and BX conducted the experiments. XM and YZ reviewed and edited the manuscript. CT supervised the experiments and prepared the manuscript and directed the final version of the manuscript. All authors reviewed and approved this manuscript.

FUNDING

This study was supported by the National Natural Science Foundation of China (Nos. 81903922 and 82130113), the China Postdoctoral Science Foundation (No. 2021MD703800), the Applied Basic Research Program of Sichuan Province (No. 2020YJ0375), the Key Research and Development Projects of Sichuan Province (No. 2021YFS0042), and the "Xinglin Scholars" Research Promotion Program of Chengdu University of TCM (Nos. BSH2019002 and BSH2021009).

ACKNOWLEDGMENTS

The authors thank XY and CZ of Waters Technology (Beijing) Co., Ltd., for their great help in mass spectrometry imaging.

SUPPLEMENTARY MATERIAL

The Supplementary Material for this article can be found online at: https://www.frontiersin.org/articles/10.3389/fphar.2022.842890/full#supplementary-material

REFERENCES

Chen, X., Tan, P., He, R., and Liu, Y.-g. (2013). Study on the Fragmentation Pathway of the Aconitine-type Alkaloids under Electrospray Ionization Tandem Mass Spectrometry Utilizing Quantum Chemistry. *J. Pharm. Innov.* 8, 83–89. doi:10.1007/s12247-013-9148-z

Chinese Pharmacopoeia Commission (2020). *The Pharmacopoeia of the People's Republic of China*. 2020 edition. Beijing: China Medical Science Press, 200.

Claude, E., Jones, E. A., and Pringle, S. D. (2017). "DESI Mass Spectrometry Imaging (MSI)," in *Imaging Mass Spectrometry: Methods and Protocols*. Editor L.M. Cole (New York, NY: Springer), 65–75. doi:10.1007/978-1-4939-7051-3_7

Dill, A. L., Ifa, D. R., Manicke, N. E., Ouyang, Z., and Cooks, R. G. (2009). Mass Spectrometric Imaging of Lipids Using Desorption Electrospray Ionization. *J. Chromatogr. B Analyt Technol. Biomed. Life Sci.* 877 (26), 2883–2889. doi:10.1016/j.jchromb.2008.12.058

Dong, S.-H., Meng, J., Wu, M.-H., Ma, Z.-G., Cao, H., and Zhang, Y. (2020). Herbalogical Study of Aconiti Lateralis Radix Praeparata (Fuzi). *Zhongguo Zhong Yao Za Zhi* 45 (22), 5567–5575. doi:10.19540/j.cnki.cjcmm.20200802.102

Fu, M., Wu, M., Qiao, Y., and Wang, Z. (2006). Toxicological Mechanisms of *Aconitum* Alkaloids. *Pharmazie* 61 (9), 735–741. PMID: 17020146.

Garza, K. Y., Feider, C. L., Klein, D. R., Rosenberg, J. A., Brodbelt, J. S., and Eberlin, L. S. (2018). Desorption Electrospray Ionization Mass Spectrometry Imaging of Proteins Directly from Biological Tissue Sections. *Anal. Chem.* 90 (13), 7785–7789. doi:10.1021/acs.analchem.8b00967

Hemalatha, R. G., and Pradeep, T. (2013). Understanding the Molecular Signatures in Leaves and Flowers by Desorption Electrospray Ionization Mass Spectrometry (DESI MS) Imaging. *J. Agric. Food Chem.* 61 (31), 7477–7487. doi:10.1021/jf4011998

Hemalatha, R. G., Naik, H. R., Mariappa, V., and Pradeep, T. (2015). Rapid Detection of *Fusarium* Wilt in Basil (*Ocimum* sp.) Leaves by Desorption Electrospray Ionization Mass Spectrometry (DESI MS) Imaging. *RSC Adv.* 5 (62), 50512–50522. doi:10.1039/C4RA16706F

Hu, R., Zhao, J., Qi, L.-W., Li, P., Jing, S.-L., and Li, H.-J. (2009). Structural Characterization and Identification of C_{19}-And C_{20}-Diterpenoid Alkaloids in Roots of *Aconitum Carmichaeli* by Rapid-Resolution Liquid Chromatography Coupled with Time-Of-Flight Mass Spectrometry. *Rapid Commun. Mass. Spectrom.* 23, 1619–1635. doi:10.1002/rcm.4038

Jiang, H., Zhang, Y., Liu, Z., Wang, X., He, J., and Jin, H. (2022). Advanced Applications of Mass Spectrometry Imaging Technology in Quality Control and Safety Assessments of Traditional Chinese Medicines. *J. Ethnopharmacol.* 284, 114760. doi:10.1016/j.jep.2021.114760

Kumara, P. M., Srimany, A., Arunan, S., Ravikanth, G., Shaanker, R. U., and Pradeep, T. (2016). Desorption Electrospray Ionization (DESI) Mass Spectrometric Imaging of the Distribution of Rohitukine in the Seedling of *Dysoxylum Binectariferum* Hook. F. *PLoS ONE* 11 (6), e0269099. doi:10.1371/journal.pone.0158099

Lei, H., Zhang, Y., Ye, J., Cheng, T., Liang, Y., Zu, X., et al. (2021). A Comprehensive Quality Evaluation of Fuzi and its Processed Product through Integration of UPLC-QTOF/MS Combined MS/MS-based Mass Spectral Molecular Networking with Multivariate Statistical Analysis and HPLC-MS/MS. *J. Ethnopharmacol.* 266, 113455. doi:10.1016/j.jep.2020.113455

Li, S. X., Zheng, F. Y., Li, Y. C., Cai, T. S., and Zheng, J. Z. (2012). Determination of Zinc and Copper in Edible Plants by Nanometer Silica Coated, Slotted Quartz Tube, Flame Atomic Absorption Spectrometry. *J. Agric. Food Chem.* 60 (47), 11691–11695. doi:10.1021/jf304485q

Liao, Y., Fu, X., Zhou, H., Rao, W., Zeng, L., and Yang, Z. (2019). Visualized Analysis of Within-Tissue Spatial Distribution of Specialized Metabolites in tea (*Camellia Sinensis*) Using Desorption Electrospray Ionization Imaging Mass Spectrometry. *Food Chem.* 292, 204–210. doi:10.1016/j.foodchem.2019.04.055

Liu, Y.-G., Yu, D.-L., Chen, Y.-J., Zhang, H.-G., and Qiao, Y.-J. (2008). Study on Chemical Reaction of Mesaconitine in Water by HPLC-ESI-MS^n. *Chin. J. New Drugs* 17 (2), 153–156.

Liu, S., Li, F., Li, Y., Li, W., Xu, J., and Du, H. (2017). A Review of Traditional and Current Methods Used to Potentially Reduce Toxicity of Aconitum Roots in Traditional Chinese Medicine. *J. Ethnopharmacol.* 207, 237–250. doi:10.1016/j.jep.2017.06.038

Liu, Y., Liu, H., Ye, Q., Fang, C., Liu, X., Liu, R., et al. (2019). Study on the Effect of Brine Processing on Contents of Alkaloids in Aconiti Lateralis Radix Praeparata. *Trad. Chin. Drug Res. Clin. Pharm.* 30 (4), 472–477. doi:10.19378/j.issn.1003-9783.2019.04.013

Luo, H., Huang, Z., Tang, X., Yi, J., Chen, S., Yang, A., et al. (2016). Dynamic Variation Patterns of Aconitum Alkaloids in Daughter Root of *Aconitum Carmichaelii* (Fuzi) in the Decoction Process Based on the Content Changes of Nine Aconitum Alkaloids by HPLC- MS- MS. *Iran. J. Pharm. Res.* 15 (1), 263–273. doi:10.22037/ijpr.2016.1780

Luo, C., Yi, F., Xia, Y., Huang, Z., Zhou, X., Jin, X., et al. (2019). Comprehensive Quality Evaluation of the Lateral Root of *Aconitum Carmichaelii* Debx. (Fuzi): Simultaneous Determination of Nine Alkaloids and Chemical Fingerprinting Coupled with Chemometric Analysis. *J. Sep. Sci.* 42 (5), 980–990. doi:10.1002/jssc.201800937

Miao, L. L., Zhou, Q. M., Peng, C., Meng, C. W., Wang, X. Y., and Xiong, L. (2019). Discrimination of the Geographical Origin of the Lateral Roots of *Aconitum Carmichaelii* Using the Fingerprint, Multicomponent Quantification, and Chemometric Methods. *Molecules* 24 (22), 4124. doi:10.3390/molecules24224124

Mohana Kumara, P., Uma Shaanker, R., and Pradeep, T. (2019). UPLC and ESI-MS Analysis of Metabolites of *Rauvolfia Tetraphylla* L. And Their Spatial Localization Using Desorption Electrospray Ionization (DESI) Mass Spectrometric Imaging. *Phytochemistry* 159, 20–29. doi:10.1016/j.phytochem.2018.11.009

Parrot, D., Papazian, S., Foil, D., and Tasdemir, D. (2018). Imaging the Unimaginable: Desorption Electrospray Ionization - Imaging Mass Spectrometry (DESI-IMS) in Natural Product Research. *Planta Med.* 84, 584–593. doi:10.1055/s-0044-100188

Qiu, Z. D., Zhang, X., Wei, X. Y., Chingin, K., Xu, J. Q., Gao, W., et al. (2021). Online Discovery of the Molecular Mechanism for Directionally Detoxification of Fuzi Using Real-Time Extractive Electrospray Ionization Mass Spectrometry. *J. Ethnopharmacol.* 277, 114216. doi:10.1016/j.jep.2021.114216

Singhuber, J., Zhu, M., Prinz, S., and Kopp, B. (2009). Aconitum in Traditional Chinese Medicine: a Valuable Drug or an Unpredictable Risk? *J. Ethnopharmacol.* 126, 18–30. doi:10.1016/j.jep.2009.07.031

Stoeckli, M., Chaurand, P., Hallahan, D. E., and Caprioli, R. M. (2001). Imaging Mass Spectrometry: a New Technology for the Analysis of Protein Expression in Mammalian Tissues. *Nat. Med.* 7 (4), 493–496. doi:10.1038/86573

Sun, H., Ni, B., Zhang, A., Wang, M., Dong, H., and Wang, X. (2012). Metabolomics Study on Fuzi and its Processed Products Using Ultra-Performance Liquid-Chromatography/electrospray-Ionization Synapt High-Definition Mass Spectrometry Coupled with Pattern Recognition Analysis. *Analyst* 137, 170–185. doi:10.1039/c1an15833c

Sun, H., Wang, M., Zhang, A., Ni, B., Dong, H., and Wang, X. (2013). UPLC-Q-TOF-HDMS Analysis of Constituents in the Root of Two Kinds of *Aconitum* Using a Metabolomics Approach. *Phytochem. Anal.* 24, 263–276. doi:10.1002/pca.2407

Sun, L., Liu, F., You, G., Feng, T., Wang, M., Liu, Y., et al. (2020). A Comparative Analysis of Aconiti Lateralis Radix and Processed Products Using UHPLC-Q-TOF-MS Combined with Multivariate Chemometrics Strategies. *J. Liq. Chromatogr. Relat. Technol.* 43 (1-2), 37–44. doi:10.1080/10826076.2019.1659150

Takáts, Z., Wiseman, J. M., Gologan, B., and Cooks, R. G. (2004). Mass Spectrometry Sampling under Ambient Conditions with Desorption Electrospray Ionization. *Science* 306 (5695), 471–473. doi:10.1126/science.1104404

Tan, M.-L., Huang, Q.-W., Xiao, F., Fan, R.-Y., Wang, Z.-L., and Yi, J.-J. (2016). Selection of Suitable Herbs for Steaming Fupian Based on the Change of Contents of Ester-Type Alkaloids. *Chin. Trad. Pat. Med.* 38 (2), 366–372. doi:10.3969/j.issn.1001-1528.2016.02.029

Tong, P., Wu, C., Wang, X., Hu, H., Jin, H., Li, C., et al. (2013). Development and Assessment of a Complete-Detoxication Strategy for Fuzi (Lateral Root of *Aconitum Carmichaeli*) and its Application in Rheumatoid Arthritis Therapy. *J. Ethnopharmacol.* 146 (2), 562–571. doi:10.1016/j.jep.2013.01.025

Wang, Y., Liu, Z., Song, F., and Liu, S. (2002). Electrospray Ionization Tandem Mass Spectrometric Study of the Aconitines in the Roots of Aconite. *Rapid Commun. Mass. Spectrom.* 16 (22), 2075–2082. doi:10.1002/rcm.828

Wang, Y., Shi, L., Song, F., Liu, Z., and Liu, S. (2003). Exploring the Ester-Exchange Reactions of Diester-Diterpenoid Alkaloids in the Aconite Decoction Process by Electrospray Ionization Tandem Mass Spectrometry. *Rapid Commun. Mass. Spectrom.* 17 (4), 279–284. doi:10.1002/rcm.914

Wu, J. J., Guo, Z. Z., Zhu, Y. F., Huang, Z. J., Gong, X., Li, Y. H., et al. (2018). A Systematic Review of Pharmacokinetic Studies on Herbal Drug Fuzi: Implications for Fuzi as Personalized Medicine. *Phytomedicine* 44, 187–203. doi:10.1016/j.phymed.2018.03.001

Xu, W., Zhang, J., Zhu, D., Huang, J., Huang, Z., Bai, J., et al. (2014). Rapid Separation and Characterization of Diterpenoid Alkaloids in Processed Roots of *Aconitum Carmichaeli* Using Ultra High Performance Liquid Chromatography Coupled with Hybrid Linear Ion Trap-Orbitrap Tandem Mass Spectrometry. *J. Sep. Sci.* 37 (20), 2864–2873. doi:10.1002/jssc.201400365

Xu, J., Li, X., Zhang, F., Tang, L., Wei, J., Lei, X., et al. (2019). Integrated UPLC-Q/TOF-MS Technique and MALDI-MS to Study of the Efficacy of YiXinshu Capsules against Heart Failure in a Rat Model. *Front. Pharmacol.* 10, 1474. doi:10.3389/fphar.2019.01474

Yan, G., Sun, H., Sun, W., Zhao, L., Meng, X., and Wang, X. (2010). Rapid and Global Detection and Characterization of *Aconitum* Alkaloids in Yin Chen Si Ni Tang, a Traditional Chinese Medical Formula, by Ultra Performance Liquid Chromatography-High Resolution Mass Spectrometry and Automated Data Analysis. *J. Pharm. Biomed. Anal.* 53 (3), 421–431. doi:10.1016/j.jpba.2010.05.004

Yang, Y., Yin, X. J., Guo, H. M., Wang, R. L., Song, R., Tian, Y., et al. (2014). Identification and Comparative Analysis of the Major Chemical Constituents in the Extracts of Single Fuzi Herb and Fuzi-Gancao Herb-Pair by UFLC-IT-TOF/MS. *Chin. J. Nat. Med.* 12 (7), 542–553. doi:10.1016/S1875-5364(14)60084-4

Yang, M., Ji, X., and Zuo, Z. (2018). Relationships between the Toxicities of Radix Aconiti Lateralis Preparata (Fuzi) and the Toxicokinetics of its Main Diester-Diterpenoid Alkaloids. *Toxins (Basel)* 10 (10), 391. doi:10.3390/toxins10100391

Ye, Q., Liu, Y.-S., Liu, H.-M., Liu, R.-J., Tang, X.-M., and Guo, L. (2019). Effects of Different Processing Technology on Contents of Alkaloids in Aconiti Lateralis Radix Praeparata. *Chin. Trad. Pat. Med* 41 (3), 601–607. doi:10.3969/j.issn.1001-1528.2019.03.024

Yue, H., Pi, Z. F., Song, F. R., Liu, Z. Q., and Liu, S. Y. (2007). Analysis of Aconite Alkaloids in the Combination of Radix Aconiti Lateralis Preparata with Different Herbs by ESI-MS Spectrometry. *Yao Xue Xue Bao* 42 (2), 201–205. PMID: 17518052. doi:10.16438/j.0513-4870.2007.02.017

Yue, H., Pi, Z., Song, F., Liu, Z., Cai, Z., and Liu, S. (2009). Studies on the Aconitine-type Alkaloids in the Roots of Aconitum Carmichaeli Debx. By HPLC/ESIMS/MS^n. *Talanta* 77, 1800–1807. doi:10.1016/j.talanta.2008.10.022

Zhang, J., Huang, Z. H., Qiu, X. H., Yang, Y. M., Zhu, D. Y., and Xu, W. (2012). Neutral Fragment Filtering for Rapid Identification of New Diester-Diterpenoid Alkaloids in Roots of *Aconitum Carmichaeli* by Ultra-high-pressure Liquid Chromatography Coupled with Linear Ion Trap-Orbitrap Mass Spectrometry. *PLOS ONE* 7 (12), e52352. doi:10.1371/journal.pone.0052352

Zhang, M., Wang, M., Liang, J., Wen, Y., and Xiong, Z. (2017). Chemical UPLC-ESI-MS/MS Profiling of Aconitum Alkaloids and Their Metabolites in Rat Plasma and Urine after Oral Administration of *Aconitum Carmichaelii* Debx. Root Extract. *Biomed. Chromatogr.* 32, e4049. doi:10.1002/bmc.4049

Zhao, Z., Liang, Z., Chan, K., Lu, G., Lee, E. L., Chen, H., et al. (2010). A Unique Issue in the Standardization of Chinese Materia Medica: Processing. *Planta Med.* 76 (17), 1975–1986. doi:10.1055/s-0030-1250522

Zhao, D., Wang, J., Cui, Y., and Wu, X. (2012). Pharmacological Effects of Chinese Herb Aconite (Fuzi) on Cardiovascular System. *J. Tradit. Chin. Med.* 32 (3), 308–313. doi:10.1016/S0254-6272(13)60030-8

Zhao, Y., Wang, J., Sun, X., Jia, L., Li, J., Shan, L., et al. (2014). Microcalorimetry Coupled with Chemometric Techniques for Toxicity Evaluation of Radix Aconiti Lateralis Preparata (Fuzi) and its Processed Products on *Escherichia coli*. *Appl. Microbiol. Biotechnol.* 98 (1), 437–444. doi:10.1007/s00253-013-5385-9

Zhou, Z.-Y., Xiong, Y.-A., Huang, Q.-W., and Yang, M. (2012). Acute Toxicity of Different Processed Products and its Parts of Aconitum Carmichalii Debx. *J. Chengdu Univ. Trad. Chin. Med* 35 (3), 63–65. doi:10.13593/j.cnki.51-1501/r.2012.03.026

Zhou, G., Tang, L., Zhou, X., Wang, T., Kou, Z., and Wang, Z. (2015). A Review on Phytochemistry and Pharmacological Activities of the Processed Lateral Root of *Aconitum Carmichaelii* Debeaux. *J. Ethnopharmacol.* 160, 173–193. doi:10.1016/j.jep.2014.11.043

Zhu, H., Wang, C., Qi, Y., Song, F., Liu, Z., and Liu, S. (2012). Rapid Quality Assessment of Radix Aconiti Preparata Using Direct Analysis in Real Time Mass Spectrometry. *Anal. Chim. Acta* 752, 69–77. doi:10.1016/j.aca.2012.09.018

Conflict of Interest: Authors XY and CZ were employed by the company Waters Technology (Beijing) Co., Ltd.

The remaining authors declare that the research was conducted in the absence of any commercial or financial relationships that could be construed as a potential conflict of interest.

Publisher's Note: All claims expressed in this article are solely those of the authors and do not necessarily represent those of their affiliated organizations, or those of the publisher, the editors and the reviewers. Any product that may be evaluated in this article, or claim that may be made by its manufacturer, is not guaranteed or endorsed by the publisher.

frontiers | Frontiers in Pharmacology

ORIGINAL RESEARCH
published: 12 April 2022
doi: 10.3389/fphar.2022.854087

High-Throughput Chinmedomics Strategy Discovers the Quality Markers and Mechanisms of Wutou Decoction Therapeutic for Rheumatoid Arthritis

Taiping Li[1,2], Fangfang Wu[1], Aihua Zhang[2], Hui Dong[2], Ihsan Ullah[2], Hao Lin[2], Jianhua Miao[1], Hui Sun[2], Ying Han[2], Yanmei He[2] and Xijun Wang[1,2]**

[1]National Engineering Laboratory for the Development of Southwestern Endangered Medicinal Materials, Guangxi Botanical Garden of Medicinal Plant, Nanning, China, [2]National Chinmedomics Research Center, National TCM Key Laboratory of Serum Pharmacochemistry, Metabolomics Laboratory, Heilongjiang University of Chinese Medicine, Harbin, China

OPEN ACCESS

Edited by:
Kornkanok Ingkaninan,
Naresuan University, Thailand

Reviewed by:
Hongxun Tao,
Jiangsu University, China
Jianxin Chen,
Beijing University of Chinese Medicine, China

***Correspondence:**
Hui Sun
sunhui7045@163.com
Xijun Wang
xijunw@sina.com

Specialty section:
This article was submitted to Ethnopharmacology, a section of the journal Frontiers in Pharmacology

Received: 13 January 2022
Accepted: 15 March 2022
Published: 12 April 2022

Citation:
Li T, Wu F, Zhang A, Dong H, Ullah I, Lin H, Miao J, Sun H, Han Y, He Y and Wang X (2022) High-Throughput Chinmedomics Strategy Discovers the Quality Markers and Mechanisms of Wutou Decoction Therapeutic for Rheumatoid Arthritis. Front. Pharmacol. 13:854087. doi: 10.3389/fphar.2022.854087

Wutou decoction (WTD) is a traditional Chinese medicine prescription for the treatment of rheumatoid arthritis (RA), and this study systematically analyzed the metabolic mechanism and key pharmacodynamic components of WTD in RA rats by combining untargeted metabolomics and serum pharmacochemistry of traditional Chinese medicine to enrich the evidence of WTD quality markers (Q-markers) studies. WTD prevented synovial edema in RA rats and reduced tumor necrosis factor-alpha and interleukin 6 levels in rat serum, according to the results of an enzyme-linked immunosorbent examination and histopathological inspection. In model rats, pattern recognition and multivariate statistical analysis revealed 24 aberrant metabolites that disrupted linoleic acid metabolism, arachidonic acid metabolism, arginine and proline metabolism, *etc*. However, continued dosing of WTD for 28 days reversed 13 abnormal metabolites, which may be an important therapeutic mechanism from a metabolomic perspective. Importantly, 12 prototypical components and 16 metabolites from WTD were characterized in RA rat serum. The results of Pearson correlation analysis showed that aconitine, L-ephedrine, L-methylephedrine, quercetin, albiflorin, paeoniflorigenone, astragaline A, astragaloside II, glycyrrhetic acid, glycyrrhizic acid, licurazide, and isoliquiritigenin are the key pharmacological components that regulate the metabolism of RA rats, and they are identified as Q-markers. In sum, utilizing metabolomics and serum pharmacochemistry of traditional Chinese medicine, the metabolic mechanisms and Q-markers of WTD therapy in RA rats were revealed, providing a theoretical basis for the quality control investigation of WTD.

Keywords: metabolomics, mass spectrometry, biomarker, pathway, quality markers, chinmedomics, effective substance

Abbreviations: ESI, electrospray ion source; IL-6, interleukin-6; OPLS-DA, orthogonal partial least squares discriminant analysis; PCA, principal component analysis; PCMS, A plotting of correlation between marker metabolites and serum constituents; Q-markers, quality markers; RA, rheumatoid arthritis; TCM, traditional Chinese medicine; TIC, total ion chromatograms; TNF-α, tumor necrosis factor-alpha; UPLC-Q/TOF-MS, ultraperformance liquid chromatography quadrupole time of flight mass spectrometry; VIP, variable importance in projection value; WTD, wutou decoction.

INTRODUCTION

Traditional Chinese medicine has a long history of application and accumulated rich clinical experience, TCM plays a pivotal role in the protection of human health, of which herbal medicine is the key medium. A large number of chemicals in herbs and prescriptions poses a difficult problem for quality control. Unlike in the past, the quality control of herbal medicines is not only concerned with the high content of the components in the herbal medicines, but the remarkable medicinal effects are more noticeable. The concept and requirements of quality markers (Q-markers) proposed by Academician Liu have promoted the development of quality control systems for TCM and herbal medicines. In general, ideal herbal medicines and prescriptions need to have five characteristics: *1*) quality transfer and traceability, *2*) component specificity, *3*) component effectiveness, *4*) component measurability, *5*) formula compatibility environment (He et al., 2018; Bai et al., 2018; Zhang et al., 2018).

Chinmedomics comprehensively blends metabolomics and serum pharmacochemistry of TCM and serves as a way for the discovery of Q-markers for herbal medicines and formulations (Zhang et al., 2019). In short, the metabolic mechanisms of herbal medicines and prescriptions for the treatment of diseases are gained through metabolomics insights (Zhang et al., 2017; Zhang et al., 2020; Qiu et al., 2020), and key pharmacodynamic components and Q-markers that regulate abnormal metabolism are identified from a large number of chemical components by correlation analysis (Wang et al., 2015; Han et al., 2020). Currently, chinmedomics was used as a research method for Q-markers to analyze the active components and therapeutic mechanisms of Shengmai San, Yinchenhao Decoction, Sijunzi Decoction, and Kaixin San (Zhang et al., 2018; Sun et al., 2019; Wang et al., 2019; Zhao et al., 2020).

Wutou decoction (WTD) is a classic prescription for treatment rheumatology, derived from "*Shang Han Lun*" of Zhang Zhongjing in the Han Dynasty and consisting of *Aconitum carmichaeli* Debeaux [Ranunculaceae], *Ephedra sinica* Stapf [Ephedraceae], *Paeonia lactiflora* Pall. [Ranunculaceae], *Astragalus mongholicus Bunge* [Leguminosae], and *Glycyrrhiza uralensis* Fisch. [Leguminosae] with a mass ratio of 10 g: 15 g: 15 g: 15 g: 15 g. Pharmacological studies have shown WTD analgesic and anti-inflammatory effects (Guo et al., 2017; Guo et al., 2020). Besides, WTD mainly contains alkaloids, triamcinolone, and flavonoid compounds that can regulate the biological signal pathways associated with rheumatoid arthritis (RA) (Qi et al., 2014; Xu et al., 2017). To enhance the Q-markers and quality control evidence of WTD, this study adopted metabolomics and serum pharmacochemistry of the TCM to carefully evaluate the global metabolic profile of WTD-treated RA rats and the components of WTD that are closely related to the therapeutic effect (**Figure 1**).

MATERIAL AND METHODS

Reagents and Medicines

HPLC grade methanol and acetonitrile were purchased from Thermo Fisher Scientific (Massachusetts, United States), analytical grade formic acid, leucine enkephalin, and Freund's complete adjuvant were purchased from Sigma-Aldrich (Shanghai, China), ultrapure water purchased from Watsons (Guangzhou, China), the kit of tumor necrosis factor-alpha (TNF-α) and interleukin-6 (IL-6) purchased from Jiancheng Biologics (Nanjing, China), the five botanical drugs that compose WTD were purchased from Tongrentang Pharmacy (Harbin, China) and were authenticated by Xijun Wang from the Department of Pharmacognosy of Heilongjiang University of Chinese Medicine.

Preparation of Wutou Decoction Extracts

The crude *Aconitum carmichaeli* Debeaux [Ranunculaceae], *Ephedra sinica* Stapf [Ephedraceae], *Paeonia lactiflora* Pall. [Ranunculaceae], *Astragalus mongholicus* Bunge [Leguminosae], and *Glycyrrhiza uralensis* Fisch. [Leguminosae] cut into small round pieces according to the mass ratio 2: 3: 3: 3: 3 and were immersed in distilled water (eight-fold volume) for 1 h and then boiled for 1.5 h. The extracted solutions were filtered through eight layers of gauze, and the filter residue was boiled with distilled water (eight-fold

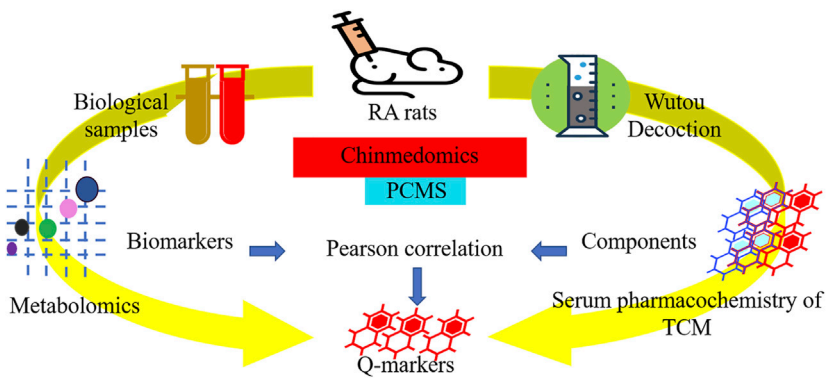

FIGURE 1 | The workflow of quality markers research for wutou decoction in the treatment of adjuvant-induced arthritis rat based on chinmedomics strategy.

volume) again for another 1 h. Finally, the two parts of the filtrates were combined, and the decoction was transformed into powder by freeze-drying. The frozen powder was dissolved with distilled water and kept at 4°C until use.

Animal Grouping and Administration

Experiments were performed with eight-week-old male Sprague-Dawley rats weighing 180–220 g (Liaoning Changsheng Biotechnology Co., Ltd., License No. SCXK [Liao] 2015-0001) under controlled environmental conditions (12/12 light/dark, 23–25°C, 50 ± 5% humidity) with unlimited access to food and water. After 7 days of acclimatization, all animals were randomly divided into the following three groups (n = 8): control group (C); model group (M), and WTD treatment group (T). The M and T rats were injected with 0.1 ml of Freund's complete adjuvant at a concentration of 2.0 $mg.ml^{-1}$ at the base of the tail, and the C rats were injected with the same volume of normal saline (Zhang et al., 2014). On the 14th day of model preparation, rats in the T were orally administered a 7.56 $g.kg^{-1}$ lyophilized powder solution of WTD once a day for 28 consecutive days (Dong et al., 2015). The C rats received the same volume of ultrapure water. The protocol was approved by the Committee on the Ethics of Animal Experiments of the College of Pharmacy of the Heilongjiang University of Chinese Medicine.

Collect and Prepare Biological Samples

Throughout the experimental period, 12 h urine from 8 p.m. to 8 a.m. the next day was collected in the metabolic cage, and the blood samples were obtained by the final stage of administration: fresh urine centrifugation for 15 min (4°C, 13,000 $r{\cdot}min^{-1}$), serum centrifugation for 15 min (4°C, 3500 $r{\cdot}min^{-1}$). Urine samples were diluted 10 times with ultrapure water, serum samples were precipitated with four times the volume of methanol and the supernatant was taken. All samples were filtered through a 0.22 μm filter before injection into the ultra-performance liquid chromatography quadrupole time of flight coupled with mass spectrometry (UPLC-Q/TOF-MS) instrument. Separately, 100 μl of urine and serum were obtained from each animal for the preparation of quality control samples in examining and optimizing the metabolomics analysis parameters.

Inflammatory Factors and Histopathological Examination

The concentrations of IL-6 and TNF- in serum were determined using the kit's instructions. X-rays of the rat feet were taken to evaluate the effects of WTD. Fresh ankles were immersed in the formalin solution, and pathological changes were observed by the affiliated hospital of the Heilongjiang University of Chinese Medicine under proper microscopic circumstances.

Metabolomic Conditions

Chromatography

The metabolomic analysis was performed using an ACQUITY UPLC® system coupled with a time-of-flight mass spectrometer (Waters Corp.). The HSS T_3 column (2.1 mm × 100 mm id, 1.8 μm; Waters Corp.) separates urine samples, whereas the BEH C_{18} column (2.1 mm × 100 mm id, 1.7 μm, Waters Corp.) separates serum samples. The column temperature is 35°C. The gradient mobile phase consisted of solvent A (0.1% FA-H_2O) and solvent B (0.1% FA-ACN). Optimized urine gradient elution status: 0–4.5 min, 1–21 A%; 4.5–7 min, 21–40% A; 7–7.5 min, 40–50% A; 7.5–9.5 min, 50–99% A. Optimized serum gradient elution status: 0–1.2 min, 1–39% A; 1.2–4.3 min, 39–68% A; 4.3–4.5 min, 68–71% A; 4.5–7.0 min, 71–78% A; 7.0–8.2 min, 78–90% A; 8.2–9.5 min, 90–99% A. The injection volume is 4 μl and the flow rate is 0.5 $ml.min^{-1}$ in both modes.

Mass Spectrometric

The Waters G2-Si mass spectrometer system (Waters Corp.) is equipped with an electrospray ion source to detect all metabolites, and the ion source temperature is 110°C. The capillary voltage in the positive ion mode (ESI^+) is 3.0 kV; in the negative ion mode (ESI^-), it is 2.7 kV. The cone voltage is 20 V, and the gas flow rate is 50 $L.h^{-1}$. Dry nitrogen is desolventizing at a flow rate of 800 $L.h^{-1}$ and a temperature of 350°C. Use the full scan mode of m/z 50–1200 Da to collect MS data. Leucine enkephalin with a concentration of 1 ng/μl and a flow rate of 10 $\mu l.min^{-1}$ in ESI^+ $[M+H]^+$ = 556.2771 and ESI^- $[M-H]^-$ = 554.2615 was used as a reference compound to obtain an accurate mass.

Constituent Analysis of Wutou Decoction

After lyophilized powder of WTD decoction was dissolved in ultrapure water and was centrifuged 15 min (4°C, 13,000 $r{\cdot}min^{-1}$), filtered with a 0.22 μm filter membrane, and injected into UPLC-MS for analysis chemical profile of WTD. The serum containing components of WTD was added with a quarter volume of 20% phosphoric acid, utilizing an OASIS MCX solid-phase extraction column (30 mg, 30 μm, Waters Corp.) to enrich the WTD components *in vivo*, dissolved in methanol for UPLC-MS data collection. Injection volume is 2 μl, the gradient mobile phase consisted of solvent A (0.1% FA-H_2O) and solvent B (0.1% FA-ACN), optimized gradient elution conditions: 0–3.0 min, 1–10% A; 3.0–7.0 min, 10–12% A; 12.0–20.0 min, 20–40% A; 20.0–22.0 min, 40–100% A. The MS^E data scanning mode of UPLC-Q/TOF-MS was combined with powerful UNIFI software (Waters Corp.) for efficient and accurate characterization of the chemical profile of the WTD and the components absorbed *in vivo*. The adduct ion is $[M+H]^+$ in ESI^+ and $[M-H]^-$ in ESI^-, respectively. To reduce false positives, select the embedded TCM database and set the tolerance error of components and fragments to 5 mDa. The study compared the serum between the M and the T and preferred the results of the high response value only in the serum of the T.

Multivariate Statistics and Data Analysis

The raw data is imported into Progenesis QI software (Waters Corp.) for noise reduction, peak alignment, and normalization to get an information matrix that includes m/z, retention time, and peak relative intensity. The EZinfo software (Waters Corp.) performs a principal component analysis (PCA) and judges differences between groups.

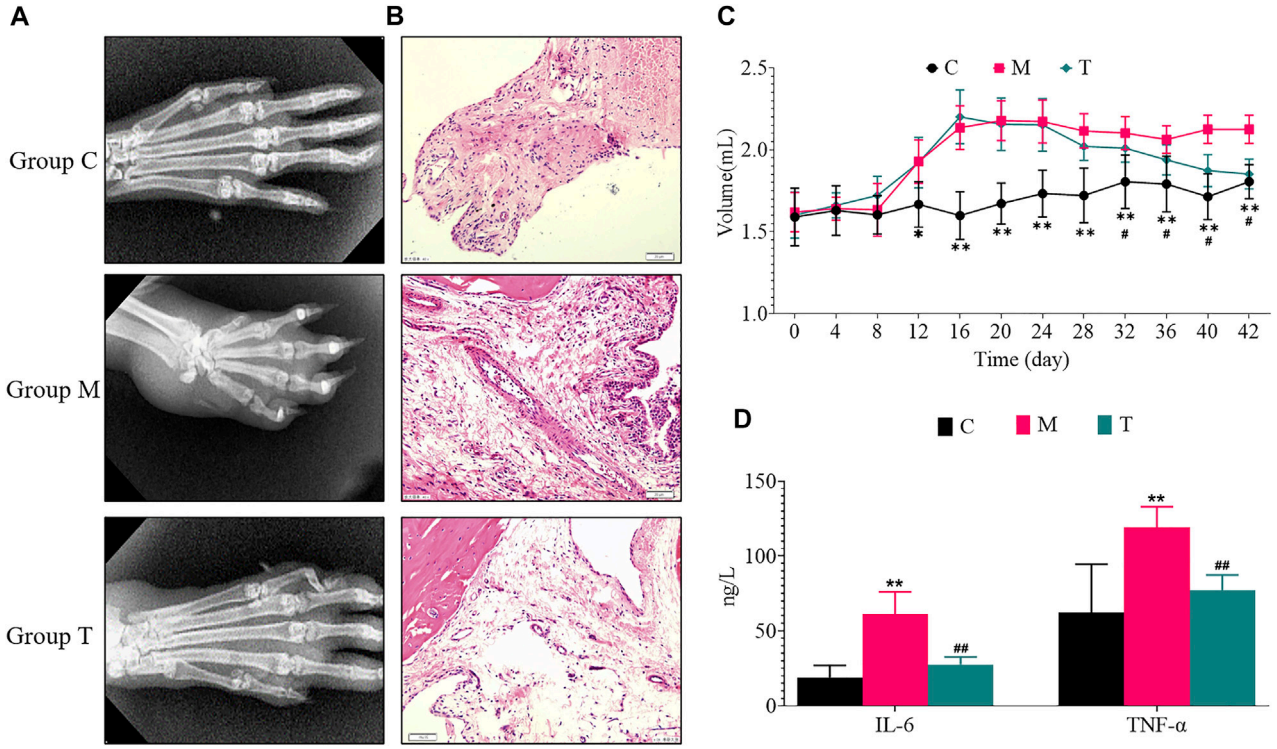

FIGURE 2 | Evaluation of the effect of wutou decoction on adjuvant-induced arthritis rat. **(A)** X-ray examination **(B)** Synovial histopathological examination (*200) **(C)** changes in paw volume before and after administration **(D)** Determination of inflammatory factors in serum. Results are expressed as mean ± SD, $n = 8$. $^{*}p < 0.05$, $^{**}p < 0.01$ vs control group. $^{\#}p < 0.05$, $^{\#\#}p < 0.01$ vs model group.

Orthogonal partial least squares discriminant analysis (OPLS-DA) calculates variable importance in projection value (VIP), a statistical normalization abundance of different ions. Finally, MS/MS information combined with HMDB (https://hmdb.ca/) and MassBank (http://www.massbank.jp/) databases identifies metabolites, VIP >1, and metabolites normalized abundance with intergroup significance are considered potential biomarkers of RA rats. Comparisons between the two groups of the quantitative data were completed using Graphpad software (California, United States) independent *t*-test and presented as mean ± standard deviation, with $p < 0.05$ indicating significant differences and $p < 0.01$ indicating extremely significant differences.

Analysis of Key Medicinal Constituents

The PCMS (plotting of correlation between marker metabolites and serum components) patented software calculates the correlation coefficient between the components absorbed into the blood of WTD and the potential biomarkers of RA rats to determine which component is most likely to have a therapeutic effect. Normalize the abundance of biomarkers and components, and then use Pearson's statistical correlation to set the reference standard for the correlation coefficient R. In this study, $0.7 \leq |R| < 0.8$ is selected as the highly correlated component; $0.8 \leq |R| \leq 1$ is regarded as extremely correlated, and extremely correlated components are regarded as Q-markers.

RESULTS

Therapeutic Effects of Wutou Decoction

Compared with the C rats, 14 days after the injection of Freund's complete adjuvant, the rats in the M reached the uttermost state of inflammation. Compared with the M, the T significantly inhibited the levels of IL-6 and TNF-α in rats and reduced the swelling of the feet (**Figure 2**).

Characterize Potential Biomarkers

Multivariate statistical analysis was performed on the metabolic fingerprint information collected from serum and urine at the end of the experiment. There are differences in serum total ion chromatograms (TIC) in C, M, and T rats in ESI^+ and ESI^- and these are reflected in PCA (**Figure 3**). Similarly, there are differences in the TIC of the urine between the three groups, suggesting a change in the metabolic profile (**Figure 4**). The OPLS-DA statistical model calculates the VIP of differential ions and is employed to screen potential biomarkers, the R2Y and Q2 values of the urine model (R2Y (cum) = 0.995, Q2(cum) = 0.927 in ESI^+, and R2Y(cum) = 0.994, Q2(cum) = 0.615 in ESI^-) and serum model (R2Y (cum) = 0.858, Q2(cum) = 0.798 in ESI^+, and R2Y (cum) = 0.872, Q2(cum) = 0.795

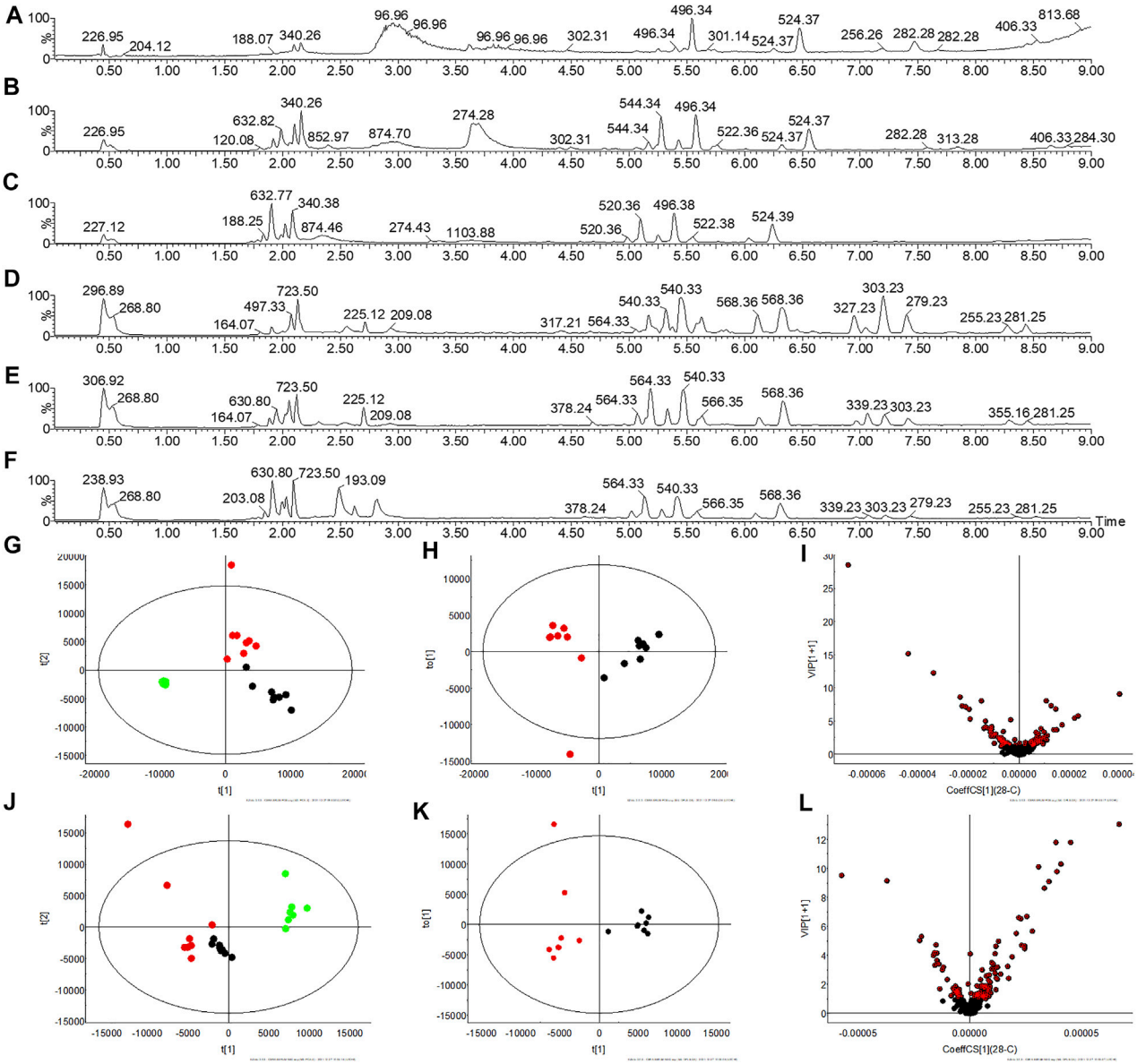

FIGURE 3 | Serum metabolic profile collection and multivariate statistical analysis. **(A–C)** TIC spectra of C, M, and T rats in ESI$^+$, respectively **(D–F)** TIC spectra of C, M, and T rats in ESI$^-$, respectively **(G,J)** PCA plot of C, M, and T in ESI$^+$ and ESI$^-$, respectively **(H,K)** OPLS-DA plot of C and M in ESI$^+$ and ESI$^-$, respectively **(I,L)** VIP plot of C and M in ESI$^+$ and ESI$^-$, respectively. Note: ●: C rats; ●: M rats; ●: T rats.

in ESI$^-$) indicated that the statistic model has good quality and predictability.

Take arachidonic acid as an example to illustrate the identification process of potential biomarkers. First, OPLS-DA calculated that the VIP of 8.09_303.2320m/z was 4.004 and the normalized abundance of this ion in the serum of the C and the M was different ($p < 0.05$). Secondly, chromatographic peak extraction and elemental composition analysis showed that the tolerance of $C_{20}H_{32}O_2$ was accepted, while m/z 304 and m/z 279 were simultaneously observed in MS extraction at 8.09 min. Finally, it was identified that m/z 304 Da is the parent ion of arachidonic acid, and the fragments of 303[M-H]$^-$ and 279[M-COOH]$^-$ were generated by high-energy bombardment in ESI$^-$ (**Supplementary Figure S1**). Eventually, 24 biomarkers are identified (**Table 1**).

Enrichment Analysis of Potential Biomarkers

The above 24 potential biomarkers of serum and urine are mostly engaged in 17 metabolic pathways, which belong to lipid metabolism, carbohydrate metabolism, and amino acid metabolism (**Table 2**). Where the impact value is greater than 0.1, linoleic acid metabolism, arachidonic acid metabolism,

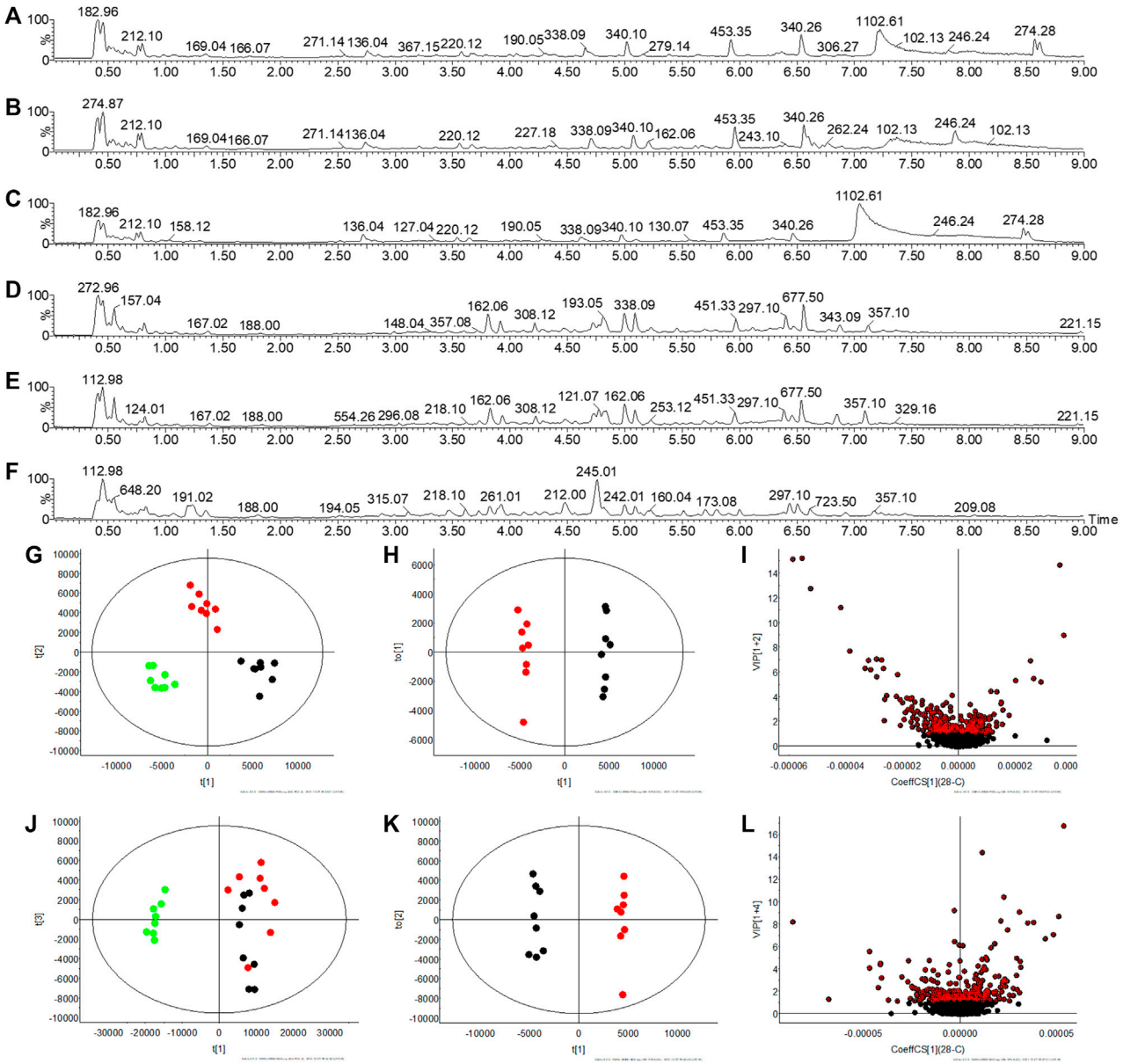

FIGURE 4 | Urine metabolic profile collection and multivariate statistical analysis. **(A–C)** TIC spectra of C, M, and T rats in ESI^+, respectively **(D–F)** TIC spectra of C, M, and T rats in ESI^-, respectively **(G,J)** PCA plot of C, M, and T in ESI^+ and ESI^-, respectively **(H,K)** OPLS-DA plot of C and M in ESI^+ and ESI^-, respectively **(I,L)** VIP plot of C and M in ESI^+ and ESI^-, respectively. Note: ●: C rats; ●: M rats; ●: T rats.

glyoxylate and dicarboxylate metabolism, arginine and proline metabolism, arginine biosynthesis, steroid hormone biosynthesis, and glycerophospholipid metabolism are considered important metabolic pathways. The WTD significantly reversed potential biomarkers with abnormal levels of 13/24 (**Figure 5**), including 4-Hydroxynonenal, L-Arginine, Prostaglandin E3, Aracidonic acid, N-Acetyltaurine, Kynurenic acid, D-Glucose, Linoleyl carnitine, Galactose-beta-1,4-xylose, Linoleic acid, Octadecenoylcarnitine, L-Palmitoylcarnitine, Sphingosine L-phosphate. WTD may correct the disturbed Linoleic acid metabolism, Arachidonic acid metabolism, Arginine and proline metabolism, Arginine biosynthesis, Steroid hormone biosynthesis, Sphingolipid metabolism, and Glycolysis/Gluconeogenesis by reversing the levels of the above markers, thereby treating Freund's complete adjuvant-induced RA rats (**Figure 6**).

Blood Components of Wutou Decoction

The UPLC-Q/TOF-MS collects the TIC of WTD before and after entering the blood in ESI^+ and ESI^- (**Figure 7**). The UNIFI software, with a powerful analysis module, can automatically

TABLE 1 | Identification results of potential biomarker groups in adjuvant-induced arthritis rats.

No	Compound	Adducts	Formula	R_t (min)	m/z	Mass error (ppm)	MS/MS	Description	HMDB ID	VIP value
1	0.48_175.1195m/z	M+H	$C_6H_{14}N_4O_2$	0.48	175.1195	3.37	M1:158[M+H-OH]$^+$ M2:130[M+H-COOH]$^+$ M3:116[M-NC(NH_2)2]$^+$	L-Arginine	HMDB0000517	1.0852
2	0.52_204.1238m/z	M+H	$C_9H_{17}NO_4$	0.52	204.1238	3.73	M1:144[M-N(CH_3)3]$^+$ M2:129[M1-CH_3]$^+$ M3:85[M1-CH_3COO]$^+$	L-Acetylcarnitine	HMDB0000201	3.0411
3	3.51_852.6867m/z	M+Na	$C_{48}H_{96}NO_7P$	3.51	852.6867	6.13	M1:829[M]$^+$ M2:184[M-$C_{43}H_{83}O_3$+2H]$^+$ M3:86[M-$C_{43}H_{83}O_7P$]$^+$	PC(22:0/P-18:0)	HMDB0008555	1.1812
4	4.01_542.3282m/z	M+H	$C_{28}H_{48}NO_7P$	4.01	542.3282	7.58	M1:523[M-H_2O]$^+$ M2:104[M-$C_{23}H_{35}O_6P$+H]$^+$ M3:86[M-$C_{23}H_{35}O_7P$]$^+$	LysoPC(20:5(5Z,8Z,11Z,14Z,17Z))	HMDB0010397	1.1387
5	4.99_424.3425m/z	M+H	$C_{25}H_{45}NO_4$	4.99	424.3425	0.92	M1:365[M+H-N(CH_3)3]$^+$ M2:85[M1-$C_{17}H_{31}COO$]$^+$ M3:71[M2-CH_2]$^+$ M4:57[M3-CH_2]$^+$	Linoleyl carnitine	HMDB0006469	2.3001
6	5.12_400.3446m/z	M+H	$C_{23}H_{45}NO_4$	5.12	400.3446	6.21	M1:341[M-CH_2COO]$^+$ M2:85[M-N(CH_3)3-$C_{15}H_{31}COO$]$^+$ M3:71[M2-CH_2]$^+$	L-Palmitoylcarnitine	HMDB0000222	1.7873
7	5.25_426.3583m/z	M+H	$C_{25}H_{47}NO_4$	5.25	426.3583	1.17	M1:426[M+H]$^+$ M2:85[M-$C_{21}H_{43}NO_2$]$^+$	Octadecenoylcarnitine	HMDB0094687	2.9946
8	6.39_481.2336m/z	M+Na	$C_{23}H_{39}O_7P$	6.39	481.2336	2.29	M1:481[M+Na]$^+$ M2:361[M-$C_{23}H_{37}O_3$]$^+$ M3:287[M-$C_{19}H_{31}CO$]$^+$ M4:185[M+2H-OH-$C_{19}H_{31}$]$^+$ M5:133[M+H-H_2PO_3-$C_{18}H_{29}$]$^+$	LPA(0:0/20:4n6)	HMDB0012496	1.1573
9	4.69_378.2401m/z	M-H	$C_{18}H_{38}NO_5P$	4.69	378.2401	−3.54	M1:379[M]$^-$ M2:378[M-H]$^-$ M3:78[M-OH-$C_{18}H_{37}NO$]$^-$	Sphingosine 1-phosphate	HMDB0000277	5.0357
10	8.09_303.2320m/z	M-H	$C_{20}H_{32}O_2$	8.09	303.2320	−3.27	M1:304[M]$^-$ M2:303[M-H]$^-$ M3:259[M-COOH]$^-$	Arachidonic acid	HMDB0001043	4.0040
11	5.12_317.2110m/z	M-H	$C_{20}H_{30}O_3$	5.12	317.2110	−3.78	M1:317[M-H]$^-$ M2:299[M1-H_2O]$^-$	15-HEPE	HMDB0010209	1.3047
12	5.45_452.2775m/z	M-H	$C_{21}H_{44}NO_7P$	5.45	452.2775	−1.76	M1:452[M-H]$^-$	LysoPE(0:0/16:0)	HMDB0011473	2.3420
13	5.06_279.2316m/z	M-H	$C_{18}H_{32}O_2$	5.06	279.2316	−4.70	M1:280[M]$^-$ M2:279[M-H]$^-$ M3:261[M2-H_2O]$^-$	Linoleic acid	HMDB0000673	3.1980
14	0.65_335.0966m/z	M+Na	$C_{11}H_{20}O_{10}$	0.65	335.0966	5.60	M1:335[M+Na]$^+$ M2:145[M-CH_2OH-$C_5H_9O_5$]$^+$	Galactose-beta-1,4-xylose	HMDB0011677	1.0580
15	0.49_103.0029m/z	M-H	$C_3H_4O_4$	0.49	103.0029	−7.93	M1:104[M]$^-$ M2:56[M-CH_2OH-OH]$^-$	Hydroxypyruvic acid	HMDB0001352	2.0564

(Continued on following page)

TABLE 1 | (*Continued*) Identification results of potential biomarker groups in adjuvant-induced arthritis rats.

No	Compound	Adducts	Formula	R_t (min)	m/z	Mass error (ppm)	MS/MS	Description	HMDB ID	VIP value
16	0.51_209.0290m/z	M-H	$C_6H_{10}O_8$	0.51	209.0290	−6.26	M1:209[M-H]$^-$ M2:165[M-COOH]$^-$ M3:103[M-OH-(COOH)2]$^-$ M4:75[M-(CHOH)3COOH]$^-$	Glucaric acid	HMDB0000663	1.0750
17	0.56_212.0219m/z	M+FA-H	$C_4H_9NO_4S$	0.56	212.0219	−9.27	M1:166[M-H]$^-$ M2:124[M-$COCH_3$]$^-$ M3:80[M-H-(CH_2)2$NHCOCH_3$]$^-$ M4:58[M-(CH_2)2SO_3H]$^-$	N-Acetyltaurine	HMDB0240253	1.9768
18	0.60_179.0549m/z	M-H	$C_6H_{12}O_6$	0.60	179.0549	−6.55	M1:179[M-H]$^-$ M2:161[M1-H_2O]$^-$ M3:143[M2-H_2O]$^-$ M4:125[M3-H_2O]$^-$ M5:59[M4-$CHOCH_2OH$]$^-$	D-Glucose	HMDB0000122	1.2602
19	1.85_131.0818m/z	M-H	$C_5H_{12}N_2O_2$	1.85	131.0818	−5.77	M1:131[M-H]$^-$ M2:99[M1-(NH_2)2]$^-$ M3:67[M2-H_2O-CH_2]$^-$	Ornithine	HMDB0000214	1.8019
20	3.28_178.0499m/z	M-H	$C_9H_9NO_3$	3.28	178.0499	−6.01	M1:178[M-H]$^-$ M2:134[M-COOH]$^-$ M3:77[M-$CONHCH_2COOH$]$^-$ M4:59[M-C_6H_5CONH]$^-$	Hippuric acid	HMDB0000714	3.3685
21	4.43_188.0345m/z	M-H	$C_{10}H_7NO_3$	4.43	188.0345	−4.29	M1:188[M-H]$^-$ M2:144[M-COOH]$^-$	Kynurenic acid	HMDB0000715	1.6490
22	5.52_201.1120m/z	M+FA-H	$C_9H_{16}O_2$	5.52	201.1120	−7.89	M1:201[M+FA-H]$^-$ M2:121[M-OH-H_2O]$^-$	4-Hydroxynonenal	HMDB0004362	1.0608
23	7.58_349.2004m/z	M-H	$C_{20}H_{30}O_5$	7.58	349.2004	−4.84	M1:349[M-H]$^-$ M2:331[M1-H_2O]$^-$ M3:313[M2-H_2O]$^-$ M4:249[M-H-H_2O-$CHCH_2C_4H_7$]$^-$	Prostaglandin E3	HMDB0002664	1.7470
24	8.78_331.1911m/z	M+FA-H	$C_{19}H_{26}O_2$	8.78	331.1911	−1.38	M1:285[M-H]$^-$ M2:225[M-$C_2H_5O_2$]$^-$	Androstenedione	HMDB0000053	1.6056

identify the structure information obtained under high and low energy, including m/z, retention time, and MS/MS fragment response values, and deduce the cleavage relationship of compounds. Compound aconitine was used as an example to describe the process of applying UNIFI software to analyze the chemical profile of WTD. The UNIFI software matched the MS^E data collected in the continuum mode. Both ion response values between groups and all m/z information at 14.12 min were obtained, and m/z 646.32 Da with a high response value in WTD samples was scanned for small molecule ions. After elemental composition and fragment matching, m/z 646.32 Da was recognized as the hydrogenation ion of aconitine and identified to 586.30 Da $[M+H-C_2H_4O_2]^+$, 568.29 Da $[M+H-C_2H_6O_3]^+$, 554.27 Da $[M+H-C_3H_8O_3]^+$ (**Supplementary Figure S2**). Finally, they characterized and identified 61 components of the WTD (**Supplementary Table S1**). Importantly, 19 components were absorbed into the blood, including 12 prototype components (**Supplementary Table S2**).

Discover the Key Medicinal Components

PCMS software was utilized in this investigation to uncover the important pharmacodynamic components of WTD in the treatment of RA rats, as well as biological activity tracking and literature analysis to identify Q-markers. The findings revealed that 19 of the WTD components were absorbed into the serum. According to correlation analysis, 12 components were confirmed as Q-markers (**Figure 8**), of which aconitine was from *Aconitum carmichaeli* Debeaux [Ranunculaceae], L-ephedrine, L-methylephedrine, quercetin, and kaempferol-3-O-rhamnoside were from *Ephedra sinica* Stapf [Ephedraceae],

TABLE 2 | Metabolic pathway analysis based on MetPA.

Pathway name	Class	Total	Expected	Hits	Raw p	$-LOG_{10}(p)$	Holm adjust	FDR	Impact	Hits/ Total	Potential biomarkers
Linoleic acid metabolism	Lipid metabolism	5	0.0530	2	0.0010	2.9850	0.0870	0.0870	1.0000	0.4000	PC(22:0/P-18:0), Linoleic acid
Arachidonic acid metabolism	Lipid metabolism	36	0.3817	2	0.0539	1.2688	1.0000	0.8310	0.3329	0.0556	PC(22:0/P-18:0), Arachidonic acid
Glyoxylate and dicarboxylate metabolism	Carbohydrate metabolism	32	0.3393	1	0.2916	0.5353	1.0000	1.0000	0.2196	0.0313	Hydroxypyruvic acid
Arginine and proline metabolism	Amino acid metabolism	38	0.4029	2	0.0594	1.2265	1.0000	0.8310	0.1685	0.0526	L-Arginine, Ornithine
Arginine biosynthesis	Amino acid metabolism	14	0.1484	2	0.0089	2.0502	0.7395	0.3742	0.1371	0.1429	L-Arginine, Ornithine
Steroid hormone biosynthesis	Lipid metabolism	77	0.8164	1	0.5693	0.2447	1.0000	1.0000	0.1275	0.0130	L-Palmitoylcarnitine
Glycerophospholipid metabolism	Lipid metabolism	36	0.3817	2	0.0539	1.2688	1.0000	0.8310	0.1118	0.0556	PC(22:0/P-18:0), LysoPC(20: 5(5Z,8Z,11Z,14Z,17Z))
Glycine, serine and threonine metabolism	Amino acid metabolism	34	0.3605	1	0.3068	0.5131	1.0000	1.0000	0.0425	0.0294	Hydroxypyruvic acid
Sphingolipid metabolism	Lipid metabolism	21	0.2227	1	0.2018	0.6951	1.0000	1.0000	0.0243	0.0476	Sphingosine 1-phosphate
Glycolysis/ Gluconeogenesis	Carbohydrate metabolism	26	0.2757	1	0.2438	0.6129	1.0000	1.0000	0.0002	0.0385	D-Glucose
Biosynthesis of unsaturated fatty acids	Lipid metabolism	36	0.3817	2	0.0539	1.2688	1.0000	0.8310	0.0000	0.0556	Linoleic acid, Arachidonic acid
Ascorbate and aldarate metabolism	Carbohydrate metabolism	10	0.1060	1	0.1014	0.9940	1.0000	1.0000	0.0000	0.1000	Glucaric acid
Phenylalanine metabolism	Amino acid metabolism	12	0.1272	1	0.1205	0.9191	1.0000	1.0000	0.0000	0.0833	Hippuric acid
alpha-Linolenic acid metabolism	Lipid metabolism	13	0.1378	1	0.1299	0.8864	1.0000	1.0000	0.0000	0.0769	PC(22:0/P-18:0)
Glutathione metabolism	Metabolism of other amino acids	28	0.2969	1	0.2601	0.5849	1.0000	1.0000	0.0000	0.0357	Ornithine
Fatty acid degradation	Lipid metabolism	39	0.4135	1	0.3437	0.4639	1.0000	1.0000	0.0000	0.0256	L-Palmitoylcarnitine
Aminoacyl-tRNA biosynthesis	Genetic Information Processing, Translation	48	0.5090	1	0.4054	0.3921	1.0000	1.0000	0.0000	0.0208	L-Arginine

albiflorin and paeoniflorigenone were from *Paeonia lactiflora* Pall. [Ranunculaceae], astragaline A, and astragaloside II were from *Astragalus mongholicus Bunge* [Leguminosae], glycyrrhetic acid, glycyrrhizic acid, licurazide, and isoliquiritigenin came from *Glycyrrhiza uralensis* Fisch. [Leguminosae].

DISCUSSION

RA is an autoimmune disease that primarily affects synovial joints and is characterized by chronic synovitis, systemic inflammation, and varying degrees of erosion of bone and cartilage. While the cause of RA is unknown, it involves a combination of genetic and environmental factors, potential mechanisms involving the body's immune system attacking joints, and researchers have focused on exploring the immune mechanisms and molecular networks of RA (Lee and Weinblatt, 2001). Nonsteroidal anti-inflammatory drugs and biologics are currently used to treat RA, but traditional medicine has attracted the attention of doctors and patients in many developing countries because these treatment methods have similar therapeutic goals: anti-inflammatory and pain suppression, slow joint injury, and prevent the development of inflammation-related complications (Moudgil and Berman, 2014; Wang et al., 2021). WTD is a Chinese prescription for rheumatoid arthritis and joint pain which was described in ancient medical writings. As a result, scientific evidence for WTD is accumulating, including clinical efficacy evaluations, characterization of complex components, and molecular mechanism analysis. The RA rat model was effectively duplicated in this work using a variety of assessment methods after injection of Freund's complete adjuvant in a short period. Through X-ray examination, histopathological analysis, and the detection of inflammatory factors, it was discovered that the model rats' feet, tails, and spinal joints were gradually swollen and stiff and that there was a severe inflammatory response in the joints of the rats, so the inflammatory response evolved into bone deformation and stiffness due to unregulated, which was the same pathological phenomenon as in previous similar studies (Pan et al., 2017; Dai et al., 2022). Although clinical features of patients

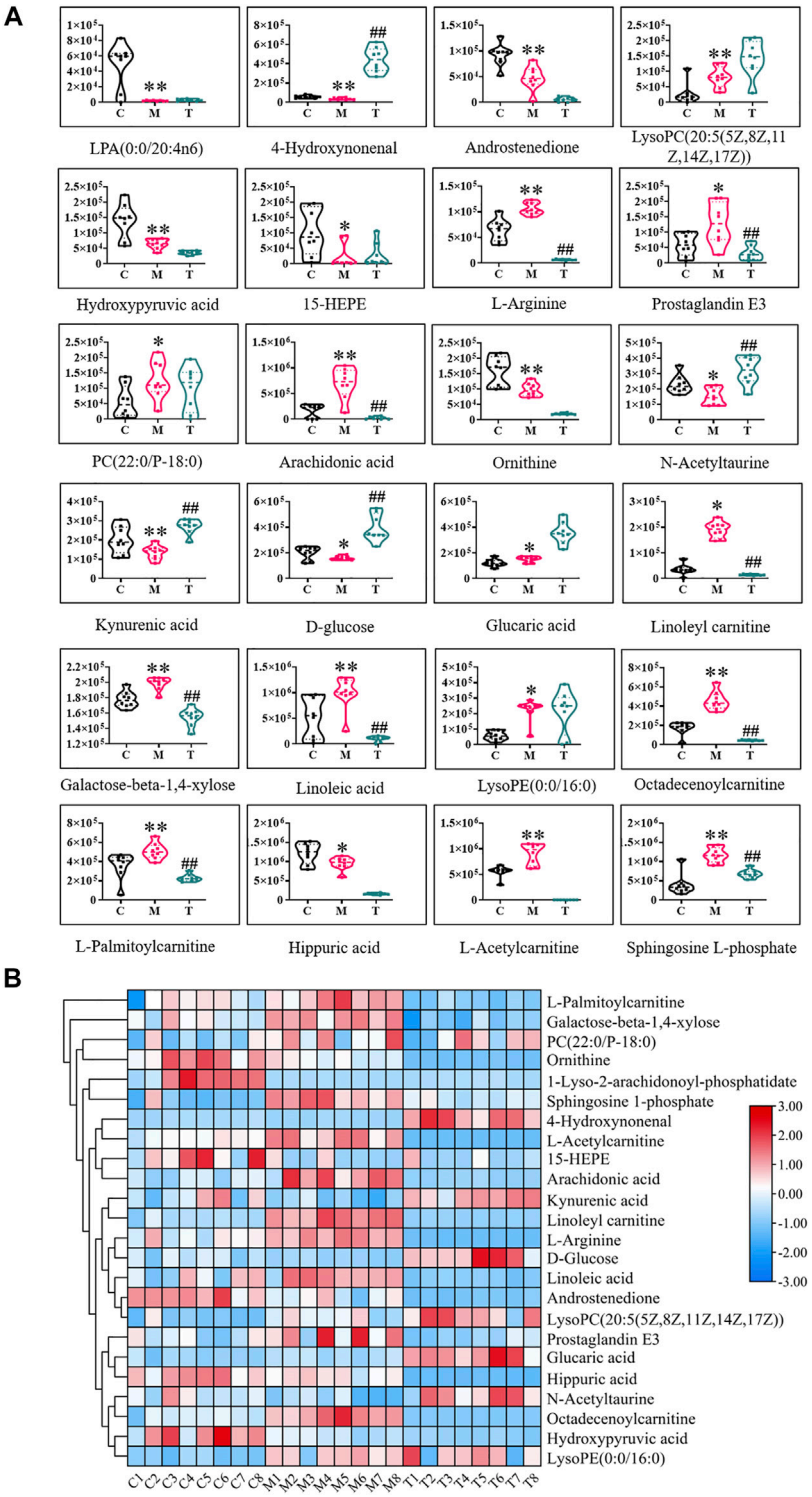

FIGURE 5 | The normalized abundance of potential biomarkers before and after wutou decoction administration. **(A)** Normalized abundance values between different groups **(B)** Heat map of the differences in the potential biomarkers of the C, M and T obtained in the ESI^+ and ESI^-. Results are expressed as mean ± SD, $n = 8$. $^*p < 0.05$, $^{**}p < 0.01$ vs control group. $^{\#}p < 0.05$, $^{\#\#}p < 0.01$ vs model group. C represents control group, M represents model group, T represents wutou decoction group.

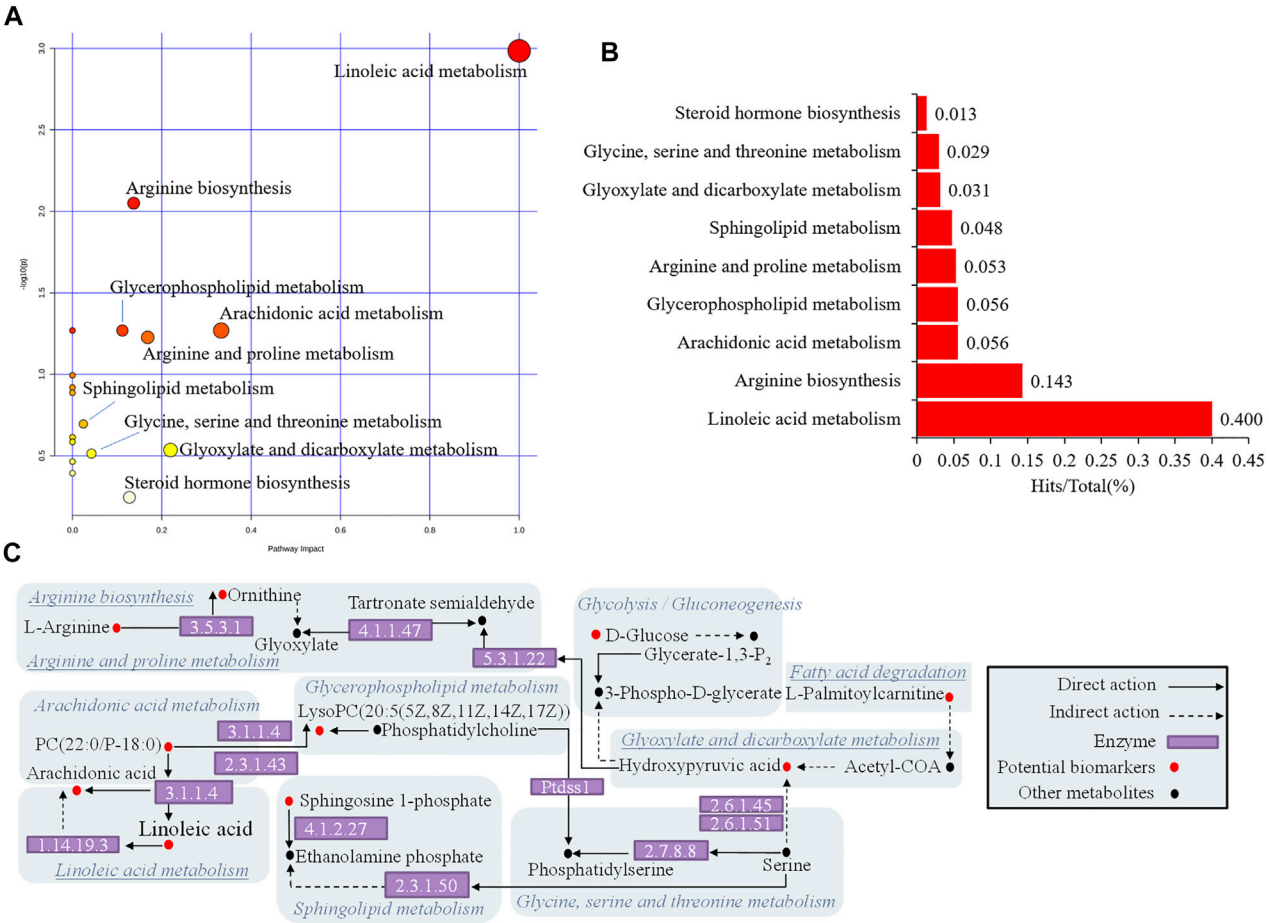

FIGURE 6 | Enrichment analysis of metabolic pathway of potential biomarkers. **(A)** Pathway impact enrichment **(B)** The proportion of biomarkers in the overall pathway **(C)** Association network of biomarker metabolic pathways.

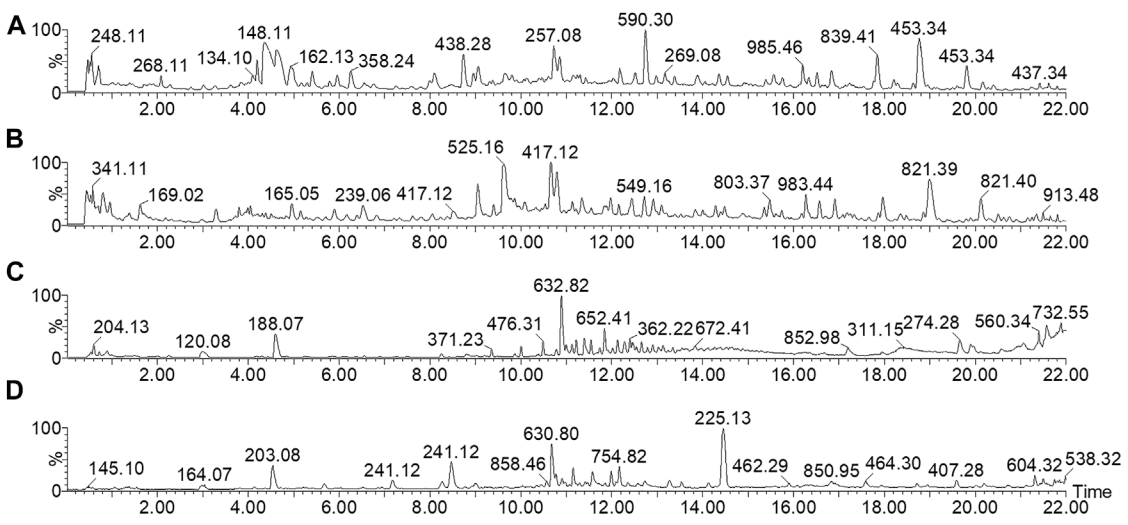

FIGURE 7 | TIC spectrum of chemical profile and absorbed components from wutou decoction. **(A,B)** The chemical profile of wutou decoction in ESI^+ and ESI^-, respectively **(C,D)** The blood components of wutou decoction in ESI^+ and ESI^-, respectively.

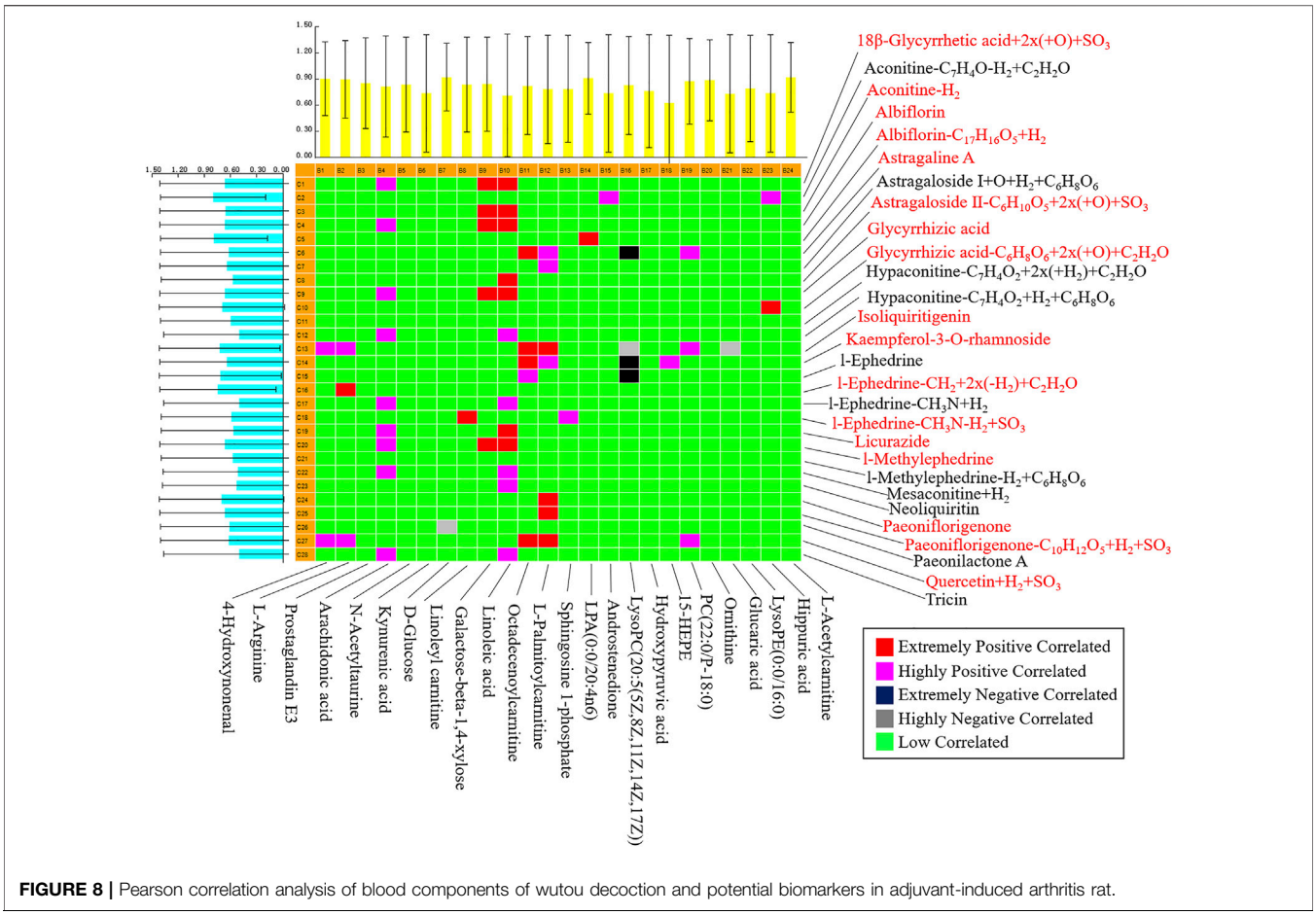

FIGURE 8 | Pearson correlation analysis of blood components of wutou decoction and potential biomarkers in adjuvant-induced arthritis rat.

with RA cannot be entirely simulated, the current results may explain why rat models of adjuvant-induced arthritis are commonly implemented in drug development.

Studies indicate metabolic disorders in biofluids in RA patients or animal models, covering lipid and glucose metabolism, and amino acid metabolism (Falconer et al., 2018). Untargeted metabolomics with pattern recognition was used to evaluate the metabolites in the serum and urine of RA rats, and 24 different metabolites were detected. Metabolic pathway enrichment results showed crosstalk of three types of pathways dominated by lipid metabolism, of which the important pathway associated with RA rats with an impact value greater than 0.1 was identified (**Table 2**). Arachidonic acid is a polyunsaturated essential fatty acid located in the body's fats, the liver, brain, and a range of other organs. Arachidonic acid performs an important role in the structure and function of the body's cell membranes; it can directly or indirectly synthesize prostaglandins and leukotrienes, and other biologically active substances, and it can cause inflammation in the body by a cascade of arachidonic acid (Charles-Schoeman et al., 2018; Szczuko et al., 2020). The level of arachidonic acid in the model group was abnormal when compared to the control group, which severely disrupted linoleic acid metabolism and arachidonic acid metabolism in lipid metabolism. However, WTD reversed the level of arachidonic acid and may modulate related metabolic pathways, suggesting that this mechanism is both underlying and noteworthy. Lysolecithin is formed by phosphatase A2 hydrolysis of lecithin, and changes in lysolecithin reflect cell renewal and phospholipid consumption (Charles-Schoeman et al., 2018). These compounds are critical in cell proliferation and inflammatory response. WTD has no positive feedback effect on LysoPC(20:5) in the pathway, but it does have a regulatory influence on steroid hormone biosynthesis of lipid metabolism *via* L-palmitoylcarnitine, and high levels of L-palmitoylcarnitine may be detrimental to energy metabolism in mitochondria (Imagawa et al., 1984). Both RA and osteoarthritis patients exhibit anomalies in arginine and proline metabolism in their synovial fluid (Carlson et al., 2018). According to KEGG, hydroxypyruvic acid interfered with glyoxylate and dicarboxylate metabolism, and it might cause cascading fluctuations by acting on arginine and proline metabolism *via* the downstream enzyme 5.3.1.22 (**Figure 6C**). Unfortunately, WTD only regulates L-arginine and cannot regulate hydroxypyruvic acid.

To discover the Q-markers of WTD, this study employed a chinmedomics strategy to analyze the correlation between the components absorbed into the blood of WTD and the potential biomarkers of RA rats, highlighting the importance of certain components in regulating RA metabolism and markers. Finally,

12 key components were determined as Q-markers for the efficacy of WTD in the treatment of RA. Aconitine, the main active component of *Aconitum carmichaeli* Debeaux [Ranunculaceae], has immunomodulatory properties that might be useful in treating autoimmune diseases, such as rheumatoid arthritis and systemic lupus erythematosus (Li et al., 2017). Ephedrine can mediate toll-like receptor 4 to encourage the production of interleukin 10 and inhibit the secretion of TNF-α to decrease inflammation (Zheng et al., 2012). Quercetin inhibits arthritis mice even stronger than methotrexate (Haleagrahara et al., 2017), and quercetin regulates the enteric nervous system to protect the jejunal inflammation caused by RA (Piovezana et al., 2019). Albiflorin and paeoniflorigenone could modulate the functions and activation of immune cells, decreases inflammatory medium production, and restore abnormal signal pathway (Zhang and Wei, 2020). Astragalin could attenuate synovial inflammation and joint destruction in RA at least partially by restraining the phosphorylation of mitogen-activated protein kinases and the activating of N-terminal kinase/activated protein 1 (Zhang and Wei, 2020). Moreover, kaempferol-3-O-rhamnoside, glycyrrhetic acid, and isoliquiritigenin all have the potential and activity to resist RA (Puchner et al., 2012; Zhu et al., 2012; Ahmed and Abd Elkarim, 2021). With the help of the correlation analysis of chinmedomics, we finally identified 12 Q-markers of WTD, which have a certain degree of anti-inflammatory and immune-regulating biological activity, but it is unclear whether the combination of these compounds has a better anti-RA effect, this needs further verification.

CONCLUSION

To summarize, this work used chinmedomics to evaluate the therapeutic effect of WTD on adjuvant-induced arthritic rats and to investigate the Q-markers of WTD. WTD helps alleviate disease states and pathological conditions in inflammatory rats, and chinmedomics as a research tool for TCM effectiveness and pharmacology promotes the discovery of WTD Q-markers and contributes to the theoretical evidence for WTD quality control.

DATA AVAILABILITY STATEMENT

The original contributions presented in the study are included in the article/**Supplementary Material**, further inquiries can be directed to the corresponding authors.

ETHICS STATEMENT

The animal study was reviewed and approved by Animal Experiment Center, Heilongjiang University of Chinese Medicine.

AUTHOR CONTRIBUTIONS

TL, FW, AZ, and IU in charge of experimental design, HD, HL, JM, YiH, and YaH in charge of data collection, XW in charge of funding.

FUNDING

This work was supported by grants from the Key Program of Natural Science Foundation of State (Grant No. 81830110, 81861168037), Scientific and Technology Development Program of Guangxi (AD18126013), the Ba Gui Scholars program of Guangxi, the Central Government Guides Local Science and Technology Development Fund Projects (ZY21195044), Natural Science Foundation of Heilongjiang Province (LH2019H056), Heilongjiang Touyan Innovation Team Program.

SUPPLEMENTARY MATERIAL

The Supplementary Material for this article can be found online at: https://www.frontiersin.org/articles/10.3389/fphar.2022.854087/full#supplementary-material

REFERENCES

Ahmed, A. H., and Abd Elkarim, A. S. (2021). Bioactive Compounds with Significant Anti-Rheumatoid Arthritis Effect Isolated for the First Time from Leaves of Bougainvillea Spectabilis. *Curr. Pharm. Biotechnol.* 22, 2048–2053. doi:10.2174/1389201021666201229111825

Bai, G., Zhang, T., Hou, Y., Ding, G., Jiang, M., and Luo, G. (2018). From Quality Markers to Data Mining and Intelligence Assessment: A Smart Quality-Evaluation Strategy for Traditional Chinese Medicine Based on Quality Markers. *Phytomedicine* 44, 109–116. doi:10.1016/j.phymed.2018.01.017

Carlson, A. K., Rawle, R. A., Adams, E., Greenwood, M. C., Bothner, B., and June, R. K. (2018). Application of Global Metabolomic Profiling of Synovial Fluid for Osteoarthritis Biomarkers. *Biochem. Biophys. Res. Commun.* 499 (2), 182–188. doi:10.1016/j.bbrc.2018.03.117

Charles-Schoeman, C., Meriwether, D., Lee, Y. Y., Shahbazian, A., and Reddy, S. T. (2018). High Levels of Oxidized Fatty Acids in HDL Are Associated with Impaired HDL Function in Patients with Active Rheumatoid Arthritis. *Clin. Rheumatol.* 37 (3), 615–622. doi:10.1007/s10067-017-3896-y

Dai, Y., Sheng, J., He, S., Wu, Q., Wang, Y., and Su, L. (2022). Dehydroevodiamine Suppresses Inflammatory Responses in Adjuvant-Induced Arthritis Rats and Human Fibroblast-like Synoviocytes. *Bioengineered* 13 (1), 268–279. doi:10.1080/21655979.2021.1999554

Dong, H., Yan, G. L., Han, Y., Sun, H., Zhang, A. H., Li, X. N., et al. (2015). UPLC-Q-TOF/MS-based Metabolomic Studies on the Toxicity Mechanisms of Traditional Chinese Medicine Chuanwu and the Detoxification Mechanisms of Gancao, Baishao, and Ganjiang. *Chin. J. Nat. Med.* 13 (9), 687–698. doi:10.1016/S1875-5364(15)30067-4

Falconer, J., Murphy, A. N., Young, S. P., Clark, A. R., Tiziani, S., Guma, M., et al. (2018). Review: Synovial Cell Metabolism and Chronic Inflammation in Rheumatoid Arthritis. *Arthritis Rheumatol.* 70 (7), 984–999. doi:10.1002/art.40504

Guo, Q., Zheng, K., Fan, D., Zhao, Y., Li, L., Bian, Y., et al. (2017). Wu-Tou Decoction in Rheumatoid Arthritis: Integrating Network Pharmacology and In Vivo Pharmacological Evaluation. *Front. Pharmacol.* 8, 230. doi:10.3389/fphar.2017.00230

Guo, Q., Mizuno, K., Okuyama, K., Lin, N., Zhang, Y., Hayashi, H., et al. (2020). Antineuropathic Pain Actions of Wu-tou Decoction Resulted from the Increase of Neurotrophic Factor and Decrease of CCR5 Expression in Primary Rat Glial Cells. *Biomed. Pharmacother.* 123, 109812. doi:10.1016/j.biopha.2020.109812

Haleagrahara, N., Miranda-Hernandez, S., Alim, M. A., Hayes, L., Bird, G., and Ketheesan, N. (2017). Therapeutic Effect of Quercetin in Collagen-Induced Arthritis. *Biomed. Pharmacother.* 90, 38–46. doi:10.1016/j.biopha.2017.03.026

Han, Y., Sun, H., Zhang, A., Yan, G., and Wang, X. J. (2020). Chinmedomics, a New Strategy for Evaluating the Therapeutic Efficacy of Herbal Medicines. *Pharmacol. Ther.* 216, 107680. doi:10.1016/j.pharmthera.2020.107680

He, J., Feng, X., Wang, K., Liu, C., and Qiu, F. (2018). Discovery and Identification of Quality Markers of Chinese Medicine Based on Pharmacokinetic Analysis. *Phytomedicine* 44, 182–186. doi:10.1016/j.phymed.2018.02.008

Imagawa, T., Watanabe, T., and Nakamura, T. (1984). Inhibition of Palmitate Oxidation in Mitochondria by Lipid Hydroperoxides. *J. Biochem.* 95 (3), 771–778. doi:10.1093/oxfordjournals.jbchem.a134668

Lee, D. M., and Weinblatt, M. E. (2001). Rheumatoid Arthritis. *Lancet* 358 (9285), 903–911. doi:10.1016/S0140-6736(01)06075-5

Li, X., Gu, L., Yang, L., Zhang, D., and Shen, J. (2017). Aconitine: A Potential Novel Treatment for Systemic Lupus Erythematosus. *J. Pharmacol. Sci.* 133 (3), 115–121. doi:10.1016/j.jphs.2017.01.007

Moudgil, K. D., and Berman, B. M. (2014). Traditional Chinese Medicine: Potential for Clinical Treatment of Rheumatoid Arthritis. *Expert Rev. Clin. Immunol.* 10 (7), 819–822. doi:10.1586/1744666X.2014.917963

Pan, T., Cheng, T. F., Jia, Y. R., Li, P., and Li, F. (2017). Anti-rheumatoid Arthritis Effects of Traditional Chinese Herb Couple in Adjuvant-Induced Arthritis in Rats. *J. Ethnopharmacol.* 205, 1–7. doi:10.1016/j.jep.2017.04.020

Piovezana Bossolani, G. D., Silva, B. T., Colombo Martins Perles, J. V., Lima, M. M., Vieira Frez, F. C., Garcia de Souza, S. R., et al. (2019). Rheumatoid Arthritis Induces Enteric Neurodegeneration and Jejunal Inflammation, and Quercetin Promotes Neuroprotective and Anti-inflammatory Actions. *Life Sci.* 238, 116956. doi:10.1016/j.lfs.2019.116956

Puchner, A., Hayer, S., Niederreiter, B., Hladik, A., Blueml, S., Bonelli, M., et al. (2012). Effects of 18β-Glycyrrhetinic Acid in hTNFtg Mice - a Model of Rheumatoid Arthritis. *Wien. Klin. Wochenschr.* 124 (5-6), 170–176. doi:10.1007/s00508-011-0103-z

Qi, Y., Li, S., Pi, Z., Song, F., Lin, N., Liu, S., et al. (2014). Chemical Profiling of Wu-tou Decoction by UPLC-Q-TOF-MS. *Talanta* 118, 21–29. doi:10.1016/j.talanta.2013.09.054

Qiu, S., Zhang, A.-h., Guan, Y., Sun, H., Zhang, T.-l., Han, Y., et al. (2020). Functional Metabolomics Using UPLC-Q/TOF-MS Combined with Ingenuity Pathway Analysis as a Promising Strategy for Evaluating the Efficacy and Discovering Amino Acid Metabolism as a Potential Therapeutic Mechanism-Related Target for Geniposide against Alcoholic Liver Disease. *RSC Adv.* 10 (5), 2677–2690. doi:10.1039/c9ra09305b

Sun, H., Zhang, A. H., Yang, L., Li, M. X., Fang, H., Xie, J., et al. (2019). High-throughput Chinmedomics Strategy for Discovering the Quality-Markers and Potential Targets for Yinchenhao Decoction. *Phytomedicine* 54, 328–338. doi:10.1016/j.phymed.2018.04.015

Szczuko, M., Kikut, J., Komorniak, N., Bilicki, J., Celewicz, Z., and Ziętek, M. (2020). The Role of Arachidonic and Linoleic Acid Derivatives in Pathological Pregnancies and the Human Reproduction Process. *Int. J. Mol. Sci.* 21 (24), 9628. doi:10.3390/ijms21249628

Wang, X., Zhang, A., Sun, H., and Yan, G. (2015). "Origin of Chinmedomics," in *Chinmedomics*. Editors X. Wang, A. Zhang, and H. Sun (Boston: Academic Press), 1–15. doi:10.1016/b978-0-12-803117-9.00001-9

Wang, X. J., Zhang, A. H., Kong, L., Yu, J. B., Gao, H. L., Liu, Z. D., et al. (2019). Rapid Discovery of Quality-Markers from Kaixin San Using Chinmedomics Analysis Approach. *Phytomedicine* 54, 371–381. doi:10.1016/j.phymed.2017.12.014

Wang, Y., Chen, S., Du, K., Liang, C., Wang, S., Owusu Boadi, E., et al. (2021). Traditional Herbal Medicine: Therapeutic Potential in Rheumatoid Arthritis. *J. Ethnopharmacol.* 279, 114368. doi:10.1016/j.jep.2021.114368

Xu, T., Li, S., Sun, Y., Pi, Z., Liu, S., Song, F., et al. (2017). Systematically Characterize the Absorbed Effective Substances of Wutou Decoction and Their Metabolic Pathways in Rat Plasma Using UHPLC-Q-TOF-MS Combined with a Target Network Pharmacological Analysis. *J. Pharm. Biomed. Anal.* 141, 95–107. doi:10.1016/j.jpba.2017.04.012

Zhang AH, A. H., Yu, J. B., Sun, H., Kong, L., Wang, X. Q., Zhang, Q. Y., et al. (2018). Identifying Quality-Markers from Shengmai San Protects against Transgenic Mouse Model of Alzheimer's Disease Using Chinmedomics Approach. *Phytomedicine* 45, 84–92. doi:10.1016/j.phymed.2018.04.004

Zhang, L., and Wei, W. (2020). Anti-inflammatory and Immunoregulatory Effects of Paeoniflorin and Total Glucosides of Paeony. *Pharmacol. Ther.* 207, 107452. doi:10.1016/j.pharmthera.2019.107452

Zhang, W., Gong, L., Zhou, L. L., Shan, J. J., Chen, L. T., Hui-Qin, X. U., et al. (2014). Effect of different compatibility of Daphnes Giraldii Cortex and Glycyrrhizae Radix et Rhizoma on adjuvant-induced arthritis in rats. *Chin. Tradit. Herbal Drugs* 45, 1418. doi:10.7501/j.issn.0253-2670.2014.10.013

Zhang, A., Fang, H., Wang, Y., Yan, G., Sun, H., Zhou, X., et al. (2017). Discovery and Verification of the Potential Targets from Bioactive Molecules by Network Pharmacology-Based Target Prediction Combined with High-Throughput Metabolomics. *RSC Adv.* 7, 51069–51078. doi:10.1039/c7ra09522h

Zhang, A.-H., Sun, H., Yan, G.-L., Han, Y., Zhao, Q.-Q., and Wang, X.-J. (2019). Chinmedomics: A Powerful Approach Integrating Metabolomics with Serum Pharmacochemistry to Evaluate the Efficacy of Traditional Chinese Medicine. *Engineering* 5, 60–68. doi:10.1016/j.eng.2018.11.008

Zhang, A. H., Ma, Z. M., Kong, L., Gao, H. L., Sun, H., Wang, X. Q., et al. (2020). High-throughput Lipidomics Analysis to Discover Lipid Biomarkers and Profiles as Potential Targets for Evaluating Efficacy of Kai-Xin-San against APP/PS1 Transgenic Mice Based on UPLC-Q/TOF-MS. *Biomed. Chromatogr.* 34 (2), e4724. doi:10.1002/bmc.4724

Zhang T, T., Bai, G., Han, Y., Xu, J., Gong, S., Li, Y., et al. (2018). The Method of Quality Marker Research and Quality Evaluation of Traditional Chinese Medicine Based on Drug Properties and Effect Characteristics. *Phytomedicine* 44, 204–211. doi:10.1016/j.phymed.2018.02.009

Zhao, Q., Gao, X., Yan, G., Zhang, A., Sun, H., Han, Y., et al. (2020). Chinmedomics Facilitated Quality-Marker Discovery of Sijunzi Decoction to Treat Spleen Qi Deficiency Syndrome. *Front. Med.* 14 (3), 335–356. doi:10.1007/s11684-019-0705-9

Zheng, Y., Guo, Z., He, W., Yang, Y., Li, Y., Zheng, A., et al. (2012). Ephedrine Hydrochloride Protects Mice from LPS challenge by Promoting IL-10 Secretion and Inhibiting Proinflammatory Cytokines. *Int. Immunopharmacol.* 13 (1), 46–53. doi:10.1016/j.intimp.2012.03.005

Zhu, L., Wei, H., Wu, Y., Yang, S., Xiao, L., Zhang, J., et al. (2012). Licorice Isoliquiritigenin Suppresses RANKL-Induced Osteoclastogenesis In Vitro and Prevents Inflammatory Bone Loss In Vivo. *Int. J. Biochem. Cel Biol.* 44 (7), 1139–1152. doi:10.1016/j.biocel.2012.04.003

Conflict of Interest: The authors declare that the research was conducted in the absence of any commercial or financial relationships that could be construed as a potential conflict of interest.

Publisher's Note: All claims expressed in this article are solely those of the authors and do not necessarily represent those of their affiliated organizations, or those of the publisher, the editors and the reviewers. Any product that may be evaluated in this article, or claim that may be made by its manufacturer, is not guaranteed or endorsed by the publisher.

frontiers | Frontiers in Pharmacology

ORIGINAL RESEARCH
published: 17 May 2022
doi: 10.3389/fphar.2022.865586

Comprehensive Analysis of *Eleutherococcus senticosus* (Rupr. & Maxim.) Maxim. Leaves Based on UPLC-MS/MS: Separation and Rapid Qualitative and Quantitative Analysis

Jianping Hu[1], Dan Wu[1,2], Yanping Sun[1], Hongquan Zhao[1], Yangyang Wang[1], Wensen Zhang[1], Fazhi Su[1], Bingyou Yang[1], Qiuhong Wang[3] and Haixue Kuang[1]**

[1]Key Laboratory of Basic and Application Research of Beiyao, Ministry of Education, Heilongjiang Touyan Innovation Team Program, Heilongjiang University of Chinese Medicine, Harbin, China, [2]Medical School, Quzhou College of Technology, Quzhou, China, [3]Department of Natural Medicinal Chemistry, College of Pharmacy, Guangdong Pharmaceutical University, Guangzhou, China

OPEN ACCESS

Edited by:
Abdul Rohman,
Gadjah Mada University, Indonesia

Reviewed by:
Alexander N. Shikov,
Saint-Petersburg State Chemical Pharmaceutical Academy, Russia
Ya-Fang Shang,
Hefei University of Technology, China

***Correspondence:**
Qiuhong Wang
qhwang668@sina.com
Haixue Kuang
hxkuang@hljucm.net

Specialty section:
This article was submitted to Ethnopharmacology, a section of the journal Frontiers in Pharmacology

Received: 30 January 2022
Accepted: 15 March 2022
Published: 17 May 2022

Citation:
Hu J, Wu D, Sun Y, Zhao H, Wang Y, Zhang W, Su F, Yang B, Wang Q and Kuang H (2022) Comprehensive Analysis of Eleutherococcus senticosus (Rupr. & Maxim.) Maxim. Leaves Based on UPLC-MS/MS: Separation and Rapid Qualitative and Quantitative Analysis. Front. Pharmacol. 13:865586. doi: 10.3389/fphar.2022.865586

Eleutherococcus senticosus (Rupr. & Maxim.) Maxim. leaves (ESL) have long been people's favorite as a natural edible green vegetable, in which phenols and saponins are the main characteristic and bioactive components. This study was first carried out to comprehensively analyze the phenols and saponins in ESL, including phytochemical, qualitative, quantitative, and bioactivity analysis. The results showed that 30 compounds, including 20 phenolic compounds and 7 saponins, were identified. Twelve of them were isolated from *Eleutherococcus* Maxim. for the first time. In the qualitative analysis, 30 phenolic compounds and 28 saponins were accurately detected. Their characteristic cleavage processes were described by UPLC-QTOF-MS/MS. Ten representative ingredients were quantitated in 29 different regions *via* a 4000 QTRAP triple quadrupole tandem mass spectrometer (UPLC-QTRAP-MS/MS), and it was found that S19 (69.89 ± 1.098 mg/g) and S1 (74.28 ± 0.733 mg/g) had the highest contents of total phenols and saponins, respectively. The newly developed analysis method for the quantitative determination was validated for linearity, precision, and limits of detection and quantification, which could be applied to the quality assessment of ESL. *In vitro* experiment, the α-glucosidase inhibitory effect of the phenolic fraction was higher than others, indicating that the phenolic content may be related to the hypoglycemic activity. It was also suggested that ESL could be developed as a natural potential effective drug or functional food.

Keywords: *Eleutherococcus senticosus* (Rupr. & Maxim.) Maxim. leaves, phenols, saponins, UPLC-MS/MS, α-glucosidase inhibitory

1 INTRODUCTION

Eleutherococcus senticosus (Rupr. & Maxim.) Maxim. (syn. *Acanthopanax senticosus* (Rupr. & Maxim.) Harms, http://www.theplantlist.org), a perennial herb belonging to the Araliaceae family, is mainly distributed in Russia, China, Korea, and Japan, especially in Heilongjiang, Jilin, and Liaoning provinces of the northeast of China (Jia et al., 2021). *Eleutherococcus senticosus* (ES), also called *Acanthopanax senticosus*, *Siberian ginseng*, or *Ciwujia*, known as a famous adaptogen—a herbal

medicine that has a non-specific inter-system anti-stress effect throughout the human body (Panossian et al., 2021), first appeared in the Pharmacopoeia of the Union of Soviet Socialist Republics (USSR) as a medicinal plant in 1962. ES was approved by monographed in Russian State Pharmacopoeia (Shikov et al., 2021) and to treat symptoms of asthenia by the European Medicines Agency (EMA), its efficacy has been proved in clinical trials (Gerontakos et al., 2021). According to Chinese Pharmacopoeia, ES is efficient in invigorating the kidney and liver, replenishing the vital essence, and calming the mind (Committee, 2020). Modern pharmacological studies have shown that it tends to stimulate immunity, prevent diseases caused by stress, and treat diseases of the cardio-cerebrovascular system (Kim et al., 2010; Liang et al., 2010; Meng et al., 2018; Xie et al., 2015). While, as a delicious renewable green vegetable and functional tea, ESL is also deeply concerned and loved by the Chinese.

Until now, most phytochemical studies have focused on the isolation and identification from ES and demonstrated that it commonly contains saponins, flavonoids, phenylpropanoids, and polysaccharides (Yang et al., 2012; Han et al., 2016; Lau et al., 2019). A few studies have currently been conducted on phenolic constituents and saponins from ESL. The intake of natural phenolic and saponin substances has considerable health benefits, especially for cardiovascular diseases, metabolic diseases, and tumors (Costa et al., 2017; Dong et al., 2019; Singh et al., 2020; Zlab et al., 2020). As the main components in ESL, phenols and saponins possess beneficial effects *in vivo* and in *vitro*, such as anti-cancer (Hayakawa et al., 2020), antiviral (Yan et al., 2018), antibacterial (Lee et al., 2003; Zhou et al., 2017), antioxidative (Tosovic et al., 2017), and inhibitory activities on nitrite production (Lee et al., 2008), and are considered as important active constituents. However, the overall analysis of the composition and content of phenols and saponins in ESL has not been reported. This study mainly investigates the composition analysis, structure cracking law, and quality evaluation of phenols and saponins of ESL (**Figure 1**).

Due to the diversity, similarity, and complexity of chemical structures, the analysis of compounds becomes a great challenge. Liquid chromatography-electrospray ionization tandem mass spectrometry (LC-MS/MS) is a powerful tool for analyzing compounds (Wang et al., 2016). Because MS can provide the information of molecular formula and fragmentation ions, researchers have identified 42 phenolic compounds in 15 min and 131 ginsenosides in 10 min by an LC-MS/MS method (Wang et al., 2016; Ren et al., 2020), which proved to be an efficient and rapid method for the characterization of compounds. Normally, the long analytical time and low sensitivity are not convenient to rapidly qualify the chemical substances in ESL. To rapidly clarify and analyze the basic chemical substances of ESL, in this study, a new rapid and sensitive ultra-high-performance liquid chromatography-triple quadrupole tandem mass spectrometry (UPLC-MS/MS) method for the thorough detection of major or trace components was firstly established to characterize and quantify phenols and saponins of ESL. Moreover, a total of 30 monomers were isolated, of which 12 compounds (**1–4**, **9**, **10**, **12**, **14**, **19**, **21–23**) were obtained from *Eleutherococcus* Maxim. for the first time and 10 compounds, including five phenols and five saponins, were used for quantitative analysis of ESL. This newly developed qualitative and quantitative method based on UPLC-MS/MS could be applied to the quality assessment of ESL. Furthermore, we also firstly compared the α-glucosidase inhibitory effect of four different active fractions of ESL *in vitro*. Overall, this study enriches the material basis of ESL to some extent and provides a standard reference for its further rational development and utilization.

2 MATERIALS AND METHODS

2.1 Plant Material

The dried ESL were collected in December 2019, Changbai Mountain, Jilin province, and identified by professor Zhenyue Wang of the School of Pharmacy, Chinese Medicine Resources Center, Heilongjiang University of Chinese Medicine.

2.2 Standard Samples, Instruments, Chemicals, and Reagents

Ten reference standards of phenols and saponins, including protocatechuic acid (**13**), chlorogenic acid (**7**), methyl 5-*O*-feruloylquinate (**3**), hyperoside (**15**), rutin (**18**), 3-*O*-α-*L*-rhamnopyranosyl-(1→2)-α-*L*-arabinopyranoside-29-hydroxy oleanolic acid (**24**), 3-*O*-β-D-glucopyranosyl-(1→2)-α-*L*-arabinopyranoside-29-hydroxy oleanolic acid (**26**), ciwujianoside C4 (**28**), saponin P_E (**29**), and ciwujianoside K (**30**) were isolated from ESL in our previous research. Their chemical structures were determined by 1D, 2D NMR spectra, and MS. The purities of all standards were above 98.0%, as elucidated by an HPLC-ELSD method. MS spectra were acquired using a Waters Synapt G2-SI Accurate-Mass Q-TOF (Waters Corp., Milford, MA, United States) and 4000 QTRAP LC/MS system (AB SCIEX, Framingham, United States). ^{1}H-NMR (600 MHz) and ^{13}C-NMR (150 MHz) data were obtained by a Bruker DPX-600 Spectrometer (Switzerland, Germany). Silica gel (200–300 mesh, Qingdao Haiyang Co., China) and ODS resin (YMC Co., Japan) were used in liquid column chromatography. The preparative HPLC column was a Diamonsil® C18 (5 μm, 10*250 mm) column (DiKMA Co., China). An ACQUITY UPLC HSS T3 column (1.8 μm, 2.1*100 mm, Waters, United States) was used to perform LC-MS analysis. LC-MS grade acetonitrile and formic acid were purchased from Thermo Fisher Scientific (Waltham, United States). Water for UPLC was purified by a Milli-Q water purification system (Darmstadt, Germany). Other reagents and solvents were of analytical grades.

2.3 Preparation of Phenolic and Saponin Fractions of *Eleutherococcus Senticosus* (Rupr. & Maxim.) Maxim. Leaves

The dried ESL (5.0 kg) were extracted with 70% ethanol (2 h, three times) under reflux. After recovering ethanol under reduced pressure, the concentrated extract of 2.006 kg (40%) was obtained. The extract was suspended with 12 L water and then successively extracted with petroleum ether and water-saturated n-butanol in a 1:1 volume ratio to obtain the n-butanol extract.

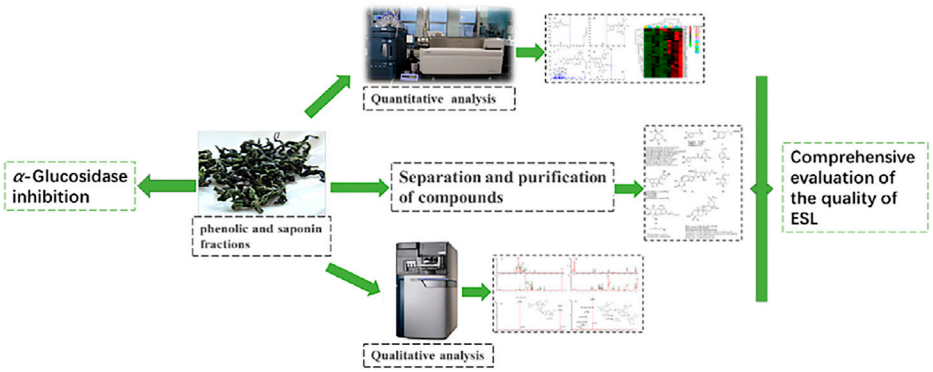

FIGURE 1 | The brief route of experimental research.

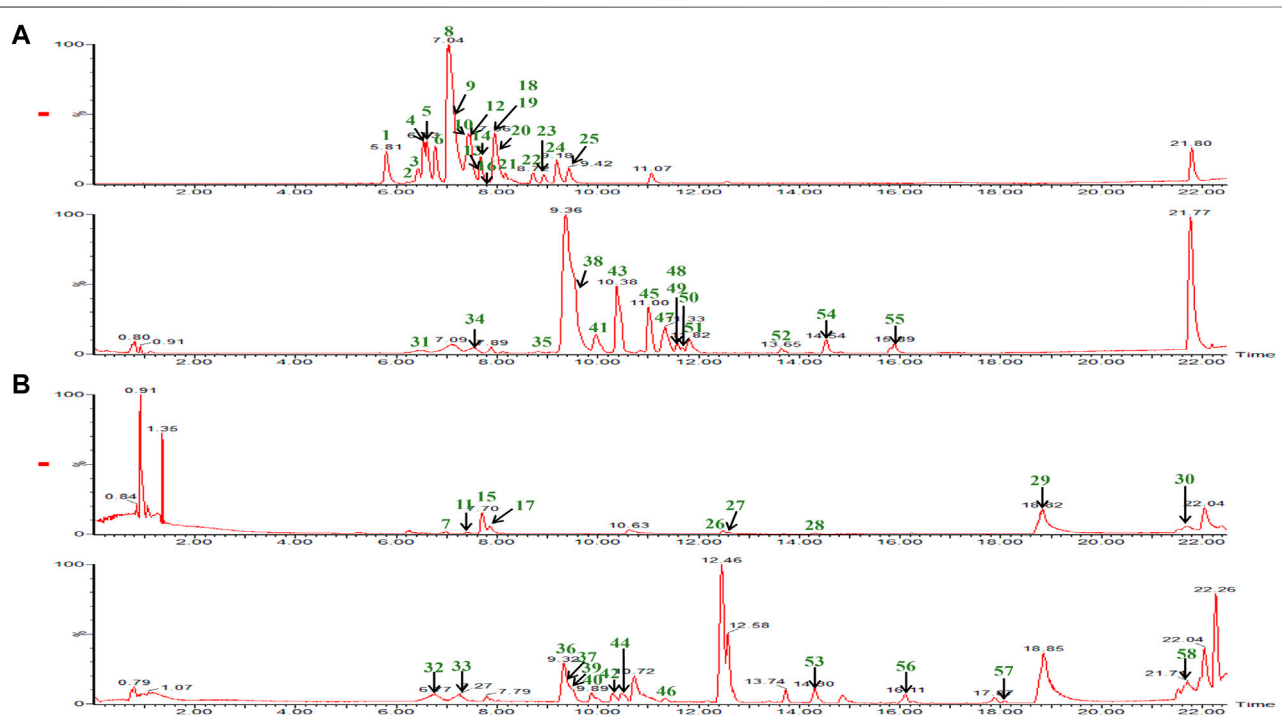

FIGURE 2 | The BPI chromatograms of 58 compounds in phenolic and saponin fractions were detected at positive ion mode **(B)** and negative ion mode **(A)**. The phenolic fraction consists of the upper part of the **(A)** and **(B)** diagram. The remaining part is the saponin fraction.

The partial n-butanol layer was subjected to PH 2-3 (337.0 g) and eluted by AB-8 macroporous adsorption resin with 30% ethanol solvent to obtain phenolic fraction (96.4 g). In the other part, the saponin fraction (109.1 g) was yielded by elution AB-8 macroporous resin in 60% ethanol.

2.4 Isolation and Identification of Chemical Constituents of Phenolic and Saponin Fractions

The above phenolic fraction (61.0 g) was chromatographed on a silica gel (200–300 mesh) column (8*150 cm), with CH_2Cl_2-MeOH (10:1, 5:1, 3:1, 2:1, 1:1, 0:1) as the eluent to produce 10 fractions (Fr.1–Fr.10) followed by TLC analysis. Fr.1 was then subjected to a reversed-phase ODS column, eluted with a mixture of MeOH (20–60%). After repeated elution of MeOH (30%, 38%, 40%) in semi-preparative HPLC chromatography, compounds **4** (9.15 mg), **7** (9.61 mg), **12** (8.32 mg), **13** (27.8 mg), and **21** (5.5 mg) were obtained. Compounds **1** (15.84 mg), **2** (80.64 mg), and **3** (33.6 mg) were obtained from Fr.2 by repeated chromatography on Diamonsil® C18 (5 μm, 10*250 mm) column using methanol (30%, 35%) as the eluent. After repeated elution with MeOH (40%), compounds **5** (8.19 mg), **6** (76.92 mg), **8** (11.01 mg), **11**

TABLE 1 | Characterization of compounds in phenolic and saponin fractions by UPLC-MS/MS.

No.	Identification	t_R (min)	Characteristic fragment ions	m/z	Formula	Neutral mass
1	Chlorogenic acid	5.81	191.0591[M-Caffeoyl-H]$^-$	353.0873[M-H]$^-$	$C_{16}H_{18}O_9$	354.12
2	Isochlorogenic acid B	6.21	431.1967 [M-$C_4H_4O_2$-H]$^-$,368.1006[M-$C_4H_4O_2$-CO_2-H_2O-H]$^-$,353.0873[M-Caffeoyl-H]$^-$,191.9475 [M-2Caffeoyl-H]$^-$	515.1202[M-H]$^-$	$C_{25}H_{24}O_{12}$	516.11
3	3-*O*-Caffeoylshikimic acid	6.43	179.0363[Caffeic acid-H]$^-$,135.0446[Caffeic acid-CO_2-H]$^-$	335.0802 [M-H]$^-$	$C_{16}H_{16}O_8$	336.04
4	1,3-Dicaffeoylquinic acid	6.50	335.0802[M-Caffeoyl-H_2O-H]$^-$,191.0530[M-2Caffeoyl-H]$^-$,179.0363[Caffeic acid-H]$^-$,135.0446 [Caffeic acid-CO_2-H]$^-$	515.1202[M-H]$^-$	$C_{25}H_{24}O_{12}$	516.13
5	3,5-Dicaffeoylquinic acid	6.60	335.0802[M-Caffeoyl-H_2O-H]$^-$, 179.0363[Caffeic acid-H]$^-$	515.1202[M-H]$^-$	$C_{25}H_{24}O_{12}$	516.12
6	Isochlorogenic acid C	6.78	368.1090[M-$C_4H_4O_2$-CO_2-H_2O-H]$^-$,335.0802[M-Caffeoyl-H_2O-H]$^-$,161.0245[Caffeic acid-H_2O-H]$^-$	515.1202[M-H]$^-$	$C_{25}H_{24}O_{12}$	516.13
7	5-*O*-Feruloylquinic acid	6.98	338.3412[M-CO_2+H]$^+$,192.1611[M-Feruloyl+H]$^+$,163.0429[Ferulic acid-OCH_3+H]$^+$,103.9565[Coumaic acid-CO_2-H_2O +H]$^+$	391.0996 [M+NA]$^+$	$C_{17}H_{20}O_9$	368.11
8	3-*O*-Feruloylquinic acid	7.04	179.0363[Ferulic acid-CH_3-H]$^-$,135.0446[Ferulic acid-CH_3-CO_2-H]$^-$	367.1090[M-H]$^-$	$C_{17}H_{20}O_9$	368.34
9	Rutin	7.20	367.1090[M-Rha-$C_2H_4O_2$-2H_2O-H]$^-$,301.0327[M-Rha-Glc-H]$^-$	609.1498[M-H]$^-$	$C_{27}H_{30}O_{16}$	610.15
10	Hyperoside	7.39	367.1090[M-$C_2H_4O_2$-2H_2O-H]$^-$,300.0257[M-Gal-2H]$^-$,271.0259[M-Gal-CO-2H]$^-$	463.0889[M-H]$^-$	$C_{21}H_{20}O_{12}$	464.38
11	5-*O*-Caffeoylshikimic acid	7.40	340.2632[M-H_2O+Na]$^+$,113.9657[M-Caffeoyl-CO_2-H_2O+H]$^+$	359.2359 [M+NA]$^+$	$C_{16}H_{16}O_8$	336.04
12	Isoquercitrin	7.46	367.1090[M-$C_2H_4O_2$-2H_2O-H]$^-$,300.0257[M-Glc-2H]$^-$,271.0259[M-Glc-CO-H]$^-$	463.0889[M-H]$^-$	$C_{21}H_{20}O_{12}$	464.38
13	Kaempferol-*3*-*O*-robinobioside	7.63	463.0889[M-Rha+H_2O-H]$^-$,285.0412[M-Rha-Gal-H]$^-$	593.1528[M-H]$^-$	$C_{27}H_{30}O_{15}$	594.16
14	Kaempferol-*3*-*O*-α-L-rhamnopyranosyl(1→2)[α-L-rhamnopyranosyl(1→6)]-β-glucopyranoside	7.68	721.5026[M-H_2O-H]$^-$,593.1528[M-Rha-H]$^-$,367.1006[M-Rha-Glc-C_2H_4O-2H_2O-H]$^-$,271.0259[M-Rha-Glc-Rha-CO-H]$^-$	739.4935[M-H]$^-$	$C_{33}H_{40}O_{19}$	740.22
15	Syringin	7.70	340.2632[M-OCH_3+H]$^+$,209.1641[M-Glc+H]$^+$	395.8013 [M+NA]$^+$	$C_{17}H_{24}O_9$	372.37
16	Quercitrin	7.79	367.1090[M-C_2H_4O-2H_2O-H]$^-$,300.0257[M-Rha-2H]$^-$,271.0259[M-Rha-CO-2H]$^-$	447.0929[M-H]$^-$	$C_{21}H_{20}O_{11}$	448.34
17	5-*O*-p-Coumaroylquinic acid butyl ester	7.86	396.3058[M+2H]$^+$,387.7999[M-H_2O+H]$^+$,113.9657 [M-C_4H_9-Coumaroyl-CO_2-H_2O+H]$^+$	417.7812 [M+NA]$^+$	$C_{20}H_{26}O_8$	394.16
18	1,4-Dicaffeoylquinic acid	7.96	353.0873[M-Caffeoyl-H]$^-$,191.0591[M-2Caffeoyl-H]$^-$	515.1202[M-H]$^-$	$C_{25}H_{24}O_{12}$	516.13
19	Isorhamnetin-3-*O*-β-D-galactopyranoside	7.96	315.0714[M-Gal-H]$^-$,284.0337[M-Gal-OCH_3-H]$^-$	477.1127[M-H]$^-$	$C_{22}H_{22}O_{12}$	478.11
20	Kaempferol-7-*O*-β-D-glucopyranoside	8.04	300.0287[M-$C_5H_8O_5$-H]$^-$,271.0259[M-$C_5H_8O_5$-CO-H]$^-$	447.1010[M-H]$^-$	$C_{21}H_{20}O_{11}$	448.10
21	Isorhamnetin	8.17	301.0327[M-CH_3-H]$^-$	315.0523[M-H]$^-$	$C_{16}H_{12}O_7$	316.06
22	Methyl 1,3-*O*-dicaffeoylquinate	8.72	405.1225[M-$C_6H_5O_2$-CH_3-H]$^-$,191.9475[M-2Caffeoyl-CH_3-H]$^-$,146.9644[M-2Caffeoyl-CH_3-CO_2-H]$^-$	529.1407[M-H]$^-$	$C_{26}H_{26}O_{12}$	530.14
23	Ferulic acid	8.93	149.9285[M-CO_2-H]$^-$,133.0272[M-CO_2-CH_3-H]$^-$	193.0503[M-H]$^-$	$C_{10}H_{10}O_4$	194.06
24	Methyl 3,4-*O*-dicaffeoylquinate	9.18	409.1496[M-$C_7H_6O_2$-H]$^-$,367.1006[M-Caffeoyl-H]$^-$,146.9644[M-2Caffeoyl-CH_3-CO_2-H]$^-$	529.1407[M-H]$^-$	$C_{26}H_{26}O_{12}$	530.14
25	Methyl 3,5-*O*-dicaffeoylquinate	9.42	409.1496[M-$C_7H_6O_2$-H]$^-$,191.9475[M-2Caffeoyl-CH_3-H]$^-$,146.9644[M-2Caffeoyl-CH_3-CO_2-H]$^-$	529.1407[M-H]$^-$	$C_{26}H_{26}O_{12}$	530.14

(Continued on following page)

TABLE 1 | (*Continued*) Characterization of compounds in phenolic and saponin fractions by UPLC-MS/MS.

No.	Identification	t_R (min)	Characteristic fragment ions	m/z	Formula	Neutral mass
26	Caffeic acid 3-*O*-glucoside	12.47	299.1089[M-CO_2+H]$^+$	343.2979 [M+H]$^+$	$C_{15}H_{18}O_9$	342.10
27	Isofraxidin 7-*O*-glucoside	12.63	223.0636[M-Glc+H]$^+$	385.3087 [M+H]$^+$	$C_{17}H_{20}O_{10}$	384.34
28	3-*O*-p-Coumaroylquinic acid	14.31	303.3065[M-2H_2O+H]$^+$, 113.9657[M-Coumaroyl-CO_2-H_2O+H]$^+$	339.3412 [M+H]$^+$	$C_{16}H_{18}O_8$	338.10
29	Quercetin	18.82	282.2811[M-H_2O+H]$^+$	303.1443 [M+H]$^+$	$C_{15}H_{10}O_7$	302.24
30	Kaempferol 3-*O*-xylopyranosyl-(1→2)-rhamnopyranosyl-(1→6)-glucopyranoside	21.71	579.5396[M-Rha+H]$^+$,378.3327[M-Rha-Glc+H]$^+$	765.1606 [M+K]$^+$	$C_{32}H_{38}O_{19}$	726.20
31	Nipponoside B	6.45	836.5967[M-Rha-$C_4H_7O_3$-H]$^-$,723.5144[M-Rha-Glc+HCOO]$^-$	1087.5569 [M-H]$^-$	$C_{53}H_{84}O_{23}$	1088.56
32	Silphioside G	6.77	454.8520[M-Glc-GlcA]$^+$,396.8013[M-OGlc-OGlcA-CO_2+H]$^+$	816.5898 [M+NA]$^+$	$C_{42}H_{66}O_{14}$	793.97
33	Songoroside A	7.27	588.4120[M]$^+$,454.3450[M-Xyl]$^+$,396.8013[M-OXyl-CO_2+H]$^+$	901.4916 [M+NA]$^+$	$C_{35}H_{56}O_7$	588.82
34	3*β*-{*O*-*β*-D-Glucopyranosyl-(1→3)-*O*-*β*-D-galactopyranosyl-(1→4)-{*O*-*α*-L-rhamnopyranosyl-(1→2)}c-*O*-*β*-D-glucuronopyranosyl}-16α-hydroxy-13*β*,28-epoxyoleanan	7.56	677.5046[M-Rha-Glc-Gal+HCOO]$^-$	1119.5756 [M-H]$^-$	$C_{54}H_{88}O_{24}$	1120.43
35	Ciwujianoside D3	8.81	557.1382[M-Rha-GlcAc-Glc-CO_2-H]$^-$,529.1407[M-Rha-GlcAc-Glc-CO_2-CH_2O-H]$^-$,409.1584[M-OAra-Rha-GlcAc-Glc-CO_2-H]$^-$	1161.5948 [M+HCOO]$^-$	$C_{55}H_{88}O_{23}$	1116.57
36	Hederagenin 3-*O*-*β*-D-glucuronopyranosyl methyl ester-28-*O*-*β*-D-glucopyranoside	9.32	635.2262[M-GlcAc+2H]$^+$,438.1238[M-OGlcAc-OGlc]$^+$	843.3132 [M+H]$^+$	$C_{43}H_{69}O_{16}$	842.45
37	Ilexoside XLVIII	9.53	588.4120[M-OGlc-CO_2]$^+$,433.1486[M-OGlcA-Glc-CO_2+Na]$^+$,411.1650[M-OGlcA-OGlc-CO_2+H]$^+$	828.3518 [M+H]$^+$	$C_{42}H_{67}O_{16}$	827.96
38	Copteroside B	9.63	409.1584[M-OGlcA-CO_2-H]$^-$,301.0403[M-OGlcA-CO_2-C_8H_{13}-H]$^-$	647.3043[M-H]$^-$	$C_{36}H_{56}O_{10}$	648.12
39	Hederacoside D	9.66	1075.5725[M]$^+$,622.2760[M-Ara-Rha-Glc-Glc+H_2O+H]$^+$,433.1486[M-OAra-Rha-Glc-Glc-CO_2+Na]$^+$	1097.5614 [M+NA]$^+$	$C_{53}H_{86}O_{22}$	1074.56
40	Ciwujianoside B	9.89	933.4871[M-Rha+K]$^+$,423.3284[M-Rha-OAra-Rha-Glc-Glc+H]$^+$	1189.6082 [M+H]$^+$	$C_{58}H_{92}O_{25}$	1188.36
41	Acanthopanaxoside C	9.95	409.1584[M-GlcA-Ara-CO_2-H]$^-$	763.4387[M-H]$^-$	$C_{41}H_{64}O_{13}$	764.43
42	Oleanolic acid 3-[rhamnosyl-(1→4)-glucosyl-(1→6)-glucoside]	10.10	749.2703[M-OGlcA+H]$^+$,455.3599[M-OGlcA-Rha-Glc+H]$^+$	949.51217 [M+NA]$^+$	$C_{48}H_{78}O_{17}$	926.22
43	Ciwujianoside C1	10.38	941.4941[M-Rha+HCOO]]$^-$,779.4745[M-Rha-Glc+HCOO]$^-$,571.3712[M-Rha-Glc-Glc-H]$^-$,391.1456[M-Rha-Glc-Glc-Ara-CO_2-H]$^-$	1087.5669 [M+HCOO]$^-$	$C_{52}H_{82}O_{21}$	1042.53
44	Hederagenin 28-O-*β*-D-glucopyranoside	10.49	439.3583[M-Glc-CH_2OH]$^+$,423.3284[M-OGlc-CH_2OH]$^+$	635.7875 [M+H]$^+$	$C_{36}H_{58}O_9$	634.14
45	3*β*-{O-*α*-L-Rhamnopyranosyl-(1→4)-O-*α*-L-rhamnopyranosyl-(1→4)-[O-*α*-L-rhamnopyranosyl-(1→2)]-O-*β*-D-glucopyranosyl-(1→x)-O-*β*-D-glucuronopyranosyl}-16*α*-hydroxy-13*β*,28-epoxyoleanane	11.00	571.3712[M-Glc-2Rha-ORha-CO_2-H]$^-$	1197.5474 [M-H]$^-$	$C_{57}H_{98}O_{26}$	1198.63
46	Silphioside F	11.31	555.1868[M-$C_2H_4O_2$-H_2O+H]$^+$,393.1572[M-OGlcA-CO_2]$^+$	655.3060 [M+NA]$^+$	$C_{36}H_{56}O_9$	632.80
47	Ciwujianoside D2	11.33	571.1937[M-Rha-GlcAc-Glc-H]$^-$	1129.5637 [M+HCOO]$^-$	$C_{54}H_{84}O_{22}$	1084.55

(Continued on following page)

TABLE 1 | (*Continued*) Characterization of compounds in phenolic and saponin fractions by UPLC-MS/MS.

No.	Identification	t_R (min)	Characteristic fragment ions	m/z	Formula	Neutral mass
48	3-*O*-*β*-D-Glucopyranoside-29-hydroxy oleanolic acid	11.57	603.3969[M-CO_2-H]$^-$,571.1937[M-CO_2-CH_2OH-H]$^-$	649.4061[M-H]$^-$	$C_{45}H_{78}O_2$	650.34
49	Eleutheroside K	11.59	649.4061[M-ORha+HCOO]$^-$,603.3969[M-Rha+H_2O-2H]$^-$,571.1937[M-ORha-H]$^-$	733.3565 [M-H]$^-$	$C_{41}H_{66}O_{11}$	734.45
50	Acanthopanaxoside E	11.68	603.3969[M-Glc-CO_2-H]$^-$,587.4081[M-OGlc-CO_2-H]$^-$	809.4473[M-H]$^-$	$C_{42}H_{66}O_{15}$	810.56
51	Ciwujianoside D1	11.82	603.3969[M-Rha-GlcAc-Glc+H_2O-2H]$^-$,571.1937 [M-Rha-GlcAc-OGlc-H]$^-$	1145.5898 [M+HCOO]$^-$	$C_{55}H_{88}O_{22}$	1100.58
52	Eleutheroside I	13.65	733.4275[M-H]$^-$,571.3712[M-ORha-H]$^-$	779.4380 [M+HCOO]$^-$	$C_{41}H_{66}O_{11}$	734.45
53	*β*-Sitosterol	14.30	346.3379[M-C_5H_{10}+2H]$^+$,302.3113[M-C_8H_{16}]$^+$,113.9657[M-$C_{21}H_{32}O$+H]$^+$	437.2013 [M+NA]$^+$	$C_{29}H_{50}O$	414.71
54	Ciwujianoside E	14.54	717.4304[M-H]$^-$,571.3712[M-Rha-H]$^-$	763.4387 [M+HCOO]$^-$	$C_{40}H_{62}O_{11}$	718.91
55	30-Norolean-12,20(29)-dien-28-oic acid-3-*O*-*β*-D-glucopyranosyl-(1→2)-*α*-L-arabinopyranoside	15.89	733.4630[M-H]$^-$,571.3712[M-Glc-H]$^-$	779.4775 [M+HCOO]$^-$	$C_{41}H_{66}O_{11}$	734.45
56	3-*O*-*α*-L-Arabinopyranoside oleanolic acid	16.11	437.1922[M-Ara-H_2O+H]$^+$·396.3492[M-OAra-CO_2+H]$^+$	589.4186 [M+H]$^+$	$C_{35}H_{56}O_7$	588.40
57	Daucosterol	18.04	577.1353[M+H]$^+$,338.3492[M-Glc-C_7H_{14}+H]$^+$,301.1434[M-Glc-C_8H_{16}]$^+$	599.1245 [M+NA]$^+$	$C_{35}H_{60}O_6$	576.85
58	Hederagenin 3-*O*-*β*-D-glucuronopyranoside-6-*O*-methyl ester	21.71	379.3438[M-OGlcAc-CO_2-CH_2OH]$^+$	685.4426 [M+NA]$^+$	$C_{37}H_{58}O_{10}$	662.40

(12.63 mg), and **14** (9.7 mg) obtained from Fr.4. Fr.5, Fr.7, and Fr.8 were purified and recrystallized with MeOH (36%, 40%) to obtain compounds **9** (7.11 mg), **10** (52.69 mg), **15** (23.8 mg), **16** (5.3 mg), and **17** (11.0 mg); compounds **18** (13.35 mg), **19** (10.1 mg), and **20** (7.49 mg); and compounds **22** (3.2 mg) and **23** (5.4 mg). In the same way as above, seven fractions Fr.11–Fr.17 were obtained from the saponin fraction (60.0 g) with TLC identified. The ODS column was applied to elute Fr.15, Fr.16, and Fr.17 with 20%–90% MeOH, further separated and purified by the C18 column, eluted with 70% and 80% MeOH solvent, followed by recrystallization to yield compounds **24** (6.61 mg), **25** (15.0 mg), **26** (11.4 mg), **27** (15.4 mg), **28** (16.7 mg), **29** (9.8 mg), and **30** (12.13 mg). The isolated compounds **1**–**30** were identified by a combination of 1D, 2D-NMR, MS data, and relevant literature.

2.5 Sample and Reference Standards Solutions Preparation

ESL from 29 different places was pulverized into powder (40 mesh). The powder (1.0 g) was accurately weighed and suspended in 20 ml MeOH and ultrasonically extracted for 30 min (40 kHz, 500 W, two times). The combined filtrate was evaporated to dryness using a rotary evaporator at 40°C. The residue was dissolved in 5 ml of MeOH. The 10 quantitative reference compounds were dissolved in MeOH and stored at 4°C until analysis. A series of mixed solutions were obtained by diluting the original solutions of these 10 compounds with MeOH. The solutions were prior filtered through a 0.22 μm syringe filter and then quantitatively analyzed.

2.6 Qualitative UPLC-QTOF-MS/MS Analysis

An ACQUITY UPLC (Waters, Milford, United States) system in tandem with a QTOF Synapt G2-SI mass spectrometer (Waters, Milford, United States) was acquired for qualitative analysis using an ACQUITY UPLC HSS T3 column (1.8 μm, 2.1*100 mm, Waters, Milford, United States). The chromatography separation was carried out at an ambient temperature of 35°C. The gradient of the eluent mobile phase included acetonitrile with 0.1% formic acid (A), and water with 0.1% formic acid (B): 0–1 min, 2% A; 1–3 min, 2%–10% A; 3–5 min, 10%–20% A; 5–9 min, 20%–55% A; 9–13 min, 55%–70% A; 13–19 min, 70%–80% A; 19–22 min, 80%–98% A; 22–22.5 min, 98%–2% A; 22.5–23 min, 2% A. The flow rate was set at 0.3 ml/min, with a 2 μL injection volume. The MS parameters were optimized as follows: scan type: positive and negative, acquire Mse over the range 100–1,300 Da; scan time: 0.25 s, collision energy: 20–35 V, cone voltage: 40 V.

2.7 Quantitation for UPLC-QTRAP-MS/MS Analysis

The quantitation analysis was done *via* an ACQUITY UPLC (Waters Corp., Milford, MA, United States) system tandem 4000 QTRAP mass spectrometer (AB SCIEX, Framingham,

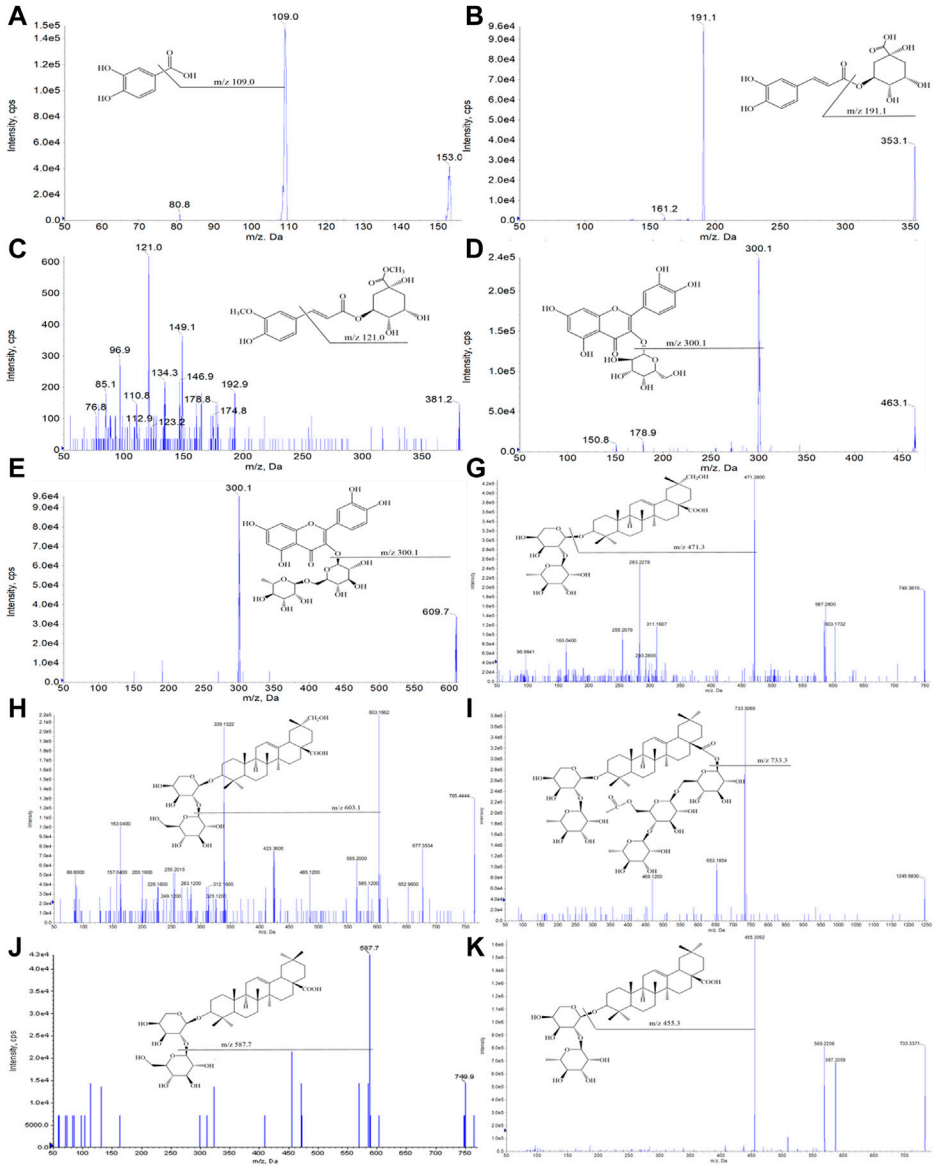

FIGURE 3 | Optimized ion pair diagrams of 10 reference compounds by the 4000 QTRAP mass spectrometry: the process of selecting the best sub-ion (Q3) according to the parent ion (Q1) of the 10 compounds.

United States) with the ACQUITY UPLC HSS T3 column (1.8 μm, 2.1*100 mm, Waters, Milford, United States).

The column temperature was 35°C. The mobile phase was the same as in the qualitative analysis. Isocratic elution was performed as follows: 0–0.5 min, 2%–30% A; 0.5–1 min, 30%–40% A; 1–1.5 min, 40%–55% A; 1.5–3.5 min, 55%–75% A; 3.5–4.5 min, 75%–98% A; 4.5–5.0 min, 98%–98% A. The flow rate was 0.4 ml/min, with 2 μL injection volume. Detection was performed in the negative electrospray ionization mode (ESI^-) in the Multiple reaction monitoring (MRM). The MS parameters were optimized as follows: TEM: 550°C, curtain gas: 10 psi, IonSpray Voltage: −4500 V, and ion source gas 1 and 2: 55 psi.

2.8 α-Glucosidase Inhibition Assay

The α-glucosidase inhibition activity of all extracts was determined as previously described with minor modifications (Zhang et al., 2017). The solutions of 20 μL different fractions and 60 μL phosphate buffer (67 mM, PH 6.8) containing 20 μL intestinal α-glucosidase solution were pre-incubated at 37°C for 5 min. Then, 8 μL PNPG (116 mM) was added to each well. The reaction mixture was incubated at 37°C for 30 min. The absorbance of the mixture was measured at 405 nm before and after incubation. Acarbose was used as the positive control. The inhibitory rate (IR) was calculated as follows:

TABLE 2 | The selective ion-pair, DP, and CE of 10 reference compounds.

No.	Compounds	Q1 [M-H]$^-$	Q3	DP/V	CE/V
A	Protocatechuic acid	153.0	109.0	–80.04	–23.74
B	Chlorogenic acid	353.1	191.1	–80.59	–19.81
C	Methyl 5-*O*-feruloylquinate	381.2	121.0	–107.28	–37.45
D	Hyperoside	463.1	300.1	–144.10	–38.99
E	Rutin	609.7	300.1	–188.87	–55.38
G	3-*O*-α-L-Rhamnopyranosyl-(1→2)-α-L-arabinopyranoside-29-hydroxy oleanolic acid	749.4	471.3	–205.60	–59.14
H	3-*O*-β-D-Glucopyranosyl-(1→2)-α-L-arabinopyranoside-29-hydroxy oleanolic acid	765.4	603.1	–212.51	–58.04
I	Ciwujianoside C4	1,245.6	733.3	–171.82	–79.83
J	Saponin P_E	749.9	587.7	–217.18	–59.35
K	Ciwujianoside K	733.5	455.3	–191.59	–61.10

TABLE 3 | The regression equation, linear range, limits of detection, and limits of quantification of 10 reference compounds.

No.	Compounds	Regression Equations	R^2	Linear ranges (μg/ml)	LOD (μg/ml)	LOQ (μg/ml)
A	Protocatechuic acid	$y = 189.394x + 231726$	0.9995	0.62–9.92	0.12	0.39
B	Chlorogenic acid	$y = 364.782x - 52129$	0.9990	0.72–22.88	0.27	0.89
C	Methyl 5-*O*-feruloylquinate	$y = 0.2943x + 162.22$	0.9997	0.75–24.0	0.21	0.71
D	Hyperoside	$y = 147.357x + 108536$	0.9992	0.97–30.72	0.48	1.61
E	Rutin	$y = 92.062x + 22102$	0.9998	0.68–21.76	0.29	0.97
G	3-*O*-α-L-Rhamnopyranosyl-(1→2)-α-L-arabinopyranoside-29-hydroxy oleanolic acid	$y = 2.1906x + 4,328.5$	0.9994	0.95–30.4	0.79	2.64
H	3-*O*-β-D-Glucopyranosyl-(1→2)-α-*L*-arabinopyranoside-29-hydroxy oleanolic acid	$y = 7.9494x + 11670$	0.9991	0.76–24.8	0.33	1.12
I	Ciwujianoside C4	$y = 19.799x + 2,157.3$	0.9995	1.1–35.2	0.28	0.92
J	Saponin P_E	$y = 1.4033x + 2,833.1$	0.9994	1.0–32.0	0.66	2.17
K	Ciwujianoside K	$y = 26.924x + 2,298.1$	0.9996	1.2–38.4	0.82	2.73

TABLE 4 | The recovery of the 10 reference compounds.

No.	Compounds	Original (ng)	Spiked (ng)	Found (ng)	Recovery (%)	RSD (%, $n = 3$)
A	Protocatechuic acid	233.69	256.00	491.83	100.43	2.15
B	Chlorogenic acid	581.95	534.00	1,111.82	99.63	1.64
C	Methyl 5-*O*-feruloylquinate	420.68	450.00	853.53	98.03	2.38
D	Hyperoside	1,206.00	1,225.55	2,332.34	95.92	2.47
E	Rutin	675.00	680.00	1,371.26	101.20	1.95
G	3-*O*-α-L-Rhamnopyranosyl-(1→2)-α-*L*-arabinopyranoside-29-hydroxy oleanolic acid	1,769.15	1,710.00	3,352.50	96.36	2.57
H	3-*O*-β-D-Glucopyranosyl-(1→2)-α-*L*-arabinopyranoside-29-hydroxy oleanolic acid	841.66	852.50	1,685.86	99.51	2.42
I	Ciwujianoside C4	694.85	715.00	1,424.51	101.04	3.72
J	Saponin P_E	1,285.40	1,250.00	2,468.97	97.38	2.84
K	Ciwujianoside K	1,670.57	1,650.00	3,330.87	100.31	1.87

TABLE 5 | The amounts of 10 reference compounds in ESL from different sources.

No.	Sources	Content (mg/g)									
		A	B	C	D	E	G	H	I	J	K
S1	Xiaoxing'anling	0.43 ± 0.007	0.71 ± 0.012	15.41 ± 0.173	1.47 ± 0.045	0.25 ± 0.006	16.20 ± 0.131	11.86 ± 0.324	0.91 ± 0.037	14.71 ± 0.094	30.60 ± 0.147
S2	Wangqing	0.39 ± 0.001	4.94 ± 0.071	10.90 ± 0.225	9.74 ± 0.044	2.78 ± 0.030	1.76 ± 0.020	1.11 ± 0.033	36.73 ± 0.582	1.74 ± 0.005	4.22 ± 0.056
S3	Huadian	0.39 ± 0.003	6.46 ± 0.253	14.00 ± 0.143	15.74 ± 0.253	3.53 ± 0.054	1.81 ± 0.032	1.07 ± 0.047	7.50 ± 0.018	1.33 ± 0.010	1.74 ± 0.038
S4	Huinan	0.61 ± 0.007	6.98 ± 0.036	5.76 ± 0.062	14.55 ± 0.117	3.79 ± 0.022	0.78 ± 0.002	1.22 ± 0.012	21.38 ± 0.360	2.32 ± 0.088	4.37 ± 0.109
S5	Huichun	0.76 ± 0.020	9.17 ± 0.192	8.40 ± 0.034	22.05 ± 0.308	3.53 ± 0.077	2.42 ± 0.055	0.48 ± 0.002	16.89 ± 0.205	3.68 ± 0.063	3.35 ± 0.088
S6	Harbin	0.63 ± 0.001	5.91 ± 0.050	15.39 ± 0.211	11.31 ± 0.135	2.44 ± 0.009	1.04 ± 0.023	0.65 ± 0.004	4.20 ± 0.037	2.25 ± 0.124	0.80 ± 0.026
S7	Linjiang	0.53 ± 0.015	6.11 ± 0.202	9.56 ± 0.042	10.66 ± 0.205	0.87 ± 0.002	1.46 ± 0.056	0.46 ± 0.013	7.84 ± 0.119	4.34 ± 0.099	1.60 ± 0.032
S8	Erdaobaihe	0.33 ± 0.001	5.25 ± 0.137	8.82 ± 0.020	10.54 ± 0.074	2.25 ± 0.028	0.60 ± 0.024	0.51 ± 0.010	6.39 ± 0.143	1.33 ± 0.026	0.42 ± 0.017
S9	Fenglin	1.19 ± 0.016	6.46 ± 0.106	3.30 ± 0.041	13.72 ± 0.012	1.64 ± 0.042	2.90 ± 0.077	1.33 ± 0.009	9.20 ± 0.311	2.09 ± 0.055	6.32 ± 0.097
S10	Baoqing	0.88 ± 0.005	6.32 ± 0.083	10.51 ± 0.067	15.22 ± 0.063	2.59 ± 0.111	1.75 ± 0.031	1.45 ± 0.033	9.04 ± 0.205	2.06 ± 0.077	4.19 ± 0.051
S11	Dunhua	0.73 ± 0.004	11.06 ± 0.108	2.55 ± 0.012	21.98 ± 0.197	3.44 ± 0.007	1.04 ± 0.013	0.41 ± 0.006	10.65 ± 0.248	1.17 ± 0.024	2.06 ± 0.018
S12	Anguo	0.95 ± 0.011	19.33 ± 0.392	9.97 ± 0.034	30.49 ± 0.439	4.94 ± 0.084	0.89 ± 0.037	0.56 ± 0.001	20.70 ± 0.414	1.66 ± 0.032	2.22 ± 0.037
S13	Shenyang	0.85 ± 0.006	13.74 ± 0.123	3.05 ± 0.015	15.53 ± 0.072	2.77 ± 0.021	1.26 ± 0.063	0.58 ± 0.013	6.83 ± 0.189	3.70 ± 0.113	0.55 ± 0.004
S14	Jingyu	0.60 ± 0.003	10.14 ± 0.272	10.69 ± 0.076	16.46 ± 0.098	2.67 ± 0.047	1.56 ± 0.019	0.46 ± 0.008	9.33 ± 0.083	0.89 ± 0.008	0.88 ± 0.003
S15	Antu	0.56 ± 0.014	6.89 ± 0.013	11.92 ± 0.162	12.92 ± 0.055	2.29 ± 0.016	0.68 ± 0.022	0.50 ± 0.016	9.40 ± 0.232	4.25 ± 0.022	1.08 ± 0.016
S16	Jiaohe	0.53 ± 0.010	6.87 ± 0.045	6.58 ± 0.043	21.28 ± 0.443	2.17 ± 0.031	1.28 ± 0.046	1.19 ± 0.003	8.51 ± 0.242	2.49 ± 0.008	1.68 ± 0.073
S17	Yanbian	0.74 ± 0.007	10.53 ± 0.101	7.60 ± 0.087	23.16 ± 0.615	3.36 ± 0.050	0.96 ± 0.039	1.52 ± 0.070	15.79 ± 0.477	6.96 ± 0.103	1.42 ± 0.066
S18	Ningan	0.74 ± 0.025	12.42 ± 0.135	5.36 ± 0.094	17.28 ± 0.250	3.59 ± 0.113	0.96 ± 0.053	0.92 ± 0.034	12.60 ± 0.233	2.80 ± 0.011	0.49 ± 0.035
S19	Huanren	0.85 ± 0.037	18.49 ± 0.374	2.89 ± 0.006	36.56 ± 0.467	11.11 ± 0.214	0.79 ± 0.022	0.31 ± 0.002	8.91 ± 0.201	1.33 ± 0.057	0.88 ± 0.072
S20	Hulin	0.54 ± 0.024	7.42 ± 0.044	9.12 ± 0.055	11.25 ± 0.015	1.92 ± 0.061	1.38 ± 0.056	0.48 ± 0.014	16.85 ± 0.003	9.09 ± 0.225	4.03 ± 0.106
S21	Chibei	0.80 ± 0.013	11.56 ± 0.067	3.20 ± 0.004	21.82 ± 0.327	3.73 ± 0.133	0.46 ± 0.018	0.52 ± 0.006	11.14 ± 0.381	1.95 ± 0.014	2.48 ± 0.054
S22	Tieli	0.70 ± 0.014	9.97 ± 0.110	4.35 ± 0.013	17.05 ± 0.088	3.27 ± 0.062	0.83 ± 0.030	1.22 ± 0.023	26.79 ± 0.694	1.60 ± 0.058	2.06 ± 0.003
S23	Fusong	8.41 ± 0.062	0.78 ± 0.005	2.89 ± 0.045	0.63 ± 0.004	0.10 ± 0.002	1.60 ± 0.043	0.93 ± 0.048	0.27 ± 0.002	2.22 ± 0.079	6.42 ± 0.039
S24	Dongning	0.88 ± 0.007	16.57 ± 0.201	5.38 ± 0.077	22.33 ± 0.171	5.99 ± 0.035	1.29 ± 0.085	1.26 ± 0.049	17.14 ± 0.401	2.92 ± 0.061	2.33 ± 0.044
S25	Raohe	1.11 ± 0.023	4.68 ± 0.093	3.18 ± 0.009	20.40 ± 0.389	8.48 ± 0.283	1.44 ± 0.069	1.00 ± 0.040	11.24 ± 0.239	3.80 ± 0.104	2.58 ± 0.112
S26	Tonghua	1.19 ± 0.034	11.70 ± 0.084	1.37 ± 0.003	20.15 ± 0.143	7.02 ± 0.075	1.28 ± 0.034	0.57 ± 0.012	15.37 ± 0.143	1.56 ± 0.040	2.04 ± 0.047
S27	Yanji	0.93 ± 0.010	7.99 ± 0.222	8.09 ± 0.041	12.47 ± 0.066	3.57 ± 0.016	0.67 ± 0.008	0.49 ± 0.005	8.38 ± 0.093	6.50 ± 0.137	0.49 ± 0.001
S28	Shihezi	0.57 ± 0.001	7.44 ± 0.099	5.87 ± 0.010	12.33 ± 0.132	1.43 ± 0.009	0.98 ± 0.011	1.13 ± 0.017	13.56 ± 0.670	5.41 ± 0.072	1.37 ± 0.046
S29	Bozhou	1.77 ± 0.043	5.67 ± 0.087	3.08 ± 0.075	18.76 ± 0.439	2.24 ± 0.017	2.07 ± 0.038	2.23 ± 0.035	9.59 ± 0.377	4.95 ± 0.091	2.49 ± 0.086

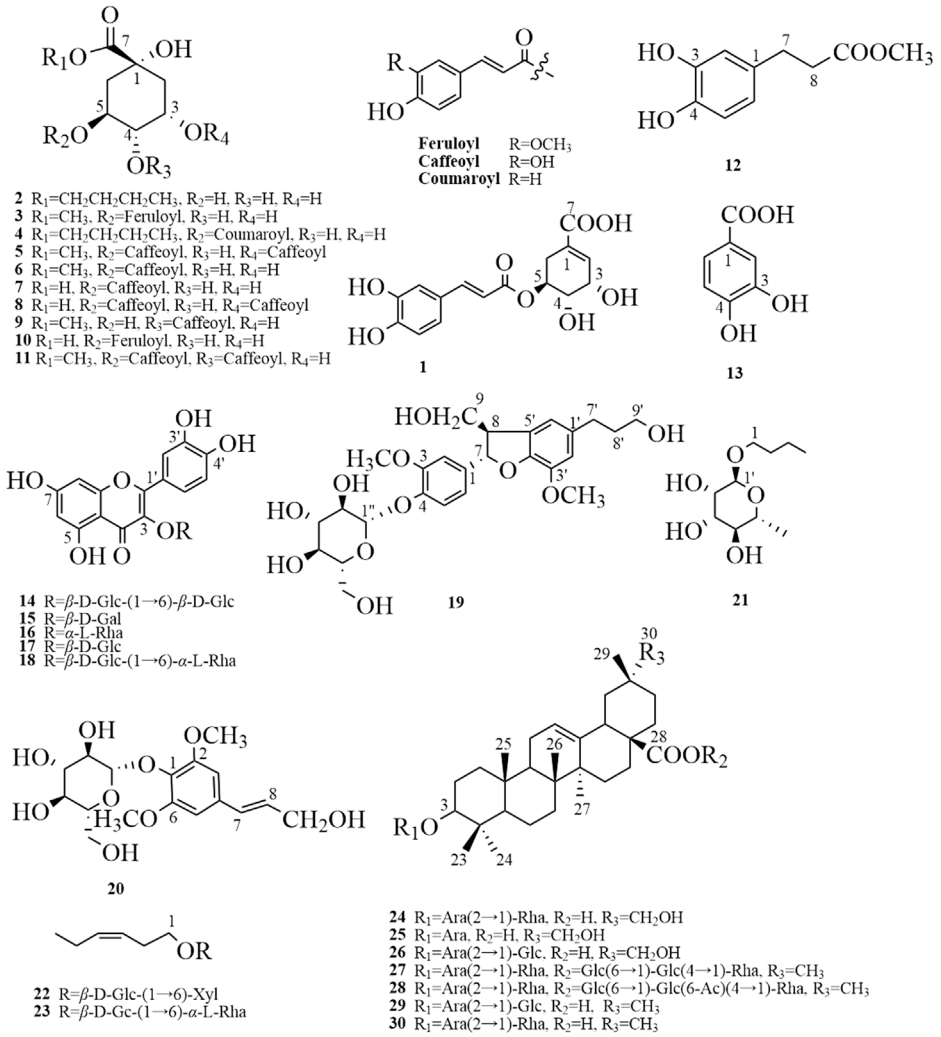

FIGURE 4 | The chemical structures of 30 compounds were isolated and identified from phenolic and saponin fractions. 5-*O*-Caffeoylshikimic acid (**1**), quinic acid butyl ester (**2**), methyl 5-*O*-feruloylquinate (**3**), 5-*O*-*p*-coumaroylquinic acid butyl ester (**4**), methyl 3,5-di-*O*-caffeoyl quinate (**5**), methyl chlorogenate (**6**), chlorogenic acid (**7**), 3,5-di-*O*-caffeoylquinic acid (**8**), 4-*O*-caffeoylquinic acid methyl ester (**9**), 5-*O*-feruloylquinic acid (**10**), methyl 3,4-di-*O*-caffeoyl quinate (**11**), 3,4-dihydroxybenzenepropionic acid methyl ester (**12**), protocatechuic acid (**13**), quercetin 3-*O*-*β*-D-glucopyranosyl-(1→6)-*β*-D-glucopyranoside (**14**), hyperoside (**15**), quercitrin (**16**), quercetin 3-*O*-*β*-D-glucopyranoside (**17**), rutin (**18**), (7S, 8R)-urolignoside (**19**), syringin (**20**), n-butyl-1-*O*-*α*-L-rhamnopyranoside (**21**), (*Z*)-Hex-3-en-1-ol *O*-*β*-D-xylopyranosyl-(1″-6′)-*β*-D-glucopyranoside (**22**), hexenyl-rutinoside (**23**), 3-*O*-*β*-L-rhamnopyranosyl-(1→2)-*α*-L-arabinopyranoside-29-hydroxy oleanolic acid (**24**), 3-*O*-*α*-arabinopyranoside 29-hydroxy oleanolic acid (**25**), 3-*O*-*α*-D-glucopyranosyl-(1→2)-*α*-L-arabinopyranoside-29-hydroxy oleanolic acid (**26**), hederasaponin B (**27**), ciwujianoside C4 (**28**), saponin P_E (**29**), and ciwujianoside K **(30)**.

$$IR(\%) = \left[\left(A_{405} \text{ of control} - A_{405} \text{ of samples}\right) \times / \left(A_{405} \text{ of control}\right)\right] \times 100$$

3 RESULTS AND DISCUSSION

3.1 Optimization of the Chromatographic Conditions

In the qualitative and quantitative analysis of ESL, desirable chromatographic separation was yielded by optimizing the column types [Waters ACQUITY UPLC HSS T3 column (1.8 μm, 2.1*100 mm)], the gradient elution procedure, the flow rate (0.3 ml/min and 0.4 ml/min, respectively), and the temperature (35°C). The mobile phase consisting of A (0.1% formic acid aqueous solution) and B (0.1% formic acid acetonitrile solution) was employed to perform gradient elution. All MS spectrometry parameters were optimized to achieve high sensitivity of phenols and saponins. Under the optimized parameters and conditions, 58 compounds were quickly identified (**Figure 2**). Their characteristic cleavage fragments were shown in **Table 1**. The optimized parameters, including declustering potential (DP), collision energy (CE) and ion pairs (**Figure 3**) of the standard compounds in the quantitative analysis were listed in **Table 2**.

3.2 Isolation of Compounds

3.2.1 Isolation of Chemical Constituents

Thirty compounds (chemical structures shown in **Figure 4**) include 20 phenols, 7 saponins, and 3 glycosides, of which 12 compounds (**1–4**, **9**, **10**, **12**, **14**, **19**, **21–23**) were isolated from *Eleutherococcus* Maxim. for the first time using a combination of chromatographic methods. The compounds were identified based on extensive NMR and MS data and comparison to published literature data when available.

3.2.2 Identification of Chemical Constituents

The isolated compounds **1–30** (chemical structures shown in **Figure 4**) were identified by a combination of 1D, 2D-NMR, and MS data. Compounds **1–4**, **9**, **10**, **12**, **14**, **19**, and **21–23** were obtained from *Eleutherococcus* Maxim. for the first time, and their NMR data were provided here.

3.2.2.1 5-O-Caffeoylshikimic Acid (1)

Yellow amorphous powder: (−) HR-ESI-MS, m/z 335.0748 $[M-H]^-$, calculated for molecular formula $C_{16}H_{16}O_8$. ^{1}H NMR (600 MHz, CD_3OD): δ 7.56 (1H, d, *J* = 15.9 Hz,H-7′), 7.04 (1H, d, *J* = 2.1 Hz, H-2′), 6.95 (1H, dd, *J* = 8.2, 2.1 Hz, H-6′), 6.86 (1H, brs, H-2), 6.78 (1H, d, *J* = 8.2 Hz, H-5′), 6.28 (1H, d, *J* = 15.9 Hz, H-8′), 5.25 (1H m, H-5), 4.41(1H, brs, H-3), 2.86 (1H, dd, *J* = 18.4, 5.2 Hz, H-6*α*), 2.32 (1H, dd, J = 18.4, 5.5 Hz, H-6*β*). ^{13}C-NMR (150 MHz, CD_3OD): δ 130.3 (C-1), 139.0 (C-2), 67.3 (C-3), 70.0 (C-4), 71.4 (C-5), 29.2 (C-6), 169.7 (C-7), 127.7 (C-1′), 115.2 (C-2′), 146.8 (C-3′), 147.3 (C-4′), 116.5 (C-5′), 123.1 (C-6′), 149.7 (C-7′), 115.1 (C-8′), 168.7 (C-9′). The NMR data were consistent with the literature (Wan et al., 2012).

3.2.2.2 Quinic Acid Butyl Ester (2)

Yellowish amorphous powder: (+) HR-ESI-MS, m/z 248.9876 $[M]^+$, calculated for molecular formula $C_{11}H_{20}O_6$. ^{1}H NMR (600 MHz, CD_3OD): δ 2.08 (2H, m, H-2), 4.09 (1H, m, H-3), 3.40(1H, dd, *J* = 8.8, 3.2 Hz, H-4), 3.99 (1H, m, H-5), 1.85(2H, m, H-6), 4.15 (2H, m, H-8), 1.65(2H, m, H-9), 1.41(2H, m, H-10), 0.96 (3H, t, *J* = 7.4 Hz, H-11). ^{13}C-NMR (150 MHz, CD_3OD): δ 76.9 (C-1), 38.3 (C-2), 71.6 (C-3), 76.8 (C-4), 68.1 (C-5), 42.2 (C-6), 175.6 (C-7), 66.3 (C-8), 31.7 (C-9), 20.1 (C-10), 14.0 (C-11). The NMR data were consistent with the literature (Shi et al., 2014).

3.2.2.3 Methyl 5-O-Feruloylquinate (3)

Yellow amorphous powder: (−) HR-ESI-MS, m/z 381.2299 $[M-H]^-$, calculated for molecular formula $C_{18}H_{22}O_9$. ^{1}H NMR (600 MHz, CD_3OD): *δ* 2.02,2.12 (each 1H, m, H-2*α*,*β*), 4.14(1H, m, H-3), 3.41(1H, dd, *J* = 8.6,3.2 Hz, H-4), 5.28(1H, m, H-5), 2.09,2.19(each 1H, m, H-6*α*, *β*), 4.03 (3H, s, 7-OCH_3), 7.04(1H, d, *J* = 2.1 Hz, H-2′), 3.69(3H, s, 3′-OCH_3), 6.78 (1H, d, *J* = 8.1 Hz, H-5′), 6.95 (1H, dd, *J* = 8.2, 2.1 Hz, H-6′), 6.22 (1H, d, *J* = 15.9 Hz, H-7′), 7.53(1H, d, *J* = 15.9 Hz, H-8′). ^{13}C-NMR (150 MHz, CD_3OD): δ 68.2 (C-1), 38.3 (C-2), 76.8 (C-3), 76.6 (C-4), 72.1 (C-5), 38.1 (C-6), 176.0 (C-7), 58.4 (7-OCH3), 123.0 (C-1′), 116.6 (C-2′), 147.2 (C-3′), 52.4 (3′-OCH_3), 146.9 (C-4′), 115.1 (C-5′), 127.7 (C-6′), 149.7 (C-7′), 112.8 (C-8′), 168.3 (C-9′). The NMR data were consistent with the literature (Ida et al., 1993).

3.2.2.4 5-O-p-Coumaroylquinic Acid Butyl Ester (4)

Light brown amorphous powder: (+) HR-ESI-MS, m/z 789.6702 $[2M+H]^+$, calculated for molecular formula $C_{20}H_{26}O_8$. ^{1}H NMR (600 MHz, CD_3OD): δ 2.20(2H, m, H-2*α*, *β*), 5.28(1H, m, H-3), 3.73(1H, dd, *J* = 7.5, 3.2 Hz, H-4),4.15(1H, m, H-5), 2.01 (1H, dd, *J* = 13.3, 6.5 Hz, H-6*α*), 2.20 (1H, dd, *J* = 13.7, 3.3 Hz, H-6*β*), 7.46(1H, d, *J* = 8.6 Hz, H-2′), 6.81(1H, d, *J* = 8.6 Hz, H-3′), 6.81 (1H, d, *J* = 8.6 Hz, H-5′), 7.46(1H, d, *J* = 8.6 Hz, H-6′), 7.60 (1H, d, *J* = 16.0 Hz, H-7′), 6.29(1H, d, *J* = 15.9 Hz, H-8′), 4.12(2H, m, H-1″), 1.64(2H, m, H-2″), 1.41(2H, m, H-3″), 0.95(3H,t,*J* = 7.4 Hz, H-4″). ^{13}C-NMR (150 MHz, CD_3OD): δ 75.9 (C-1), 35.8 (C-2), 72.2 (C-3), 72.7 (C-4), 70.4 (C-5), 38.1 (C-6), 175.5 (C-7), 127.1 (C-1′), 131.2 (C-2′), 115.9 (C-3′), 161.4 (C-4′), 115.9 (C-5′), 131.2 (C-6′), 145.8 (C-7′), 115.2 (C-8′), 168.3 (C-9′), 66.1 (C-1″), 31.7 (C-2″), 20.1 (C-3″), 14.0 (C-4″). The NMR data were consistent with the literature (Osawa et al., 2001).

3.2.2.5 4-O-Caffeoylquinic Acid Methyl Ester (9)

White amorphous powder: (+) HR-ESI-MS, m/z 391.1035 $[M+Na]^+$, calculated for molecular formula $C_{17}H_{20}O_9$. ^{1}H NMR (600 MHz, CD_3OD): *δ* 2.07, 2.20 (each 1H, m, H-2*α*, *β*), 4.29 (1H, m, H-3), 4.82 (1H, m, H-4), 4.25 (1H, m, H-5), 2.03, 2.19 (each 1H, H-6*α*, *β*), 7.63 (1H,d, *J* = 15.9 Hz, H-7), 7.07 (1H, d, *J* = 2.1 Hz, H-2′), 6.78 (1H, d, *J* = 8.2 Hz, H-5′), 6.97 (1H, dd, *J* = 8.3, 2.1 Hz, H-6′), 7.63 (1H, d, *J* = 15.9 Hz, H-7′), 6.36 (1H, d, *J* = 15.9 Hz, H-8′), 3.75 (3H, s, 7-OCH_3). ^{13}C-NMR (150 MHz, CD_3OD): δ 76.5 (C-1), 42.2 (C-2), 69.1 (C-3), 78.6 (C-4), 65.7 (C-5), 38.5 (C-6), 175.7 (C-7), 53.0 (7-OCH3), 127.9 (C-1′), 115.2 (C-2′), 146.9 (C-3′), 149.6 (C-4′), 116.5 (C-5′), 123.0 (C-6′), 147.2 (C-7′), 115.4 (C-8′), 169.0 (C-9′). The NMR data were consistent with the literature (Chen et al., 2016).

3.2.2.6 5-O-Feruloylquinic Acid (10)

White amorphous powder: (+) HR-ESI-MS, m/z 391.1035 $[M+Na]^+$, calculated for molecular formula $C_{17}H_{20}O_9$. ^{1}H NMR (600 MHz, CD_3OD): δ 2.12 (4H, m, H-2, 6), 4.14 (1H, m, H-3), 3.73 (1H, dd, *J* = 7.5, 3.1 Hz, H-4), 5.28 (1H, m, H-5), 7.04 (1H, d, *J* = 2.1 Hz, H-2′), 6.78 (1H, d, *J* = 8.1 Hz, H-5′), 6.95 (1H, dd, *J* = 8.2, 2.1 Hz, H-6′), 7.53 (1H, d, *J* = 15.9 Hz, H-7′), 6.22 (1H, d, *J* = 15.9 Hz, H-8′), 3.69 (3H, s, 3′-OCH_3). ^{13}C-NMR (150 MHz, CD_3OD): δ 75.8 (C-1), 38.0 (C-2), 72.1 (C-3), 70.3 (C-4), 72.6 (C-5), 37.8 (C-6), 175.5 (C-7), 53.0 (7-OCH3), 127.7 (C-1′), 115.2 (C-2′), 149.7 (C-3′), 146.9 (C-4′), 116.6 (C-5′), 123.0 (C-6′), 147.2 (C-7′), 115.1 (C-8′), 168.3 (C-9′). The NMR data were consistent with the literature (Menozzi-Smarrito et al., 2011).

3.2.2.7 3,4-Dihydroxybenzenepropionic Acid Methyl Ester (12)

Yellow oily matter: (−) HR-ESI-MS, m/z 195.0631 $[M-H]^-$, calculated for molecular formula $C_{10}H_{12}O_4$. ^{1}H NMR (600 MHz, CD_3OD): δ 6.62 (1H, d, *J* = 2.1 Hz, H-2), 6.66 (1H, d, *J* = 8.0 Hz, H-5), 6.50 (1H, dd, *J* = 8.0, 2.1 Hz, H-6), 2.55 (2H, t, *J* = 7.6 Hz, H-7), 2.76 (2H, t, *J* = 7.6 Hz, H-8), 3.63 (3H, s, 9-OCH_3). ^{13}C-NMR (150 MHz, CD_3OD): δ 133.5 (C-1), 116.4 (C-

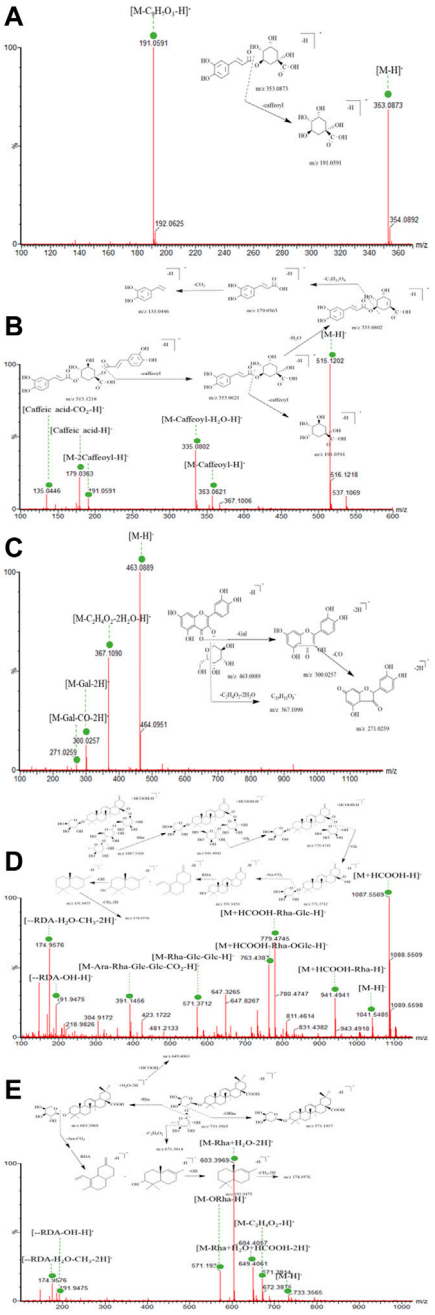

FIGURE 5 | UPLC-QTOF-MS/MS spectra and the cleavage pathways of chlorogenic acid **(A)**, 1,3-dicaffeoylquinic acid **(B)**, hyperoside **(C)**, ciwujianoside C1 **(D),** and eleutheroside K **(E)**.

2), 144.7 (C-3), 146.2 (C-4), 116.4 (C-5), 120.5 (C-6), 31.4 (C-7), 37.1 (C-8), 175.4 (C-9), 52.0 (9-OCH_3). The NMR data were consistent with the literature (Meng et al., 2014).

3.2.2.8 Quercetin 3-O-β-D-Glucopyranosyl-(1→6)-β-D-glucopyranoside (14)

White amorphous powder: (+) HR-ESI-MS, m/z 627.5396 $[M+H]^+$, calculated for molecular formula $C_{27}H_{30}O_{17}$.^{1}H NMR (600 MHz, CD_3OD): δ 6.21 (1H, d, *J* = 2.1 Hz, H-6), 6.40 (1H, d, *J* = 2.1 Hz, H-8), 7.84 (1H, d, *J* = 2.2 Hz, H-2′), 6.87 (1H, d, *J* = 8.5 Hz, H-5′), 7.59 (1H, dd, *J* = 8.5, 2.2 Hz, H-6′), 5.25 (1H, d, *J* = 7.7 Hz, H-1″), 5.17 (1H, d, *J* = 7.8 Hz, H-1‴). ^{13}C-NMR (150 MHz, CD_3OD): δ 158.5 (C-2), 135.8 (C-3), 179.6 (C-4), 163.1 (C-5), 99.9 (C-6), 166.1 (C-7), 94.7 (C-8), 158.8(C-9), 105.6 (C-10),123.0 (C-1′), 117.8 (C-2′), 145.8 (C-3′), 150.0 (C-4′), 116.1 (C-5′), 123.2 (C-6′), 105.4 (C-1″), 75.8 (C-2″), 78.4 (C-3″), 73.2 (C-4″), 77.2 (C-5″), 70.1 (C-6″), 104.3 (C-1‴), 75.1 (C-2‴), 77.2 (C-3‴), 71.3 (C-4‴), 78.2 (C-5‴), 62.0 (C-6‴). The NMR data were consistent with the literature (Zeng et al., 2020).

3.2.2.9 (7S, 8R)-Urolignoside (19)

White amorphous powder: (+) HR-ESI-MS, m/z 545.1989 $[M+Na]^+$, calculated for molecular formula $C_{26}H_{34}O_{11}$. ^{1}H NMR (600 MHz, CD_3OD): δ 7.03 (1H, d, *J* = 1.4 Hz, H-2), 3.86 (3H, s, 3- OCH_3), 7.14 (1H, d, *J* = 8.4 Hz, H-5), 6.93 (1H, dd, *J* = 8.4, 2.0 Hz, H-6), 5.56 (1H, d, *J* = 5.9 Hz, H-7), 3.45 (1H, m, H-8), 3.68, 3.76 (each 1H, H-9α, β), 6.72 (1H, brs, H-2′), 3.83 (3H, s, 3′-OCH_3), 6.74 (1H, brs, H-6′), 2.63 (2H, *t*, *J* = 7.5 Hz, H-7′), 1.82 (2H, m, H-8′), 3.57 (2H, *t*, *J* = 6.5 Hz, H-9′), 4.89 (1H, d, *J* = 7.4 Hz, H-1″). ^{13}C-NMR (150 MHz, CD_3OD): δ 138.4(C-1), 111.2 (C-2), 151.0 (C-3), 56.8 (3-OCH_3), 147.1 (C-4), 116.2 (C-5), 119.4 (C-6), 88.5 (C-7), 55.7 (C-8), 65.1 (C-9), 137.1 (C-1′), 114.2 (C-2′), 143.5 (C-3′), 56.7(3′-OCH_3), 145.3 (C-4′), 129.6 (C-5′), 118.0 (C-6′), 32.9 (C-7′), 35.8 (C-8′), 62.3 (C-9′), 102.8 (C-1″), 74.9 (C-2″), 77.9 (C-3″), 71.4 (C-4″), 78.2 (C-5″), 62.5 (C-6″). The NMR data were consistent with the literature (Zhao et al., 2018).

3.2.2.10 N-Butyl-1-O-α-L-Rhamnopyranoside (21)

Colorless oily matter: (−) HR-ESI-MS, m/z 255.8209$[M+2H_2O-H]^-$, calculated for molecular formula $C_{10}H_{20}O_5$. 1H, m, NMR (600 MHz, CD_3OD): δ 4.65 (1H, brs, H-1), 3.77 (1H, dd, *J* = 3.4 Hz, H-2), 3.63 (1H, dd, *J* = 1.7 Hz, H-3), 3.31 (H-4), 3.57 (1H, m, H-5), 1.26 (3H, d, *J* = 6.3 Hz, H-6) 3.39, 3.67 (each 1H, m, H-1′), 1.57 (2H, m, H-2′), 1.41 (2H, m, H-3′), 0.94 (3H, t, *J* = 7.4 Hz, H-4′). ^{13}C-NMR (150 MHz, CD_3OD): δ 101.7 (C-1), 72.5 (C-2), 74.0 (C-3), 72.4 (C-4), 69.8 (C-5), 18.0 (C-6), 68.3 (C-1′), 32.8 (C-2′), 20.5 (C-3′), 14.2 (C-4′). The NMR data were consistent with the literature (Mallavadhani and Narasimhan, 2009).

3.2.2.11 (Z)-Hex-3-en-1-ol O-β-D-Xylopyranosyl-(1″-6′)-β-D-Glucopyranoside (22)

White amorphous powder; (+) HR-ESI-MS, m/z 417.1705 $[M+Na]^+$, calculated for molecular formula $C_{17}H_{30}O_{10}$.^{1}H NMR (600 MHz, CD_3OD): δ 3.55,3.83 (each 1H, m, H-1), 2.38 (2H, q, *J* = 7.2 Hz, H-2), 5.39 (1H, dtt, *J* = 10.8, 5.1, 1.4 Hz, H-3), 5.45 (1H, dtt, *J* = 12.1, 6.9, 1.4 Hz, H-4), 2.08 (2H, qd, *J* = 7.4, 1.4 Hz, H-5), 0.97 (3H, t, *J* = 7.6 Hz, H-6) 4.32 (1H, d, *J* = 7.5 Hz, H-1′), 4.08 (1H, dd, *J* = 11.5, 2.1 Hz, H-6′α), 3.74 (1H, dd, *J* = 11.5, 5.6 Hz, H-6′β), 4.27 (1H, d, *J* = 7.8 Hz, H-1″). ^{13}C-NMR (150 MHz, CD_3OD): δ 70.7 (C-1), 28.8 (C-2), 125.9 (C-3), 134.5 (C-4), 21.6 (C-5), 14.7 (C-6), 104.4 (C-1′), 74.9 (C-2′), 78.0 (C-3′), 71.2 (C-4′), 77.7 (C-5′), 69.8 (C-6′), 105.5 (C-1″), 75.1 (C-2″), 77.0 (C-3″), 71.5 (C-4″), 67.0 (C-5″). The NMR data were consistent with the literature (Iha et al., 2012).

3.2.2.12 Hexenyl-Rutinoside (23)

White amorphous powder: (+) HR-ESI-MS, m/z 408.3348 $[M]^+$, calculated for molecular formula $C_{18}H_{32}O_{10}$. ^{1}H NMR (600 MHz, CD_3OD): δ 3.54,3.83 (each 1H, m, H-1), 2.39 (2H, m, H-2), 5.39 (1H, m, H-3), 5.46 (1H, m, H-4), 2.08 (2H, m, H-5), 0.97 (3H, t, J = 7.8 Hz, H-6) 4.25 (1H, d, J = 7.5 Hz, H-1′), 4.74 (1H, d, J = 1.7 Hz, H-1″), 1.26 (3H, d, J = 6.2 Hz, H-6″). ^{13}C-NMR (150 MHz, CD_3OD): δ 70.6 (C-1), 28.9 (C-2), 125.9 (C-3), 134.6 (C-4), 21.6 (C-5), 14.7 (C-6), 104.5 (C-1′), 75.1 (C-2′), 78.1 (C-3′), 71.7 (C-4′), 76.9 (C-5′), 68.1 (C-6′), 102.3 (C-1″), 72.6 (C-2″), 73.6 (C-3″), 74.1 (C-4″), 69.8 (C-5″), 18.1 (C-6″). The NMR data were consistent with the literature (Kil et al., 2019).

3.3 Identity Assignment and Confirmation of the Phenolic Compounds and Saponins in ESL

In the present study, the phenolic and saponin fractions of ESL extracted in Method 2.3 were used as the representative sample for qualitative analysis because of its most comprehensive phenolic and saponins profile. According to the accurate fragmentation law of fragment ions and the literature, 58 compounds (**Figure 2**; **Table 1**), including 30 phenols and 28 saponins, were identified. All compounds were divided into three categories: phenolic acids, flavonoids, and saponins.

3.3.1 Phenolic Compounds

To date, phenols in ESL have not been systematically characterized through UPLC-MS/MS. As shown in **Table 1**, 30 phenolic compounds were identified, mainly divided into phenolic acids and flavonoids based on their structural characteristics. Among them, most of these phenolic acids were composed of one or two caffeic acids and one quinic acid or their derivatives by dehydration condensation, such as compounds **1–8**, **11**, **17**, **18**, **22–26**, and **28**. Generally, due to the readily dissociated ester bond, these phenolic acids were inclined to lose quinic acid moieties (156 Da), caffeoyl (162 Da), feruloyl (176 Da), or coumaroyl moieties (146 Da) in the MS spectra as one characteristic of them. Moreover, the further CO_2 (44 Da) and OCH_3/CH_3 (31/15 Da) loss were other characteristic fragmentation behavior of compounds **2–8**, **11**, **17**, **22–26**, and **28** because of the oxygen methyl or carboxyl group in their structures (Ren et al., 2020). For example, the 191 Da, 192 Da, 113 Da, 179 Da, 353 Da, and 367 Da fragment ions in compounds **1–5**, **7**, **8**, **17**, **18**, **24**, and **28** were caused by the loss of caffeoyl, feruloyl, coumaroyl, and/or quinic acid ion. Fragment 135 Da, 338 Da, 179 Da, 299 Da, 149 Da, 163 Da, and 103 Da in compounds **3–4**, **8**, **26**, **23**, and **7** were typically obtained by direct loss of CO_2 or OCH_3/CH_3 fragment ions. Chlorogenic acid (**1**, **Figure 5A**) and 1,3-dicaffeoylquinic acid (**4**, **Figure 5B**) were used as representative phenolic acids to clarify the unique fragmentation pathway in this study.

Among the 11 flavonoids rapidly identified (**Table 1**), all but two flavonoid aglycones belong to the *O*-glycosyl type. For flavonoid *O*-glycoside, the most typical fragmentation behavior was C-*O* bond cleavage, which frequently produced a glycosyl moiety (Huang et al., 2015). In addition, all flavonoids had the same mother nucleus, which was quercetin (302 Da), kaempferol (286 Da), and rhamnetin (316 Da), respectively. Accordingly, compounds **9**, **10**, **12**, and **16** caused the parent nuclear fragment ion 301/300 Da $[quercetin\text{-}H/2H]^-$ due to the loss of rutinose (308 Da), galactose (162 Da), glucose (162 Da), and rhamnoside (146 Da). The representative fragments $[M\text{-}H\text{-}146\text{–}162]^-$ in compound **13** was $[kaempferol\text{-}H]^-$, which were obtained by losing one robinobioside (308 Da) group. Similarly, compound **19** lost one galactose (162 Da) to produce fragmentation 315 Da $[rhamnetin\text{-}H/M\text{-}H\text{-}162]^-$. Flavonoid *O*-glycosides, such as compounds **9**, **10**, and **12**, often showed the loss of $C_2H_4O_2$ (60 Da), attributed to the split through the sugar moiety. Moreover, the loss of partial division of sugar unit has also been found in some compounds (**14**, **16**, **20**) of this type, which might be a characteristic fragmentation behavior of these compounds with splitting through the glycosyl. Due to the reverse Diels–Alder reaction (RDA), flavonoids were trend to produce characteristic fragmentation (CO, 28 Da) behavior (Ren et al., 2020; L.; Xie et al., 2019). Hyperoside (**10**, **Figure 5C**) was used as the example of flavonoid *O*-glycosides and flavones, respectively, to illuminate their characteristic fragmentation pathway.

3.3.2 Saponins

According to the fragmentation features and combined with literature verification (Li et al., 2010), 28 saponins were quickly identified, most of which belonged to the oleanolic acid type. In the positive and negative ion mode, the additive ions of saponins were mainly $[M+Na]^+$, $[M+H]^+$, $[M-H]^-$ and $[M+HCOO]^-$. The mother nucleoside fragments were obtained by breaking or continuously breaking *O*-glycosyl or sugar groups, including glucose (162 Da), rhamnoside(146 Da), glucuronic acid (176 Da), galactose (162 Da), xylose (132 Da), and arabinose (132 Da) and so on. (Xia et al., 2019). In addition, the further characteristic fragment ions such as 191 Da and 174 Da were obtained by RDA rearrangement. For example, peak 43 showed a molecular formula of $C_{52}H_{82}O_{21}$ (m/z 1087.5569 $[M+HCOO]^-$. The fragment ion m/z 571.3712 $[M\text{-}Rha\text{-}Glc\text{-}Glc\text{-}H]^-$ indicated that its mother nucleus was 30-noroleanolic acid, when combined with the loss of one rhamnose fragment ion to obtain m/z 941.4941 $[M\text{-}Rha+HCOO]^-$ and one glucose fragment ion to get m/z 779.4745 $[M\text{-}Rha\text{-}Glc+HCOO]^-$, which was preliminarily identified as ciwujianoside C1 (**Figure 5D**). Due to the existence of carboxyl structure, it was easy to lose fragment CO_2 (44 Da) and gain m/z 391.1456 $[M\text{-}Rha\text{-}Glc\text{-}Glc\text{-}Ara\text{-}CO_2\text{-}H]^-$. A similar process also happened to ciwujianoside K (**Figure 5E**). Furthermore, the RDA rearrangement and partial loss of sugar phenomenon (**Figures 5D,E**) often occurred due to the presence of cycloolefin structure in the parent nucleus, which was a common and typical feature of saponins. The identification data of other compounds are shown in detail in **Table 1**.

3.4 Validation of the Quantitative Analytical Method

In the process of quantitative analysis, the contents of phenols and saponins from 29 different places were evaluated by the content determination of 10 reference compounds, which were selected

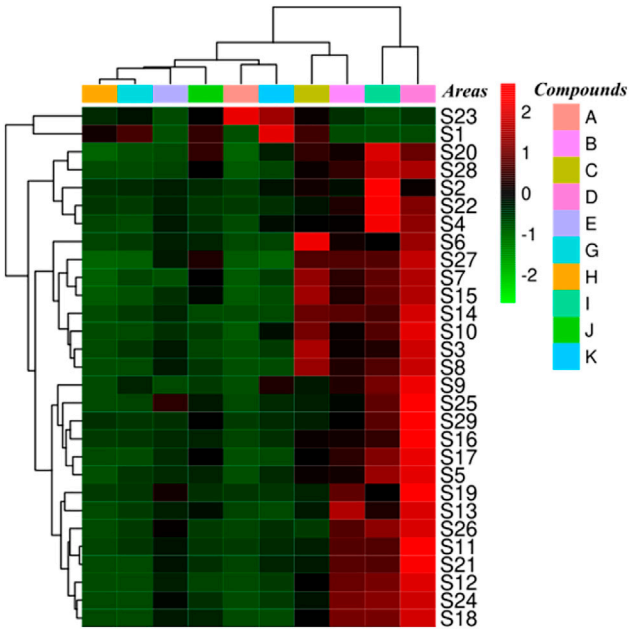

FIGURE 6 | Cluster analysis of ESL from 29 different areas based on the content differences of 10 reference compounds.

because of their properties, structure, and content. The linearity, quantitative limit (LOQ), detection limit (LOD), repeatability, precision, stability, and recovery of the UPLC-QTRAP-MS/MS quantitative analysis method were verified. The integral peak area (Y) and concentration (X) of 10 reference compounds in six different concentration standard solutions were analyzed by linear regression analysis. The regression equation, determination coefficient, and linear range of the reference compounds were listed in **Table 3**. The LOD and LOQ under the present chromatographic conditions were determined at a signal-to-noise ratio (S/N) of about 3 and 10, respectively.

Intra-day and inter-day changes were selected to evaluate the precision of the test. For the intra-day difference test, the mixed standard solution was analyzed within 1 day, while for the inter-day difference test, the solution was detected repeatedly in a continuous 3-day cycle. Variations were expressed by the relative standard deviation (RSD). Verification studies showed that the overall intra-day and inter-day variations (RSD) were less than 2.27% and 2.73%, respectively. In the stability test, the contents of 10 components in the sample solution were determined at 0, 2, 4, 8, 12, 24, and 48 h, respectively, and the RSD values were all less than 3.75%. In the repetitive test, the same samples were extracted six times and analyzed as mentioned above. The RSD values of 10 compounds were all less than 2.85%. The accuracy of the method was evaluated by recovery rate. A known amount of reference compounds was added to a certain amount of sample. The mixed solution of the standard was extracted and analyzed by the above-mentioned method. The experiment was repeated three times, and the accuracy of the method was good. The total recovery rate was 95.92%–101.04%, and the RSD was 1.64%–3.72% (**Table 4**). The results indicated that the determination of phenols and saponins by UPLC-QTRAP-MS/MS had high precision, accuracy, and sensitivity.

TABLE 6 | Results of α-glucosidase inhibition assay.

	IC50 (μg/ml)	Inhibition (%) at 500 μg/ml
Phenolic fraction	471.4 ± 17.7	53.7 ± 7.0
Saponin fraction	1094.0 ± 28.4	22.7 ± 3.4
n-BuOH fraction	1004.3 ± 30.8	27.3 ± 2.6
Alcohol extract	1386.4 ± 44.5	18.4 ± 2.1

Values represent the mean ± SEM (n = 3).

3.5 Constituents Analysis of Samples

Ten standard compounds in ESL samples from 29 locations were quantitatively determined by UPLC-QTRAP-MS/MS to comprehensively evaluate the contents of phenols and saponins. Each sample was analyzed three times to determine the mean contents (**Table 5**). The results showed that the contents of these compounds varied greatly among the samples collected from different habitats. The contents of protocatechuic acid (**A**, 8.41 ± 0.062 mg/g) and chlorogenic acid (**B**, 19.33 ± 0.392 mg/g) were the highest in S23 and S12, respectively, and methyl 5-*O*-feruloylquinate (**C**, 15.41 ± 0.173 mg/g), 3-*O*-α-L-rhamnopyranosyl-(1→2)-α-L-arabinopyranoside-29-hydroxy oleanolic acid (**G**, 16.20 ± 0.131 mg/g), 3-*O*-β-D-glucopyranosyl-(1→2)-α-L-arabinopyranoside-29-hydroxy oleanolic acid (**H**, 11.86 ± 0.324 mg/g), saponin P_E (**J**, 14.71 ± 0.094 mg/g), and ciwujianoside K (**K**, 30.60 ± 0.147 mg/g) were the highest in S1. The content of ciwujianoside C4 (**I**, 36.73 ± 0.582 mg/g) in S2, hyperoside (**D**, 36.56 ± 0.467 mg/g) and rutin (**E**, 11.11 ± 0.214 mg/g) in S19 was highest, respectively. Comprehensive analysis showed that the content of phenols in S19 was up to 69.89 ± 1.098 mg/g; the highest content of saponins in S1 was 74.28 ± 0.703 mg/g. This indicated that S19 and S1 will be better choices when these ingredients are required for further research. Cluster analysis (**Figure 6**) divided 29 locations into five categories. S2, S4, S20, S22, and S28 were the same categories. S1 and S23; S3, S6, S7, S8, S10, S14, S15, and S27; S5, S9, S16, S17, S25, and S29 were one category, respectively, and the rest were one category. These results suggested that different areas have different contents of phenols and saponins.

3.6 α-Glucosidase Inhibition Assay of ESL

α-Glucosidase inhibition assay was used to evaluate the hypoglycemic property of the extracted parts of ESL, respectively. As shown in **Table 6**, all extracts showed effective hypoglycemic activity. The results indicated that the hypoglycemic activity of different extracts was different. Among them, phenolic fraction had the best hypoglycemic activity (471.4 ± 17.7 μg/ml), followed by n-butanol (1004.3 ± 30.8 μg/ml), saponins (1094.0 ± 28.4 μg/ml), and alcohol extract (1386.4 ± 44.5 μg/ml). These results might be correlated with phenols content, suggesting that ESL could be a new plant source of natural hypoglycemic.

4 CONCLUSION

This study established a new rapid and sensitive UPLC-QTOF-MS/MS method to identify phenols and saponins in ESL. Under the optimized conditions, 30 phenols and 28 saponins were detected and identified within 23.0 min *via* comparing the characteristic fragments of mass spectrometry with the information of the published literature (**Figure 2**; **Table 1**). Most phenolic acids were formed by dehydration condensation of one or two caffeic acids and one quinic acid or their derivatives. Due to the dissociation of oxygen methyl, carboxyl, and ester bond in their structures, losing OCH_3/CH_3 (31/15 Da), CO_2 (44 Da), quinic acid (156 Da), caffeoyl (162 Da), caffeoyl (176 Da), or coumaroyl (146 Da) was their main cleavage characteristics. Flavonoids and saponins tended to be *O*-glycosides, and the most typical fragmentation behavior was the cleavage of the C-*O* bond. Their mother nucleus was obtained by destroying or continuously destroying *O*-glycosyl or sugar groups. The glycosyl of flavonoids mainly included rutinose (308 Da), galactose (162 Da), glucose (162 Da), and rhamnoside (146 Da), and saponins mainly lost glucose, rhamnoside, glucuronic acid (176 Da), galactose, xylose (132 Da), arabinose (132 Da), and so on. Because of the reverse Diels–Alder reaction (RDA), flavonoids were apt to produce characteristic fragments (CO, 28 Da), and saponins obtained characteristic ions such as 191 Da and 174 Da. Moreover, partial sugar loss was also a typical common feature of flavonoids and saponins. The exact or complete chemical structures of 30 compounds from the phenolic and saponin fractions of ESL were further clarified by nuclear magnetic resonance spectroscopy, of which 12 (including eight phenols) were isolated from this genus for the first time (**Figure 4**). To quantitatively determine 10 components in ESL from 29 different areas to evaluate the contents of phenols and saponins, a UPLC-QTRAP-MS/MS method was established. The results showed that the highest contents of phenols and saponins in S19 and S1 were 69.89 ± 1.098 and 74.28 ± 0.733 mg/g, respectively (**Table 5**). Cluster analysis (**Figure 6**) divided 29 locations into five categories, suggesting that different areas have different contents of phenols and saponins. The methodological investigation suggested that the established qualitative and quantitative methods could be used to evaluate the quality of ESL. In addition, the α-glucosidase inhibitory activity of phenolic fraction was the highest *in vitro* (**Table 6**), indicating that the phenolic content may be related to the hypoglycemic activity. It was suggested that ESL could be developed as a natural potential effective drug or functional food. However, its pharmacological effects *in vivo* and related mechanisms need to be further studied.

DATA AVAILABILITY STATEMENT

The original contributions presented in the study are included in the article/Supplementary Material. Further inquiries can be directed to the corresponding author.

AUTHOR CONTRIBUTIONS

JH: conceived the experiment, drafted the manuscript. DW: critical evaluation of the manuscript, literature review. YS, HZ, YW, WZ, FS, and BY: experimental studies, data collection, and manuscript preparation. QW and HK: approved the final manuscript.

ACKNOWLEDGMENTS

Chief Scientist of Qi-Huang Project of National Traditional Chinese Medicine Inheritance and Innovation "One Hundred Million" Talent Project (2021), Qi-Huang Scholar of National Traditional Chinese Medicine Leading Talents Support Program (2018), Heilongjiang Touyan Innovation Team Program (2019).

REFERENCES

Chen, B., Cai, W., Liu, F., and Liu, Z. B. (2016). *Chemical Constituents in Mailuoning Injection(I)*. Central South Pharmacy.

Committee, N. P. (2020). *Pharmacopoeia of the People's Republic of China*. Beijing: China Medical And Technology Press, 310–313.

Costa, C., Tsatsakis, A., Mamoulakis, C., Teodoro, M., Briguglio, G., Caruso, E., et al. (2017). Current Evidence on the Effect of Dietary Polyphenols Intake on Chronic Diseases. *Food Chem. Toxicol.* 110, 286–299. doi:10.1016/j.fct.2017.10.023

Dong, J., Liang, W., Wang, T., Sui, J., Wang, J., Deng, Z., et al. (2019). Saponins Regulate Intestinal Inflammation in colon Cancer and IBD. *Pharmacol. Res.* 144, 66–72. doi:10.1016/j.phrs.2019.04.010

Gerontakos, S., Taylor, A., Avdeeva, A. Y., Shikova, V. A., Pozharitskaya, O. N., Casteleijn, D., et al. (2021). Findings of Russian Literature on the Clinical Application of Eleutherococcus Senticosus (Rupr. & Maxim.): A Narrative Review. *J. Ethnopharmacol* 278, 114274. doi:10.1016/j.jep.2021.114274

Han, J., Liu, L., Yu, N., Chen, J., Liu, B., Yang, D., et al. (2016). Polysaccharides from Acanthopanax Senticosus Enhances Intestinal Integrity through Inhibiting TLR4/NF-Kb Signaling Pathways in Lipopolysaccharide-Challenged Mice. *Anim. Sci. J.* 87 (8), 1011–1018. doi:10.1111/asj.12528

Hayakawa, S., Ohishi, T., Miyoshi, N., Oishi, Y., Nakamura, Y., and Isemura, M. (2020). Anti-Cancer Effects of Green Tea Epigallocatchin-3-Gallate and Coffee Chlorogenic Acid. *Molecules* 25 (19). doi:10.3390/molecules25194553

Huang, M., Zhang, Y., Xu, S., Xu, W., Chu, K., Xu, W., et al. (2015). Identification and quantification of phenolic compounds in Vitex negundo L. var. cannabifolia (Siebold et Zucc.) Hand.-Mazz. using liquid chromatography combined with quadrupole time-of-flight and triple quadrupole mass spectrometers. *J. Pharm. Biomed. Anal.* 108, 11–20. doi:10.1016/j.jpba.2015.01.049

Ida, Y., Satoh, Y., Ohtsuka, M., Nagasao, M., and Shoji, J. (1993). Phenolic Constituents of Phellodendron Amurense Bark. *Phytochemistry* 35 (1), 209–215. doi:10.1016/s0031-9422(00)90536-3

Iha, A., Matsunami, K., Otsuka, H., Kawahata, M., Yamaguchi, K., and Takeda, Y. (2012). Three new aliphatic glycosides from the leaves of Antidesma japonicum Sieb. et Zucc. *J. Nat. Med.* 66 (4), 664–670. doi:10.1007/s11418-012-0635-1

Jia, A., Zhang, Y., Gao, H., Zhang, Z., Zhang, Y., Wang, Z., et al. (2021). A Review of Acanthopanax Senticosus (Rupr and Maxim.) Harms: From Ethnopharmacological Use to Modern Application. *J. Ethnopharmacol* 268, 113586. doi:10.1016/j.jep.2020.113586

Kil, H. W., Rho, T., and Yoon, K. D. (2019). Phytochemical Study of Aerial Parts of Leea Asiatica. *Molecules* 24 (9). doi:10.3390/molecules24091733

Kim, K. J., Hong, H. D., Lee, O. H., and Lee, B. Y. (2010). The Effects of Acanthopanax Senticosus on Global Hepatic Gene Expression in Rats

Subjected to Heat Environmental Stress. *Toxicology* 278 (2), 217–223. doi:10.1016/j.tox.2010.04.010

Lau, K. M., Yue, G. G., Chan, Y. Y., Kwok, H. F., Gao, S., Wong, C. W., et al. (2019). A Review on the Immunomodulatory Activity of Acanthopanax Senticosus and its Active Components. *Chin. Med.* 14, 25. doi:10.1186/s13020-019-0250-0

Lee, S., Park, H. S., Notsu, Y., Ban, H. S., Kim, Y. P., Ishihara, K., et al. (2008). Effects of Hyperin, Isoquercitrin and Quercetin on Lipopolysaccharide-Induced Nitrite Production in Rat Peritoneal Macrophages. *Phytother Res.* 22 (11), 1552–1556. doi:10.1002/ptr.2529

Lee, S., Shin, D. S., Oh, K. B., and Shin, K. H. (2003). Antibacterial Compounds from the Leaves of Acanthopanax Senticosus. *Arch. Pharm. Res.* 26 (1), 40–42. doi:10.1007/BF03179929

Li, S. L., Lai, S. F., Song, J. Z., Qiao, C. F., Liu, X., Zhou, Y., et al. (2010). Decocting-induced Chemical Transformations and Global Quality of Du-Shen-Tang, the Decoction of Ginseng Evaluated by UPLC-Q-TOF-MS/MS Based Chemical Profiling Approach. *J. Pharm. Biomed. Anal.* 53 (4), 946–957. doi:10.1016/j.jpba.2010.07.001

Liang, Q., Yu, X., Qu, S., Xu, H., and Sui, D. (2010). Acanthopanax Senticosides B Ameliorates Oxidative Damage Induced by Hydrogen Peroxide in Cultured Neonatal Rat Cardiomyocytes. *Eur. J. Pharmacol.* 627 (1-3), 209–215. doi:10.1016/j.ejphar.2009.10.055

Mallavadhani, U. V., and Narasimhan, K. (2009). Two Novel Butanol Rhamnosides from an Indian Traditional Herb, Euphorbia Hirta. *Nat. Prod. Res.* 23 (7), 644–651. doi:10.1080/14786410802214009

Meng, L. J., Liu, B. L., Zhang, Y., and Zhou, G. X. (2014). Chemical Constituents in Root Barks of Lycium Chinense. *Chin. Traditional Herbal Drugs* 45 (15), 2139–2142.

Meng, Q., Pan, J., Liu, Y., Chen, L., and Ren, Y. (2018). Anti-tumour Effects of Polysaccharide Extracted from Acanthopanax Senticosus and Cell-Mediated Immunity. *Exp. Ther. Med.* 15 (2), 1694–1701. doi:10.3892/etm.2017.5568

Menozzi-Smarrito, C., Wong, C. C., Meinl, W., Glatt, H., Fumeaux, R., Munari, C., et al. (2011). First Chemical Synthesis and *In Vitro* Characterization of the Potential Human Metabolites 5-O-Feruloylquinic Acid 4'-sulfate and 4'-O-Glucuronide. *J. Agric. Food Chem.* 59 (10), 5671–5676. doi:10.1021/jf200272m

Osawa, K., Arakawa, T., Shimura, S., and Takeya, K. (2001). *New Quinic Acid Derivatives from the Fruits of Chaenomeles Sinensis (Chinese Quince)*. Tokyo: Natural Medicines.

Panossian, A. G., Efferth, T., Shikov, A. N., Pozharitskaya, O. N., Kuchta, K., Mukherjee, P. K., et al. (2021). Evolution of the Adaptogenic Concept from Traditional Use to Medical Systems: Pharmacology of Stress- and Aging-Related Diseases. *Med. Res. Rev.* 41 (1), 630–703. doi:10.1002/med.21743

Ren, M., Xu, W., Zhang, Y., Ni, L., Lin, Y., Zhang, X., et al. (2020). Qualitative and Quantitative Analysis of Phenolic Compounds by UPLC-MS/MS and Biological Activities of Pholidota Chinensis Lindl. *J. Pharm. Biomed. Anal.* 187, 113350. doi:10.1016/j.jpba.2020.113350

Shi, L. I., Liu, D. Y., Shi, X. F., and Lei, Y. P. (2014). Chemical Constituents in N-Butanol Extract from pine needles of Cedrus Deodara. *Chin. Traditional Herbal Drugs* 45 (18), 2602–2606.

Shikov, A. N., Narkevich, I. A., Flisyuk, E. V., Luzhanin, V. G., and Pozharitskaya, O. N. (2021). Medicinal Plants from the 14th Edition of the Russian Pharmacopoeia, Recent Updates. *J. Ethnopharmacol* 268, 113685. doi:10.1016/j.jep.2020.113685

Singh, B., Singh, J. P., Kaur, A., and Singh, N. (2020). Phenolic Composition, Antioxidant Potential and Health Benefits of Citrus Peel. *Food Res. Int.* 132, 109114. doi:10.1016/j.foodres.2020.109114

Tošović, J., Marković, S., Dimitrić Marković, J. M., Mojović, M., and Milenković, D. (2017). Antioxidative Mechanisms in Chlorogenic Acid. *Food Chem.* 237, 390–398. doi:10.1016/j.foodchem.2017.05.080

Wan, C., Yuan, T., Cirello, A. L., and Seeram, N. P. (2012). Antioxidant and α-glucosidase Inhibitory Phenolics Isolated from Highbush Blueberry Flowers. *Food Chem.* 135 (3), 1929–1937. doi:10.1016/j.foodchem.2012.06.056

Wang, H. P., Zhang, Y. B., Yang, X. W., Zhao, D. Q., and Wang, Y. P. (2016). Rapid Characterization of Ginsenosides in the Roots and Rhizomes of Panax Ginseng by UPLC-DAD-QTOF-MS/MS and Simultaneous Determination of 19 Ginsenosides by HPLC-ESI-MS. *J. Ginseng Res.* 40 (4), 382–394. doi:10.1016/j.jgr.2015.12.001

Xia, Y. G., Gong, F. Q., Guo, X. D., Song, Y., Li, C. X., Liang, J., et al. (2019). Rapid Screening and Characterization of Triterpene Saponins in Acanthopanax Senticosus Leaves *via* Untargeted MSAll and SWATH Techniques on a Quadrupole Time of Flight Mass Spectrometry. *J. Pharm. Biomed. Anal.* 170, 68–82. doi:10.1016/j.jpba.2019.02.032

Xie, L., Lin, Q., Guo, K., Tong, C., Shi, S., and Shi, F. (2019). HPLC–DAD–QTOF-MS/MS Based Comprehensive Metabolomic Profiling of Phenolic Compounds in Kalimeris Indica Anti-inflammatory Fractions. *Ind. Crops Prod.* 140, 111636. doi:10.1016/j.indcrop.2019.111636

Xie, Y., Zhang, B., and Zhang, Y. (2015). Protective Effects of Acanthopanax Polysaccharides on Cerebral Ischemia-Reperfusion Injury and its Mechanisms. *Int. J. Biol. Macromol* 72, 946–950. doi:10.1016/j.ijbiomac.2014.09.055

Yan, W., Zheng, C., He, J., Zhang, W., Huang, X. A., Li, X., et al. (2018). Eleutheroside B1 Mediates its Anti-influenza Activity through POLR2A and N-Glycosylation. *Int. J. Mol. Med.* 42 (5), 2776–2792. doi:10.3892/ijmm.2018.3863

Yang, F., Yang, L., Wang, W., Liu, Y., Zhao, C., and Zu, Y. (2012). Enrichment and Purification of Syringin, Eleutheroside E and Isofraxidin from Acanthopanax Senticosus by Macroporous Resin. *Int. J. Mol. Sci.* 13 (7), 8970–8986. doi:10.3390/ijms13078970

Zeng, J., Zhang, S. N., Song, H. Z., Ma, R. J., and Tan, Q. G. (2020). Flavonoid and Lignan Glycosides from the Leaves of Melia Azedarach. *Chem. Nat. Comp.* 56 (2). doi:10.1007/s10600-020-03019-w

Zhang, H., Su, Y., Wang, X., Mi, J., Huo, Y., Wang, Z., et al. (2017). Antidiabetic Activity and Chemical Constituents of the Aerial Parts of Heracleum Dissectum Ledeb. *Food Chem.* 214, 572–579. doi:10.1016/j.foodchem.2016.07.065

Zhao, X.-C., Du, J.-L., Xie, Y.-G., Zhang, Y., and Jin, H.-Z. (2018). Chemical Constituents of the Flowers of Hemerocallis Minor. *Chem. Nat. Compd.* 54 (3), 556–558. doi:10.1007/s10600-018-2405-0

Zhou, T., Li, Z., Kang, O. H., Mun, S. H., Seo, Y. S., Kong, R., et al. (2017). Antimicrobial Activity and Synergism of Ursolic Acid 3-O-α-L-Arabinopyranoside with Oxacillin against Methicillin-Resistant *Staphylococcus aureus*. *Int. J. Mol. Med.* 40 (4), 1285–1293. doi:10.3892/ijmm.2017.3099

Zlab, C., Wxab, C., Ying, Z. D., Ld, C., and Jsab, C. (2020). A Review of Saponin Intervention in Metabolic Syndrome Suggests Further Study on Intestinal Microbiota. *Pharmacol. Res.* 160.

Conflict of Interest: The authors declare that the research was conducted in the absence of any commercial or financial relationships that could be construed as a potential conflict of interest.

Publisher's Note: All claims expressed in this article are solely those of the authors and do not necessarily represent those of their affiliated organizations or those of the publisher, the editors, and the reviewers. Any product that may be evaluated in this article, or claim that may be made by its manufacturer, is not guaranteed or endorsed by the publisher.

frontiers | Frontiers in Pharmacology

REVIEW
published: 02 June 2022
doi: 10.3389/fphar.2022.853023

Advances in Fingerprint Analysis for Standardization and Quality Control of Herbal Medicines

Eka Noviana[1], *Gunawan Indrayanto*[2] *and Abdul Rohman*[1,3]*

[1]Departement of Pharmaceutical Chemistry, Faculty of Pharmacy, Universitas Gadjah Mada, Yogyakarta, Indonesia, [2]Faculty of Pharmacy, Universitas Surabaya, Surabaya, Indonesia, [3]Center of Excellence, Institute for Halal Industry and Systems, Universitas Gadjah Mada, Yogyakarta, Indonesia

Herbal drugs or herbal medicines (HMs) have a long-standing history as natural remedies for preventing and curing diseases. HMs have garnered greater interest during the past decades due to their broad, synergistic actions on the physiological systems and relatively lower incidence of adverse events, compared to synthetic drugs. However, assuring reproducible quality, efficacy, and safety from herbal drugs remains a challenging task. HMs typically consist of many constituents whose presence and quantity may vary among different sources of materials. Fingerprint analysis has emerged as a very useful technique to assess the quality of herbal drug materials and formulations for establishing standardized herbal products. Rather than using a single or two marker(s), fingerprinting techniques take great consideration of the complexity of herbal drugs by evaluating the whole chemical profile and extracting a common pattern to be set as a criterion for assessing the individual material or formulation. In this review, we described and assessed various fingerprinting techniques reported to date, which are applicable to the standardization and quality control of HMs. We also evaluated the application of multivariate data analysis or chemometrics in assisting the analysis of the complex datasets from the determination of HMs. To ensure that these methods yield reliable results, we reviewed the validation status of the methods and provided perspectives on those. Finally, we concluded by highlighting major accomplishments and presenting a gap analysis between the existing techniques and what is needed to continue moving forward.

Keywords: herbal medicines, fingerprint analysis, chemometrics, chemical fingerprint, DNA fingerprint

OPEN ACCESS

Edited by:
George Qian Li,
Western Sydney University, Australia

Reviewed by:
Srinivas Patnala,
Rhodes University, South Africa
Anoop Kumar,
Delhi Pharmaceutical Sciences and Research University, India

***Correspondence:**
Abdul Rohman
abdulkimfar@gmail.com

Specialty section:
This article was submitted to Ethnopharmacology, a section of the journal Frontiers in Pharmacology

Received: *12 January 2022*
Accepted: *26 April 2022*
Published: *02 June 2022*

Citation:
Noviana E, Indrayanto G and Rohman A (2022) Advances in Fingerprint Analysis for Standardization and Quality Control of Herbal Medicines. Front. Pharmacol. 13:853023. doi: 10.3389/fphar.2022.853023

1 INTRODUCTION

Herbal medicines (HMs) or herbal drugs have been known for centuries and empirically used to treat diseases by people across different cultures throughout history. Approximately 40% of the drugs used nowadays are directly or indirectly originated from natural products [plants 25%, microorganisms (13%), animals (3%)] (Calixto, 2019). While herbal medicines are generally perceived to be safer than synthetic drugs, the lack of regulations on HMs, especially in the past, has led to many adverse events (Walji et al., 2009). The contamination and adulteration of HMs also become a major concern (Posadzki et al., 2013). With the growing market of HMs, many countries have provided some regulations and guidance to ensure the safe use of the medicines by the patients or consumers. According to WHO, in 2018 about 90% of member states/countries have had national regulations on HMs (WHO, 2019). Many of these countries have 1) reported the use of national or other

pharmacopeias (typically those from Britain, the United States, and Europe) or monographs that include HMs, 2) provided guidance for good manufacturing practices and mechanisms to ensure compliance with the manufacturing requirements, and 3) enforced special regulatory requirements for HMs or similar requirements to those for conventional pharmaceuticals. These regulations or policies are made and put into practice to create a standardized quality of herbal medicines and ensure their safety and efficacy.

The standardization and quality control of HMs involve the physicochemical evaluation of the raw/crude materials, assessment of the stability, efficacy, and safety of the finished products, and provision of product information to ensure the appropriate use by the consumers. To perform the evaluation, macroscopic and microscopic observations on the specimen as well as chemical and biological analyses are typically done. Analytical approaches to this evaluation generally fall into three categories: marker compound analysis or single component analysis (targeted analysis), fingerprinting/profiling, and metabolomic studies (Riedl et al., 2015). Marker compounds are commonly chosen from the abundant compounds in a botanical specimen and used as potency standards. However, the standardization of HMs based on marker compounds often yields unreliable results, especially when the chosen marker is not the biologically active component of the plant (Ruiz et al., 2016). In addition, the therapeutic effects of HMs may result from a complex interaction among various herbal constituents, and thus, a single or a few markers may not be a good predictor of the overall efficacy.

Fingerprinting techniques, on the other hand, interrogate the whole chemical profile of the botanical specimen. In combination with multivariate data analysis or chemometrics, this complex profile can be extracted into a common pattern that correlates with certain biological or pharmacological activities and set as a criterion for assessing the individual material or formulation (Kharbach et al., 2020). Tasks such as differentiating between authentic and adulterated HMs as well as distinguishing the origins of plant species have been performed using fingerprinting techniques (Wang and Yu, 2015; Sima et al., 2018). Chemical fingerprints are often generated using chromatographic techniques such as high-performance liquid chromatography (HPLC) and thin-layer chromatography (TLC) (Fan et al., 2006; Wagner et al., 2011; Custers et al., 2017). However, other techniques such as molecular spectroscopy, mass spectrometry, capillary electrophoresis, and DNA-based methods can also provide chemical or molecular fingerprints for such purposes. This review aimed to evaluate the progress and applications of these various fingerprinting techniques for the standardization and quality controls of herbal drugs.

2 STANDARDIZATION OF HERBAL DRUGS: CURRENT CRITERIA, LIMITATIONS, AND CHALLENGES

Official methods for general standardization of herbal drugs or botanicals have been described by the current compendia and regulatory agencies (EMA, 2011; FDA, 2016; WHO, 2017; Farmakope Herbal Indonesia, 2017; Taiwan Herbal Pharmacopeia, 2019; British Pharmacopoeia, 2020; Hong Kong Chinese Materia Medica Standards, 2020; USP Herbal Medicine Compendium, 2021; USP44-NF39, 2021b, 2021c). Sampling methods for botanical samples have also been described (USP44-NF39, 2021b). The common standardization methods described by those official guidelines are macroscopic/microscopic characterizations, chemical tests, chromatographic fingerprinting, DNA profiling, quantitative determination of certain compounds/markers or a group of compounds, test for chemical contaminants/microorganisms, and physicochemical tests. According to WHO, non-specific chemical tests (e.g., phytochemical screening for alkaloids, flavonoids, terpenes, steroids, saponins, tannins, etc.) must not be applied for the identification (WHO, 2017). The general guidance for the development, validation, and standardization of new or non-official methods of analysis for botanicals/herbs and dietary supplements has been published by the Association of Official Analytical Chemists (AOAC, 2019). In this section, only the specific methods of herbal standardization/validation will be discussed in detail.

Some compendia and reference standards have described comprehensive macroscopic and microscopic characterizations of each of the herbs, including their pictures (Farmakope Herbal Indonesia, 2017; British Pharmacopoeia, 2020; Hong Kong Chinese Materia Medica Standards, 2020). However, due to phenotypic variations between different populations of identical species in commercial samples, these techniques may be insufficient for correct identification. To overcome this problem, the application of a DNA-based approach can be recommended for plant identification/authentication (Klein-Junior et al., 2021). It is worth noting that the DNA-based approach works well for plant authentication, but not for assessing the quality of plant materials. Many external factors can affect the (secondary) metabolites content of a plant both qualitatively and quantitatively. Plants with similar DNA profiles may not produce similar compositions of metabolites. Therefore, a quality control tool solely based on DNA profiling is not recommended. A combination of chemical characterization (both qualitative and quantitative) and DNA profiling/barcoding would serve as a more comprehensive method of herbs identification (Indrayanto, 2018a; Leong et al., 2020).

All the official guidelines described above generally apply high-performance thin-layer chromatography (HPTLC) for the method of identification of the herbs. Detailed HPTLC methods of identification for the article on botanical origins or herbs have been described (USP44-NF39, 2021a, 2021f). TLC identification of each herb, as described in USP, BP, Indonesian Herbal Pharmacopeia, Taiwan Pharmacopeia, USP Herbal Compendium, and Hong Kong Chinese Materia Medica Standards, is generally carried out by observation of the TLC plates under white light and UV light. For example, adulterants of *Sclerocarya birrea* leaves and leaf products could be visually detected on HPTLC images using white light and UV-366 nm (Do et al., 2020). Retardation factors (R_f) of the target spots, their colors, and intensities can be compared between the sample and

the standard. However, this visual observation may show poor reproducibility due to the strong influences of experimental conditions (Klein-Junior et al., 2021). To have more reliable results for the visual identification of botanicals using TLC profiles, a complete and comprehensive method validation should be performed (Reich et al., 2008; Do et al., 2021). The application of densitometry for the evaluation of TLC chromatograms is preferred due to its accuracy and precision. Method validation for the assessment of TLC fingerprinting using HPTLC-densitogram has been reported in which coefficient correlations (R), congruence coefficient (c), similarity index (SI), and dendrogram were applied for evaluating the densitograms of samples and standards (Srivastava et al., 2019). HPTLC-profile plots could also be directly generated using Image^{R} software after auto processing and enhancing the TLC images by XnView 2.40^{R} freeware, followed by chemometrics evaluation (Ibrahim and Zaatout, 2019). To obtain a more accurate and reproducible assessment of the TLC profile, the application of similarity analysis as described in the Chinese Pharmacopoeia 2015 is recommended (Shen et al., 2021). The applications of HPLC fingerprints for the authentication of Chinese herbs have also been described by Hongkong Chinese Materia Medica Standards. Typical HPLC chromatograms and relative retention time (RR_t) of specific compounds are provided in each monograph (Hong Kong Chinese Materia Medica Standards, 2020).

Various analytical techniques can be applied for generating chemical fingerprinting of HMs. These include spectrometric methods (e.g., infrared (IR), near-infrared (NIR), nuclear magnetic resonance (NMR), and mass spectrometry (MS)), chromatographic methods (e.g., HPLC, gas chromatography (GC), HPTLC), and capillary electromigration methods (e.g, capillary electrophoresis (CE)) combined with various detectors. The quality of the fingerprints depends on sample pre-treatment and the selected chemical techniques (Klein-Junior et al., 2021). Typically, the more sophisticated the instruments, the more reliable the results. However, the operational cost for these sophisticated methods could be expensive. These methods also need highly trained personnel and large amounts of reagents and solvents. It is well known that all methods used at a QC laboratory should not only be simple, cost-effective, and fast, but they also need to be accurate and precise. Therefore, direct attenuated total reflectance-Fourier transform infrared (ATR-FTIR) spectroscopy combined with chemometrics could be recommended as an alternative QC tool to the HPTLC (i.e., the commonly used method in pharmacopeias). The ATR-FTIR requires minimum to no sample preparations. To apply FTIR methods, the availability of official botanical reference materials (BRMs) is crucial (Indrayanto, 2018a). If the BRM is not yet available, the botanical or herb reference materials must be standardized first using liquid chromatography-high resolution tandem mass spectrometry (LC-HR-MS/MS) to evaluate their exact biochemical components.

All official guidelines describe the method of quantification of a certain compound(s) or a group of compounds using spectroscopic and/or chromatographic methods. Minimum concentrations of the compounds are generally described and used as the acceptance criteria. However, these criteria are not appropriate to be applied as a parameter of the quality of herbs (Länger et al., 2018). The assayed compounds/markers must be considered as purely analytical markers without correlation to quality or efficacy. Chemical constituents (compounds) in botanical articles can be categorized as active principles, active markers, analytical markers, or negative markers (USP44-NF39, 2021c). Unfortunately, in all monographs of botanicals in the current USP 44-NF 39, those terms of markers are not described. Only the name of the compounds or a group of compounds and their minimum concentrations or specification range concentrations (for certain preparations) are described by each monograph. Analyzing a certain compound or a group of compounds in herbs will only be useful for QC if the compounds have a direct correlation to the efficacy or toxicity of the herbs. For this purpose, some researchers have recommended new criteria for the QC markers e.g. Herb MarRS system, Q-marker, Bioactive chemical markers, etc., or in general terms referred to as "quality markers" (Indrayanto, 2018a). If an herb is already known for its quality markers, there is no need to evaluate the quality of the herb using the fingerprinting method.

Most commercial herbal drug preparations consist of a mixture of herbs and/or extracts. Therefore, methods for standardization of individual herbs that are described in the Pharmacopeia cannot be applied directly as a quality control (QC) tool for all stages of the manufacturing processes i.e. incoming materials, in-process control, finished product, and sample storage. To obtain a consistent quality of HMs, all stages of the production line need to be evaluated by QC (Indrayanto, 2018a). If the quality marker of each component of the assessed herbal product is known, the QC can be performed by analyzing those markers in all stages of production. However, if the quality markers are not yet known, the QC should be performed by using a combination of fingerprinting methods and chemometrics, both qualitatively and quantitatively. Each batch of a commercial herbal drug should show identical efficacy. Thus, the exact composition of herbs and/or extracts should be determined (Heinrich et al., 2020). For this purpose, the combination of chemical profiling and chemometrics seems to be the method of choice. Generally, a combination of various analytical techniques needs to be applied to the analysis of HM preparations (Muyumba et al., 2021). The authors recommend starting with a sophisticated method to define the exact composition of the HM (e.g., LC-HR-MS/MS or NMR 400 MHz), and then transferring the method to a relatively cost-effective method (e.g., ATR-FTIR, HPTLC, LC-UV/Vis) for routine QC assessment. Procedures for the method transfer have been described in compendia (USP44-NF39, 2021d).

3 FINGERPRINT DATA ANALYSIS USING CHEMOMETRIC APPROACH

Quality assessment of HMs using a combination of fingerprinting and chemometrics is the method of choice if the quality markers are not yet specified. Chemical profiles/fingerprints of HMs

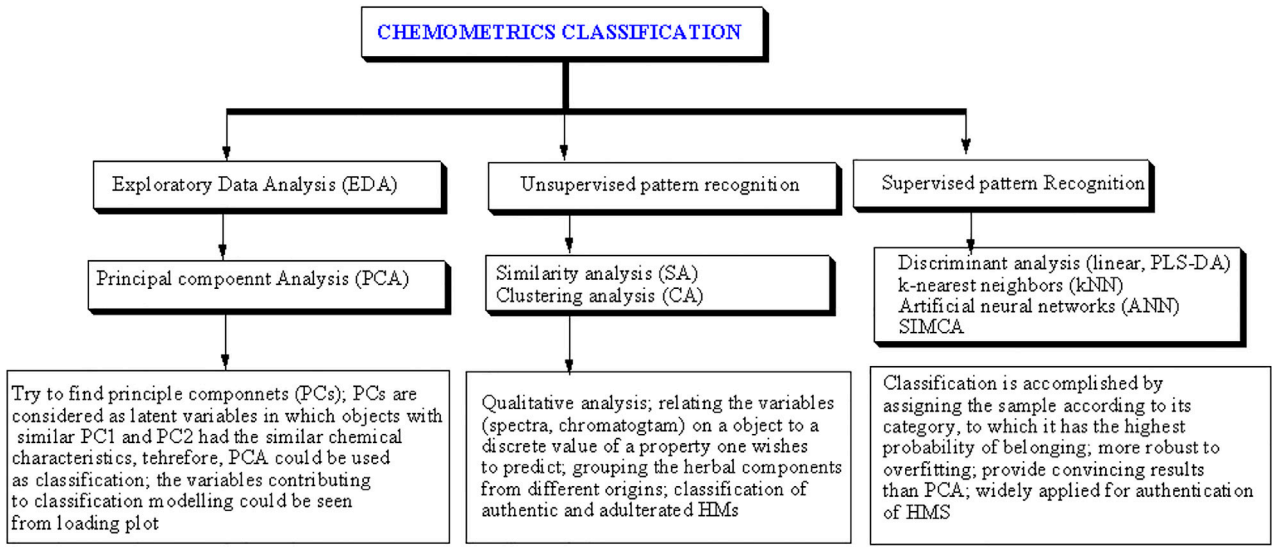

FIGURE 1 | The chemometrics classification techniques widely applied for the identification of objects. Reproduced from (Rohman and Windarsih, 2020) under the terms and conditions of the Creative Commons Attribution (CC BY) license. PLS-DA = partial least squares discriminant analysis, SIMCA = soft independent modeling of class analogy.

obtained by instrumental methods such as LC-MS/MS and ^{1}H-NMR spectroscopy feature similarities and differences among one another. These sets of similarities and differences enable classifications of samples into certain categories, for instance, authentic and adulterated HMs. However, in any HMs, there are a large number of chemical responses from unknown components, which make the data handling challenging. And hence, powerful statistical techniques known as chemometrics are typically employed to treat these large chemical data (Nikam et al., 2012). The combination of chemical fingerprints and chemometrics enables accurate identification of samples even if the samples do not contain chemically characteristic constituents at exactly similar concentrations.

Chemometrics can be defined as the utilization of statistics and mathematics to analyze chemical data (Rohman and Putri, 2019). The International Chemometrics Society defined chemometrics as "*the science of relating chemical measurements made on a chemical system to the property of interest (such as concentration) through the application of mathematical or statistical methods*" (Huang et al., 2015). Chemometrics is widely applied to chemical data obtained from measurements using spectroscopic and chromatographic methods (Rohman and Windarsih, 2020). Chemometrics of classification is the most common chemometrics technique applied in fingerprint profiling of HMs. The aim of classification chemometrics is to correlate the chemical data or variables obtained from instrumental measurements to a discrete value of a property the analyst wishes to predict (Biancolillo and Marini, 2018). These techniques include exploratory data analysis and pattern recognition (either supervised or unsupervised) (**Figure 1**). Exploratory data analysis and unsupervised pattern recognition can be applied to reduce the amount of original data and gain a better understanding of the chemical data sets (Berrueta et al., 2007). Multivariate calibrations can be used for building the prediction models for the analyte(s) of interest. The most popular multivariate calibrations applied in standardization and quality controls of HMs included principal component regression, partial least squares regression (PLSR), and multiple linear regression (MLR) (Singh et al., 2013).

Principal component analysis (PCA) is widely used for exploratory data analysis. PCA is capable of reducing the dimensionality of the datasets and increasing the interpretability of the data while retaining the most important piece of information of the datasets (Jollife and Cadima, 2016). This task is achieved by generating principal components (PCs) as an orthogonal linear transformation that considers variances from different variables in the data (Rawat et al., 2021). Unsupervised pattern recognition algorithms such as similarity analysis (SA) and hierarchical clustering analysis (HCA) are also commonly applied. SA can be applied to classify HMs samples based on the correlation and congruence coefficients. If the correlation and congruence coefficients are close to 1, it can be stated that the two fingerprints are similar (Chuchote and Somwong, 2019). HCA, on the other hand, can be performed to reveal the highest similarity within a cluster and the highest dissimilarity among clusters (Chuchote and Somwong, 2019).

Supervised pattern recognition algorithms are typically used to generate classification models and determine which class a sample belongs to. Classification models are built based on data obtained from chemical measurements of known samples. Unknown samples are then assigned to a previously determined class based on the similarity of chemical properties between the sample and the known class members. Supervised pattern recognition algorithms such as linear discriminant analysis (LDA), partial least squares discriminant analysis (PLS-DA),

soft independent modeling of class analogy (SIMCA), artificial neural networks (ANN), k-nearest neighbors (KNN), and least squares-support vector machine (LS-SVM) are often applied in HM authentication (Huang et al., 2015). LDA can maximize the distance between classified samples or groups, enabling better differentiation among HM classes (Luo and Shao, 2013). In the case of the number of samples is less than the number of measured variables (often referred to as 'ill-conditioned), PLS-DA can be applied to improve the capability of the predictive models to classify the samples (Razmovski-Naumovski et al., 2010). By applying PCA to each class, SIMCA classification can be generated to produce predictive models using the significant components only (Qu and Hu, 2011). KNN algorithm places samples and their relative distances among one another based on the level of similarity (Harrison). Similar things exist in proximity and *vice versa*. Another supervised method, LS-SVM which is based on the theory of statistical learning using classification and regression techniques, can also be employed in HM fingerprint profiling (Samui and Kothari, 2011).

3.1 Validation of Chemometrics Techniques

Chemometrics is mainly based on the application of empirical models intended for building predictive models either for qualitative (classification) or quantitative (calibration) purposes. The experimental measurements could provide large data containing a lot of information which allows the analyst to make the predictions of one or more properties of interest. The selection of an appropriate chemometrics model and the way to verify the model reliability are fundamental aspects to consider. The chemometrics strategies for performing these tasks are collectively referred to as validation. Validation aims to evaluate whether reliable conclusions can be drawn from the chemometrics modeling (Brereton et al., 2018). During the validation process, it is suggested to include some criteria such as the appropriateness of the chemometrics model, the adequacy of computational calculations used in the fitting procedure, the statistical reliability of models, and the generalizability of any resulting interpretations (Westad and Marini, 2015).

To assess the performance of the developed models, some diagnostic parameters based on the model or the calculation of residuals (i.e., differences between actual and predictive parameters) are often used as error criteria. Validation of chemometrics models can be performed using two approaches, internal validation (cross-validation) and external validation (Miller and Miller, 2018). Cross-validation is required to avoid overfitting the model. Cross-validation is based on the repeated resampling of the dataset into the sub-sets of training and testing. In multivariate calibration models, this validation is typically done using the leave-one-out technique. In this technique, one of the calibration samples is taken out and the remaining calibration samples are used to establish a new calibration model. The removed sample is then evaluated using the newly established model. This process is repeated to evaluate each calibration sample. Cross-validation can be chosen if the number of the evaluated samples is small and it is not feasible to build an external test set. The main disadvantage of cross-validation is that the resulting estimates may still be biased because the calibration and validation datasets are never completely independent. External validation employed two separate data sets for the calibration and validation. In this approach, the residuals are calculated from independent samples which mimic how the developed model will be routinely used. Therefore, this strategy is recommended whenever possible (Biancolillo and Marini, 2018). The validation approach should be selected based on the sample size (Kos et al., 2003). When the dataset or number of samples is small (less than 50), cross-validation is preferred, while external validation should be used if the number of samples is more than 50.

To evaluate the classification chemometrics, some performance characteristics including sensitivity, specificity, precision, accuracy and model efficiency are used (Oliveri and Downey, 2012; Oliveri et al., 2020):

$$\text{Sensitivity} = \frac{\text{TP}}{\text{TP} + \text{FN}} \tag{1}$$

$$\text{Specificity} = \frac{\text{TN}}{\text{TN} + \text{FP}} \tag{2}$$

$$\text{Efficiency} = \sqrt{\frac{\text{TP} \times \text{TN}}{(\text{TP} + \text{FN}) \times (\text{TN} + \text{FP})}} \tag{3}$$

$$\text{Precision} = \frac{\text{TP}}{\text{TP} + \text{FP}} \tag{4}$$

$$\text{Accuracy} = \frac{\text{TN} + \text{TP}}{\text{TN} + \text{TP} + \text{FN} + \text{FP}} \tag{5}$$

where TN is true negative, TP is true positive, FN is false negative, and FP is false positive. A parameter known as Matthews's correlation coefficient (r_M) can also be used as a comprehensive evaluation of model efficiency which considers all four possible outcomes (i.e. TP, TN, FP, and FN).

$$r_M = \frac{(\text{TP} \times \text{TN}) - (\text{FP} \times \text{FN})}{\sqrt{(\text{TP} + \text{FP}) \times (\text{TP} + \text{FN}) \times (\text{TN} + \text{FP}) \times (\text{TN} + \text{FN})}} \tag{6}$$

Some statistical parameters typically used for the performance characteristics are coefficient of determination (R^2) and root mean square error (RMSE). R^2 determines the relationship between two variables: actual values and predicted values from the instrument (accuracy). The precision of the validated analytical method is assessed by root mean square error of calibration (RMSEC) for error evaluation in the calibration model and root mean square error of prediction (RMSEP) for error evaluation in the prediction model. RMSEC and RMSEP can be obtained using the following equations:

$$\text{RMSEC} = \sqrt{\frac{\sum_{i=1}^{m} (\hat{\text{Y}}\text{i} - \text{Yi})^2}{\text{M} - 1}} \tag{7}$$

$$\text{RMSEP} = \sqrt{\frac{\sum_{i=1}^{n} (\hat{\text{Y}}\text{i} - \text{Yi})^2}{\text{N}}} \tag{8}$$

M and N are the numbers of samples used in calibration and validation, respectively. Yi and Δi are the predicted and actual values, respectively. Root mean square error of cross-validation (RMSECV) is used to express RMSEC if cross-validation using the leave-one-out technique is used.

For qualitative identification of HM, validation samples should consist of specified inferior test material (SITM) and specified superior test material (SSTM) (AOAC, 2019). SITM is a botanical (herb) mixture that has the maximum concentration of target material (herb) that is considered unacceptable (negative result) as specified by its standard method performance requirements (SMPR). SSTM is a mixture of herbs that has the minimum concentration of the target herb that is considered acceptable (positive result). The detailed procedure can be found in the AOAC guidelines (AOAC, 2019). BRM of each specified herb should be used for preparing SITM and SSTM. The availability of authentic herb/botanical reference materials and/or stable standardized mixtures of herbs and/or extracts with exact compositions as validation samples are crucial for qualitative and quantitative assessment of HMs using chemical profiling or fingerprinting (Wulandari et al., 2022).

General official validation methods for chemometrics analysis have been described in USP 44-NF39 general chapter (1039) Chemometrics (USP44-NF39, 2021e) and EP 10.0, 5.21 Chemometrics methods applied to analytical data (European Pharmacopoeia, 2021). Quantitative methods of analysis using chemometrics should be validated in two steps. First, calibration models are evaluated based on the R^2, RMSEC or RMSECV, and RMSEP (European Pharmacopoeia, 2021; USP44-NF39, 2021e). If the model meets the requirements of the analytical target profile, then the validation can be continued to step 2, which is the evaluation of general validation parameters of drugs (i.e., accuracy, precision, and robustness). This evaluation should be performed according to the general chapters of the USP 44-NF 39 (1225) (USP44-NF39, 2021 h), (1210) (USP44-NF39, 2021 g), and/or the AOAC guidelines (AOAC, 2019). Unfortunately, many published works do not report the method validation completely, as described in Tables 6, 7, and 8 of our recent book chapter (Wulandari et al., 2022). Without method validation, the reliability of the reported data cannot be ascertained. Detailed discussions regarding the development, validation, and standardization of analytical methods (qualitative and quantitative) using chemometrics have been previously described (Rohman and Windarsih, 2020; Wulandari et al., 2022).

4 APPLICATIONS OF FINGERPRINTING METHODS

Due to their separation capability, FDA and the European Medicines Agency recommend chromatographic techniques for the standardization of HMs. Consequently, many chromatographic methods have been developed for fingerprinting/profiling different HMs samples in the past decades. Among these, TLC, HPTLC, HPLC, LC-MS/MS, capillary electrophoresis, and GC equipped with several detectors were used (Sima et al., 2018). Vibrational spectroscopy and NMR spectroscopy combined with chemometrics have also emerged as analytical tools for the standardization of HMs. Vibrational spectroscopy (VS) methods including FTIR, NIR, and Raman spectroscopy generate spectra containing useful information for the standardization of HMs and have been widely used (Moros et al., 2010). VS methods are rapid and the generated fingerprint spectra can be treated using chemometrics to yield more interpretable results for answering different biological questions (Wang and Yu, 2015; Rohaeti et al., 2021). NMR spectroscopy has also emerged as a powerful analytical technique for the QC of HMs because it can be used for simultaneous and rapid analysis of primary or secondary metabolites with good sensitivity (Kim et al., 2010; Imai et al., 2020). Chemical fingerprints can also be obtained from MS spectra which readily provide information on the presence of certain metabolites or elements within the HM samples based on their masses (Yang and Deng, 2016). Besides chemical fingerprints, molecular fingerprints from the plant DNA can serve as a great authentication and standardization tool (Zhokhova et al., 2019). Some advantages and disadvantages of these different methods in combination with chemometrics are shown in **Table 1**.

4.1 Spectroscopic Fingerprinting

FTIR and NMR spectroscopies are commonly used for QC and herbal authentication through fingerprint profiling. FTIR is one of the most commonly used spectroscopic techniques, which can detect microgram levels of samples (Arendse et al., 2021). FTIR spectroscopy operates in the mid-IR region which corresponds to wavenumbers of 4,000–400 cm^{-1}. Functional groups of HM components can absorb IR photons at specific frequencies (or wavenumbers), resulting in fingerprint spectra that can be used for herbal authentication (Azlah et al., 2020). To assist data interpretation, chemometrics tools, mainly exploratory data analysis and pattern recognition, can be used.

The QC of different extracts of *Sonchus arvensis* (known locally in Indonesia as *Tempuyung*) was successfully carried out by FTIR spectroscopy combined with chemometrics (Rafi et al., 2021). PCA was used for the classification of the extracts, while PLS was applied for finding functional groups responsible for the antioxidant activity. FTIR spectra at combined wavenumbers of 3,200–2,800 cm^{-1} and 1800–400 cm^{-1} that were previously subjected to pre-processing using standard normal variate provided distinct clusters for the different extracts. PC1 and PC2 described 95% of the total variance within the dataset (PC1 and PC2 explained 79% and 16% of the variance, respectively). According to the loading plot of the PLS regression, the O–H (at 3,500–3,300 cm^{-1}) and C–O (at 1,205–1,124 cm^{-1}) bonds, which are attributed to the phenolic compounds, gave a significant contribution to the antioxidant activity of *S. arvensis* leaf extracts. A similar approach was also used for the QC of *Phyllanthus niruri* plants that were grown at different altitudes (Kartini et al., 2021).

ATR-FTIR and Raman spectroscopy have been used for the QC of turmeric that was adulterated with metanil yellow (MY), a toxic azo dye (Dhakal et al., 2016). Due to its similar appearance to turmeric, MY may be added to turmeric powder. FTIR spectra at 650–4,000 cm^{-1} can be used to detect the presence of MY in turmeric. Peaks between 1,628–1740 cm^{-1} were specific to turmeric. These peaks are

TABLE 1 | Advantages and disadvantages of fingerprinting methods for the standardization and quality control of herbal medicines.

Methods	Advantages	Disadvantages	References
Vibrational spectroscopy (NIR; mid-IR and Raman)	Rapid, applicable to both raw materials and processed samples (e.g,. extracts, finished HM products), requires minimum to no chemical solvents and reagents during sample pretreatment, non-destructive, enables online analysis	No separation capacity, standardization and quality control of HMs with complex components must be supported by chemometrics methods	Li et al. (2020c), Huck (2015)
NMR spectroscopy	Non-destructive and non-invasive, environmentally friendly, relatively rapid and easy to use on a regular basis, minimum sample preparation, can provide structural information of components of complex mixtures without pre-isolation/purification, suitable for metabolite fingerprinting of HMs	Low sensitivity, signal overlapping in complex HMs, relatively sophisticated and expensive instruments, the use of chemometrics software is inevitable to treat the large data generated	Pacholczyk-Sienicka et al. (2021)
Chromatography	Can separate target compounds in HM matrices into fractions or isolated compounds, wide suitability, high resolution, selectivity, sensitivity, and can be fully automatable operation; By using HR-MS/MS detector, the chemical structure of target peaks can be predicted and determined	Time-consuming, needs extraction and stability studies for standards and samples, high cost for sophisticated instruments (LC-MS/MS); Needs peak alignments and retention time correction for each of samples prior to multivariate analysis	Kharbach et al. (2020), Li et al. (2020b)
Capillary electrophoresis	High separation capability, can be applied in either single marker analysis, fingerprinting, or metabolomic studies for quality control of HMs, low sample and reagent consumption, relatively lower cost of instrumentation compared to HPLC/GC.	Low resolution for nonpolar or noncharged analytes unless coupled with other partition-based separation techniques, lower sensitivity compared to chromatographic techniques due to the low amount of sample used	Hou et al. (2019), Gong et al. (2021)
Direct MS	Capable of rapidly separating analytes in complex HM matrices based on the mass per charge, many ambient MS techniques are available and require only minimal to no sample preparation, some techniques support the imaging of chemical fingerprints	MS detector is relatively more expensive than other detectors, ionization efficiency may vary among techniques and/or sample matrices which could result in low reproducibility	Freitas et al. (2019), Pereira et al. (2021), Zhang et al. (2022)
DNA barcoding/ fingerprinting	Enable authentication of medicinal samples to species level, can detect adulteration from even closely related species, suitable for plant genotyping to create standardized medicinal crops	Does not provide any information on metabolite contents of the HMs, cannot detect adulterants from different parts of plants from the same species	Hadipour et al. (2020), Hadipour et al. (2020)

correlated to the vibration of carbonyl groups, which are absent in MY. Moreover, the peak at 1,140 cm^{-1} was specific to MY and demonstrated a linear correlation between the actual and predicted concentrations of MY (R = 0.95). Raman spectroscopy at 100–3,700 cm^{-1} could also be used for the quantification of the adulterant. A Raman peak at 1,406 cm^{-1} showed a linear correlation (R = 0.93) between the actual and predicted concentrations of MY. FTIR could detect MY at 5% concentration, whereas Raman could detect down to 1%. However, the performance characteristics including accuracy and precision were not stated. Both parameters are required to assess systematic and random errors, respectively.

Proton (^{1}H) and carbon (^{13}C) NMR spectroscopy are extensively applied for the QC of HMs due to the unique fingerprints generated from the interaction between molecules and certain radio waves. This interaction results in changes in the spin direction. With the development of two-dimensional (2D) NMR techniques such as J-resolved, heteronuclear single quantum correlation, and heteronuclear multiple bonds correlation, the techniques have the potential to be standardized as analytical fingerprinting techniques for HM standardization (Sun et al., 2018).

NMR combined with chemometrics have been applied to classify HM samples based on their geographical origins. Recently, the suitability of ^{1}H-NMR coupled with PCA and orthogonal PLS-DA (OPLS-DA) was reported for the differentiation of three *Curcuma* species namely *C. longa, C. xanthorrhiza*, and *C. manga* from different origins in Indonesia (Nurani et al., 2021). There are 14 metabolites identified from the ^{1}H-NMR spectra that are responsible for generating the classification model. These metabolites include curcuminoids (curcumin, dimethoxy- and bis-desmethoxycurcumin), some carbohydrates, and amino acids. In addition, NMR in combination with PCA and OPLS-DA could differentiate *C. longa, C. xanthorrhiza, and C. manga* from different origins as shown in **Figure 2**. The validation results, as carried out using the permutation test, indicate that the developed model demonstrated goodness of fit (R^2 value >0.8) and good predictivity (Q^2 >0.45).

Another geographical classification was reported for Asian red pepper powders that were distributed in Korea (Lee et al., 2020). Analysis of the ^{1}H-NMR spectra showed that several metabolites played significant roles in differentiating the samples. For example, higher tyrosine and alanine contents were found in

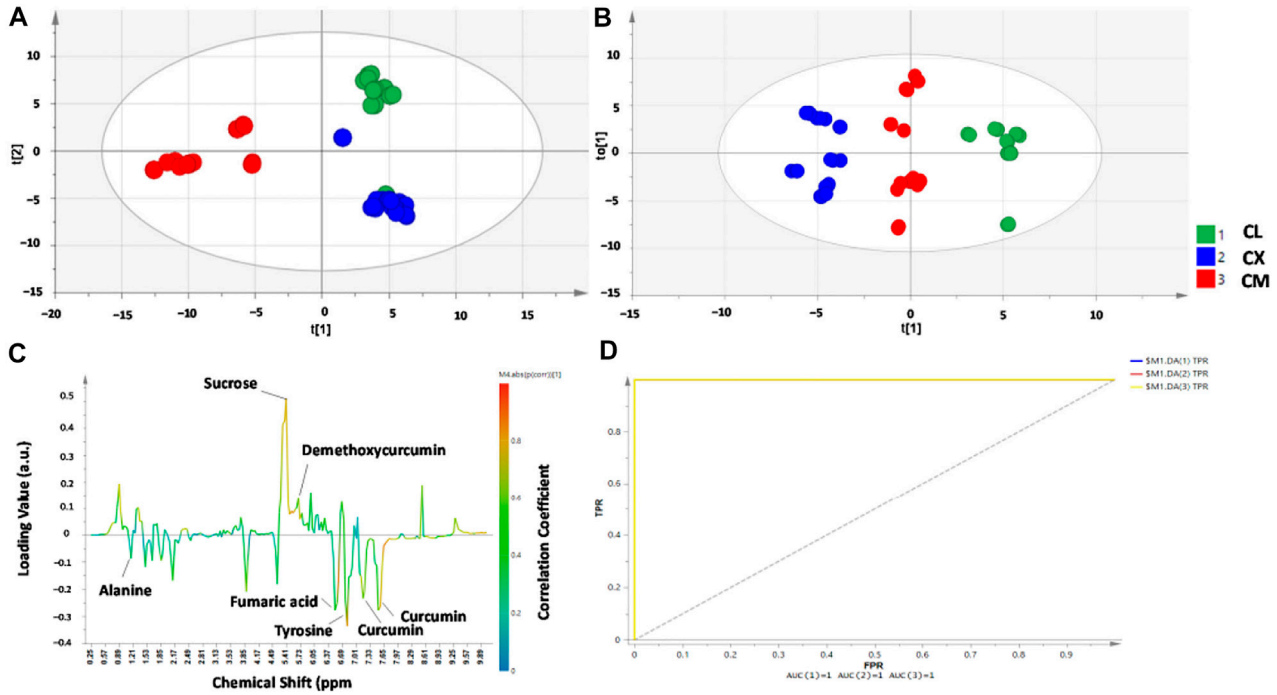

FIGURE 2 | Partial least square-discriminant analysis (PLS-DA) score plot **(A)**, orthogonal projections to latent structures-discriminant analysis (OPLS-DA) score plot **(B)**, OPLS-DA S-line correlation plot **(C)**, and receiver operating characteristic (ROC) curve **(D)** for differentiation and classification of *C. longa* (CL), *C. xanthorrhiza* (CX), *and C. manga* (CM) from different origins. Reproduced from Nuraini et al. (2021) under the terms of Creative Commons Attribution (CC BY) license (https://creativecommons.org/licenses/by/4.0/).

samples from Vietnam, whereas the quantities of *a*-glucose, *ß*-glucose, adenosine, and tryptophan were higher in samples from Korea. Using canonical DA, 15 blind samples were correctly classified and one sample from China was misclassified due to the high contents of *a*-glucose and *ß*-glucose. Difference in sugar contents between HMs was also reported from serrano pepper grown in two areas in Mexico: Veracruz and Oaxaca (Becerra-Martínez et al., 2017). There was a distinct difference in the concentrations of metabolites including glucose, fructose, sucrose, and citrate between the two sample groups. In addition, lactate was only present in samples from Oaxaca whilst succinate was only detected in Veracruz samples. Differentiation using PCA provided R^2 and Q^2 values of 0.936 and 0.875, respectively. A better classification was obtained with OPLS-DA with $R^2X = 0.923$, $R^2Y = 0.999$, and $Q^2 = 0.996$. NMR in combination with PCA and OPLS-DA is also successful for the classification and authentication of *C. xanthorrhiza* from adulterant of *C. aeruginosa*. The decreased contents of curcumin as determined by HPTLC in adulterant levels of ≥40% of *C. aeruginosa* in *C. xanthorrhiza* rhizome could indicate the adulteration practice of *C. xanthorrhiza* with other rhizomes. Morever, OPLS-DA is successfully applied for the classification of pure and adulterated *C. xanthorrhiza* with higher R2X (0.965), R2Y (0.958), and Q2 (cum) (0.93) as shown in **Figure 3** (Rohman et al., 2020).

Using an appropriate selection of variables obtained from molecular spectroscopic measurements (NIR, FTIR, NMR) and suitable chemometrics techniques, quality and standardized HMs can be obtained. In addition, the combination of chemometrics and spectral datasets is a proven tool to authenticate HMs from adulterants and assure the geographical origins of the HMs. Authentication by spectroscopic methods must be accompanied by the analysis of certified reference herbal materials or product formulations containing similar compositions to those of raw materials or products being investigated (Coskun et al., 2021).

4.2 Chromatographic Fingerprinting

Due to the complexity of plant materials and their extracts, chromatographic methods (e.g., TLC, HPLC, and GC) coupled with spectroscopic detectors (UV/diode array detector (DAD), MS, NMR) are mostly applied as standardization methods of herbal drugs. Since different compounds could have identical UV spectra, MS or HR-MS/MS becomes the detector of choice. While LC-NMR can also be applied, the cost of analysis using this instrument could be expensive. Some recent reviews (2020–2021) discussing the application of a combination of chromatographic fingerprinting and chemometrics for the quality assessment of herbal drugs have been published (Balekundri and Mannur, 2020; Li et al., 2020b; Kharbach et al., 2020; Shen et al., 2020; Klein-Junior et al., 2021). Generally, the objectives of fingerprinting methods are 1) to determine seasonal and geographical locations, 2) taxonomic identification, 3) assessment of extraction processes, and 4)

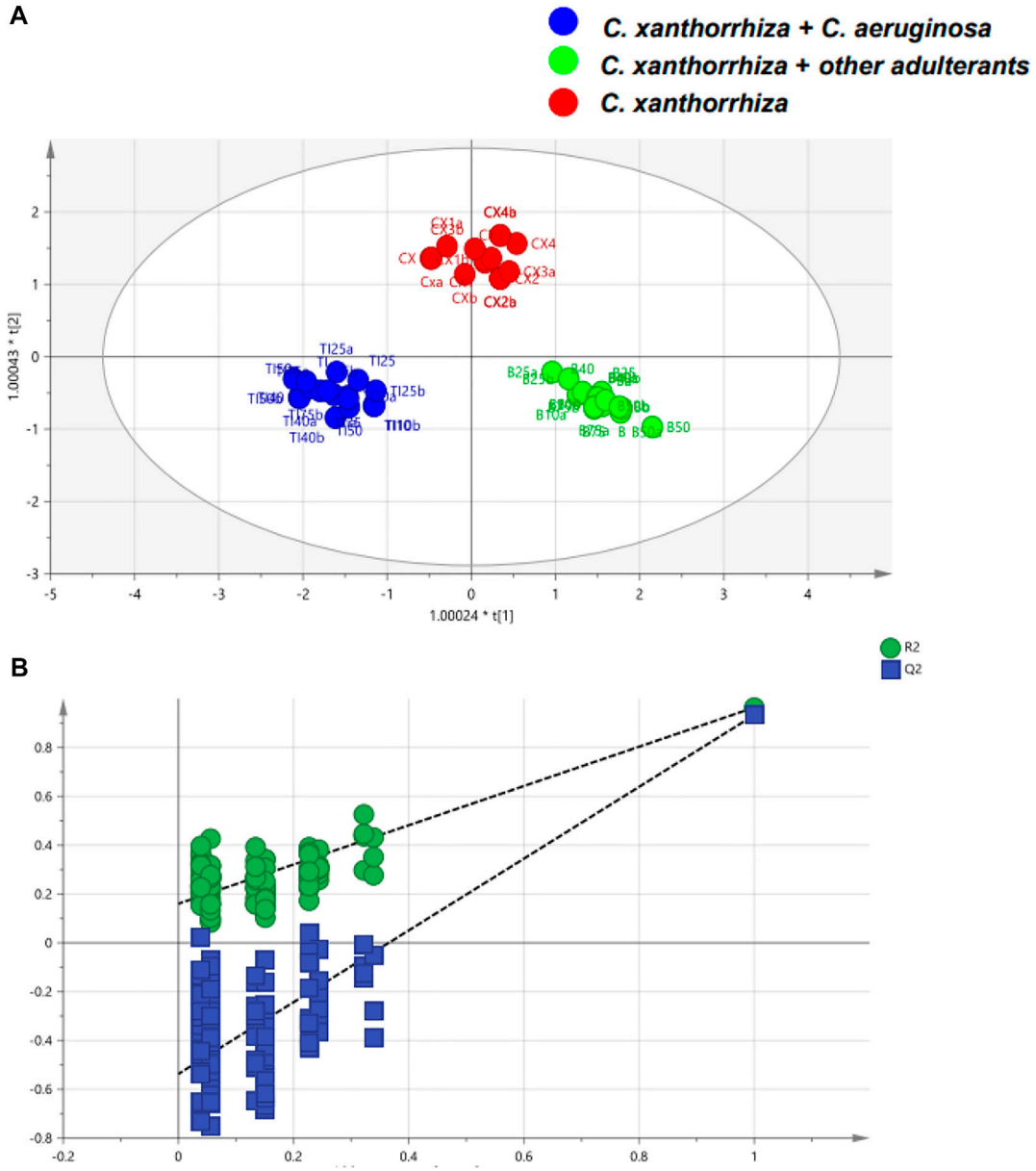

FIGURE 3 | The orthogonal projections to latent structures-discriminant analysis (OPLS-DA) score plot of pure and adulterated *C. xanthorrhiza* with *C. aeruginosa* **(A)** and permutation test of OPLS-DA model **(B)**. Reproduced from Rohman et al. (2020) under the terms of Creative Commons Attribution (CC BY) license (https://creativecommons.org/licenses/by/4.0/).

quality control and authentication of the herbal drugs (Kharbach et al., 2020). If the chromatographic fingerprint of an herbal drug is identical to its botanical reference material or standardized extract, it can be assumed that the herb shows a phyto equivalence to the standard (Sahoo et al., 2010). Phyto equivalence means the bioactivities and/or toxicities of the herbal drug are identical to its standard based on the similarity of their metabolite contents. Therefore, chromatographic fingerprinting can be applied as a standardization tool for ensuring the efficacy and safety of herbal drugs if their quality markers have not been yet specified.

Chromatographic fingerprinting can be categorized into characteristic chromatograms and fingerprints. A characteristic chromatogram is a chromatogram that allows the selection of one or several components/peaks as an identification marker for the quality control of HMs. Fingerprint analysis is a semi-quantitative analysis based on the whole peaks or components in the samples. Both methods are described in the Chinese Pharmacopoeia 2015 (Shen et al., 2020). Most of the current Pharmacopoeias, as described in **Section 2**, applied HPTLC fingerprints for the identification of herbs. The accuracy of the fingerprint as a standardization tool depends on the instrument,

the more sophisticated the instrument the more accurate the fingerprints are. To our knowledge, LC-HR-MS/MS is the most accurate method for performing chromatographic fingerprinting. GC-MS is the method of choice for thermo-stable samples. For complex samples, pre-treatments using headspace solid-phase microextraction (HS-SPME) can be applied (Balekundri and Mannur, 2020).

The drawbacks of chromatography are time-consuming sample preparation and/or extraction prior to chromatographic measurements (Li et al., 2020b). The extraction method could affect the metabolite profile of the samples. Thus, the selection of extraction solvents is crucial. The stability of the metabolites in the selected solvents must also be evaluated. The stability of metabolites can be evaluated by calculating the similarity values (i.e., R and c must be close to 1), performing PCA on the chromatograms, and observing variation/relative standard deviation (RSD) in the retention time of 5–10 important peaks of the QC samples (tight clustering) that are stored for a certain time. For example, the metabolites are considered stable if the RSD of the R_t is less than 5% (Indrayanto, 2018b). Bingbing et al. recently studied the stability of herbal extracts at 0, 4, 6, 8, 12, and 24 h time intervals (Bingbing et al., 2021). Six peaks in the GC-MS total ion chromatogram were selected as markers for determining the retention time (R_t) and peak area (PA). RSDs of the R_t and peak area from the 6 peaks were <0.04% and <10%, respectively. For the validation of chromatographic fingerprinting methods, precision (intra- and inter-day) should be then evaluated using QC samples if the stability of QC samples can be confirmed (Indrayanto, 2018b).

The raw data of the first order chromatographic fingerprinting (R_t/R_f vs intensity of detector response) should undergo pre-processing prior to further evaluation using chemometrics. Some of these pretreatments include baseline correction, smoothing, and peak alignment. Numerous approaches for peak alignment and retention-time correction, including correlation optimized warping, parametric time warping, target peak alignment, dynamic time warping, fuzzy warping, and semi-parametric time warping, have been generally applied (Li et al., 2020b; Kharbach et al., 2020). Examples of chromatographic methods applicable for the first-order chromatographic fingerprinting are HPLC-fixed UV/Vis, HPLC-evaporative light scattering detector (ELSD), HPLC-refractive index detector (RID), GC-flame ionization detector (FID), HPTLC-densitometry. However, the identity and purity of the observed peaks cannot be confirmed absolutely by the first-order fingerprint method. Peaks that have identical R_t or R_f do not necessarily represent identical compounds, and a single peak may contain more than one compound.

Second-order chromatographic fingerprints can be obtained using HPLC-DAD, LC-MS, and GC-MS. The data consist of pair data of R_t or mass-per-charge (m/z) or wavelength vs intensity. Because many structurally related compounds have similar UV/Vis spectra, the applications of HPLC-DAD fingerprinting have limitations (Klein-Junior et al., 2021), leaving LC-MS as the method of choice. LC-MS fingerprint data are typically processed as follows prior to chemometrics analysis: 1) determining molecular features, then 2) retention time alignment, 3) bucketing, 4) filtering, scaling, normalization, and finally 5) data analysis (Indrayanto, 2018b). Automatic time alignment of R_t-m/z pairs for certain time intervals and mass ranges (e.g. 100–1,000 Da) can be performed using software supplied with the LC-HRMS instrument. Data can be grouped automatically into buckets with R_t-m/z pairs (x minutes-a Da) with a mass tolerance of b Da (Ratih et al., 2019). Detailed methods for processing and bucketing the raw LC-MS data have been discussed in a previous publication (Thiele et al.). Recently, a new algorithm based on sub-window factor analysis (SFA)-HRMS for peak alignment of LC-HR-MS data was proposed (Zeng et al., 2021). Initially, region of interest (ROI) searching and fuzzy matching are combined to transform the raw data sets into equidistant matrices effectively. Protocols for data pre-treatment, processing, and validation for chromatographic fingerprinting using LC-MS and GC-MS have been described in detail in previous publications (Want et al., 2010; Blaise et al., 2021).

Third-order chromatographic fingerprints can be generated by using LC-MS/MS, GC-MS/MS (R_t, m/z_1, m/z_2), or 2D-LC/GC-DAD/MS (data: R_{t1}, R_{t2}, wavelength, or m/z) (Li et al., 2020b). Algorithms and workflows for effective chromatographic fingerprinting are available within the majority of commercial software packages dedicated to GCxGC and other comprehensive two-dimensional chromatography platforms (Stilo et al., 2020). The theory, experiments, and various chemometrics processing methods of multi-way chromatographic methods (e.g., 2D-LC- DAD/MS, 2D-GC-MS, GC-MS/MS, three-dimensional (3D)-GC-MS) have been previously discussed (Escandar and Olivieri, 2019). The application of multivariate curve resolution-alternating least-squares (MCR-ALS) and parallel factor analysis (PARAFAC) for multi-way chromatographic methods have also been recently reviewed (Anzardi et al., 2021).

Qualitative and quantitative chromatographic fingerprinting methods can be applied as QC tools in all stages of herbal drugs production i.e., incoming materials, in-process control, finished products, and stored samples (Indrayanto, 2018a). As described in **Section 2**, the official identification method for herbs (incoming materials) is comparing the HPTLC fingerprint of the samples to the authentic standards or BRMs visually. Due to some limitations in visual observation, evaluation of the chromatographic fingerprints by calculating similarity values (R, c) and/or multivariate analysis (PLS-DA, SIMCA, LDA, etc.) is more recommended. The application of second-order chromatographic fingerprinting (GC-MS, LC-MS) will yield more accurate results for herb identification.

To have the best consistency in each production batch, the composition of herbs/extracts should be evaluated qualitatively and quantitatively for every stage of the production process (Heinrich et al., 2020; Wei et al., 2020). The quality assessment of herbal drug preparations is typically not easy due to the complex nature of the metabolite contents and their possible variation. It is well known that many external factors can affect the metabolite contents qualitative and quantitatively. Extraction methods and material processing

could also affect the stability of the metabolites. The availability of BRMs and stable standardized extracts are crucial for the quality assessment of each stage of herbal drug production. Some recent publications on the application of chromatographic fingerprinting for QC assessment of herbal drugs during their production are discussed below.

Yan et al. proposed the applications of macro qualitative similarity (S_m) and macro quantitative similarity (P_m) for evaluating the compositions (qualitative, semi-quantitative) of the herbal drug preparations during production using HPLC-UV fingerprint (Yan et al., 2021). Reference fingerprint (RFP) of the standard preparation (SP) was used. Establishing an SP for an herbal drug requires multi-source raw materials or preparations; generally, not less than 15 batches of samples for a single raw material and 100 batches of samples for a herbal preparation. A qualified product requires its $S_m \geq 0.90$, $80\% \leq P_m \leq 120\%$, and qualified content of markers. The standard value of RFP should be $S_m \geq 0.95$ and $P_m \approx 100$. Yao et al. applied a multi evaluation method for a non-prescription herbal drug mixture using ultra-performance liquid chromatography (UPLC) fingerprinting at 254 nm, compound identification via UPLC-triple time of flight (Triple-TOF)-MS analysis, and quantitative determination of the compounds via UPLC-UV-254 nm (Yao et al., 2019). Although similarity levels of the fingerprints were 0.935–0.984, PCA using 7 detected compounds showed 2 clusters. These results showed that the application of first-order chromatographic fingerprinting has limitations. Ji et al. compared the profiles of compounds in traditional Chinese medicine (TCM) tablets and their herbal components using 2D-LC-quadrupole-TOF (q-TOF) MS (Ji et al., 2018). Fifty-four compounds were identified from the total 465 peaks found in the tablet samples. Twelve out of 465 peaks could not be found in the chromatograms of the herbal components, suggesting further investigation on the compatibility of the herbal components. Differences in LC-q-TOF MS profiles of raw materials and processed Chinese herb preparation have also been reported (Li et al., 2021). These differences affected the disposition of metabolites in an *in-vivo* study using rats. Another group (Li H. et al., 2020) applied multiple fingerprint profiling of polysaccharides in Chinese traditional drugs using FTIR, HPLC-UV, and size exclusion chromatography (SEC)-RID for quality determination. Twelve batches of these herbal drugs showed a high degree of similarity. Unfortunately, the authors did not discuss the advantages of using fingerprints from polysaccharides in comparison with those from the whole metabolites. Zhao et al. studied the LC-MS profiles and anti-proliferative effects of 22 commercial gingers (Zhao et al., 2020). These data were then evaluated using PCA. The study demonstrated that variation in the fingerprint profiles that results from differences in chemical compositions could have a significant impact on the efficacy and bioactivity of the ginger extracts.

The discussions above show that the quality assessment of herbs and/or plant extracts for research and QC purposes can be only well performed using chromatographic fingerprinting if the authentic BRM and/or standardized extract are available and possess desired pharmacological activities. Identical chromatographic fingerprints mean the sample is phyto equivalent to its standard (Sahoo et al., 2010). It would also be useful if the regulatory agency in each country could produce official BRMs for all herbs. Due to many environmental factors that can affect the metabolite contents, the application of official BRMs from other countries is not recommended (Bensoussan et al., 2015; Indrayanto, 2018b). For QC in the production lines, pharmaceutical industries should develop a standardized mixture of herbs and/or extracts with exact compositions. Without these standardized mixtures, it is impossible to have herbal drugs with consistent efficacy. Further research should be conducted to determine the quality markers of each herb/product to avoid the need for performing chemical profiling at the QC laboratories in pharmaceutical industries.

4.3 Electrophoretic Fingerprinting

Fingerprinting using electrophoresis presents great advantages for the analysis of complex herbal medicines due to its separation capability. Electrophoretic techniques have been used for decades to assist both molecular and chemical fingerprinting. Charged molecules such as nucleic acids and metabolites can be well separated using these techniques to obtain fingerprints (Shen et al., 2019; Gong et al., 2021). Gel electrophoresis using agarose or polyacrylamide gel is often employed to quickly confirm the presence of certain amplification products or perform sequencing in DNA barcoding and fingerprinting (Shen et al., 2019; Hadipour et al., 2020). Capillary electrophoresis (CE) has also been extensively explored in chemical fingerprinting for the standardization and quality control of herbal medicines (Johnson and Lunte, 2016; Gong et al., 2021).

CE has been used for fingerprint analyses of various raw materials and products containing medicinal plants such as *Ginkgo biloba* (Johnson and Lunte, 2016), *Smilax glabra* Roxb. (Zhang and Cheung, 2011), *Carthamus tinctorius* L.(Sun et al., 2003), *Scutellaria baicalensis* (Yu et al., 2007; Wang Y. et al., 2014), *Dendrobium candidum* (Zha et al., 2009), *Glycyrrhiza uralensis* (Ma et al., 2017; Gong et al., 2021), etc. Gong et al. recently reported a quality evaluation of Compound Liquorice Tablets (a Western-Chinese herbal preparation containing liquorice extract, powdered poppy, camphor, star anise oil, and sodium benzoate) using CE with UV detection (Gong et al., 2021). Tablets were ground, dissolved in 0.5% phosphoric acid-acidified methanol-water (80:20 v/v) mixture, filtered, and subjected to CE separation using a fused silica capillary at 15 kV separation voltage and 25 mM sodium tetraborate: acetonitrile (5:1) background electrolyte.

The composition of background electrolyte (BGE) plays a pivotal role in fingerprint analysis using CE. The electrophoretic mobility of the analytes is dictated by the hydrated radius and overall charge of the molecules. Therefore, buffered solution at a certain pH is often used as a component in BGE to protonate or deprotonate neutral molecules. For example, the pH of the BGE may be set in the range of 8.7–10.0 using borate buffer in the analysis of HMs containing flavonoids and phenolic compounds so that the compounds will carry at least one negative charge (Chen et al., 2011; Johnson and Lunte, 2016; Roblová et al., 2016). In addition to providing buffering capacity in this pH range, borate can form complexes with the phenolic compounds and

increase their overall sizes and effective charges (Johnson and Lunte, 2016). For example, Johnson and Lunte used 25 mM ammonium biborate in 10% methanol (pH 9.3) to perform CE separation of 14 flavones, flavanones, and flavonols with similar structures and several representative glycosides from plants (Johnson and Lunte, 2016). Acidic BGE such as a mixture of methanol-acetonitrile (85:15 v/v) containing acetic acid 0.5% and ammonium acetate 90 mM was reported for the analysis of alkaloids from Amaryllidaceae (Gotti et al., 2006). Under this condition, the alkaloids (i.e., galanthamine and haemanthamine) are protonated and can be resolved from one another using CE. In another experiment on CE fingerprinting of alkaloids from *Sophora flavescens* (Hou et al., 2019), coordination additives were found to play a larger role in CE separation than pH condition does. The additives possibly assisted the boron anion complexation with alkaloids, enhancing the differences in mobility among analytes.

Similar to chromatographic fingerprints, qualitative and quantitative analysis using CE fingerprints can be performed in multiple ways. One of the reported approaches is classification into several quality grades based on the quantitative fingerprinting method (QFM). In this method, the similarity of a sample to reference material is evaluated based on several criteria and then the sample is assigned to one of the 8 grades (i.e., 1 = best, 2 = better, 3 = good, 4 = fine, 5 = moderate, 6 = common, 7 = defective, and 8 = inferior) based on the similarity level (Liu et al., 2015; Gong et al., 2021). Samples that fall into grades 1–5 are considered qualified. QFM typically uses 3 criteria to determine the quality grade of the sample: 1) qualitative similarity, which represents the similarity in the number and distribution of fingerprint peaks between the sample and reference, 2) quantitative similarity, which reflects the similarity in the overall content of the fingerprints, and 3) fingerprint variation coefficient, which represents the qualitative variation/dissimilarity of the fingerprints (Liu et al., 2015). Based on how these 3 criteria are calculated, several QFMs have been reported such as the simple quantified ratio fingerprint method (Liu et al., 2015), limited ratio quantified fingerprint method (Chen et al., 2018), equal weight ratio quantitative fingerprint method (Gong et al., 2021), linear quantitative profiling method (Hou et al., 2019), averagely linear quantified fingerprint method (Zhang et al., 2019), systematic quantified fingerprint method (Lan et al., 2019), and average method of systematic quantified fingerprint method (Wang et al., 2021b).

The relationship between the CE fingerprints and other properties such as biological activities can also be further investigated using PLSR (Chen et al., 2018; Hou et al., 2019). Other chemometric methods for classification such as PCA and HCA have also been explored on CE fingerprints (Iino et al., 2012; Roblová et al., 2016; Hou et al., 2019). Validation of CE methods typically follows the same protocols and criteria as those of chromatographic methods. CE methods are validated by evaluating their linearity, limit of detection and quantification, precision, and accuracy, whereas the chemometric calibration models are evaluated based on the R^2 and RMSE values (Hou et al., 2019).

CE fingerprinting methods offer advantages for the standardization and quality control of herbal medicine such as low reagent consumption, relatively high analysis speed, and improved separation efficiency. However, since analytes are separated based on their electromigration, the separation of neutral metabolites such as terpenes in CE may be challenging. This could be a problem if neutral metabolites are major constituents and play a significant role in HM differentiation/classification. Adding another separation dimension by performing micellar electrokinetic chromatography (MEKC) and/or using an MS detector could potentially solve the issue. MEKC improves the separation of neutral compounds by combining the electrophoretic-electroosmotic mobility of the analytes and their partitioning between BGE and surfactant micelles (Liu et al., 2015). MS can help separate unresolved peaks into their constituents, provided that none of the constituents experiences severe ionization suppression under the CE-MS condition. Alternatively, chromatographic separation can be opted for.

4.4 Direct MS Fingerprinting

Not only is MS a powerful detector in hyphenated techniques such as HPLC-MS and CE-MS, but it has also been utilized to perform direct fingerprint analyses for herbal standardization and quality control. Direct MS has been used to collect fingerprints of herbal materials from a variety of plants such as *Allium sativum* (Pereira et al., 2021), *Fritillaria sp.* (Xin et al., 2014; Wang et al., 2017), *Panax quinquefolium* L. (Chan et al., 2011), *Origanum sp.* (Massaro et al., 2021), *Gastrodiae elata* (Wong et al., 2016), *Cynanchum sp.* (Jun et al., 2016), etc. Ambient MS in which analytes are ionized at ambient pressure is often employed (Xin et al., 2014; Massaro et al., 2021; Pereira et al., 2021), although inductively coupled plasma (ICP) MS for multi-element fingerprinting (Zhao et al., 2017) and matrix-assisted laser desorption/ionization (MALDI) MS (Lai et al., 2012) have also been reported. Ambient ionization techniques applicable to herbal materials and products include desorption electrospray ionization (DESI) (Talaty et al., 2005; Freitas et al., 2019), ESI on solid substrates (Deng and Yang, 2013; Hu et al., 2014; Wang H. et al., 2014; Xin et al., 2014; Jun et al., 2016), tissue ESI and related techniques (Chan et al., 2011; Liu et al., 2011; Hu et al., 2013), extractive ESI (Lee et al., 2021; Zhang et al., 2022), direct analysis in real-time (DART) (Kumar et al., 2015; Wang et al., 2021a), and desorption atmospheric pressure chemical ionization (DAPCI) (Pi et al., 2011).

In DESI, analytes in herbal samples are ionized/desorbed by impinging the surface of the samples using charged solvent droplets. This technique allows for the analysis of samples without any pretreatment. DESI also enables surface imaging for mapping the spatial distribution of secondary metabolites within the sample specimen (Freitas et al., 2019). DESI has been applied to raw herbal materials such as leaves, stems, roots, and flowers as well as dosage forms such as tablets and capsules (Yang and Deng, 2016). DESI on powdered samples may be challenging because the powder could spatter after being hit by the solvent droplets, hindering analyte desorption and/or ion transfer to the mass analyzer. To overcome this problem, powdered samples can

be compressed into thin tablets or dissolved in a volatile solvent and applied as a thin film on a solid surface prior to MS analysis (Crawford et al., 2017).

Similar strategies are used in solid substrate-based ESI techniques in which samples are placed onto/into solid supports such as triangular paper (Deng and Yang, 2013), wooden toothpicks (Xin et al., 2014; Pereira et al., 2021), aluminum foil (Hu et al., 2014), and pipette tips (Wang H. et al., 2014). Paper and wooden toothpicks are porous materials that can hold samples. Paper-spray ionization is typically applied to liquid samples (Deng and Yang, 2013), whereas the wooden tip ESI can be applied to both liquid and solid samples (Xin et al., 2014; Pereira et al., 2021). The toothpick can be directly dipped into liquid samples or pre-wetted with a suitable solvent followed by dipping into solid samples. A larger quantity of samples such as bulk materials can be loaded into a folded aluminum foil or pipette tip (Wang H. et al., 2014; Hu et al., 2014). The pointed side/tip of the triangular paper, toothpick, folded foil, or pipette tip is then placed toward the MS inlet while applying a high voltage to the sample/support for ionizing the analytes. Alternatively, the high voltage can be applied to the MS inlet while the sample is grounded (Hu et al., 2013). This technique can preserve the sample and therefore, is suitable for real-time monitoring of secondary metabolites in unharvested medicinal crops. Pipette tips loaded with powdered samples can also be connected to a solvent-filled syringe to perform simultaneous extraction and spray ionization (Wang H. et al., 2014).

DART produces analytical results similar to those of DESI. The difference between the techniques lies in the medium used to ionize the samples. In DESI, the sample surface is exposed to an electrospray plume, while an ionizing noble gas stream (i.e., metastable He) is used in DART (Gross, 2006). Using DART, botanical samples can be directly analyzed without any sample preparation (Kumar et al., 2015; Wang et al., 2021a). Ionizing gas is also used in DAPCI to desorb/ionize analytes from the plant samples (Pi et al., 2011). A high voltage is applied to produce a corona discharge that ionizes the carrier gas (e.g., He, N_2, or Ar). This gas is then pneumatically directed to the sample surface.

After obtaining mass spectra fingerprints, multivariate data analysis can then be applied to the datasets to extract the information of interest. Exploratory data analysis via PCA is often done to reveal certain grouping or clustering of medicinal samples based on the characteristics of MS fingerprints (Pi et al., 2011; Xin et al., 2014; Pereira et al., 2021). The exploratory analysis only tells whether known samples can be differentiated from one another based on the score plot. To predict which class or cluster an unknown sample belongs to, prediction models using supervised classification methods can be implemented. For example, Zhang et al. recently performed PCA and OPLS-DA on 90 *P. notoginseng* samples grown under different conditions (Zhang et al., 2022). Results from the PCA and OPLSDA are in agreement in which there were 12–14 MS peaks that mainly contributed to the differentiation. These peaks, included sucrose, fructose, several ginsenosides (Rg1, Rf, Rb1, Noto-R1, malonyl-Rb1, malonyl-Rg1, malonyl-Rf, Rd, and Re), linoleic acid, palmitic acid, and malic acid, can be used as key indicators to discriminate samples of different origins, commercial specifications, and growing conditions. The parameters R^2Y and Q^2 of the OPLS-DA model were 0.939 and 0.875, respectively, showing good predictive ability. Prediction models based on PLS-DA and MS fingerprints have also been built for other plant materials, providing up to 97% accuracy in the prediction rate (Xin et al., 2014; Pereira et al., 2021).

Massaro et al. validated a DART-MS fingerprinting method for oregano authentication by SVM (Massaro et al., 2021). They first conducted exploratory PLS-DA on 4 independent data sets (i.e. spectra collected with two different extraction solvents and two ion modes in MS). The most discriminated variables were selected from each data set and then merged using a mid-level data fusion approach. These variables were used to build an SVM classifier which was then validated by Monte Carlo cross-validation and against an independent set of oregano samples (external validation). A 90% prediction accuracy was reported with specificity and sensitivity of 92% and 95%, respectively. Incorrectly classified samples included samples containing adulterants not used in building the prediction models, showing that the classification ability of the model largely depends on the calibration data sets. Another authentication study based on direct MS fingerprints was carried out by Wang et al. using PLSR (Wang et al., 2017). Pure *Fritillaria unibactreata* was mixed with adulterants at 0%–100% w/w concentrations to develop the prediction model. Linearity and reproducibility of the method were assessed using QC samples containing pure herbs at several concentrations in five replicates. The R^2 and RMSEP of the prediction model were 0.9072 and 0.1004, respectively. The model especially suffered from a lack of accuracy when used to analyze samples at low concentrations of target herbs (<10%). Although this was not the best system, the model can still be useful for the rapid screening of adulterated samples. Better results were obtained from PLSR models constructed using hyphenated techniques such as UPLC-q-TOF/MS and UPLC-triple quadrupole (TQ)/MS fingerprints (Wang et al., 2017), suggesting that interference from matrix components may be prominent in direct MS.

The main advantage of performing direct MS over hyphenated methods is the speed of analysis and high sampling throughput. In addition, several direct MS techniques allow minimum destruction to the sample which is desirable in real-time monitoring/fingerprinting of metabolites in living organisms. This benefit can be exploited for rapid monitoring of metabolite profiles in unharvested plants to determine the optimum growing conditions or harvesting age. However, direct MS may suffer from matrix effects which could yield inaccurate identification and/or quantification. Increasing the number of sampling spots and/or using extractive ESI to selectively take the metabolites out of the plant matrix could potentially mitigate the issue. Nevertheless, the method must be thoroughly validated to ensure the reliability of the results.

4.5 DNA Barcoding and Fingerprinting

DNA analysis has been used in herbal drug research to perform 1) authentication of medicinal plants, 2) detection of adulteration or

substitution with other closely related species, 3) breeding of medicinal plants, and 4) quality control and standardization of medicinal plant materials. In the context of plant authentication, DNA analysis is mostly used to differentiate among plant species, not individual plants within the species. This technique is often referred to as DNA barcoding. For example, Shen and coworkers reported authentication of *Drynaria rosii*, a traditional Chinese herb using DNA barcodes (Shen et al., 2019). To develop the barcodes, genomic DNA of *D. rosii* and other 6 closely related species (*D. sinica, D. bonii, D. delavayi, D. quercifolia, D. propinqua*, and *Pseudodrynaria coronans*) were polymerase chain reaction (PCR)-amplified, sequenced using the Sanger method, and aligned to generate a phylogenetic tree. The tree provided an evident clustering in which plant samples from the same species were clustered into one clade, showing its potential for differentiating *D. rosii* from adulterants. However, complications may arise if the tested sample is a mixture of herbs. The presence of sequences from multiple species may affect the placement of the sample within the clusters, hampering definite identification. Chosen markers for the authentication of articles of botanical origin must be specific enough to identify target and adulterant species in the samples, but also universal enough to prevent false-negative from closely related species (USP44-NF39, 2021c).

Various DNA barcodes have been made available online to assist authentication of herbal materials. Several barcoding databases that can be used include the Barcode of Life Data System (http://www.boldsystems.org), IdIt-ITS2 (http://its2-plantidit.dnsalias.org), PTIGS-IdIt (http://psba-trnh-plantidit.dnsalias.org), and Medicinal Materials DNA Barcode Database (http://www.cuhk.edu.hk/icm/mmdbd.htm) (Chen et al., 2014). The Consortium for the Barcode for Life (CBOL) proposed 7 plastid DNA regions for plant DNA barcoding including *atp*F-*atp*H, *rbc*L, *rpo*B, *rpo*C1, *mat*K, *psb*K-*psb*I, and *trn*H-*psb*A (CBOL-Plant-Working-Group et al., 2009). Many other barcodes have been reported in the literature and the choice of barcodes has been discussed in several review articles (Hollingsworth et al., 2011; Li et al., 2015; Zhokhova et al., 2019). Typically, these barcodes were evaluated based on their discriminating abilities. Combinations of barcodes from different loci are typically proposed to improve efficiency in plant species discrimination. CBOL recommended the 2-locus combination of *rbc*L and *mat*K for its ability to successfully discriminate species in 72% of cases and discriminate congeneric species in 100% of cases (CBOL-Plant-Working-Group et al., 2009). Another study revealed barcodes derived from the ITS2 region provided better discrimination efficiency for medicinal plants than the commonly used *rbc*L gene, with a discrimination efficiency of more than 90% at the species level (Chen et al., 2010; Zhang et al., 2015). ITS2 barcodes are relatively short (~200 bp) which are favorable for identification and quality control in herbal preparations, since plant DNA in these samples is often significantly degraded to <500 bp fragments (Zhokhova et al., 2019). A combination of ITS2 and *psb*A-*trn*H barcodes are available for most herbal plants listed in the Chinese, Japanese, Korean, Indian, United States, and European Pharmacopoeias (Chen et al., 2014). DNA barcodes for common medicinal plants in the tropics have also been reported (Tnah et al., 2019).

While these barcodes can discriminate even closely related species, co-amplification of the barcoding sequences in herbal preparations containing multiple plant species or excipients may negatively impact the DNA decoding. Also, the addition of excipients in large amounts may cause the barcode primers to preferentially amplify DNA from the excipients (Zhokhova et al., 2019). To overcome these problems, digital PCR or next-generation sequencing (NGS) can be integrated into the barcoding protocol. In digital PCR, DNA samples are diluted in a suitable buffer at several dilution ratios such that the final DNA concentration for the PCR template is approximately 1 molecule per μL (Morley, 2014; Zhokhova et al., 2019). Using this approach, a mixture of DNA from different plant sources or materials can be deconvoluted to improve the chance of low-abundant DNA molecules being amplified and detected. This method has been used for authentication of *Ginkgo biloba* in herbal dietary supplements (Little, 2014). Droplet digital PCR was reported by Yu et al. for qualitative and quantitative analysis of *Panax notoginseng* powder samples mixed with several adulterants (Yu et al., 2021). NGS allows for independent amplification of individual DNA sequences within the mixture and excludes any overlapping DNA sequences, enabling more accurate DNA decoding in multi-component herbal preparations. This approach has been applied to the authentication of various herbal supplements containing *Echinacea purpurea*, *Valeriana officinalis*, *Ginkgo biloba*, *Hypericum perforatum*, and *Trigonella foenum-graecum* (Ivanova et al., 2016). The applications of NGS for the identification and authentication of herbal products have been discussed in several review articles (Haynes et al., 2019; Lo and Shaw, 2019).

Although significant progress has been made, DNA barcoding in herbal preparations containing multiple components remains challenging. Method validation should always be performed to evaluate the reliability of the results. AOAC International has published guidelines for the validation of botanical identification methods (qualitative) and quantitative chemical methods for dietary supplements and botanicals (AOAC, 2019). However, translating these guidelines to DNA-based methods may not be trivial. DNA barcoding methods are often validated using raw plant materials and therefore become less appropriate for detecting adulterants in finished products. When developing a DNA barcoding method for detecting adulteration, it is also important to determine the limit of detection for each adulterant by creating mixtures of the target species with known amounts of possible adulterants.

DNA fingerprinting is a method for simultaneously detecting mini- or microsatellites (i.e., short sequences of repetitive DNA that show greater variations among individuals) to create a unique pattern for identification. DNA fingerprinting techniques are especially useful for plant genotyping and controlling the quality of medicinal crops (Zhokhova et al., 2019). Because variations in the plant genetic materials may affect the phenotypes, including the production of secondary metabolites, identification of plant varieties with desired traits could assist in preparing more standardized plant materials with similar characteristics. In the early days of DNA fingerprinting,

restriction fragment length polymorphism (RFLP) in conjunction with Southern blot hybridization became the main technique for profiling plants' DNA (Dallas, 1988; Antonius and Nybom, 1994). This technique, however, is time-consuming and requires multiple species-specific probes, limiting its applications mainly to economically important plants.

PCR-based DNA fingerprinting techniques have been reported in which single oligonucleotide primers with random sequences were used to produce PCR fragments from multiple loci in the genomic DNA (Welsh and McClelland, 1990; Caetano-Anolles, 1991). One of the techniques that became popular was random amplified polymorphic DNA (RAPD), in which single primers were used to amplify nonspecific sites of the DNA (Chang et al., 2017; Rafalski et al., 2020). For example, RAPD markers were used to assess the genetic diversity of *Curcuma comosa* Roxb and other *Curcuma* sp. collected from different regions in Thailand. Fifteen RAPD primers were used to amplify the genomic DNA from 30 plant samples (Boonsrangsom, 2020). The RAPD profiles were then used to classify the samples into two major clusters: Cluster I which consists of *C. comosa* Roxb samples from different regions and Cluster II which consists of other *Curcuma* sp. Cluster I was divided into 6 sub-clusters which may be useful for conservation and breeding programs by further analyzing the metabolite profiles of the samples and the correlation between the genetic and metabolite profiles.

Amplified fragment length polymorphism (AFLP) and inter-simple sequence repeat (ISSR) techniques are also common (Paun and Schönswetter, 2012; Hassan et al., 2020; Junior et al., 2020; Leipold et al., 2020). AFLP uses selective amplification of digested DNA fragments to generate unique DNA fingerprints, while ISSRs are DNA fragments (100–3,000 bp) located between two adjacent, oppositely oriented microsatellite regions. Hadipour et al. investigated the genetic variation of wild *Papaver bracteatum* L. from 9 different populations in Iran using AFLP and ISSR markers (Hadipour et al., 2020). The genetic diversities were 52% and 48% among different populations; 38% and 41% within the populations for ISSR and AFLP, respectively. AFLP and ISSR also similarly grouped the samples into 3 major groups and 1 minor group, which correlated well with the geographical distribution of the samples.

While DNA barcoding and fingerprinting are powerful tools for medicinal plant genotyping and authentication, there are several limitations associated with these methods. The successful application of DNA barcoding/fingerprinting relies on the quality of DNA, primer affinity, amplification, and amplicon sequencing. Intact plant DNA can typically be extracted from fresh or dried materials using standard DNA extraction methods (Shen et al., 2019; Hadipour et al., 2020). However, significant degradation of DNA can occur during the manufacturing process of herbal products (de Boer et al., 2015). Thus, DNA-based methods are more appropriate for the initial stage of raw material preparation and standardization rather than for the quality control of highly processed herbal preparations. These methods will also not be able to determine from which plant part the materials come and cannot be used in the case of adulteration with different parts of the same plant species. Plant DNA profiles may not be well correlated with the secondary metabolite contents as genomic DNA remains unaffected by seasonal variations, whereas metabolite production can vary between seasons (Ahmed et al., 2019). In addition, the removal of certain metabolites during extraction or other processes will not be reflected on the DNA profiles. Therefore, DNA barcoding/fingerprinting cannot be single-handedly used to predict the efficacy of raw materials or finished products and must be used to complement the chemical analysis and macroscopic/microscopic evaluation of the herbal specimen/samples.

5 CONCLUSION, CHALLENGES, AND FUTURE PERSPECTIVES

Due to the complex nature of herbal drug preparations, the method of standardizations for individual herbs that are described in the herbs' monographs in the pharmacopeia cannot be applied directly as a QC tool for all stages in the manufacturing processes, except for the quality assessment for the incoming herbs/extracts. The visual evaluation based on the HPTLC method described by the Pharmacopoeias and official guidelines should be completed using similarity- and/or chemometrics-methods. Chemical profiling or fingerprinting is the method of choice for performing quality control if the quality markers are not yet specified for each of the herbs.

Using fingerprinting methods, various tasks in the research and development of herbal drugs can be performed. Chemical fingerprints can be used to evaluate the quality of raw materials, extracts, and finished products. With the help of chemometrics, information can be extracted from the fingerprints to find similarities/differences which are useful to group samples based on certain characteristics (e.g., authentic vs adulterated samples, samples from different geographical origins, etc.) and establish correlations between the chemical profiles and biological/pharmacological activity of interest. Relationships between chemical profiles/fingerprints and biological/pharmacological activities such as antioxidant, antibacterial, antihypertensive, anti-inflammatory, and antitumor have been successfully established in multiple plant materials and HM preparations (Zhang et al., 2018). Results obtained from these studies have also led to the discovery of quality markers that can be used for future QC applications.

Chemical fingerprints can be obtained using various separation-based (e.g., LC, TLC, and CE) or nonseparation-based (e.g., FTIR and NMR spectroscopy) techniques. Due to their ability to rapidly generate chemical fingerprints, chemical profiling using direct spectroscopy and MS methods may offer more benefits over chromatographic methods. The application of FTIR is preferred due to its relatively lower operation cost. Using single measurements, spectroscopic/spectrometric methods can generate a large number of spectral data which can be characterized by wavenumbers, intensities, chemical shifts, or mass-per-charge. By optimizing spectral treatments (pre-processing), selection of fingerprint regions, and the use of appropriate chemometric techniques, these methods can be applied for the standardization and quality control of HMs.

Assessment of both chemical dan DNA fingerprints would provide a more comprehensive outlook on the authenticity and overall quality of the HMs, and thus are recommended to be used in conjunction when appropriate. The combined assessment would be especially useful to determine plant genotypes that result in desirable phenotypes such as high contents of certain bioactive metabolites. In addition, collaborative studies through proficiency testing are required to get comparable results for these fingerprinting methods and to finally propose them as standard methods in the future.

To have reliable results for the quality assessment using chemical profiles, the availability of authentic botanical reference materials and stable standardized extracts is crucial. Although the current pharmacopeias have described the physicochemical specifications of each raw plant material, the active component(s) and associated pharmacology activities are not specified. In addition, these individual specifications cannot be directly applied to determine the specification of HM containing multiple plant materials. Therefore, pharmaceutical industries should prepare and provide stable standardized extracts that have certain pharmacological applications for their QC. It would be practical if specifications of commonly used HM preparations including their active components and desired therapeutic applications are provided in the herbal or general compendia in the near future.

Many studies reported to date are still limited to plant materials, dried mixtures of plant materials, or extracts without reporting their exact chemical compositions, making comparison among results found in the literature and replicating the experiments difficult. To prevent these problems, the chemical compositions of extracts or HM preparations should be accurately determined, and all methods used for the chemical, biological, and/or pharmacological testing (*in-vitro*, *in-vivo*, *ex-vivo*) should be fully validated according to the newest guidelines, prior to routine application (Indrayanto, 2022). Finally, appropriate clinical trials should be conducted before HMs can be prescribed and used in clinical settings. The exact chemical compositions of the HMs and their stability must be determined to assure similar efficacy from batch to batch. Knowing the exact composition of the HM may also assist in determining incompatibilities between the active components and excipients, and possible unwanted interactions between the HM components and other drugs or food. The pharmacokinetic parameters of the HMs must be evaluated to ensure effective and safe use of HMs.

AUTHOR CONTRIBUTIONS

EN formulated the idea of the manuscript; EN, GI, and AR wrote the initial draft, reviewed, and edited the draft. All authors have read and approved the final manuscript.

ACKNOWLEDGMENTS

The authors thank Universitas Gadjah Mada's Publishers and Publications Board (BPP UGM) for the publication support. The authors wish to acknowledge Ms. Nurliya Irfiani (PT Merck Sharp Dohme Pharma Tbk, Pandaan, Pasuruan, Indonesia) for providing references for European Pharmacopoeia 10, Mrs. Wahyu Dewi Tamayanti (Institute of Life, National Yang Ming Chiao Tung University, Taipei, Taiwan) for supplying references of Taiwan Pharmacopeia 2019 and British Pharmacopoeia 2020, and the Library of Universitas Surabaya, Surabaya, Indonesia, for providing access to the USP-NF online databases.

REFERENCES

Ahmed, S., Griffin, T. S., Kraner, D., Schaffner, M. K., Sharma, D., Hazel, M., et al. (2019). Environmental Factors Variably Impact Tea Secondary Metabolites in the Context of Climate Change. *Front. Plant Sci.* 10, 939. doi:10.3389/fpls.2019.00939

Antonius, K., and Nybom, H. (1994). DNA Fingerprinting Reveals Significant Amounts of Genetic Variation in a Wild raspberryRubus Idaeuspopulation. *Mol. Ecol.* 3, 177–180. doi:10.1111/j.1365-294x.1994.tb00119.x

Anzardi, M. B., Arancibia, J. A., and Olivieri, A. C. (2021). Processing Multi-Way Chromatographic Data for Analytical Calibration, Classification and Discrimination: a Successful Marriage between Separation Science and Chemometrics. *TrAC Trends Anal. Chem.* 134, 116128. doi:10.1016/j.trac.2020.116128

AOAC (2019). Guidelines for Dietary Supplements and Botanicals (AOAC Official Method of Analysis, Appendix K). Available at: http://www.eoma.aoac.org/app_k.pdf (Accessed November 1, 2021).

Arendse, E., Nieuwoudt, H., Magwaza, L. S., Nturambirwe, J. F. I., Fawole, O. A., and Opara, U. L. (2021). Recent Advancements on Vibrational Spectroscopic Techniques for the Detection of Authenticity and Adulteration in Horticultural Products with a Specific Focus on Oils, Juices and Powders. *Food Bioprocess Technol.* 14, 1–22. doi:10.1007/s11947-020-02505-x

Azlah, M. A. F., Chua, L. S., Abdullah, F. I., and Yam, M. F. (2020). A Fast and Reliable 2D-IR Spectroscopic Technique for Herbal Leaves Classification. *Vib. Spectrosc.* 106, 103014. doi:10.1016/j.vibspec.2019.103014

Balekundri, A., and Mannur, V. (2020). Quality Control of the Traditional Herbs and Herbal Products: a Review. *Future J. Pharm. Sci.* 6, 1–9. doi:10.1186/s43094-020-00091-5

Becerra-Martínez, E., Florentino-Ramos, E., Pérez-Hernández, N., Gerardo Zepeda-Vallejo, L., Villa-Ruano, N., Velázquez-Ponce, M., et al. (2017). 1 H NMR-Based Metabolomic Fingerprinting to Determine Metabolite Levels in Serrano Peppers (Capsicum Annum L.) Grown in Two Different Regions. *Food Res. Int.* 102, 163–170. doi:10.1016/j.foodres.2017.10.005

Bensoussan, A., Lee, S., Murray, C., Bourchier, S., van der Kooy, F., Pearson, J. L., et al. (2015). Choosing Chemical Markers for Quality Assurance of Complex Herbal Medicines: Development and Application of the Herb MaRS Criteria. *Clin. Pharmacol. Ther.* 97, 628–640. doi:10.1002/cpt.100

Berrueta, L. A., Alonso-Salces, R. M., and Héberger, K. (2007). Supervised Pattern Recognition in Food Analysis. *J. Chromatogr. A* 1158, 196–214. doi:10.1016/j.chroma.2007.05.024

Biancolillo, A., and Marini, F. (2018). Chemometric Methods for Spectroscopy-Based Pharmaceutical Analysis. *Front. Chem.* 6, 576. doi:10.3389/fchem.2018.00576

Bingbing, L., Qian, W., Caixia, L., Wenjing, H., Guoliang, C., Yongxia, G., et al. (2021). Study on GC-MS Fingerprint of Petroleum Ether Fraction of Shenqi

Jiangtang Granules. *Digit. Chin. Med.* 4, 32–41. doi:10.1016/j.dcmed.2021.03.004

Blaise, B. J., Correia, G. D. S., Haggart, G. A., Surowiec, I., Sands, C., Lewis, M. R., et al. (2021). Statistical Analysis in Metabolic Phenotyping. *Nat. Protoc.* 16, 4299–4326. doi:10.1038/s41596-021-00579-1

Boonsrangsom, T. (2020). Genetic Diversity of 'Wan Chak Motluk' (Curcuma Comosa Roxb.) in Thailand Using Morphological Characteristics and Random Amplification of Polymorphic DNA (RAPD) Markers. *South Afr. J. Bot.* 130, 224–230. doi:10.1016/j.sajb.2020.01.005

Brereton, R. G., Jansen, J., Lopes, J., Marini, F., Pomerantsev, A., Rodionova, O., et al. (2018). Chemometrics in Analytical Chemistry-Part II: Modeling, Validation, and Applications. *Anal. Bioanal. Chem.* 410, 6691–6704. doi:10.1007/s00216-018-1283-4

British Pharmacopoeia (2020). London: The Department of Health and Social Care, British Pharmacopoeia Commission Office.

Caetano-Anollés, G., Bassam, B. J., and Gresshoff, P. M. (1991). DNA Amplification Fingerprinting Using Very Short Arbitrary Oligonucleotide Primers. *Biotechnol. (N Y)* 9, 553–557. doi:10.1038/nbt0691-553

Calixto, J. B. (2019). The Role of Natural Products in Modern Drug Discovery. *An. Acad. Bras. Cienc.* 91 Suppl 3, e20190105. doi:10.1590/0001-3765201920190105

Chan, S. L., Wong, M. Y., Tang, H. W., Che, C. M., and Ng, K. M. (2011). Tissue-spray Ionization Mass Spectrometry for Raw Herb Analysis. *Rapid Commun. Mass Spectrom.* 25, 2837–2843. doi:10.1002/rcm.5177

Chang, Y., Oh, E. U., Lee, M. S., Kim, H. B., Moon, D.-G., and Song, K. J. (2017). Construction of a Genetic Linkage Map Based on RAPD, AFLP, and SSR Markers for Tea Plant (*Camellia Sinensis*). *Euphytica* 213, 1–15. doi:10.1007/s10681-017-1979-0

Chen, J., Zhu, H., Chu, V. M., Jang, Y. S., Son, J. Y., Kim, Y. H., et al. (2011). Quality Control of a Herbal Medicinal Preparation Using High-Performance Liquid Chromatographic and Capillary Electrophoretic Methods. *J. Pharm. Biomed. Anal.* 55, 206–210. doi:10.1016/j.jpba.2010.12.022

Chen, S., Pang, X., Song, J., Shi, L., Yao, H., Han, J., et al. (2014). A Renaissance in Herbal Medicine Identification: from Morphology to DNA. *Biotechnol. Adv.* 32, 1237–1244. doi:10.1016/j.biotechadv.2014.07.004

Chen, S., Sun, G., Ma, D., Yang, L., and Zhang, J. (2018). Quantitative Fingerprinting Based on the Limited-Ratio Quantified Fingerprint Method for an Overall Quality Consistency Assessment and Antioxidant Activity Determination of Lianqiao Baidu Pills Using HPLC with a Diode Array Detector Combined with Chemometric Methods. *J. Sep. Sci.* 41, 548–559. doi:10.1002/jssc.201700566

Chen, S., Yao, H., Han, J., Liu, C., Song, J., Shi, L., et al. (2010). Validation of the ITS2 Region as a Novel DNA Barcode for Identifying Medicinal Plant Species. *PloS One* 5, e8613. doi:10.1371/journal.pone.0008613

Chuchote, C., and Somwong, P. (2019). Similarity Analysis of the Chromatographic Fingerprints of Thai Herbal Ya-Ha-Rak Remedy Using HPLC. *Interprof. J. Health Sci.* 17, 55–63.

Coskun, S. H., Wise, S. A., and Kuszak, A. J. (2021). The Importance of Reference Materials and Method Validation for Advancing Research on the Health Effects of Dietary Supplements and Other Natural Products. *Front. Nutr.* 8, 786241. doi:10.3389/fnut.2021.786261

Crawford, E. A., Gerbig, S., Spengler, B., and Volmer, D. A. (2017). Rapid Fingerprinting of Lignin by Ambient Ionization High Resolution Mass Spectrometry and Simplified Data Mining. *Anal. Chim. Acta* 994, 38–48. doi:10.1016/j.aca.2017.09.012

Custers, D., van Praag, N., Courselle, P., Apers, S., and Deconinck, E. (2017). Chromatographic Fingerprinting as a Strategy to Identify Regulated Plants in Illegal Herbal Supplements. *Talanta* 164, 490–502. doi:10.1016/j.talanta.2016.12.008

Dallas, J. F. (1988). Detection of DNA "fingerprints" of Cultivated Rice by Hybridization with a Human Minisatellite DNA Probe. *Proc. Natl. Acad. Sci. U. S. A.* 85, 6831–6835. doi:10.1073/pnas.85.18.6831

de Boer, H. J., Ichim, M. C., and Newmaster, S. G. (2015). DNA Barcoding and Pharmacovigilance of Herbal Medicines. *Drug Saf.* 38, 611–620. doi:10.1007/s40264-015-0306-8

Deng, J., and Yang, Y. (2013). Chemical Fingerprint Analysis for Quality Assessment and Control of Bansha Herbal Tea Using Paper Spray Mass Spectrometry. *Anal. Chim. Acta* 785, 82–90. doi:10.1016/j.aca.2013.04.056

Dhakal, S., Chao, K., Schmidt, W., Qin, J., Kim, M., and Chan, D. (2016). Evaluation of Turmeric Powder Adulterated with Metanil Yellow Using FT-Raman and FT-IR Spectroscopy. *Foods* 5, 1–15. doi:10.3390/foods5020036

Do, T. K. T., Trettin, I., de Vaumas, R., Cañigueral, S., Valder, C., and Reich, E. (2021). Proposal for a Standardised Method for the Identification of Essential Oils by HPTLC. *Pharmeur. Bio Sci. Notes* 2021, 157–166.

Do, T. K. T., Clark, K., Christen, P., and Reich, E. (2020). Quality Assessment of Sclerocarya Birrea Leaves and Leaves Products from Burkina Faso Based on Fingerprinting Using HPTLC. *JPC-J Planar Chromat* 33, 439–448. doi:10.1007/s00764-020-00058-5

EMA (2011). Guideline on Declaration of Herbal Substances and Herbal Preparations 1 in Herbal Medicinal Products 2/traditional Herbal Medicinal Products. Available at: https://www.ema.europa.eu/en/documents/scientific-guideline/guideline-declaration-herbal-substances-herbal-preparations-herbal-medicinal-products/traditional-herbal-medicinal-products-spc_en.pdf (Accessed August 26, 2021).

Escandar, G. M., and Olivieri, A. C. (2019). Multi-way Chromatographic Calibration-A Review. *J. Chromatogr. A* 1587, 2–13. doi:10.1016/j.chroma.2019.01.012

European Pharmacopoeia (2021). , 1–18. Available at: https://pheur.edqm.eu/internal/99b060ac937f4ef4b8b7cd48d98097b7/10-5/default/page/52100E.pdf (Accessed May 16, 2021).5.21 Chemometrics Method Applied to Analytical Data.

Fan, X.-H., Cheng, Y.-Y., Ye, Z.-L., Lin, R.-C., and Qian, Z.-Z. (2006). Multiple Chromatographic Fingerprinting and its Application to the Quality Control of Herbal Medicines. *Anal. Chim. Acta* 555, 217–224. doi:10.1016/j.aca.2005.09.037

Farmakope Herbal Indonesia (2017). *Edisi II*. Jakarta: Kementrian Kesehatan Republik Indonesia.

FDA (2016). Botanical Drug Development, Guidance for Industry, U.S. Department of Health and Human Services Food and Drug Administration Center for Drug Evaluation and Research (CDER). Available at: https://www.fda.gov/media/93113/download (Accessed August 26, 2021).

Freitas, J. R. L., Vendramini, P. H., Melo, J. O. F., Eberlin, M. N., and Augusti, R. (2019). Assessing the Spatial Distribution of Key Flavonoids in *Mentha Piperita* Leaves: An Application of Desorption Electrospray Ionization Mass Spectrometry Imaging (DESI-MSI). *J. Braz. Chem. Soc.* 30, 1437–1446.

Gong, D., Zheng, Z., Chen, J., Pang, Y., and Sun, G. (2021). Holistic Quality Evaluation of Compound Liquorice Tablets Using Capillary Electrophoresis Fingerprinting Combined with Chemometric Methods. *New J. Chem.* 45, 2563–2572. doi:10.1039/d0nj05461e

Gotti, R., Fiori, J., Bartolini, M., and Cavrini, V. (2006). Analysis of Amaryllidaceae Alkaloids from Narcissus by GC-MS and Capillary Electrophoresis. *J. Pharm. Biomed. Anal.* 42, 17–24. doi:10.1016/j.jpba.2006.01.003

Gross, J. H. (2006). *Mass Spectrometry: A Textbook*. Heidelberg: Springer Science & Business Media.

Hadipour, M., Kazemitabar, S. K., Yaghini, H., and Dayani, S. (2020). Genetic Diversity and Species Differentiation of Medicinal Plant Persian Poppy (*Papaver Bracteatum* L.) Using AFLP and ISSR Markers. *Ecol. Genet. Genomics* 16, 100058. doi:10.1016/j.egg.2020.100058

Harrison, O. (2021). Machine Learning Basics with the K-Nearest Neighbors Algorithm. *Toward Data Sci.* Available at: https://towardsdatascience.com/machine-learning-basics-with-the-k-nearest-neighbors-algorithm-6a6e71d01761 (Accessed November 17, 2021).

Hassan, R., Waheed, M. Q., Shokat, S., Rehman-Arif, M. A., Tariq, R., Arif, M., et al. (2020). Estimation of Genomic Diversity Using Sequence Related Amplified Polymorphism (SRAP) Markers in a Mini Core Collection of Wheat Germplasm from Pakistan. *Cereal Res. Commun.* 48, 33–40. doi:10.1007/s42976-019-00006-y

Haynes, E., Jimenez, E., Pardo, M. A., and Helyar, S. J. (2019). The Future of NGS (Next Generation Sequencing) Analysis in Testing Food Authenticity. *Food control.* 101, 134–143. doi:10.1016/j.foodcont.2019.02.010

Heinrich, M., Appendino, G., Efferth, T., Fürst, R., Izzo, A. A., Kayser, O., et al. (2020). Best Practice in Research - Overcoming Common Challenges in Phytopharmacological Research. *J. Ethnopharmacol.* 246, 112230. doi:10.1016/j.jep.2019.112230

Hollingsworth, P. M., Graham, S. W., and Little, D. P. (2011). Choosing and Using a Plant DNA Barcode. *PloS One* 6, e19254. doi:10.1371/journal.pone.0019254

Hollingsworth, P. M., Forrest, L. L., Spouge, J. L., Hajibabaei, M., Ratnasingham, S., van der Bank, M., et al. (2009). A DNA Barcode for Land Plants. *Proc. Natl. Acad. Sci.* 106, 12794–12797.

Hong Kong Chinese Materia Medica Standards (2020). *Chinese Medicine Regulatory Office*. Kowloon: Department of Health. Available at: https://www.cmro.gov.hk/html/eng/useful_information/hkcmms/volumes.html (Accessed November 1, 2021). The Government of Hong Kong Special Administrative Region.

Hou, Z., Sun, G., Guo, Y., Yang, F., and Gong, D. (2019). Capillary Electrophoresis Fingerprints Combined with Linear Quantitative Profiling Method to Monitor the Quality Consistency and Predict the Antioxidant Activity of Alkaloids of *Sophora Flavescens*. *J. Chromatogr. B Anal. Technol. Biomed. Life Sci.* 1133, 121827. doi:10.1016/j.jchromb.2019.121827

Hu, B., So, P. K., and Yao, Z. P. (2014). Electrospray Ionization with Aluminum Foil: a Versatile Mass Spectrometric Technique. *Anal. Chim. Acta* 817, 1–8. doi:10.1016/j.aca.2014.02.005

Hu, B., Wang, L., Ye, W. C., and Yao, Z. P. (2013). *In Vivo* and Real-Time Monitoring of Secondary Metabolites of Living Organisms by Mass Spectrometry. *Sci. Rep.* 3, 2104–4. doi:10.1038/srep02104

Huang, Y., Wu, Z., Su, R., Ruan, G., Du, F., and Li, G. (2015). Current Application of Chemometrics in Traditional Chinese Herbal Medicine Research. *J. Chromatogr. B Anal. Technol. Biomed. Life Sci.* 1026, 27–35. doi:10.1016/j.jchromb.2015.12.050

Huck, C. (2015). "Infrared Spectroscopic Technologies for the Quality Control of Herbal Medicines," in *Evidence-Based Validation of Herbal Medicine*. Editor P. K. Mukherjee (Elsevier), 477–493. doi:10.1016/b978-0-12-800874-4.00022-2

Ibrahim, R. S., and Zaatout, H. H. (2019). Unsupervised Pattern Recognition Chemometrics for Distinguishing Different Egyptian Olive Varieties Using a New Integrated Densitometric Reversed-phase High-Performance Thin-Layer Chromatography-Image Analysis Technique. *JPC - J. Planar Chromatogr. - Mod. TLC* 32, 453–460. doi:10.1556/1006.2019.32.6.2

Iino, K., Sugimoto, M., Soga, T., and Tomita, M. (2012). Profiling of the Charged Metabolites of Traditional Herbal Medicines Using Capillary Electrophoresis Time-Of-Flight Mass Spectrometry. *Metabolomics* 8, 99–108. doi:10.1007/s11306-011-0290-7

Imai, A., Lankin, D. C., Gödecke, T., Chen, S. N., and Pauli, G. F. (2020). Differentiation of Actaea Species by NMR Metabolomics Analysis. *Fitoterapia* 146, 104686. doi:10.1016/j.fitote.2020.104686

Indrayanto, G. (2022). The Importance of Method Validation in Herbal Drug Research. *J. Pharm. Biomed. Anal.* 214, 114735. doi:10.1016/j.jpba.2022.114735

Indrayanto, G. (2018a). Recent Development of Quality Control Methods for Herbal Derived Drug Preparations. *Nat. Prod. Commun.* 13, 1934578X1801301208. doi:10.1177/1934578x1801301208

Indrayanto, G. (2018b). Validation of Chromatographic Methods of Analysis: Application for Drugs that Derived from Herbs. *Profiles Drug Subst. Excipients, Relat. Methodol.* 43, 359–392. doi:10.1016/bs.podrm.2018.01.003

Irnawati, I., Dika, F., Riswanto, O., Riyanto, S., and Martono, S. (2021). The Use of Software Package of R Factoextra and FactoMineR and Their Application in Principal Component Analysis for Authentication of Oils. *Indones. J. Chemom. Pharm. Anal.* 1, 1–10.

Ivanova, N. V., Kuzmina, M. L., Braukmann, T. W., Borisenko, A. V., and Zakharov, E. V. (2016). Authentication of Herbal Supplements Using Next-Generation Sequencing. *PloS One* 11, e0156426. doi:10.1371/journal.pone.0156426

Ji, S., Liu, Z. Z., Wu, J., Du, Y., Su, Z. Y., Wang, T. Y., et al. (2018). Chemical Profiling and Comparison of Sangju Ganmao Tablet and its Component Herbs Using Two-Dimensional Liquid Chromatography to Explore Compatibility Mechanism of Herbs. *Front. Pharmacol.* 9, 1167. doi:10.3389/fphar.2018.01167

Johnson, R. T., and Lunte, C. E. (2016). A Capillary Electrophoresis Electrospray Ionization-Mass Spectrometry Method Using a Borate Background Electrolyte for the Fingerprinting Analysis of Flavonoids in *Ginkgo Biloba* Herbal Supplements. *Anal. Methods* 16, 3325–3332. doi:10.1039/C6AY00463F

Jolliffe, I. T., and Cadima, J. (2016). Principal Component Analysis: A Review and Recent Developments. *Phil. Trans. R. Soc. A* 374, 20150202. doi:10.1098/rsta.2015.0202

Jun, G., Park, T.-M., and Cha, S. (2016). Fast and Simple Chemical Fingerprinting Analysis of Medicinal Herbs by Paper Cone Spray Ionization Mass Spectrometry (PCSI MS). *Bull. Korean Chem. Soc.* 37, 1337–1343. doi:10.1002/bkcs.10868

Junior, C. A. D. K., Manechini, J. R. V., Corrêa, R. X., Pinto, A. C. R., da Costa, J. B., Favero, T. M., et al. (2020). Genetic Structure Analysis in Sugarcane (Saccharum spp.) Using Target Region Amplification Polymorphism (TRAP) Markers Based on Sugar- and Lignin-Related Genes and Potential Application in Core Collection Development. *Sugar Tech.* 22, 641–654. doi:10.1007/s12355-019-00791-0

Kartini, K., Hardianti, D., and Hadiyat, M. A. (2021). Identification of *Phyllanthus Niruri* by FTIR Spectroscopy with Chemometrics. *Pharmaciana* 11, 251–260. doi:10.12928/pharmaciana.v11i2.15954

Kharbach, M., Marmouzi, I., el Jemli, M., Bouklouze, A., and vander Heyden, Y. (2020). Recent Advances in Untargeted and Targeted Approaches Applied in Herbal-Extracts and Essential-Oils Fingerprinting - A Review. *J. Pharm. Biomed. Anal.* 177, 112849. doi:10.1016/j.jpba.2019.112849

Kim, H. K., Choi, Y. H., and Verpoorte, R. (2010). NMR-based Metabolomic Analysis of Plants. *Nat. Protoc.* 5, 536–549. doi:10.1038/nprot.2009.237

Klein-Junior, L. C., de Souza, M. R., Viaene, J., Bresolin, T. M. B., de Gasper, A. L., Henriques, A. T., et al. (2021). Quality Control of Herbal Medicines: From Traditional Techniques to State-Of-The-Art Approaches. *Planta Med.* 87, 964–988. doi:10.1055/a-1529-8339

Kos, G., Lohninger, H., and Krska, R. (2003). Validation of Chemometric Models for the Determination of Deoxynivalenol on Maize by Mid-infrared Spectroscopy. *Mycotoxin Res.* 19, 149–153. doi:10.1007/BF02942955

Kumar, S., Bajpai, V., Singh, A., Bindu, S., Srivastava, M., Rameshkumar, K. B., et al. (2015). Rapid Fingerprinting of *Rauwolfia* Species Using Direct Analysis in Real Time Mass Spectrometry Combined with Principal Component Analysis for Their Discrimination. *Anal. Methods* 7, 6021–6026. doi:10.1039/c5ay01249j

Lai, Y. H., So, P. K., Lo, S. C., Ng, E. W., Poon, T. C., and Yao, Z. P. (2012). Rapid Differentiation of *Panax Ginseng* and *Panax Quinquefolius* by Matrix-Assisted Laser Desorption/ionization Mass Spectrometry. *Anal. Chim. Acta* 753, 73–81. doi:10.1016/j.aca.2012.09.047

Lan, L., Zhang, Y., Zhang, M., and Sun, G. (2019). Evaluation of the Quality of Compound Liquorice Tablets by DSC and HPLC Fingerprints Assisted with Dissolution. *J. Pharm. Biomed. Anal.* 175, 112715. doi:10.1016/j.jpba.2019.06.012

Länger, R., Stöger, E., Kubelka, W., and Helliwell, K. (2018). Quality Standards for Herbal Drugs and Herbal Drug Preparations–Appropriate or Improvements Necessary? *Planta Med.* 84, 350–360.

Lee, C. H., Huang, H. C., Tseng, M. C., and Chen, C. J. (2021). An Extractive Nanoelectrospray Ionization-Mass Spectrometry Method for Chinese Herbal Medicine Authentication. *J. Food Drug Anal.* 29, 468–499. doi:10.38212/2224-6614.3368

Lee, D., Kim, M., Kim, B. H., and Ahn, S. (2020). Identification of the Geographical Origin of Asian Red Pepper (Capsicum Annuum L.) Powders Using 1 H NMR Spectroscopy. *Bull. Korean Chem. Soc.* 41, 317–322. doi:10.1002/bkcs.11974

Leipold, M., Tausch, S., Hirtreiter, M., Poschlod, P., and Reisch, C. (2020). Sampling for Conservation Genetics: How Many Loci and Individuals Are Needed to Determine the Genetic Diversity of Plant Populations Using AFLP? *Conserv. Genet. Resour.* 12, 99–108. doi:10.1007/s12686-018-1069-1

Leong, F., Hua, X., Wang, M., Chen, T., Song, Y., Tu, P., et al. (2020). Quality Standard of Traditional Chinese Medicines: Comparison between European Pharmacopoeia and Chinese Pharmacopoeia and Recent Advances. *Chin. Med.* 15, 76–20. doi:10.1186/s13020-020-00357-3

Li, H., Cao, J., Wu, X., Deng, Y., Ning, N., Geng, C., et al. (2020a). Multiple Fingerprint Profiling for Quality Evaluation of Polysaccharides and Related Biological Activity Analysis of Chinese Patent Drugs: Zishen Yutai Pills as a Case Study. *J. Ethnopharmacol.* 260, 113045. doi:10.1016/j.jep.2020.113045

Li, X., Yang, Y., Henry, R. J., Rossetto, M., Wang, Y., and Chen, S. (2015). Plant DNA Barcoding: from Gene to Genome. *Biol. Rev. Camb Philos. Soc.* 90, 157–166. doi:10.1111/brv.12104

Li, Y., Shen, Y., Yao, C. L., and Guo, D. A. (2020b). Quality Assessment of Herbal Medicines Based on Chemical Fingerprints Combined with Chemometrics Approach: A Review. *J. Pharm. Biomed. Anal.* 185, 113215. doi:10.1016/j.jpba.2020.113215

Li, Y., Shen, Y., Yao, C. L., and Guo, D. A. (2020c). Quality Assessment of Herbal Medicines Based on Chemical Fingerprints Combined with Chemometrics

Approach: A Review. *J. Pharm. Biomed. Anal.* 185, 113215. doi:10.1016/j.jpba.2020.113215

Li, Z., Ryenchindorj, L., Liu, B., Shi, J., Zhang, C., Hua, Y., et al. (2021). Chemical Profiles and Metabolite Study of Raw and Processed *Cistanche Deserticola* in Rats by UPLC-Q-TOF-MSE. *Chin. Med.* 16, 95. doi:10.1186/s13020-021-00508-0

Little, D. P. (2014). Authentication of *Ginkgo Biloba* Herbal Dietary Supplements Using DNA Barcoding. *Genome* 57, 513–516. doi:10.1139/gen-2014-0130

Liu, J., Wang, H., Cooks, R. G., and Ouyang, Z. (2011). Leaf Spray: Direct Chemical Analysis of Plant Material and Living Plants by Mass Spectrometry. *Anal. Chem.* 83, 7608–7613. doi:10.1021/ac2020273

Liu, Y., Sun, G., Wang, Y., Yang, L., and Yang, F. (2015). Monitoring the Quality Consistency of Weibizhi Tablets by Micellar Electrokinetic Chromatography Fingerprints Combined with Multivariate Statistical Analyses, the Simple Quantified Ratio Fingerprint Method, and the Fingerprint-Efficacy Relationship. *J. Sep. Sci.* 38, 2174–2181. doi:10.1002/jssc.201500145

Lo, Y. T., and Shaw, P. C. (2019). Application of Next-Generation Sequencing for the Identification of Herbal Products. *Biotechnol. Adv.* 37, 107450. doi:10.1016/j.biotechadv.2019.107450

Luo, D. H., and Shao, Y. W. (2013). Classification of Chinese Herbal Medicine Based on Improved LDA Algorithm Using Machine Olfaction. *Amm* 239-240, 1532–1536. doi:10.4028/www.scientific.net/AMM.239-240.1532

Ma, D., Yang, L., Yan, B., and Sun, G. (2017). Capillary Electrophoresis Fingerprints Combined with Chemometric Methods to Evaluate the Quality Consistency and Predict the Antioxidant Activity of Yinqiaojiedu Tablet. *J. Sep. Sci.* 40, 1796–1804. doi:10.1002/jssc.201601155

Massaro, A., Negro, A., Bragolusi, M., Miano, B., Tata, A., Suman, M., et al. (2021). Oregano Authentication by Mid-level Data Fusion of Chemical Fingerprint Signatures Acquired by Ambient Mass Spectrometry. *Food control.* 126, 108058. doi:10.1016/j.foodcont.2021.108058

Miller, J., and Miller, J. C. (2018). *Statistics and Chemometrics for Analytical Chemistry*. London: Pearson Education.

Morley, A. A. (2014). Digital PCR: A Brief History. *Biomol. Detect. Quantif.* 1, 1–2. doi:10.1016/j.bdq.2014.06.001

Moros, J., Garrigues, S., and Guardia, M. d. l. (2010). Vibrational Spectroscopy Provides a Green Tool for Multi-Component Analysis. *TrAC Trends Anal. Chem.* 29, 578–591. doi:10.1016/j.trac.2009.12.012

Muyumba, N. W., Mutombo, S. C., Sheridan, H., Nachtergael, A., and Duez, P. (2021). Quality Control of Herbal Drugs and Preparations: the Methods of Analysis, Their Relevance and Applications. *Talanta Open* 4, 100070. doi:10.1016/j.talo.2021.100070

Nikam, P. H., Kareparamban, J., Jadhav, A., Kadam, V., and Jadhav, A. (2012). Future Trends in Standardization of Herbal Drugs. *J. Appl. Pharm. Sci.* 2, 38–44. doi:10.7324/JAPS.2012.2631

Nurani, L. H., Rohman, A., Windarsih, A., Guntarti, A., Riswanto, F. D. O., Lukitaningsih, E., et al. (2021). Metabolite Fingerprinting Using 1H-NMR Spectroscopy and Chemometrics for Classification of Three Curcuma Species from Different Origins. *Molecules* 26, 7626. doi:10.3390/molecules26247626

Oliveri, P., and Downey, G. (2012). Multivariate Class Modeling for the Verification of Food-Authenticity Claims. *TrAC Trends Anal. Chem.* 35, 74–86. doi:10.1016/j.trac.2012.02.005

Oliveri, P., Malegori, C., Mustorgi, E., and Casale, M. (2020). "Application of Chemometrics in the Food Sciences," in *Comprehensive Chemometrics*. Editors S. Brown, R. Tauler, and B. Walczak. Second Edition (Elsevier), 99–111. doi:10.1016/b978-0-12-409547-2.14748-1

Pacholczyk-Sienicka, B., Ciepielowski, G., and Albrecht, Ł. (2021). The Application of NMR Spectroscopy and Chemometrics in Authentication of Spices. *Molecules* 26, 382. doi:10.3390/molecules26020382

Paun, O., and Schönswetter, P. (2012). "Amplified Fragment Length Polymorphism: an Invaluable Fingerprinting Technique for Genomic, Transcriptomic, and Epigenetic Studies," in *Plant DNA Fingerprinting and Barcoding* (Springer), 75–87. doi:10.1007/978-1-61779-609-8_7

Pereira, H. V., Pinto, F. G., dos Reis, M. R., Garret, T. J., Augusti, R., Sena, M. M., et al. (2021). A Fast and Effective Approach for the Discrimination of Garlic Origin Using Wooden-Tip Electrospray Ionization Mass Spectrometry and Multivariate Classification. *Talanta* 230, 122304. doi:10.1016/j.talanta.2021.122304

Pi, Z., Yue, H., Ma, L., Ding, L., Liu, Z., and Liu, S. (2011). Differentiation of Various Kinds of *Fructus Schisandrae* by Surface Desorption Atmospheric Pressure Chemical Ionization Mass Spectrometry Combined with Principal Component Analysis. *Anal. Chim. Acta* 706, 285–290. doi:10.1016/j.aca.2011.07.013

Posadzki, P., Watson, L., and Ernst, E. (2013). Contamination and Adulteration of Herbal Medicinal Products (HMPs): an Overview of Systematic Reviews. *Eur. J. Clin. Pharmacol.* 69, 295–307. doi:10.1007/s00228-012-1353-z

Qu, B., and Hu, Y. (2011). Non-negative Matrix Factorization-Based SIMCA Method to Classify Traditional Chinese Medicine by HPLC Fingerprints. *J. Chromatogr. Sci.* 49, 189–197. doi:10.1093/chrsci/49.3.189

Rafalski, J. A., Hanafey, M. K., Tingey, S. V., and Williams, J. G. K. (2020). "Technology for Molecular Breeding: RAPD Markers, Microsatellites and Machines," in *Plant Genome Analysis*. Editor P. M. Gresshoff (Boca Raton: CRC Press), 19–27. doi:10.1201/9781003068907-3

Rafi, M., Rismayani, W., Sugiarti, R. M., Syafitri, U. D., Wahyuni, W. T., and Rohaeti, E. (2021). FTIR-based Fingerprinting Combined with Chemometrics for Discrimination of *Sonchus Arvensis* Leaves Extracts of Various Extracting Solvents and the Correlation with its Antioxidant Activity. *Indones. J. Pharm.* 32, 132–140. doi:10.22146/ijp.755

Ratih, G. A. M., Imawati, M. F., Purwanti, D. I., Nugroho, R. R., Wongso, S., Prajogo, B., et al. (2019). Metabolite Profiling of Justicia Gendarussa Herbal Drug Preparations. *Nat. Prod. Commun.* 14, 1934578X19856252. doi:10.1177/1934578x19856252

Razmovski-Naumovski, V., Tongkao-on, W., Kimble, B., Qiao, V. L., Beilun, L., Li, K. M., et al. (2010). Multiple Chromatographic and Chemometric Methods for Quality Standardisation of Chinese Herbal Medicines. *World Sci. Technol.* 12, 99–106. doi:10.1016/s1876-3553(11)60003-3

Reich, E., Schibli, A., and DeBatt, A. (2008). Validation of High-Performance Thin-Layer Chromatographic Methods for the Identification of Botanicals in a cGMP Environment. *J. AOAC Int.* 91, 13–20. doi:10.1093/jaoac/91.1.13

Roblová, V., Bittová, M., Kubáň, P., and Kubáň, V. (2016). Capillary Electrophoresis Fingerprinting and Spectrophotometric Determination of Antioxidant Potential for Classification of *Mentha* Products. *J. Sep. Sci.* 39, 2862–2868.

Rohaeti, E., Karunina, F., and Rafi, M. (2021). FTIR-based Fingerprinting and Chemometrics for Rapid Investigation of Antioxidant Activity from Syzygium Polyanthum Extracts. *Indones. J. Chem.* 21, 128–136. doi:10.22146/ijc.54577

Rohman, A., Wijayanti, T., Windarsih, A., and Riyanto, S. (2020). The Authentication of Java Turmeric (Curcuma Xanthorrhiza) Using Thin Layer Chromatography and 1H-NMR Based-Metabolite Fingerprinting Coupled with Multivariate Analysis. *Molecules* 25, 3928. doi:10.3390/molecules25173928

Rohman, A., and Windarsih, A. (2020). The Application of Molecular Spectroscopy in Combination with Chemometrics for Halal Authentication Analysis: A Review. *Int. J. Mol. Sci.* 21, 1–18. doi:10.3390/ijms21145155

Rohman, A., and Putri, A. R. (2019). The Chemometrics Techniques in Combination with Instrumental Analytical Methods Applied in Halal Authentication Analysis. *Indones. J. Chem.* 19, 262–272. doi:10.22146/ijc.28721

Ruiz, G. G., Nelson, E. O., Kozin, A. F., Turner, T. C., Waters, R. F., and Langland, J. O. (2016). A Lack of Bioactive Predictability for Marker Compounds Commonly Used for Herbal Medicine Standardization. *PloS One* 11, e0159857. doi:10.1371/journal.pone.0159857

Sahoo, N., Manchikanti, P., and Dey, S. (2010). Herbal Drugs: Standards and Regulation. *Fitoterapia* 81, 462–471. doi:10.1016/j.fitote.2010.02.001

Samui, P., and Kothari, D. P. (2011). Utilization of a Least Square Support Vector Machine (LSSVM) for Slope Stability Analysis. *Sci. Iran.* 18, 53–58. doi:10.1016/j.scient.2011.03.007

Shen, M. R., He, Y., and Shi, S. M. (2021). Development of Chromatographic Technologies for the Quality Control of Traditional Chinese Medicine in the Chinese Pharmacopoeia. *J. Pharm. Anal.* 11, 155–162. doi:10.1016/j.jpha.2020.11.008

Shen, M. R., He, Y., and Shi, S. M. (2021). Development of Chromatographic Technologies for the Quality Control of Traditional Chinese Medicine in the Chinese Pharmacopoeia. *J. Pharm. Anal.* 11, 155–162. doi:10.1016/j.jpha.2020.11.008

Shen, Z., Lu, T., Zhang, Z., Cai, C., Yang, J., and Tian, B. (2019). Authentication of Traditional Chinese Medicinal Herb "Gusuibu" by DNA-Based Molecular

Methods. *Industrial Crops Prod.* 141, 111756. doi:10.1016/j.indcrop.2019.111756

Sima, I. A., Andrási, M., and Sârbu, C. (2018). Chemometric Assessment of Chromatographic Methods for Herbal Medicines Authentication and Fingerprinting. *J. Chromatogr. Sci.* 56, 49–55. doi:10.1093/chromsci/bmx080

Singh, I., Juneja, P., Kaur, B., and Kumar, P. (20132013). Pharmaceutical Applications of Chemometric Techniques. *ISRN Anal. Chem.* 2013, 1–13. doi:10.1155/2013/795178

Srivastava, M., Maurya, P., Mishra, S., Kumar, N., and Shanker, K. (2019). Chemotaxonomic Differentiation of *Clerodendrum* Species Based on High-Performance Thin-Layer Chromatographic Fingerprinting of Key Secondary Metabolites and Chemometric Data Analysis. *JPC - J. Planar Chromatogr. - Mod. TLC* 32, 211–222. doi:10.1556/1006.2019.32.3.6

Stilo, F., Bicchi, C., Jimenez-Carvelo, A. M., Cuadros-Rodriguez, L., Reichenbach, S. E., and Cordero, C. (2020). Chromatographic Fingerprinting by Comprehensive Two-Dimensional Chromatography: Fundamentals and Tools. *Trac. Trends Anal. Chem.*, 116133.

Sun, L., Wang, M., Ren, X., Jiang, M., and Deng, Y. (2018). Rapid Authentication and Differentiation of Herbal Medicine Using 1H NMR Fingerprints Coupled with Chemometrics. *J. Pharm. Biomed. Anal.* 160, 323–329. doi:10.1016/j.jpba.2018.08.003

Sun, Y., Guo, T., Sui, Y., and Li, F. (2003). Fingerprint Analysis of *Flos Carthami* by Capillary Electrophoresis. *J. Chromatogr. B Anal. Technol. Biomed. Life Sci.* 792, 147–152. doi:10.1016/s1570-0232(03)00255-1

Taiwan Herbal Pharmacopeia (2019). 3rd ed. TaiwanRepublic of China: Ministry of Health and Welfare.

Talaty, N., Takáts, Z., and Cooks, R. G. (2005). Rapid *In Situ* Detection of Alkaloids in Plant Tissue under Ambient Conditions Using Desorption Electrospray Ionization. *Analyst* 130, 1624–1633. doi:10.1039/b511161g

Thiele, H., Fischer, C., and Decker, J. Statistical Data Analysis of Metabolomics Data, Generated by MS and NMR Spectroscopy Produces Compound Identifications Not Possible with Either Technology Alone. Available at: http://citeseerx.ist.psu.edu/viewdoc/download?doi=10.1.1.570.9695&rep=rep1&type=pdf (Accessed September 28, 2021).

Tnah, L. H., Lee, S. L., Tan, A. L., Lee, C. T., Ng, K. K. S., Ng, C. H., et al. (2019). DNA Barcode Database of Common Herbal Plants in the Tropics: a Resource for Herbal Product Authentication. *Food control.* 95, 318–326. doi:10.1016/j.foodcont.2018.08.022

USP Herbal Medicine Compendium (2021). General-Noticesresources. Available at: https://hmc.usp.org/about/general-noticesresources (Accessed August 26, 2021).

USP44-NF39 (2021d). General Chapters, General Test and Assay, <1010> Analytical Data-Interpretation and Treatment. Available at: https://online.uspnf.com/uspnf/document/1_GUID-5C0818CD-E76F-44B8-B504-C202CA762F2A_5_en-US (Accessed July 5, 2021).

USP44-NF39 (2021e). General Chapters, General Test and Assay, <1039> Chemometrics. Available at: https://online.uspnf.com/uspnf/document/1_GUID-9E862365-D262-4D50-8CA9-CFF0D4577262_2_en-US (Accessed August 20, 2021).

USP44-NF39 (2021f). General Chapters, General Test and Assay, <1064> Identification of Articles of Botanical Origin by HPTLC Procedure. Available at: https://online.uspnf.com/uspnf/document/1_GUID-A80A5CE0-E573-4DE1-90C3-0B1A098FA991_1_en-US (Accessed August 27, 2021).

USP44-NF39 (2021g). *General Chapters, General Test and Assay, <1210>, Statistical Tool for Procedure Validation. 1–14.* Available at: https://online.uspnf.com/uspnf/document/1_GUID-13ED4BEB-4086-43B5-A7D7-994A02AF25C8_6_en-US (Accessed August 6, 2021).

USP44-NF39 (2021h). General Chapters, General Test and Assay, <1225>, Validation of Compendial Procedure. Available at: https://online.uspnf.com/uspnf/document/1_GUID-E2C6F9E8-EA71-4B72-A7BA-76ABD5E72964_4_en-US (Accessed September 4, 2021).

USP44-NF39 (2021a). *General Chapters, General Test and Assay, <203> HPTLC Procedure for Identification of Articles of Botanical Origin*, 1–3. Available at: https://online.uspnf.com/uspnf/document/1_GUID-AC55337F-C4CA-4792-9D64-59C649957B03_2_en-US (Accessed August 27, 2021).

USP44-NF39 (2021b). General Chapters, General Test and Assay, <561> Articles of Botanical Origin. Available at: https://online.uspnf.com/uspnf/document/1_GUID-E8A1366F-9657-41FC-9EDC-C20F4BE473B6_5_en-US (Accessed August 26, 2021).1–15.

USP44-NF39 (2021c). General Chapters, General Test and Assay, <563> Identification of Articles of Botanical Origin. Available at: https://online.uspnf.com/uspnf/document/1_GUID-C265E70B-F143-40B5-BE1B-3C74F9986762_3_en-US (Accessed August 27, 2021).1–11.

Wagner, H., Bauer, R., Melchart, D., Xiao, P. G., and Staudinger, A. (2011). *Chromatographic Fingerprint Analysis of Herbal Medicines*. Berlin: Springer.

Walji, R., Boon, H., Barnes, J., Austin, Z., Baker, G. R., and Welsh, S. (2009). Adverse Event Reporting for Herbal Medicines: a Result of Market Forces. *Healthc. Policy* 4, 77–90. doi:10.12927/hcpol.2009.20820

Wang, H., So, P. K., and Yao, Z. P. (2014a). Direct Analysis of Herbal Powders by Pipette-Tip Electrospray Ionization Mass Spectrometry. *Anal. Chim. Acta* 809, 109–116. doi:10.1016/j.aca.2013.11.060

Wang, L., Liu, L. F., Wang, J. Y., Shi, Z. Q., Chang, W. Q., Chen, M. L., et al. (2017). A Strategy to Identify and Quantify Closely Related Adulterant Herbal Materials by Mass Spectrometry-Based Partial Least Squares Regression. *Anal. Chim. Acta* 977, 28–35. doi:10.1016/j.aca.2017.04.023

Wang, P., and Yu, Z. (2015). Species Authentication and Geographical Origin Discrimination of Herbal Medicines by Near Infrared Spectroscopy: A Review. *J. Pharm. Anal.* 5, 277–284. doi:10.1016/j.jpha.2015.04.001

Wang, X., Jiang, Q., Li, H., and Chen, D. D. Y. (2021a). Rapid Fingerprint Analysis for Herbal Polysaccharides Using Direct Analysis in Real-Time Ionization Mass Spectrometry. *Rapid Commun. Mass Spectrom.* 35, e9139. doi:10.1002/rcm.9139

Wang, X., Liu, X., Wang, J., Wang, G., Zhang, Y., Lan, L., et al. (2021b). Study on Multiple Fingerprint Profiles Control and Quantitative Analysis of Multi-Components by Single Marker Method Combined with Chemometrics Based on Yankening Tablets. *Spectrochimica Acta Part A Mol. Biomol. Spectrosc.* 253, 119554. doi:10.1016/j.saa.2021.119554

Wang, Y., Sun, G., Liu, Z., Liu, Y., Gao, Y., Zhang, J., et al. (2014b). Capillary Electrophoresis Fingerprinting Coupled with Chemometrics to Evaluate the Quality Consistency and Predict the Antioxidant Activity of Sanhuang Tablet as Part of its Quality Control. *J. Sep. Sci.* 37, 3571–3578. doi:10.1002/jssc.201400765

Want, E. J., Wilson, I. D., Gika, H., Theodoridis, G., Plumb, R. S., Shockcor, J., et al. (2010). Global Metabolic Profiling Procedures for Urine Using UPLC-MS. *Nat. Protoc.* 5, 1005–1018. doi:10.1038/nprot.2010.50

Wei, X. C., Cao, B., Luo, C. H., Huang, H. Z., Tan, P., Xu, X. R., et al. (2020). Recent Advances of Novel Technologies for Quality Consistency Assessment of Natural Herbal Medicines and Preparations. *Chin. Med.* 15, 56–24. doi:10.1186/s13020-020-00335-9

Welsh, J., and McClelland, M. (1990). Fingerprinting Genomes Using PCR with Arbitrary Primers. *Nucleic Acids Res.* 18, 7213–7218. doi:10.1093/nar/18.24.7213

Westad, F., and Marini, F. (2015). Validation of Chemometric Models - a Tutorial. *Anal. Chim. Acta* 893, 14–24. doi:10.1016/j.aca.2015.06.056

WHO (2017). Good Pharmacopeial Practices: Draft Chapter on Monographs on Herbal Medicines. Available at: https://www.who.int/medicines/areas/quality_safety/quality_assurance/GPhP-HerbalsChapter_QAS15-621_Rev4-07_09_2017.pdf?ua=1 (Accessed August 26, 2021).

WHO (2019). *WHO Global Report on Traditional and Complementary Medicine 2019.* Luxembourg: World Health Organization.

Wong, H. Y., Hu, B., So, P. K., Chan, C. O., Mok, D. K., Xin, G. Z., et al. (2016). Rapid Authentication of *Gastrodiae Rhizoma* by Direct Ionization Mass Spectrometry. *Anal. Chim. Acta* 938, 90–97. doi:10.1016/j.aca.2016.07.028

Wulandari, L., Idroes, R., Noviandy, T. R., and Indrayanto, G. (2022). "Application of Chemometrics Using Direct Spectroscopic Methods as a QC Tool in Pharmaceutical Industry and Their Validation," in *Profile of Drug Substances, Excipients and Related Methodology*. Editor A. A. Almajed (Academic Press, Elsevier Inc.). doi:10.1016/bs.podrm.2021.10.006

Xin, G. Z., Hu, B., Shi, Z. Q., Lam, Y. C., Dong, T. T., Li, P., et al. (2014). Rapid Identification of Plant Materials by Wooden-Tip Electrospray Ionization Mass Spectrometry and a Strategy to Differentiate the Bulbs of *Fritillaria*. *Anal. Chim. Acta* 820, 84–91. doi:10.1016/j.aca.2014.02.039

Yan, H., Sun, G., Zhang, J., Sun, W., Hou, Z., Li, X., et al. (2021). Overall Control Herbal Medicine in Best Consistency. *J. Pharm. Biomed. Anal.* 195, 113867. doi:10.1016/j.jpba.2020.113867

Yang, Y., and Deng, J. (2016). Analysis of Pharmaceutical Products and Herbal Medicines Using Ambient Mass Spectrometry. *TrAC Trends Anal. Chem.* 82, 68–88. doi:10.1016/j.trac.2016.04.011

Yao, Z., Yu, J., Tang, Z., Liu, H., Ruan, K., Song, Z., et al. (2019). Multi-evaluating Strategy for Siji-Kangbingdu Mixture: Chemical Profiling, Fingerprint Characterization, and Quantitative Analysis. *Molecules* 24, 3545. doi:10.3390/molecules24193545

Yu, K., Gong, Y., Lin, Z., and Cheng, Y. (2007). Quantitative Analysis and Chromatographic Fingerprinting for the Quality Evaluation of *Scutellaria Baicalensis* Georgi Using Capillary Electrophoresis. *J. Pharm. Biomed. Anal.* 43, 540–548. doi:10.1016/j.jpba.2006.08.011

Yu, N., Han, J., Deng, T., Chen, L., Zhang, J., Xing, R., et al. (2021). A Novel Analytical Droplet Digital PCR Method for Identification and Quantification of Raw Health Food Material Powder from *Panax Notoginseng*. *Food Anal. Methods* 14, 552–560. doi:10.1007/s12161-020-01887-0

Zeng, J., He, M., Wu, H., Fu, S., and Zhang, Z. (2021). Peak Alignment for Herbal Fingerprints from Liquid Chromatography-High Resolution Mass Spectrometry via Diffusion Model and Bi-directional Eigenvalues. *Microchem. J.* 167, 106296. doi:10.1016/j.microc.2021.106296

Zha, X.-Q., Luo, J.-P., and Wei, P. (2009). Identification and Classification of Dendrobium Candidum Species by Fingerprint Technology with Capillary Electrophoresis. *South Afr. J. Bot.* 75, 276–282. doi:10.1016/j.sajb.2009.02.002

Zhang, C., Zheng, X., Ni, H., Li, P., and Li, H. J. (2018). Discovery of Quality Control Markers from Traditional Chinese Medicines by Fingerprint-Efficacy Modeling: Current Status and Future Perspectives. *J. Pharm. Biomed. Anal.* 159, 296–304. doi:10.1016/j.jpba.2018.07.006

Zhang, Q. F., and Cheung, H. Y. (2011). Development of Capillary Electrophoresis Fingerprint for Quality Control of *Rhizoma Smilacis Glabrae*. *Phytochem. Anal.* 22, 18–25. doi:10.1002/pca.1245

Zhang, X., Chen, Z. Y., Qiu, Z. D., Liu, M., Xu, J., Lai, C. J., et al. (2022). Molecular Differentiation of *Panax Notoginseng* Grown under Different Conditions by Internal Extractive Electrospray Ionization Mass Spectrometry and Multivariate Analysis. *Phytochemistry* 194, 113030. doi:10.1016/j.phytochem.2021.113030

Zhang, Y., Yang, F., Zhang, J., Sun, G., Wang, C., Guo, Y., et al. (2019). Quantitative Fingerprint and Quality Control Analysis of Compound Liquorice Tablet Combined with Antioxidant Activities and Chemometrics Methods. *Phytomedicine* 59, 152790. doi:10.1016/j.phymed.2018.12.013

Zhang, Z.-L., Song, M.-F., Guan, Y.-H., Li, H.-T., Niu, Y.-F., Zhang, L.-X., et al. (2015). DNA Barcoding in Medicinal Plants: Testing the Potential of a Proposed Barcoding Marker for Identification of *Uncaria* Species from China. *Biochem. Syst. Ecol.* 60, 8–14. doi:10.1016/j.bse.2015.02.017

Zhao, L., Rupji, M., Choudhary, I., Osan, R., Kapoor, S., Zhang, H. J., et al. (2020). Efficacy Based Ginger Fingerprinting Reveals Potential Antiproliferative Analytes for Triple Negative Breast Cancer. *Sci. Rep.* 10 (19182), 1–11. doi:10.1038/s41598-020-75707-0

Zhao, Y., Ma, X., Fan, L., Mao, F., Tian, H., Xu, R., et al. (2017). Discrimination of Geographical Origin of Cultivated Polygala Tenuifolia Based on Multi-Element Fingerprinting by Inductively Coupled Plasma Mass Spectrometry. *Sci. Rep.* 7 (12577), 1–10. doi:10.1038/s41598-017-12933-z

Zhokhova, E. V., Rodionov, A. V., Povydysh, M. N., Goncharov, M. Y., Protasova, Y. A., and Yakovlev, G. P. (2019). Current State and Prospects of DNA Barcoding and DNA Fingerprinting in the Analysis of the Quality of Plant Raw Materials and Plant-Derived Drugs. *Biol. Bull. Rev.* 9, 301–314. doi:10.1134/s2079086419040030

Conflict of Interest: The authors declare that the research was conducted in the absence of any commercial or financial relationships that could be construed as a potential conflict of interest.

Publisher's Note: All claims expressed in this article are solely those of the authors and do not necessarily represent those of their affiliated organizations, or those of the publisher, the editors and the reviewers. Any product that may be evaluated in this article, or claim that may be made by its manufacturer, is not guaranteed or endorsed by the publisher.

frontiers | Frontiers in Pharmacology

SYSTEMATIC REVIEW
published: 08 June 2022
doi: 10.3389/fphar.2022.855384

Authentication of *Marantodes pumilum* (Blume) Kuntze: A Systematic Review

Ida Syazrina Ibrahim[1], *Mazlina Mohd Said*[1], *Noraida Mohammad Zainoor*[2] *and Jamia Azdina Jamal*[1]*

[1]*Drug and Herbal Research Centre, Faculty of Pharmacy, Universiti Kebangsaan Malaysia, Kuala Lumpur, Malaysia,* [2]*National Pharmaceutical Regulatory Agency, Petaling Jaya, Malaysia*

Botanical drug products consist of complex phytochemical constituents that vary based on various factors that substantially produce different pharmacological activities and possible side effects. *Marantodes pumilum* (Blume) Kuntze (Primulaceae) is one of the most popular Malay traditional botanical drugs and widely recognized for its medicinal use. Many studies have been conducted focusing on the identification of bioactive substances, pharmacological and toxicological activities in its specific varieties but less comprehensive study on *M. pumilum* authentication. Lack of quality control (QC) measurement assessment may cause different quality issues on *M. pumilum* containing products like adulteration by pharmaceutical substances, substitution, contamination, misidentification with toxic plant species, which may be detrimental to consumers' health and safety. This systematic literature review aims to provide an overview of the current scenario on the quality control of botanical drug products as determined by pharmacopoeia requirements specifically for *M. pumilum* authentication or identification. A systematic search for peer-reviewed publications to document literature search for *M. pumilum* authentication was performed using four electronic databases: Web of Science, PubMed, Scopus and ScienceDirect for related studies from January 2010 to December 2021. The research studies published in English and related articles for identification or authentication of *M. pumilum* were the main inclusion criteria in this review. A total 122 articles were identified, whereby 33 articles met the inclusion criteria. Macroscopy, microscopy, chemical fingerprinting techniques using chromatography, spectroscopy and hyphenated techniques, and genetic-based fingerprinting using DNA barcoding method have been used to identify *M. pumilum* and to distinguish between different varieties and plant parts. The study concluded that a combination of approaches is necessary for authenticating botanical drug substances and products containing *M. pumilum* to assure the quality, safety, and efficacy of marketed botanical drug products, particularly those with therapeutic claims.

Keywords: authentication, identification, fingerprinting, *Marantodes pumilum*, quality control

OPEN ACCESS

Edited by:
Abdul Rohman,
Gadjah Mada University, Indonesia

Reviewed by:
Faezah Mohd Salleh,
University of Technology Malaysia, Malaysia
Kwabena F.M. Opuni,
University of Ghana, Ghana

***Correspondence:**
Jamia Azdina Jamal
jamia@ukm.edu.my

Specialty section:
This article was submitted to Ethnopharmacology, a section of the journal Frontiers in Pharmacology

Received: *15 January 2022*
Accepted: *27 April 2022*
Published: *08 June 2022*

Citation:
Ibrahim IS, Mohd Said M, Mohammad Zainoor N and Jamal JA (2022) Authentication of Marantodes pumilum (Blume) Kuntze: A Systematic Review. Front. Pharmacol. 13:855384. doi: 10.3389/fphar.2022.855384

INTRODUCTION

Since ancient times, botanical drugs have been employed in the daily lives of the world population due to their medicinal efficacy in promoting well-being and health. Around 80% of the world's population consumes botanical drugs as health supplements since they are thought to be effective in disease management and have been recognized as safe for decades owing to their natural origin. Despite the widespread use of botanical drug products for a long time, problems with quality control persist. The increased demand for botanical drug products may expose them to various types of adulteration, such as substitution, contamination, or the use of fillers, all of which represent a threat to the health and safety of consumers (Techen et al., 2014; Abubakar et al., 2018). In fact, different countries define botanical drug products differently and use different systems for registering, licensing, dispensing, manufacturing, and trading them to ensure their safety, efficacy, and quality. As a result, there is a disparity in registration requirements between countries and variation in the botanical drugs quality.

Recognizing the need, for the past few decades, WHO has consistently issued various guidelines and policies related to botanical drugs, such as Guidelines for the Assessment of Herbal Medicines, Good Agricultural and Collection Practices (GACP) and Quality Control Methods for Medicinal Plant Materials, with the goal of standardizing and harmonizing botanical drugs regulation globally (Yadav and Dixit, 2008). Currently, botanical drug products must meet pharmacopoeia identification requirements for organoleptic evaluation (touch, smell, sight, and taste), macroscopic evaluation (shape, color, and texture), microscopic assessment and chemical fingerprint techniques such as chromatography and spectroscopy (Li et al., 2020). Additionally, the British Pharmacopoeia has included DNA barcoding as a means of identifying botanical drugs (Heinrich and Anagnostou, 2017). In fact, Malaysia's regulatory body has consistently adopted various international guidelines issued by the World Health Organization (WHO), Medicines and Healthcare Products Regulatory Agency (MHRA), European Medicines Agency (EMA), Therapeutic Goods Administration (TGA), and Food and Drug Administration (FDA) to strengthen the registration requirements for botanical drug products since 1992. It is vital to identify and authenticate botanical drugs and products utilizing a variety of approaches, whether during the final product phase for clinical study evaluation or throughout product development for the market (Smillie and Khan, 2010).

Due to the open online market, the botanical drug-based industry has also piqued the interest of Asian countries. Malaysia's forest is home to a diverse array of medicinal plants with a great potential for use in the botanical drugs industry. Malaysia's botanical drugs domestic market was expected to grow at a 15% annual rate from RM7 billion in 2010 to around RM29 billion by 2020 (Fadzil et al., 2018). The increase in the number of botanical drug products registered with the National Pharmaceutical Regulatory Agency (NPRA) demonstrates the growing demand for botanical drug products (Fadzil et al., 2018). Realizing the huge economic opportunities in the local botanical drugs industry and the requirements that need to be complied with, the agricultural National Key Economic Areas (NKEA) Entry Point Project 1 (EPP1) was focused on potential growth that might contribute to Malaysia's gross national income (GNI). Due to their potential therapeutic properties, Malaysia's government has identified 11 important plants, including *Eurycoma longifolia* Jack (Simaroubaceae), *Marantodes pumilum* (Blume) Kuntze (Primulaceae), *Andrographis paniculata* (Burm.f.) Nees (Acanthaceae), and others, to be commercialized as high-value botanical drug products. *M. pumilum*, locally known as Kacip Fatimah, is widely spread in Southeast Asian tropical forests and is well-known for its medicinal properties. It is a member of the Primulaceae family and was formally recognized as a member of the family Myrsinaceae and known as *Labisia pumila* (Blume) Fern.-Vill (WFO, 2022). In various parts of Malaysia, *M. pumilum* is referred to as kachip patimah, selusuh fatimah, rumput siti fatimah, akar fatimah, kachit fatimah, pokok pinggang, rumput palis, tadah matahari, mata pelandok rimba, bunga belangkas hutan (Chua et al., 2011) and sangkoh (Iban) (Abdullah et al., 2013). There are eight *M. pumilum* varieties and only three varieties; var. *alata* (Scheff.) Mez., var. *pumila* and var. *lanceolata* (Scheff.) Mez. are widely distributed in Malaysia rain forest and have attracted the researcher's interest thus far (Sunarno, 2005; Chua et al., 2012). The three varieties can be distinguished by their petioles and leaf characteristics. *M. pumilum* var. *alata* has red veins and broad winged petioles, whereas var. *pumila* has an emarginate winged petiole and an ovate leaf blade, and var. *lanceolata* has a long, non-winged or terete petiole (**Figure 1**). However, due to the close macromorphological features, it was extremely difficult to visually separate them based on petiole characteristics, particularly when the petioles were not fully formed (Abdullah et al., 2012).

Traditionally, indigenous women of the Malay Archipelago consumed water decoctions of *M. pumilum* to aid in labor and delivery, while the botanical drug is believed to tone the abdominal muscles, assist in tightening the birth canal, and enhance overall body strength during postpartum (Zakaria and Mohd, 1994). Additionally, ancient communities employed the *M. pumilum* to treat diarrhoea, rheumatism, gonorrhea and flatulence (Burkill, 1966). Numerous research has shown that *M. pumilum* has a wide range of pharmacological activities, including antibacterial, antifungal, anti-inflammatory, cytotoxicity, antioxidative, xanthine oxidase inhibitory, phytoestrogenic, anticarcinogenic, anti-aging, anti-hyperuricemia, anti-osteoporotic, anti-obesity, cardioprotective effect, and uterotonic (Norhaiza et al., 2009; Choi et al., 2010; Karimi et al., 2011, 2013; Pihie et al., 2011; Jamal et al., 2012; Mamat et al., 2014; Pandey et al., 2014; Dianita et al., 2016; Hairi et al., 2018; Wan Omar et al., 2019; Aladdin et al., 2020; Rahmi et al., 2020).

Phytochemical constituents found in *M. pumilum* varieties include flavonoids, phenolics, methyl gallate, carotenoids, ascorbic acids, fatty acids, saponins, alkenyl compounds and benzoquinone derivatives (Ahmad et al., 2018). Many variables influence the phytochemical constituents, such as environmental

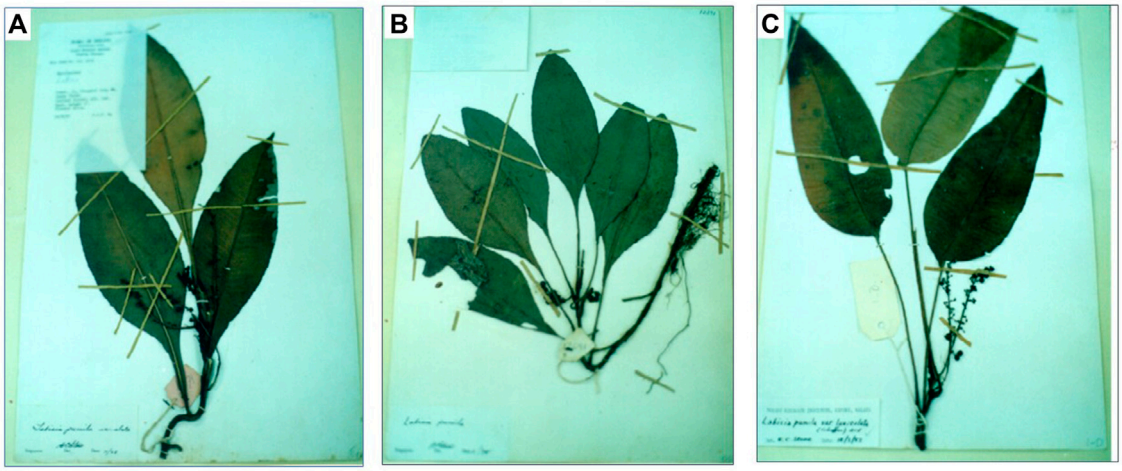

FIGURE 1 | Voucher specimens of **(A)** *Marantodes pumilum* var. *alata*, **(B)** *Marantodes pumilum* var. *pumila* and **(C)** *Marantodes pumilum* var. *lanceolata* (obtained from the Kepong Herbarium of Forest Research Institute Malaysia).

factors, species varieties and plant parts. The variation in phytochemical contents between batches often results in markedly variable pharmacological actions and probable side effects (Liang et al., 2004; Goodarzi et al., 2013). According to Karimi et al. (2011), the phytochemical constituent presence and abundance differs between *M. pumilum* varieties and plant parts. The study indicated that gallic acid was highest in var. *alata* leaves, followed by var. *lanceolata* leaves and var. *pumila* leaves. Several studies have established that different *M. pumilum* species and plant parts possess distinct pharmacological properties, including phytoestrogenic activity of var. *alata* leaves (Giaze et al., 2018; Hairi et al., 2018), xanthine oxidase inhibitory activity of var. *pumila* leaves (Aladdin et al., 2020) and anti-inflammatory effect of var. *pumila* roots (Rahmi et al., 2020).

Due to the wide range of phytochemicals found in this plant that can contribute to different pharmacological effects and side effects, majority of research on *M. pumilum* has focused on the bioactive substances, pharmacological and toxicological activities and less studies conducted specifically on its identification and authentication. As such, the aim of this review is to present an overview of the current state of authentication for *M. pumilum* in the global botanical drug products industry.

MATERIALS AND METHODS

Search Strategy

A systematic review of the literature was conducted in accordance with the Preferred Reporting Items for Systematic Reviews and Meta-Analyses (PRISMA) guideline (Moher et al., 2009). A search strategy based on a combination of relevant keywords and Boolean operators was used [ALL = (authentication or identification or quality control or chemical profiling or fingerprint) and (marantodes pumilum or labisia pumila or kacip fatimah)] for Web of Science database and [("authentication" OR "identification" OR "quality control" OR "chemical profiling" OR "fingerprint") AND ("marantodes pumilum" OR "labisia pumila" OR "kacip Fatimah")] for PubMed, Scopus and ScienceDirect databases. Following the search conducted on 18 November 2021, the option "search alert" was selected to receive weekly updates for all four literature databases. All the selected articles were saved in Mendeley Desktop Version 1.19.8 (2008–2020) reference manager.

Selection Process and Criteria

Identification: Database searches identified 606 records (WoS = 22, PubMed = 4, Scopus = 499 and ScienceDirect = 81).

Screening: Articles were screened manually in four stages. Initially, articles that were published as a review, book chapter, or conference proceeding were excluded. Secondly, articles that were published between January 2010 and December 2021 were considered. Thirdly, articles without data or information on the identification or authentication of *Marantodes pumilum* (Kacip Fatimah) as botanical drug substances or botanical drug products were omitted. Following screening, 552 articles were deleted. Finally, duplicate entries were removed from the databases, leaving 37 eligible articles.

Eligibility: A total of 37 full-text papers were evaluated and screened for eligibility using the following criteria:

1. The tested sample was required to be made up of botanical drug substances or botanical drug products. A variety of scientific names, that is, *Labisia pumila* (synonym), *Marantodes pumilum*, and the common name Kacip Fatimah were accepted for the review.
2. The details of the tested sample, including the collection site, plant species, plant parts and sample processing, were clearly documented and described.
3. All pertinent methodologies within the scope of the studies were accepted. The tested samples were authenticated using several techniques, including macroscopic and microscopic

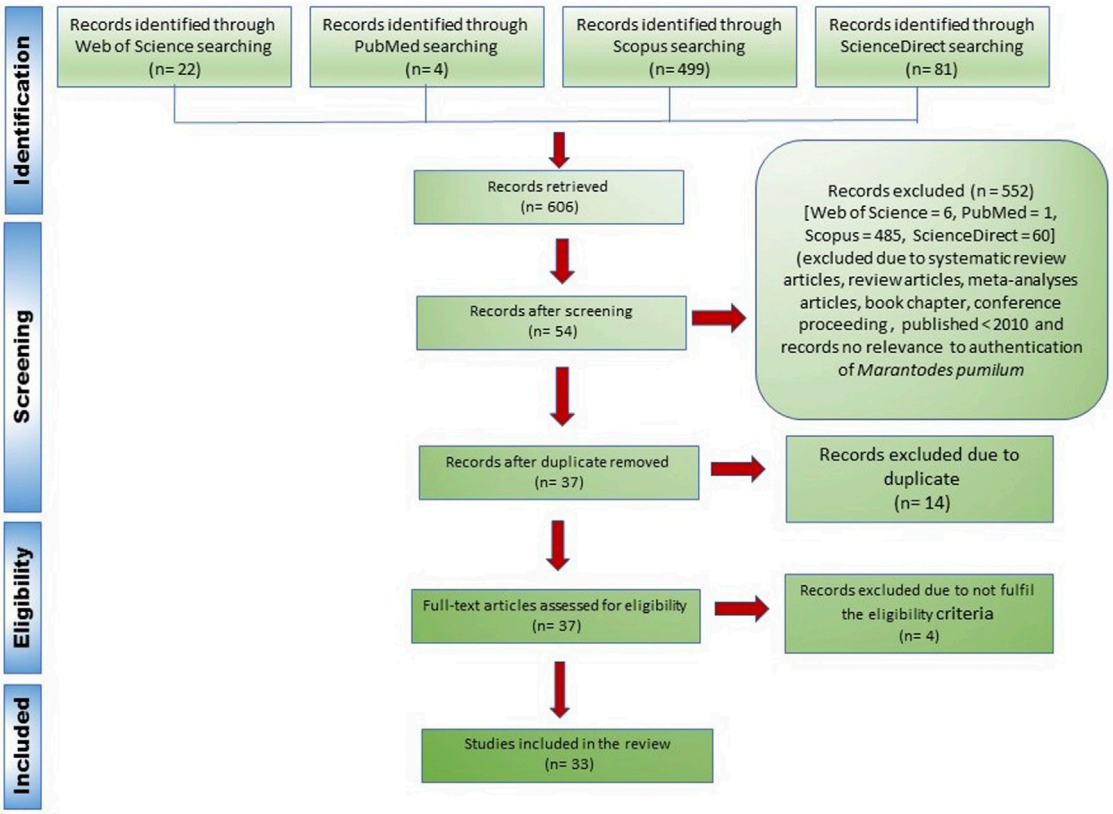

FIGURE 2 | Flowchart of the article search process according to the PRISMA guidelines (Moher et al., 2009).

methods, chemical fingerprinting, genetic fingerprinting, and phytochemical analysis.

Included: 33 peer-reviewed articles were included in the systematic review of the literature, as described in **Figure 2**. The flowchart was made in accordance with PRISMA guidelines (Moher et al., 2009).

RESULTS

All selected articles were published between January 2010 and December 2021 (**Table 1**). Thirty-three full-text articles met the inclusion criteria and were classified as research articles in this review. Majority of the included full-text articles were conducted locally at various universities and institutions in Malaysia, while six were conducted abroad in China (study 24), Sweden (studies 1 and 5), the United States of America (studies 6 and 7) and India (study 2). Even though the genus *Labisia* was reclassified as *Marantodes* in 2012, 81% (n = 27) of publications cited *Labisia pumila* rather than *Marantodes pumilum*. Four studies were conducted on all three common varieties of *M. pumilum* var. *alata*, var. *pumila*, and var. *lanceolata*; one study used *M. pumilum* var. *alata* and var. *pumila*, sixteen studies focused exclusively on *M. pumilum* var. *alata*, one study used only *M. pumilum* var. *pumila* and ten studies made no mention of the *M. pumilum* variety. On average, 70% of publications indicated the variety used in the study, with the remaining 30% of articles lacking identification at variety level. Apart from that, 60.6% (n = 20) studies used *M. pumilum* leaves, whereas other studies used whole plants (21.2%, n = 7), leaves and stem/roots (15.15%, n = 5), and stem-roots (3%, n = 1). According to the review, (72.7%, n = 24) majority of the researchers used wild plant sources rather than cultivated sources.

Notably, all investigations included in this review employed at least one approach for identifying or authenticating *M. pumilum*. Generally, about (66.70%, n = 22) of the study conducted morphological tests on the *M. pumilum* samples and 67.7% (n = 23) of the 33 study included the voucher specimen number for the test samples except for studies 1, 3, 9, 11, 12, 14, 15, 22, 24, and 29. Multiple sources of *M. pumilum* from different areas in Malaysia were used in 18.2% (n = 6) of research conducted abroad. Botanists authenticated most test samples based on morphological identification, except for those used in studies 1 and 24 that were conducted in China and Sweden, respectively, due to the lack of information on morphological identification and voucher specimen for *M. pumilum* in the articles compared to other studies. Qualified botanists in public educational institutions and government research institutions performed the plant authentication.

TABLE 1 | Authentication and identification methods of *Marantodes pumilum* botanical drug substances and commercial products.

No.	Study	Species and sources	Voucher specimen	Identification/Authentication Methods
1	Mannerås et al. (2010)	Whole plant of *L. pumila* var. *alata,* (Wild plant from rainforest of Peninsular Malaysia)	Not available	Not available
2	Pandey et al. (2010)	Leaf of *L. pumila,* (Wild plant from Perak)	21648	Morphology
3	Pattiram et al. (2011)	Leaf of *L. pumila,* [Wild plant (unkown source)]	Not available	GCMS
4	Chua et al. (2011)	Leaf of *L. pumila* var. *alata, L. pumila* var. *pumila,* [Cultivated plant from Forest Research Institute Malaysia (FRIM)]	FRI 59810	Phytochemical screening, UPLC/ESI/MS/MS, chemometrics
5	Fazliana et al. (2011)	Whole plant of *L. pumila* var. *alata*, (Wild plant from Pahang)	FRI54816	Morphology
6	Ali and Khan (2011)	Root of *L. pumila,* (Cultivated plant supplied by Holista Biotech Sdn. Bhd.)	PID26	Morphology, NMR, IR, TLC, HPLC
7	Avula et al. (2011)	Leaf and stem-root of *L. pumila* var. *alata,* (Cultivated plant supplied by Holista Biotech Sdn. Bhd.)	3809, 3810, 8400, 5002, 5003, 5004 (United States)	TLC, IR, HPLC/UV/ELSD, LC/ESI/TOF, NMR, HRESI/MS
8	Al-Mekhlafi et al. (2012)	Leaf of *L. pumila,* (Wild plant from Pahang)	ACP0084/08	UV, IR, NMR
9	Abdullah et al. (2012)	Leaf of *L. pumila* var. *alata, L. pumila* var. *pumila* and *L. pumila* var. *lanceolata,* (Wild plant from Negeri Sembilan, Johor, Pahang, and Kedah)	Not available	IR, chemometric analysis
10	Pan et al. (2012)	Whole plant of *L. pumila,* (Wild plant from Perak)	I/LP/3547	Morphology, HPLC
11	Abdah et al. (2014)	Leaf of *L. pumila* var. *alata,* (Cultivated plant from FRIM)	Not Available	HPLC
12	Effendy et al. (2014)	Whole plant of *L. pumila* var. *alata*, (Wild plant from Kedah)	Not available	Morphology, phytochemical screening
13	Tnah et al. (2014)	Leaf of *L. pumila* var. *alata,* var. *pumila* and var. *lanceolata*, (Wild plant from Pasoh Forest Reserve, Negeri Sembilan)	KEP 223663—223665	Morphology, DNA barcoding
14	Norhayati et al. (2014)	Whole plant of *L. pumila* var. *alata,* [Wild plant (unknown source)]	Not available	HPLC
15	Karimi et al. (2015)	Leaf of *L. pumila* var. *alata, L. pumila* var. *pumila* and *L. pumila* var. *lanceolata*, (Wild plant from Sungkai, Perak; Hulu Langat, Selangor; and Kota Tinggi, Johor)	Not available	Phytochemical screening
16	Aladdin et al. (2016)	*M. pumilum* var. *alata, M. pumilum* var. *pumila* and *M. pumilum* var. *lanceolata,* (Wild plant from Bujang Melaka Forest Reserve, Kampar, Perak)	UKMB 30006/SM 2622, UKMB 30007/SM s.n., UKMB 30008/SM s.n, respectively	Morphology, microscopy, HPTLC, HPLC, ATR-FTIR
17	Dianita et al. (2016)	Whole plant of *L. pumila* var. *alata,* (Wild plant from Perak]	UKMB 30010	Morphology, HPLC
18	Karimi et al. (2016)	Leaf of *L. pumila* var. *alata,* [Cultivated plant from Universiti Putra Malaysia (UPM)]	Stone 6030 (KLU) (UPM)	Morphology, HPLC, GC and GC/MS
19	Adam et al. (2017)	Leaf of *M. pumilum,* (Wild plant from Perak)	KLU49047 (UM)	Morphology, LC/MS
20	Latiff et al. (2018)	Leaf of *L. pumila* var. *alata,* (Cultivated plant from FRIM)	FRI 59810	Morphology, LC/MS/MS
21	Giribabu et al. (2018)	Leaf of *M. pumilum,* (Wild plant from Tapah, Perak)	KLU 46767	Morphology, UPLC/MS/MS
22	Tnah et al. (2019)	Leaf of *L. pumila*, (Wild plant from forest reserves, botanical gardens and medicinal plant nurseries in Peninsular Malaysia and commercial products)	Not available	Morphology, DNA barcoding
23	Giaze et al. (2019)	Leaf and stem-root of *M. pumilum* var. *alata*, (Wild plant from Simpang Empat, Kedah)	UKM-HF131	Morphology, LC/MS
24	Wu et al. (2019)	Leaf and stem of *L. pumila,* (Cultivated plant from FRIM)	Not available	UPLC/MS/MS
25	Tan et al. (2019)	Leaf of *M. pumilum,* (Wild plant from Tapah, Perak)	KLU49047 (UM)	Morphology, LC/MS/MS
26	Muhamad et al. (2019)	Leaf of *L. pumila* var. *alata,* (Wild plant from Tapah, Perak)	FF/UiTM/KF/02/13	Morphology, LC/MS
27	Wan Omar et al., (2019)	Leaf of *M. pumilum* var. *alata,* (Wild plant from Tapah, Perak)	KLU49047 (UM)	Morphology, LC/MS
28	Dharmani et al. (2019)	Leaf and stem-root of *L. pumila* var. *alata,* (Wild plant supplied by Delima Jelita Herbs, Kedah)	UKMHF131	Morphology, LC/MS/MS
29	Salehan et al. (2020)	Leaf of *L. pumila* var. *alata*, (Wild plant from Alor Setar, Kedah)	Not available	LC/MS Q-TOF
30	Radzali et al. (2020)	Leaf of *L. pumila* var. *pumila,* ((unknown) from Batu Pahat, Johor)	UKMB 30007/SM sn	Morphology, HPLC
31	Manshor et al. (2020)	Aerial part and leaf of *L. pumila,* (Wild plant from Sungai Siput Utara, Perak)	11632	Morphology, HPLC

(Continued on following page)

TABLE 1 | (*Continued*) Authentication and identification methods of *Marantodes pumilum* botanical drug substances and commercial products.

No.	Study	Species and sources	Voucher specimen	Identification/Authentication Methods
32	Yeop et al. (2021)	Whole plant of *L. pumila* var. *alata*, (Wild plant from Bentong, Pahang)	PIIUM 0321	Morphology, UPLC/PDA, UPLC/QTOF/MS
33	Tarmizi et al. (2021)	*Labisia pumila* var. *alata* and *L. pumila* var. *pumila (red and green leaf)* (Cultivated plant from Batu Pahat, Johor)	PID 250817-17 (LPPG), PID 260817-17 (LPPR), PID 270817-17 (LPA)	Morphology, HPLC, DNA barcoding

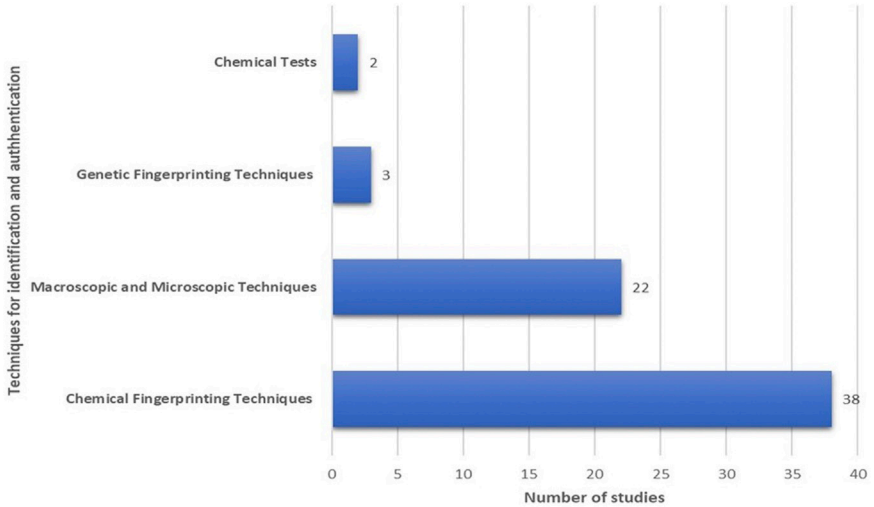

FIGURE 3 | *Marantodes pumilum* identification and authentication techniques reported between 2010 and 2021.

The researchers' choice of approaches for detecting phytochemical characteristics varies according to the sensitivity of the procedures. Most studies employed chemical fingerprinting techniques (58.46%, n = 38), followed by macroscopic and microscopic techniques (33.85%, n = 22), genetic fingerprinting techniques (4.6%, n = 3) and chemical tests (3.07%, n = 2) (**Figure 3**). Less sensitive techniques such as ultraviolet (UV) spectroscopy, thin layer chromatography (TLC), high performance thin layer chromatography (HPTLC) and Fourier transform infrared (FTIR) spectroscopy were complemented by high-end instruments such as liquid chromatography-mass spectrometry (LC/MS/MS) or nuclear magnetic resonance (NMR). Among the chromatographic techniques, HPLC is the mostly used method (30.30%, n = 10), followed by HPTLC/TLC (12.12%, n = 4) and gas chromatography (GC) (3.03%, n = 1). Over the past 10 years, a total of 36.6% (n = 12) studies have applied the hyphenated chromatographic and mass spectrometric techniques in their research.

Two studies (12 and 15) used phytochemical screening, whereas study 4 combined phytochemical analysis with a more advanced instrument, ultra-performance liquid chromatography coupled with electrospray ionization tandem mass spectrometry (UPLC/ESI/MS/MS), to identify the nine flavanols and nine phenolics in various fractions of *M. pumilum*. Additionally, the study 4 used a chemometric approach such as principal component analysis (PCA) to demonstrate the similarities and differences in phytochemical profiles of different fractions. Chemometrics was also used in conjunction with the chemical fingerprinting technique in study 9, which reported on the use of macroscopy, IR spectroscopy, and chemometric analysis as a powerful technique for differentiating 84 test samples from seven different locations in Peninsular Malaysia. The first method for simultaneous determination of triterpenes, saponins and alkenated-phenolics in the leaves, stems, and roots of *M. pumilum* var. *alata* was developed in study 7 using high performance liquid chromatography-ultraviolet-evaporative light scattering detector (HPLC-UV-ELSD) in conjunction with other structure elucidation techniques such as TLC, IR, liquid chromatography coupled with electrospray ionization quadrupole time of flight mass spectrometry (LC/ESI/TOF), NMR and high resolution electrospray ionization mass spectrometry (HRESI/MS). Spectroscopic and chemical analyses were used in study 6 to elucidate the structures of alkyl phenols and saponins found in the roots of *M. pumilum*. Three investigations (studies 13, 22. and 33) used DNA fingerprinting to identify *M. pumilum*.

Table 2 summarises selected characteristic features derived from the 33 articles used to distinguish *M. pumilum* varities using various analytical techniques.

TABLE 2 | Characteristic features to distinguish *Marantodes pumilum* varieties based on different analytical techniques.

No.	Techniques	Plant Parts	Analysis		*M. pumilum* var. *alata*	*M. pumilum* var. *pumila*	*M. pumilum* var. *lanceolata*	References
1	Microscopic analysis (anatomy)	Leaf epidermis	Type of trichome	Adaxial epidermis	Absent	Simple, 2-armed, scale	Absent	Aladdin et al. (2016)
				Abaxial epidermis	Scale, capitate glandular	Scale	Scale	
			Type of stomata	Adaxial epidermis	Absent	Absent	Absent	
				Abaxial epidermis	Anisocyatic, staurocytic	Anisocyatic, diacytic	Anisocyatic	
			Pattern of anticlinal walls	Adaxial epidermis	Straight to curved	Straight to curved	Straight to curved	
				Abaxial epidermis	Straight to wavy	Straight to wavy	Straight to wavy	
		Leaf venation	Marginal venation		Incomplete	Incomplete	Marginal venation	
			Areolar venation		Closed, a few opened, minority free ending veinlets	Closed, free ending veinlets	Areolar venation	
		Leaf lamina and margin	Main mascular bundle		Equidistant to abaxial and adaxial epidermis	Equidistant to abaxial and adaxial epidermis	Close to the adaxial epidermis	
			Marginal outline		Rounded	Rounded	Tapering	
			Marginal direction		10–30° upwards	10–30° upwards	30–45° downwards	
		Midrib	Outline	Adaxial	Slightly convex	Flat/straight	Flat/straight	
				Abaxial	U-shaped	¾ of circle	¾ of circle	
			Cell inclusion		Solitary crystal calcium oxalate (rectangular), druses, scattered starch grains	Solitary crystal calcium oxalate (cubic), clustered starch grains	Solitary crystal calcium oxalate (cubic), druses, scattered starch grains	
			Type of trichome		Scale, capitate glandular	Scale, capitate glandular	Scale	
		Petiole	Outline		Wing presence at the left and right of adaxial side, ¾ of oval at abaxial side	Wing presence at the left and right of adaxial side, ¾ of oval at abaxial side	Oval	
			Cell inclusion		Brachyscelereids, solitary crystals calcium oxalate (cubic), druses	Brachyscelereids, starch grains, solitary crystals calcium oxalate (cubic), druses	Starch grains, solitary crystals calcium oxalate (cubic), druses	
		Stem	Type of trichome		Scale	Scale, capitate glandular	Scale	
			Outline		Circular	Circular	Circular	
			Parenchyma cortex		Ca. 10–20	Ca. 8–10	Ca. 8–10	
			Number of additional vascular bundle in cortex		6	6	5	
			Pith		Relatively wide	Relatively medium	Relatively medium	
			Cell inclusion		Brachyscelereids, solitary crystals, druses, starch grains	Brachyscelereids, solitary crystals, druses, starch grains	Brachyscelereids, solitary crystals, druses, starch grains	
			Type of trichome		Scale	Scale, capitate glandular	Scale, capitate glandular	
			Secretory canals		Present in pith parenchyma	Present in pith and parenchyma cortex	Present in pith and parenchyma cortex	
2	FTIR with KBR disk	Leaf	IR spectra		1733 (C = O stretching) 1204 (C-H in plane deformation)	1733 (C = O stretching)	Absent	Abdullah et al. (2012)
			Second derivative IR spectra	1597 (C = C stretching)	Present	Absent	Absent	
				1331 (O-H bending)	Absent	Absent	Present	
			2D correlation IR spectra	1660 (C = O vibration)	Present	Absent	Present	
				1559 and 1600	More intense	Low intensity	Low intensity	
				Cross-peaks at (1600, 1640), (1560, 1640) and (1560, 1600)	Strong intensity	Low intensity	Low intensity	
				Cross-peaks at (545–688, 662–740)	Strong broad	Weak	Narrow	
			Principal component analysis (PCA)	The varieties are clustered differently				

(Continued on following page)

TABLE 2 | (*Continued*) Characteristic features to distinguish *Marantodes pumilum* varieties based on different analytical techniques.

No.	Techniques	Plant Parts	Analysis	*M. pumilum* var. *alata*	*M. pumilum* var. *pumila*	*M. pumilum* var. *lanceolata*	References
3	ATR-FTIR	Leaf	IR spectra	3341 (O-H stretching) 1242 (C-O stretching)	3340 (O-H stretching) 1235 (C-O stretching) 1157 (C-O stretching)	3285 (O-H stretching) 1237 (C-O stretching) 1159 (C-O stretching)	Aladdin et al. (2016)
		Stem-root		3326 (O-H stretching) 1614 (C-C stretching) 1021 (C-O stretching)	3329 (O-H stretching) 1615 (C-C stretching) 1021 (C-O stretching)	3330 (O-H stretching) 1611 (C-C stretching) 1021 (C-O stretching)	
4	HPTLC	Leaf Stem-root	Fingerprint chromatogram	Presence of peaks at R_f 0.20–0.70 Presence of peaks at R_f 0.22 at different intensities			Aladdin et al. (2016)
5	HPLC	Whole plant	Detection of phytochemical compounds on chromatogram	• Ardisicrenoside B • Ardisiacrispin A • 3-O-α-L-rhamnopyranosyl-(1 → 2)-β-D-glucopyranosyl-(1 → 4)-αl-arabinopynanosyl cyclamiretin A • Ardisimamilloside H • Irisresorcinol • Belamcandol B • Demethylbelamcan-daquinone B	No information	No information	Avula et al. (2011)
		Leaf		• Gallic acid • Rutin	• Gallic acid • Rutin	No information	Tarmizi et al. (2021)
				No information	• Gallic acid • Methyl gallate • Caffeic acid	No information	Radzali et al. (2020)
				• Belamcandol B, 5-pentadec-10′-(Z)-enyl resorcinol • 1,3-dihydroxy-5- pentadecylbenzene, 5-(heptadec-12′-(Z)-enyl) resorcinol • Demethylbelamcanda-quinone B	No information	No information	Muhamad et al. (2019)
				• Quercetin • Myricetin	No information	No information	Latiff et al. (2018)
				• Gallic acid • Pyrogallol • Myricetin • Quercetin • Naringin • Daidzein • Catechin • Epicatechin	No information	No information	Karimi et al. (2016)
				• Gallic acid	No information	No information	Salehan et al. (2020)
				• Gallic acid	No information	No information	Abdah et al. (2014)
6	LCMS	Whole plant	Detection of phytochemical compounds on chromatogram	• Gallic acid • Caffeic acid • Ellagic acid • Apigenin • Kaempferol • Quercetin • Myricetin	No information	No information	Giaze et al. (2019)
		Whole plant		• Ardisicrenoside B • Ardisiacrispin A, 3-O-α-L-rhamnopyranosyl-(1 → 2)-β-D-glucopyranosyl-(1 → 4)-αl-arabinopynanosyl cyclamiretin A	No information	No information	Avula et al. (2011)

(Continued on following page)

TABLE 2 | (*Continued*) Characteristic features to distinguish *Marantodes pumilum* varieties based on different analytical techniques.

No.	Techniques	Plant Parts	Analysis	*M. pumilum* var. *alata*	*M. pumilum* var. *pumila*	*M. pumilum* var. *lanceolata*	References
		Leaf		• Ardisimamilloside H • Belamcandol B • Demethylbelamcanda-quinone B • Irisresorcinol • Benzoic acid • Gallic acid • Vanillic acid • Syringic acid • Salicylic acid • Cinnamic acids • Protocatechuic acid • Coumaric acid • Caffeic acid • Chlorogenic acid • Quercetin • Myricetin • Kaempferol • Catechin • Epigallocatechin	No information	No information	Chua et al. (2011)
7	DNA Genetic Fingerprinting	Leaf	DNA References barcode	*ITS2* (MK249864) *rbc*L (MH828448)	*ITS2* (MK249864) *rbc*L (MH838008)	*ITS2* (MH749147) *rbc*L (MH766971)	Tarmizi et al. (2021)
				rbcL *trnH-psbA*			Tnah et al. (2019)
			Microsatellites	84 alleles	48 alleles	66 alleles	Tnah et al. (2014)

TABLE 3 | Strengths and limitations of analytical techniques for *Marantodes pumilum* authentication.

Techniques		Strengths	Limitations
Organoleptic, macroscopy and microscopy		• Quick physical evaluation for adulteration, contamination, and substitution (Upton et al., 2020)	• Conventional method, imprecise and inconsistent result (Smillie & Khan, 2010) • Requires expertise and skilled or well-trained personnel (Smillie & Khan, 2010) • Microscopy is not applicable for materials in extracted or prepared (e.g., resins) form (Upton et al., 2020)
Chemical fingerprinting	IR/NIR Spectroscopy	• Quick, non-destructive, and high throughput method with minimal sample preparation (Upton et al., 2020) • Able to generate chemical fingerprint to differentiate plant varieties and plant parts (Aladdin et al., 2016)	• Affected by variables such as moisture, particle size and homogeneity of test samples (Upton et al., 2020)
	TLC	• Manual, rapid, simple, flexible, low-cost, and minimal sample preparation (Liang et al., 2004) • Test sample and References standard can be analysed simultaneously (Liang et al., 2004)	• Issues with reproducibility, resolutions, sensitivity and difficulty to detect trace phytochemical components (Yongyu et al., 2011)
	HPTLC	• Automated sample application allows for improved separation, band resolution and reproducibility of results (Aladdin et al., 2016) • High throughput and screen multiple samples in a single assay (Upton et al., 2020)	
	HPLC	• High selectivity, sensitivity, resolution, and fully automatable operation (Smillie and Khan, 2010) • Enable qualitative and quantitative analysis (Upton et al., 2020)	• Unable to distinguish between closely related species or non-target species that have similar chemical profiles (Upton et al., 2020) • Affected by factors related to variation in climate, phenotype, storage condition, age, and cultivation time (Mohammed et al., 2017)
	MS hyphenated techniques	• Powerful for rapid identification of phytochemical constituents in plant extracts (Liang et al., 2004) • High resolution, high speed, accurate mass-measurement and able to retrieve more information in a complex botanical drug substance (Yongyu et al., 2011)	• High cost
Biological fingerprinting	DNA Barcode	• Rapid, sensitive, and effective tool for identification of species (Tarmizi et al., 2021) • Widely used to differentiate individual plant, genus, homogeneity analysis, and detection of adulterants (Upton et al., 2020) • Less affected by plant age, physiological conditions, environmental factors, harvest, storage, and processing methods (Yongyu et al., 2011)	• Unable to identify extracted form or processed botanical drugs (Tarmizi et al., 2021) • Highly dependent on the availability of References standard data sequences (Tarmizi et al., 2021) • Unable to provide information related to concentration of compounds with therapeutic value (Yongyu et al., 2011) • Genome information only as a complement tool of other quality control techniques (Yongyu et al., 2011)

DISCUSSION

Between 2016 and 2020, almost 3,000 botanical drug products were registered, increasing by 16% and accounting for 50% of all registered products in Malaysia within 5 years (NPRA, 2020). The figures indicate the significant growth of botanical drug products in the Malaysian market because of persistent client demand. Authentication of botanical drugs is critical to ensuring the consistency of their quality, safety, and efficacy prior to production. Numerous experts have emphasized the importance of certification of botanical drugs to assure their purity and safety. As a result, rigorous authentication must be performed to ascertain the quality and safety of botanical drug products prior to registration approval. Standardization and quality control of raw materials must follow the pharmacopoeia-defined process of identification and authentication.

The systematic review assessed current quality control trends for *M. pumilum* in the botanical drug research and development setting, as described by pharmacopoeia. In general, the 33 peer-reviewed articles demonstrate that a variety of techniques have been used to identify and authenticate different varieties and plant parts of *M. pumilum*. Most of the articles reviewed collected wild *M. pumilum* specimens. The continued reliance on raw materials derived from wild resources, whether for research or commercial purposes, will eventually deplete the supply of *M. pumilum*. This has become a source of concern for botanical drugs suppliers, as wild *M. pumilum* is known to grow slowly in its natural habitat. As a result, several research institutions have conducted extensive tissue culture breeding for *M. pumilum* to keep up with the expanding market demand (Tarmizi et al., 2021).

Additionally, it is discovered that most of the reviewed studies employed at least one method of identification, and that awareness of the requirement has gradually increased since 2010. Effective identification and authentication tools are critical for monitoring the source of high-demand raw materials to avoid undesirable activities such as adulteration of raw materials, which negatively impacts the quality of botanical drug products. As recently reported, this approach was widely

used for ginseng products, supplements, commercial botanical drug products, and Kadsura crude drugs (Liu et al., 2019; Ichim et al., 2020; Ichim and de Boer, 2021).

Organoleptic evaluation, macroscopy, and microscopy are the first three fundamental principal methods of identification and authentication used to ensure the quality of botanical drugs (World Health Organization, 2011). Due to the morphological and phytochemical complexity of interspecific hybrids, within-species variation, and the difficulty associated with recognizing species in some plant genera, voucher specimens are critical for organoleptic and macroscopic verification of source material utilized in botanical drugs research (Eisenman et al., 2012). From this review, ten of the articles did not provide information on voucher specimens of *M. pumilum* used in the studies. Lack of adequate voucher specimens has resulted in major issues, such as the inability to duplicate crucial experimental results and the incorrect assignment of phytochemical and pharmacological data to the correct genus and species. Authentication is especially important for *M. pumilum* since previous studies have shown that different varieties, plant parts and types of extracts have varying phytochemical compositions and pharmacological actions (Karimi et al., 2015; Aladdin et al., 2020; Rahmi et al., 2020). Thus, prior to producing botanical drug products containing *M. pumilum* for a particular intended pharmacological action, accurate plant variety and plant part identification must be performed. Adhering to the pharmacopoeia monograph specification for identification tests of botanical drugs would confirm the material's authenticity. Microscopic examination enables primary species identification, as well as the detection of adulteration, contamination, and substitution of botanical drugs (Upton et al., 2020) (**Table 3**). Aladdin et al. (2016) reported the first effective distinction of three *M. pumilum* varieties and plant parts utilizing microscopic approach. The microscopical characteristics, such as stomata, trichomes, stem and leaf margin, petiole, midrib, vascular system, anticlinal walls, secretory canals, and cell inclusion, can all be used to differentiate and identify each variety of *M. pumilum* and its plant part (**Table 2**). As previously reported, 41% of 508 botanical drug products sold in 13 countries that were microscopically authenticated were found to be adulterated (Ichim et al., 2020). However, macroscopic, and microscopic analyses alone are insufficient for reliably identifying plant species and determining their quality (Smillie & Khan 2010; Srirama et al., 2017). Plant tissues with little or no cellular variations, processed materials, and extensive dehydration of plants can eliminate diagnostic features, making analysis challenging with these methods (Smillie and Khan, 2010). The issues are compounded by the lack of appropriate reference material and a scarcity of qualified taxonomists (Ichim et al., 2020). Therefore, additional identification techniques should be included to verify the authenticity of plant materials.

Numerous papers describe the use of fingerprint profiling for botanical drugs identification and authentication by spectroscopy and chromatography. Guo (2017) demonstrated that evaluating the botanical drugs quality based on a single or specified markers overlooks the synergistic effects of the multi-phytochemical components of botanical drugs, suggesting that a holistic quality assessment approach using chemical fingerprinting method is relevant. In a prior work, fingerprints of different plant parts of *Panax notoginseng* (Burkill) F.H. Chen (Araliaceae) were generated using a combination of near infrared spectroscopy (NIR), HPLC, UPLC, and capillary electrophoresis (CE) (Zhu et al., 2014). Aladdin et al. (2016) have reported the usage of a more simple, convenient, and non-destructive phytochemical fingerprinting technique, namely attenuated total reflectance-FTIR (ATR-FTIR) without the usage of KBr (**Table 2**). The work was an advance on a prior study that used multi-step infrared spectroscopy and a KBR disc (Abdullah et al., 2012). Even though the method without KBr has a lower resolution than the method with KBr disc (Zou et al., 2005), the results of the different profiles between the three *M. pumilum* varieties and plant parts clearly demonstrated that the ATR-FTIR fingerprinting technique can be used to determine the identity and quality control of *M. pumilum* raw materials. However, this technique alone may be best suited for a single authentic plant ingredient because it may be difficult to gain accurate information of the phytochemical compositions and to detect adulterants based only on the chemical functional groups from the infrared spectrum. Moisture, particle size, and homogeneity of test samples all have an impact on analytical precision (Upton et al., 2020) (**Table 3**).

The phytochemical fingerprint profile of botanical drugs generates a large amount of data in the form of chromatograms or spectra, making it nearly impossible for the analyst to visually inspect each data point and exploit the useful chemical information contained in the fingerprint data *via* univariate analysis. As a result, a multivariate data analysis technique was developed to analyze chemical fingerprinting data to eliminate or reduce undesired sources of variation caused by various variables or instrumental responses from the analytical techniques, as well as to extract useful and meaningful information from the fingerprint data (Gad et al., 2013; Huang et al., 2016). Chemometric techniques have been widely used in quality control of botanical drug products due to their capacity to tackle a variety of problems in a variety of domains, including similarity analysis and exploratory learning. Apart from that, the chemometric approach can analyze a variety of data, both qualitatively and quantitatively, *via* a classification algorithm and a multivariate calibration algorithm (Li et al., 2020). The combination of chemometric techniques such as principal component analysis (PCA) and multilayer perceptron classifier (MLPC) modelling with ATR-FTIR has been reported as a rapid and effective method for botanical drugs quality evaluation of *Gastrodia elata* Blume (Orchidaceae) powder (Zhan et al., 2022). From this systematic review study, Abdullah et al. (2012) successfully characterized leaves of three *M. pumilum* varieties using IR and chemometrics (**Table 2**), whereas Chua et al. (2011) used an integrated approach of chemical fingerprinting with UPLC-ESI-MS/MS and chemometric technique to differentiate *M. pumilum* var. *alata* and var. *pumila* leaves based on the compositions of nine flavonols, two flavanols, and nine phenols.

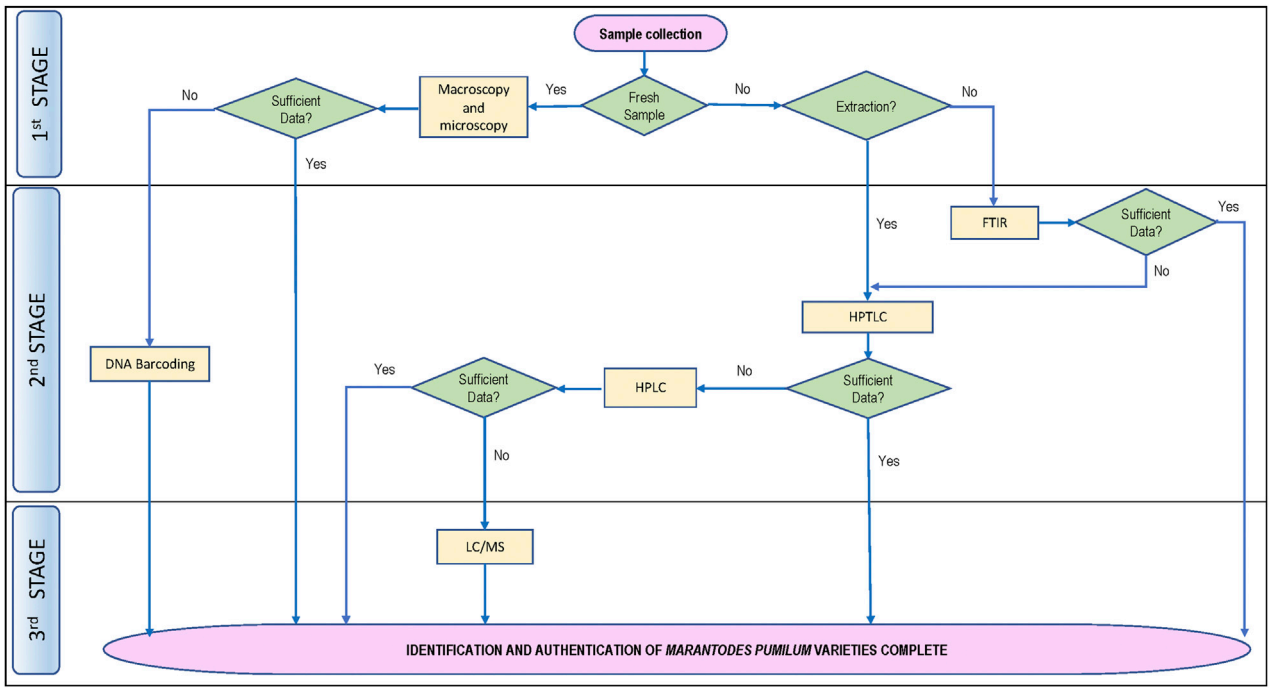

FIGURE 4 | Proposed flow chart for authentication of *Marantodes pumilum* varieties.

TLC technique has been widely recognized as a preliminary screening approach to HPLC, owing to its ability to rapidly generate a fingerprint of varied plant materials in a single, simple, and low-cost analysis while producing high sample throughput. TLC is used for preliminary screening or identification of phytochemical components that provide the plant's unique fingerprint (Liang et al., 2004). The HPTLC technique, when combined with automated sample application and densitometric scanning, offers numerous advantages, including high throughput samples, low analytical costs, and the ability to separate test samples and reference standards concurrently (Upton et al., 2020) (**Table 3**). These methods are described in most international pharmacopoeias, including the British Pharmacopoeia, the United States Pharmacopeia, and the Chinese Pharmacopoeia. There are numerous studies that used TLC and HPTLC for authentication such as ginseng, Radix Puerariae and *M. pumilum* (Xie et al., 2006; Siyumbwa, 2015). Aladdin et al. (2016) reported that the HPTLC fingerprint profiles of three varieties of *M. pumilum* leaves and stem-roots gathered from a wild source at a single location were somewhat comparable with varying intensities, implying the presence of identical phytochemicals in varying concentrations (**Table 2**). According to Karimi et al. (2015), total phenolics, total flavonoids, and fatty acid concentration also varied between *M. pumilum* var. *alata*, var. *pumila*, and var. *lanceolata* leaves obtained from three separate locations from the wild. The presence of identical compounds with varying compositions complicates accurate authentication of commercial plant materials, as phytochemical compound concentrations are influenced by a variety of extrinsic factors, such as geographic (latitude, altitude, and soil type), climatic (light, temperature, rainfall, and atmospheric compositions) and agricultural practice (cultivation, harvesting and processing methods, and storage conditions), as well as intrinsic factors, such as plant age, genetics, chemotypes and botanical parts (Liang et al., 2004; Yongyu et al., 2011). *M. pumilum* has been reported to contain potential pharmacologically active phytochemicals such as quercetin, myricetin, kaempferol, naringin, rutin, apigenin, catechin, epigallocatechin, pyrogallol, gallic acid, ascorbic acid, salicylic acid, syringic acid, vanillic acid, protocatechuic acid, coumaric acid, caffeic acid, chlorogenic acid, daidzein, genistein, β-carotene, anthocyanins, demethylbelamcandaquinone B, and 3,7-dihydroxy-5-methoxy-4,8-dimethyl-isocoumarin (Norhaiza et al., 2009; Ali and Khan, 2011; Chua et al., 2011; Ehsan et al., 2011; Hairi et al., 2018; Wu et al., 2018; Aladdin et al., 2020). Gallic acid and caffeic acid were identified as the major phenolic acids in the methanol extracts of three *M. pumilum* varieties (Karimi et al., 2011). Due to their widespread presence in other plants, the two compounds cannot be considered a unique biomarker for *M. pumilum*. Hence, the diverse class of phytochemicals necessitates the use of more sensitive approaches for *M. pumilum* identification and authentication.

Liquid chromatography is one of the most efficient analytical techniques for phytochemical profiling since the stationary phase column, mobile phase gradient system and detector can all be modified to suit the analysis of a variety of phytochemical components. For the development of a

validated analytical method, statistically significant representative set of plant samples from multiple populations is used to establish a fingerprint profile, whereas reference standards, whether commercially available, extracted, or isolated, are necessary (Smillie and Khan, 2010). In this review, Avula et al. (2011) used HPLC to assess the phytochemicals content isolated from *M. pumilum* var. *alata* leaves, stems, and roots (**Table 2**), whereas Aladdin et al. (2016) distinguished three varieties of *M. pumilum* and their plant parts based on fingerprinting profile. However, both studies utilized only botanical drugs obtained from a single location, indicating that additional research is necessary. Closely related plant species with similar chemical profiles will not be discriminated using HPLC (**Table 3**). Researchers have used hyphenated chromatographic and mass spectrometric techniques, such as liquid chromatography-mass spectrometry (LC/MS), gas chromatography-mass spectrometry (GC/MS), and capillary electrophoresis-mass spectrometry (CE/MS), to authenticate plant materials. In this systematic review study, LC/MS (Giaze et al., 2019), LC/MS/MS (Dharmani et al., 2019), UPLC/MS/MS (Wu et al., 2019), and LC/ESI/TOF (Avula et al., 2011) were used to determine phytochemical compositions of different *M. pumilum* plant parts, whereas UPLC-ESI/MS/MS was used to detect components between *M. pumilum* var. *alata* and var. *pumila* leaves (Chua et al., 2011). To date, the combination of chromatography and mass spectrometry is the most advanced approach and is often used by researchers to analyze the composition of botanical drugs qualitatively and quantitatively to determine the consistency of their quality. Mass spectrometry imaging may be used to visually assess quality variations (Wei et al., 2020). However, the cost of the hyphenated equipment is a significant constraint (**Table 3**).

The researchers are currently interested in the other tool for botanical drugs authentication using genetic fingerprinting techniques. DNA barcoding enabled a rapid examination of the botanical drugs composition and was found to be an effective technique for authenticating dried and powdered plant materials for quality control purposes (Gesto-Borroto et al., 2021). Tnah et al. (2014) were the first to report the use of a genetic-based fingerprint technique to differentiate leaves of three *M. pumilum* varieties collected in the wild, followed by another investigation of botanical drug products containing *M. pumilum* (Tnah et al., 2019) (**Table 2**). According to the latter study, DNA barcoding was able to detect 56.7% of 30 selected botanical drug products containing *M. pumilum* and were found to be authentic, 10% were substituted with other plant taxa, and 6.7% were contaminated. DNA information was not detected in 26.6% of botanical drug products due to the low concentration or degradation of the processed botanical drug preparations. The study reported the authenticity of a product containing a single ingredient of *M. pumilum*, however, for a product containing a mixture of *M. pumilum* and *Querqus lusitanica* Lam. (Fagaceae) had no DNA sequence. Additionally, a recent study by Tarmizi et al. (2021) effectively used DNA barcoding and HPLC techniques for the identification of cultivated *M. pumilum* var. *alata* and var. *pumila* leaves, as well as investigation of the authenticity of botanical drug products containing *M. pumilum*. However, nine of test samples (60%) reported not amplifiable due to the lack or low concentration of DNA recovered from degradation. This demonstrated that the primary limitation of the current DNA barcoding approach is its inability to identify *M. pumilum* at the variety level due to inaccuracies in selecting the targeted sequence, use of a large barcode size and DNA degradation in processed materials (**Table 3**). As a result, DNA barcoding may not be suitable as a stand-alone method of identification of processed botanical drug products and should be combined with additional authentication techniques such as morphological features and chemical analyses.

The various techniques used to identify *M. pumilum* varieties and plant parts in the articles reviewed in this study (**Table 1**, **2**), such as macroscopy, microscopy, chromatography, spectroscopy and chemometrics, suggest that a combination of approaches is required to authenticate botanical drug substances and products. However, the existing reports did not address phytochemical variation of a plant variety or plant part collected from various locations, differences between those collected from the wild sources and those collected from cultivated sources, as well as adulteration with other plant parts or varieties. When producing a standardized botanical drug product, obtaining botanical drug substance from a cultivated plantation location rather than the wild will assure plant homogeneity. Phytochemical indicators are frequently used to standardize botanical drug products. A guideline for selecting marker substances for quality control of botanical drug is provided by the World Health Organization (2017). To facilitate correct identification and authentication of *M. pumilum* utilized in botanical drug products development, it is vital to identify the phytochemical constituents with known therapeutic activity. As shown in **Figure 4**, a flow procedure for *M. pumilum* authentication up to the variety level is proposed based on an existing approach.

CONCLUSION

This review found that no one technique for authenticating *M. pumilum* botanical drug substances and products can be used. Each technique has its own distinct interpretation of the plant, ranging from simple morphological characteristics to a more comprehensive comprehension of the *M. pumilum*'s phytochemical constituents. Developing proper authentication procedures is critical for the development and manufacturing of botanical drugs, whether for clinical trials or before the product reaches the consumer. Thus, additional research is necessary to determine the most effective authentication techniques for differentiating the varieties of *M. pumilum* and their plant parts to ensure that the correct species is used in the manufacturing process of

botanical drug products and to avoid adulterations that could pose a health risk to consumers.

DATA AVAILABILITY STATEMENT

The raw data supporting the conclusions of this article will be made available by the authors, without undue reservation.

AUTHOR CONTRIBUTIONS

II is a Phd. candidate who conducted a systematic literature search, assessed the findings and prepared a systematic literature review draft. JJ, MS, and NZ contributed ideas for the systematic literature review design and reviewed the manuscript. JJ is the project leader and revised the manuscript.

FUNDING

The study was supported by the UKM research grant scheme (GUP 2021-007).

ACKNOWLEDGMENTS

We would like to express our gratitude to Universiti Kebangsaan Malaysia for the financial support and the usage of library facilities.

REFERENCES

Abdah, S. N. M., Sarmidi, M. R., Yaakob, H. Y., and Ware, I. (2014). Fractionation of *Labisia pumila* Using Solid-phase Extraction for Extraction of Gallic Acid. *J. Teknol.* 69 (4), 65–68. doi:10.11113/jt.v69.3176

Abdullah, F., Ling, S. K., Man, S., Tan, A. L., Tan, H. P., and Abdullah, Z. (2012). Characterization and Identification of *Labisia pumila* by Multi-Steps Infrared Spectroscopy. *Vib. Spectrosc.* 62, 200–206. doi:10.1016/j.vibspec.2012.06.004

Abdullah, N., Chermahini, S. H., Chua, L. S., and Sarmidi, M. R. (2013). *Labisia pumila*: A Review on its Traditional, Phytochemical and Biological Uses. *World Appl. Sci. J.* 27 (10), 1297–1306. doi:10.5829/idosi.wasj.2013.27.10.1391

Abubakar, B. M., Salleh, F. M., Shamsir Omar, M. S., and Wagiran, A. (2018). Assessing Product Adulteration of *Eurycoma longifolia* (Tongkat Ali) Herbal Medicinal Product Using DNA Barcoding and HPLC Analysis. *Pharm. Biol.* 56 (1), 368–377. doi:10.1080/13880209.2018.1479869

Adam, S. H., Giribabu, N., Bakar, N. M. A., and Salleh, N. (2017). *Marantodes pumilum* (Kacip Fatimah) Enhances Iin-Vvitro Glucose Uptake in 3T3-L1 Adipocyte Cells and Reduces Pancreatic Complications in Streptozotocin-Nicotinamide Induced Male Diabetic Rats. *Biomed. Pharmacother.* 96, 716–726. doi:10.1016/j.biopha.2017.10.042

Ahmad, S. U., Azam, A., Shuid, A. N., and Mohamed, I. N. (2018). Antioxidant and Anti-inflammatory Activities of *Marantodes pumilum* (Blume) Kuntze and Their Relationship with the Phytochemical Content. *Rec. Nat. Prod.* 12 (6), 518–534. doi:10.25135/rnp.58.17.11.188

Al-Mekhlafi, N. A., Shaari, K., Abas, F., Kneer, R., Jeyaraj, E. J., Stanslas, J., et al. (2012). Alkenylresorcinols and Cytotoxic Activity of the Constituents Isolated from *Labisia pumila*. *Phytochemistry* 80, 42–49. doi:10.1016/j.phytochem.2012.04.008

Aladdin, N.-A., Jamal, J. A., Talip, N., Hamsani, N. A. M., Rahman, M. R. A., Sabandar, C. W., et al. (2016). Comparative Study of Three *Marantodes pumilum* Varieties by Microscopy, Spectroscopy and Chromatography. *Rev. Bras. Farmacogn.* 26 (1), 1–14. doi:10.1016/j.bjp.2015.10.002

Aladdin, N. A., Husain, K., Jalil, J., Sabandar, C. W., and Jamal, J. A. (2020). Xanthine Oxidase Inhibitory Activity of a New Isocoumarin Obtained from *Marantodes pumilum* var. *pumila* Leaves. *BMC Complement. Med. Ther.* 20 (1), 324–412. doi:10.1186/s12906-020-03119-8

Ali, Z., and Khan, I. A. (2011). Alkyl Phenols and Saponins from the Roots of *Labisia pumila* (Kacip Fatimah). *Phytochemistry* 72 (16), 2075–2080. doi:10.1016/j.phytochem.2011.06.014

Avula, B., Wang, Y. H., Ali, Z., Smillie, T. J., and Khan, I. A. (2011). Quantitative Determination of Triperpene Saponins and Alkenated-Phenolics from *Labisia pumila* Using an LC-UV/ELSD Method and Confirmation by LC-ESI-TOF. *Planta Med.* 77 (15), 1742–1748. doi:10.1055/s-0030-1271037

Burkill, I. H. (1966). *A Dictionary of the Economic Products of the Malay Peninsula*. Kuala Lumpur: Ministry of Agriculture and Cooperatives.

Choi, H. K., Kim, D. H., Kim, J. W., Ngadiran, S., Sarmidi, M. R., and Park, C. S. (2010). *Labisia pumila* Extract Protects Skin Cells from Photoaging Caused by UVB Irradiation. *J. Biosci. Bioeng.* 109 (3), 291–296. doi:10.1016/j.jbiosc.2009.08.478

Chua, L. S., Latiff, N. A., Lee, S. Y., Lee, C. T., Sarmidi, M. R., and Aziz, R. A. (2011). Flavonoids and Phenolic Acids from *Labisia pumila* (Kacip Fatimah). *Food Chem.* 127, 1186–1192. doi:10.1016/j.foodchem.2011.01.122

Chua, L. S., Lee, S. Y., Abdullah, N., and Sarmidi, M. R. (2012). Review on *Labisia pumila* (Kacip Fatimah): Bioactive Phytochemicals and Skin Collagen Synthesis Promoting Herb. *Fitoterapia* 83 (8), 1322–1335. doi:10.1016/j.fitote.2012.04.002

Dharmani, M., Kamarulzaman, K., Giribabu, N., Choy, K. W., Zuhaida, M. Z., Aladdin, N. A., et al. (2019). Effect of *Marantodes pumilum* Blume (Kuntze) var.Alata on β-cell Function and Insulin Signaling in Ovariectomised Diabetic Rats. *Phytomedicine* 65, 153101. doi:10.1016/j.phymed.2019.153101

Dianita, R., Jantan, I., Jalil, J., and Amran, A. Z. (2016). Effects of *Labisia pumila* var. *alata* Extracts on the Lipid Profile, Serum Antioxidant Status and Abdominal Aorta of High-Cholesterol Diet Rats. *Phytomedicine* 23 (8), 810–817. doi:10.1016/j.phymed.2016.04.004

Effendy, N. M., Khamis, M. F., Soelaiman, I. N., and Shuid, A. N. (2014). The Effects of *Labisia pumila* on Postmenopausal Osteoporotic Rat Model: Dose and Time-dependent Micro-CT Analysis. *J. Xray Sci. Technol.* 22 (4), 503–518. doi:10.3233/XST-140441

Ehsan, K., Hawa, Z. E. J., and Sahida, A. (2011). Phytochemical Analysis and Antimicrobial Activities of Methanolic Extracts of Leaf, Stem and Root from Different Varieties of *Labisia pumila* Benth. *Molecules* 16, 4438–4450.

Eisenman, S. W., Tucker, A. O., and Struwe, L. (2012). Voucher Specimens Are Essential for Documenting Source Material Used in Medicinal Plant Investigations. *JAMP* 1 (1), 30–43.

Fadzil, N. F., Wagiran, A., Salleh, F. M., Shamsiah, A., and Izham, N. H. M. (2018). Authenticity Testing and Detection of *Eurycoma longifolia* in Commercial Herbal Products Using Bar-High Resolution Melting Analysis. *Genes* 9 (8), 408. doi:10.3390/genes9080408

Fazliana, M., Ramos, N. L., Luthje, P., Sekikubo, M., and Holm, A. (2011). *Labisia pumila* var. *alata* Reduces Bacterial Load by Inducing Uroepithelial Cell Apoptosis. *J. Ethnopharmacol.* 136 (1), 111–116. doi:10.1016/jep.2011.04.01810.1016/j.jep.2011.04.018

Gad, H. A., El-Ahmady, S. H., Abou-Shoer, M. I., and Al-Azizi, M. M. (2013). Application of Chemometrics in Authentication of Herbal Medicines: A Review. *Phytochem. Anal.* 24 (1). doi:10.1002/pca.2378

Gesto-Borroto, R., Medina-Jiménez, K., Lorence, A., and Villarreal, M. L. (2021). Application of DNA Barcoding for Quality Control of Herbal Drugs and Their Phytopharmaceuticals. *Rev. Bras. Farmacogn.* 31, 127–141. doi:10.1007/s43450-021-00128-7

Giaze, T. R., Shuid, A. N., Soelaiman, I. N., Mohamed, N., Jamal, J. A., and Fauzi, M. B. (2019). Comparative Anti-osteoporotic Properties of the Leaves and Roots of *Marantodes pumilum* var. *alata* in Postmenopausal Rat Model. *J. Tradit. Complement. Med.* 9 (4), 393–400. doi:10.1016/j.jtcme.2019.01.002

Giaze, T. R., Shuid, A. N., Soelaiman, I. N., Muhammad, N., Fauzi, M. B., and Arlamsyah, A. Z. (2018). *Marantodes pumilum* Leaves Promote Repair of

Osteoporotic Fracture in Postmenopausal Sprague-Dawley Rats. *Int. J. Pharmacol.* 14 (7), 973–980. doi:10.3923/ijp.2018.973.980

Giribabu, N., Karim, K., and Salleh, N. (2018). Effects of *Marantodes pumilum* (Kacip Fatimah) on Vaginal pH and Expression of Vacoular ATPase and Carbonic Anhydrase in the Vagina of Sex-Steroid Deficient Female Rats. *Phytomedicine* 49, 95–105. doi:10.1016/j.phymed.2018.05.018

Goodarzi, M., Russel, P. J., and Heyden, Y. V. (2013). Similarity Analyses of Chromatographic Herbal Fingerprints: A Review. *Anal. Chim. Acta* 804, 16–28. doi:10.1016/j.aca.2013.09.017

Guo, D. (2017). Quality Marker Concept Inspires the Quality Research of Traditional Chinese Medicines. *Chin. Herb. Med.* 9 (1), 1–2. doi:10.1016/S1674-6384(17)60069-8

Hairi, H. A., Jamal, J. A., Aladdin, N. A., Husain, K., Sofi, N. S. M., Mohamed, N. I., et al. (2018). Demethylbelamcandaquinone B (Dmcq B) Is the Active Compound of *Marantodes pumilum* var. *alata* (Blume) Kuntze with Osteoanabolic Activities. *Molecules* 23 (7), 1–19. doi:10.3390/molecules23071686

Heinrich, M., and Anagnostou, S. (2017). From Pharmacognosia to DNA-Based Medicinal Plant Authentication – Pharmacognosy through the Centuries. *Planta Med.* 83 (14-15), 1110–1116. doi:10.1055/s-0043-108999

Huang, Y., Wu, Z., Su, R., Ruan, G., Du, F., and Li, G. (2016). Current Application of Chemometrics in Traditional Chinese Herbal Medicine Research. *J. Chromatogr. B Anal. Technol. Biomed. Life Sci.* 1026, 27–35. doi:10.1016/j.jchromb.2015.12.050

Ichim, M. C., and de Boer, H. J. (2021). A Review of Authenticity and Authentication of Commercial Ginseng Herbal Medicines and Food Supplements. *Front. Pharmacol.* 11, 2185. doi:10.3389/fphar.2020.612071

Ichim, M. C., Hasser, A., and Nick, P. (2020). Microscopic Authentication of Commercial Herbal Products in the Globalized Market: Potential and Limitations. *Front. Pharmacol.* 11, 876. doi:10.3389/fphar.2020.00876

Jamal, J. A., Ramli, N., Stanslas, J., and Husain, K. (2012). Estrogenic Activity of Selected Myrsinaceae Species in MCF-7 Human Breast Cancer Cells. *Int. J. Pharm. Pharm. Sci.* 4 (4), 547–553.

Karimi, E., Jaafar, H. Z. E., and Ahmad, S. (2013). Antifungal, Anti-inflammatory and Cytotoxicity Activities of Three Varieties of *Labisia pumila* Benth: From Microwave Obtained Extracts. *BMC Complement. Altern. Med.* 13, 1–20. doi:10.1186/1472-6882-13-20

Karimi, E., Jaafar, H. Z. E., and Ahmad, S. (2011). Phytochemical Analysis and Antimicrobial Activities of Methanolic Extracts of Leaf, Stem and Root from Different Varieties of *Labisa pumila* Benth. *Molecules* 16 (6), 4438–4450. doi:10.3390/molecules16064438

Karimi, E., Jaafar, H. Z. E., and Ghasemzadeh, A. (2016). Chemical Composition, Antioxidant and Anticancer Potential of *Labisia pumila* Variety *alata* under CO_2 Enrichment. *NJAS - Wagen. J. Life Sci.* 78, 85–91. doi:10.1016/j.njas.2016.05.002

Karimi, E., Jaafar, H. Z. E., Ghasemzadeh, A., and Ebrahimi, M. (2015). Fatty Acid Composition, Antioxidant and Antibacterial Properties of the Microwave Aqueous Extract of Three Varieties of *Labisia pumila* Benth. *Biol. Res.* 48, 1–6. doi:10.1186/0717-6287-48-9

Latiff, N. A., Chua, L. S., Sarmidi, M. R., Ware, I., and Rashid, S. N. A. A. (2018). Liquid Chromatography Tandem Mass Spectrometry for the Detection and Validation of Quercetin-3-*O*-Rutinoside and Myricetin from Fractionated *Labisia pumila* var. *alata*. *Malays. J. Anal. Sci.* 22 (5), 817–827.

Li, Y., Shen, Y., Yao, C. L., and Guo, D-A. (2020). Quality Assessment of Herbal Medicines Based on Chemical Fingerprints Combined with Chemometrics Approach: A Review. *J. Pharm. Biomed. Anal.* 185, 113215. doi:10.1016/j.jpba.2020.22321510.1016/j.jpba.2020.113215

Liang, Y. Z., Peishan, X., and Chan, K. (2004). Quality Control of Herbal Medicines. *J. Chromatogr. B Anal. Technol. Biomed. Life Sci.* 812, 53–70. doi:10.1016/j.jchromb.2004.08.041

Liu, J., Wei, X., Zhang, X., Qi, Y., Zhang, B., Liu, H., et al. (2019). A Comprehensive Comparative Study for the Authentication of the Kadsura Crude Drug. *Front. Pharmacol.* 9, 1576. doi:10.3389/fphar.2018.01576

Mamat, N., Jamal, J. A., Jantan, I., and Husain, K. (2014). Xanthine Oxidase Inhibitory and DPPH Radical Scavenging Activities of Some Primulaceae Species. *Sains Malays* 43 (12), 1827–1833. doi:10.17576/jsm-2014-4312-03

Mannerås, L., Fazliana, M., Nazaimoon, W. M. W., Lonn, M., Gu, H. F., and Ostenson, C. G. (2010). Beneficial Metabolic Effects of the Malaysian Herb *Labisia pumila* var. *alata* in a Rat Model of Polycystic Ovary Syndrome. *J. Ethnopharmacol.* 127 (2), 346–351. doi:10.1016/j.jep.2009.10.032

Manshor, N. M., Razali, N., Jusoh, R. R., Asmawi, M. Z., Mohamed, N., and Zainol, S. (2020). Vasorelaxant Effect of Water Fraction of *Labisia pumila* and its Mechanisms in Spontaneously Hypertensive Rats Aortic Ring Preparation. *Int. J. Cardiol. Hypertens.* 4, 100024. doi:10.1016/j.ijchy.2020.100024

Moher, D., Liberati, A., Tetzlaff, J., and Altman, D. G. The PRISMA Group (2009). Preferred Reporting Items for Systematic Reviews and Meta-Analyses: The PRISMA Statement. *PLoS Med.* 6 (7). doi:10.1371/journal.pmed.100009710.1136/bmj.b2535

Muhamad, M., Choo, C. Y., Hasuda, T., and Hitotsuyanagi, Y. (2019). Estrogenic Phytochemical from *Labisia pumila* (Myrsinaceae) with Selectivity towards Estrogen Receptor Alpha and Beta Subtypes. *Fitoterapia* 137, 104256. doi:10.1016/j.fitote.2019.104256

Norhaiza, M., Maziah, M., and Hakiman, M. (2009). Antioxidative Properties of Leaf Extracts of a Popular Malaysian Herb, *Labisia pumila*. *J. Med. Plants Res.* 3 (4), 217–223.

Norhayati, M. N., George, A., Hazlina, N. H. N., Azidah, A. K., Indiana, H. I., and Law, K. S. (2014). Efficacy and Safety of *Labisia pumila* var. *alata* Water Extract Among Pre- and Postmenopausal Women. *J. Med. Food* 17 (8), 929–938. doi:10.1089/jmf.2013.2953

NPRA (2020). Annual Report 2020. Published on the Internet. Avilable from https://npra.gov.my/index.php/en/informationen/annual-reports/npra-annual-reports.html. Accessed at 03 June 2021

Pan, Y., Tiong, K. H., Rashid, B. A. A., Ismail, Z., Ismail, R., and Mak, J. W. (2012). Inhibitory Effects of Cytochrome P450 Enzymes CYP2C8, CYP2C9, CYP2C19 and CYP3A4 by *Labisia pumila* Extracts. *J. Ethnopharmacol.* 143 (2), 586–591. doi:10.1016/j.jep.2012.07.024

Pandey, A., Bani, S., Sangwan, P., and Koul, S. (2010). Selective Th1 Upregulation by Ethyl Acetate Fraction of *Labisia pumila*. *J. Ethnopharmacol.* 132 (1), 309–315. doi:10.1016/j.jep.2010.08.039

Pandey, A., Sarang, B., and Sangwan, P. L. (2014). Anti-obesity Potential of Gallic Acid from *Labisia pumila*, through Augmentation of Adipokines in High Fat Diet Induced Obesity in C57BL/6 Mice. *Adv. Res.* 2 (10), 556–570. doi:10.9734/air/2014/10182

Pattiram, P. D., Lasekan, O., Tan, C. P., and Zaidul, I. S. M. (2011). Identification of the Aroma-Active Constituents of the Essential Oils of Water Dropwort (*Oenanthe javanica*) and "Kacip Fatimah" (*Labisia pumila*). *Int. Food Res. J.* 18 (3), 1021–1026.

Pihie, A. H. L., Othman, F., and Zakaria, Z. A. (2011). Anticarcinogenic Activity of *Labisia pumila* against 7,12- Dimethylbenz (A) Anthracene (DMBA)/croton Oil-Induced Mouse Skin Carcinogenesis. *Afr. J. Pharm. Pharmacol.* 5 (7), 823–832. doi:10.5897/AJPP11.140

Radzali, S. A., Markom, M., and Saleh, N. M. (2020). Co-solvent Selection for Supercritical Fluid Extraction (SFE) of Phenolic Compounds from *Labisia pumila*. *Molecules* 25 (24), 1–15. doi:10.3390/molecules25245859

Rahmi, E. P., Kumolosasi, E., Jalil, J., Husain, K., Buang, F., Abd. Razak, A. F., et al. (2020). Anti-hyperuricemic and Anti-inflammatory Effects of *Marantodes pumilum* as Potential Treatment for Gout. *Front. Pharmacol.* 11, 289. doi:10.3389/fphar.2020.00289

Salehan, N. A. M., Naila, A., Ajit, A., and Sulaiman, A. Z. (2020). Effect of Solid to Water Ratio, Time and Temperature on Aqueous Extraction of Gallic Acid from *Labisia pumila* var. *alata* of Malaysia. *Pak. J. Sci. Ind. Res. B Biol. Sci.* 63 (2), 93–99. doi:10.52763/pjsir.biol.sci.63.2.2020.93.99

Siyumbwa, S., Kamran, S., Akowuah, G., Teo, S. S., Amini, F., and Patrick, N. (2015). The HPTLC Validated Method Development for the Quantification of Naringin from the Partially Purified *Labisia pumila* Dichloromethane Extract. *J. Chromatogr. Sep. Tech.* 6 (4), 271–274. doi:10.4172/2157-7064.1000271

Smillie, T. J., and Khan, I. A. (2010). A Comprehensive Approach to Identifying and Authenticating Botanical Products. *Clin. Pharmacol. Ther.* 87 (2), 175–185. doi:10.1038/clpt.2009.287

Srirama, R., Kumar, J. U. S., Seethapathy, G. S., Newmaster, S. G., Ragupathy, S., and Ganeshaiah, K. N. (2017). Species Adulteration in the Herbal Trade: Causes, Consequences and Mitigation. *Drug Saf.* 40 (8), 651–661. doi:10.1007/s40264-017-0527-0

Sunarno, B. (2005). Revision of the Genus *Labisia* (Myrsinaceae). *Blumea J. Plant Taxon. Plant Geogr.* 50 (3), 579–597. doi:10.3767/000651905x622879

Tan, N. A. S., Giribabu, N., Karim, K., Nymathulla, S., and Salleh, N. (2019). Intravaginal Treatment with *Marantodes pumilum* (Kacip Fatimah) Ameliorates Vaginal Atrophy in Rats with Post-menopausal Condition. *J. Ethnopharmacol.* 236, 9–20. doi:10.1016/j.jep.2019.02.027

Tarmizi, A. A. A., Wagiran, A., Mohd Salleh, F., Chua, L. S., Abdulllah, F. I., and Hasham, R. (2021). Integrated Approach for Species Identification and Quality Analysis for *Labisia pumila* Using DNA Barcoding and HPLC. *Plants* 10, 717. doi:10.3390/plants10040717

Techen, N., Parveen, I., Zhiqiang, P., and Khan, I. A. (2014). DNA Barcoding of Medicinal Plant Material for Identification. *Curr. Opin. Biotechnol.* 25, 103–110. doi:10.1016/j.copbio.2013.0901010.1016/j.copbio.2013.09.010

Tnah, L. H., Lee, C. T., Lee, S. L., Ng, C. H., and Ng, K. K. S. (2014). Development of Microsatellites in *Labisia pumila* (Myrsinaceae), an Economically Important Malaysian Herb. *Appl. Plant Sc.* 2 (6), 1400019. doi:10.3732/apps.1400019

Tnah, L. H., Lee, S. L., Tan, A. L., Lee, C. T., Ng, K. K. S., and Ng, C. H. (2019). DNA Barcode Database of Common Herbal Plants in the Tropics: a Resource for Herbal Product Authentication. *Food control.* 95, 318–326. doi:10.1016/j.foodcont.2018.08.022

Upton, R., David, B., Stefan, G., and Glasl, S. (2020). Botanical Ingredient Identification and Quality Assessment: Strengths and Limitations of Analytical Techniques. *Phytochem. Rev.* 19 (5), 1157–1177. doi:10.1007/s11101-019-09625-z

Wan Omar, W. F. N., Giribabu, N., Karim, K., and Salleh, N. (2019). *Marantodes pumilum* (Blume) Kuntze (Kacip Fatimah) Stimulates Uterine Contraction in Rats in Post-partum Period. *J. Ethnopharmacol.* 245, 112175. doi:10.1016/j.jep.2019.112175

Wei, X. C., Cao, B., Luo, C. H., Huang, H. Z., Tan, P., Xu, X. R., et al. (2020). Recent Advances of Novel Technologies for Quality Consistency Assessment of Natural Herbal Medicines and Preparations. *Chin. Med. (United Kingdom)* 15 (1), 1–24. doi:10.1186/s13020-020-00335-9

WFO (2022). *Marantodes pumilum* (Blume) Kuntze. Available at: http://www.worldfloraonline.org/taxon/wfo-0001039157 (Accessed on Apr 21, 2022).

World Health Organization (2017). "WHO Guidelines for Selecting Marker Substances of Herbal Origin for Quality Control of Herbal Medicines," in *WHO Expert Committee on Specifications for Pharmaceutical Preparation: Fifty First Report. Annex 1. WHO Technical Report Series, No. 1003* (Geneva: World Health Organization).

World Health Organization (2011). Quality Control Methods for Herbal Materials. Geneva: World Health Organization.

Wu, H., Xi, H., Lai, F., Ma, J., Chen, W., and Liu, H. (2019). Cellular Antioxidant Activity and Caco-2 Cell Uptake Characteristics of Flavone Extracts from *Labisia pumila*. *Int. J. Food Sci. Technol.* 54 (2), 536–549. doi:10.1111/ijfs.13968

Wu, H., Xi, H., Lai, F., Ma, J., and Liu, H. (2018). Chemical and Cellular Antioxidant Activity of Flavone Extracts of *Labisia pumila* before and after *In Vitro* Gastrointestinal Digestion. *RSC Adv.* 8, 12116–12126. doi:10.1039/c8ra00142a

Xie, P., Chen, S., Liang, Y., Wang, X., Tian, R., and Upton, R. (2006). Chromatographic Fingerprint Analysis-A Rational Approach for Quality Assessment of Traditional Chinese Herbal Medicine. *J. Chromatogr. A* 1112 (1–2), 171–180. doi:10.1016/j.chroma.2005.12.091

Yadav, N. P., and Dixit, V. K. (2008). Recent Approaches in Herbal Drug Standardization. *Int. J. Integr. Biol.* 2 (3), 195–203.

Yeop, A., Sandanasamy, J., Pang, S. F., and Gimbun, J. (2021). Stability and Controlled Release Enhancement of *Labisia pumila*'s Polyphenols. *Food Biosci.* 41, 101025. doi:10.1016/j.fbio.2021.101025

Yongyu, Z., Shujun, S., Wenyu, W., Huijuan, C., and Jianbing, W. (2011). *Quality Control Method for Herbal Medicine - Chemical fingerprint Analysis*. Quality Control of Herbal Medicines and Related Areas, 171–194.

Zakaria, M., and Mohd, M. A. (1994). *Traditional Malay Medicinal Plants*. Kuala Lumpur: Fajar Bakti.

Zhan, W., Yang, X., Lu, G., Deng, Y., and Yang, L. (2022). A Rapid Quality Grade Discrimination Method for *Gastrodia elata* Powder Using ATR-FTIR and Chemometrics. *Spectrochim. Acta A Mol. Biomol. Spectrosc.* 264, 120189. doi:10.1016/j.saa.2021.120189

Zhu, J., Fan, X., Cheng, Y., Agarwal, R., Moore, C. M. V., and Chen, S. T. (2014). Chemometric Analysis for Identification of Botanical Raw Materials for Pharmaceutical Use: A Case Study Using *Panax notoginseng*. *PLoS ONE* 9 (1), 1–10. doi:10.1371/journal.pone.0087462

Zou, P., Hong, Y., and Koh, H. L. (2005). Chemical Fingerprinting of *Isatis indigotica* Root by RP-HPLC and Hierarchical Clustering Analysis. *J. Pharm. Biomed. Anal.* 38 (3), 514–520. doi:10.1016/j.jpba.2005.01.022

Conflict of Interest: The authors declare that the research was conducted in the absence of any commercial or financial relationships that could be construed as a potential conflict of interest.

Publisher's Note: All claims expressed in this article are solely those of the authors and do not necessarily represent those of their affiliated organizations, or those of the publisher, the editors and the reviewers. Any product that may be evaluated in this article, or claim that may be made by its manufacturer, is not guaranteed or endorsed by the publisher.

frontiers | Frontiers in Pharmacology

ORIGINAL RESEARCH
published: 24 June 2022
doi: 10.3389/fphar.2022.832590

Shuangxinfang Prevents S100A9-Induced Macrophage/Microglial Inflammation to Improve Cardiac Function and Depression-Like Behavior in Rats After Acute Myocardial Infarction

Yize Sun[1†], Zheyi Wang[2†], Jiqiu Hou[3], Jinyu Shi[3], Zhuoran Tang[1], Chao Wang[3] and Haibin Zhao[3*]*

[1]Third Affiliated Hospital, Beijing University of Chinese Medicine, Beijing, China, [2]Qilu Hospital, Cheeloo College of Medicine, Shandong University, Jinan, China, [3]Oriental Hospital, Beijing University of Chinese Medicine, Beijing, China

OPEN ACCESS

Edited by:
Abdul Rohman, Gadjah Mada University, Indonesia

Reviewed by:
Rebecca J. Henry, University of Maryland, Baltimore, United States
Min Yang, Jiangsu Institute of Nuclear Medicine, China

***Correspondence:**
Chao Wang
wangchaozhongyi@sina.cn
Haibin Zhao
haibin999@126.com

[†]*These authors have contributed equally to this work*

Specialty section:
This article was submitted to Ethnopharmacology, a section of the journal Frontiers in Pharmacology

Received: *10 December 2021*
Accepted: *06 May 2022*
Published: *24 June 2022*

Citation:
Sun Y, Wang Z, Hou J, Shi J, Tang Z, Wang C and Zhao H (2022) Shuangxinfang Prevents S100A9-Induced Macrophage/Microglial Inflammation to Improve Cardiac Function and Depression-Like Behavior in Rats After Acute Myocardial Infarction. Front. Pharmacol. 13:832590. doi: 10.3389/fphar.2022.832590

Background: Depression is a common complication of cardiovascular disease, which deteriorates cardiac function. Shuangxinfang (psycho-cardiology formula, PCF) was reported to alleviate myocardial ischemia injury and improve depression-like behavior. Interestingly, our previous proteomics study predicted that the protein S100A9 appeared as an important target, and macrophage/microglial inflammation might be involved in the process of PCF improving depression induced by acute myocardial infarction (AMI). This study aims to validate the proteomics results.

Methods: AMI rat models were established *in vivo*, followed by the administration of PCF or ABR-215757 (also named paquinimod, inhibiting S100A9 binding to TLR4) for 5 days. Forced swimming test (FST) and open field test (OFT) were applied to record depression-like behavior, and echocardiography was employed to evaluate cardiac function. Morphological changes of cardiomyocytes were assessed by HE staining and TUNEL staining on day 7 after cardiac surgery, as well as Masson trichrome staining on day 21. Hippocampal neurogenesis was determined by Nissl staining, while 5-hydroxytryptamine (5-HT), tryptophan/kynurenine ratio, and brain-derived neurotrophic factor (BDNF) in the hippocampus were analyzed as biochemical indicators of depression. We employed RT-qPCR, western blotting, and immunofluorescence to detect the expression of pathway-related genes and proteins. Myocardial and hippocampal expression of inflammatory factors were performed by ELISA. The activation of macrophage and microglia was assessed *via* immunoreaction using CD68 and Iba1, respectively. For *in vitro* confirmation, BV2 cells were primed with recombinant protein S100A9 and then treated with PCF serum or ferulic acid to determine alterations in microglial inflammation.

Results: Rats in the AMI group showed heart function deterioration and depression-like behavior. Coronary ligation not only brought about myocardial inflammation, cell apoptosis, and fibrosis but also reduced the neurogenesis, elevated the tryptophan/

kynurenine ratio, and decreased the content of 5-HT. PCF could ameliorate the pathological and phenotypic changes in the heart and brain and inhibit the expression of the S100A9 protein, the activation of the microglial cell, and the secretion of IL-1β and TNF-α raised by AMI. ABR-215757 showed therapeutic effect and molecular biological mechanisms similar to PCF. Treatment with PCF serum or ferulic acid *in vitro* was proved to efficiently block the hyperactivation of BV2 cells and increment of cytokine contents induced by recombinant protein S100A9.

Conclusion: We identify S100A9 as a novel and potent regulator of inflammation in both the heart and brain. Macrophage/microglia inflammation mediated by S100A9 is considered a pivotal pathogenic in depression after AMI and a major pathway for the treatment of PCF, suggesting that PCF is a promising therapeutic candidate for psycho-cardiology disease.

Keywords: Shuangxinfang, traditional Chinese medicine, acute myocardial infarction, epressive disorder, S100A9, inflammation, microglia, macrophages

1 BACKGROUND

The reported prevalence of depression after acute myocardial infarction (AMI) for the last few years varied across studies and generally ranged from 18% to 40% (Smolderen et al., 2017; Feng et al., 2019; Trajanovska et al., 2019; Worcester et al., 2019). The TRIUMPH study, an observational multicenter cohort study published in *Circulation*, which enrolled 4,062 patients with AMI and recognized depression between 24 and 72 h of admission, declared that one-fifth of patients with AMI had significant depressive symptoms (Smolderen et al., 2017). The research assessed depression in patient survivors during hospitalization at 3 and 12 months after AMI, and the three groups presented almost equal representation of depression according to beck depression inventory (BDI) with 34.1%, 30.8%, and 30%, respectively (Trajanovska et al., 2019). These results implied that acute coronary events might directly induce depression, regardless of other socioeconomic factors. It is reported that only patients with incident post-AMI depression, rather than ongoing or recurrent depressions, had an impaired cardiovascular prognosis (de Jonge et al., 2006), suggesting that the pathological mechanism of AMI-induced depression may be different from other types and worthy of further investigation.

Depression has been classified as a risk factor for poor prognosis among patients with cardiovascular diseases, which is closely related to decreased heart rate variability, sympathetic nervous excitement, and ventricular arrhythmias, ulteriorly leading to fatal and non-fatal cardiovascular events, loss of life quality, an increase in healthcare expenditure, and suicide risk (Gehi et al., 2005; Rodrigues et al., 2015; Hawkins et al., 2016; AbuRuz and Al-Dweik, 2018; Wilkowska et al., 2019; Bangalore et al., 2020). Selective serotonin reuptake inhibitors (SSRIs) are currently preferred choices for depressed patients with cardiovascular disease. However, associations of antidepressant treatment with long-term cardiac outcomes in depression following AMI have been inconclusive (Coupland et al., 2016; Kim et al., 2018; Iasella et al., 2019; Kim et al., 2019). It means that new therapeutic strategies still need to be developed to make up for the deficiency of current antidepressants.

Shuangxinfang (psycho-cardiology formula, PCF) consists of four kinds of botanical drugs, including *Salvia miltiorrhiza* Bunge (Lamiaceae; *Salviae miltiorrhizae* radix et rhizoma), the roots and rhizomes of *Chuanxiong Rhizoma* (Umbelliferae; *Ligusticum chuanxiong* Hort.), the bulb of *Lilium pumilum* DC (Liliaceae; Lilii Bulbus), and the dried seeds of *Ziziphi Spinosae Semen* [Rhamnaceae; *Ziziphus jujuba* Mill. var. spinosa (Bunge) Hu ex H.F.Chou], which are beneficial in promoting blood circulation, removing stasis, lifting the spirit, and gaining the vitality to be away from gloomy mood and somatic distress. The main active substances of *Salvia miltiorrhiza* Bunge include the phenolic acids, the diterpenoid tanshinones, and related quinone derivatives (Pang et al., 2016). *Lilium pumilum* DC contains various chemical components, in which steroidal saponins, flavonoids, and polysaccharides are the main active ingredients (Zhou et al., 2021). *Ziziphi Spinosae Semen* contains flavonoids, saponins, alkaloids, and fatty oils (Hua et al., 2021). Besides, 174 components have been identified from *Chuanxiong Rhizoma*, among which phthalides and alkaloids would be the main bioactive ingredients for the pharmacological properties (Chen et al., 2018). Our previous clinical trials have already confirmed that PCF could relieve angina pectoris and improve depressive symptoms (Wang et al., 2021). The pharmacological mechanism of PCF concentrates on the regulation of inflammatory response and the neuroendocrinology system. PCF could inhibit the expression of inflammatory factors such as tumor necrosis factor-α (TNF-α) in AMI rats and meanwhile appease the neural system by modulating the γ-aminobutyric acid (GABA) system (Wang et al., 2019). The above data highlighted a critical role for the PCF in inhibiting inflammation caused by injured myocardium and alleviating depression following AMI.

To systematically identify possible targets and explore the biological mechanism of PCF in depression after AMI, we have performed pharmacoproteomic profiling of the myocardium and hippocampus in rats from the sham, AMI, and PCF groups using label-free liquid chromatography-mass spectrometry (LC-MS/MS) (Sun et al., 2021). The intersection of differentially expressed proteins (DEPs) in the peri-infarct border zone and

hippocampus produces a unique protein, that is S100A9, which has become a topic molecule in the cardiovascular field during these years (Nagareddy et al., 2020; Wang et al., 2021). The role of S100A9 in driving inflammatory response after MI has attracted much attention and has been identified as a potential therapeutic target (Li et al., 2019). Also, the alarmin S100A9 mediating neuroinflammation in depressive-like behaviors begins to come into focus (Gong et al., 2018). According to alteration of the proteomics profile in biological fraction and pertinent pathways, macrophage/microglia inflammation might be a biological mechanism for PCF to protect against the pathological progress of depression after AMI. As reported, S100A9 modulates macrophage inflammation in AMI and regulates microglial inflammation in depression (Ma et al., 2017; Marinković et al., 2019), yet the evidence of it is not quite adequate in post-AMI depression. Indeed, the regulation of S100A9 in macrophage/microglia inflammation guides a direction for molecular mechanisms in psycho-cardiology diseases. In this study, systematic experiments were performed in AMI rats with depression-like behavior to verify the hypothesis derived from proteomics.

2 MATERIALS AND METHODS

2.1 Preparation of PCF

One dosage of PCF was composed of the roots and rhizomes of *Salvia miltiorrhiza* Bunge (Lamiaceae; *Salviae miltiorrhizae* radix et rhizoma) (Dan Shen, 20 g), the roots and rhizomes of *Chuanxiong Rhizoma* (Umbelliferae; *Ligusticum chuanxiong* Hort.) (Chuan Xiong, 12 g), the bulb of *Lilium pumilum* DC (Liliaceae; Lilii Bulbus) (Bai He, 30 g), and the dried seeds of *Ziziphi Spinosae Semen* (Rhamnaceae; *Ziziphus jujuba* Mill. var. spinosa [Bunge] Hu ex H.F.Chou) (Suan Zao Ren, 30 g). PCF granules, purchased from Beijing Pharmaceutical Co., Ltd., were made of the above four botanical drugs by the process of water heating, extraction, separation, concentration, drying, and granulation. The process was operated according to the "Technical Requirements for Quality Control and Standard Formulation of Chinese Medicine Granule," issued by the National Medical Products Administration. One dosage of PCF granule was dissolved in 100 ml distilled water which was heated at a temperature of 100°C. According to the long-term clinical practice, the adult daily dosage of PCF was 1 ml (PCF solution)/600 g (body weight)/d. The optimal dosage of the PCF solution for rats was six times greater than the adult dosage based on the body surface areas in accordance with the Chinese Medicine Pharmacology Research Technology. Furthermore, the converted lavage dose has been applied and verified on the efficacy for depression post-AMI in previous experiments (Wang et al., 2019). Thus, the optimal lavage dose was 1 ml/100 g/d.

2.2 Drugs and Reagents

Paquinimod (Apexbio, Houston, TX, United States), also called ABR-215757 (a specific inhibitor of S100A9), binds to S100A9 in a Ca^{2+}/Zn^{2+} dependent way and blocks interaction with TLR4 (Björk et al., 2009; Liang et al., 2019). It has been applied to the experimental research of depression, atherosclerosis, and other diseases (Stenström et al., 2016; Kraakman et al., 2017). According to the literature and the results of previous studies, ABR-215757 was successively dissolved in 10% DMSO, 40% polyethylene glycol 400 (PEG400), 5% Tween 80, and 45% normal saline, and injected intraperitoneally at a dose of 5 mg/kg/d, once a day for 5 consecutive days (Masouris et al., 2017; Tahvili et al., 2018). Recombinant protein S100A9 (Bio-Techne, Minnesota, MN, United States) was prepared into 300 μg/ml mother solution with sterile water and then diluted to 0.01 μM, 0.02 μM, 0.05 μM, and 0.1 μM with a complete medium in the initial experiments. A concentration of 0.1 μM was adopted in the subsequent experiments. C34 (Apexbio, Houston, TX, United States) inhibited toll-like receptor 4 *in vitro*, which was dissolved in DMSO to prepare mother liquor with a concentration of 10 mM and diluted to the final concentration of 10 μM when used (Adegoke et al., 2019). Ferulic acid (Yuanye Bio-Technology, Shanghai, China) was dissolved in DMSO and configured to a concentration of 80 μM.

2.3 *In Vitro* Study

2.3.1 Preparation of Medicated Sera

The rats were given PCF or distilled water as above and anesthetized by intraperitoneal injection of pentobarbital 1 hour after administration. Blood was collected from the abdominal aorta and centrifuged, heat-inactivated at 56°C for 30 min, and filtered by a 0.22 μm filter membrane. The serum was packed separately and frozen at −80°C until use.

2.3.2 Cell Culture

The microglial cell line BV-2 was received from the Scientific Research Center of Shanghai 10th People's Hospital and cultured in high-glucose Dulbecco's-modified eagle's medium (H-DMEM, Invitrogen, United States) with 10% fetal bovine serum (FBS Gibco, United States) and 1% penicillin/streptomycin (Gibco, United States) at 37°C in a humidified atmosphere with 5% CO2. Cells at 80% confluency were supplied for experimental treatments or trypsinized for passage.

2.3.3 Group Design

BV2 microglia cells were divided into six groups: control, recombinant protein S100A9 (S100A9), C34, PCF serum (PCF), ferulic acid (FA), and control serum (CS). Except for the control group treated with complete medium, cells in the C34, FA, PCF, and CS groups were cultured in 0.1 μM of recombinant S100A9 protein for 6 h, followed by complete medium, respectively, supplemented with 10 μM C34, 80 μM FA, 5% PCF serum, and 5% control serum for 6 h.

2.3.4 CCK-8 Assay

Cells were cultured in 96-well plates (2×10^4 cells per well) with 100 μl complete medium containing various doses of recombinant S100A9 protein (0.01/0.02/0.05/0.1 μM), control serum (5%, 10%, 20%), or PCF serum (5%, 10%, 20%), to determine the dose-dependent effects of reagents. Cell viability was measured *via* the CCK-8 assay kits. The absorbance at 450 nm was measured with a microplate reader.

2.3.5 Enzyme-Linked Immunosorbent Assay

The cell supernatants from each sample were collected for ELISA assays. Concentrations of inflammation markers, including S100A9, TNF-α, and IL-1β, were determined by pre-coated ELISA kits (MLBIO, Shanghai, China) according to the manufacturer's instructions.

2.4 *In Vivo* Experiment

2.4.1 Animals

Male Sprague-Dawley (SD) rats (220 ± 20 g) were purchased from Beijing Vital River Laboratory Animal Technology Co., Ltd., [License No. SCXK (Beijing) 2016–0006]. All rats were fed in a specific pathogen-free facility with controlled temperature (22 ± 1°C), relative humidity (65–70%), and a 12:12 light/dark cycle.

2.4.2 Ethics

Experiments were in accordance with protocols approved by the Institutional Animal Care and Use Committee of the University of Chinese Medicine, Beijing, China (Ethical number: BUCM-4-2020091108-3141).

2.4.3 Establishment of AMI Rat Model

As described previously, ligation of the left anterior descending (LAD) coronary artery was used to construct the AMI rat model, while only threading was operated without knotting in the sham group (Wang et al., 2019; Hou et al., 2021). Penicillin was injected intraperitoneally to prevent infection. The success of the AMI model was marked of pathological Q wave by more than six leads of ECG I, AVL, and V1~V6 in electrocardiograph on the second day after surgery.

2.4.4 Design and Allocation

After 7 days of acclimatization, the rats were randomly divided into the sham group (n = 16), AMI group (n = 18), PCF group (n = 18), and ABR-215757 group (n = 18). All the rats received LAD operation other than the sham group. Rats in the PCF group were administered intragastrically PCF solution (1 ml/100 g/d) at 8 a.m. every day for 5 days, while the rats in the other groups received the same volume of distilled water (1 ml/100 g/d) on the same schedule. Paquinimod (5 mg/kg/d) was injected into the rats of the ABR-215757 group intraperitoneally at 8:30 a.m. every day for 5 days, and the rats in the other groups were intraperitoneally injected with the same volume of 0.9% normal saline. After the last treatment administration, the rats underwent behavioral tests and echocardiography. Then, half of the rats randomly selected in each group were given a peritoneal injection of 1% pentobarbital sodium, and blood samples were collected from the abdominal aorta. The hearts and brain tissues were immediately isolated and snap-frozen in liquid nitrogen. On the 21st day after surgery, the remaining rats were sacrificed to detect neurogenesis in the hippocampus and cardiac fibrosis in the myocardium.

2.5 Behavioral Tests

Behavioral tests were performed in a double-blinded manner and operated in a dark and quiet room, and all rats were transported to which 1 hour earlier to acclimatize. The behavior in the open field test and forced swimming test was videotaped and further analyzed by SuperMaze (Softmaze, Shanghai, China), specialized animal behavior video analysis software.

2.5.1 Open Field Test (OFT)

The first step was to set up the software program. In SuperMaze, the grayscale was set as the recognition algorithm and three points were determined to track the position of the rats. The open field is a square wooden chest (100 × 100 × 60 cm) with a black floor and divided into 25 identical areas with white lines. A single rat was placed in the central square and allowed to move freely for 5 min. The number of verticalities (times of rat stood on its hind limbs) was recorded by an observer blind to the group, while the total distance and distance in the central region were recorded in the software. The field was wiped clean with 75% alcohol before each test.

2.5.2 Forced Swimming Test

The dynamic background method was selected, and the rats were located by the center of gravity in SuperMaze. The FST was operated in a transparent glass cylindrical tank with 60 cm in height, 38 cm in width, and 40 cm in depth. Rats were put into the glass tank filled with 22°C–24°C fresh water and allowed to swim freely for 5 min. The immobility time was recorded by the video camera and analyzed by SuperMaze software.

2.6 Echocardiography

The rats were anesthetized and fixed on a board with fur shaved. Three continuous cardiac cycles were captured from the left ventricular short axial section to detect the M-shaped curve. Left ventricular ejection fraction (LVEF) and left ventricular fractional shortening (LVFS) were measured to assess cardiac function. The left ventricular end-diastolic inner diameter (LViDd), left ventricular end-systolic inner diameter (LViDs), left ventricular end-diastolic volume (LVEDV), and left ventricular end-systolic volume (LVESV) were measured to evaluate the ventricular structure.

2.7 H&E and Masson Staining

The tissues extracted were embedded in paraffin and cut at a 4 μm thickness after fixation in 10% neutral formalin for 72 h. These slices were stained with hematoxylin/eosin (H&E) or Masson trichrome and observed under an optical microscope (Carl Zeiss Microscopy, Germany) to evaluate histopathological changes and collagen deposition. The percentage of collagen deposition area was analyzed by the ratio of fibrosis area to the total myocardial area.

2.8 Nissl Staining

The brains were dyed with toluidine blue O to assess neurogenesis. Brain sections were immersed in xylene and then rehydrated in graded alcohol solutions and distilled water. Subsequently, tissue slices were stained with toluidine blue (Servicebio, Wuhan, China) for 10 min, quickly rinsed in distilled water, dried at a 60°C environment, made transparent by xylene, and sealed with neutral gum. Three sample sections were selected from each group and observed using an optical

microscope. The mean integrated optical density (IOD) of the dentate gyrus (DG) region in the hippocampus was measured by Image-Pro Plus 6.0 software (Media Cybernetics Inc., Rockville, MD, United States).

2.9 TUNEL Assay

Cardiac cell death was evaluated utilizing a TdT-mediated dUTP nick end labeling (TUNEL) assay kit (Roche, United States) in accordance with the manufacturer's protocol. The kit was labeled with FITC fluorescein, and the positive apoptotic nucleus was dyed green. The cells were stained with DAPI (1:30, Beyotime Biotechnology, China) for nuclear counterstaining and observed under a fluorescence microscope (Zeiss Axio Scope A1). Three fields of each slice were selected for quantification. ImageJ software (NIH, MD, United States) was applied to calculate the number of TUNEL positive cells. Apoptosis index (AI) = (number of apoptotic nucleus/number of total nucleus) × 100%.

2.10 Immunofluorescence Staining

Paraffin sections of heart and brain tissue were processed as previously described. After routine dewaxing, hydration, and antigen retrieval, the tissues were incubated in bovine serum albumin (BSA) for 30 min. After blocking, the slices were incubated with an anti-Iba1 (1:500, Abcam, United Kingdom), anti-CD68 (1:200, Abcam, United Kingdom), or anti-S100A9 (1:500, Proteintech, United States) overnight at 4°C, followed by secondary antibodies conjugated to CY3 (1:300, Servicebio, China) or HRP (1:500, Servicebio, China). As for anti-S100A9, the slices were incubated with FITC at room temperature in the dark for 10 min. Subsequently, the tissues were stained with DAPI for nuclear counterstaining. The stained slides were photographed under a fluorescence microscope. The number of $CD68^+$ cells in the myocardium or $Iba1^+$ cells in the hippocampus was counted by ImageJ software (NIH, MD, United States) in a blinded manner. The data were expressed as the mean number of cells per square millimeter. For intensity measurements, three sections from each sample at the same level were used to determine the mean optical density (mean optical density = IOD/area). The mean values were calculated from three randomly selected microscopic fields from each section.

2.11 Western Blotting

The hippocampal and myocardial samples were lysed; then, proteins were extracted with RIPA buffer (Thermo Fisher Scientific, United States) and measured by the BCA protein concentration Determination kit (Glpbio, United States). Protein mixtures were separated *via* 10% SDS-PAGE and transferred to polyvinylidene difluoride (PVDF) membranes (Millipore, United States). TBST containing non-fat dried milk was used to block non-specific binding to the membranes, and the membranes were incubated with primary antibodies at 4°C overnight, followed by incubation with the secondary antibodies (1:3000, Thermo Fisher Scientific) at room temperature for 30 min and reaction with enhanced chemiluminescence (ECL). The primary antibodies for immunoblotting were as follows: anti-TLR4 (1:1000, Abcam), anti-NF-κB (1:1000, Abcam), anti-BDNF (1:1000, Abcam), anti-GAPDH (1:1000, Servicebio), and anti-ACTIN (1:1000, Servicebio). The exposure condition was adjusted on the basis of luminescence intensity. The results were scanned and color-modulated, and the target band intensities were analyzed by the BandScan software (Glyko, United States).

2.12 Real-Time Quantitative PCR

TRIzol and chloroform were used to extract mRNA from tissues and cells. Purity was assessed by the ratio of A260/A280, and RNA with a purity between 1.8 and 2.0 was used for the next actions. The complementary strand DNA was synthesized from RNA *via* first-strand cDNA synthesis mix with gDNA Remover F0201-100T Kit (LABLEAD, China). The real-time PCR reaction system was formulated as requested by QuantiNova SYBR Green PCR Kit (QIAGEN, Germany). Each reaction was run in 35–40 cycles consisting of the following steps: initial heat activation at 95°C for 2 min followed by a set cycle of denaturation at 95°C for 5 s and combined annealing/extension at 60°C for 10 s. Melt curve analysis was performed to confirm the specificity of the amplicon. As a final step, relative mRNA expression levels were analyzed using the formula ΔΔCt method and normalized to the GAPDH.

2.13 Sequences of PCR Primers

Gene symbol	Forward	Reverse
S100A9	GACATCCTGACA CCCTGAACAAG	CCCATCAGCATCAT ACACTCCTC
NF-κB	TTATGGGCAGGATGGACCTA	CTCCTTCGGAACGA TATGAT
GAPDH	CTGGAGAAACCTGCCAAGTATG	GGTGGAAGAATGGGA GTTGCT

2.14 LC–MS/MS Method

The hippocampus tissue samples were weighed and ground in the frozen grinding machine. 80% methanol was added at a ratio of 1:10, followed by vortex, low-temperature ultrasound for 10 min, and centrifugation at 13000 rpm for 10 min. Then, the supernatant was removed to frozen centrifugation and concentrated to dry, and 100 ul of solvent was added for redissolution. The analysis was performed on the AB SCIEX QTRAP 4500 (United States) triple quadrupole mass spectrometer in SRM and positive ionization mode. The LC separation was run on an ACQUITY HSS PFP column (2.1 × 100 mm, 1.7 μm, United States) equipped with Waters ACQUITY UPLC I-Class infinite binary pump. Acetonitrile containing 10 mM amine acetate and 0.1% formic acid was used as solvent A, and water containing 10 mM amine acetate and 0.1% formic acid was used as solvent B. The flow rate was 0.2 ml/min. The steps of gradient elution were as follows: the

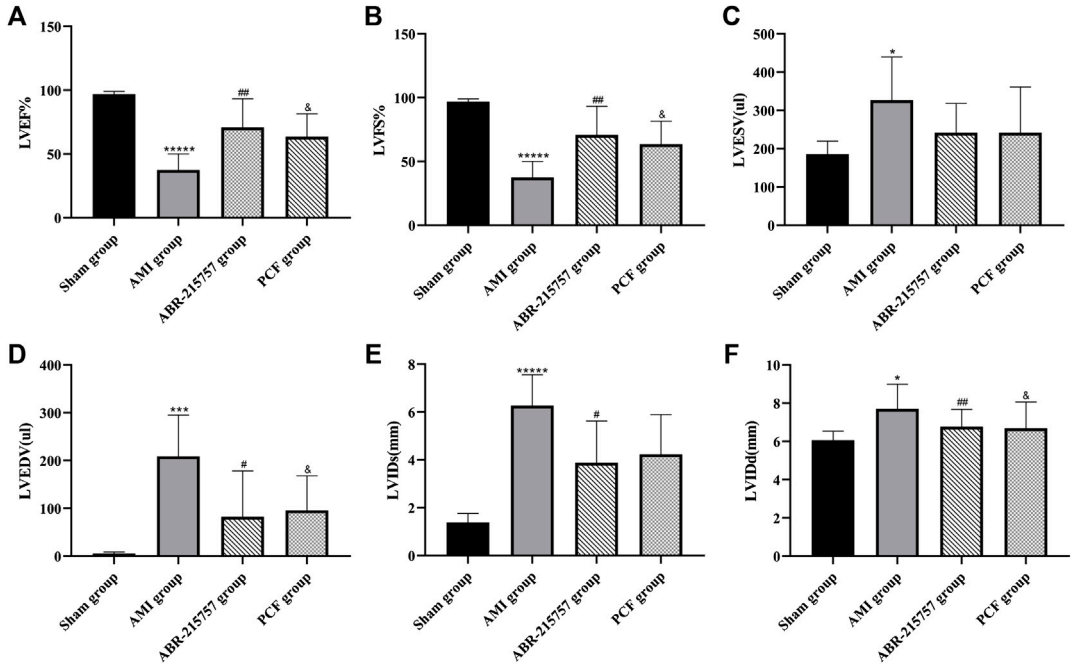

FIGURE 1 | Cardiac function parameters of rats after myocardial infarction in echocardiography from each group (n = 7). Values were expressed as mean ± SD. LVEF: left ventricular ejection fraction. LVFS: left ventricular fractional shortening. LViDd: left ventricular end-diastolic inner diameter; LViDs: left ventricular end-systolic inner diameter. LVEDV: left ventricular end-diastolic volume. LVESV: left ventricular end-systolic volume. *p < 0.05, ***p < 0.001, *****p < 0.00001, compared with the sham group. #p < 0.05, ##p < 0.01, compared with the AMI group. & p < 0.05, compared with the AMI group.

initial conditions were 98% solvent B starting from 0 min, 8 min to 0% solvent B, returning to the initial state of 98% solvent B after 2 min, and 12 min to end a collection. The column temperature was 35°C, while the sample was kept at 10°C and the injection volume was 10 μl. The MS parameters were as follows: ESI ion source temperature, 500°C; air curtain, 30 psi; collision activated dissociation gas settings, medium; and ion spray voltage, 5500 V. All data were processed by Analyst 1.6.3 Software.

2.15 Statistical Analysis

The data were presented as mean ± standard deviation (SD). Statistical graphing was performed using GraphPad Prism software (version 8.0; Inc., San Diego, CA, United States). For multiple comparison tests, one-way analysis of variance (ANOVA) was performed, followed by a Tukey *post hoc* test. Data were analyzed for normality and homogeneity of variances as a justification for parametric or nonparametric analyses. For all analyses, an average value of $p < 0.05$ was considered statistically significant.

3 RESULTS

3.1 PCF Improved Cardiac Function and Ventricular Remodeling in AMI Rats

As shown in **Figure 1**, myocardial infarction led to wall thinning, dilated left ventricular chambers, and an obvious decrease in cardiac function. The LVEF and LVFS were decreased in the AMI groups compared with the sham group ($p < 0.00001$). In contrast, the LVEF and LVFS in the PCF group were significantly elevated compared with the AMI group ($p < 0.05$) and showed a similar trend in the ABR-215757 group ($p < 0.01$). Thus, PCF and ABR-215757 could overcome the inhibitory effects of AMI on the LVEF and LVFS. The LVIDd and LVIDs, respectively, indicated end-diastolic and end-systolic left ventricle internal dimension, while LVESV and LVEDV, respectively, showed the maximum volume of the ventricle in systole and diastole. The four indicators in the PCF group and ABR-215757 group were declined in contrast with the AMI group.

3.2 PCF Alleviated Histological Injury in Myocardial Tissue of AMI Rats

The severity of cardiac damage was evaluated by morphological observations (**Figure 2**). Hematoxylin/eosin staining showed an orderly arrangement of myocardial fibers in the sham group. Conversely, the myocardial fibers became loosely and irregularly arranged in the AMI group. Instead, PCF and ABR-215757 alleviated the morphological injuries after AMI. Compared with the sham group, the apoptosis index was significantly increased in the AMI group on day 7 after coronary ligation ($p < 0.001$); then, a large number of fibrotic scars were observed on day 21 ($p < 0.0001$). TUNEL assay revealed that PCF and ABR-215757 significantly ameliorated AMI-induced cell apoptosis (**Figure 2D**), and Masson staining showed that both of them significantly decreased the fibrosis area in the peri-infarct border zone ($p < 0.001$, **Figure 2E**), indicating their beneficial effects to reduce impairment of cardiac function.

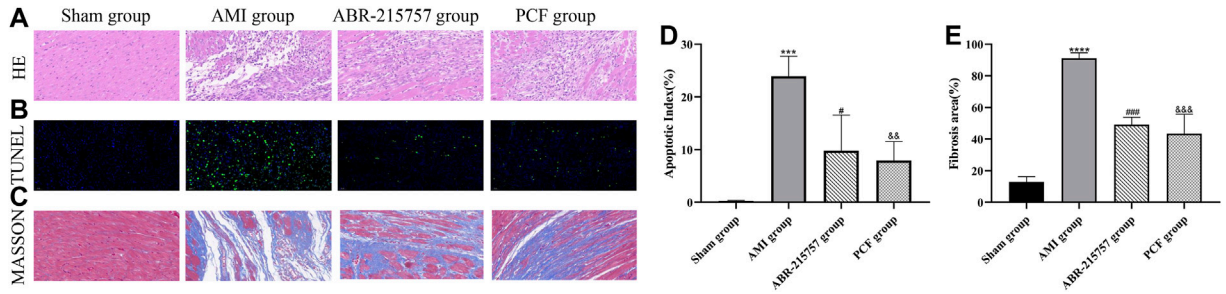

FIGURE 2 | Effect of PCF on AMI-induced pathological changes in the myocardial tissue. **(A)** H&E staining showed different levels of inflammatory infiltration in the peri-infarct border zone. Scale bar, 40 μm. **(B)** TUNEL staining showed cardiac apoptosis on 7 days after MI surgery. Green staining of the nucleus indicated apoptosis, and blue staining marked DAPI. **(C)** Masson trichrome staining of heart slides at 21 days after MI. Red, myocardium; blue, scarred fibrosis. **(D)** Quantitative analysis of TUNEL-positive cells in the border zone of infarction area. Three separate fields were calculated from each group. **(E)** Fibrosis area as a percentage (three samples from each group). ***$p < 0.001$, ****$p < 0.0001$, compared with the sham group. #$p < 0.05$, ###$p < 0.001$, compared with the AMI group. && $p < 0.01$, &&& $p < 0.001$, compared with the AMI group.

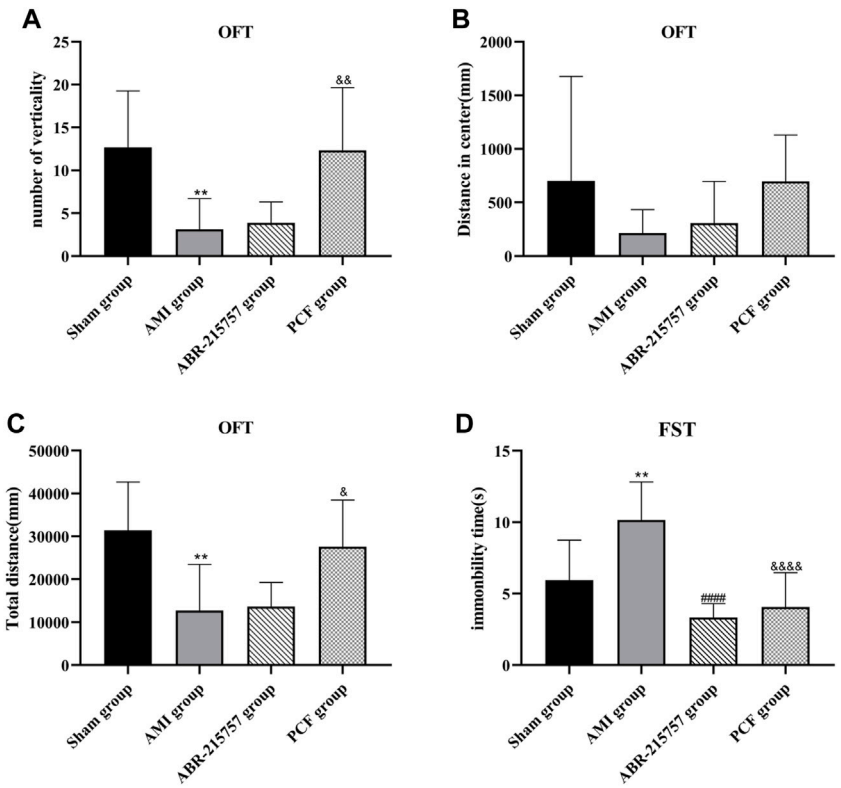

FIGURE 3 | PCF significantly ameliorated depression-like behavior in rats after myocardial infarction. **(A)** The number of verticality in open field test (OFT). **(B)** Distance in center. **(C)** Total distance. **(D)** Immobility time of rats in forced swimming test (FST). $n = 9$ per group. **$p < 0.01$, compared with the sham group. ####$p < 0.0001$, compared with the AMI group. & $p < 0.05$, && $p < 0.01$, &&&& $p < 0.0001$, compared with the AMI group.

3.3 PCF Improved Depression in Rats After AMI

Compared with the sham group, rats in the AMI groups showed depression-like behaviors, such as a reduction of crossing zones and rearing times in OFT and longer immobility time in FST ($p < 0.01$, **Figure 3**). In contrast, rats in the PCF group were much more active, such as extended total distance ($p < 0.05$) and increased verticality number ($p < 0.01$) in OFT and much shorter immobility duration in FST ($p < 0.0001$). Interestingly, rats after intraperitoneal injection of paquinimod showed less horizontal movement and fewer rearing times in OFT ($p > 0.05$) but shorter immobility time in FST ($p < 0.0001$).

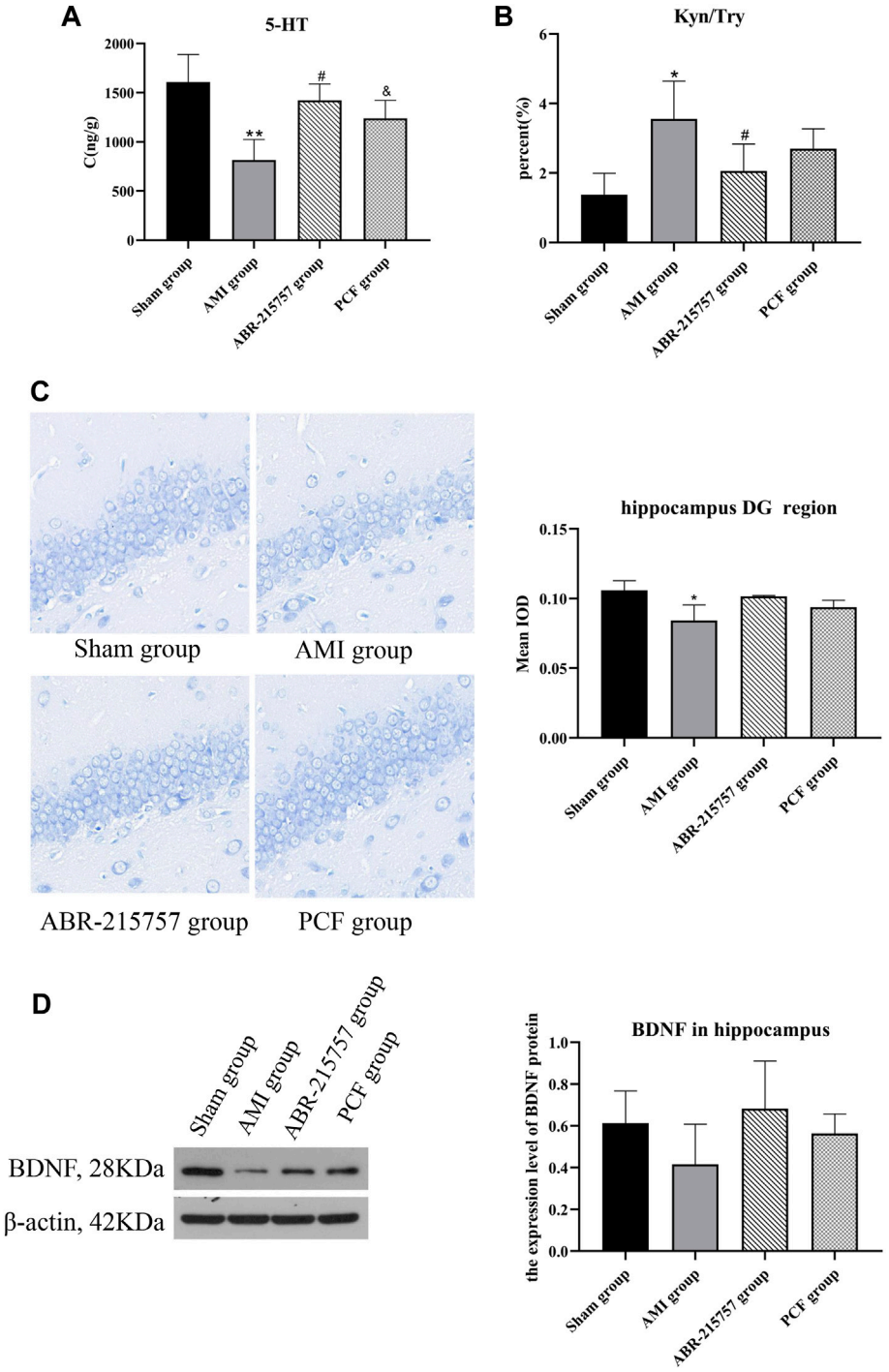

FIGURE 4 | The effect of PCF on the neurotransmitter disorder and decreased neurogenesis caused by myocardial infarction. **(A)** HPLC analysis of 5-HT in the hippocampus of rats ($n = 3$). **(B)** Ratio of kynurenine to tryptophan. **(C)** Nissl's staining in the dentate gyrus region of hippocampus from different groups. **(D)** Western blotting detected the protein expression levels of BDNF in the hippocampus ($n = 3$). 5-HT: 5-hydroxytryptamine; Kyn: kynurenine; Try: tryptophan; BDNF: brain-derived neurotrophic factor; DG: dentate gyrus. *$p < 0.05$, **$p < 0.01$, compared with the sham group. #$p < 0.05$, compared with the AMI group. &$p < 0.05$, compared with the AMI group.

The mainstay of antidepressant therapy directs at serotonin (5-hydroxytryptamine, 5-HT) metabolism, in detail, blocking the reuptake of 5-HT from the extracellular space. As a precursor for serotonin, 95% of tryptophan is degraded in the liver through the kynurenine pathway, and the remaining is used for the synthesis of 5-HT (Oxenkrug, 2013). Abnormalities in the tryptophan-

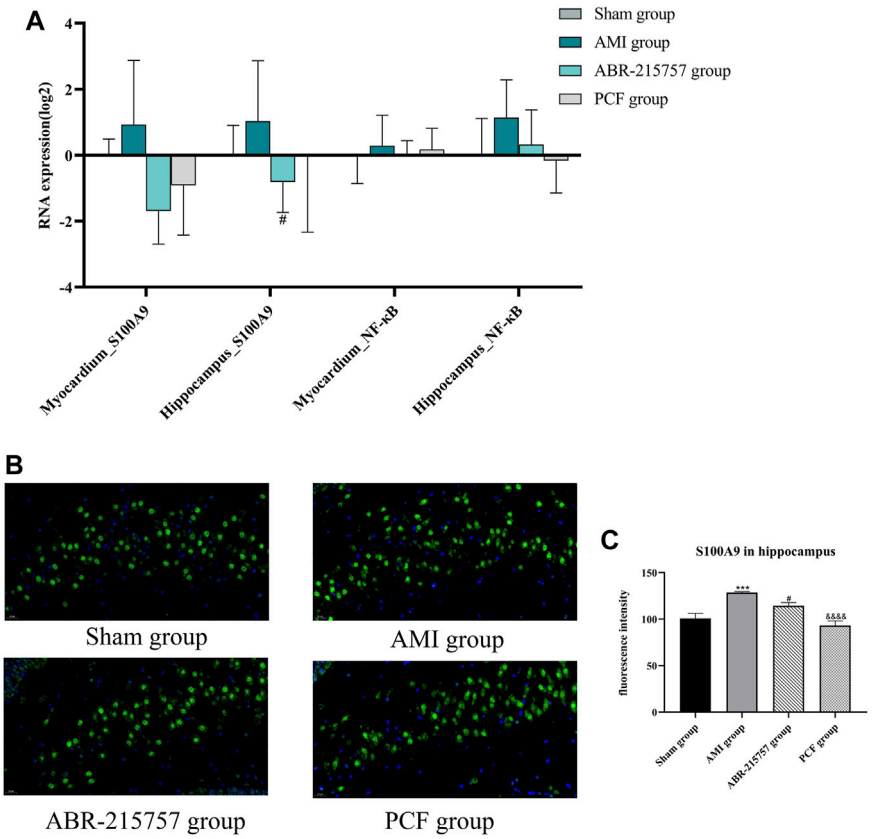

FIGURE 5 | The effect of PCF on the S100A9/NF-κB pathway in the hippocampus and myocardium. **(A)** The gene expression of S100A9 and NF-κB in the hippocampus and myocardium detected by RT-qPCR. Data were presented as mean ± SD, $n = 3$ per group. **(B)** Immunofluorescence analysis of S100A9 in hippocampus tissues. S100A9 immunostaining was shown in green and DAPI in blue. **(C)** Mean optical density of S100A9-positive cells. Three fields were selected from each slide. ***$p < 0.001$, compared with the sham group. #$p < 0.05$, compared with the AMI group. &&&& $p < 0.0001$, compared with the AMI group.

kynurenine pathway are implicated in the pathophysiology of depressive disorder (Muneer, 2020). To examine the effects of AMI on neurotransmitters in the brain, we analyzed the hippocampus tissues by liquid chromatography-mass spectrometry (LC-MS). As shown in **Figures 4A**, significant decrease in 5-HT level was observed in AMI rats ($p < 0.01$), while PCF and ABR-215757 treatment led to a degree of recovery ($p < 0.05$). The level of tryptophan (Try) was altered in a manner similar to that of 5-HT. Proinflammatory cytokines catalyze the conversion of Try to kynurenine (Kyn), and the kynurenine pathway may elucidate the phenomenon of inflammation in depression (Vancassel et al., 2018). It has evoked widespread concern that the ratio of kynurenine to tryptophan is significantly enhanced in patients with depression (Maes et al., 2002; Zhang et al., 2016). Our results showed an increased hippocampal Kyn/Try ratio in the AMI group ($p < 0.05$), and the ratio declined with the administration of S100A9 inhibitors ($p < 0.05$, **Figure 4B**).

Depression is associated with neuroplasticity in the brain regions, particularly the hippocampus. Nissl bodies, easily stained by toluidine blue, reflects the synthesis of Nissl bodies and the survival of nerve cells. Nissl staining revealed that the rats had fewer neurons with the loose arrangement in the hippocampal DG regions on day 21 after coronary artery ligation ($p < 0.05$, **Figure 4C**), whereas no obvious hippocampal neuron loss was observed in the PCF group and ABR-215757 group. Brain-derived neurotrophic factor (BDNF), a topic neurotrophic factor of intensive research in the mammalian brain, contributing to the maintenance and survival of neurons and activity-dependent regulation of synapse number and function, is integral to the pathophysiology of depression (Zhang et al., 2016). Multiple lines of evidence implied that administration of BDNF into either hippocampus or midbrain in rodent models produces an antidepressant-like effect (Monteggia et al., 2007). In this study, the expression level of BDNF was downregulated in the AMI group compared with the sham group and showed an upward trend after administration of PCF and ABR-215757, but there was no statistical significance between groups (**Figure 4D**).

3.4 PCF Inhibited the Activation of S100A9/TLR4/NF-κB Signaling Pathway

Our present proteomic study revealed that S100A9 was the only molecule intersected from numerous proteins in the myocardium and hippocampus and one of the differentially expressed proteins among the sham, AMI, and PCF groups. We first verified the *in*

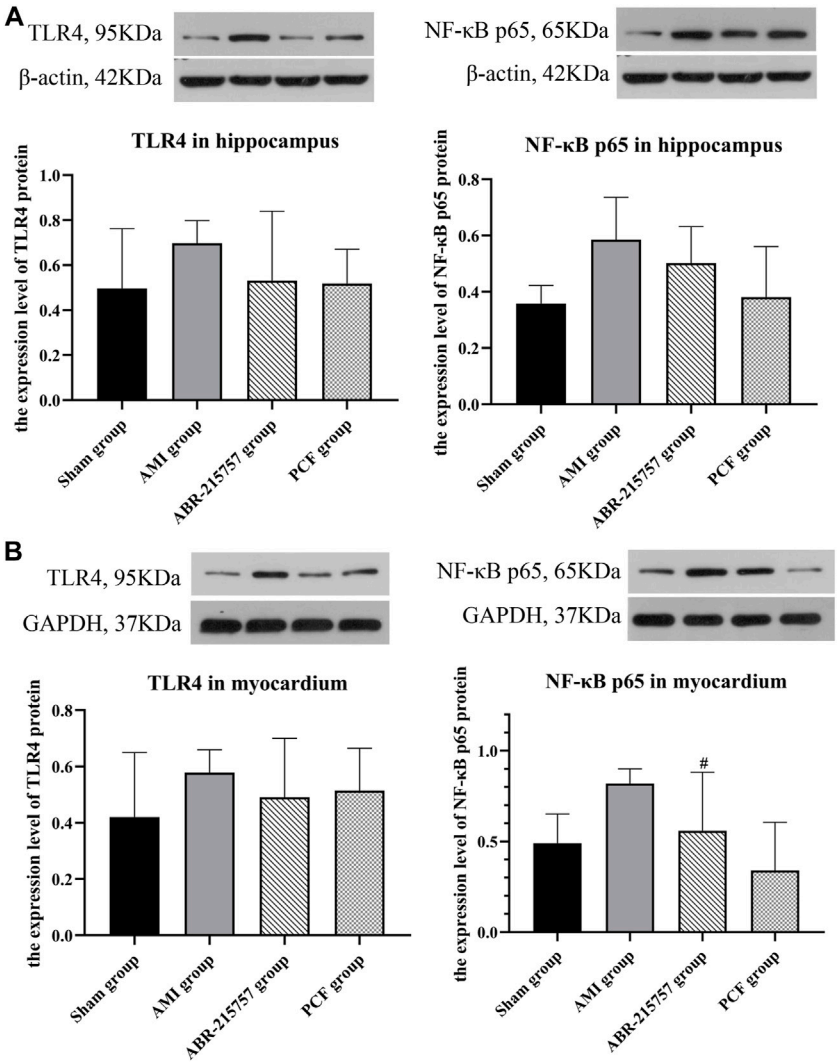

FIGURE 6 | Protein expression of TLR4 and NF-κB detected by western blotting. **(A)** The protein bands of TLR4 and NF-κB in the hippocampus. β-actin was reused as the loading control for protein TLR4 and NF-κB p65. **(B)** The protein bands of TLR4 and NF-κB in the myocardium. Data were presented as mean ± SD. $n = 3$ per group. #$p < 0.05$, compared with the AMI group.

vivo effect of coronary ligation on the S100A9 expression by RT-qPCR. Consistent with proteomic data, the expression level of S100A9 gene was elevated in the AMI group compared with the sham group and was returned to the basal level by PCF treatment (**Figure 5A**). The expression of S100A9 protein in the hippocampus was also visualized by immunofluorescence. Expression analysis showed increased expression of S100A9 in the AMI group ($p < 0.001$), and S100A9-positive fluorescence intensity were markedly decreased in the PCF group ($p < 0.0001$) and ABR-215757 group ($p < 0.05$, **Figure 5B**). In addition, the immunoblotting analysis showed that the expression of TLR4 and NF-κB protein was changed in a manner similar to that of S100A9 (**Figure 6**). Interestingly, the protein expression trend was observed in the myocardium and hippocampus. In order to explore the effect of S100A9 on inflammatory factors, the ABR-215757 group was set and the expression pattern was found to be parallel to that in the PCF group. As shown in **Figure 5A** and **Figure 6A**, compared with the AMI group, the expression of the S100A9 gene in the hippocampus and NF-κB protein in the myocardium from the ABR-215757 group was downregulated ($p < 0.05$). However, it is regrettable that there was no statistically significant difference in protein expression between the PCF and AMI group.

3.5 PCF Reduced the Contents of Proinflammatory Factor

Furthermore, we detected the expression of inflammatory cytokines (S100A9, IL-1β, and TNF-α) in the hippocampus and myocardium by ELISA. As shown in **Figure 7**, S100A9 levels in the myocardium were significantly increased in the AMI group ($p < 0.01$), while those in the sham group

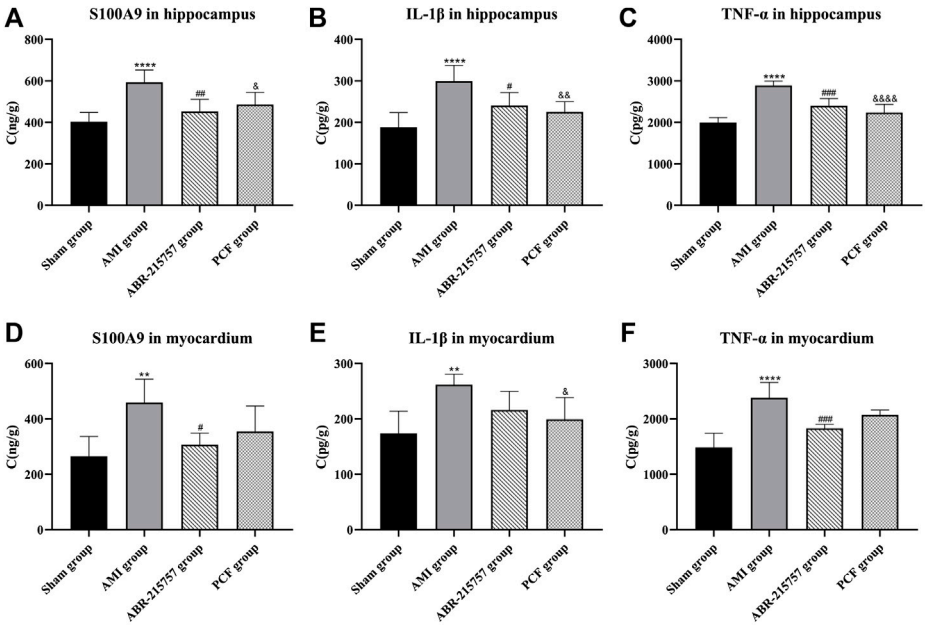

FIGURE 7 | Levels of S100A9, IL-1β, and TNF-α in the hippocampus and myocardium were determined by an ELISA assay. Values were expressed as mean ± SD. $n = 6$ per group. $^{**}p < 0.01$, $^{****}p < 0.0001$ compared with the sham group. $\#p < 0.05$, $\#\#p < 0.01$, $\#\#\#p < 0.001$, compared with the AMI group. $\&p < 0.05$, $\&\&p < 0.01$, $\&\&\&\&p < 0.0001$, compared with the AMI group.

remained low. In contrast with the sham group, coronary ligation not only significantly increased the IL-1β ($p < 0.01$) and TNF-α levels ($p < 0.0001$) in the myocardium but also elevated the levels of inflammatory factors in the hippocampus to promote neuroinflammation ($p < 0.0001$). On the contrary, the results showed that relative to the AMI group, the hippocampal S100A9 ($p < 0.01$), IL-1β ($p < 0.05$), and TNF-α ($p < 0.001$) levels were obviously downregulated after ABR-215757 intervention, while the myocardial S100A9 ($p < 0.05$) and TNF-α ($p < 0.001$) levels also showed a clear trend of descending. Besides, we found that PCF reduced myocardial IL-1β level compared with the AMI group ($p < 0.05$), and the levels of S100A9 ($p < 0.05$), IL-1β ($p < 0.01$), and TNF-α ($p < 0.0001$) were declined in the hippocampus.

3.6 PCF Inhibited the Activation of Macrophages/Microglia

CD68 and Iba1 are recognized as specific markers, respectively, for macrophage and microglia. In order to investigate the effect of AMI on the activation of the macrophage in the heart, immunofluorescence staining for myocardial sections was performed. Results indicated that acute myocardial ischemia significantly increased the number of CD68 positive cells ($p < 0.01$, **Figures 8A,B**). However, PCF and ABR-215757 treatment inhibited macrophage activation and decreased the number of $CD68^+$ cells ($p < 0.01$). We further interrogated the effect of cardiac surgery on hippocampal microglia. As the results indicated, hippocampal microglia were activated by coronary ligation, while PCF and ABR-215757 treatment decreased the number of $Iba1^+$ cells in the hippocampal region ($p < 0.01$ for ABR-215757, $p < 0.05$ for PCF, **Figures 8C,D**).

3.7 The Effect of Recombinant Protein S100A9 on the Viability of BV2 Cells

CCK-8 assay was applied to determine the effect of recombinant protein S100A9 on the viability of BV2 cells. As shown in **Figure 9A**, the administration of protein S100A9 with 0.01 μmol–0.05 μmol for 6 h had no significant effect on the viability of microglia cells, while 0.1 μmol of S100A9 could observably promote microglial cell proliferation ($p < 0.05$). Therefore, 0.1 μmol of S100A9 was utilized in the following experiments.

3.8 S100A9 Induced Morphological Changes of Microglia Cells

As "sentinels" of the nervous system, it is fitting that microglia respond to changes in biological signaling. Further investigation in BV2 cells observed two major morphological phenotypes, amoeboid *versus* ramified (**Figure 9C**). Resting microglia cells existed mostly with oblate bodies, as well as stretched and elongated synapses. Under the activation of recombinant S100A9 protein, microglia cells became enlarged, retracted their processes, formed new motile protrusions, and transformed into spherical or ameboid form. Parameters such as cell area and radius can be used to describe the microglia activation state. Then, a more detailed morphological characterization was carried out. The results revealed that compared with the control serum group, S100A9 induced decreases in radius ratio ($p < 0.05$, **Figure 9D**). These morphological modulations indicated that the activation of microglia was attributed to the S100A9 stimulation.

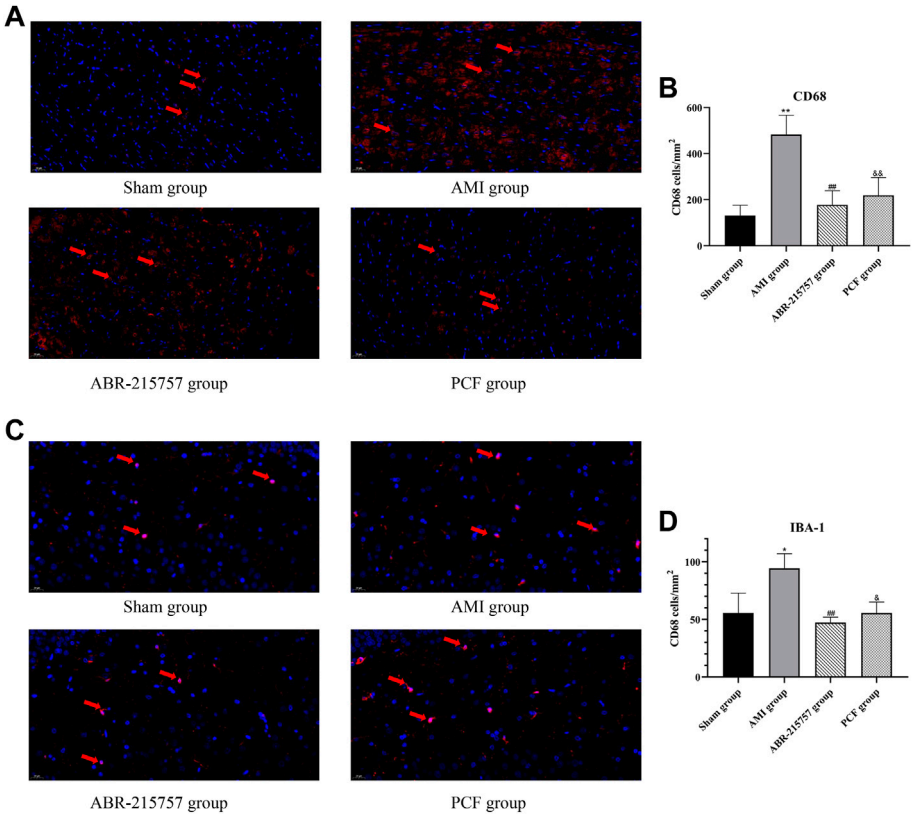

FIGURE 8 | Macrophage activation in the myocardium and microglial activation in the DG region of AMI rats by immunofluorescence staining. **(A)** Representative images of CD68 positive cells in the myocardium. **(B)** Quantification of the $CD68^+$ cell number. **(C)** Representative images of Iba1 positive cells in the DG region of the hippocampus. **(D)** Quantification of the $Iba1^+$ cell number. $n = 3$ slices from each group. $^*p < 0.05$, $^{**}p < 0.01$, compared with the sham group. $\#\#p < 0.01$, compared with the AMI group. & $p < 0.05$, && $p < 0.01$, compared with the AMI group.

3.9 Effect of PCF Serum on S100A9-Induced Activation of Inflammatory Factors

This study investigated whether PCF serum was involved in the suppression of the inflammatory response induced by S100A9. As shown in **Figure 9E**, inflammatory factors including S100A9, TNF-α, and IL-1β were markedly increased following treatment with the recombinant S100A9 protein, compared with those in the control group ($p < 0.05$). No marked reduction in inflammatory factors was observed in the control serum group. However, treatment with PCF serum resulted in a significant reduction in protein S100A9 ($p < 0.05$). There might be viewpoints that components cannot be identified in drug serum, which represents a "black box operation" with unclear pharmacodynamic substance. Indeed, we have previously detected pharmaceutical ingredients in serum from rats intragastrically by PCF utilizing LC-MS and found that ferulic acid might be a major molecule component of PCF. Therefore, the inhibitory effect of ferulic acid on S100A9-induced inflammatory factors was also examined. The result turned out that ferulic acid could not only reduce S100A9 content ($p < 0.05$) but also inhibit the expression of TNF-α and IL-1β ($p < 0.05$). In addition, C34 (TLR4 inhibitor) was proved to reverse the proinflammatory effects of S100A9 ($p < 0.05$).

3.10 Effect of PCF Serum on the Viability of BV-2 Cells

In order to confirm that the anti-inflammatory property of PCF serum was not due to cytotoxic effects on the BV-2 microglial cells, the drug serum group was further divided into three subgroups with a concentration of 5%, 10%, and 20%, respectively. As can be seen from **Figure 9B**, the viability of the BV-2 cells was not reduced following treatment with low and medium concentrations of PCF. BV-2 cell viability was slightly decreased in the high dose group, but there was no statistical significance compared with the control group. These results indicated that the inhibitory effects of drug serum on the S100A9-induced inflammatory response did not result from its cytotoxic action.

4 DISCUSSION

Related proteins and immunoinflammatory phenotypes predicted by previous proteomics were examined in this study. Our research highlighted that PCF inhibited macrophage/microglia inflammation by the suppression of S100A9

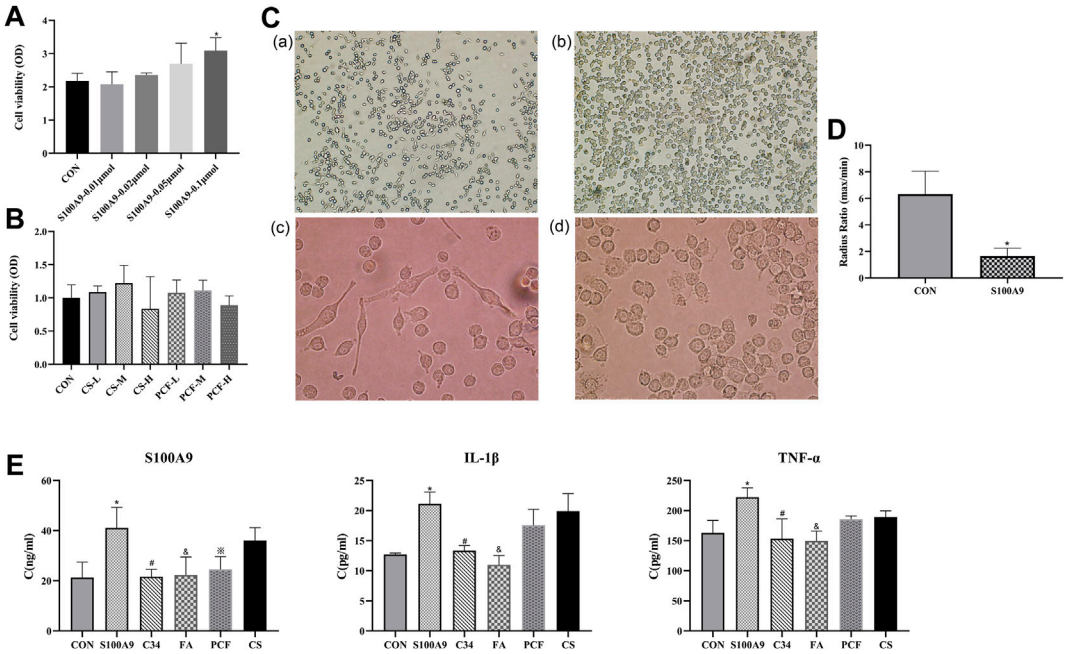

FIGURE 9 | PCF serum reduced the proinflammatory effect of recombinant protein S100A9 in BV2 cells *via* inhibiting TLR4. **(A)** Microglia cells were treated with protein S100A9 (0.01,0.02, 0.05, 0.1 μmol) for 6 h. CCK-8 assay was used to detect the viability of BV2 cells. **(B)** Effect of PCF serum with a concentration of 5%, 10%, and 20% on the viability of BV-2 cells. **(C)** Resting microglia (a, ×100 magnification; c, ×400 magnification) and activated microglia (b, ×100 magnification; d, ×400 magnification). Morphological changes of BV2 microglia after incubation with S100A9 protein for 6 h (b,d). **(D)** The ratio of the maximum radius to the minimum radius in BV2 microglia. **(E)** The level of S100A9, IL-1β, and TNF-α in the culture media was measured with ELISA. Each value represented the mean ± SD of three independent experiments. CS: control serum; CS-L: control serum low dose; CS-M: control serum medium dose; CS-H: control serum high dose; PCF: PCF serum; PCF-L: PCF serum low dose; PCF-M: PCF serum medium dose; PCF-H: PCF serum high dose; C34: TLR4 inhibitor; FA: ferulic acid; *$p < 0.05$, compared with the control group. #$p < 0.05$, compared with the S100A9 group. & $p < 0.05$, compared with the S100A9 group. ※ $p < 0.05$, compared with the S100A9 group.

signaling after AMI, thus improving cardiac function and depression-like behavior. PCF serum and ferulic acid alleviated microglia inflammation *in vitro*.

According to proteomics results from our previous studies, we speculated that PCF might regulate S100A9-mediated over-activation of macrophage/microglia inflammation, thus leading to mitigation in subsequent inflammatory processes involved in AMI. The dramatic cardiomyocyte death initiates a cascade of inflammation in AMI, in the process of which the role of alarmin S100A9 in deteriorating cardiac function has become a hot topic supported by several top journals of clinical and experimental evidence in these years (Li et al., 2019; Marinković et al., 2020; Sreejit et al., 2020). S100A9, as a potent activator of the innate immune response, as well as the damage-associated molecular pattern (DAMP) protein, is abundantly expressed in neutrophils and rapidly released from activated neutrophils, monocytes/macrophages, and dying cardiomyocytes into the coronary and systemic circulation after myocardial ischemia (Schiopu and Cotoi, 2013). S100A9 interacted locally with toll-like receptor 4 (TLR4) or receptor of advanced glycation end products (RAGE) to promote the expression of NF-κB and release IL-1β and TNF-α (Ehrchen et al., 2009; Riva et al., 2012). The regulatory role of S100A9 in macrophage activation has been brought into focus. The continuous activation of macrophages might be actuated by the S100A9 protein, which acts as a character at the center of the stage to orchestrate the functions of the individual players in cooperation with other proinflammatory cytokines (Ganta et al., 2019; Marinković et al., 2020). Stankiewicz et al. recently analyzed the hippocampal transcriptome of mice subjected to acute and chronic social stress of different durations and found that hippocampal S100A9 mRNA increased (Stankiewicz et al., 2015). In addition, central injection of recombinant S100A9 proteins could evoke depressive-like behaviors, the activation of TLR4/NF-κB signaling, and microglia. The effects of S100A9 protein were attenuated by TLR4 inhibitor TAK-242, indicating that the dysfunction of S100A9/TLR4 signaling in the hippocampus could generate neuroinflammation and depression-like behaviors (Gong et al., 2018). *In vitro* studies also showed that S100A9 observably increased the secretion of proinflammatory cytokines, including TNF-α and IL-6, in cultured BV-2 microglial cells, the process of which was suppressed by TLR4 inhibitors (Ma et al., 2017). Microglia activation is not only a hallmark of neuroinflammation but also contributes to the development of depressive-like behaviors. Recent studies demonstrated that the impairment of the normal structure and function of microglia caused by intense inflammatory activation can result in depression and associated impairments in neuroplasticity and neurogenesis. Accordingly, some forms of depression can be recognized as a microglial disease (microgliopathy) (Yirmiya et al., 2015). Hippocampal

microglial activation was demonstrated to originate from stress and be implicated in the pathophysiology of depression. Thus, the hippocampus, a region with a high density of microglial cells (Brites and Fernandes, 2015), was selected to be tested instead of other brain organs. Similar to the above results, in AMI-induced depressive rats, the level of S100A9 showed an increasing trend in the myocardium and the hippocampus, accompanied by the activation of transcription factor NF-κB and the release of proinflammatory factors. Also, our research showed a higher content of S100A9 in the myocardium and the hippocampus by ELISA in the AMI group. Coronary ligation promoted the activation of macrophage/microglia, respectively evidenced by an increase in the number of myocardial CD68 positive cells and hippocampal Iba1 positive cells. Intragastric administration of PCF downregulated the expression of S100A9 and other inflammatory factors and inhibited the activation of microglia. Our results revealed that PCF intervention inhibited inflammation, which might partly attribute to a reduction in the content of S100A9 and the inhibiting effect of macrophage/microglia activation.

For additional verification of the mechanism, ABR-215757 was used to inhibit S100A9. Paquinimod exerts consistent and robust immunomodulatory effects on systemic lupus erythematosus, positively evaluated in a phase 2 randomized controlled trial (Bengtsson et al., 2012). The application range of paquinimod has gradually expanded in preclinical studies and mainly lies in its inhibition of inflammatory reaction by blocking the interaction with TLR4 and RAGE (Kraakman et al., 2017; Boros and Vécsei, 2020). Paquinimod is second-generation quinoline-3-carboxamides and may be a novel promising therapeutic way for depressive disorder (Boros and Vécsei, 2020). At the moment, *in vivo* studies demonstrate that ABR-215757 effectively ameliorates depressive symptoms (Gong et al., 2018). In our research, after continuous administration of ABR-215757 in the whole acute phase, the expression levels of S100A9, NF-κB, IL-1β, and TNF-α were significantly downregulated. Moreover, the inhibition of macrophage/microglia activation by ABR-215757 was shown to alleviate inflammation and modulate 5-HT metabolism. As a result of TLR4 signaling blocking, the desperate behavior was successfully rescued, and the cardiac function was partially restored. It is noteworthy that ABR-215757 could ameliorate depression-like behavior, characterized by improvement in despair rather than interest and exploration. Separate depressive symptoms may be encoded by differential changes in distinct circuits in the nervous system. An article published in *Cell* in 2017 reported that distinct neuronal projections to the lateral habenula and ventral tegmental area subserved different depressive behaviors: behavioral despair and social withdrawal, respectively (Knowland et al., 2017). The results of the behavioral test implied that ABR-215757 had distinct effects on different depressive phenotypes. Reviewing the related literature, we hypothesized that the separate effect of ABR-215757 on different phenotypes of depression might originate from the diverse projection of neurons, deserving further exploration.

However, it is still not clearly identified that S100A9 induced an inflammatory response *via* the TLR4 receptor nor that PCF inhibited microglial inflammation through this pathway. Therefore, we conducted cell experiments in which BV2 microglia were stimulated by recombinant S100A9 protein at a concentration of 0.1 μmol to construct a model group. Our results showed that S100A9 could induce the release of IL-1β and TNF-α in microglial cells. Cellular morphology revealed the characters of recombinant S100A9 in the activation of microglia. An increase in IL-1β and TNF-α levels derived from activated microglia may promote depressive symptoms. In addition, the C34 (TLR4 inhibitor) group and PCF (PCF serum) group were set up to elucidate the mechanisms that *in vivo* studies have failed to elucidate. The inhibition of TLR4 attenuated these effects of S100A9, indicating that S100A9-induced microglia activation depended on TLR4 signaling. We examined whether or not the expression of TNF-α and IL-1β induced by S100A9 was inhibited by the treatment with PCF serum on the BV2 microglia. The expression of inflammatory markers was significantly upregulated by S100A9 and showed a downward trend by the co-treatment with PCF serum.

In the infarcted myocardium caused by prolonged coronary occlusion, the DAMP proteins released from necrotic cells trigger both myocardial and systemic inflammatory responses. Inflammatory cells clear the infarct of dead cells and matrix debris and activate repair by myofibroblasts and vascular cells, but they may also lead to adverse fibrotic remodeling of viable segments and accentuate cardiomyocyte apoptosis (Huang and Frangogiannis, 2018). Induction of cytokines and upregulation of endothelial adhesion molecules modulate leukocyte recruitment in the infarcted heart tissues. Apoptosis, a process of programmed cell death, has been proposed to occur in response to proinflammatory cytokines after myocardial ischemia (Frangogiannis, 2015). In the present study, we measured the inflammation level and occurrence of apoptosis severally by HE staining and TUNEL staining in the heart tissues on day 7 after coronary ligation. Also, Masson staining was applied to assess myocardial fibrosis at 21 days after AMI. Severe inflammatory infiltrates, myocardial fiber rupture, increased apoptosis index, and fibrotic regions were shown in the AMI group. Conversely, these pathological phenomena were alleviated by the administration of PCF.

There is considerable evidence that behavioral impairments observed after AMI are consistent with a model of human post-MI depression (Wann et al., 2007; Bah et al., 2011a; Bah et al., 2011b). A majority of studies accorded closely with the conclusion, and Wann et al. (2007) put much effort into making it convincing (Bah et al., 2011a). Wann et al. (2007) reported that MI rats display behavioral signs compatible with depression 2 weeks after the cardiovascular event, including anhedonia (i.e., less sucrose intake) and behavioral despair (i.e., decreased forced swimming) (Wann et al., 2007). Our study declared that rats in the AMI group showed depression-like behavior, as performed by the reduced ability of movement in OFT and longer immobility time in FST. These findings implied that depression-like performance in rodents with MI was demonstrated by diverse behavioral tests.

Depression is recognized as a circuit disease influencing multiple encephalic regions connected in functional networks.

The hippocampus, as a primary zone in the cerebral limbic system, has been identified as a major role in the pathological progress of depression. Many factors that may interact with hippocampal damage to trigger depressive episodes, neurotransmitter disturbance, and altered neurotrophic signaling are included (Kraus et al., 2017). The 5-HT hypothesis is supported by vast amounts of data that serotonin metabolism is altered in depression (Dell'Osso et al., 2016). The shunt of Try from 5-HT to Kyn formation is a dominating etiological factor of depression. Kyn was reported to be a proinflammatory metabolite in the neuroimmune signaling network mediating depressive-like behavior (Zhang et al., 2020). The Kyn/Try ratio, an indicator of the activation of the first step of the Kyn pathway, the elevation of which indicated a decrease in the conversion of tryptophan to 5-HT. Activation of the Kyn pathway *via* inflammation has been substantiated in clinical and preclinical research (Savitz, 2020; Troubat et al., 2021). Inflammation-driven alterations in kynurenine metabolic pathways result in substantial alterations in the metabolism of 5-HT. Our study showed a low content of 5-HT on day 7 postoperatively, accompanied by a rise in Kyn/Try ratio. Myocardial infarction might disturb tryptophan metabolism through the kynurenine pathway, thereby resulting in a decrease in 5-HT synthesis. PCF might change the expression of 5-HT directly *via* the kynurenine pathway, thus improving depression-like behaviors in AMI rats.

One of the most attractive features of the hippocampus is the unusual capacity for adult neurogenesis. In the sub-granular zone of the dentate gyrus (DG) of the hippocampus, newborn neurons are continuously generated, developed into mature neurons, and functionally integrated into the existing neural circuitry. It is now well established that adult hippocampal neurogenesis is decreased in rodent models of depression (Tanti et al., 2013). Proinflammatory cytokines are involved in immune system-to-brain communication by activating resident microglia in the brain. Activated microglia reduce neurogenesis by suppressing neuronal stem cell proliferation, promoting apoptosis of neuronal progenitor cells, and decreasing the survival of newly developing neurons and their integration into existing neuronal circuits (Cope and Gould, 2019). The process of neurogenesis is strongly stimulated by a brain-derived neurotrophic factor (BDNF), a neurotrophic factor that modulates functional and structural plasticity in the central nervous system, thus affecting dendritic spines and adult neurogenesis. A mass of studies reported the association of a decrease in BDNF mRNA and protein levels in the hippocampus with an increase in susceptibility to develop depressive disorders (Karege et al., 2002; Weinstock, 2017). For synaptic plasticity, we observed the morphology and number of neurons in the hippocampus through Nissl staining. The experimental results showed that the neuronal body of the hippocampus in the AMI group was lost. In our study, the effects of the AMI model on the expression of the synaptic-plasticity protein in the hippocampus were explored by western blotting. The decrease in BDNF might account partly for the depression-like behavior in AMI rats. The results were opposite for rats treated with PCF, although no significant statistical difference was found.

Some experimental studies, until now, have evaluated the anti-inflammatory efficacy of various drug therapies in depression after MI. Ge et al. demonstrated that Ginkgolide B significantly increased the 5-HT content in the brain median raphe nucleus and cortex *via* the reduction of IL-1β to ameliorate depression in MI mice (Ge et al., 2020). Wang et al. revealed that oral minocycline could prevent increases in plasma cytokines and microglia activation, thus causing some improvement in cardiac function and depression-like behavior (Wang et al., 2019). Our study focuses not only on the role of PCF in improving depression-like behavior after MI but also on the function of controlling the upstream switch of microglial inflammation. Microglia express pattern recognition receptors (PRR) that are designed to identify DAMP (e.g., S100A9) and mediate inflammatory responses. The administration of PCF led to a reduction of the S100A9 level, which meant that PCF might cut the pathological chain of the S100A9-microglial activation-inflammatory cascade from the early stage.

There are some laboratory achievements for the molecule compounds of components in PCF consistent with the inflammatory mechanism obtained in our study. The published literature showed that ferulic acid, an important active ingredient in *Chuanxiong Rhizoma*, was proven to be antidepressive *via* increasing monoamine neurotransmitter levels in the hippocampus (Zhang et al., 2011). Also, the antioxygenation property of ferulic acid was implicated in the alleviation of myocardial injury in ischemia-reperfusion rats (Liu et al., 2021). Our *in vitro* study found that ferulic acid had an inhibitory effect on S100A9-induced microglial inflammation, providing evidence for the mechanism underlining the anti-depressed function. Neocryptotanshinone, a natural product isolated from Salvia miltiorrhiza Bunge, showed anti-inflammatory effects by inhibiting NF-κB and iNOS signaling pathways in LPS-stimulated mouse macrophages (RAW264.7) cells (Wu et al., 2015). It is implied that a percentage of agents showed therapeutic effects similar to PCF in psycho-cardiology diseases. The future for active ingredients in PCF within standardized quality control ensures repeatable pharmacological action.

There are limitations to our study. Only a single group was set in this research instead of several dose groups. Although the efficacy of PCF in depression after AMI was performed and confirmed in preliminary experiments, the absence of multi-dose groups cannot ensure a dose-response relationship. S100A9 is a small calcium-binding protein of the S100 family that is expressed, in most biological settings, as a heterodimer complexed with its partner, S100A8. Future research concentrating on the functional and pathological difference between the monomer and heterodimer is urgently needed. Due to the limited sample in our experiments, no significant statistical difference was observed in the expression of some indicators between groups. Moreover, nothing but *in vitro* evidence was provided that S100A9 triggered microglial activation through the TLR4 pathway, yet animal experiments in which a biological metabolism was more similar to the human body remained absent.

5 CONCLUSION

Taken together, PCF, a modified TCM formula, promotes the recovery of cardiac function and improves depression-like behavior after MI. The possible mechanism involved in the protective effects of PCF *in vivo* includes the reduction of inflammation, apoptosis, and fibrosis in the myocardium, the inhibition of the Kyn pathway, and a boost of neurogenesis in the hippocampal tissue. Our results identify S100A9 as a promoter of macrophage/microglia inflammation, with a central role in depressive disorder induced by AMI. The concept of a common modifier driving both myocardial and hippocampal immune response to AMI is novel and of major significance for realizing the immunopathology of this disease. Indeed, the effects of short-term S100A9 blockade closely recapitulate the consequences of reduced inflammation on cardiac function and depression. PCF is also proved to be efficacious for targeting local and systemic inflammatory phases after MI. *In vitro* experiments conclude that protein S100A9 promotes the production of proinflammatory cytokines in microglia *via* TLR4, while PCF serum inhibiting the release of S100A9 may provide a therapeutic approach in microglial-mediated neuroinflammatory diseases. These findings provide scientific evidence for the cardioprotective and antidepressive effects of PCF, particularly in the process of suppressing macrophage/microglia inflammation.

DATA AVAILABILITY STATEMENT

The datasets presented in this study can be found in online repositories. The names of the repository/repositories and accession number(s) can be found below: MetaboLights-MTBLS4527. Supplementary data can be found online at http://proteomecentral.proteomexchange.org/cgi/GetDataset?ID=PXD027832. The mass spectrometry proteomics data have been deposited to the ProteomeXchange Consortium (http://proteomecentral.proteomexchange.org) *via* the iProX partner repository with the dataset identifier PXD027832.

ETHICS STATEMENT

The study was approved by the Institutional Animal Care and Use Committee of the University of Chinese Medicine, Beijing, China (Ethical number: BUCM-4-2020091108-3141).

AUTHOR CONTRIBUTIONS

HZ and CW conceived the project, designed and supervised this study. YS and JS and carried out animal experiments. JH and ZT assisted with the establishment of the AMI model. YS and ZW performed in vitro experiments, as well as sample preparation and detection. ZW performed the statistical analysis. YS completed the manuscript. All authors approved the final version of the manuscript.

FUNDING

This research was supported by the Beijing Natural Science Foundation Program (no. 7202126) and the National Natural Science Foundation of China (NSFC, no. 82174332).

ACKNOWLEDGMENTS

We are thankful for the support of the DongFang Hospital of Beijing University of Chinese Medicine.

REFERENCES

AbuRuz, M. E., and Al-Dweik, G. (2018). Depressive Symptoms and Complications Early after Acute Myocardial Infarction: Gender Differences. *Open Nurs. J.* 12, 205–214. doi:10.2174/1874434601812010205

Adegoke, E. O., Adeniran, S. O., Zeng, Y., Wang, X., Wang, H., Wang, C., et al. (2019). Pharmacological Inhibition of TLR4/NF-κB with TLR4-IN-C34 Attenuated Microcystin-Leucine Arginine Toxicity in Bovine Sertoli Cells. *J. Appl. Toxicol.* 39 (6), 832–843. doi:10.1002/jat.3771

Bah, T. M., Benderdour, M., Kaloustian, S., Karam, R., Rousseau, G., and Godbout, R. (2011a). Escitalopram Reduces Circulating Pro-inflammatory Cytokines and Improves Depressive Behavior without Affecting Sleep in a Rat Model of Post-cardiac Infarct Depression. *Behav. Brain Res.* 225 (1), 243–251. doi:10.1016/j.bbr.2011.07.039

Bah, T. M., Kaloustian, S., Rousseau, G., and Godbout, R. (2011b). Pretreatment with Pentoxifylline Has Antidepressant-like Effects in a Rat Model of Acute Myocardial Infarction. *Behav. Pharmacol.* 22 (8), 779–784. doi:10.1097/FBP.0b013e32834d1385

Bangalore, S., Shah, R., Gao, X., Pappadopulos, E., Deshpande, C. G., Shelbaya, A., et al. (2020). Economic Burden Associated with Inadequate Antidepressant Medication Management Among Patients with Depression and Known Cardiovascular Diseases: Insights from a United States-based Retrospective Claims Database Analysis. *J. Med. Econ.* 23 (3), 262–270. doi:10.1080/13696998.2019.1686311

Bengtsson, A. A., Sturfelt, G., Lood, C., Rönnblom, L., van Vollenhoven, R. F., Axelsson, B., et al. (2012). Pharmacokinetics, Tolerability, and Preliminary Efficacy of Paquinimod (ABR-215757), a New Quinoline-3-Carboxamide Derivative: Studies in Lupus-Prone Mice and a Multicenter, Randomized, Double-Blind, Placebo-Controlled, Repeat-Dose, Dose-Ranging Study in Patients with Systemic Lupus Erythematosus. *Arthritis Rheum.* 64 (5), 1579–1588. doi:10.1002/art.33493

Björk, P., Björk, A., Vogl, T., Stenström, M., Liberg, D., Olsson, A., et al. (2009). Identification of Human S100A9 as a Novel Target for Treatment of Autoimmune Disease via Binding to Quinoline-3-Carboxamides. *PLoS Biol.* 7 (4), e1000097. doi:10.1371/journal.pbio.1000097

Boros, F., and Vécsei, L. (2020). Progress in the Development of Kynurenine and Quinoline-3-Carboxamide-Derived Drugs. *Expert Opin. Investig. Drugs* 29 (11), 1223–1247. doi:10.1080/13543784.2020.1813716

Brites, D., and Fernandes, A. (2015). Neuroinflammation and Depression: Microglia Activation, Extracellular Microvesicles and microRNA Dysregulation. *Front. Cell Neurosci.* 9, 476. doi:10.3389/fncel.2015.00476

Chen, Z., Zhang, C., Gao, F., Fu, Q., Fu, C., He, Y., et al. (2018). A Systematic Review on the Rhizome of Ligusticum Chuanxiong Hort. (Chuanxiong). *Food Chem. Toxicol.* 119, 309–325. doi:10.1016/j.fct.2018.02.050

Cope, E. C., and Gould, E. (2019). Adult Neurogenesis, Glia, and the Extracellular Matrix. *Cell Stem Cell* 24 (5), 690–705. doi:10.1016/j.stem.2019.03.023

Coupland, C., Hill, T., Morriss, R., Moore, M., Arthur, A., and Hippisley-Cox, J. (2016). Antidepressant Use and Risk of Cardiovascular Outcomes in People

Aged 20 to 64: Cohort Study Using Primary Care Database. *BMJ* 352, i1350. doi:10.1136/bmj.i1350

de Jonge, P., van den Brink, R. H., Spijkerman, T. A., and Ormel, J. (2006). Only Incident Depressive Episodes after Myocardial Infarction are Associated with New Cardiovascular Events. *J. Am. Coll. Cardiol.* 48 (11), 2204–2208. doi:10.1016/j.jacc.2006.06.077

Dell'Osso, L., Carmassi, C., Mucci, F., and Marazziti, D. (2016). Depression, Serotonin and Tryptophan. *Curr. Pharm. Des.* 22 (8), 949–954. doi:10.2174/1381612822666151214104826

Ehrchen, J. M., Sunderkötter, C., Foell, D., Vogl, T., and Roth, J. (2009). The Endogenous Toll-like Receptor 4 Agonist S100A8/S100A9 (Calprotectin) as Innate Amplifier of Infection, Autoimmunity, and Cancer. *J. Leukoc. Biol.* 86 (3), 557–566. doi:10.1189/jlb.1008647

Feng, L., Li, L., Liu, W., Yang, J., Wang, Q., Shi, L., et al. (2019). Prevalence of Depression in Myocardial Infarction: A PRISMA-Compliant Meta-Analysis. *Med. Baltim.* 98 (8), e14596. doi:10.1097/md.0000000000014596

Frangogiannis, N. G. (2015). Pathophysiology of Myocardial Infarction. *Compr. Physiol.* 5 (4), 1841–1875. doi:10.1002/cphy.c150006

Ganta, V. C., Choi, M., Farber, C. R., and Annex, B. H. (2019). Antiangiogenic VEGF165b Regulates Macrophage Polarization via S100A8/S100A9 in Peripheral Artery Disease. *Circulation* 139 (2), 226–242. doi:10.1161/circulationaha.118.034165

Ge, Y., Xu, W., Zhang, L., and Liu, M. (2020). Ginkgolide B Attenuates Myocardial Infarction-Induced Depression-like Behaviors via Repressing IL-1β in Central Nervous System. *Int. Immunopharmacol.* 85, 106652. doi:10.1016/j.intimp.2020.106652

Gehi, A., Haas, D., Pipkin, S., and Whooley, M. A. (2005). Depression and Medication Adherence in Outpatients with Coronary Heart Disease: Findings from the Heart and Soul Study. *Arch. Intern Med.* 165 (21), 2508–2513. doi:10.1001/archinte.165.21.2508

Gong, H., Su, W. J., Cao, Z. Y., Lian, Y. J., Peng, W., Liu, Y. Z., et al. (2018). Hippocampal Mrp8/14 Signaling Plays a Critical Role in the Manifestation of Depressive-like Behaviors in Mice. *J. Neuroinflammation* 15 (1), 252. doi:10.1186/s12974-018-1296-0

Hawkins, M., Schaffer, A., Reis, C., Sinyor, M., Herrmann, N., and Lanctôt, K. L. (2016). Suicide in Males and Females with Cardiovascular Disease and Comorbid Depression. *J. Affect Disord.* 197, 88–93. doi:10.1016/j.jad.2016.02.061

Hou, J., Wang, C., Ma, D., Chen, Y., Jin, H., An, Y., et al. (2021). The Cardioprotective and Anxiolytic Effects of Chaihujialonggumuli Granule on Rats with Anxiety after Acute Myocardial Infarction is Partly Mediated by Suppression of CXCR4/NF-κB/GSDMD Pathway. *Biomed. Pharmacother.* 133, 111015. doi:10.1016/j.biopha.2020.111015

Hua, Y., Guo, S., Xie, H., Zhu, Y., Yan, H., Tao, W. W., et al. (2021). Ziziphus Jujuba Mill. Var. Spinosa (Bunge) Hu Ex H. F. Chou Seed Ameliorates Insomnia in Rats by Regulating Metabolomics and Intestinal Flora Composition. *Front. Pharmacol.* 12, 653767. doi:10.3389/fphar.2021.653767

Huang, S., and Frangogiannis, N. G. (2018). Anti-inflammatory Therapies in Myocardial Infarction: Failures, Hopes and Challenges. *Br. J. Pharmacol.* 175 (9), 1377–1400. doi:10.1111/bph.14155

Iasella, C. J., Kreider, M. S., Huang, L., Coons, J. C., and Stevenson, J. M. (2019). Effect of Selective Serotonin Reuptake Inhibitors on Cardiovascular Outcomes after Percutaneous Coronary Intervention: A Retrospective Cohort Study. *Clin. Drug Investig.* 39 (6), 543–551. doi:10.1007/s40261-019-00776-7

Karege, F., Perret, G., Bondolfi, G., Schwald, M., Bertschy, G., and Aubry, J. M. (2002). Decreased Serum Brain-Derived Neurotrophic Factor Levels in Major Depressed Patients. *Psychiatry Res.* 109 (2), 143–148. doi:10.1016/s0165-1781(02)00005-7

Kim, J. M., Stewart, R., Lee, Y. S., Lee, H. J., Kim, M. C., Kim, J. W., et al. (2018). Effect of Escitalopram vs Placebo Treatment for Depression on Long-Term Cardiac Outcomes in Patients with Acute Coronary Syndrome: A Randomized Clinical Trial. *JAMA* 320 (4), 350–358. doi:10.1001/jama.2018.9422

Kim, Y., Lee, Y. S., Kim, M. G., Song, Y. K., Kim, Y., Jang, H., et al. (2019). The Effect of Selective Serotonin Reuptake Inhibitors on Major Adverse Cardiovascular Events: A Meta-Analysis of Randomized-Controlled Studies in Depression. *Int. Clin. Psychopharmacol.* 34 (1), 9–17. doi:10.1097/yic.0000000000000238

Knowland, D., Lilascharoen, V., Pacia, C. P., Shin, S., Wang, E. H., and Lim, B. K. (2017). Distinct Ventral Pallidal Neural Populations Mediate Separate Symptoms of Depression. *Cell* 170 (2), 284. doi:10.1016/j.cell.2017.06.015

Kraakman, M. J., Lee, M. K., Al-Sharea, A., Dragoljevic, D., Barrett, T. J., Montenont, E., et al. (2017). Neutrophil-derived S100 Calcium-Binding Proteins A8/A9 Promote Reticulated Thrombocytosis and Atherogenesis in Diabetes. *J. Clin. Invest.* 127 (6), 2133–2147. doi:10.1172/jci92450

Kraus, C., Castrén, E., Kasper, S., and Lanzenberger, R. (2017). Serotonin and Neuroplasticity - Links between Molecular, Functional and Structural Pathophysiology in Depression. *Neurosci. Biobehav Rev.* 77, 317–326. doi:10.1016/j.neubiorev.2017.03.007

Li, Y., Chen, B., Yang, X., Zhang, C., Jiao, Y., Li, P., et al. (2019). S100a8/a9 Signaling Causes Mitochondrial Dysfunction and Cardiomyocyte Death in Response to Ischemic/Reperfusion Injury. *Circulation* 140 (9), 751–764. doi:10.1161/circulationaha.118.039262

Liang, X., Xiu, C., Liu, M., Lin, C., Chen, H., Bao, R., et al. (2019). Platelet-neutrophil Interaction Aggravates Vascular Inflammation and Promotes the Progression of Atherosclerosis by Activating the TLR4/NF-κB Pathway. *J. Cell Biochem.* 120 (4), 5612–5619. doi:10.1002/jcb.27844

Liu, X., Qi, K., Gong, Y., Long, X., Zhu, S., Lu, F., et al. (2021). Ferulic Acid Alleviates Myocardial Ischemia Reperfusion Injury via Upregulating AMPKα2 Expression-Mediated Ferroptosis Depression. *J. Cardiovasc. Pharmacol.* 79 (4), 489–500. doi:10.1097/fjc.0000000000001199

Ma, L., Sun, P., Zhang, J. C., Zhang, Q., and Yao, S. L. (2017). Proinflammatory Effects of S100A8/A9 via TLR4 and RAGE Signaling Pathways in BV-2 Microglial Cells. *Int. J. Mol. Med.* 40 (1), 31–38. doi:10.3892/ijmm.2017.2987

Maes, M., Verkerk, R., Bonaccorso, S., Ombelet, W., Bosmans, E., and Scharpé, S. (2002). Depressive and Anxiety Symptoms in the Early Puerperium Are Related to Increased Degradation of Tryptophan into Kynurenine, a Phenomenon Which is Related to Immune Activation. *Life Sci.* 71 (16), 1837–1848. doi:10.1016/s0024-3205(02)01853-2

Marinković, G., Grauen Larsen, H., Yndigegn, T., Szabo, I. A., Mares, R. G., de Camp, L., et al. (2019). Inhibition of Pro-inflammatory Myeloid Cell Responses by Short-Term S100A9 Blockade Improves Cardiac Function after Myocardial Infarction. *Eur. Heart J.* 40 (32), 2713–2723. doi:10.1093/eurheartj/ehz461

Marinković, G., Koenis, D. S., de Camp, L., Jablonowski, R., Graber, N., de Waard, V., et al. (2020). S100A9 Links Inflammation and Repair in Myocardial Infarction. *Circ. Res.* 127 (5), 664–676. doi:10.1161/circresaha.120.315865

Masouris, I., Klein, M., Dyckhoff, S., Angele, B., Pfister, H. W., and Koedel, U. (2017). Inhibition of DAMP Signaling as an Effective Adjunctive Treatment Strategy in Pneumococcal Meningitis. *J. Neuroinflammation* 14 (1), 214. doi:10.1186/s12974-017-0989-0

Monteggia, L. M., Luikart, B., Barrot, M., Theobold, D., Malkovska, I., Nef, S., et al. (2007). Brain-derived Neurotrophic Factor Conditional Knockouts Show Gender Differences in Depression-Related Behaviors. *Biol. Psychiatry* 61 (2), 187–197. doi:10.1016/j.biopsych.2006.03.021

Muneer, A. (2020). Kynurenine Pathway of Tryptophan Metabolism in Neuropsychiatric Disorders: Pathophysiologic and Therapeutic Considerations. *Clin. Psychopharmacol. Neurosci.* 18 (4), 507–526. doi:10.9758/cpn.2020.18.4.507

Nagareddy, P. R., Sreejit, G., Abo-Aly, M., Jaggers, R. M., Chelvarajan, L., Johnson, J., et al. (2020). NETosis is Required for S100A8/A9-Induced Granulopoiesis after Myocardial Infarction. *Arterioscler. Thromb. Vasc. Biol.* 40 (11), 2805–2807. doi:10.1161/atvbaha.120.314807

Oxenkrug, G. (2013). Serotonin-kynurenine Hypothesis of Depression: Historical Overview and Recent Developments. *Curr. Drug Targets* 14 (5), 514–521. doi:10.2174/1389450111314050002

Pang, H., Wu, L., Tang, Y., Zhou, G., Qu, C., and Duan, J. A. (2016). Chemical Analysis of the Herbal Medicine Salviae miltiorrhizae Radix et Rhizoma (Danshen). *Molecules* 21 (1), 51. doi:10.3390/molecules21010051

Riva, M., Källberg, E., Björk, P., Hancz, D., Vogl, T., Roth, J., et al. (2012). Induction of Nuclear Factor-κB Responses by the S100A9 Protein is Toll-like Receptor-4-dependent. *Immunology* 137 (2), 172–182. doi:10.1111/j.1365-2567.2012.03619.x

Rodrigues, G. H., Gebara, O. C., Gerbi, C. C., Pierri, H., and Wajngarten, M. (2015). Depression as a Clinical Determinant of Dependence and Low Quality of Life in Elderly Patients with Cardiovascular Disease. *Arq. Bras. Cardiol.* 104 (6), 443–449. doi:10.5935/abc.20150034

Savitz, J. (2020). The Kynurenine Pathway: A Finger in Every Pie. *Mol. Psychiatry* 25 (1), 131–147. doi:10.1038/s41380-019-0414-4

Schiopu, A., and Cotoi, O. S. (2013). S100A8 and S100A9: DAMPs at the Crossroads between Innate Immunity, Traditional Risk Factors, and Cardiovascular Disease. *Mediat. Inflamm.* 2013, 828354. doi:10.1155/2013/828354

Smolderen, K. G., Buchanan, D. M., Gosch, K., Whooley, M., Chan, P. S., Vaccarino, V., et al. (2017). Depression Treatment and 1-Year Mortality after Acute Myocardial Infarction: Insights from the TRIUMPH Registry (Translational Research Investigating Underlying Disparities in Acute Myocardial Infarction Patients' Health Status). *Circulation* 135 (18), 1681–1689. doi:10.1161/circulationaha.116.025140

Sreejit, G., Abdel-Latif, A., Athmanathan, B., Annabathula, R., Dhyani, A., Noothi, S. K., et al. (2020). Neutrophil-Derived S100A8/A9 Amplify Granulopoiesis after Myocardial Infarction. *Circulation* 141 (13), 1080–1094. doi:10.1161/circulationaha.119.043833

Stankiewicz, A. M., Goscik, J., Majewska, A., Swiergiel, A. H., and Juszczak, G. R. (2015). The Effect of Acute and Chronic Social Stress on the Hippocampal Transcriptome in Mice. *PLoS One* 10 (11), e0142195. doi:10.1371/journal.pone.0142195

Stenström, M., Nyhlén, H. C., Törngren, M., Liberg, D., Sparre, B., Tuvesson, H., et al. (2016). Paquinimod Reduces Skin Fibrosis in Tight Skin 1 Mice, an Experimental Model of Systemic Sclerosis. *J. Dermatol. Sci.* 83 (1), 52–59. doi:10.1016/j.jdermsci.2016.04.006

Sun, Y., Wang, Z., Wang, C., Tang, Z., and Zhao, H. (2021). Psycho-cardiology Therapeutic Effects of Shuangxinfang in Rats with Depression-Behavior Post Acute Myocardial Infarction: Focus on Protein S100A9 from Proteomics. *Biomed. Pharmacother.* 144, 112303. doi:10.1016/j.biopha.2021.112303

Tahvili, S., Törngren, M., Holmberg, D., Leanderson, T., and Ivars, F. (2018). Paquinimod Prevents Development of Diabetes in the Non-obese Diabetic (NOD) Mouse. *PLoS One* 13 (5), e0196598. doi:10.1371/journal.pone.0196598

Tanti, A., Westphal, W. P., Girault, V., Brizard, B., Devers, S., Leguisquet, A. M., et al. (2013). Region-dependent and Stage-specific Effects of Stress, Environmental Enrichment, and Antidepressant Treatment on Hippocampal Neurogenesis. *Hippocampus* 23 (9), 797–811. doi:10.1002/hipo.22134

Trajanovska, A. S., Kostov, J., and Perevska, Z. (2019). Depression in Survivors of Acute Myocardial Infarction. *Mater Sociomed.* 31 (2), 110–114. doi:10.5455/msm.2019.31.110-114

Troubat, R., Barone, P., Leman, S., Desmidt, T., Cressant, A., Atanasova, B., et al. (2021). Neuroinflammation and Depression: A Review. *Eur. J. Neurosci.* 53 (1), 151–171. doi:10.1111/ejn.14720

Vancassel, S., Capuron, L., and Castanon, N. (2018). Brain Kynurenine and BH4 Pathways: Relevance to the Pathophysiology and Treatment of Inflammation-Driven Depressive Symptoms. *Front. Neurosci.* 12, 499. doi:10.3389/fnins.2018.00499

Wang, C., Hou, J., Du, H., Yan, S., Yang, J., Wang, Y., et al. (2019a). Anti-depressive Effect of Shuangxinfang on Rats with Acute Myocardial Infarction: Promoting Bone Marrow Mesenchymal Stem Cells Mobilization and Alleviating Inflammatory Response. *Biomed. Pharmacother.* 111, 19–30. doi:10.1016/j.biopha.2018.11.113

Wang, H. W., Ahmad, M., Jadayel, R., Najjar, F., Lagace, D., and Leenen, F. H. H. (2019b). Inhibition of Inflammation by Minocycline Improves Heart Failure and Depression-like Behaviour in Rats after Myocardial Infarction. *PLoS One* 14 (6), e0217437. doi:10.1371/journal.pone.0217437

Wang, L., Wang, Z., Yang, Z., Yang, K., and Yang, H. (2021a). Study of the Active Components and Molecular Mechanism of Tripterygium Wilfordii in the Treatment of Diabetic Nephropathy. *Front. Mol. Biosci.* 8, 664416. doi:10.3389/fmolb.2021.664416

Wang, Y., Zhang, X., Duan, M., Zhang, C., Wang, K., Feng, L., et al. (2021b). Identification of Potential Biomarkers Associated with Acute Myocardial Infarction by Weighted Gene Coexpression Network Analysis. *Oxid. Med. Cell Longev.* 2021, 5553811. doi:10.1155/2021/5553811

Wann, B. P., Bah, T. M., Boucher, M., Courtemanche, J., Le Marec, N., Rousseau, G., et al. (2007). Vulnerability for Apoptosis in the Limbic System after Myocardial Infarction in Rats: a Possible Model for Human Postinfarct Major Depression. *J. Psychiatry Neurosci.* 32 (1), 11–16.

Weinstock, M. (2017). Prenatal Stressors in Rodents: Effects on Behavior. *Neurobiol. Stress* 6, 3–13. doi:10.1016/j.ynstr.2016.08.004

Wilkowska, A., Rynkiewicz, A., Wdowczyk, J., Landowski, J., and Cubała, W. J. (2019). Heart Rate Variability and Incidence of Depression during the First Six Months Following First Myocardial Infarction. *Neuropsychiatr. Dis. Treat.* 15, 1951–1956. doi:10.2147/ndt.S212528

Worcester, M. U., Goble, A. J., Elliott, P. C., Froelicher, E. S., Murphy, B. M., Beauchamp, A. J., et al. (2019). Mild Depression Predicts Long-Term Mortality after Acute Myocardial Infarction: A 25-Year Follow-Up. *Heart Lung Circ.* 28 (12), 1812–1818. doi:10.1016/j.hlc.2018.11.013

Wu, C., Zhao, W., Zhang, X., and Chen, X. (2015). Neocryptotanshinone Inhibits Lipopolysaccharide-Induced Inflammation in RAW264.7 Macrophages by Suppression of NF-κB and iNOS Signaling Pathways. *Acta Pharm. Sin. B* 5 (4), 323–329. doi:10.1016/j.apsb.2015.01.010

Yirmiya, R., Rimmerman, N., and Reshef, R. (2015). Depression as a Microglial Disease. *Trends Neurosci.* 38 (10), 637–658. doi:10.1016/j.tins.2015.08.001

Zhang, Y. J., Huang, X., Wang, Y., Xie, Y., Qiu, X. J., Ren, P., et al. (2011). Ferulic Acid-Induced Anti-depression and Prokinetics Similar to Chaihu-Shugan-San via Polypharmacology. *Brain Res. Bull.* 86 (3-4), 222–228. doi:10.1016/j.brainresbull.2011.07.002

Zhang, J. C., Yao, W., and Hashimoto, K. (2016). Brain-derived Neurotrophic Factor (BDNF)-TrkB Signaling in Inflammation-Related Depression and Potential Therapeutic Targets. *Curr. Neuropharmacol.* 14 (7), 721–731. doi:10.2174/1570159x14666160119094646

Zhang, Q., Sun, Y., He, Z., Xu, Y., Li, X., Ding, J., et al. (2020). Kynurenine Regulates NLRP2 Inflammasome in Astrocytes and its Implications in Depression. *Brain Behav. Immun.* 88, 471–481. doi:10.1016/j.bbi.2020.04.016

Zhou, J., An, R., and Huang, X. (2021). Genus Lilium: A Review on Traditional Uses, Phytochemistry and Pharmacology. *J. Ethnopharmacol.* 270, 113852. doi:10.1016/j.jep.2021.113852

Conflict of Interest: The authors declare that the research was conducted in the absence of any commercial or financial relationships that could be construed as a potential conflict of interest.

Publisher's Note: All claims expressed in this article are solely those of the authors and do not necessarily represent those of their affiliated organizations or those of the publisher, the editors, and the reviewers. Any product that may be evaluated in this article, or claim that may be made by its manufacturer, is not guaranteed or endorsed by the publisher.

GLOSSARY

AI, apoptosis index
AMI, acute myocardial infarction
Arg-1, arginase-1
BDI, beck depression inventory
BDNF, brain-derived neurotrophic factor
BSA, bovine serum albumin
BZ, peri-infarct border zone
C34, TLR4 inhibitor
CD68, cluster of differentiation 68
DAMP, damage-associated molecular pattern
DAPI, 4,6-diamino-2-phenyl indole
DEPs, differentially expressed proteins
DG, dentate gyrus
DMEM, Dulbecco-modified eagle's medium
DMSO, dimethyl sulfoxide
ECG, electrocardiograph
ECL, enhanced chemiluminescence
ELISA, enzyme linked immunosorbent assay
FA, ferulic acid
FBS, fetal bovine serum
FST, Forced swimming test
GABA, γ-aminobutyric acid
GAD67, glutamic acid decarboxylase-67
GAPDH, glyceraldehyde-3-phosphate dehydrogenase
GC-MS, gas chromatography-mass spectrometry
HE, hematoxylin and eosin
HRP, horseradish peroxidase
Iba1, ionized calcium-binding adapter molecule 1
IL-1β, interleukin-1β
iNOS, inducible nitric oxide synthase
IOD, integrated optical density
LAD, left anterior descending
LC-MS/MS, label-free liquid chromatography-tandem mass spectrometry
LVEF, left ventricular ejection fractions
LVFS, left ventricular fractional shortening
LViDd, left ventricular end-diastolic inner diameter
LViDs, left ventricular end-systolic inner diameter
LVEDV, left ventricular end-diastolic volume
LVESV, left ventricular end-systolic volume
Kyn, kynurenine
NF-κB, nuclear factor kappa-B
NO, nitric oxide
OFT, open field test
PCF, psycho-cardiology formula (Shuangxinfang)
PEG400, 40% polyethylene glycol 400
PRR, pattern recognition receptors
PVDF, polyvinylidene difluoride
RAGE, receptor of advanced glycation end products
S100A9, $Ca2^{+}$ binding proteins belonging to the S100 family
SD, standard deviation
SSRIs, selective serotonin reuptake inhibitors
TCM, traditional Chinese medicine
TLR4, toll-like receptor 4
TNF-α, tumor necrosis factor-α
Try, tryptophan
TSPO, translocator protein
TUNEL, TdT-mediated dUTP Nick-End Labeling.

frontiers | Frontiers in Pharmacology

ORIGINAL RESEARCH
published: 30 June 2022
doi: 10.3389/fphar.2022.852604

Clinical Efficacy Protocol of Yinhuapinggan Granules: A Randomized, Double-Blind, Parallel, and Controlled Clinical Trial Program for the Intervention of Community-Acquired Drug-Resistant Bacterial Pneumonia as a Complementary Therapy

Jiaoli Wang[1,2†], Haoran Hu[3†], Haixia Du[4], Man Luo[2], Yilan Cao[3], Jiaping Xu[3], Tianhang Chen[4], Yilei Guo[3], Qixiang Li[3], Wen Chen[3], Yifei Zhang[5], Jin Han[3] and Haitong Wan[1,4]**

[1]Zhejiang Chinese Medical University, Hangzhou, China, [2]Department of Respiratory Medicine, Hangzhou First People's Hospital, Hangzhou, China, [3]College of Basic Medical Science, Zhejiang Chinese Medical University, Hangzhou, China, [4]College of Life Science, Zhejiang Chinese Medical University, Hangzhou, China, [5]Dongzhimen Hospital, Beijing University of Chinese Medicine, Beijing, China

OPEN ACCESS

Edited by:
Kornkanok Ingkaninan,
Naresuan University, Thailand

Reviewed by:
Rolf Teschke,
Hospital Hanau, Germany
Surasak Saokaew,
University of Phayao, Thailand

***Correspondence:**
Jin Han
3232168@163.com
Haitong Wan
whtong@126.com

[†]These authors have contributed equally to this work

Specialty section:
This article was submitted to Ethnopharmacology, a section of the journal Frontiers in Pharmacology

Received: 11 January 2022
Accepted: 08 June 2022
Published: 30 June 2022

Citation:
Wang J, Hu H, Du H, Luo M, Cao Y, Xu J, Chen T, Guo Y, Li Q, Chen W, Zhang Y, Han J and Wan H (2022) Clinical Efficacy Protocol of Yinhuapinggan Granules: A Randomized, Double-Blind, Parallel, and Controlled Clinical Trial Program for the Intervention of Community-Acquired Drug-Resistant Bacterial Pneumonia as a Complementary Therapy. Front. Pharmacol. 13:852604. doi: 10.3389/fphar.2022.852604

Background: Community-acquired bacterial pneumonia (CABP) is an important health care concern in the worldwide, and is associated with significant morbidity, mortality, and health care expenditure. *Streptococcus pneumoniae* is the most frequent causative pathogen of CABP. Common treatment for hospitalized patients with CABP is empiric antibiotic therapy using β-lactams in combination with macrolides, respiratory fluoroquinolones, or tetracyclines. However, overuse of antibiotics has led to an increased incidence of drug-resistant S. *pneumoniae*, exacerbating the development of community-acquired drug-resistant bacterial pneumonia (CDBP) and providing a challenge for physicians to choose empirical antimicrobial therapy.

Methods: Traditional Chinese medicine (TCM) is widely used as a complementary treatment for CDBP. *Yinhuapinggan* granules (YHPG) is widely used in the adjuvant treatment of CDBP. Experimental studies and small sample clinical trials have shown that YHPG can effectively reduce the symptoms of CDBP. However, there is a lack of high-quality clinical evidence for the role of YHPG as a complementary drug in the treatment of CDBP. Here, we designed a randomized, double-blind, placebo-controlled clinical trial to explore the efficacy and safety of YHPG. A total of 240 participants will be randomly assigned to the YHPG or placebo group in a 1:1 ratio. YHPG and placebo will be added to standard treatment for 10 days, followed by 56 days of follow-up. The primary outcome is the cure rate of pneumonia, and the secondary outcomes includes conversion rate of severe pneumonia, lower respiratory tract bacterial clearance, lactic acid (LC) clearance rate, temperature, C-reactive protein (CRP), criticality score (SMART-COP score), acute physiological and chronic health assessment system (APACHEII score) and clinical

endpoint events. Adverse events will be monitored throughout the trial. Data will be analyzed according to a pre-defined statistical analysis plan. This research will disclose the efficacy of YHPG in acquired drug-resistant pneumonia.

Clinical Trial Registration: https://clinicaltrials.gov, identifier ChiCTR2100047501

Keywords: Yinhuapinggan (YHPG,), traditional Chinese medicine (TCM), community-acquired drug-resistant bacterial pneumonia (CDBP), multidrug resistance, clinical trial, clinical efficacy

INTRODUCTION

Community-acquired bacterial pneumonia (CABP) is a frequent clinical condition and one of the most common infectious diseases (Sheam et al., 2020). Commonly used treatments include anti-infective therapy, general therapy and symptomatic treatment, of which antibiotic medication is the most important. However, as a double-edged sword, antimicrobial drugs are also an important cause of community-acquired bacterial drug-resistant pneumonia (CDBP) (Kollef and Betthauser, 2019; Wongsurakiat and Chitwarakorn, 2019). With the increasing use of antibiotics worldwide (Klein et al., 2018), the crisis of drug resistance has become more and more serious, and has been listed as a major public health problem by the World Health Organization (Emily et al., 2011). Management of CDBP has been further complicated due to the emergence of antibiotic resistance, particularly from *Streptococcus pneumoniae* strains (Liapikou et al., 2019). Published guidelines for the management of CDBP provide health care practitioners with current, evidence-based standards for antimicrobial therapy, yet even this expert guidance sometimes conflicts (van Duin and Paterson, 2016; Cao et al., 2018; Froes et al., 2019; Torres et al., 2019). Inflammatory diseases of the respiratory system caused by drug-resistant bacterial infections are commonly in respiratory, emergency and intensive care wards. Recently there has been an increasing number of highly hypervirulent carbapenem-resistant *K. pneumoniae* infections (Nair and Niederman, 2021), which might cause blood stream infection or nosocomial pneumonia related sepsis (Lee et al., 2017). As the drug resistance of bacteria makes antibacterial drugs less effective, it is difficult to suppress the expansion of inflammatory cells, which in turn leads to increased lung damage. If the inflammation spreads further, it can cause serious conditions such as waterfall uncontrolled systemic inflammatory response and multi-organ failures, where the morbidity and mortality rate are extremely high (He et al., 2018).

Recent studies, including multiple randomized controlled trials and systematic reviews, have demonstrated that short-term antibiotic therapy is safe and equally effective for most patients with pneumonia (Avdic et al., 2012; Haas et al., 2016; Li et al., 2016; Uranga et al., 2016; Royer et al., 2018; van Duin and Paterson, 2020). Conversely, a longer treatment period puts patients at risk of antibiotic-associated adverse events, such as clostridioides difficile infection and multidrug-resistant (MDR) microorganisms (Vaughn et al., 2019; Wattengel et al., 2019; Du et al., 2021). Antibiotic abuse is becoming more and more serious in China. With its wide application in bacterial pneumonia, the detection rate and infection rate of various drug-resistant bacteria have also increased dramatically (Hu et al., 2018), resulting in a significant increase in the incidence of drug-resistant bacterial pneumonia. Overuse of antibiotics, particularly fluoroquinolones (Møller Gundersen et al., 2019; Gilbert et al., 2020), may increase the risk of MDR bacteria selection and nosocomial pneumonia, though convincing clinical data to support these possibilities are lacking (Tamma et al., 2012). The clinical research of Adrie et al. (2013) showed that the rates of secondary identification rate of MDR bacteria in the monotherapy and dual therapy groups was similar to the incidence of nosocomial pneumonia. This finding should not be construed as supporting evidence that unnecessary antibiotic use is harmless. Widespread abuse of antibiotic does generate more MDR bacteria. Facing the drug-resistant bacterial pneumonia, the choice of antimicrobial drugs based on results of drug sensitivity is very limited, and it is difficult to adequately balance the antimicrobial effect with adverse reactions. At the same time, the development of new antimicrobial drugs is difficult and time consuming (Chellat et al., 2016), making their clinical application very difficult.

For CDBP, the Modern Medical Association refers to the Guidelines for the Diagnosis and Treatment of Chinese Adult Community-Acquired Pneumonia (2016 Edition) and recommends rational use of antibacterial drugs based on the patient's severity and possible pathogen infection. For example, MRSA is given vancomycin, ESBLs *Klebsiella pneumoniae* is given imipenem/statin sodium (Qu & Cao, 2016) to assist mechanical ventilation, enhance sputum removal, maintain the balance of the internal environment, and encourage the patients to cough, turn, or pat the back to promote sputum excretion, give expectorant and anticonvulsant drugs, and nebulize normal saline when necessary. In addition, immunomodulators such as immunoglobulin, transfer factor, thymidine, etc., can be used in adjuvant therapy to help prevent and treat MOF.

Traditional Chinese medicine (TCM) is a popular complementary treatment and complementary medicine with unique advantages in the treatment of drug-resistant bacterial pneumonia. Modern pharmacological studies have shown that TCM is rich in active ingredients, less prone to drug resistance, and has antibacterial, anti-inflammatory, anti-endotoxic and immune enhancing effects (Han et al., 2016; Cheng et al., 2019). Although Western medicine antibacterial drugs have strong antibacterial effects, they have many side effects, such as allergies, double infection, bacterial resistance, which limit their clinical application. Studies have shown that the antibacterial spectrum of single Chinese medicine is narrow, and the antibacterial effect is difficult to adapt to the needs of complex diseases. Traditional Chinese medicine compound has the characteristics of multi-component, multi-channel and multi-target. It has a wide antibacterial spectrum, and has the

TABLE 1 | Components of YHPG (intervention drug).

Scientific name	Chinese Pinyin	Latin scientific name	Parts and form used
Lonicera japonica Thunb.	Jin Yin Hua	*Lonicerae japonicae flos*	Dried flower bud
Ephedra sinica Stapf.	Ma Huang	*Ephedrae herba*	Dried root and rhizome
Prunus armeniaca L. var. ansu Maxim.	Ku Xing Ren	*Armeniacae semen amarum*	Dried mature seeds
Polygonum cuspidatum Sieb.et Zucc.	Hu Zhang	*Polygoni cuspidi rhizoma et radix*	Dried root and rhizome
Pueraria lobata (Willd.) Ohwi.	Ge Gen	*Puerariae lobatae radix*	Dried root
Glycyrrhiza uralensis Fisch.	Gan Cao	*Glycyrrhizae radix et rhizoma*	Dried root and rhizome

advantages of high efficiency, low toxicity and non-resistance. The combination of TCM prescriptions and western drugs not only give full play to the therapeutic characteristics of individualized TCM identification, dose reduction and multi-channel overall regulation, but also can better alleviate clinical symptoms and improve the patient's regression and prognosis. In recent years, a large number of studies have been conducted to find effective alternative or supplements for the treatment of drug-resistant bacterial pneumonia with TCM or a combination of Chinese and Western medicine.

Yinhuapinggan granules (YHPG) were developed by Shaanxi Dongke Pharmaceutical Company Limited (Shaanxi, China) and approved by the Chinese Food and Drug Administration (CFDA) for CDBP treatment in 2002 (Patent No. ZL031 51188.0; Approval No. Z20184088). YHPG consists of six herbs (**Table 1**) that clear heat, detoxify the body and promote lung penetration to expel the evil influence. Studies on animal and cellular pharmacodynamic and mechanism of action of YHPG have shown that it has various effects such as antiviral, antibacterial, antipyretic, analgesic, cough suppressant and immune regulator. Toxicological studies did not show any significant toxic side effects. YHPG have significant preventive and curative effects on influenza virus pneumonia in mice, which can be achieved by regulating the secretion of inflammatory factors in the body and reducing the inflammatory response of respiratory organs (Peng et al., 2016a). After treatment, YHPG can significantly reduce the lung index and lung tissue viral load of influenza virus H1N1-infected mice, and alleviate the pathological changes of lung tissue, which can inhibit influenza virus replication and regulate the decrease of immune function in influenza virus mice (Peng et al., 2015). The mechanism of anti-influenza viral action of YHPG may be related to the attenuation of lung injury in influenza virus-infected mice and the regulation of gene and protein expression of key targets of TLRs signaling pathway (Peng et al., 2016b; Du et al., 2017). However, current clinical data on YHPG as CDBP complementary therapy lack high quality and have limited methodology and sample size. Therefore, we designed a double-blind clinical trial to investigate the efficacy and safety of YHPG for the treatment of acquired pneumonia (Wang et al., 2020). The main hypothesis of this research was as follows: in combination with conventional standard therapy, YHPG was superior to placebo in patients with acquired pneumonia.

METHODS AND DESIGN

Design and Settings

This research is a prospective, randomized, double-blind, placebo-controlled, superior trial (Wang et al., 2021). The trial will be conducted at Hangzhou First People's Hospital and will enroll 240 participants. Participants will be randomly assigned to either the YHPG group or the placebo group in a 1:1 ratio after enrolling and obtaining written informed consent. This trial includes a 7-day baseline period, a 10-day intervention period, and a 56-day follow-up period. A flow chart of the research process is shown in **Figure 1** investigators will monitor and assess participants at each visit. The design follows the rules of the Interventional Trial Standards Protocol Project Proposal (Chan et al., 2013) and the Consolidated Standards for Reporting Trials (CONSORT) (Schulz et al., 2010).

Recruitment

The research will be conducted at Hangzhou First People's Hospital. The recruitment strategy will include advertising in local free newspapers, social media, online publications and posters displayed by participating institutions. Recruitment begins in August 2021 and will be completed over a 2-year period. Patients who agree to participate will be examined and diagnosed by an associate attending physician to confirm their inclusion in the research and will be enrolled in the online allocation system after written informed consent is obtained.

Study Population

Inclusion Criteria

- Voluntary participation, understanding and signing the informed consent form. Be aged 18–85 years, regardless of gender.
- Meet the diagnostic criteria for community-acquired drug-resistant bacterial pneumonia (positive bacterial culture for drug-resistant bacteria in lower respiratory tract specimens).
- Chinese medicine evidence of evil stagnation of the lung and Wei evidence or phlegm-heat congestion of the lung (pneumonia mild to moderate, evidence of Wei-Qi division).
- Satisfy all of the above at the same time.

Exclusion Criteria

- Those whose family or patients do not agree or cannot comply with the treatment.
- Patients with lung infections caused by lung tumors, tuberculosis; or other non-infectious pneumonia; combined with severe heart and brain disease.
- Hospital-acquired drug-resistant bacterial pneumonia; those who are allergic to western or Chinese medicine and have already used Chinese medicine to treat patients.

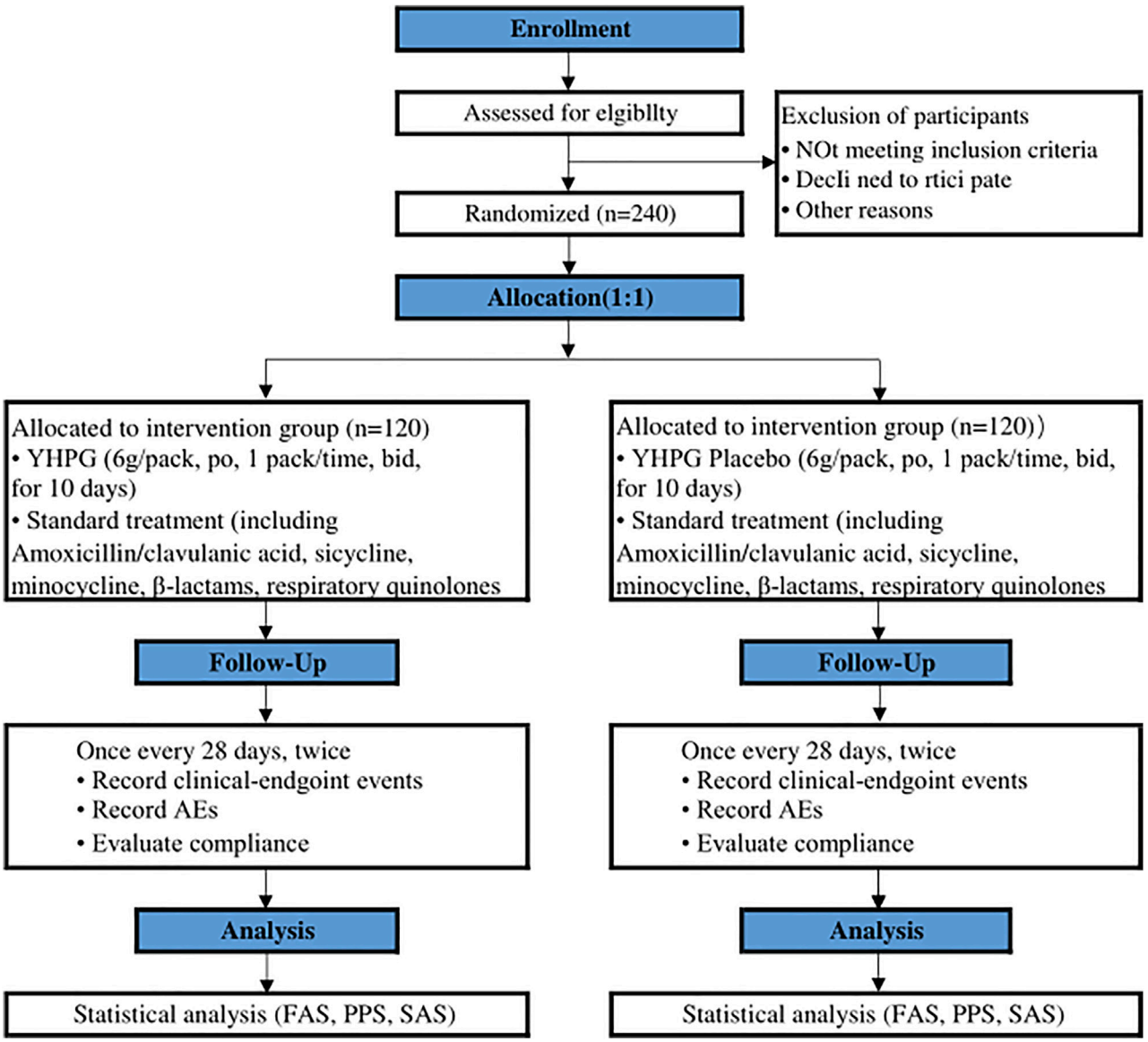

FIGURE 1 | Flowchart of the clinical trial design. The template is from the CONSORT 2010 flowchart. YHPG, Yinhuapinggan; AEs, adverse events; FAS, full analysis set; PPS, per protocol analysis; SAS, safety assessment set.

- Multi-drug resistant patients.

Criteria for Withdrawal, Removal, Dropout and Termination

The investigator's decision to withdraw the case from the trial refers to a situation in which a subject who has been enrolled in the trial becomes unfit to continue the trial, for example: 1) if the subject's condition worsens during the course of the research, the subject is allowed to complete the safety examination and withdraw from the trial to receive other effective treatment in order to protect the subject; 2) during the clinical trial, the subject develops certain comorbidities, complications or special physiological changes that make the subject unfit to continue the trial. 3) the use of other treatments or drugs that are prohibited from being used together, which affects the determination of efficacy and safety; 4) the occurrence of adverse events or serious adverse events that make the subject unfit to continue with the trial; 5) the use of less than 80% or more than 120% of the prescribed amounts of drugs; 6) blinding or emergency blinding.

Subjects have the right to withdraw from the trial in the middle of the trial according to the provisions of the informed consent form; or subjects who have not explicitly requested to withdraw from the trial but are no longer receiving the drug and testing and are lost to follow-up are referred to as disenrollment. The reasons for withdrawal or drop-out should be known and recorded

whenever possible. For example, if the subject feels that the treatment is not effective, if he/she has difficulty tolerating certain discomforts, if there is something that prevents him/her from continuing with the clinical research, if there are financial factors, or if he/she has not given a reason for dropping out.

When a subject withdraws from the trial, the investigator must complete the reason for withdrawal in the eCRF, contact the subject if possible, complete the assessment items that can be completed, and complete an end-of-treatment follow-up record form, recording the last dosing time if possible. For those discharges due to adverse events that are finally judged to be related to the trial drug after follow-up, this must be recorded in the eCRF and the sponsor notified.

The entire research will be terminated if 1) a serious adverse event related to the trial drug occurs during trial implementation; 2) major deviations or human errors are identified during trial implementation that seriously affect the quality of the trial and make it difficult to achieve the trial objectives; 3) termination is requested by the sponsor with full protection of the rights and safety of the subjects (e.g., funding reasons, administrative reasons, etc.); 4) termination is ordered by the State Food and Drug Administration or the Ethics Committee for one reason or another.

All requirements set out in the research protocol must be strictly enforced. Any intentional or unintentional deviation or violation of the trial protocol and GCP principles can be classified as a deviation from the protocol or violation of the protocol. In the course of monitoring, if a deviation from the protocol is found by the supervisor, a deviation record should be completed by the investigator or supervisor, detailing the time of discovery, the time and process of the event, the cause and the corresponding handling measures, signed by the investigator and communicated to the Ethics Committee and the sponsor. In the data statistics and summary report, the investigator analyses and reports on the impact of protocol deviations or breaches that occur on the final data and conclusions.

When serious protocol breaches occur, an assessment should be made. If necessary, the sponsor may terminate the research early.

Randomization, Allocation Concealment Mechanism, and Blinding

After obtaining informed consent from all patients, participants are assigned to two random factors in a 1:1 ratio. The randomization list was generated by computer based on randomly arranged blocks from the test statistician. According to the list, the test drug (including placebo) was blind-labeled and packaged by Shaanxi Dongke Pharmaceutical Co., Ltd., for shipment to the trial site; treatments were randomly assigned by removing sequentially numbered treatments from the relevant supply.

Double-blind controlled trials are blinded to the investigator and the subject. The blinding process is carried out by the person in charge of the clinical research unit in conjunction with the sponsor and the statistician, and the test and control drugs are packaged in a uniform manner, while ensuring that there is no difference in appearance between the two groups of drugs, and the numbering of the drug boxes is blinded. The blinding process should be documented and signed by all staff involved in the blinding process. The blinded base must be sealed on the spot after the drug has been dispensed and kept in two separate locations by the institutional staff responsible for the clinical research and the sponsor. Emergency letters should be sent to each center with the trial drug and kept by the person in charge of the institution until the end of the trial.

In case of emergency, the investigator should ask the head of the center for permission to open the emergency blinded letter and notify the clinical research team leader within 24 h after the blind is broken.

Interventions

Eligible participants will be randomly assigned to either the YHPG group or the placebo group. If YHPG was used prior to randomization, a 2-week drug washout period should be implemented to avoid any potential complications from YHPG. All participants will receive standard treatment.

The YHPG group will receive YHPG (batch no. 20210602, 6 g per packet, manipulated, one packet at a time, 2 times per day). The placebo group will receive YHPG simulant (batch no. 20210602, 6 g per packet, operated, one packet at a time, 2 times per day).

Regarding standard treatment, oral anti-infective drugs with good therapeutic bioavailability such as amoxicillin/clavulanic acid, ciclosporin, minocycline, β-lactams, and respiratory quinolones should be used during the intervention period according to CDBP treatment guidelines (Qu & Cao, 2016). Herbal formulations containing similar ingredients and efficacy to YHPG will not be permitted. Concomitant treatment of comorbidities (e.g., hypertension, diabetes, hyperlipidemia, and other chronic conditions) is permitted during the intervention. Investigators should document concomitant medications faithfully and maintain dose stability during the trial.

With regard to emergency treatment, participants should be treated first in the event of SAE or acute deterioration during treatment and treatment status should be recorded as AE record sheet and combined drug record sheet. If the participant's condition worsens during treatment and continuation of the trial is not recommended (e.g., local or systemic complications such as PE, ARDS, empyema, lung abscess, phlebitis, sepsis, and metastatic abscess), the trial should be considered for termination and conversion to surgery or other types of clinical therapy. Patients will be categorized as "treatment ineffective" in the analysis.

YHPG and capsule mimics will be supplied by Shaanxi Dongke Pharmaceutical Co. The quality control of YHPG is important. The method of determining the composition of YHPG is based on the general principles of "The Chinese Pharmacopoeia (2020 Edition)." Using gas chromatography (General Principle 0512) (Compiled by the National Pharmacopoeia Commission, 2019), each package of YHPG should contain chlorogenic acid ($C_{16}H_{18}O_9$) ≥ 7.5 mg, lignan ($C_{21}H_{20}O_{11}$) ≥ 0.25 mg, rhodopsin ($C_{15}H_{10}O_5$) ≥ 1.5 mg, polydatin ($C_{20}H_{22}O_8$) ≥ 0.38 mg and puerarin ($C_{21}H_{20}O_9$) ≥ 6 mg. The main

TABLE 2 | Research schedule.

Research phase time	Baseline period	Intervention period		Follow-up	
	Visit 1	Visit 2	Visit 3	Visit 4	Visit 5
	−7 to 0 days	5 days	10 days	28 days	56 days
Data collection at baseline	×				
Informed consent	×				
Inclusion/exclusion criteria	×				
Demographic data	×				
Obtain the central random number	×				
Previous history, medical history, and allergies	×				
Comorbidities and co-medications	×				
Safety evaluation					
Vital signs	×	×	×		
Physical examination	×	×	×		
Blood routine	×		×		
Urine routine	×		×		
Blood biochemistry	×		×		
ECG	×		×		
Urine pregnancy test	×		×		
Efficiency evaluation					
Pneumonia cure rate		×	×		
Diagnosis of severe pneumonia	×	×	×		
Laboratory tests	×	×	×		
APACHEII score	×		×		
SMART-COP score	×		×		
Lower respiratory tract bacterial clearance		×	×		
LC clearance rate		×	×		
Clinical-endgoint events		×	×	×	×
Other work					
Dispense drug	×				
Recovery and record of research drug			×		
Record AEs		×	×	×	×
Complications due to medications		×	×		
Evaluate compliance		×	×	×	×

ECG, Electrocardiogram Laboratory tests, C-reactive protein, Lactic acid, Procalcitonin, Oxygenation index; APACHEII score, Acute Physiology, Age and Chronic Health Evaluation; LC, lactic acid; AEs, adverse events.

contents of the capsule mimics are corn starch, silica, caramel (liquid) and sunset yellow. We added 2% YHPG powder to the capsule mimic to achieve an odor, color, taste, and texture comparable to YHPG. After treatment, the packages will be returned to the researchers.

OUTCOMES

Primary and Secondary Outcomes

Details of the items to be measured and the time window for data collection are shown in **Table 2**. The primary outcome was the cure rate of pneumonia (at different time periods). The efficacy was determined by referring to the "Guidelines for Clinical Research on New Chinese Medicines" evaluation method (Editor-in-Chief Zheng Xiaoyu, 2002), and the nimodipine method was used.

$$\text{n (efficacy index)} = (\text{pre} - \text{treatment score} - \text{post} - \text{treatment score})/\text{pre} - \text{treatment score} \times 100\%$$

Markedly effective: clinical symptoms and signs improved significantly, $70\% \leq n < 100\%$; Effective: clinical symptoms and signs improved, $30\% \leq n < 70\%$; Ineffective: clinical symptoms and signs did not improve significantly, or even worsened, $n < 30\%$.

$$\textit{Pneumonia cure rate} = (\textit{number of effective cases} + \text{number of effective cases})/\text{total number of cases} \times 100\%$$

Secondary outcomes were 1) rate of severe pneumonia; 2) criticality score (SMART-COP score) (Charles et al., 2008); 3) acute physiological and chronic health assessment system (APACHEII score) (Knaus et al., 1985); 4) temperature, lower respiratory bacterial clearance, LC clearance rate, CRP, Procalcitonin (PCT), and oxygenation index (PaO2/FiO2); 5) clinical endpoint event incidence (acute respiratory failure, septic shock, acute heart failure, acute coronary syndrome, and all-cause death).

Safety Evaluation Standard

Safety evaluation standard include AEs, SAEs, concomitant medication, changes in clinical laboratory results (e.g., blood routine, blood biochemistry, urine routine, etc.), clinical symptoms, results of vital sign measurements such as

temperature, heart rate, respiratory rate, blood pressure, 12-lead ECG and physical examination.

System Biological Index

Fifty subjects in each group will be randomly selected for metabolic, proteomics, and transcriptional examinations to explore the biomarkers of YHPG for the treatment of CBAP (Wang et al., 2020).

Regarding the collection of blood samples, participants will fast for 10 h before sampling at the start of the research (day 0) and after treatment (day 10). 5 ml of blood will then be drawn and centrifuged and the serum stored in EP tubes at −80°C. Regarding the collection of urine samples, participants will fast for 10 h (and be allowed to drink water) before taking the medication. They will be fasted and water consumption will be prohibited up to 2 h before urine collection 1 h after taking the drug. After taking the drug, water will be rationed to 200 ml/h for 2–8 h and low-fat meals may be consumed for 4 h after taking the drug. Urine samples will be collected at baseline and after treatment (10 days) and stored in EP tubes at −80°C.

Collection and Management of Data

The EDC (eCRF) system will used for this research. The investigator will complete the electronic case report form completely and accurately. Only one clinical research subject's data information will be recorded on each case report form.

After data entry into the eCRF at the research center, quality control staff should check the consistency of the eCRF data with the original records to ensure that the data are accurately completed into the eCRF. The supervisor verifies 100% that the trial data entry in the eCRF system is complete, accurate and consistent with the original medical record information. Data items that are in doubt, or inconsistent with the original medical record information, are promptly challenged. Data entry clerks and investigators were urged to respond to queries and to verify and correct inconsistent data.

Data management staff use logical verification to verify the quality of data entry, and the results of queries are sent to the investigator in the form of a challenge, which is verified and corrected by the investigator. Quality control staff verify data management files and database data.

The research center quality assurance staff carry out random checks on data transfer files and statistical report data to ensure that the data are accurate. The sponsor conducts audits in different areas of the above clinical trial process, sample testing process, data, reporting and calculation process as needed, taking into account the progress of the trial and the results of the quality control staff/monitors' verification.

Throughout the trial, all data obtained during the clinical research will be handled appropriately to ensure the rights and privacy of the subjects participating in the clinical research and the investigators will maintain the confidentiality of the data for a period of 5 years after the completion of the trial.

Sample Size

The formula for calculating the sample size was based on superior clinical trial sample size estimates (Wan et al., 2017a). According to the need of the research, the clinical research part was focused on preliminary exploration, and a small sample size was selected to conduct the research on the early effects of herbal interventions in pneumonia (whether the interventions turned into severe pneumonia) with reference to previous relevant clinical studies on exogenous fever in our project group (unpublished data).

Refer to the clinical research literature of our team for treating pneumonia (Wan et al., 2017b), the healing rate was 85%–89% in the treatment group and the placebo group was 69%–74%. Given an error rate of $\alpha = 0.025$ for the treatment group and $\beta = 0.2$ for the control group. Taking into account the dropout rate of 10%, it is calculated that 216 patients should be allocated to the treatment group and the placebo group in a 1:1 ratio. In conjunction with the need for clinical laboratory sample analysis, a total of 240 cases are therefore proposed to be enrolled, 120 in each group.

Trial Completion

The trial will end after 240 patients have been randomized and all patients have completed 56 days of treatment and follow-up.

Statistical Analyses

EPI 3.0 software was used for data management; SAS software package was used for statistical analysis. All statistical tests were performed using a two-sided test, and a p-value less than or equal to 0.05 was considered statistically significant for the difference tested. Different subgroups of drug-resistant bacteria were also analyzed according to pathogen detection.

Measures for each visit in the different treatment groups will be statistically described using the mean ± standard deviation. Comparisons will be made with the basal values of the screening period and paired t-tests will be used to compare pre- and post-group differences. Changes in the two groups before and after treatment for the primary indicators are compared using analysis of covariance (COANOVA). Comparisons between groups for measures of secondary indicators were made using paired t-tests or rank sum tests.

The statistical description of the count data for each visit in the different treatment groups was done using frequency (composition ratio). Changes before and after treatment in the two groups were tested using the χ^2 test or the exact probability test. Grade information was compared between groups using the rank sum test. **Table 3** displays the analysis method for a specific result.

Adverse Events

All clinical events and clinically significant laboratory adverse reactions will be handled in accordance with the harmonized guidelines detailed in the Common Adverse Events Evaluation Criteria NCI CTCAE Version 4.03 and Emergency Response Reference Plan. Clinical events and clinically significant laboratory test abnormalities will be graded in accordance with NCI CTCAE 4.03. Treatment-induced adverse reactions will be documented by the investigator and brought to the attention of the sponsor's medical monitor, who will discuss with the investigator and determine appropriate action steps. All subjects experiencing AEs, whether or not they are considered treatment-related, must be monitored regularly (if feasible) until symptoms subside, any abnormal laboratory values return to

TABLE 3 | Outcomes and methods of analyses.

Outcome/variable	Hypothesis	Measures	Methods of analyses
Baseline balance test		Quantitative outcomes (age, temperature, heart rate, respiratory rate and blood pressure)	t-test/Wilcoxon rank-sum test
		Qualitative outcomes (sex, marriage and previous treatment)	Chi-squared test/Fisher's exact test/ rank-sum test
Adherence at post-Intervention		Percent and cases Of adherence <80% and ≥80%	Chi-squared test/Fisher's exact test
Concomitant treatments		Percent and cases of concomitant treatments	Chi-squared test/Fisher's exact test
Primary outcome			
Pneumonia cure rate	Improvement occurred		t-test/Wilcoxon rank-sum test Covariance analysis
Secondary outcomes			
Severe pneumonia rate	Improvement occurred		t-test/Wilcoxon rank-sum test
Laboratory tests	Improvement occurred		t-test/Wilcoxon rank-sum test
APACHEII score	Improvement occurred		t-test/Wilcoxon rank-sum test
SMART-COP score			t-test/Wilcoxon rank-sum test
Lower respiratory tract bacterial clearance rate			t-test/Wilcoxon rank-sum test
LC clearance rate			t-test/Wilcoxon rank-sum test
Safety outcomes			
AEs, SAE		Percent and cases Of AEs and SAEs	Chi-squared test/Fisher's exact test
Vital signs		Change value relative to baseline	t-test/Wilcoxon rank-sum test

Laboratory tests, C-reactive protein, Lactic acid, Procalcitonin, Oxygenation index; APACHEII score, Acute Physiology, Age and Chronic Health Evaluation; LC, lactic acid; AEs, adverse events; SAE, serious adverse events.

normal or to baseline levels or until they are considered irreversible, or until the observed changes can be appropriately interpreted. Abnormalities in laboratory tests of clinical significance at level 3 or 4 should be confirmed by repeat testing, if practicable, preferably within 3 working days of receipt of the initial test result.

Quality Control of the Intervention

In order to further ensure the quality of clinical trials, a multi-center trial coordination committee is established, with the general director of the clinical research and acting as the coordinator of the research among the centers of the clinical trial, and the research director of each participating research unit and the director of the sponsor as members of the coordination committee, which is responsible for the implementation of the entire trial and the research and resolution of trial-related issues.

Supervisors are appointed by the sponsor to ensure that the rights and interests of subjects in clinical trials are protected, that data in trial records and reports are accurate and complete, to oversee the implementation of clinical trial protocols, drug clinical trial management norms and relevant regulations, and to conduct regular on-site supervision visits to each center. The investigator shall agree that the clinical trials conducted are subject to inspection and audit by the State Food and Drug Administration, or visual inspection or audit by the sponsor or CRO.

Clinical supervisors have the right to propose amendments to eCRF forms that do not comply with the protocol during the monitoring process. Investigators participating in clinical trials are responsible for making corrections to eCRF forms that are not standardized, such as input errors, but must follow the authenticity of the information.

Through pre-clinical trial training, researchers should be fully aware of and understand the clinical trial protocol and the specific content of its indicators. For the objective indicators specified, they should be checked at the time points and methods specified in the protocol, and attention should be paid to observing adverse reactions or unanticipated toxic effects and following up on them.

Trial Status

This is an ongoing trial. The first participant was enrolled in 16 August 2021; As of 31 December 2021, a total of 78 patients have been enrolled. Recruitment is scheduled to be completed in December 2022 and analysis will be completed by April 2023. The trial will end after the last follow-up visit of the last random participant.

DISCUSSION

CDBP is a common and prevalent clinical condition and one of the most common infectious diseases, in which the use of antimicrobial drugs is most important. And in the face of drug-resistant bacterial pneumonia arising from the proliferation of antimicrobial drugs, the choice of antimicrobial drugs based on drug sensitivity results is very limited, and it is difficult to make an adequate balance between antimicrobial effects and adverse effects (Møller Gundersen et al., 2019; Spellberg and Rice, 2019). Meanwhile,

novel antimicrobial drugs are difficult to develop and have long lead times (Chellat et al., 2016), making their clinical treatment very difficult. A growing body of evidence suggests that the combination of TCM and Western medicine may be the best approach to achieve greater therapeutic efficacy in patients with CDBP.

YHPG is a widely used herbal formulation for the treatment of acquired pneumonia in China. Pharmacological results have shown that YHPG is effective in a variety of mechanistic pathways for the treatment of CDBP, such as anti-influenza virus (Peng et al., 2016b; Du et al., 2017), preventing and controlling influenza virus pneumonia, reducing the viral load of influenza virus in lung tissue, attenuating lung histopathological changes, inhibiting influenza virus replication and regulating immune function (Emily et al., 2011). However, whether YHPG is effective in CDBP patients' needs to be confirmed by a large sample, randomized controlled clinical trial. Therefore, we designed a randomized, double-blind, placebo-controlled clinical trial in the hope of validating the efficacy and safety of CDBP for the treatment of CDBP (Wang et al., 2021). The results of the research may provide a strategy for the combined treatment of Chinese and Western medicine in CDBP.

We chose the efficacy index of pneumonia (different time periods) (efficacy determination was based on the evaluation method of the "Guidelines for Clinical Research on New Chinese Medicines", using the nimodipine method) to assess the cure of CDBP patients (Editor-in-Chief Zheng Xiaoyu, 2002). The efficacy index for pneumonia (different time periods) is a convenient and intuitive criterion that does not require special equipment or advanced training for physicians and is well tolerated by patients. The degree of patient recovery is then assessed by the criticality score (SMART-COP score) (Charles et al., 2008), and the Acute Physiological and Chronic Health Assessment System (APACHEII score) (Knaus et al., 1985). In the meantime, patient temperature, lower respiratory bacterial clearance, LC clearance rate, CRP, PCT, and oxygenation index (PaO2/FiO2) together form part of the efficacy index.

In addition, we applied metabolic and proteomics analyses to explore therapeutic biomarkers of YHPG for CDBP and to improve CDBP treatment by providing an objective basis for precise treatment (Wang et al., 2020).

However, several limitations need to be considered. Firstly, the YHPG used in this trial is for the treatment of early and mid-stage CDBP, so these findings may not be applicable to severe CDBP. secondly, the AEs will only be recorded and treated during the 10-day intervention period and 56-day follow-up period, which is a relatively short period, but the short-term results could encourage further prospective studies with different treatment regimens and longer follow-up times. Finally, this trial will be conducted at Hangzhou First People's Hospital, and the results of treatment effects and individual differences in YHPG in other areas are not available. More efforts should be made to optimize these shortcomings and answer these questions in future research.

DATA AVAILABILITY STATEMENT

The original contributions presented in the study are included in the article/supplementary material, further inquiries can be directed to the corresponding authors.

ETHICS STATEMENT

The studies involving human participants were reviewed and approved by the Research Ethics Committee of Hangzhou First People's Hospital (IRB#2021-20210408-01). The patients/participants provided their written informed consent to participate in this study.

AUTHOR CONTRIBUTIONS

HW and JH designed this study. JW, HH, and HD were responsible for the drafting of the manuscript. ML and TC were responsible for ensuring the implementation of the clinical study. YC, JX, and YG participated in the revision of the manuscript, QL, WC, and YZ participated in modifications to the research protocol. All authors have read and approved the final version of the manuscript.

FUNDING

This project was supported by the National Natural Science Foundation of China (No. 81930111).

ACKNOWLEDGMENTS

We appreciate the efforts and cooperation of all research staff and patients involving this study. We appreciate the great technical support from the Key Laboratory of TCM Encephalopathy of Zhejiang Province (grant No. 2020E10012).

REFERENCES

Adrie, C., Schwebel, C., Garrouste-Orgeas, M., Vignoud, L., Planquette, B., Azoulay, E., et al. (2013). Initial Use of One or Two Antibiotics for Critically Ill Patients with Community-Acquired Pneumonia: Impact on Survival and Bacterial Resistance. *Crit. Care* 17 (6), R265. doi:10.1186/cc13095

Avdic, E., Cushinotto, L. A., Hughes, A. H., Hansen, A. R., Efird, L. E., Bartlett, J. G., et al. (2012). Impact of an Antimicrobial Stewardship Intervention on Shortening the Duration of Therapy for Community-Acquired Pneumonia. *Clin. Infect. Dis.* 54, 1581–1587. doi:10.1093/cid/cis242

Cao, B., Huang, Y., She, D. Y., Cheng, Q. J., Fan, H., Tian, X. L., et al. (2018). Diagnosis and Treatment of Community-Acquired Pneumonia in Adults: 2016 Clinical Practice Guidelines by the Chinese Thoracic Society, Chinese Medical Association. *Clin. Respir. J.* 12 (4), 1320–1360. doi:10.1111/crj.12674

Chan, A. W., Tetzlaff, J. M., Altman, D. G., Laupacis, A., Gøtzsche, P. C., Krleža-Jerić, K., et al. (2013). SPIRIT 2013 Statement: Defining Standard Protocol Items for Clinical Trials. *Ann. Intern. Med.* 158, 200–207. doi:10.7326/0003-4819-158-3-201302050-00583

Charles, P. G., Wolfe, R., Whitby, M., Fine, M. J., Fuller, A. J., Stirling, R., et al. (2008). SMART-COP: a Tool for Predicting the Need for Intensive Respiratory or Vasopressor Support in Community-Acquired Pneumonia. *Clin. Infect. Dis.* 47, 375–384. doi:10.1086/589754

Chellat, M. F., Luka, R., and Rainer, R. (2016). Targeting Antibioticresistance. *Angew. Chem. Int. Ed. Engl.* 55 (23), 6600–6626. doi:10.1002/anie.201506818

Cheng, C., Zhang, W., Zhu, B., and Shi, L. (2019). Research Progress on the Effect of Traditional Chinese Medicine Against Common Drug-Resistant Bacteria and its Mechanism. *J. Nanjing Univ. Traditional Chin. Med.* 35 (2), 229–233.

Compiled by the National Pharmacopoeia Commission (2019). *Draft of the Four General Rules of the 2020 Edition of the Chinese Pharmacopoeia*. Beijing: China Medical Science and Technology Press.

Du, H., Wan, H., He, Y., Yang, J., Lu, Y., and Zhou, H. (2017). *In Vitro* Anti-Influenza A H1N1 Virus Effect of Yinhuapinggan Granules. *J. Traditional Chin. Med.* 58 (23), 2039–2044.

Du, S., Wu, X., Li, B., Wang, Y., Shang, L., Huang, X., et al. (2021). Clinical Factors Associated with Composition of Lung Microbiota and Important Taxa Predicting Clinical Prognosis in Patients with Severe Community-Acquired Pneumonia. *Front. Med.* 24, 1–14. doi:10.1007/s11684-021-0856-3

Editor-in-Chief Zheng Xiaoyu (2002). *Guiding Principles for Clinical Research of New Traditional Chinese Medicine Drugs Trial*. Beijing: China Medical Science and Technology Press.

Emily, L., Weil, D. E., Mario, R., and Hiroki, N. (2011). The Who Policypackage to Combat Antimicrobial Resistance. *Bull World Health Organ* 8 (95), 390–392. doi:10.2471/BLT.11.088435

Froes, F., Pereira, J. G., and Póvoa, P. (2019). Outpatient Management of Community-Acquired Pneumonia. *Curr. Opin. Pulm. Med.* 25 (3), 249–256. doi:10.1097/MCP.0000000000000558

Gilbert, T. T., Arfstrom, R. J., Mihalovic, S. W., Dababneh, A. S., Varatharaj Palraj, B. R., Dierkhising, R. A., et al. (2020). Effect of β-Lactam Plus Macrolide versus Fluoroquinolone on 30-Day Readmissions for Community-Acquired Pneumonia. *Am. J. Ther.* 27 (2), e177–e182. doi:10.1097/MJT.0000000000000788

Haas, M. K., Dalton, K., Knepper, B. C., Stella, S. A., Cervantes, L., Price, C. S., et al. (2016). Effects of a Syndrome-specific Antibiotic Stewardship Intervention for Inpatient Community-Acquired Pneumonia. *Open Forum Infect. Dis.* 3, ofw186. doi:10.1093/ofid/ofw186

Han, F., Xing, R.-H., Chen, L., Xiong, W., Yang, M., and Zhao, Z.-D. (2016). Research Progress on Antibacterial Resistance of Traditional Chinese Medicine. *Chin. J. Chin. Materia Medica* 4 (15), 813–817. doi:10.4268/cjcmm20160509

He, X., Li, D., Qiao, L., and Kang, Y. (2018). Research Progress on the Epidemiology and Prognosis of Sepsis. *Chin. J. Crit. Care Med.* 30 (5), 486–489. doi:10.3760/cma.j.issn.2095-4352.2018.05.019

Hu, F., Guo, Y., Zhu, D., Wang, F., Jiang, X., Xu, Y., et al. (2018). Surveillance of Bacterial Drug Resistance in China by CHINET in 2017. *Chin. J. Infect. Chemother.* 18 (3), 241–251. doi:10.16718/j.1009-7708.2018.03.001

Klein, E. Y., van Boeckel, T. P., Martinez, E. M., Pant, S., Gandra, S., Levin, S. A., et al. (2018). Global Increase and Geographic Convergence in Antibiotic Consumption between 2000 and 2015. *Proc. Natl. Acad. Sci. U. S. A.* 115 (515), E3463–E3470. doi:10.1073/pnas.1717295115

Knaus, W. A., Draper, E. A., Wagner, D. P., and Zimmerman, J. E. (1985). Apache II: a Severity of Disease Classification System. *Crit. Care Med.* 13 (10), 818–829. doi:10.1097/00003246-198510000-00009

Kollef, M. H., and Betthauser, K. D. (2019). New Antibiotics for Community-Acquired Pneumonia. *Curr. Opin. Infect. Dis.* 32 (2), 169–175. doi:10.1097/QCO.0000000000000526

Lee, C. R., Lee, J. H., Park, K. S., Jeon, J. H., Kim, Y. B., Cha, C. J., et al. (2017). Antimicrobial Resistance of Hypervirulent *Klebsiella pneumoniae*: Epidemiology, Hypervirulence-Associated Determinants, and Resistance Mechanisms. *Front. Cell. Infect. Microbiol.* 7, 483. doi:10.3389/fcimb.2017.00483

Li, D. X., Ferrada, M. A., Avdic, E., Tamma, P. D., and Cosgrove, S. E. (2016). Sustained Impact of an Antibiotic Stewardship Intervention for Community-Acquired Pneumonia. *Infect. Control Hosp. Epidemiol.* 37, 1243–1246. doi:10.1017/ice.2016.165

Liapikou, A., Cilloniz, C., Palomeque, A., and Torres, T. (2019). Emerging Antibiotics for Community-Acquired Pneumonia. *Erratum Expert Opin Emerg Drugs* 24 (4), 221–231. doi:10.1080/14728214.2019.1685494

Møller Gundersen, K., Nygaard Jensen, J., Bjerrum, L., and Hansen, M. P. (2019). Short-course vs Long-Course Antibiotic Treatment for Community-Acquired Pneumonia: A Literature Review. *Basic Clin. Pharmacol. Toxicol.* 124 (5), 550–559. doi:10.1111/bcpt.13205

Nair, G. B., and Niederman, M. S. (2021). Updates on Community Acquired Pneumonia Management in the ICU. *Pharmacol. Ther.* 217, 107663. doi:10.1016/j.pharmthera.2020.107663

Peng, X., He, Y., Zhou, H., Zhang, Y., Yang, J., Chen, J., et al. (2015). *In Vivo* Anti-Influenza A H1N1 Influenza Virus Effect of Yinhua Pinggan Granules. *Chin. J. Chin. Materia Medica* 40 (19), 3845–3850. doi:10.4268/cjcmm20151926

Peng, X. Q., Zhou, H. F., Lu, Y. Y., Chen, J.-K., Wan, H.-T., and Zhang, Y.-Y. (2016). Protective Effects of Yinhuapinggan Granule on Mice with Influenza Viral Pneumonia. *Int. Immunopharmacol.* 30 (1), 85–93. doi:10.1016/j.intimp.2015.11.029

Peng, X. Q., He, Y., Zhou, H. F., Wang, H. T., Zhang, Y. Y., and Yang, J. H. (2016). Antiviral Effects of Yinhuapinggan Granule against Influenza Virus Infection in the ICR Mice Model. *J. Nat. Med.* 70 (1), 75–88. doi:10.1007/s11418-015-0939-z

Qu, J. M., and Cao, B. (2016). Chinese Society of Respiratory Medicine. Guidelines for the Diagnosis and Treatment of Adult Community-Acquired Pneumonia in China (2016 Edition). *Chinese J. Tubercul. Respir. Med.* 39 (4), 253–279. doi:10.3760/cma.j.issn.1001-0939.2016.04.005

Royer, S., DeMerle, K. M., Dickson, R. P., and Prescott, H. C. (2018). Shorter versus Longer Courses of Antibiotics for Infection in Hospitalized Patients: A Systematic Review and Meta-Analysis. *J. Hosp. Med.* 13, 336–342. doi:10.12788/jhm.2905

Schulz, K. F., Altman, D. G., and Moher, D. (2010). CONSORT 2010 Statement: Updated Guidelines for Reporting Parallel Group Randomised Trials. *BMJ* 340, c332–2. doi:10.1136/bmj.c332

Sheam, M. M., Syed, S. B., Nain, Z., Tang, S. S., Paul, D. K., Ahmed, K. R., et al. (2020). Community-acquired Pneumonia: Aetiology, Antibiotic Resistance and Prospects of Phage Therapy. *J. Chemother.* 32 (8), 395–410. doi:10.1080/1120009X.2020.1807231

Spellberg, B., and Rice, L. B. (2019). Duration of Antibiotic Therapy: Shorter Is Better. *Ann. Intern Med.* 171 (3), 210–211. doi:10.7326/M19-1509

Tamma, P. D., Cosgrove, S. E., and Maragakis, L. L. (2012). Combination Therapy for Treatment of Infections with Gram-Negative Bacteria. *Clin. Microbiol. Rev.* 25, 450–470. doi:10.1128/CMR.05041-11

Torres, A., Chalmers, J. D., Dela Cruz, C. S., Dominedò, C., Kollef, M., Martin-Loeches, I., et al. (2019). Challenges in Severe Community-Acquired Pneumonia: a Point-Of-View Review. *Intensive Care Med.* 45 (2), 159–171. doi:10.1007/s00134-019-05519-y

Uranga, A., España, P. P., Bilbao, A., Quintana, J. M., Arriaga, I., Intxausti, M., et al. (2016). Duration of Antibiotic Treatment in Community-Acquired Pneumonia: A Multicenter Randomized Clinical Trial. *JAMA Intern Med.* 176, 1257–1265. doi:10.1001/jamainternmed.2016.3633

van Duin, D., and Paterson, D. L. (2016). Multidrug-Resistant Bacteria in the Community: Trends and Lessons Learned. *Infect. Dis. Clin. North Am.* 30 (2), 377–390. doi:10.1016/j.idc.2016.02.004

van Duin, D., and Paterson, D. L. (2020). Multidrug-Resistant Bacteria in the Community: An Update. *Infect. Dis. Clin. North Am.* 34 (4), 709–722. doi:10.1016/j.idc.2020.08.002

Vaughn, V. M., Flanders, S. A., Snyder, A., Conlon, A., Rogers, M. A. M., Malani, A. N., et al. (2019). Excess Antibiotic Treatment Duration and Adverse Events in Patients Hospitalized with Pneumonia: A Multihospital Cohort Study. *Ann. Intern Med.* 171 (3), 153–163. doi:10.7326/M18-3640

Wan, X., Zhang, L., and Liu, J. (2017). Estimation of Sample Size in Clinical Studies: (1) Clinical Trials. *J. Tradit. Chin. Med.* 48, 504–507. doi:10.3390/molecules25225319

Wan, H, Jin, Y, He, Y, Yang, J, Zhou, H., Yu, Li, et al. (2017). Diagnosis and Curative Effect Evaluation Criteria for the Syndrome of Exogenous Febrile

Disease and Stagnation of Lung Health (Trial Implementation). *World J. Integr. Traditional Chin. West. Med.* 12 (10), 1469–1471.

Wang, Y., Xu, J., Yang, J., Zhang, L., Pan, Y., Dou, L., et al. (2020). Effects of Guanxinshutong Capsules as Complementary Treatment in Patients with Chronic Heart Failure: Study Protocol for a Randomized Controlled Trial. *Front. Pharmacol.* 11, 571106. doi:10.3389/fphar.2020.571106

Wang, Y., Guo, Y., Lei, Y., Huang, S., Dou, L., Li, C., et al. (2021). Design and Methodology of a Multicenter Randomized Clinical Trial to Evaluate the Efficacy of Tongmai Jiangtang Capsules in Type 2 Diabetic Coronary Heart Disease Patients. *Front. Pharmacol.* 12, 625785. doi:10.3389/fphar.2021.625785

Wattengel, B. A., Sellick, J. A., Skelly, M. K., Napierala, R., Jr, Schroeck, J., and Mergenhagen, K. A. (2019). Outpatient Antimicrobial Stewardship: Targets for Community-Acquired Pneumonia. *Clin. Ther.* 41 (3), 466–476. doi:10.1016/j.clinthera.2019.01.007

Wongsurakiat, P., and Chitwarakorn, N. (2019). Severe Community-Acquired Pneumonia in General Medical Wards: Outcomes and Impact of Initial Antibiotic Selection. *BMC Pulm. Med.* 19 (1), 179. doi:10.1186/s12890-019-0944-1

Conflict of Interest: The authors declare that the research was conducted in the absence of any commercial or financial relationships that could be construed as a potential conflict of interest.

Publisher's Note: All claims expressed in this article are solely those of the authors and do not necessarily represent those of their affiliated organizations, or those of the publisher, the editors and the reviewers. Any product that may be evaluated in this article, or claim that may be made by its manufacturer, is not guaranteed or endorsed by the publisher.

Frontiers in Pharmacology

Explores the interactions between chemicals and living beings

The most cited journal in its field, which advances access to pharmacological discoveries to prevent and treat human disease.

Discover the latest Research Topics

See more →

Frontiers

Avenue du Tribunal-Fédéral 34
1005 Lausanne, Swizerland
frontiersin.org

Contact us

+41 (0)21 510 17 00
frontiersin.org/about/contact